Journal of

Published to provide a continuing, authoritative, and up-to-date record of technologic, engineering, and economic progress in all branches of the metals industry by the

Metals Branch

American Institute of Mining and Metallurgical Engineers, Inc.
29 West 39th Street, New York 18

o o o

T. W. LIPPERT
Manager of Publications
Editor, Journal of Metals

o o o

JAMES A. STANGARONE
Advertising Manager

o o o

WINIFRED D. GIFFORD, HAROLD N. UNDERHILL, *Assistant Editors;* GRACE PUGSLEY, *Production Manager;* WALTER J. SEWING, *Assistant.*

o o o

OFFICERS, AIME

Lewis E. Young	*President*
A. B. Kinzel	*Vice President*
Philip Kraft	*Vice President*
R. W. Thomas	*Vice President*
C. H. Benedict	*Vice President*
D. H. McLaughlin	*Vice President*
Andrew Fletcher	*VP & Treasurer*

o o o

AIME STAFF

E. H. Robie	*Secretary*
H. A. Maloney	*Asst. Treasurer*
E. J. Kennedy, Jr.	*Asst. Secretary*
Ernest Kirkendall	*Asst. Secretary*
William H. Strang	*Asst. Secretary*
H. Newell Appleton	*Asst. to Secretary*

o o o

Technical Publications Comittee

E. C. Meagher	*Chairman*
E. J. Kennedy, Jr.	*Secretary*

o o o

Auxiliary Publications Committee

O. B. J. Fraser	*Chairman, IMD*
Michael Tenenbaum	*Chairman, ISD*
Philip T. Stroup	*Chairman, EMD*

o o o

Publications Advisory Committee

J. B. Austin, F. N. Rhines, C. D. King, John D. Sullivan, Fred P. Peters, A. W. Schlechten, Frank T. Sisco, M. Tenenbaum, Felix Wormser

o o o

The AIME Also Publishes
Mining Engineering
and
Journal of Petroleum Technology

METALS

IN THIS ISSUE

VOL. 188, NO. 1 JANUARY, 1950

COVER

The new induction-furnace melting dept. at Eastern Stainless Steel Corp., Baltimore. There are four Ajax furnaces, each of 5000-lb capacity, 1200 cycles and 840 kw. Both home and bought stainless steel scrap is used. The ingots are hot-rolled by Lukens at Coatesville and cold-rolled in the Eastern plant.

FEATURES

NEWS

TECHNICAL ARTICLES

TRANSACTIONS

Technical Notes

Published the first day of each month by the American Institute of Mining and Metallurgical Engineers, Inc., 29 West 39th Street, New York 18, N. Y. Telephone: PEnnsylvania 6-9220. Subscription $8 per year for non-AIME members in United States and North, South and Central America; $9, foreign; $6 for AIME members, or $4 in combination with a subscription to *Mining Engineerng* or the *Journal of Petroleum Technology*. Single copies, 75 cents; special issues, $1.50 . . . The AIME is not responsible for any statement made or opinion expressed in its publications. . . . Copyright 1949 by the American Institute of Mining and Metallurgical Engineers, Inc. . . . Registered cable address, AIME New York . . . Indexed in Engineering Index, Industrial Arts Index and Chemical Abstracts . . . Reentered as second-class matter Sept. 21, 1949, at the post office at New York, N. Y., under the Act of March 3, 1879.

J. J. Green (p. 16F): born in Highspire, Pa., and attended Midland high school, graduating from Carnegie Tech with B.S. degree. He now lives in Rosslyn Farms, Carnegie, Pa. Was with Crucible Steel Co. Midland Plant and is now Assistant Superintendent of Melting at the Universal Cyclops Steel Corp., Bridgeville, Pa. . . . **H. R. Hanley** (p. 16G): born in Paxton, Ill. Went to Rice Collegiate Inst. and graduated from Missouri School of Mines & Metallurgy with degrees of B.S.-Min. Eng.; Met. Eng., D. Engineering (Hon.). Is a member of AIME and lives in Rolla Mo. Was connected with the Bully Hill Copper Mining & Smelting Co., U. S. Smelting Refining & Mining Co., and Consulting Engineer; extractive and refining metallurgy, secondary metals, galvanizing, for miscellaneous companies; was Prof. of Met. Eng. Missouri School of Mines & Met. (now Emeritus). Mr. Hanley has previously presented fourteen AIME papers on Insoluble Anodes Electrolytic Zinc; Adherence of Zinc to Aluminum Cathode; Metallurgy of Zinc; Misch. Papers on Furnaces, etc. . . . **Sven Fornander** (p. 22): born in Karlstad, Sweden, attending high school there and graduated from Royal Institute of Technology, Stockholm as Bergsingeniör. He is a member of AIME and lives in Surahammar. Was formerly Assistant to Dr. G. Phragmen, Metallografiska Institutet, Melting Shop Manager and currently Research Manager Surahammars Bruks AB. Mr. Fornander's chief recreation is trout fishing. . . . **Folke Nilsson** (p. 22): born in Nyed, Sweden, attending high school in Karlstad and graduating from Royal Technical University, Stockholm, with degree of Bergsingeniör. He resides in Hagfors, Sweden. Was for a time Metallurgist, becoming General Superintendent of Metallurgical Dept. and currently General Manager of Hagfors Steelworks, Uddeholm AB, Hagfors, Sweden. Enjoys fishing, golf, mountain climbing and skiing. . . . **Samuel F. Carter** (p. 30): born in Bessemer, Ala., went to high school there and received degrees of B.S. and M.S. from Birmingham-Southern College and University of Wisconsin. He is a Junior Member of AIME and lives in Birmingham. Mr. Carter has previously presented an AIME paper on Effect of Some Melting Variables on Tensile Properties. His major interests are hunting, fishing and tennis. . . . **Rolland S. French** (p. 53): born in Providence, R. I., attended Newton high school, graduating from M.I.T. and Yale Univ. with B.Sc. and M.Eng. Is a member of AIME and lives in Nichols, Conn. Is Metallurgical Eng. in Research Dept. Bridgeport Brass Co., and for some years instructor in Bridgeport Engineering Inst. Mr. French has previously presented a paper before the AIME on Grain Growth & Recryst. of 70-30 Cartridge Brass. His chief recreations are color photography, singing and (in his own words) "matching wits with children, two boys and two girls—average success!" . . . **Herbert S. Kalish** (p. 59): born New York City, attending Brooklyn Technical high school, graduating from Missouri School of Mines with B.S. degree also from Univ. of Pennsylvania, with M.S., B.S. in Met. E., M.S. in Met. E. degrees. Is a member of AIME and lives in Jamaica, N. Y. He was connected with the Gary Wks. of Carnegie-Illinois Steel Corp as Met. Observer; Research Eng. at Battelle Memorial Inst.; Research Asst. Thermodynamics Lab, University of Penn., Research Met. Electric Storage Battery Co., Senior Engineer Sylvania Electric Products, Inc., Bayside, N. Y. Mr. Kalish has previously presented an AIME paper on Low Temperature Properties of Tin and Tin-Lead Alloys. He enjoys outdoor sports

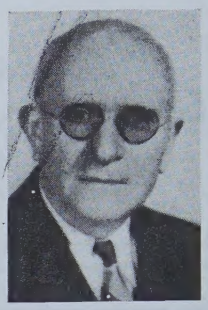

H. R. Hanley

S. Fornander

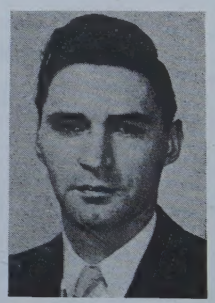

S. F. Carter

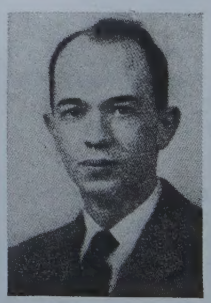

R. S. French

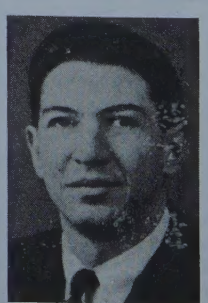

H. S. Kalish

and photography. . . . **M. H. Caron** (p. 67): born in Java, attended high schools at Soerabaia and Semarang, Java, graduating from Technical University, Delft, Holland, with degree of Mining Engineer. Is a member of AIME and lives in Ryswyk (Z-H). Molenlaan 6, Netherlands. Was in employ of the N.E.I., Bureau of Mines, for some years as Chief Engineer; elected as full professor of Metallurgy at Delft, Holland. . . . **Bruno B. A. Luzzatto** (p. 105): born in Trieste, Italy, attended Liceo Classico Marco Polo in Venice, Italy and graduated from the Engineering School of Univ. of Milano, Italy, with Ph.D. degree. Is a member of AIME and resides in Washington. Was Production Manager of Aluminum Factories (Montecatini) in Italy; worked in France as manager of Electrodes factory for Alais, Froges & Camargue; Consulting Engineering work for the Elektrokemisk

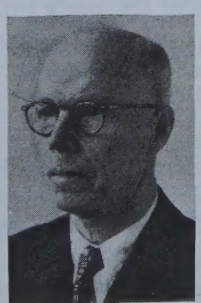

M. H. Caron

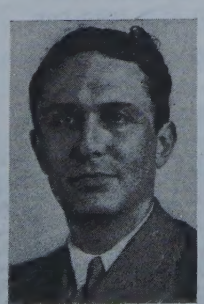

B. Luzzatto

of Oslo, Norway. Board of Economic Warfare and Foreign Economic Administration in Washington, D. C., Chief industrial rehabilitation in Italy for UNRRA. Now with Economic Cooperation Administration, Washington, D. C. His major interests are tennis, tinkering, and . . . economics. . . . **Chih-Chung Wang** (p. 136): born in Wusih, Kiangsu, China. Attended Nankai Middle School, Chungking, China, and graduated from Tangshan Eng. College of Chalo-Tung University, China, with B.S. in Mining & Met. Eng. Is a Student Associate AIME and lives in Chicago. Is now Teaching Asst. in the Dept. of Metallurgical Eng. at Illinois Inst. of Tech. and is working for M.S. degree. Mr. Wang's chief interests are photography, music and traveling. . . . **P. W. Ramsey** (p. 139): born in Wilkinsburg, Pa., and attended high school there. Graduated from W & J. College and Carnegie Tech with B.S.-Met. Eng. degree. Is a member of AIME and lives in Palmerton, Pa. Served in the U. S. Navy (Destroyers) for two years and is now Metallurgical Investigator for N. J. Zinc Co. Mr. Ramsey has previously presented an AIME paper on Rolled Zinc-Titanium Alloys as co-author. His chief recreation is deer-hunting in the Poconos and the activities of the Choral and Clambake Society of Lower Towamensing along with several other AIME members. . . . **G. L. Werley** (p. 139): born in New Tripoli, Pa., attended high school in Palmerton, Pa. and graduated from Pennsylvania State College with degree of B.S. He lives in Palmerton, and is associated with the New Jersey Zinc Co. Mr. Werley has previously presented papers before various technical societies. He enjoys golf and is a stamp collector. . . . **B. L. Averbach** (p. 150): born in Rochester, N. Y., went to Benjamin Franklin high school and Rensselaer Polytechnic Inst. receiving degree of M. Met. Eng., and Sc.D. degree from M.I.T. Is a member of AIME and lives in Cambridge, Mass. Was Chief Metallurgist at U. S. Radiator Corp.; Metallurgist at General Electric Co., Schenectady and currently Asst. Prof. Dept. of Met., M.I.T. Mr. Averbach has previously presented papers on retained austenite, recrystallization. His chief activities are squash racquets, baseball, golf. . . . **A. R. Elsea** (p. 154): born in Columbus, Ohio, attended high schools in Columbus and Joliet, Ill., and graduated from Ohio State University with degree of B. Met. Engr. Is a mem-

C. C. Wang

P. W. Ramsey

G. L. Werley

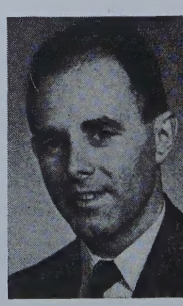

B. L. Averback

A. B. Elsea

ber of AIME and makes his home in Columbus, Ohio. Was Research Engineer for some time and currently Asst. Supervisor at Battelle Memorial Institute. Mr. Elsea has previously presented AIME papers as co-author on Cobalt Chromium Binary System and on Investigation of Temper Brittleness in Low Alloy Steels. His chief recreations are camping, fishing, gardening and photography. . . . **A. E. Nehrenberg** (p. 162); born in Draper, S. Dak., attended Rapid City high school and graduated from S. Dak. School of Mines, Rapid City, S. D. with B.S. degree. Also studied at Armour Inst. and was a night school student at Columbia Univ. Is a member of AIME and lives in Bloomfield, N. J. Worked as Met. Observer and Asst. Met. at Carnegie-Illinois Steel Corp., S. Chicago. Metallurgist in Charge at Amertop, Forest Park, Ill., Naval Ordnance Plant. Enjoys bowling, golf and contract bridge. . . . **H. A. Lepper, Jr.,** (p. 175): born in Washington, D. C. and attended McKinley high school there, graduating with degrees of B.S. in C.E. from George Washington Univ., M.S. at University of Illinois, Dr. Eng. at Yale Univ. Was for a time Graduate Assistant, Reinforced Concrete Slab Investigation, at Univ. Illinois and now Instructor, Asst. Professor in Civil Engineering Dept. at Yale. Mr. Lepper's home is in Hamden, Conn. . . . **R. W. Fenn, Jr.** (p. 175) born in Torrington, Conn., attended Crosby high school in Waterbury, Conn., graduating from Rensselaer Polytechnic Inst. with B. in Met. Eng. degree, Yale University, M.Eng., D.-Eng. Is a Student Associate member of AIME and lives in Midland, Mich. Was for some time Asst. Metallurgist at General Elec. Co., Lynn, Mass. and currently Research Metallurgist at Dow Chemical Co., Magnesium Division. Mr. Fenn is interested in woodworking, tennis, volley ball and skiing. . . . **Paul Gordon** (p. 182): born in Hartford, Conn., went to Weaver High in that city, and graduated from Wesleyan Univ. and M.I.T. with degrees of B.S., M.S. and Sc.D. in Metallurgy. Is a member of AIME and lives in Chicago. Was Research Asst., Dept. of Metallurgy, M.I.T.; Group Leader, Phys. Met. Research, M.I.T. Metallurgical Project for the Manhattan Project and AEC: Research Associate, Dept. of Met., M.I.T., and is at the present time Asst. Prof. Dept. of Met.Eng., Illinois Inst. of Technology, Chicago. Mr. Gordon's chief recreation is contract bridge.

A. R. Kaufmann (p. 182); born in Philadelphia, went to Cheltenham high school in Elkins Park, Pa. and received B.Sc. degree from Lafayette Univ. and Sc.D. in Met. from M.I.T. Mr. Kaufmann is a member of AIME and lives in Lexington, Mass. He is now an Associate Professor of Metallurgy at M.I.T. His chief interest is farming.

A. E. Nehrenberg

ATTENTION AUTHORS

The Fall Meeting of the Institute of Metals Div., AIME, will be at the Sheraton Hotel, Chicago, Oct. 23-25. Deadline for papers for this meeting is April 15, 1950.

* With reladling a much closer control of electric furnace steel analyses is possible according to J. J. Green (p. 16F). It is also possible to melt to relatively narrow aims within any given specification.

* Automatic current settings for arc-furnace operation result in great savings, according to L. A. Wynd (p. 17), who gives a detailed report on results in the Republic plant.

* Inductive stirring, a new Swedish device for arc furnaces, is described on p. 22.The relations between this equipment and the melting-down period, power consumption, oxidizing period and slag removal are dealt with in detail.

* Quantitative hydrogen analyses of electric arc-furnace carbon steels with varied melting practices are given by Sam F. Carter (p. 30).

* The U. S. Steel Corp. has a seventeen-man mission of experts in Pakistan making a study of the country's industrial potential. In steel, a modest rolling mill is planned. Mr. E. E. Robbins, the Corporation's Far East regional director, heads the mission which is the outgrowth of conversations last August between Mr. Fairless and Mr. Ghulam Mohammed, the Pakistani Finance Minister. Corporation willingness to help Pakistan has already had a great influence in improving political relations with that country.

* The commercial treaty recently signed between the U. S. and Uruguay is regarded as a model for others under President Truman's famous Fourth Point. American investors are assured the very maximum of protection and the terms are reciprocal in that Uruguayan business men are accorded the same set of rights in the U. S. if they wish to make use of them.

The Uruguayan agreement is called a Treaty of Friendship, Economic Development and Commerce. A similar agreement is in prospect with India.

* American steel exports to Canada are facing difficulties. Britain is stepping up deliveries and Germany has just sent an energetic trade mission to capture a share of the Canadian market. If Germany were to replace 5 pct of American steel exports to Canada it would represent $30 million annually, which would buy a lot of Canadian grains.

* The Hopkins electric hot-top process which had its trial runs at Allegheny-Ludlum's Watervliet plant, is now being installed by three other companies--Eastern Stainless, Braeburn and Universal-Cyclops. Better ingot yields is the objective.

* Several alloy producers also report excellent increases in ingot yields by using "Thermatomic" compounds (Pittsburgh Metals Purifying Co.).

* The most detailed data ever published on the process developed for handling nickel and cobalt ores (Nicaro, Cuba) are presented by M. H. Caron (p. 67).

* Greater efficiency in the extraction of aluminum from alumina is obtained by using improved self-baking electrodes as a substitute for multiple prebaked electrodes as a substitute for multiple prebaked electrodes or also the conventional self-baking electrodes now in use (p. 105).

* New data on plastic deformation in the rolling process have been developed by B. L. Averbach (p. 150). The distribution of principal strains was determined by radiographing a lead grid embedded in a cast tin bar.

Dr. Schmidt

Says . . . .

"Happy 1950"

Ed. Note: Dr. Emerson P. Schmidt has for many years been the Director of Economic Research for the Chamber of Commerce of the United States, Washington. He has an admirable record of economic analyses and forecasts proven accurate by subsequent developments.

Q: I remember particularly, Dr. Schmidt, your publication . . . before the end of the war projecting postwar economic developments.
A: Well . . . that's kind of you . . . not many people have remembered that.
Q: Looking back now, was there anything you missed . . . were you off the beam in anything . . . in your own opinion?
A: Well, I think that I did not forecast the height and the duration of the prosperity although I thought we were certainly going to have some very prosperous times . . . so that in a sense I underestimated the strength of our economy. I guess none of us really expected that we would have as much reconstructing in productive facilities of the rest of the planet as has actually taken place and providing relief to the foreigner.
Q: Well, most people thought prosperity would taper off . . . it looked as if almost anything could happen! In general, what do you think 1950 will bring?
A: Well, if you look at the stock market it looks pretty good . . . the stock market has been known to be wrong so we ought to look a little further. My own general feeling is that 1950 will be a pretty good year although not quite as prosperous as 1949 . . . certainly not as good as 1948 which was the best in the country's history.
Q: Do you think unemployment may reach 4 million in 1950?
A: I certainly wouldn't be surprised if it did . . . but still that would be only fairly moderate unemployment considering the volume of people who are changing jobs and the constant flow of new entrants into the labor market.
Q: Jobs will be harder to get, eh?
A: Yes, they will . . . and harder to keep, too.
Q: How about taxes—higher or lower?
A: Only a confirmed optimist would look for them to be lower . . . state and local taxes . . . although not in all states and communities . . . may on the average be a little higher. I think Federal taxes will stay about the way they are except that possibly the wartime excise taxes may be repealed, as they ought to be, because there is no justification for penalizing certain types of goods.
Q: As, for instance, the pocketbooks the women are always complaining about!
A: Yes, that's a good example of unjustified penalization.
Q: What about the budget . . . do you think it will remain unbalanced?
A: Everything certainly points in that direction! The estimated deficit is around $5 billion for fiscal 1950 and I would be surprised if it were in balance during 1950 . . . I think this Congress will look at expenditures a little more critically than it did in 1949 but living comes high these days and everyone has his hand out . . . it'll be tough going.
Q: Do you ever expect in your lifetime to see any period when the budget is in balance? I mean actually is, without financial tricks and sleight-of-hand?
A: Well, if the American people continue to make as heavy demands on the government, and if the politicians think they can get elected by catering to special interests, I'm afraid that the chances for balancing the budget are remote. Maybe we'll be lucky to balance the budget once in five years!
Q: If the past 20 yr is any indication we're not likely to do even that well!
A: Oh well, let's try to be optimistic about it . . . a balanced budget today has lots of friends in theory . . . everyone wants someone else to get it in balance.
Q: Somebody has to pay for the welfare state, eh?
A: The New Zealanders and the Australians, I think, expressed their opinion on that during the last couple of weeks.
Q: How will we handle the welfare state?
A: For the time being it looks like inflation . . . it appears painless that way.
Q: I notice some pension victories, in steel, for instance, have been followed by price increases. Is that something that would inevitably follow?
A: Yes. We have a lot of misinformation on the nature of prices and costs and profits . . . any increase in costs that goes across the board . . . across the whole industry . . . is certain to find its way not only into the cost structure of that industry but the price structure as well.
Q: Will recent pension victories result in greater pressure on Federal Social Security payments?

A: Well, yes. The House has already adopted HR 6000 which will lift government pensions by about 70 pct. It is almost certain that the Senate will do something similar. But the Chamber of Commerce and most business groups . . . most businessmen have favored some correction in this prewar benefit formula . . . and favored extension of coverage so that all groups will have minimum protection from the government system.

Q: In interviews a month or so ago with the steel strikers, all seemed to prefer government protection to company protection because they are rather fearful of change of job or company bankruptcy, and all recognize that sometimes they might be frozen to a job unnecessarily by a company pension.

A: Well, yes. That's one of the evils of these private pension schemes although there is much to be said for them. But I remember Justice Brandeis one time calling these pension schemes "the new industrial peonage" and I often wonder what he would be saying now if he saw these Union administrators pushing these compensation and welfare schemes . . . I imagine that workers are pretty beholden to labor leaders otherwise they may be cut off . . . I think that most of the workers feel they are to some extent the prisoners of the Union leaders. It is a serious matter for them.

Q: When looking far ahead some economists—not you—have made some important announcements, Sumner Slichter, for instance, as far ahead as 1980. He says in 1980 the workers may well work only a 30-hr week and have twice the standard of living as in 1949. What do you think of that?

A: Well, we have made our own analysis of trends and if you project the trends of the last 60 yr into the next 30 yr, that is, up to 1980, wages will be $5 an hr and the gross national product will be up around $900 billion. It won't be quite as good a dollar as we have now . . . but certainly growth factors in our economy are strong and the inflation pressures over the long pull are pretty potent. One of the most serious factors, however, which I think Professor Slichter and other people have not taken into account, is the failure of productivity to rise. The output has not risen during the past few years as it did in the prewar period. Our studies indicate that perhaps instead of the normal 2½ pct rise in productivity per manhour per year, compounded, the figure is nearer 1 pct . . . and if this trend continues then this brave new world we are hoping for is somewhat less certain . . . we are going to have to work to produce this brave new world . . . or a lot of people will find it neither brave nor new!

Q: Technical men take a very dim view of extrapolating curves . . . there may be too much calm assumption that we will always have a steady increase in productivity . . . curves sometimes have a habit of leveling off.

A: Yes, or even reversing themselves . . . we must not believe—or blindly believe—that a rise in productivity will inevitably come. It will come only if we do the right thing, which in my book means plenty of research, development of new techniques and products, good discipline on the job, no undue amount of absenteeism on the job . . . and management and labor must work as a team. If we do that, then, and only then, can the expectations of Professor Slichter and others be realized.

Q: As he said . . . we might expect two cars in every garage. Maybe some people won't want two cars—or two television sets!

A: Well, you know what the communist said to his comrade who remarked he didn't like caviar . . . "after the revolution he would eat it whether or no." Anyhow those two cars will present quite a traffic problem . . . or maybe they won't if everyone is inside looking at their two television sets.

Q: Maybe one of the television sets will be in one of the cars!

A: That'll be the day . . . it'll be a real test of bravery in the brave new world!

Q: Maybe everyone will have two psychoses . . . two nervous breakdowns, too!

A: Why not?

Q: How about war and the cold war?

A: We have got to do some fundamental thinking, I believe, on that score. It is quite probable we will be in a state of semi-war, or cold war . . . or even actual combat. My own viewpoint has been that the likelihood of a Third World War in the near-term future is not too great, partly because the Soviet Union is getting pretty much what it wants through our own default, and the failure of an adequate high policy. So, as long as the Soviet Union is getting largely what it wants and fears no threat from outside, why should it go to war? If more Titos develop, as we all hope, then they might in desperation strike out somewhere and that might precipitate a Third World War. But it seems to me that from now on we will be in a state of semi-war economy . . . and hoping we can keep it to a minimum so we won't have elaborate controls and government directives of the economy . . . because they will do more harm than good.

Q: To return to the domestic economy . . . do you think the government, irespective of its being a Republican or Democratic administration, would tolerate for long, say six milion unemployed?

A: No, I don't think they would . . . I think any government would feel the pressures and do something about it. Whether they would actually solve the problem or simply patch up some spots is difficult to say. It would certainly mean more deficit spending and probably mean expanded public works . . . a lot of noise and a lot of make-believe . . . and might even put some people back to work.

Q: As regards the farmer. How long do you think this astounding accumulation of farm products can last without something cracking some place?

A: Well, our population is steadily expanding and our agricultural acreage is, after all, limited . . . so over the long pull I think American farmers are going to be reasonably prosperous. But if we have an artificial support of prices and the government standing ready to purchase any surplus I think it's going to be rather fatal . . . and if we must have a farm program I think the type of program which the 80th Congress developed—a flexible support program under which the support would decline when the surpluses increase thereby giving the farmer an incentive to divert his energies to other farm products—is the sensible type of approach. But Mr. Brannan, who is trying to make political hay, has got another scheme . . . as a matter of fact he says his plan will mean for him either a palace or the backhouse!

Q: Which do you think it will be?

A: So far it looks more like the backhouse . . . but you can never tell about these things that promise something to everyone with no pain.

Q: Is it possible that today certain industries, certain older industries, have management that has lost some of its adventurous spirit and drive?

A: Well, I don't know as I could identify any cases, but it certainly would not be surprising if that were true. With the kind of market economy that we have, with consumers constantly being offered alternatives and substitutes, any industry that rests on its oars is likely to be liquidated pretty darn soon. Recently we submitted some testimony to the Celler Monopoly Investigating Committee . . . we gave quite a portrayal of how the invention of substitutes is the greatest single powerful force to prevent monopoly and stagnation . . . and in our search we couldn't find an industry that is really stagnant.

Q: I would think perhaps that the railroad industry seemingly is slowly working progressively toward a crisis of some sort.

A: Well, there you have a special problem . . . you have got substitute methods of transport that are making the railroads in part obsolete. In addition you have very aggressive, militant, powerful unions. With a good deal of upward pressure on wage costs and a growing tendency to featherbedding that means the wage dollar is buying less service except as it is offset by greater investment in large locomotives, larger cars and faster trains. So it is a difficult situation . . . but I think the competitive pressures on the railroads will force them to adopt techniques in order to survive. Years ago I think the railroads were stagnating a great deal more than they are today.

Q: Do you expect there's going to be any great action on President Truman's "Fourth Point" regarding greater investment abroad on the part of American industry?

A: Well, the primary investment or the predominant type of investment in recent years has been for the development of oil resources and insofar as the American people will need foreign produced commodities . . . certainly some American dollars will go out and try to create the physical capital to produce those commodities . . . but I don't look for any great flood of export capital from this country. You can't expect widows or orphans . . . or even a Wall St. banker . . . to send dollars to a foreign country unless that country has a reasonably stable government and constitutional guarantees, and some prospect for converting local currency back into dollars. Such situations do not prevail on too wide a front. So I don't look for too much from Point Four.

Q: To sum up the year 1950 again . . . it looks like a reasonably prosperous year to you?

A: Well, the first half . . . unless something unusual shows up . . . is almost assuredly to be satisfactory. We have had the biggest housing starts in history for this time of year, beating all records, and much of these starts will carry over into 1950 . . . and government construction, government building will offset the decline, at least in part, in plant and equipment investment. We have got the soldiers' insurance payments coming along in the first part and there are a lot of other factors of strength . . . we have actually created a backlog of demand due to the strikes in steel and coal, and while they have destroyed some income by virtue of close-downs, part of the backlogs will carry over into 1950. We have a very considerable backlog of coal stockpiles to fill up . . . and there will be some inventory accumulation in the first half so that business should be quite good.

". . . . The yearly increment in productivity is nearer 1 pct, not 2½ pct as generally quoted."

Q: In general, it will be happy 1950, eh?

A: Yes, although the last half is not so certain . . . as a matter of fact it might end on a less optimistic note than 1949 is ending.

Q: Just one more question . . . I notice in Britain . . . a great deal of attention is being paid to the Rignano plan . . . a system to get more revenue whereby a person cannot bequeath anything beyond the immediate first generation—his wife and children—and from there on the residue reverts to the State. Eventually in our search to support some of the economic luxuries . . . do you think we may eventually end by considering the same thing?

A: It wouldn't be too surprising. For what happens in Britain tends to happen in this country . . . a decade or two later. But perhaps when Britain makes a flop of their socialistic experiment we will learn a lesson and recognize the dangers of drying up the sources of know-how and venture capital, and investment, and ability . . . it is always well to remember that dollars frequently go with ability. Take the dollars . . . you destroy ability. If we go in that direction I think we will have a more slowly rising standard of living than what we otherwise have, and I hope the American people are smart enough not to import any ideologies and practices of decadent Europe.

Q: Well, happy 1950 to you.

A: Happy 1950 to you too . . . and all the members of AIME!

It's Everyone's Business

DEC. 20—The spirit of Christmas and good will toward men has managed a few brief appearances on the front pages, welcome relief from man's usual ill-will toward man. A couple politicos did their best to brighten the scene by well-publicized romances. There was a general exodus to Florida to patch up nervous systems, and even the UNO quieted down as Mr. Vyshinsky departed for home via Eastern Germany. Before going he opened up a preliminary bombardment for the worldwide "communist peace offensive," and it is now the duty of the 600 million (according to the Cominform) ideological converts to press home the attack.

In Washington, Mr. Lilienthal resigned as Chairman of the Atomic Energy Commission and demonstrated again the difficulty of government to retain the services of capable men. The President has yet to appoint another victim—possibly someone nicely noncontroversial and timid. So might the critics be appeased, but it would bode ill for the rapid exploitation of peaceful uses of atomic energy, the relaxation of excessive secrecy, wider sharing of developmental work with friendly nations and possible revision of the Acheson-Lilienthal proposals for international control of the atomic bomb.

Mr. Clark Gifford, one of the President's closest aids, also resigned, he to go after the rewards of private work and better take care of three children. It was Mr. Gifford who in the dark summer of 1948 pumped conviction into the President that the Fair Deal could win and it was he who wrote the speeches showing the President to be a homespun humanitarian. And over in the Interior Department, Mr. Krug (who expected a Dewey victory) dropped off without fanfare. Mr. Oscar Chapman got the job, a victory for merit and devotion. Mr. Chapman is sincere and able. Furthermore he campaigned vigorously for Mr. Truman.

Along the pension front the Bell Telephone System has ordered an immediate increase in monthly payments from $50 to $100, less Federal Security payments. The union, however, is very annoyed at such cutting of the ground from under one of their main claims and has proposed bringing charges of unfair labor practices against the System for making the increase without proper consultation and collective bargaining. With steel, coal and telephone well pensioned, and a foothold secured in Detroit, the growing campaign to pry open the Federal treasury to increase old-age pensions (now at $26 monthly) has won some formidable allies in private industry. Even Senator Taft, who calls the welfare state the "farewell state," inquires as to why some workers should have superior protection.

In mid-November some 59,518,000 Americans were employed, an unknown number were on short shifts and unemployment had dropped to 3,490,000, a goodly decline from the July peak of 4,000,000 unemployed which had resulted in such fretful concern in many quarters. In mid-July there were 35 areas in 14 states with 12 pct or more of the working population hunting jobs. However, by the end of September some $80 million in Federal procurement and construction contracts and loans had been funneled into these depressed areas, and there has resulted considerable alleviation of distress. To the generally improved business conditions throughout the country, however, goes some of the credit. The country still has a goodly number of families on the lower rungs of the economic ladder (see graph), and these groups are now the subject of several studies of the factors contributing to low income and the circumstances in which low-income families live, in cities and farms.

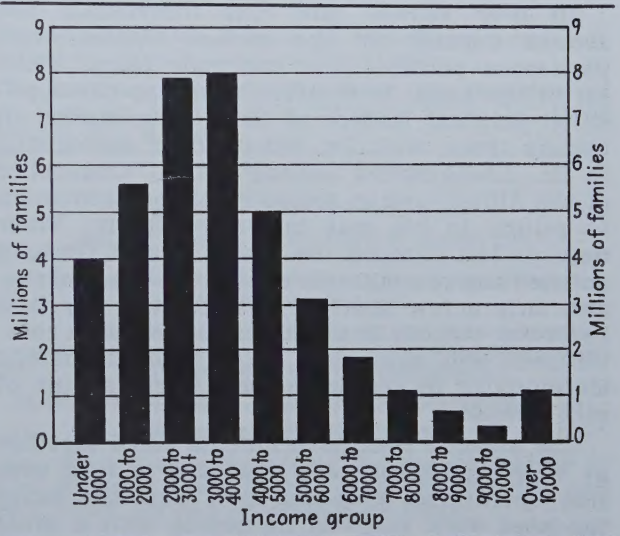

Among the base metals copper alone has remained firm during recent weeks at 18½¢ per lb. The demand which comes mainly from the building industry is strong, and is not expected to slacken in the immediate future. Copper consumption is currently estimated as being well above current production plus imports, but stocks were built up fairly well during the first half of the year. Contrary to expectations the ending of the steel strike did not bolster the zinc price and quotations have fallen off to 9¾¢ per lb. Lead broke on Nov. 25 to 12¢ a lb, the level in effect last June. Demand for lead has tended to weaken within recent months although Europe is still shipping supplies in search of dollars. In tin, prices have persisted on the downward side to today's quotation of 78.25¢. Turnover has not been large. Tin activity will not begin to look like a real market until more supplies are available from competitive sources in the Far East. But already weakness in the tin price has led to a special meeting of certain member countries of the Tin Study Group in The Hague to consider

reestablishment of the prewar buffer-stock scheme.

Now that Paul Hoffman has laid down the dictum that countries in the Marshall area must liberalize trade relations to stimulate recovery, many producers are taking fright and exploring trick ideas to protect their industries from the searching winds of foreign competition. There are signs that the prewar coke cartel is being revived, similar moves are underway in scrap steel and chemicals, and steel and coal may join the list. Certain European steel producers are toying with the idea of transplanting the American basing point mechanism from American to European soil. The French have also come up with the scheme whereby high-cost producers would sell out to their more efficient competitors. The NAM has already started to prod Mr. Hoffman's organization, and it is unlikely that ECA will remain passive to all these maneuverings for long.

All over Europe and Asia individuals bob around uneasily on the surface ripples while ponderous political and economic forces clash far in the deep. In Western Germany the opposition political leaders at Bonn have struck an uneasy truce, with Dr. Schumacher apologizing to Dr. Adenauer for calling him a "Chancellor of the Allies," and in return receiving permission to return to his seat in the Assembly. Their wrangle has dumped the whole idea of German defense and rearmament into the political arena, and only a few short years after the war it is becoming obvious to the Allies that either a commitment will soon have to be made to defend Germany or to accede to some German plan of self-defense.

The Atlantic Pact governments allied together in Western Defense are now face to face with real operational planning now that the fancy top-level work has run its course with a great deal of committee-breeding, air visits back and forth, and paper swapping. Even with the support of $900 million worth of American arms it is obvious that commitments of money and men of all the countries involved must materially increase if principles and plans are to be turned into acts and pledges. One shake of Stalin's fist is worth far more than any number of General Montgomery's plans. The governments involved face grave and far-reaching decisions. The United States has belatedly assured the Europeans that they will not be the receptacle for American arms surpluses and that they will not be fobbed off with articles for which they have no genuine need.

All through the satellite countries bordering Russia a witch-hunt of extraordinary proportions continues to fell the mighty. Speeches of various party functionaries present a picture of party membership a jumble of agents provocateurs, spies and saboteurs. No party member can be trusted, however long his standing. Stalin is convinced that Titoism and the Anglo-American cold war in the "peoples democracies" merely repeats the Western interventionist campaign and Trotskyist subversion that were overcome in Russia. Stalin himself has given the warning that "a double-faced saboteur with a Party card, often hiding behind a screen of servility, seeming enthusiasm and high-flown dialectics is a much more dangerous enemy than an ordinary survivor of the hostile classes."

The Cominform met a few weeks ago in Budapest minus a number of familiar faces. Bulgarian Premier Dimitrov is dead and his Vice-Premier, Kostov, is being readied for the hangman for trying to "physically annihilate" him. The father of the Cominform, Zhdanov, is dead. Rumanian Foreign Minister, Anna Pauker, wasn't there. The survivors issued the usual pronouncements with all the euphemistic charm and grotesque self-deception of the communist vocabulary. Anyone opposing Soviet policies is a warmonger. Tito is now a fascist, and against fascism no holds are barred.

Over in the Asian theater of the cold war, the World Federation of Trade Unions (WFTU) met with great fanfare in Peking during the third week of November. But trade union affairs were not on the agenda—rather a blueprint of action for an Eastern Cominform was laid down, a blueprint of revolutions from Persia to Japan, comparable to that given by the late Zhdanov for

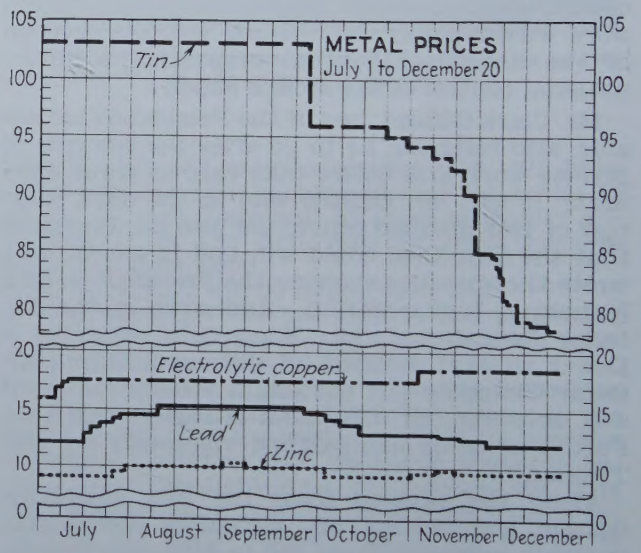

Europe at the initial meeting of the Western Cominform in 1947. The Western Cominform was devised to battle the Marshall Plan and the Eastern Cominform is to counter President Truman's "Fourth Point" of technical help for underdeveloped areas. Mao Tse-tung was kept in the background (Moscow doesn't want another Tito). Rather the main Moscow man in his cabinet, Liu Shao-chi, laid down the strategy: "Armed revolution must be the main theme in the people's liberation struggle, to be coordinated with other methods such as legal and illegal mass resistance in enemy-controlled areas and cities."

All this looks like 1950 will have pretty much the same impact on the nervous system as 1949. Or maybe more so!

Program for th

New York, Sta

IRON & STEEL DIV.

General Session

Tuesday, Feb. 14, 9:00 A.M.

Powder Cutting and Scarfing Processes, by R. S. Babcock, Linde Air Products Co.

Tin Fusion Method for the Determination of Hydrogen in Steel, by D. J. Carney, Carnegie-Illinois Steel Corp., J. Chipman and N. J. Grant. Mass. Inst. of Tech. Jl. of Metals, Feb.

Sampling and Analysis of Liquid Steel for Hydrogen, by D. J. Carney, Carnegie-Illinois Steel Corp., J. Chipman and N. J. Grant, Mass. Inst. of Tech. Jl. of metals, Feb.

Experimental Production of Ferrochromium from Mouat, Mont., Chromite, by F. W. Wessel and R. T. C. Rasmussen, U. S. Bureau of Mines.

Metallurgical Slags

Tuesday, Feb. 14, 2:00 P.M.

Mechanism of the Sulphur Reaction between Liquid Iron and Slag, by G. Derge, W. O. Philbrook and K. M. Goldman, Carnegie Inst. of Tech.

Evaluation of pH Measurements with Regard to the Basicity of Metallurgical Slags, by C. W. Sherman and N. J. Grant, Mass. Inst. of Tech. Jl. of Metals, Nov.

Use of Radiocalcium to Study the Distribution of Calcium between Molten Slags and Iron Saturated with Carbon, by W. O. Philbrook, K. M. Goldman and M. M. Helzel, Carnegie Inst. of Tech. Jl. of Metals, Feb.

Manganese Equilibrium under Simple Oxide Slags, by J. Chipman and J. B. Gero, Mass. Inst. of Tech., and T. B. Winkler, Bethlehem Steel Co. Jl. of Metals, Feb.

Metals Branch Dinner

Tuesday, Feb. 14. Cocktail Party at 6:00 and dinner at 7:00 P.M.

Physical Chemistry of Liquid Iron

Wednesday, Feb. 15, 9:00-10:45 A.M.

Equilibrium in the Reaction of Hydrogen with Oxygen in Liquid Iron, by M. N. Dastur, H. A. Brassert & Co., and J. Chipman, Mass. Inst. of Tech. Jl. of Metals, Aug.

Activity of Sulphur in Liquid Steel: The Influence of Copper, by E. M. Cox, and T. Rosenqvist, University of Chicago.

Optical Temperature Scale and Emissivity of Liquid Iron, by M. N. Dastur, H. A. Brassett & Co., and N. A. Gokcen, Mass. Inst. of Tech. Jl. of Metals, Oct.

Physical Chemistry of Steel Making Committee Luncheon Meeting

Wednesday, Feb. 15, 12:15 P.M.

Physical Chemistry of Liquid Iron

Wednesday, Feb. 15, 2:00 P.M.

Solubility of Oxygen in Liquid Iron Containing Aluminum, by D. C. Hilty and Walter Crafts, Union Carbide & Carbon Res. Labs., Inc. Jl. of Metals, Feb.

Solubility of Oxygen in Liquid Iron Containing Silicon and Manganese, by D. C. Hilty and Walter Crafts, Union Carbide & Carbon Res. Labs., Inc. Jl. of Metals, Feb.

Thermodynamic Properties of Sulphur in Molten Iron-Sulphur Alloys, by C. W. Sherman, Mass. Inst. of Tech., H. I. Elvander, Degerfors Jernverks A.B., Degerfors, Sweden, and J. Chipman, Mass. Inst. of Tech. Jl. of Metals, Feb.

Effect of Carbon on the Activity of Sulphur in Liquid Iron, by J. P. Morris and R. C. Buehl, Bureau of Mines. Jl. of Metals, Feb.

Bessemer Converter Operations

(Sponsored by the Committee on Bessemer Steel)

Thursday, Feb. 16, 9:00-11:00 A.M.

Blowing Problems Related to Iron Quality, by R. E. Edwards, Jones & Laughlin Steel Corp.

The Bessemer Converter Process in the Manufacture of Steel, by A. B. Wilder, National Tube Co. Jl. of Metals, Nov. & Dec.

Howe Memorial Lecture

Thursday, Feb. 16, 11:00 A.M.

By F. B. Foley, International Nickel Co.

Iron & Steel Division Executive Committee Luncheon Meeting

Thursday, Feb. 16, 12:15 P.M.

Converter Process Developments

(Sponsored by the Committee on Bessemer Steel)

Thursday, Feb. 16, 2:00 P.M.

Side Blow Converter Process for the Production of Low Nitrogen Steel Ingots, by R. R. Webster, and H. T. Clark, Jones & Laughlin Steel Corp.

Experimental Operation of a Basic-Lined Surface-Blown Hearth for Steel Production, by C. E. Sims, Battelle Memorial Inst., and F. L. Toy, Carnegie-Illinois Steel Corp.

Some Observations on Continental Bessemer Practice, by S. J. Cresswell, Carnegie-Illinois Steel Corp.

INSTITUTE OF METALS DIV.

Reviews of Aspects of Metallurgy

Sunday, Feb. 12, 9:30 A.M.

Solidification of Metals and Alloys arranged by C. S. Smith

This Sunday program will bring the audience up to date on the present status of solidification without introducing new data. These sessions will be repeated each year on various subjects and should prove invaluable in reviewing and summarizing the tremendous amount of research work done in a particular field.

The Liquid Metal: Nature of Structural Change During Solidification, Nucleation of Solid, by J. H. Hollomon, General Electric Co.

1:30 P.M.

Growth of Crystals from the Melt: Pure Metals, Solid Solutions, Dendrite Formation, Coring, Diffusion, Morphology of Cast Metals and Alloys, by R. F. Mehl, Carnegie Institute of Technology.

8:00 P.M.

Solidification of Steel Ingots: Columnar vs. Equiaxed Structure, Ingot Defects, Gas Evolution, Segregation, etc., by B. R. Queneau, Carnegie-Illinois Steel Co.

950 Annual Meeting

otel, Feb. 12-16

Alloy Systems: Nitrogen and Carbon in Steel

Monday, Feb. 13, 9:00 A.M.

Iron-Nitrogen System, by V. G. Paranjpe, Morris Cohen, M. B. Bever and C. F. Floe, Mass. Inst. of Tech. Jl. of Metals, Feb.

Effects of Nitrogen, Iron, or Nickel Upon the Alpha-Beta Transformation and Gamma Precipitation in Cobalt-Chromium Alloys, by A. R. Elsea and C. C. McBride, Battelle Memorial Inst. Jl. of Metals, Jan.

System Chromium-Carbon, by D. S. Bloom and N. J. Grant, Mass. Inst. of Tech. Jl. of Metals, Jan.

Carbides in Isothermally Transformed Chromium Steels, by Walter Crafts and J. L. Lamont, Union Carbide & Carbon Research Lab., Inc. Jl. of Metals, Dec.

Carbides in Long-Tempered Vanadium Steels, by J. L. Lamont and Walter Crafts, Union Carbide & Carbon Research Lab., Inc. Jl. of Metals, Feb.

Symposium on Tube Production Practice

Monday, Feb. 13, 9:00 A.M.

Theory of Tube Production Methods, by R. J. Ripling, Case Inst. of Tech.

Aluminum Alloy Production, by R. F. McCormick, Aluminum Co. of America.

Copper Alloy Production, by Horace Y. Bassett, Calumet & Hecla Cons. Copper Co.

Ferrous Alloy Production, by J. W. Schroeder, National Tube Co.

Alloy Systems: Structure and Stability

Monday, Feb. 13, 2:30 P.M.

Iron-Chromium-Nickel Ternary System, by J. W. Pugh and J. D. Nisbet, General Electric Co. Jl. of Metals, Feb.

Faults in the Structure of Copper-Silicon Alloys, by C. S. Barrett, University of Chicago. Jl. of Metals, Jan.

Undercooling of Minor Liquid Phases in Binary Alloys, by Chih-Chung Wang and C. S. Smith, University of Chicago. Jl. of Metals, Jan.

Measurement of Relative Interface Energies in Twin Related Crystals, by C. G. Dunn, F. W. Daniels and M. J. Bolton, General Electric Co. Jl. of Metals, Feb.

Thermodynamic Properties of the Alpha Brasses, by A. W. Herbenar, Ohio Crankshaft Co., C. A. Siebert and O. S. Duffenback, University of Michigan. Jl. of Metals, Feb.

Symposium on Tube Production Practice

Monday, Feb. 13, 2:30 P.M.

Lead Tube Production, by George Hiers, National Lead Co.

Nickel Tube Production, by W. A. Dickenson, International Nickel Co.

Nickel Tube Production, by H. F. Hendershott, International Nickel Co.

F. N. Rhines, Prof. of Metallurgy, Carnegie Institute of Technology, Pittsburgh, and chairman IMD, is shown with C. D. King, U. S. Steel Corp., chairman ISD (left) and J. D. Sullivan, Battelle Memorial Institute, chairman EMD (right).

Magnesium Tube Production, by C. J. Huffman, Dow Chemical Co.

Magnesium Tube Production, by G. Ansel, Dow Chemical Co.

IMD Membership Committee Meeting

Monday, Feb. 13, 4:00 P.M.

Alloy Systems: New Alloys

Tuesday, Feb. 14, 9:00 A.M.

Titanium Binary Alloys, by C. M. Craighead, O. W. Simmons and L. W. Eastwood, Battelle Memorial Inst. Jl. of Metals, Feb.

Ternary Alloys of Titanium, by C. M. Craighead, O. W. Simmons and L. W. Eastwood, Battelle Memorial Inst. Jl. of Metals, Feb.

Quaternary Alloys of Titanium, by C. M. Craighead, O. W. Simmons and L. W. Eastwood, Battelle Memorial Inst. Jl. of Metals, Feb.

The Alloy Systems Uranium-Aluminum and Uranium-Iron, by Paul Gordon, and A. R. Kaufmann, Mass. Inst. of Tech. Jl. of Metals, Jan.

The Alloy Systems Uranium-Tungsten, Uranium-Tantalum and Tungsten-Tantalum, by C. H. Schramm, P. Gordon and A. B. Kaufmann, Mass. Inst. of Tech. Jl. of Metals, Jan.

Institute of Metals Division Executive Committee Luncheon Meeting

Tuesday, Feb. 14, 12:15 P.M.

Mechanical Properties: Theory and Light Metals

Tuesday, Feb. 14, 2:00 P.M.

Plastic Deformation in the Rolling Process, by B. L. Averbach, Mass. Inst. of Tech. Jl. of Metals, Jan.

Some Observations on the Recovery of Cold-Worked Alumium, by T. V. Cherian, P. Pietrokowsky and J. E. Dorn, University of Calif. Jl. of Metals, Dec.

Effect of Prestraining Temperatures on the Recovery of Cold-Worked Aluminum, by T. E. Tietz, R. A. Anderson and J. E. Dorn, University of Calif. Jl. of Metals, Dec.

Properties of Sand-Cast Magnesium-Rare Earth Alloys, by T. E. Leontis, Dow Chemical Co. Jl. of Metals, Dec.

Aging Behavior of a Zinc Alloy Containing 25 pct Manganese, 15 pct Copper, 0.1 pct Aluminum, by P. W. Ramsey and J. L. Werley, N. J. Zinc Co. Jl. of Metals, Jan.

Metals Branch Dinner

Tuesday, Feb. 14. Cocktail Party at 6:00 and Dinner at 7:00 P.M.

Mechanical Properties: Steel

Wednesday, Feb. 15, 9:00 A.M.

Some Effects of Phosphorus and Nitrogen on Properties of Low-Carbon Steel, by G. Enzian, Jones & Laughlin Steel Corp. Jl. of Metals, Feb.

Flow and Fracture Characteristics of a Die Steel at High Hardness Levels, by L. J. Klingler and C. C. Chow, Case Inst. of Tech., and G. Sachs, Metals Research Assoc. Jl. of Metals, Dec.

Effects of Molybdenum and Phosphorus Upon the Toughness of Manganese Steels, by M. Baeyertz, W. F. Craig, Jr. and J. P. Sheehan, Armour Res. Foundation. Jl. of Metals, Feb.

Institute of Metals Division General Business Meeting

Feb. 15, 10:30 A.M.

Institute of Metals Division Lecture

Feb. 15, 11:00 A.M.

By E. E. Schumacher, Bell Tel. Labs.

Properties: Effect of Alloy Elements

Wednesday, Feb. 15, 2:00 P.M.

Intergranular Parting of Brass During Anneals, by F. H. Wilson and E. W. Palmer, American Brass Co. Jl. of Metals, Dec.

Effect of Solute Elements on the Tensile Deformation of Copper, by R. S. French, Bridgeport Brass Co. and W. R. Hibbard, Jr., Yale Univ. Jl. of Metals, Jan.

Low-Temperature Properties of Tin-Antimony and Tin-Cadmium Alloys, by F. J. Dunkerley, H. B. Hunter, and F. G. Stone, Univ. of Penn. Jl. of Metals, Dec.

Electrical Resistivity and Thermoelectric Power of Antimony-Selenium Alloys, by B. P. Cullity and Maria Telkes, Mass. Inst. of Tech. Jl. of Metals, Jan.

Effects of Interstitial Solutes on the Mechanical Properties of Alpha Titanium, by W. L. Finlay and J. A. Snyder, Remington Arms Co., Inc. Jl. of Metals, Feb.

Powder Metallurgy

Wednesday, Feb. 15, 2:00 P.M.

Zirconium-Berryllium System by Powder Metallurgy Methods, by H. H. Hausner and H. S. Kalish, Sylvania Electric Prods., Inc. Jl. of Metals, Jan.

Cemented Titanium Carbide, by J. G. Redmond and E. N. Smith, Kennametal, Inc. Jl. of Metals, Dec.

Extrusion of Powder Magnesium Alloys, by R. S. Busk and T. E. Leontis, Dow Chemical Co. Jl. of Metals, Feb.

Iron-Silicon Alloys by the Powder-Metallurgy Process, by R. Wachtell, American Electro Metal Corp. Jl. of Metals, Feb.

Effect of Annealing in a Magnetic Field upon Iron-Cobalt and Iron-Cobalt-Nickel Alloys Prepared by Powder Metallurgy, by J. F. Libsch, G. W. Beckman and D. Warren, Lehigh Univ., and R. J. Franklin and E. Both, U.S.A. Signal Corps. Jl. of Metals, Feb.

Properties: Elasticity and Anelasticity

Thursday, Feb. 16, 9:00 A.M.

Elastic Coefficients of Single Crystals of Alpha Brass, by R. W. Fenn, Jr., Dow Chemical Co., W. R. Hibbard, Jr., and H. A. Lepper, Jr., Yale Univ. Jl. of Metals, Jan.

Thermoelastic Effect in Iron and Nickel as a Function of Temperature, by R. Rocca and M. B. Bever, Mass. Inst. of Tech. Jl. of Metals, Feb.

Internal Friction of Cold-Worked Metals at Various Temperatures, by T'ing Sui Ke, Univ. of Chicago. Jl. of Metals, Feb.

Study of Recrystallization and Grain Growth by Measurements of Internal Friction, by T'ing Sui Ke, Univ. of Chicago, Jl. of Metals, Feb.

Powder Metallurgy

Thursday, Feb. 16, 9:00 A.M.

Control of Atmospheric Beryllium, by N. P. Pinto, Sylvania Elec. Prods., Inc.

Behavior of Pores during the Sintering of Copper Compacts, by F. N. Rhines, C. E. Birchenall and L. A. Hughes, Carnegie Inst. of Tech. Jl. of Metals, Feb.

Powder Metallurgy Committee Luncheon Meeting

Feb. 16, 12:15 P.M.

Kinetics

Feb. 16, 2:00 P.M.

Self-Diffusion in Alpha and Gamma Iron, by C. E. Birchenall and R. F. Mehl, Carnegie Institute of Technology. Jl. of Metals, Jan.

Diffusion Coefficient of Carbon in Austenite, by Cyril Wells, Walter Batz and R. F. Mehl, Carnegie Institute of Technology. Jl. of Metals, Feb.

Growth of Austenite as Related to Prior Structure, by A. E. Nehrenberg, Crucible Steel Co. of America. Jl. of Metals, Jan.

Kinetics of the Eutectoid Transformation in Alloys of Iron and Nitrogen, by B. N. Bose, and M. F. Hawkes, Carnegie Institute of Technology. Jl. of Metals, Feb.

Kinetics of the Reactions of Columbium and Tantalum With O_2, N_2 and H_2, by E. A. Gulbransen and K. F. Andrew, Westinghouse Electric Corp. Jl. of Metals, Feb.

Thermodynamic Investigation of the System Silver-Silver Sulphide, by Terkel Rosenqvist, Institute for the Study of Metals, Jl. of Metals, Aug.

Powder Metallurgy Seminar

Feb. 16, 2:30 P.M.

Dr. O. W. Ellis, Chairman

Methods of Powder Preparation, by J. J. Cordiano, U. S. Metals Refining Co., Carteret, N. J.

EXTRACTIVE METALLURGY DIV.

Aluminum (Primary and Secondary)—Magnesium

Monday, Feb. 13, 9:00 A.M.

Extractive Metallurgy of Aluminum, by R. S. Sherwin, Reynolds Metals Co.

Metallurgy of Secondary Aluminum and Magnesium Alloys, by Walter Bonsack, Apex Smelting Co.

Production of Aluminum from Kalunite Alumina, by Arthur Fleischer, Nickel Cadmium Battery Corp. and Julian Glasser, Armour Research Foundation.

Amex Modification of the Kalunite Process for the Production of Alumina, by Arthur Fleischer, Nickel Cadmium Battery Corp.

Aluminum Recovers Itself, by Stanley H. Brown, Permanente Metals Corp.

Titanium-Zirconium-Manganese

Feb. 13, 2:30 P.M.

Continuous Method of Producing Ductile Titanium, by P. J. Maddex and L. W. Eastwood, Battelle Memorial Institute.

Electrical Resistivity of Titanium Slags, by James L. Wyatt, Titanium Div., National Lead Co.

Recent Practice at the Boulder City Titanium Plant, by F. S. Wartman, H. C. Fuller and D. H. Baker, Jr., U. S. Bureau of Mines.

Pilot Plant Production of Malleable Zirconium, by W. J. Kroll, W. W. Stephens and H. I. Holmes, U. S. Bureau of Mines.

Metallic Manganese Metallurgy in Japan, by P. B. Dettmer, Oakland, Calif.

Copper

Tuesday, Feb. 14, 9:00 A.M.

Core Type Induction Furnaces of Large Capacity for Melting Nonferrous Metals, by Manuel Tama, Ajax Engineering Co.

Treatment of Electrolytic Copper Refinery Slimes, by J. H. Schloen and E. M. Elkin, Canadian Copper Refiners, Ltd.

History of the Development of Mechanical Tuyere Punching at the McGill Smelter, by Leonard Larson, Kennecott Copper Corp.

Review and Preview of the Physical Chemistry of Copper Smelting, by R. Schuhmann, Jr., Mass. Inst. of Tech.

Zinc

Tuesday, Feb. 14, 2:00 P.M.

Recovery of Zinc Dithionate Sulphur-dioxide Leaching Process, by S. F. Ravitz and A. E. Back, Bureau of Mines.

Calbeck Process for Refining Zinc Oxide, by John H. Calbeck, William T. Maidens and Oscar J. Hassel, American Zinc Oxide Co.

Low-Pressure Distillation of Zinc from Aluminum-Zinc Alloy, by M. J. Spendlove and H. W. St. Clair, Bureau of Mines. Jl. of Metals, Sept.

Refining of Zinc, by Stanley Robson, Zinc Corporation, Ltd.

Brief History of Filtering Practice at Risdon, by V. A. Corstorphan, Electrolytic Zinc Co. of Australia.

Design and Operation of a Counter Current Gas Scrubbing System, by F. H. C. Kelley, Electrolytic Zinc Co. of Australia.

Metals Branch Dinner

Tuesday, Feb. 14. Cocktail Party at 6:00 and Dinner at 7:00 P.M.

Round Table Symposium on Fume and Dust Collection

Wednesday, Feb. 15, 9:00 A.M.

Fume and Dust Problem in Industry, by Harry V. Welch, Western Precipitation Co. Jl. of Metals, Dec.

Hygiene Program Control of Dust and Fume in a Smelting Industry, by J. M. Abersold, American Smelting & Refining Co.

An Improved Automatic Smoke Sampler, by J. J. Donoso, American Smelting & Refining Co.

Modern Baghouse Practice for the Recovery of Metallurgical Fumes, by A. L. Labbe and J. J. Donoso, American Smelting & Refining Co.

Conditioning Dwight-Lloyd Gases to Increase Bag Life, by R. E. Shinkoskey, American Smelting & Refining Co.

Extractive Metallurgy Division Executive Committee Meeting

Wednesday, Feb. 15, 12:15 P.M.

Round Table Symposium on Fume and Dust Collection

Wednesday, Feb. 15, 2:00 P.M.

Acid Conditioning of Metallurgical Smoke for Cottrell Precipitation, by A. L. Labbe, American Smelting & Refining Co.

Treatment of Dwight-Lloyd Gases Tooele Plant (Anaconda), by B. L. Sackett, Anaconda Copper Mining Co.

How the Operation of a Cottrell Precipitator is Affected by the Resistivity of the Collected Material, by Walter A. Schmidt, Wayne T. Sproull and Y. Nakada, Western Precipitation Co.

Ultrasonic Precipitation, by Harold Danser, Ultrasonic Corp.

Extractive Metallurgy Division General Meeting

Wednesday, Feb. 15, 4:45 P.M.

Lead-Antimony

Thursday, Feb. 16, 9:00 A.M.

The Relationship between Electrical Conductivity and Composition of Molten Lead Silicate Slags, by A. K. Schellinger and R. P. Olsen, Stanford University. Jl. of Metals, Dec.

Water Sealed Wind Boxes for Dwight-Lloyd Sintering Machines, by E. McL. Tittmann and E. A. Hase, American Smelting & Refining Co.

Development of the Lead Blast Furnace at Port Pirie, South Australia, by L. A. White, Broken Hill Associated Smelters.

Electroyltic Refining of Antimony Bullion, by David Schlain, J. D. Prater and S. F. Ravitz, Bureau of Mines.

Cobalt—Nickel—Tin

Thursday, Feb. 16, 2:00 P.M.

Tin Metallurgy in Japan, by P. B. Dettmer, Oakland, Calif.

Thermodynamic Relationships in Chlorine Metallurgy, by Herbert H. Kellogg, Assistant Professor of Mining Engineering, Columbia University.

Fundamental and Practical Factors in Ammonia Leaching of Nickel and Cobalt Ores, by M. H. Caron, Delft, Netherlands. Jl. of Metals, Jan.

Separation of Nickel and Cobalt, by M. H. Caron. Jl. of Metals, Jan.

Production of Cobalt Oxide, Cobalt Sulphate and Electrolytic Cobalt, by Alan S. Gill, Electrolytic Zinc Co. of Australia.

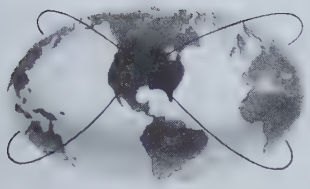

SECTION ACTIVITIES

North Pacific Section

The 23rd annual Mineral Industry Institute will be held on Thursday, Jan. 19, 1950, on the University of Washington Campus. This year the Institute will present a program devoted entirely to metallurgy, according to Edward A. Rowe. Prominent speakers in the field will address the guests on various phases of metallurgy with emphasis on importance of some of the lesser known metals.

As in past years, the evening meeting of the Institute will be held jointly with North Pacific Section of the AIME. The banquet will be followed by an address by a speaker of national reputation.

Cleveland Section

William M. Baldwin, research professor at Case Institute of Technology, presented the first lecture of the fall series on Nov. 17 before the Cleveland Section. Dr. Baldwin repeated his Marburg Lecture of the annual ASTM meeting on residual stresses in metals, illustrating his talk with colored slides, thereby simplifying description of a complete stress system to his listeners. The direction and amount of all three principal stresses was clearly indicated in perspective.

Commonplace subjects such as round rods, tubing, and flat bars were described as to typical residual stress conditions which usually exist in them. Another striking illustration of the use of colored slides was seen in the depth of penetration of residual stresses which arise when rolling sheet. Effect of variables such as roll diameter, stock thickness, and percentage reduction were considered.

Detroit Section

The theory of pressing metal powders and the design of presses and auxiliary pressing equipment were the subjects of L. H. Bailey's lecture on Nov. 21 to the Detroit Section. Mr. Bailey pointed out that the pressing operation is one of the most important steps leading to the finished product. Sometimes pressing is only a means of compacting loose particles of powder into a solid mass prior to sintering. For most applications, however, it is used as a molding operation with the object of shaping metal powders into a desired part whose shape is not changed by subsequent sintering.

Philadelphia Section

E. M. Wise, of the International Nickel Co., spoke on Oct. 27 before the Philadelphia Section on the magnetic properties of nickel, iron-nickel, iron-nickel-chromium, and many related alloys. He presented the fundamentals of magnetism, citing the evidence for the existence of magnetic "domains," as commonly accepted by research physicists today.

The ferromagnetic properties of the transition metals, iron, nickel, cobalt, and the para- and di-magnetic properties of other metals were specifically explained on the basis of electron configuration. It was also pointed out that certain metals such as platinum, paladium, and others, had electronic structures which facilitate ferromagnetic behavior when alloyed with suitable metals.

The magnetic characteristics of numerous specific alloys of nickel as a function of temperature were also presented. The interesting history of "Alnico" was related and several possible explanations for the superb magnetic properties of this and other similar permanent magnet alloys were offered.

By the masterful presentation of these and many other aspects of the general subject, Mr. Wise showed an enviable familiarity with the subject of magnetism from its infancy to the present advanced stage of development of the science. The lecture was well received and a lively and interesting discussion of many magnetic phenomena followed the formal talk.

Carnegie Institute of Technology

The Metals Club at Carnegie Tech is looking forward to an active 1950 season, and if last year's accomplishments are an indication, the Club will continue to hold successful meetings.

Ingenious Club members arranged last year to hold their monthly meetings at various fraternity houses on the campus and at a minimum of expense. Industrial leaders aired their views of labor relations, what industry expects of metallurgists, and other interesting topics at informal sessions. The Club also co-operated with a modern metallurgical methods course given at the school, attended more informal meetings, and went on several field trips. Last fall plans were made for a dance, a banquet for membership and faculty, and a printed Club paper, The Ladle. The publication, aided by alumni contributions and the metallurgical engineering department, is now operating in the black and will continue publication.

Members have carried out an extensive AIME membership drive and made noteworthy efforts to bridge the gap between alumni and undergraduates. All metallurgical students at Tech are now eligible for voting memberships. According to M. F. Stavish, Secretary, the officers elected for the school year are: Lee Horigan, President; John Brown, Vice-President and Treasurer; M. F. Stavish, Secretary; William Lambert, "Ladle" Editor; and Howard Cannon, Social Chairman.

University of Michigan

The University of Michigan Affiliated Student Society got off to a good start last fall with its annual picnic and had plans for meetings and field trips for the season. John Carlson is President; Alan F. Busto, Vice-President; Charles W.

Phillips, Secretary; Fred M. Baker, Recording Secretary; Charles W. Phillips, Secretary-Treasurer; C. A. Siebert, Faculty Sponsor; and Clarence L. Raynor, of the Hoskins Mfg. Co., Industry Counselor.

University of Pennsylvania

The Metallurgical Engineering Society of the University of Pennsylvania began its fall activities on Oct. 3 with election of officers and the announcement that the Society was accepted as an Affiliated Student Chapter of the AIME. James Fulton is President; Victor Damiano, Vice-President; and Leroy Anderson, Secretary-Treasurer.

The Oct. 12 meeting with the metallurgical engineering department of Drexel Institute of Technology featured short talks by the directors of the two departments, Professor Brick and Professor Grosvenor, of Penn and Drexel respectively. On Oct. 17 plans were made for speakers and evening meetings for the duration of the term. Further plans for 1950 are in the development stage, and with increased membership the Society hopes to have a highly successful year.

New York

The latest meeting of powder metallurgists, Nov. 16, in the New York metropolitan area was again very well attended.

The main feature of the evening was an outline of modern sintering theories presented by Dr. Ben H. Alexander, Sylvania Electric Products Laboratories in Bayside, Long Island. This talk was based on theories of recrystallization, grain growth, diffusion, and flow presented at the Sylvania Symposium in August.

In addition to this presentation, Dr. F. V. Lenel of Rensselaer Polytechnical Institute reviewed the high spots of his work on sintering in the presence of liquid phase.

Dr. H. H. Hausner of Sylvania touched on his research in the field of Conductivity measurements as related to the sintering process.

Dr. Kamillo Konopicky of Austrian-American Magnasite Corp., who was in New York on a visit from Austria, described his method of powder classification which, although originally developed for refractory materials, is applicable to metal powders. His particular size distribution and density versus pressure curves, which have already been published in this country, were discussed.

It was only the late hour of the evening that interrupted the lively discussion on all the matters presented by the speakers.

Electric Furnace Conference

The Seventh Annual Electric Furnace Steel Conference of the Iron and Steel Division established an all time record for attendance of 585 on Dec. 8 and 9 at the William Penn Hotel in Pittsburgh. This figure does not include the more than fifty of the two hundred that attended the Saturday morning free Educational Session without registering.

Unusual technical sessions included one on materials handling, a whole session devoted to temperature and composition measurements and one on refractories. The other technical sessions dealt with operating improvements, use of oxygen and gases in steel. The educational session covered the chemistry of electric furnace steelmaking and included two movies, a lecture and a panel of experts to answer the questions submitted by the audience. Some of the principle papers have appeared in the **Journal of Metals.** The complete Proceedings with discussion will be available next summer.

James W. Kinnear, Jr., President of Firth Sterling Steel and Carbide Corp., was an excellent toastmaster at the annual banquet. (Picture at banquet is shown below.) Gene Flack, Sales Counsel and Director of Advertising for Sunshine Biscuits, thoroughly entertained the registrants as the principal speaker. Executive Committee Chairman Norman Stotz presented Past Chairman John Caine with a certificate and perpetual Electric Furnace Steel Conference registration. He thanked the Westinghouse Male Quartet for their fine musical program and expressed appreciation to J. W. Harvey and his local committee for providing such a sucessful cocktail party and dinner. The new officers announced for the year 1950 are James Bowers, Chairman of the Executive Committee, T. J. McLoughlin, Chairman, and R. H. Frank, Vice Chairman of the Conference Committee.

• • •

At the Seventh Annual Electric Furnace Steel Conference, Dec. 8-10, Pittsburgh. At the Annual Dinner, James W. Kinnear, Jr., President, Firth Sterling Steel & Carbide Corp., was Toastmaster. In the background is Norman I. Stotz, President, Braeburn Alloy Steel Corp., who is Chairman of the Electric Furnace Steel Executive Committee.

• • •

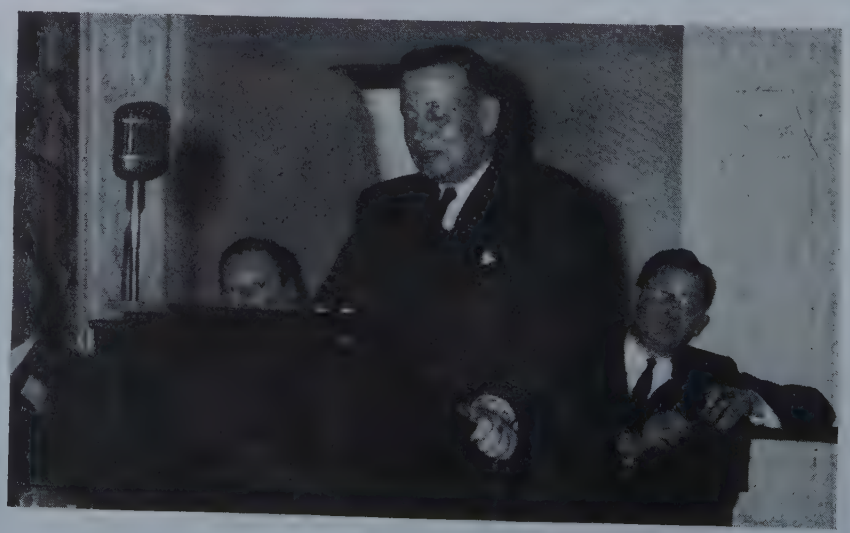

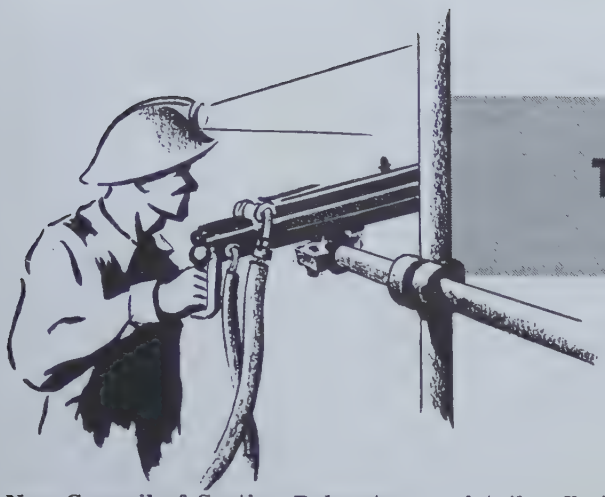

THE DRIFT OF THINGS

. . . as followed by EDWARD H. ROBIE

New Council of Section Delegates

Among other features of the forthcoming Annual Meeting will be the first gathering of the newly organized Council of Section Delegates. Thus is another of the recommendations of the Committee on Divisionalization and Publication Program (Hjalmar W. Johnson, chairman, with M. M. Leighton and Clayton G. Ball) coming to fruition. This Committee suggested "some form of representative assembly serving as a co-ordinating link between Sectional units of organization and the Central Administration. . . . The Council thus evolved should be made truly representative, with duly acredited delegates representative of the Local Sections, and possibly of the Divisions, possessing sufficient tenure of office to ensure continuity in its deliberations. . . . It should function in an advisory capacity only. . . . It would, in the first place, provide the electorate with orderly means of periodically informing the Directorate concerning membership views to a degree not now available, and in turn would provide the means by which the heavy responsibility and problems of the Central Administration could be better appreciated by the membership than is now often the case."

Following receipt of the Johnson Committee report, a "Committee on Democratization," consisting of Joseph L. Gillson, chairman, with E. A. Anderson and George B. Corless, was appointed to investigate the problem of democratization further and to activate the ideas of the Johnson Committee. It reported at the Annual Meeting in San Francisco last year, and one of its six points was the reorganization of the Section Delegates' group and replanning of its meetings. The Committee was asked to amplify its suggestion, and at the recent September meeting of the Board reported its recommendations in detail, offering provisional bylaws for the operation of the proposed Council. The forthcoming meeting will be organized and will operate under these bylaws.

Section Delegates' meetings are nothing new; they have long been on the program for our Annual Meetings. But heretofore the delegate has usually functioned as such for that meeting only; the agenda has been drawn up by the Secretary's office; the President of the Institute has presided; and the meetings have conflicted with technical sessions.

As envisaged by the Gillson committee, the principal duties of the new Council would be "(a) To receive proposals, complaints, and suggestions from individual members or Local Sections. It may appoint committees to investigate such and to formulate recommendations to present to the Board. (b) To keep the President of the Institute informed on affairs in the Local Sections. (c) To receive information about Institute affairs from the Board through the President of the Institute and to pass such information on to Local Sections."

Each delegate will be elected for two years, but to assure continuity of at least half of the group the two-year terms will be staggered; that is, half of the Local Sections are appointing a delegate to serve until Nov. 14, 1950, and half a delegate to serve until Nov. 14, 1951. To get the meeting started next February, the delegate from the Colorado Section, M. I. Signer, will be Chairman pro tem, and the delegate from the Permian Basin Section, Secretary pro tem. However, at the meeting, a Nominating Committee consisting of the delegates from the Boston, Gulf Coast, and Pennsylvania Authracite Sections will report, offering a full slate of officers—Chairman, Vice-Chairman, Secretary, and four Executive Committeemen—who will, if elected, take office immediately.

The agenda for the meeting will be prepared by the delegates from the New York, Permian Basin, San Francisco, Upper Peninsula, and Colorado Sections.

Any Director or officer of the Institute may attend the Council's meetings as an observer, without vote, but only if invited.

Two meetings of the Council each year are authorized, but railroad expenses of the delegates will be paid only to the Annual Meeting of the Institute for the present. If a delegate cannot attend, an observer may take his place, or an observer may accompany a delegate, but an observer will in no case have a vote.

The Gillson committee suggested that "whenever possible, the meeting shall precede by a day or so, a scheduled Board meeting." The Council meeting therefore has been scheduled for 10 a.m., Saturday, Feb. 11, 1950, and it can continue through the afternoon and evening if need be. The Board will meet Sunday at 10 a.m. and all Section Delegates and observers are invited to be present and to participate in any discussion by the Directors of matters brought to the Board by the Delegates, or in any other topics in which they may be interested. The meeting of the Council will be entirely free of any conflicting sessions, and the meeting of the Board largely so. Time should be sufficient for full discussion of important matters.

Some skepticism has been expressed as to whether the proposed plan will be more satisfactory than the procedure that has been followed before. But the mechanics are available for a true and uninhibited expression of the sentiment of the rank and file. The success of the meeting is entirely in the hands of the delegates.

Branch Organization

Another of the important recommendations of the Johnson committee was the organization of the Institute into three major professional groups—the Mining, Metals,

and Petroleum Branches. With the organization of the Mining, Geology, and Geophysics Division now recognized by the Board, the Divisional structure is complete and the Branch organization can now be consummated. The bylaws of the Institute provide definitely for a governing council for each branch, made up of at least six members, including one each from the Mineral Economics and Mineral Industry Education Divisions, the other members being equally divided among the constituent Divisions. This means, in practice, that the Petroleum Branch council shall consist of six or more members, the Branch and the Division here being synonymous; the Metals Branch council must consist of at least eight members (there being three Divisions in this Branch); and the Mining Branch council shall consist of six members or more (there being four Divisions in this Branch).

The Petroleum Branch council has already been set up and is the same as the officers and executive committee of the Petroleum Division; in fact, the Division prefers to be known as the Petroleum Branch. Likewise, the Metals Branch council has been named, with A. A. Smith Jr. as Chairman, E. O. Kirkendall as Secretary, and an executive committee of six, including the Chairmen of its three constituent Divisions. It is hoped that the Mining Branch Council can be named at the Annual Meeting, at which time a meeting of the officers of its constituent Divisions is planned. Possibly for want of a directive, the Metals Branch council has so far been inactive but it is organized to act if it should be called upon.

So far, the responsibilities and duties of the Branch Councils have not been established, and this is a matter for early Board action. Certainly, general supervision over the Branch journals and the activities of component Divisions would seem to be within the province of the Branch councils. Fair appropriations from the national treasury for Divisional activities should be studied. One of the first responsibilities of the Mining Branch council, which will be discussed at the Annual Meeting, would presumably be to recommend to the Board whether or not a paid secretary should be employed, and if so, what his field of activity should be. The Johnson committee suggested a field secretary for the Institute as a whole, and the Gillson committee specifically recommended a field secretary for the Mining Branch, with headquarters preferably in Salt Lake City.

The Noble Prize

Honors, awards, and prizes bestowed by the Institute are becoming so numerous that many of them are not as well known to the membership as they deserve to be. The Alfred Noble Prize is an example. It is not strictly an AIME prize, since it may be granted to the author of "a technical paper of particular merit" published by any of the Founder Societies or by the Western Society of Engineers. However, AIME members have frequently won it, as they did in both 1948 (John H. Hollomon) and 1949 (Robert L. Hoss). The cash prize is $350, and the expenses of the recipient are paid to the meeting at which the award is made. Competition for the prize is not severe, for it is limited to authors who have not passed their 31st birthday when the paper is accepted, and only a small proportion of the members of the societies in this category have reached the professional stature where they feel they can write an acceptable technical paper.

Here is an opportunity that should interest Junior Members, and those of our Members who are still in their twenties. The prize is decidedly worth while, as is the trip to the Annual Meeting, and the prestige of being the prizewinner may easily be worth considerably more than either, when it comes to looking for a job. All you have to do is to write a more outstanding paper than a dozen or so of your fellows. It's worth a try.

Continuing the Trip

In the November issue, the travels of the Secretary ended in El Paso on a rum note. This department got crowded out of the December issue, but the complaints thereby aroused from disappointed readers could have been counted by the Venus de Milo on the fingers of one hand.

From El Paso we drove to Silver City, N. Mex., where we found the small properties discouraged about the declining metal prices, but Kennecott's big open pit at Santa Rita was producing as usual, and a leaching project on some 125,000,000 tons of capping, containing about 0.35 pct. of copper, was underway, which should add a total of 400,000 tons to the country's copper production in the years to come. The ore for the concentrator runs a bit over 1 pct. in copper, about a tenth of which is oxidized. At the smelter at Hurley we found that the vibrating feeders on the reverberatories had been abandoned as they did not work satisfactorily on material containing around 9 pct. moisture.

Next stop, Inspiration, where we saw its open-pit operations for the first time, 15-yd. Dart trucks (24 tons) dumping 5,500 tons of ore daily direct to a 42-in. gyratory. An equal amount of waste has to be disposed of at present, but later on the waste should be but about 0.7 ton per ton of ore. At the leaching plant, capacity has had to be increased because of lower-grade ore. How was it done? By raising the walls of the leaching tanks 18 in., which increased their capacity by 12 pct., but involved a big job in rearranging piping. We were interested in the grizzly bars used in the belt discharge into the tanks to lessen segregation in the ore bed.

At Tucson we ran into a dads' and moms' day at the university, but T. G. Chapman had time for a good visit. Enrollment in the mining school there is at a peak and up a third over last year, with 216 undergraduates and 22 graduate students, though enrollment in the other engineering courses declined about 10 pct., to 660. Particularly close relationships with the mining companies are maintained, which helps in getting jobs in the summer and after graduation, and in securing scholarships.

Hollywood Sponsors Purity

Smog, which as everybody should know by this time, is a combination of smoke, fog, and any other troublesome matter that gets into the air of industrial communities when there is no wind, is a problem in many cities of the country. Metallurgical and chemical plants in the vicinity are viewed with extreme suspicion when smog persists, so that engineers concerned with dust and fume control are expected to contribute to the solution of the problem.

George E. Lynch, who has recently been working on the dustless incineration of some (but not all, of course) of the refuse of a movie company at Hollywood, as well as on the cleaning of openhearth gases in Pittsburgh, sends us a clipping about a new method to prevent smog in Los Angeles. Apparently almost everything has been tried, but still the September smog season last fall was the worst yet. The latest device is to name one of the Paramount girls—starlet we believe is the technical term—to be Miss Pure Air. She was to call on the mayors of Los Angeles County's 45 cities to seek their co-operation in National Smog Abatement Week. Her blond personality was supposed to spur the mayors to greater efforts, and her glamor was felt likely to be as effective as anything else in charming away the smog.

Proposed for Membership

Total AIME membership on Nov. 30, 1949, *was* 16,130, *in addition* 4,658 *Student Associates were enrolled.*

ADMISSIONS COMMITTEE

James L. Head, Chairman; Albert J. Phillips, Vice-Chairman; George B. Corless, T. B. Counselman, Ivan A. Given, Robert L. Hallett, Richard D. Mollison, and John Sherman.

Institute members are urged to review this list as soon as the issue is received and immediately to wire the Secretary's office, night message collect, if objection is offered to the admission of any applicant. Details of the objection should follow by air mail. The Institute desires to extend its privileges to every person to whom it can be of service but does not desire to admit persons unless they are qualified.

In the following list C/S means change of status! R, reinstatement; M, Member; J, Junior Member; AM, Associate Member; S, Student Associate.

Alabama

Birmingham—Kirkwood, Walter Robert. (M). Moore, Melvin Carl. (J).
Tarrant—Ruff, William B., Jr. (M).
Tuscaloosa—Dodd, Dorace Carr. (C/S—S-M).

Arizona

Ajo—Keener, William Hayes. (C/S—J-M).
Bisbee—Stuart, Herbert Zimmerly. (R, C/S—J-M).
Globe—Bamerio, Ralph Victor. (C/S—J-M).
Tucson—Fruitman, Frank W. (C/S—J-M).

Arkansas

El Dorado—Ragsdale, John G. (J).
Little Rock—Brown, Frederick Isaac, Jr. (C/S—S-J).
Malvern—Vincent, Kenneth Chapman. (C/S—J-M).

California

Avenal—Knowlton, Drexel Robert. (R, C/S—S-M).
Belmont—Wharton, Bruce Alan. (C/S—J-M).
Coalinga—Harris, Donald Fred. (J). Ustick, Ronald Errol. (J).
Desert Center—Wick, Dave Ervin (C/S—S-J).
Folsom—Wells, John H. (C/S—J-M).
Glendale—Lockwood, R. Bruce. (M).
Grass Valley—Abell, Herbert Emery. (M). Courtney, Humphrey M. (AM).
Los Angeles—Kaplan, Maxwell Henry. (C/S—S-J). McMurray, Thomas Richard. (J). Sparkman, Richard Myron. (J). Townsend, Robert Dawson. (J). White, Robert Thompson. (M).
Menlo Park—Horn, Alvah Jordan. (C/S—J-M).
Modesto—Hocknan, Albert Benjamin. (M).
Monterey—Thurston, George Henry. (C/S—J-AM).
Modesto—Hockman, Abert Benjamin. (M).
Oakland—Byrns, A. C. (M). Lundquist, Raynard Victor. (R, C/S—AM-M).
Pasadena—Howell, Baber Noyes. (R, C/S—J-M).
Riverdale—Graves, Charles Dennis. (R, C/S—S-M).

San Francisco—Crosby, James Winfield, III. (C/S—S-J). Hoskins, Charles Becker. (C/S—J-M).
Santa Barbara—Kamprath, Harry Erhard. (R—M).
Taft—Oliphant, John Joseph. (M).

Colorado

Climax—Boone, James Robert. (C/S—J-M). Enzmann, Robert Duncan. (J).
Denver—Bush, Herbert Howard. (J). Carlile, Jessie Crawford. (M). Humphreys, Ira Boyd. (M). Owens, Marvin Franklin. (C/S—J-AM). White, Robert. (M). Wilson, Glenn Ogden. (M).
Grand Junction—Freeman, Val LeRoy. (C/S—S-J).
Leadville—Tyler, Edmund Andrew. (R, C/S—J-M).
Rifle—Russell, Paul Latimer. (C/S—J-M).

Connecticut

Bridgeport—French, Rolland Sydney. (C/S—J-M).
New Canaan—Goodyear, Austin. (AM).
Woodbury—Heslin, Gerard Matthew. (M).

District of Columbia

Washington—Lillie, Charles Robert. (C/S—S-M).

Florida

Lakeland—Gabeler, William H. (M).
Plant City—Bender, John Andrew. (J).

Idaho

Kellogg—Preston, Kenneth L. (R, C/S—S-M).
Wallace—Hollister, Victor Frederick. (C/S—S-J).

Illinois

Champaign—Jackman, Harold Wesley. (M).
Chicago—Berman, Frank. (R, C/S—S-J). Koehler, Ernest L. (C/S—J-M). Murphy, John Benedict. (M).
East St. Louis—Hicks, Harold Newton. (M).
Salem—Hockman, James Noah. (M).

Indiana

East Chicago—Andberg, Ernest J. (R, C/S—S-M).
Fort Wayne—Mancini, Peter Vincent. (J).
Gary—Sadowsky, Maurice J. (C/S—S-J).

Kansas

Augusta—Holsapple, Lawrence William. (M).
Eureka—Campbell, James Leslie. (C/S—S-J).
Garden City—Miller, Loyle Pope. (C/S—S-J).
Hays—Rogers, Arthur Marion. (M).

Kentucky

Henderson—Mefford, Nace Fennell, Jr. (C/S—S-J).
Pikeville—Batten, Otho Smith. (M).
Wayland—Howard, Noah Daniel. (M).

Louisiana

New Orleans—Reynaud, Richard Burke. (C/S—S-J). Yeager, John Glenn. (R, C/S—J-M).

Massachusetts

Brookline—Castleman, Louis Samuel. (C/S—J-M).
Cambridge—Cremens, Walter Samuel. (C/S—S-J).
Hinsham—Pepper, Edward Lanning. (C/S—J-M).
Milton—Stewart, Robert William. (C/S—J-M).

Michigan

Ann Arbor—Sinnott, Maurice J. (C/S—J-M). Strong, Richard. (C/S—S-J).
Clare—Burgess, David Miller, Jr. (C/S—S-J).
Wakefield—Haller, Harry Frederick. (C/S—J-M).

Minnesota

Hibbing—Miller, William Chellis. (C/S—S-J).
Duluth—Netschert, Bruce Carlton. (C/S—S-J).
St. Paul—Sorenson, Roy T. (C/S—S-J).

Missouri

Bonne Terre—Tittman, David William. (C/S—S-J).
Flat River—Henry, Ralph Lavern. (C/S—J-M).
Rolla—Nelson, Harve Preston. (C/S—J-M).

Montana

Butte—Lyons, John Seth. (C/S—J-M).

Nebraska

Omaha—Parsons, John Steven. (C/S—S-J).

New Jersey

Carlstadt—Dwyer, Thiel Enos. (C/S—J-M).
Cedar Grove—Faulkner, Ross Hilton. (M).
Clifton—Jackson, Reuben Ulirich. (M).
Englewood—Ruprecht, Charles Mattlage. (AM).
Glen Rock—Peck, Charles Bert. (AM).
Highlands—Weis, George Henry. (M).
Linden—Breitenstein, John Stuart. (M).
Montclair—Tillson, Benjamin Franklin, Jr. (C/S—J-M).
Murray Hill—Treuting, Robert Graham. (C/S—J-M).
Nutley—Perebinossoff, Andre A. (M).
Perth Amboy—Muccilli, Philip Carmin. (M).
Plainfield—Spaulding, Hugh Kenneth. (C/S—J-M).
Short Hills—Kennedy, Edwin L. (AM).
Summit—Murphree, Eger Vaughan. (M).
Weehawken—Pinel, Maurice Louis. (C/S—J-M).
West Orange—Bivens, George Allen. (C/S—S-J).
Westwood—Seibert, Walter Emil, Jr. (C/S—S-J).

New Mexico

Carlsbad—Erskine, Neil Markham. (M).

New York

Bronxville—Lyon, Emmett Jefferson. (M).
Carle Place—Ried, Robert C. (C/S—J-M).
Elmhurst—Silk, Edmond John. (M).
Glen Cove—Drury, Maynard Kane. (C/S—J-M).
Glen Head—Doubleday, G. Chester. (M).
Hamburg—Creighton, James A. (M).
Laurel Hill—Barkell, Howard. (R, C/S—J-M).
Lockport—Clark, Donald L. (C/S—J-M).
Malverne—Kretschmann, Raymond Joseph. (J).
Mamaroneck—Wachtell, Richard Lloyd. (J).
Manhasset—Conkey, Henry George. (M).
New York—Bowman, Thomas Parker. (M). Callery, Francis Anthony. (M). Carberry, T. Frank. (AM). Friedlander, Kurt A. (AM). Glaser, Frank W. (J). Johnson, Donald S. (M). Kalil, Eugene Joseph. (C/S—J-M). Sherman, Arthur. (C/S—J-M). Steinitz, Robert. (M). Van Paasschen, Jacob. (C/S—J-M).
Scarsdale—Garretson, Mrs. Mary Welleck. (M). Godinez, Manuel. (M).
Tuckahoe—Stern, James Alan. (C/S—J-AM).
Waccabuc—Parker, Robert Boyd. (AM).

North Carolina

Asheville—Hudspeth, William Roy, Jr. (J).

Ohio

Cadiz—Mills, Edwin Lewis. (R, C/S—AM-M).
Cleveland—Perout, Emil. (C/S—S-J). Ricksecker, Ralph E. (M). Rozalsky, Irving. (J). Steinberg, Morris Albert. (C/S—J-M).
Columbus—DuMont, Charles Siereon. (C/S—J-M).
Cuyahoga Falls—Thompson, James Robert. (M).
Gates Mills—Bigler, William Paul. (M).
Mansfield—Uhl, Marion C. (C/S—J-M).
North Jackson—Fisher, Edward J. P. (R—M).
Worthington—Flint, Norman K. (R, C/S—S-J).

Oklahoma

Bartlesville—Bartz, Mahlon Hugh. (C/S—J-M). Wey, John Edward. (C/S—S-J).
Duncan—Lowary, Thomas Blaine. (J).
Norman—Wolbert, George Smith, Jr. (C/S—J-M).
Oklahoma City—Eisner, Stephan M. (C/S—S-J). Janovy, John. (C/S—J-M).
Tulsa—Davis, Warren B. (C/S—J-M). Hall, Albert Le Clair. (M). Kaye, Emby. (M). Schluntz, E. Kenneth. (C/S—J-M).

Pennsylvania

Apollo—Kommel, Arthur Richard. (C/S—J-M).
Bethlehem—Hoy, Robert Beck. (C/S—J-M). Kaulfuss, Ernest J. (C/S—J-M).
Butler—Hindman, Robert Paul. (M).
Coraopolis—Maratta, William. (C/S—J-M).
Cornwall—Bingham, John Paul. (R, C/S—S-M).
DuBois—Bromfield, Rendle T. (M).
Glenshaw—Newhall, Henry Sylvanus. (C/S—J-M).
Hazleton—Boddorf, Raymond Deane. (M). Middleton, Harold Rosencrans. (M). Owens, Harry Casselberry. (AM). Schwartz, Arthur Dick. (AM).
Lancaster—Biemesderfer, George Keener. (AM).
New Castle—Klugh, Howard E. (M). Lewis, Hamilton Ward. (M).
Philadelphia—Eckmann, Henry Adolph. (C/S—J-M).
Pittsburgh—Coonrod, Forrest Pinkston. (C/S—S-J). Hull, Frederick Charles. (C/S—J-M). Joy, Joseph Francis. (R—M). Loria, Edward Albert. (C/S—J-M). Myers, Howard Burton. (C/S—J-M).
Temple—Myers, Philip Benham. (C/S—J-M).
Vandergrift—Godleski, Stephen. (M).
Verona—Anderson, William Albert. (C/S—J-M).
Waynesburg—Robson, Orval. (M).

South Dakota

Philip—O'Neal, Lewis Merle. (C/S—S-AM).
Rapid City—Van Duzee, Gerald Robert. (C/S—J-M).

Tennessee

Oak Ridge—Murray, George Thomas. (R, C/S—S-J).

Texas

Bellaire—Simpson, Raymond Ellsworth, Jr. (J).
Dallas—Coles, Burton Everett, Jr. (J). Cook, Evin Lee. (M). Davis, Roger Hugh. (C/S—J-AM). Fort, Ellsworth William. (R, C/S—J-M). Haynes, James Morton. (M). Jenkins, Rodman. (J). Mitchell, Joseph Augustus. (AM). Scott, Erwin Ralph. (R, C/S—J-M).
Fort Worth—Robinson, Reginald Lawrence. (AM).
Freeport—Elder, Harvey Bernard, Jr. (C/S—S-J).
Freer—Pittman, Pitser Paul. (R, C/S—S-J).
Houston—Pollard, John Harrison. (R—M). Whitmore, Clifford Monroe. (M).
Kilgore—Jay, Wilburn Reagan. (AM).
Liberty—Drushel, William H. (C/S—J-M).

Midland—Loos, De Lasso. (J). West, Robert Van Osdell, Jr. (J).
Odessa—Greene, Page Osmond. (C/S—S-J). Maurice, James Matthew. (C/S—J-AM).
Orange—Howard, Forrest Conrad. (J).
Plains—Catlett, R. John. (J).
Sherman—Sinclair, Thomas Graham. (C/S—S-J).
Sunray—Forbes, Frank Henry. (C/S—J-M).
Wichita Falls—Gearhart, Marvin. (J).

Utah

Bingham Canyon—Rauer, Richard Conrad. (C/S—J-M).
Garfield—Speers, Elmer Charles. (C/S—J-M).
Heber City—Hawn, George. (M).
Salt Lake City—Bernard, Lynn Daston. (M). De Haven, Addison C. (AM). Hanchett, Hughes Byron. (M). Payne, O. Anthony. (C/S—S-AM). Pearcey, John Guy. (M).

Virginia

Blacksburg—Nevitt, Michael Vogt. (J).
Bluefield—Pero, John William. (M).

Washington

Evans—Vervaeke, Robert G. (C/S—J-M).
Olympia—Purdy, Charles Phillips, Jr. (C/S—J-M).
Seattle—Collins, Willis Erdman, Jr. (AM). Heinzinger, Lee Wilber. (AM).
Spokane—Kirkemo, Harold. (C/S—J-M).

West Virginia

Bluefield—Fox, John Joseph. (M).
Everettville—Kerns, Lawrence F. (M).
Fairmont—Hanna, Robert Wilson. (M). McCandless, Richard Charles. (J).
Kayford—Cannon, Joseph Michael. (C/S—J-M).
Oak Hill—Anderson, Charles Preston. (M).
Sutton—McNary, Harry Bane. (M).
Tioga—Davies, Harold B. (R—M).
Webster Springs—Stacy, Marlis. (M).

Wisconsin

Madison—Porter, Lew Forster. (M).
Milwaukee—Anderson, Richard Carl. (C/S—S-J).

Wyoming

Laramie—Biggs, Paul. (C/S—J-M). Lipstate, Philip H., Jr. (R, C/S—S-M).

Alaska

Fairbanks—MacDonald, Donald, III. (C/S—J-M).
Juneau—Stejer, Francis Adrien, Jr. (C/S—J-AM).

Northwest Territory

Yellowknife—Chalmers, Herbert James. (C/S—J-M).

Ontario

Madsen—Pittson, Victor Jackson. (C/S—S-J).
Ottawa—Monture, Gilbert Clarence. (M).
Virginiatown—Stanlow, Malcolm Morris. (AM).

Quebec

Amos—Almond, Lloyd Beemer. (M).
Portnauf—Pare, Guy. (J).

Coahuila

Rosita—Cushman, Edward Henry. (M).
Torreon—Von Friedrich, William Bataille. (C/S—J-M).

Chile

Chuquicamata—Winkle, Robert Frederick. (C/S—J-M).

Peru

La Oroya—Pagel, Richard Frederick. (C/S—S-J).
Lima—Fagan, Thomas James. (M).

Venezuela

Caracas—Mead, Homer Nathan. (C/S—J-M). Patton, William Richard. (C/S—J-M). Rosales, Cesar Miguel. (C/S—J-M).
Maracaibo—Forrer, Martin. (J).

France

Paris—Steidle, Edward, Jr. (C/S—J-M).

Netherlands

The Hague—Haffner, Bernhard Kinsey. (C/S—J-M).

Southwest Africa

Tsumeb—Boyce, John Howard. (C/S—J-M).

Federated Malay States

Kuala Lumpur—Dunne, William Thomas. (M).
Sungei Lembing—Evans, Arthur Francis. (C/S—J-M).

India

Calcutta—Mathew, Poonithra Mathai. (J).
Rajsthan—Bhattacharyya, Byom Kesh. (M).

Indonesia

Billiton—Van Arkel, Hubertus. (C/S—J-M).

New South Wales

Hillgrove—Trestrail, Hugh Alexander. (C/S—J-M).
Wollongong—Holland, Thomas Whatley. (C/S—J-M).

Philippine Islands

Cebu City, Cebu—Santos-Ynigo, Luis Marcial. (C/S—J-M).

Business Session

Covers Magazines, Officers, and Committees

WITH twenty Directors present, the Board again held a lengthy meeting on Nov. 16, gathering for an informal luncheon at the Engineers' Club at 12:30 and moving over to the Board room at Institute headquarters immediately thereafter for a business session that lasted until 5:20. President Young presided, as he has at all Board meetings during his term of office.

T. W. Lippert, Manager of Publications, announced certain changes in Mining Engineering and the Journal of Metals to be effective with the January issues. The volume number of each journal will hereafter correspond with the number of the Transactions volume containing the technical papers published in the journal during the year. Thus, instead of Vol 2 of ME and JM during 1950, the volume numbers will be 187 and 188 respectively. Also, the page numbers of each journal will hereafter be continuous from month to month throughout the year and will include all sections of the journal, thus avoiding the complex system that has obtained in 1949. Though these changes will result in gaps in the numbering of volumes, and in the paging of the Transactions volumes, they seem to be the best solution yet devised to objections offered by the Post Office and by readers to discontinuous paging in the monthly issues, and to difficulties in indexing.

Another change will be made which has been the subject of much controversy during the year: the editor of each of the three journals published by the AIME will select only those personals that he wishes to use, and the section of personals and obituaries common to all journals will be discontinued. All the items will be prepared at Institute headquarters as formerly but a selection will be made by each journal. This does not necessarily mean that each journal will limit its personals to items about the members of its own Branch, for it is expected that each editor will also carry the more important items about Institute members in other Branches as well. The reaction of readers is invited. To save space, the company connections and street addresses of applicants for membership are also being discontinued,

and the possibility of complete elimination of the names of applicants is being studied.

Plans for increasing the advertising in all three journals were also announced. The Journal of Petroleum Technology will turn over advertising solicitation of new prospects in eleven Western states to the firm of McDonald-Thompson, of San Francisco and Los Angeles, and the Mining and Metals journals will appoint an advertising man with headquarters in Chicago, who may also be asked to solicit advertising in the Petroleum journal. Final approval for the appointment of the Chicago representative was voted at the meeting of the Executive and Finance Committees on Dec. 7.

In line with recommendations made in the Johnson Committee report two years ago, H. Newell Appleton was appointed in charge of internal business administration and office management at AIME headquarters. He will report to the Secretary, as before, but will have authority and responsibility for the conduct of business at Institute headquarters with the maximum efficiency. Mr. Appleton has served the AIME most effectively for 21 years in many capacities and is favorably known to many of those who have attended its conventions.

Further attention was given by the Board to a matter that had come up at the October meeting of the Finance Committee: what to do about the Engineering Societies Building. Costly repairs are imminent and the building is inadequate to meet the needs of its occupants. The feeling of the committee that has been studying the matter, as reported in person by William N. Carey, chairman, and secretary of the ASCE, is that serious consideration should be given to securing, or constructing, a new building and selling the present one. Many have also questioned whether or not the Founder Societies should continue to give the present substantial support to the Engineering Societies Library, and a home for this also enters into the picture. The United Engineering Trustees Real Estate Committee was encouraged by the Board to continue its study of the possibility of new quarters for the societies.

Official announcement was made of the election of the AIME officers presented by the Nominating Committee and published in the July issues of the journals. The ticket is headed by Donald H. McLaughlin as President for 1950, with Andrew Fletcher and Robert W. Thomas as Vice-Presidents, and Harold Decker, Francis B. Foley, E. C. Meagher, C. V. Millikan, Gail F. Moulton, and Howard I. Young, Directors. Divisional Chairmen, and Directors ex officio for next year, are: Mining, Geology, and Geophysics, P. J. Shenon; Minerals Beneficiation, Grover J. Holt; Coal, Carroll F. Hardy; Industrial Minerals, Richard M. Foose; Institute of Metals, Maxwell Gensamer; Iron and Steel, H. K. Work; Extractive Metallurgy, Carleton C. Long; Petroleum, John E. Sherborne; Mineral Economics, Charles H. Behre Jr.; and Mineral Industry Education, Allison Butts.

Some discussion was devoted to a recommendation of the Coal Division that the initiation fee for Members and Associate Members be reduced from $20 to $10; this would reduce AIME income from that source by about $9000 a year, which might be offset by the enrollment of a larger number of new members. It was thought that greater publicity should be given to the fact that the present initiation fee could be paid in four annual installments of $5 each on request, about 17 percent of new members now taking advantage of this privilege. One suggestion was that no initiation fee be charged Junior Members when they must change their status to Associate or Member at age 33 but that the fee be charged in gradually increasing amounts, according to age, thereafter. It was decided to discuss the matter further at the Annual Meeting. How to handle the finances of Institute, Branch, and Divisional meetings, carrying out the idea that they should be self-supporting, also received attention by the Directors, with final decision to be made later.

The Mineral Industry Education Division was authorized to proceed with the implementation of its suggestion that a new major AIME award be given for notable contributions to mineral industry education. Approval was voted to the "Canons of Ethics for Engineers" adopted two years ago by the Engineers' Council for Professional Development; the AIME had previously not subscribed to any such code. An invitation was presented for the AIME to suggest a candidate for the award of the Kelvin Medal in 1950 by the Institution of Civil Engineers, of Great Britain. The medal is given for "distinguished service in the application of science to engineering." The Secretary will be glad to have AIME members suggest names for this honor.

Appointments to committees authorized by the Board include: Jack I. Laudermilk as vice-chairman of the Technical Publications Committee in lieu of Anthony Anable, resigned; Harold M. Bannerman on the Auxiliary Publications Committee of the Industrial Minerals Division, Oliver Bowles having declined; Francis B. Foley reappointed to represent AIME in the American Documentation Institute; James A. Barr to represent the AIME on the Committee on Deep Well Vertical Pumps, of the American Standards Association; A. Rodger Denison reappointed to represent AIME in the American Geological Institute; C. B. Sawyer to take the place of C. H. Mathewson, resigned, on the Council of the American Association for the Advancement of Science; Morris Muskat to represent AIME on the Committee on Fluid Permeation of the American Standards Association; and Manuel B. Llosa A. and A. Russell Merz to represent AIME at a meeting of the Peruvian Institute of Technical Valuations at Lima, Dec. 8-15.

Sherwin F. Kelly reported on a meeting that he had attended as an AIME delegate—that of the First Pan-American Engineering Congress at Rio de Janeiro, July 15-23. He urgently recommended that AIME lend its wholehearted support to the continued existence of PAEC (UPADI) and take an active interest in the work of that organization.

Directors present, besides President Young, were: Messrs. Alford, Benedict, Daveler, Elkins, Head, Kinzel, Kraft, McLaughlin, Meyerhoff, Millikan, Peirce, Phillips, Rhines, Schumacher, Sullivan, Swainson, Swift, Williams, and Wrather.

At a meeting of the Executive and Finance Committees on Dec. 7, with President Young and Messrs. McLaughlin, Schumacher, Daveler, Weed, and Fletcher present, various more or less routine and minor matters were disposed of. Approval was voted of a new Affiliated Student Society at the College of Engineering, New York University, with John P. Nielsen as Faculty Sponsor and Edmund M. Wise as Counselor.

The following prices were set on volumes in the Institute of Metals Symposium Series (superseding previous prices): Vol. 1, Nonferrous Melting Practice, and Vol. 3, Rod and Wire Production Practice, $2 to members and $3 to nonmembers; Vol. 2, Nonferrous Rolling Practice, $3 to members and $4.50 to nonmembers.

Reladling

to obtain uniform bath composition

by J. J. Green

THE matter of uniform bath composition has always been of great concern to makers of electric-furnace steels. This problem is considerably accentuated in the manufacture of steels containing high chromium contents, because of the processes involved. In melting high chromium steels by using a process involving high percentages of chromium-bearing scrap and chrome ore, with a subsequent chromium reduction from slag to metal at high temperatures, or by a practice involving large ferrochrome additions, the stratification of chromium has been regarded as a matter of vital importance.

Obtaining a bath of uniform chemical composition by the usual method of stirring with steel rabbles has not always proved satisfactory. It is particularly difficult to stir the bath properly by the use of steel rabbles when excessively high temperatures are obtained after slag reduction because of the consequent rapid melting of the rabbles. A number of companies have made mechanical mixers for stirring the bath, but these devices are usually quite large and could not be readily adapted to our practices.

J. J. Green is Melting Dept. Metallurgist for Universal-Cyclops Steel Corp., Bridgeville, Pa.

This was a paper presented before the Seventh Annual Electric Furnace Steel Conference, Iron and Steel Div., AIME, Dec. 8-10, Pittsburgh.

In an attempt to obtain a more uniform bath, the idea of tapping out a portion of the metal was conceived, and then pouring it back into the furnace over the lip of the ladle, thus duplicating to some extent, the type of mechanical mixing that occurs during the tapping of a heat.

This plan could easily be fitted into practice in the Universal-Cyclops plant, since on all of the furnaces the roofs can be lifted and the furnace shells proper can be moved out from under the electrodes, thus making the return of the metal to the furnace a simple operation.

This process, which is now a standard practice for all straight-chrome stainless iron alloys and chrome-nickel stainless grades, is termed "reladling". The mechanical mixing of the bath thus obtained has resulted in the complete elimination of discrepant results due to an insufficiently mixed bath.

Before the reladling practice was started, 4.7 pct of off-analysis heats could be attributed directly to stratification of chromium in the fluid bath. Since the reladling practice has been in effect, this figure has been reduced to under 2 pct, the over-all improvement from this cause being approximately 70 pct. The other elements, such as manganese, silicon and nickel, have not given as much trouble as chromium. However, after reladling, it has been possible to control bath composition of all elements more closely.

In taking a preliminary test to check bath composition, two samples are taken from different parts of the furnace. An examination of the chromium results on the last 600 stainless heats made has disclosed that on 80.5 pct of the heats the variation in chromium on the two tests was less than 0.10 pct, and on only 1.3 pct of the heats was the variation over 0.25 pct. The high percentage of heats showing such good agreement in analysis has saved much furnace time otherwise lost while waiting for a second preliminary determination when the first two samples were not in agreement. It has also reduced the number of determinations required of the chemical laboratory, and only on very rare occasions is it felt necessary to send a second preliminary test to check the first test.

In using the reladling process, other advantages have been found that were not anticipated when it was put into general practice. One advantage of this procedure is that it cools the bath considerably. This is a distinct help, since the reladling operation takes place after reduction of chromium from the slag, and the bath is quite hot. A temperature drop in the bath of from 100° F to 200° F is found, depending on the length of time in the ladle, the rate of tap, and the rate at which the metal is poured back into the furnace. This is a matter of furnace control, and the operator is trained to regulate the reladling process so that he is able to control the bath temperature during the final stage of the heat.

Another advantage of reladling has been that it has eliminated an objectionable job performed by the furnace crews. Standing in front of a hot furnace rabbling a heat with a heavy steel bar is not a very desirable job. This is one case when there is no need for insisting that a furnace operator perform an undesirable job, as it can be done so easily by reladling. Needless to say, the furnace crews are sold 100 pct on reladling.

Since the reladling operation has been in regular use, a much closer control of our analyses has been obtained, and it has been possible to melt to relatively narrow aims within any given specification. Before reladling, the chemical specification to which Type 301 stainless was melted included a 1½ pct chromium range, and a 1 pct nickel range. With the institution of the reladling practice, these ranges have been substantially narrowed, and it is of interest to know that on the last 300 heats of this grade that have been made, 87 pct of such heats have finished within a plus or minus range of 0.35 pct for chromium, and 95 pct of the heats have finished within a plus or minus range of 0.25 pct for nickel.

Steelmakers have always been faced with the necessity of making heats within a desired specification, and today the limits to which heats must be melted are becoming closer and closer. By using the reladling operation it is possible to melt heats to close chemical analysis by having a uniform bath composition before making final alloy additions.

by H. R. Hanley

Zinc Metallurgy in 1949

IN the zinc industry progress has been made in newly designed equipment of unprecedented size and functional characteristics. This is evidenced by flash roasters, sintering machines, high frequency melting furnaces, zinc condensers, and other large units. Progress has been made also by improved operating features with old equipment.

Desulfurization: Two Herreshoff roasters of the National Zinc Co. at Bartlesville, which have been in service over 21 yr, were given major repairs during the summer and are again in operation.

The staff of the Blackwell, Oklahoma plant of the American Metal Co., probably the largest of the horizontal retort plants in existence (11,200 retorts, 5600 of which are charged daily) has been conducting small scale experimental work on sintering green ore. Successful operations of this type of sintering have been carried on by the National Smelting Co. in Swansea Vale and Avonmouth for the past 20 yr. As a result of this experimental work a large sintering plant has been authorized to desulfurize and sinter all incoming sulfide concentrates. This will be done on one large machine, 168 ft long and 12 ft wide over the wind boxes. It is being designed and built by the American Ore Reclamation Co. of Chicago, which firm is also designing the entire plant. A Northern Co. automatic bag house is being installed to collect the cadmium dust from the sintering operation.

H. R. Hanley is Professor of Metallurgy, School of Mines and Metallurgy, University of Missouri, Rolla, Mo.

The plant is designed to produce sinter from more than 600 tons of sulfide concentrates per day and will operate 5 days a week. This will allow 2 days a week for inspection and maintenance of plant equipment. No acid plant is contemplated at this time but the plant is so designed that acid could be made when conditions warrant. This method of operating eliminates the necessity of carrying swing crews and therefore reduces the normally required number of skilled operators.

The New Jersey Zinc Co. (Pa.) has put into operation the largest flash roasting unit built to date, with a capacity of 250 tons of zinc sulfide concentrates per day. The roaster is built with drying hearths at the bottom, permitting the use of a stub shaft to carry the rabble arms and eliminating the necessity for extending the shaft through the entire height of the furnace.

A new sintering machine has been installed, 72 in. wide, built by the American Ore Reclamation Co. with a daily capacity of 600 tons of sulfide concentrates. A new acid plant of 250 tons daily capacity, using Monsanto designed vanadium catalyst with three stages of conversion, has also been installed at Palmerton.

During 1948-49, at their Westport, Conn. laboratories, the Dorr Co. has conducted a long series of roasting tests on zinc flotation concentrates using their Fluo-Solids process. It has produced successfully a sweet roast yielding a calcine having many advantages for the electrolytic zinc process. In a similar manner desulfurization was terminated at 5 pct; this amount supplying fuel for subsequent sintering prior to distilling. Again the calcine appears to be ideal for the purpose intended. The very close control of temperature and stack gas composition seems to make the Fluo-Solids process ideal for zinc roasting. When acid is to be made, the strength of the SO_2 gas can be adjusted to suit desired conditions up to a maximum of about 14 pct SO_2 with a minimum production of SO_3. No commercial or pilot plant installations have been made as yet but may be shortly.

The sintering of raw zinc concentrates, yielding SO_2 for acid production, by the National Zinc Co., Avonmouth and Swansea Vale, continues at the customary ratio 5:1 (return sinter:raw concentrates). Some modifications of this process are envisaged which should be implemented in the near future.

The large sulfuric acid interests of this company has taken it into the fluorine field and a commercial plant for the production of high grade anhydrous hydrofluric acid has been in operation during the year. Note: Considerable interest has been aroused in diecast electrical conduit fittings made by this company from Mazak alloys. Considerable care, however, is necessary in their installation in certain surroundings.

Developments at the Selby plant of the American Smelting & Refining Co. represent the first commercial operation employing only two stages of sintering raw lead concentrate, with recirculation of part of the SO_2 gases for making contact acid or liquid SO_2. The concentrated gases from the second-over machine are actually higher in SO_2 content than those from the higher sulfur first-over charge, both being above 6 pct. This type of desulfurization has replaced the multiple-hearth roaster at this plant except for shutdowns or other contingencies; its extension to zinc concentrates will be of interest.

Retorts: Controlled drying of retorts was developed at the Donora (Pa.) Works of the American Steel & Wire Co. and a paper on this development was published in the July issue of the Journal of Metals (R. R. Fuslang and D. H. Wertz, authors).

The controlled drying process depends upon circulation at low velocity of a large volume of conditioned air among the moist retorts. After placement of the retorts in the drying room with the stack dampers and room doors closed, they stand at the existing temperatures until the following morning. Then air circulation is started and continued for 48 hr at a dry-bulb temperature of 120°F and 72 pct humidity. The wet-bulb temperature for this humidity is 110°F which remains constant throughout the drying cycle. Then the dry-bulb temperature is raised according to a routine which develops a pro-

gressively decreasing humidity for 80 hr, ending at 170°F, with a final relative humidity of 17 pct. At this point the fresh air and stack dampers are opened and fresh air heated to 170°F sweeps through the room for the next 16 hr to complete the drying cycle. These 96-hr dried retorts are in a condition equivalent to the retorts dried for 45 days in the conventional manner.

The National Zinc Co. at Bartlesville, Okla., has installed deairing equipment in the pottery department with indicated improvements in quality and life of retorts thus fabricated.

Distilling Furnaces (Horizontal Retorts): A new block of furnaces was built during the first half of the year by the National Zinc Co. (Bartlesville) and put in operation in June, replacing two old and smaller blocks. The new block is of the split type with 208 retorts on a corner or 832 for the full block. Its capacity is 50 tons of oxidized or sintered zinc material per cycle (48 hr). One stove or end is charged one day, the opposite end the following day. Retort residues, when commercially valuable, are beneficiated by a magnetic concentration process.

A new rod mill for mixing charges immediately before charging into retorts has been installed at the Machovec Smelter of the American Zinc Co. of Illinois, at Dumas, Texas. This provides a heavier charge per retort and is a notable improvement.

Some progress has been made in mechanical charging of retorts at the Amarillo plant of the American Smelting & Refining Co.

Continuous Distilling: The New Jersey Zinc Co. (Pa.) has installed additional vertical retort furnaces, replacing the remaining horizontal ones.

A new type of condenser has been developed by this company and placed in commercial operation during the year. A motor-driven impeller is employed which maintains showers of liquid zinc to scrub the gas-vapor stream. The heat of condensation is removed by water-cooled coils immersed in the zinc bath. This is an innovation in the field of metal vapor condensation and is one of the outstanding achievements of the year. Note: A complete pilot plant for flotation was added to the research facilities at Palmerton.

Because of the extensive installation of new furnaces and accessory equipment by the St. Joseph Lead Co. in 1948, none is reported for 1949. Their greatly expanded facilities have required considerable development work of an operational nature. This company is continuing full scale commercial testing of various designs of the Weatan-Najarian condensers. Fifty tons of zinc per day have been tapped from one unit, regular production usually running between 30 and 40 tons daily.

Electrolytic Treatment: Operations at Rhodesia Broken Hill, Northern Rhodesia, have not changed materially. Excessive amounts of impurities are removed from solutions as routine practice. Oxidizing of iron with MnO_2 ore at about 15 mg per L H_2SO_4 prevents the loss of this reagent in attacking zinc sulfide.

Soluble silica at high concentration is precipitated after neutralizing acidity with powdered limestone plus an excess of 3 gm per L, when heated to 70-75°C with live steam. During this step V_2O_5 and P_2O_5 are precipitated as ferric vanodate and phosphate respectively and the surplus iron as hydroxide. The dissolved silica passes from a gel to a granular form, readily filterable.

Purification of solution of electrolytic zinc solution at Risdon Tasmania[1] is of interest. Superior results are obtained in precipitation of iron at a pH above 4 when the hydroxide is formed rather than a basic sulfate. The former is easily filtered and washed without cracking of cakes, the latter behaves in an adverse manner.

Experience at Risdon has shown that the presence of a reasonably high concentration of soluble silica is necessary for the co-precipitation of germanium; the latter appears to be substantially absorbed on the silica in passing from colloidal to granular condition.

A new large induction melting furnace is to be installed at Risdon with a power loading of 540 kw which will be supplied through three electric induction transformers attached to the base of a rotating furnace unit.

The furnace should be capable of melting 118 tons of cathode zinc per day with a power consumption of 110 Kw-hr per ton. The cost of power is expected to be less than equivalent fuel oil as at present used. Melting in an experimental furnace indicates an improved melting efficiency of 1 to 1½ pct over previous fuel oil operation.

Experimental work is being performed on mechanical slab casting of zinc at the plant of the Cons Mining & Smelting Company of Canada (Trail). When this work reaches the production line it will be of interest to all electrolytic plants.

Zinc Fuming: The zinc fuming plant of the Hudson Bay Mining & Smelting Co., Flin Flon, is under construction for the treatment of the large accumulation of zinc plant residues.

The latter is to be charged to the copper roaster, and to pass with the regular calcine to the reverberatory copper smelting furnace. The usual sequences follow, viz: the copper and precious metals will enter the matte while the zinc, to a great extent, will enter the slag. This procedure is essentially that of zinc slag enrichment; the copper reverberatory slag, without the zinc plant residue addition, already carries an appreciable zinc percentage. The slag is treated by a fuming process in which the zinc is recovered primarily, as oxide in the following steps:

(1) Holding furnaces (2) Fuming furnaces (3) Boilers (4) Cooling tubes (5) Bag house (6) Oxide leaching plant.

The bag house oxide is to be leached with acid and the resulting zinc sulfate solution will join the primary solution flow of the present electrolytic zinc circuit.

The existing zinc plant is being expanded for higher production tonnage by increasing the solution purification section of the leaching plant, adding two electrolytic cell sections and a 100-ton melting furnace in the casting plant.

---

1. **Harry Hey, "The Electrolytic Zinc Industry", Fourth Empire Mining and Metallurgical Congress, G. B. 1949.**

Results of

Optimum Current Control

On Electric Furnaces

by L. A. Wynd

With today's emphasis on very fast and efficient melting practice, these operating data are particularly timely. The author shows records of actual heats to indicate the great advantages accruing from automatic current settings, as compared with the results obtained with the furnace operator adjusting current settings by hand and by guess.

Technically, there isn't anything today that is very new about optimum current settings for fast melting except the apparatus described by R. M. Bayle, of Westinghouse, earlier in the Conference. (See *Journal of Metals*, December 1949.) This equipment does, automatically and better, some of the things previously left to the furnace operator to do by guess and by hand.

N. R. Stansel thoroughly and completely explained the fundamentals of optimum current in the arc, in his book "Industrial Electric Heating", published in 1933 and now out of print.

N. J. Roberts appeared before the Electric Furnace Steel Conference in October 1944 and presented his excellent paper entitled, "Use of Power for Fast Melting", in which basic fundamentals were outlined. This paper summarized attractive benefits obtainable by applying these principles to arc-furnace melting.

L. A. Wynd is Electrical Supt., Republic Steel Corp., Chicago. **This paper was presented before the Seventh Annual Electric Furnace Steel Conference, Iron and Steel Div., AIME, Pittsburgh, Dec. 8-10.**

The opening remarks in Mr. Robert's paper alluded to Mark

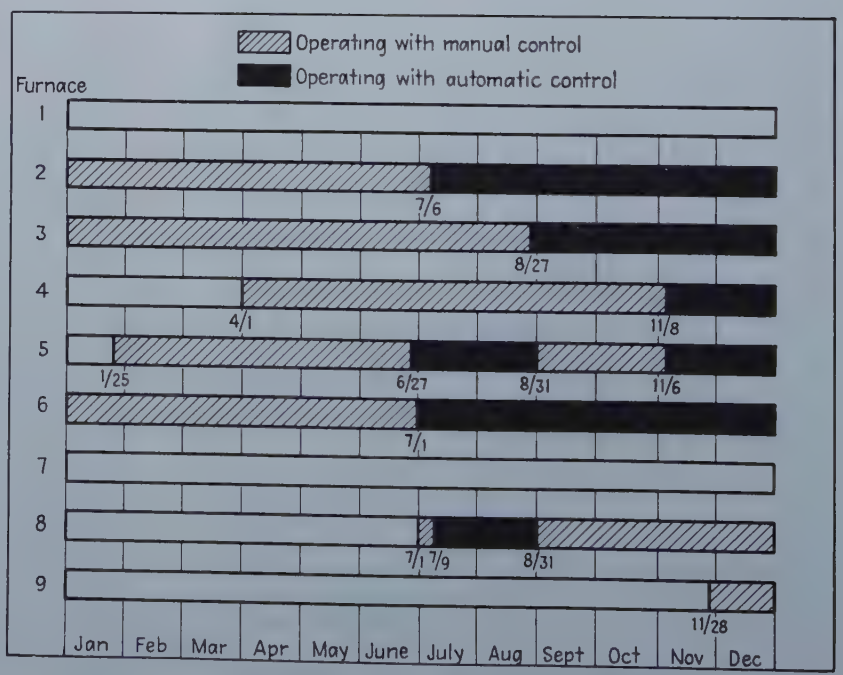

FIG 1—Electric Furnaces operated in the year 1948 showing periods with and without automatic control.

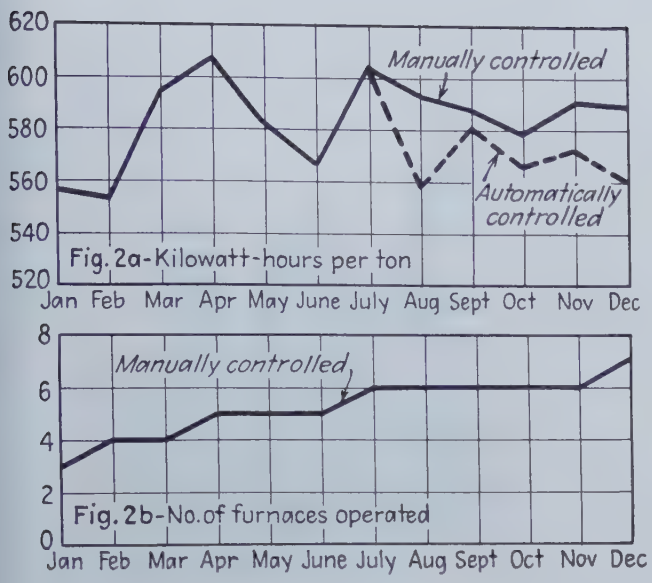

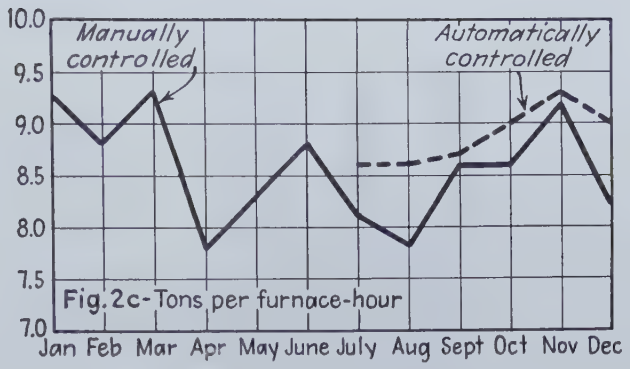

FIG 2—(Above and Left) Number of furnaces operated and operating results with manual and with automatic control.

FIG 3—(Below) Tons of rimmed steel per furnace-hour; December 1948.

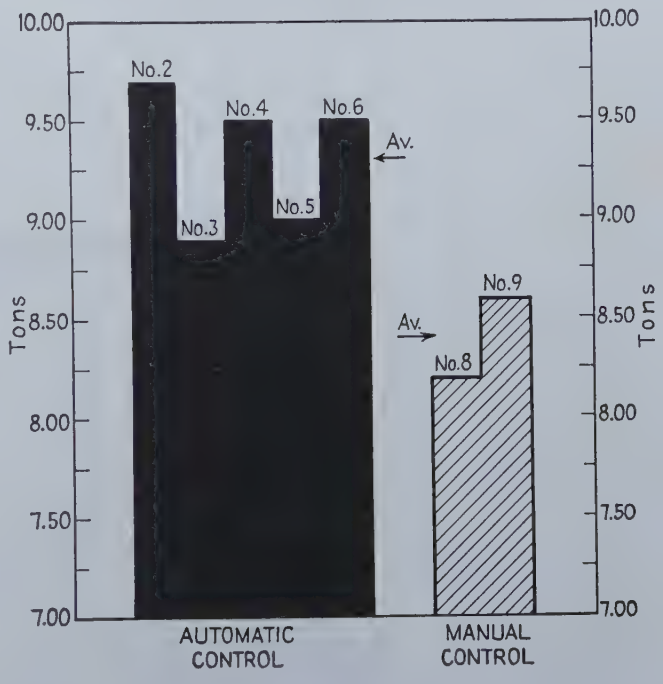

Twain's classic statement about the weather as being applicable to the situation with respect to the actual practical application of these principles. The author of this paper intends to show that the principles were not only talked about but also something was done about them. Results to date substantiate the claims made in the closing paragraph of Mr. Robert's paper.

The accompanying graphs show the results obtained with furnaces operating with and without the control which produces maximum power in the arc and attendant high-speed melting.

All furnaces represented are duplicates. Each was a 70-ton, 20-ft shell, Heroult type, powered with a three-phase, 12000 kva transformer having secondary voltages of 124, 159, 200, 230 and 275. Automatic control is used only on the three highest voltages. Twenty-inch graphite electrodes were used throughout.

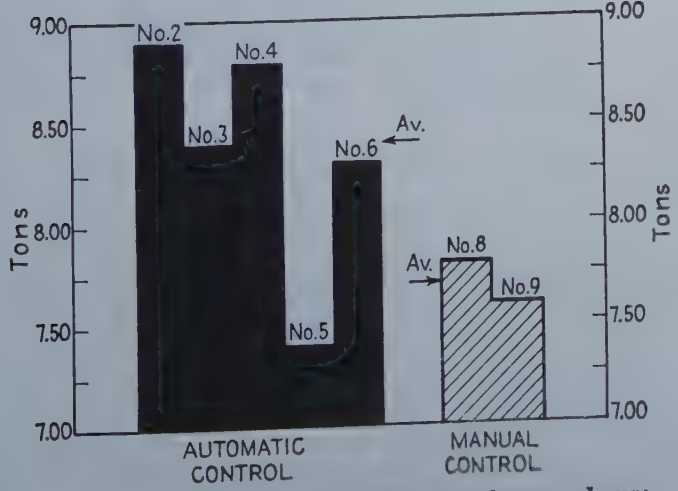

FIG 4—Tons of alloy steel per furnace-hour; December 1948.

Data for the charts were taken from the "Daily Report of Electric Furnace Operations" log sheets kept in the Melt-Shop Superintendent's office.

Fig. 1 graphically pictures 1948 electric furnace operations with specific dates of application of automatic control. It ties in with slide fig. 2, curves in fig. 2a, fig. 2b and fig. 2c, which show trends due to the automatic features.

The wide variance in these curves is attributable to the fact that starting up a furnace calls for considerable crew training and also results in increased charging delays. These factors obscure some of the benefits attained by automatic control.

The month of December was chosen

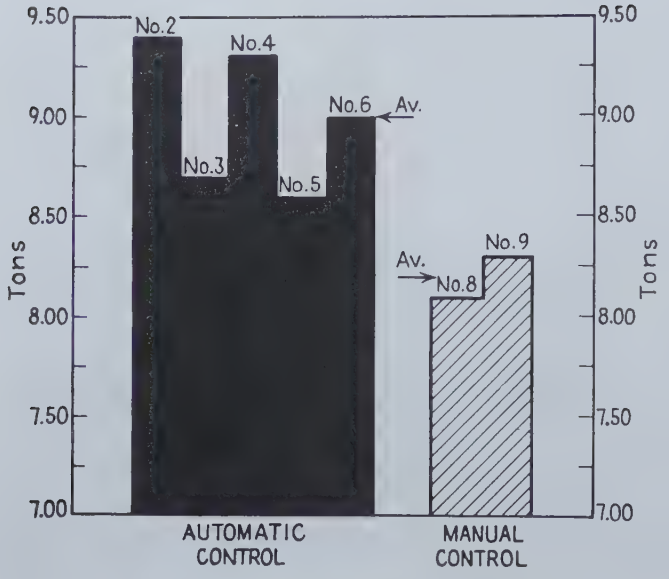

FIG 5—Tons of steel (all grades) per furnace-hour; December 1948.

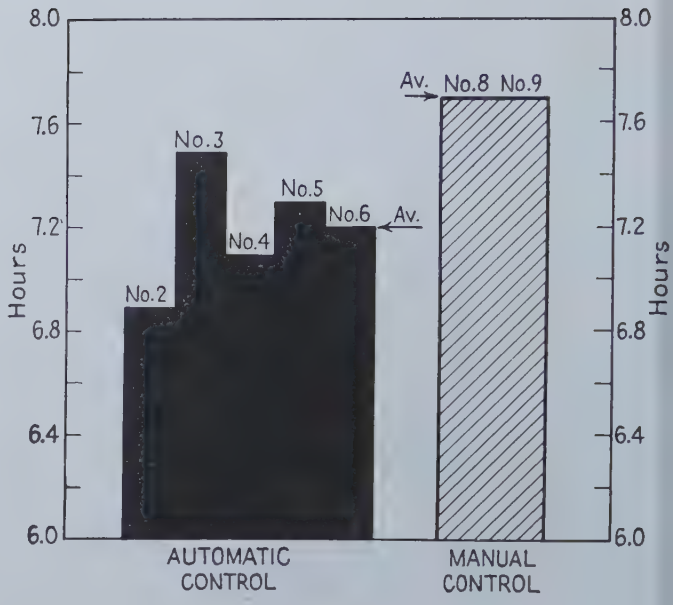

FIG 7—Power on to tap—hours per heat for rimmed heats; December 1948.

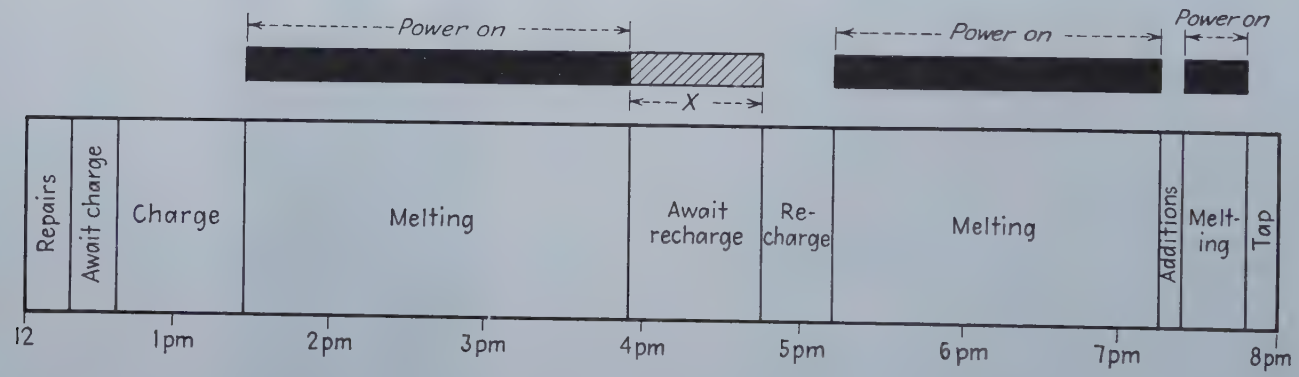

FIG 6—(Above) Electric furnace heat cycle. Time values shown are only approximate, and chart is used to show relation and sequence of elements only. X varies with floor and stock-house conditions and number of furnaces charging.

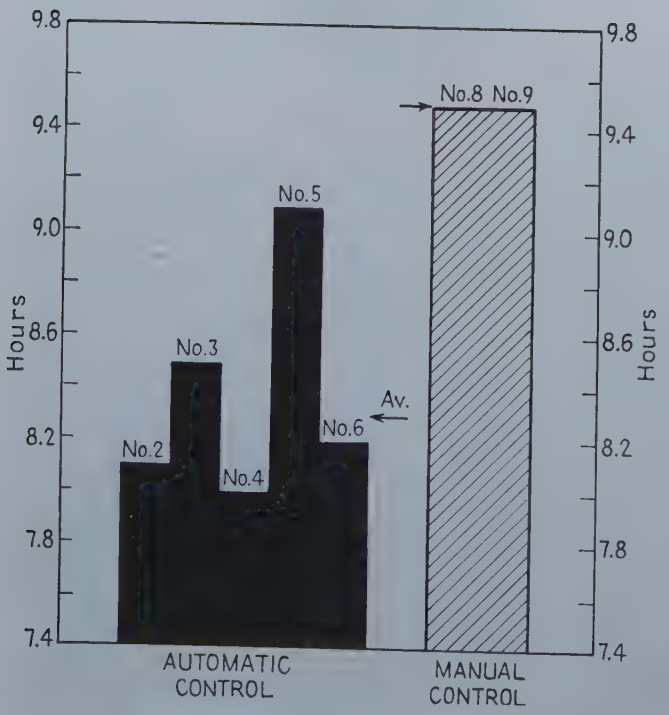

FIG 8—(Left) Power on to tap—hours per heat for alloy heats; December 1948.

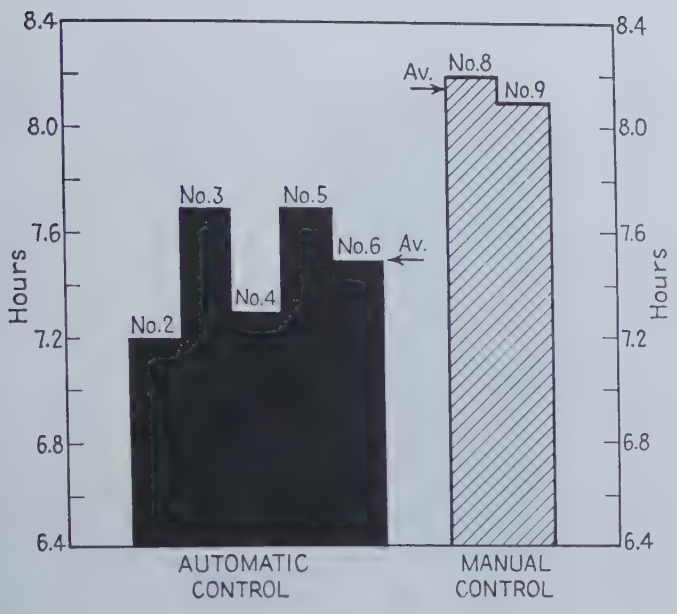

FIG 9—Power on to tap—hours per heat for all grades of steel; December 1948.

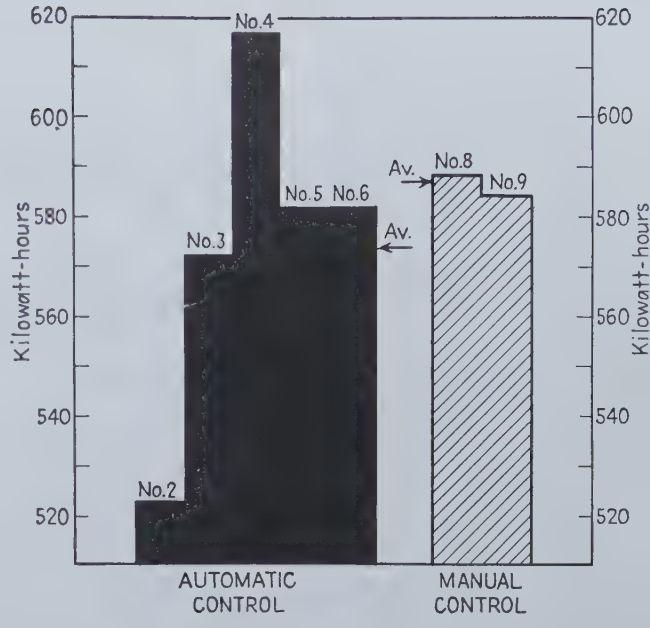

FIG 10—Kilowatt-hours per ton of steel; December 1948.

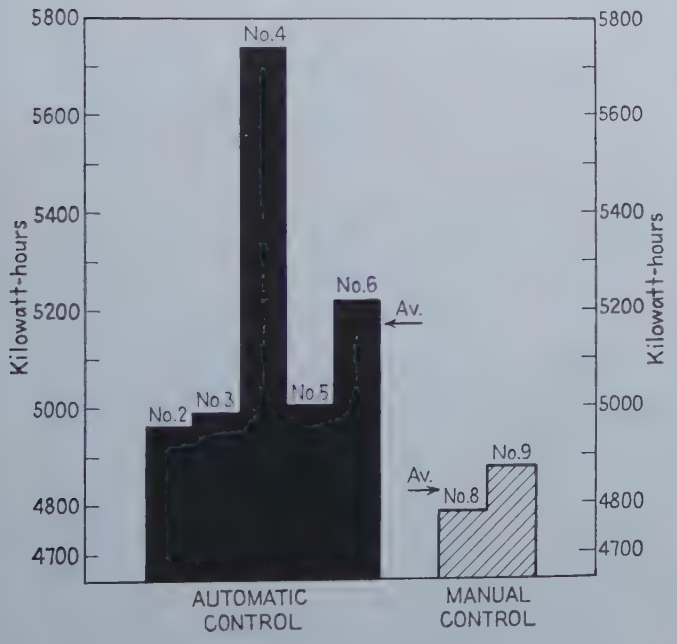

FIG 11—Kilowatt-hours per furnace-hour; December 1948.

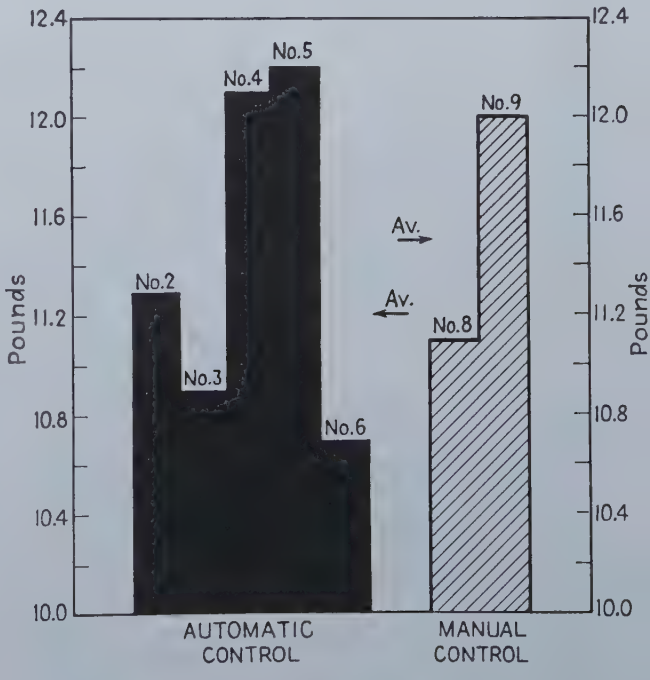

FIG 12—Pounds of electrodes per ton of steel; December 1948.

as a period to compare performances of furnaces having automatic controls with those operated manually. During this period, five furnaces (Nos. 2, 3, 4, 5 and 6) operating automatic on the three highest voltages were compared with furnaces (Nos. 8 and 9) which operated manually on all voltages.

The graphs in figs. 3, 4 and 5 show comparative performance in tons per furnace hour for different types of heats and indicate improved performance on all types where automatic controls were in use.

Fig. 6 graphically represents a typical heat cycle for an 8-hr heat from tap to tap. Time values are only approximate but the elements are in proper sequence.

Melting of the original charge and the recharging elements are shown as continuous, but actually these are broken into small increments of charging and melting as a few cars of scrap become available from time to time.

If the charge in a furnace has melted down sufficiently to receive the recharge, the energy

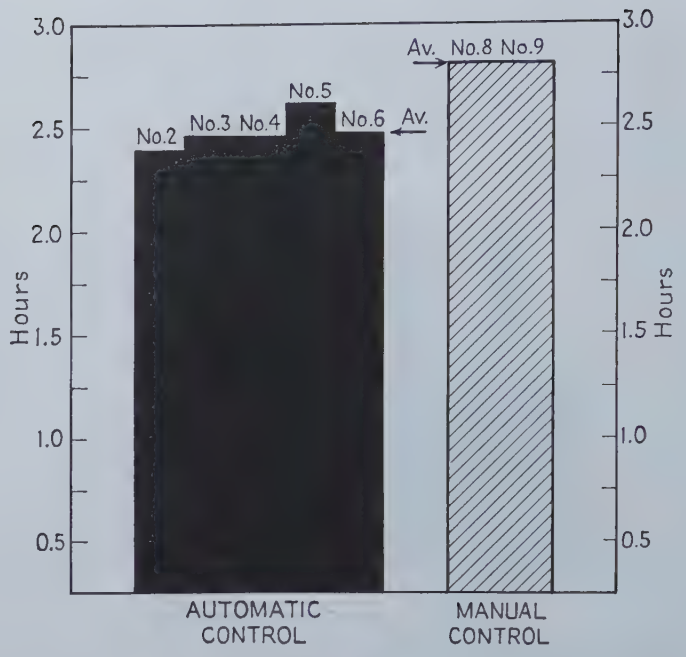

FIG 13—Average delay per heat; December 1948.

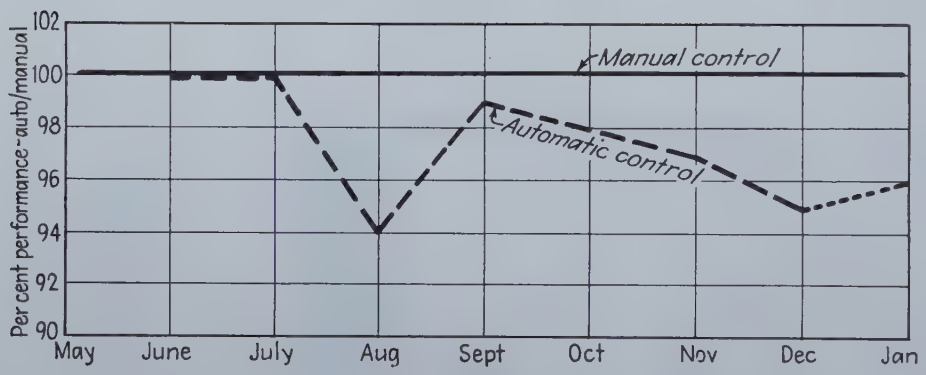

FIG 14—Index of performance. Kilowatt-hours per ton for furnaces with automatic control v. furnaces with manual control.

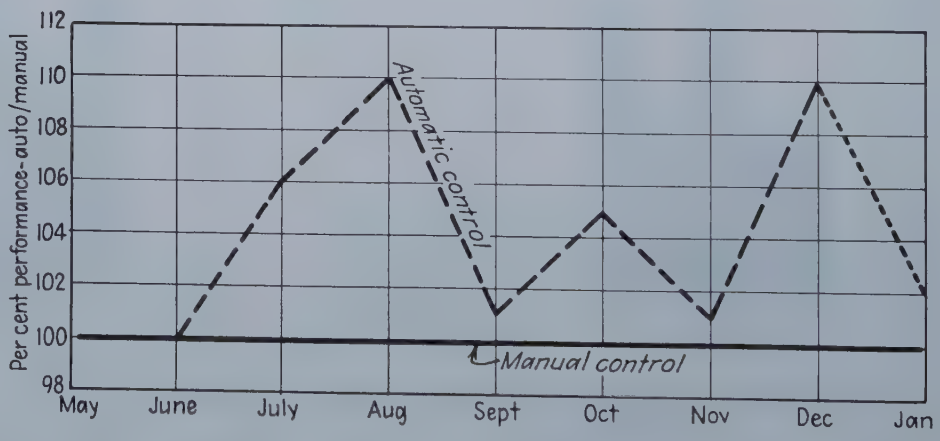

FIG 15—Index of performance. Tons of steel (all grades) per furnace-hour for furnaces with automatic control v. furnaces with manual control.

put into the furnace from that point until scrap is actually charged is partially wasted. This will vary from heat to heat and this loss obscures the actual benefits from automatic control and results in radical differences in energy used per ton of scrap melted.

In order to throw out the time variable of repairs, awaiting charging and actual charging, the charts in figs. 7, 8 and 9 were developed. These show a comparison of hours from "power on to tap". However the losses resulting from recharging delays are still in these figures.

The data in figs. 10, 11 and 12, covering pertinent data on power and electrodes, are self explanatory.

Fig. 13 shows average of all delays per heat. Included in these delays are: charging, melting, finishing, pit, mason, mechanical, electrical and power demand.

The final graphs in figs. 14 and 15 show the index of performance and summarize two of the most important results every electric furnace operator is striving for.

Inductive Stirring in Arc Furnaces

by Sven Fornander

and

Folke Nilsson

DURING the reducing period in the arc furnace it is possible to refine the steel with respect to sulphur and oxygen to a larger extent than in other types of furnaces used in steel-making. However, as this refining requires a long time, it is a fairly expensive process. The reason why it takes time is that the reactions in which sulphur and oxygen are removed from the steel, take place mainly in the surface of contact between slag and steel, and thus diffusion processes come into the picture.

Trials have been made to accelerate these reactions by means of various kinds of stirring. In this paper an account will be given of the results obtained with a new type of stirring device, which has been developed and tested in Sweden during the last 10 yrs.

Sven Fornander is Research Manager of Surahammars Bruks AB, Surahammar, Sweden, and Folke Nilsson is General Manager, Hagfors Steelworks, Uddeholms AB, Uddeholm, Sweden.

This paper was presented before the Seventh Annual Electric Furnace Steel Conference, Iron and Steel Div., A.I.M.E., Pittsburgh, Dec. 8-10.

In 1936 the Swedish electrical firm ASEA was asked by a steelworks whether it would be possible to produce a stirring movement in a hot metal mixer by electric means. The problem was taken up for study by Dr. Ludwig Dreyfus. He succeeded in solving it according to a principle which had not been applied before to this purpose, and laboratory experiments with small tin melts showed that the stirring effect wanted could be produced. However, the project of using electric stirring in a hot-metal mixer was never carried out.

Instead, the first electric stirrer was installed on a 15-ton arc furnace at Surahammars Bruks AB in 1939. The technical director of this works, Yngve Törneman had long realized the possibilities of increased stirring and therefore took the responsibility for the installation. This first test was not successful from an economical point of view, but the results obtained paved the way for further developments.*

** Due to the furnace construction, the stirring coil had to be placed inside the furnace shell on top of the bottom plate. It was in operation for about one month only and was then damaged by overheating.*

As a result of the war it was a long time before the next electric stirrer was put into operation. This was done in the autumn of 1947 on a 15-ton furnace, constructed by Demag at Hagfors Steelworks, belonging to the Uddeholms AB. Shortly afterwards, in June 1948 a new furnace provided with an electric stirrer, was put into operation at Surahammars Bruks AB. This furnace, which was constructed and manufactured by ASEA, has a nominal capacity of 10 tons.

Thus, the electric stirrer in its present form is the last link in a rather long chain of developments. It fulfills all the requirements that are essential for operation and for steel-making.

The principle of the stirrer has been described by Dreyfus[1], who called it the induction motor principle. The stirrer, which is placed under the nonmagnetic bottom plate of the furnace, works on two phases. The electric currents in the two phases induce electric current paths in the liquid

In this first part of a two-part article, the authors for the first time describe in this country a new type of stirring device to accelerate metallurgical reactions in arc furnaces. Herein the authors describe the history of inductive stirring, the type of equipment used in these latest experiments, and results during the melting down period, power consumption for melting, the oxidizing period and slag removal.

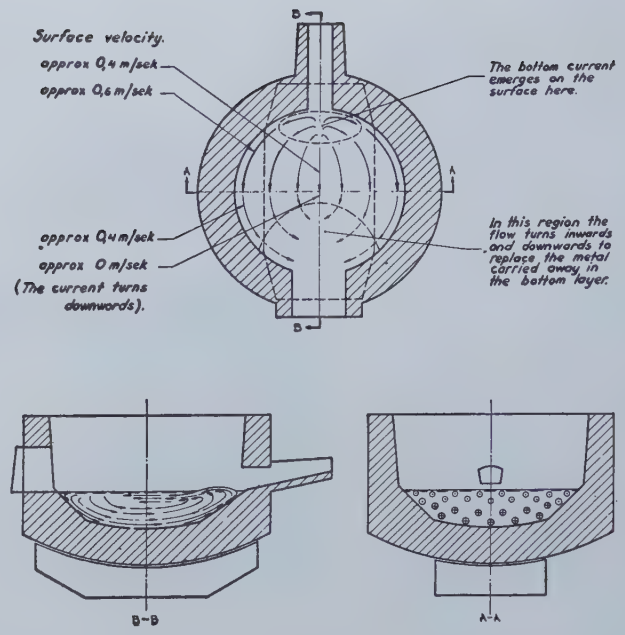

Fig 1—Bath motion in a 15-ton furnace.

steel bath. At the same time the two phases generate a moving magnetic field, which reacts upon the steel composing the current paths with forces parallel to the furnace bottom. The result is that those parts of the bath which are close to the furnace bottom are set in motion in a direction parallel to the bottom.

Fig. 1 is a diagram of the stirring motion in the Uddeholm-furnace. With the direction of bath motion normally employed a strong bottom current of molten metal goes from the furnace door towards the taphole. As a result of the shape of the bottom, the current turns off upwards at the taphole. Just inside the furnace door the current goes downwards, and to this area the metal flows from the middle and the sides of the furnace. The values of speed indicated on the diagram were determined by observation on pieces of burnt lime floating on a clean metal bath. When the bath is covered by a slag layer the latter probably retards the motion, and therefore the speed of the surface layer of a slag-covered bath will be lower than indicated by the observations on a clean bath.

The slagging-off operation is considerably facilitated when the stirrer is in operation. The deslagging is carried out simply by raking off the slag from the area just inside the furnace door. The stirrer does the rest of the work: it transports the slag from the backwall and the sides on to the door. The importance of this is great, since the deslagging is the hottest and most unpleasant job at an arc furnace. The stirrer guarantees that the deslagging will be effectively done: the operation will be no harder to carry out even though it is thoroughly done.

The direction of motion shown in fig 1 is usually employed. The motion can be reversed by means of a simple device. This is done occasionally when alloying additions are made in order to move them towards the middle of the furnace.

In table I a few data are given on the electrical stirrers used at the two furnaces mentioned above.

TABLE I
Data on Electrical Stirrers

Company	Nominal Furnace Capacity, Tons	Motor Power, KW	Generator Power, KVA	Power Consumption, KWH per ton	Relative Stirring Effect
Surahammar .	10	63	105	17	a
Uddeholm	15	109	212	18	1.3 a

Metallurgical experience with the ASEA electric stirrer: During the last year two investigations were carried out in Sweden in order to clarify the influence of inductive stirring on the course of a heat in the arc furnace. One of these investigations was made at the 15-ton furnace at Uddeholm[2] and the other at the 10-ton furnace at Surahammar[3]. The method employed was the same in both cases: a number of experimental heats were made with or without the aid of the inductive stirring coil but in other respects as nearly identical as possible. The heats were studied in some detail. The results from the two groups of heats were compared and conclusions were drawn.

Special studies were made at the two works of the influence of stirring upon the temperature distribution in the bath as well as upon the concentrations in different parts of the bath after alloy additions.

Sampling: The steel samples were taken with a device suggested by N. Rudberg, see fig. 2. The

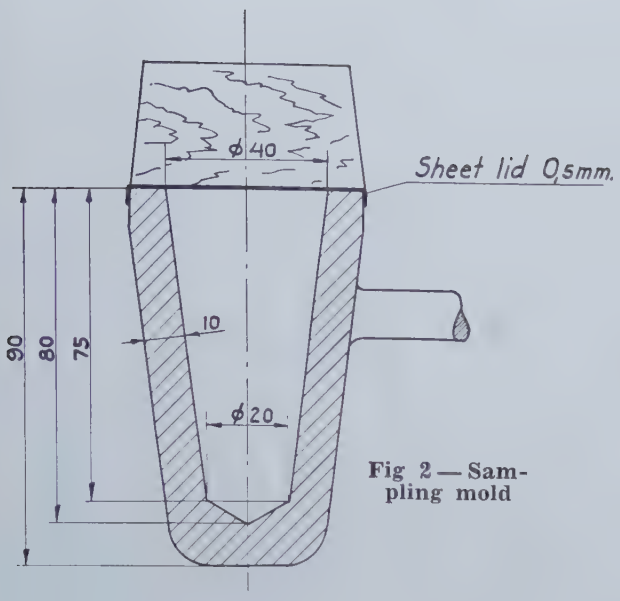

Fig 2 — Sampling mold

mold is made from mild steel. In sampling unkilled steel about 2 g of an aluminium wire of 1 mm diam (about 0.5 pct Al) is placed inside the mold. In sampling during the reducing period, when the steel is killed, the mold is used empty. The mold is furnished with a sheet lid, about 0.5 mm thick. The lid is covered by a piece of wood, fixed in position by an iron wire. After slagging up to the edge, the mold is dipped into the steel bath. When the wire has melted, the wooden piece rises to the slag surface uncovering the slag-free sheet lid. The lid melts and the mold is filled with steel. The samples obtained are free from furnace slag, and since they are not affected by the atmosphere during solidification their composition and especially their oxygen content will be representative of that of the steel bath.

This method of sampling was developed at Surahammar[4], where it has been used rather frequently during the last 7 yr. To test the reproducibility of the method some 200 duplicate

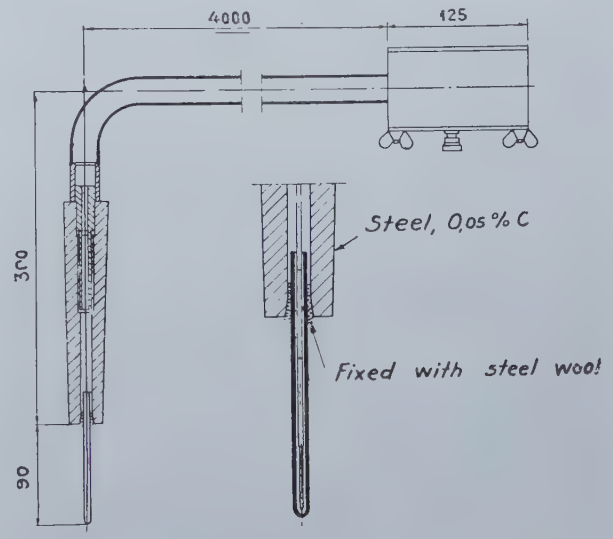

samples have been taken in various kinds of furnaces. The samples were analyzed for oxygen by the vacuum-fusion method. The reproducibility of the sampling method is regarded as satisfactory. It lies approximately between the same limits as that of the analysis: the difference between the oxygen contents obtained was larger than 0.003 pct 0 in only five cases out of 200.

The slag samples were taken with a spoon in the usual way and poured into a flat mold.

The steel temperatures were determined with a somewhat modified type of the Schofield quick-immersion pyrometer, the main feature of which is that it contains no parts which can give off gases when heated. As a result of the pyrometer design, the thermocouple wires will not be contaminated during the measurements, and it is possible to use the same hot junction for 50 successive determinations without getting any measurable change in the emf of the couple. Fig 3 shows the pyrometer construction. This method was developed at Surahammar a few years ago° under the auspices of the Jernkontorets Fors-

Fig 3—(Right) Pyrometer design.

Fig 4—(Below) Heat No. 1; 10-ton furnace, without stirrer.

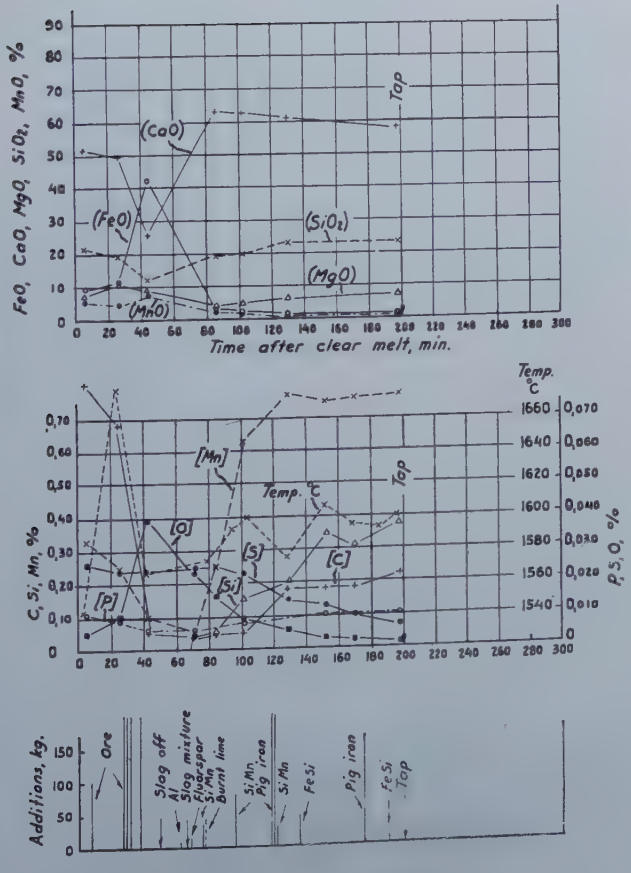

kningsverksamhet (the research organization of the Swedish Ironmasters Association).

Results: At each of the two steelworks mentioned, about 15 experimental heats were studied in some detail making a total of 30 heats. In this paper detailed information will be given about only eight experimental heats, which are regarded as typical. The data are given in the form of diagrams, see figs 4 to 11. Table II shows the analyses of the ingots made in the heats.

TABLE II
Pit Sample Analysis of Experimental Heats

Heat No.	Company	Kind of Stirring	Pit Sample Analysis C	Si	Mn	P	S
1	Surahammar	Rabbling	0.23	0.32	0.71	0.010	0.005
2		Rabbling	0.24	0.28	0.72	0.008	0.005
3		Inductive	0.15	0.25	0.58	0.008	0.005
4		Inductive	0.22	0.21	0.69	0.011	0.005
5	Uddeholm	Rabbling	0.16	0.34	1.41	0.014	0.013
6		Inductive	0.17	0.26	1.33	0.009	0.010
7		Rabbling	0.65	0.14	0.61	0.016	0.015
8		Inductive	0.67	0.17	0.68	0.007	0.013

The inductive stirring was used on four of the heats during the period of time from just before "clear melt" to "tap". On the other four heats rabbling by hand was made when it was considered necessary.

From the data collected in the two investigations the following results were obtained.

(1) The melting down period: At the Uddeholm furnace a study was made of the power consumption during the melting down period in order to ascertain whether the inductive stirring would exert any influence. In all, 104 heats were included in this study. The stirrer was working during the latter third of the melting period. The result is shown in table III. As will be seen from the table, the stirrer does not affect the melting down process.

TABLE III
Power Consumption for Melting

	With Inductive Stirring	Heats for Comparison
Number of heats	50	54
Total kWh to "clear melt" (stirrer excluded)	424,100	445,000
Total production, tons	848	912
kWh per ton for melting (stirrer excluded)	499	499
Total kWh for stirrer	3,077	
Working time for stirrer	41 min	
kWh per ton for stirrer (to "clear melt")	3.6	
Melting time per heat	2h, 29 min	2h, 30 min
Bath carbon at "clear melt", percent	0.89	0.97

(2) The oxidizing period: The raw materials for the experimental heats one to four were selected in such proportions that the carbon content at "clear melt" was high enough for a long oxidizing period to be required. It was thought that the influence of the inductive stirring upon the carbon refining could be studied best in this way. Fig 12 shows the decarburization curves for the four heats. The rate of carbon drop is about the same in all cases, 1.2 pct C per hr, and thus the rate of carbon drop is not affected by the in-

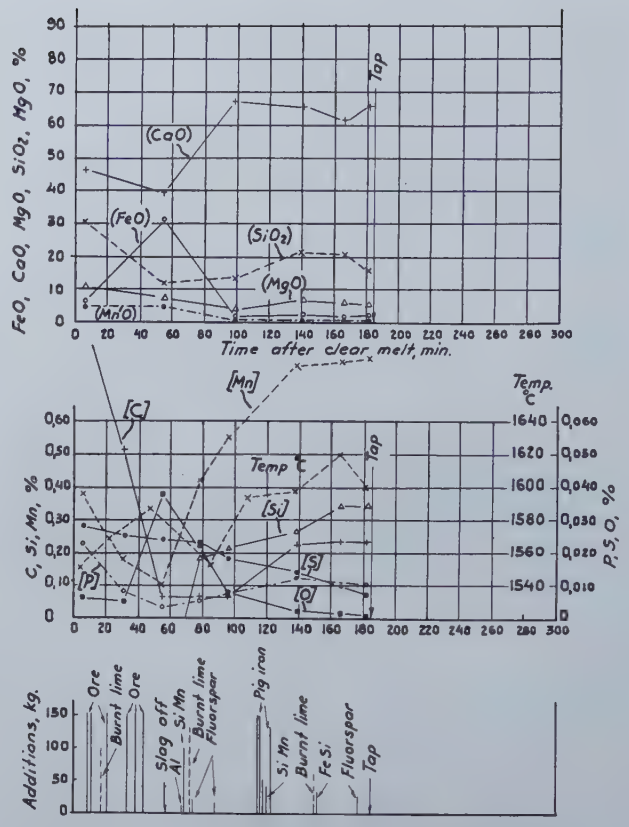

Fig 5—(Above) Heat No. 2; 10-ton furnace, without stirrer.

Fig 6—(Below) Heat No. 3; 10-ton furnace, with stirrer.

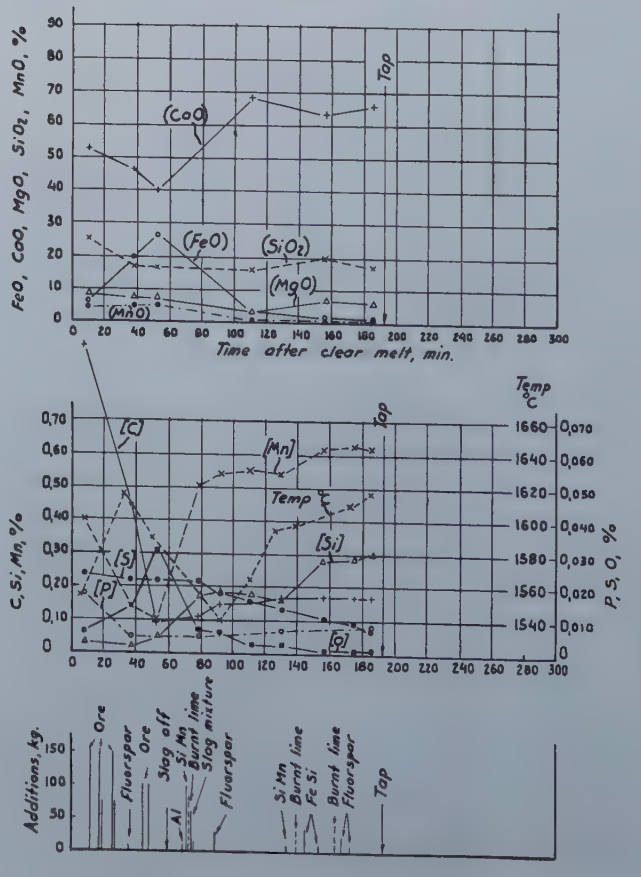

Fig 7—(Below) Heat No. 4; 10-ton furnace, with stirrer.

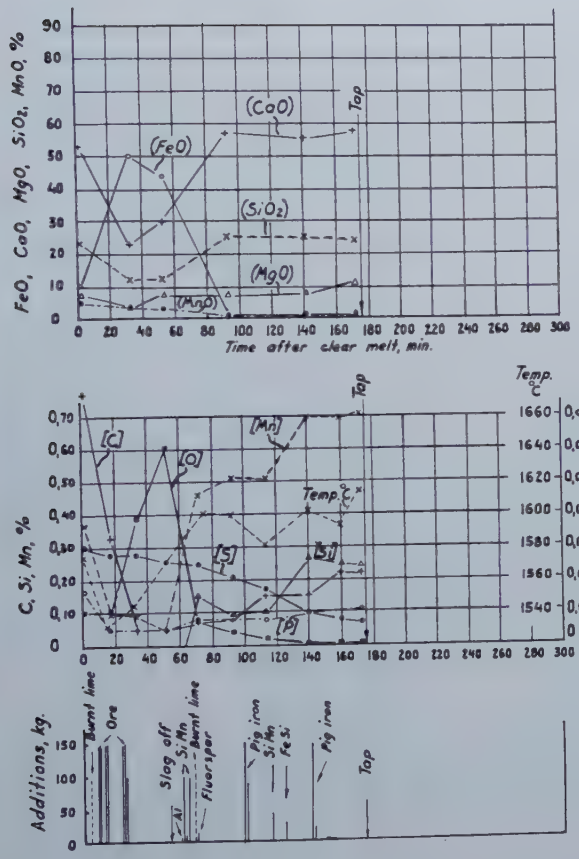

Fig 8—Heat No. 5; 15-ton furnace, without stirrer.

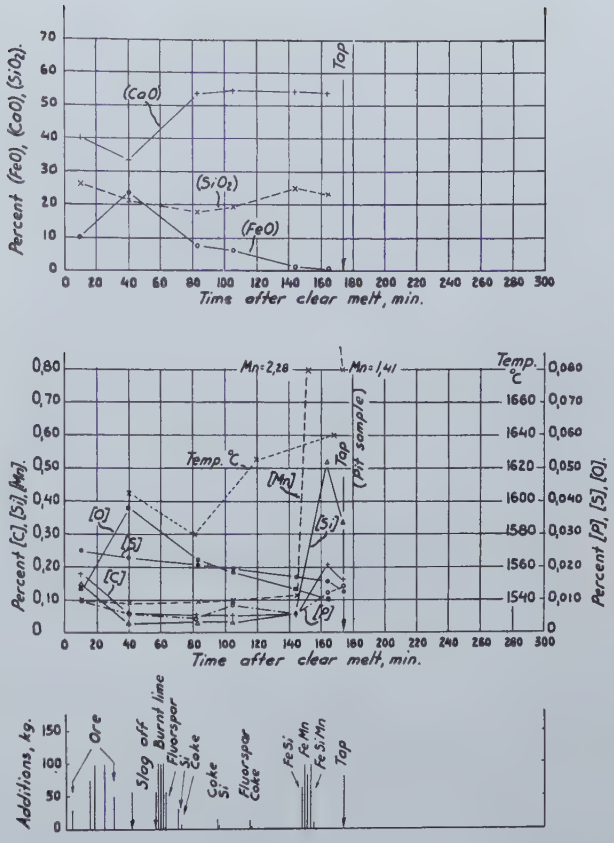

Fig 9—(Right) Heat No. 6; 15-ton furnace, with stirrer.

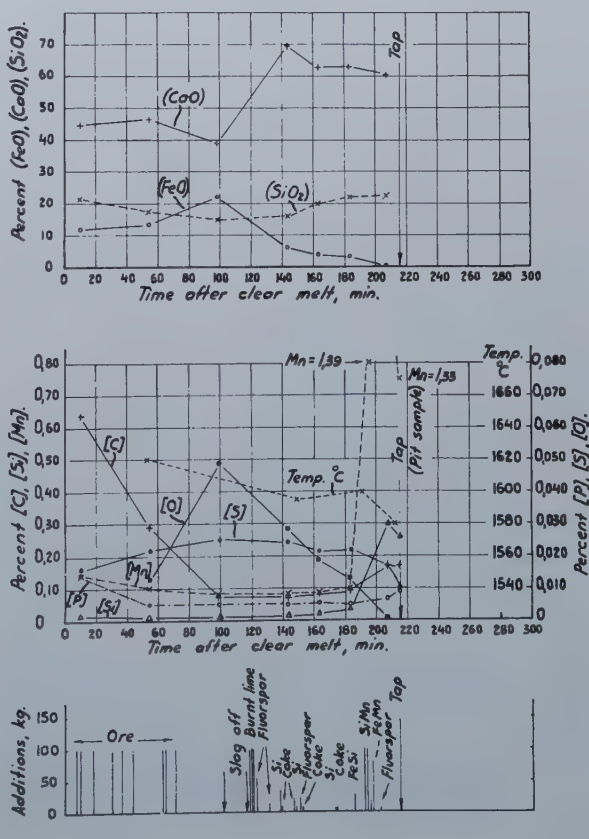

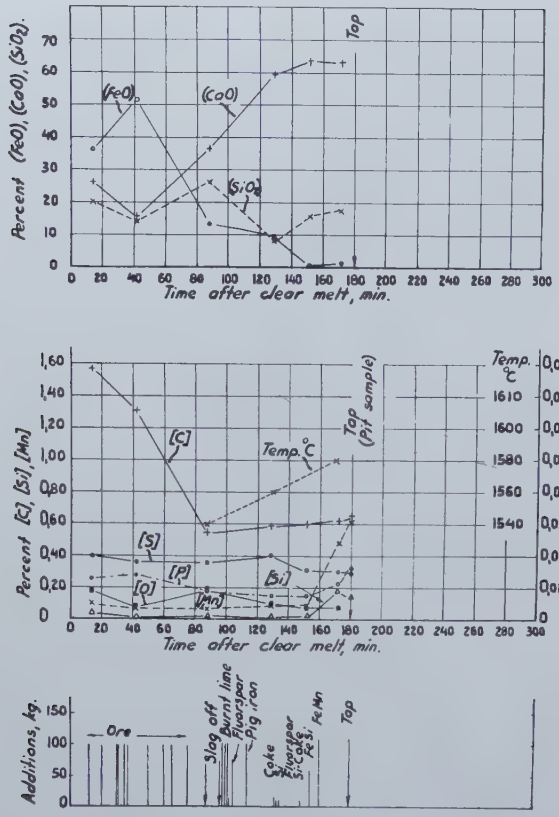

Fig 10—(Left) Heat No. 7; 15-ton furnace, without stirrer.

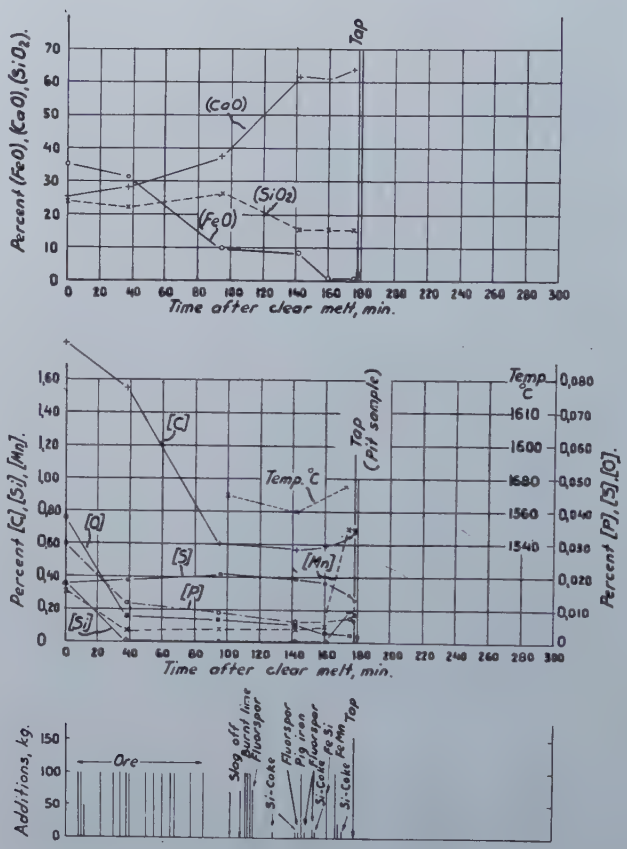

Fig 11—(Above) Heat No. 8; 15-ton furnace, with stirrer.

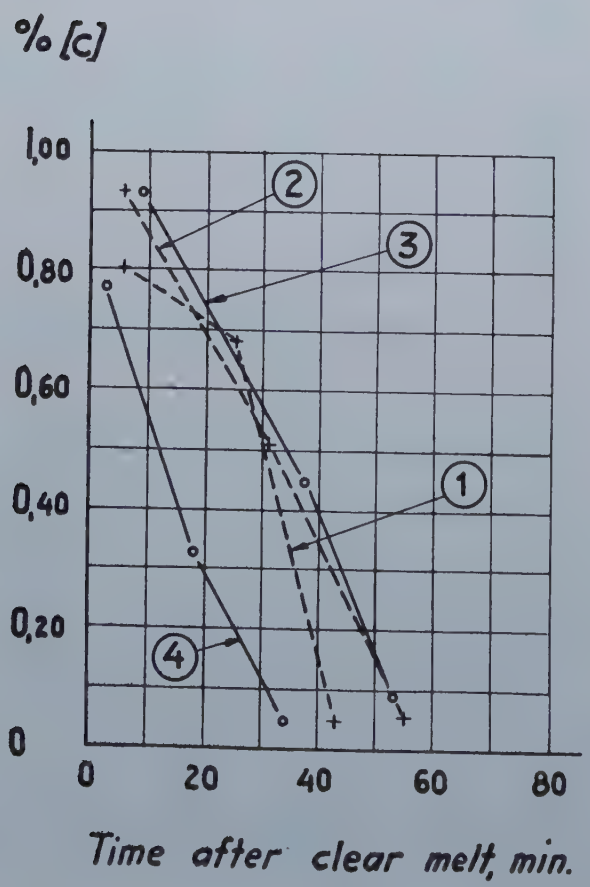

Fig 12—(Left) Decarburization curves, heats Nos. 1 to 4.

ductive stirring. The diagram shows that a high rate of carbon drop can be attained in the arc furnace.

The same conclusion was drawn at Uddeholm, where the following experiment was made, see fig 13. In heat No. 10 the stirrer was switched on only during the last part of the oxidizing period and in heat No. 12 only during its first part. In both heats the power input was the same (2200 kw) and the ore additions were equal (70 kg every 5 min). The curves of decarburization are similar.

In fig 14 the oxygen content of the steel bath during the oxidizing period is plotted against the carbon content. The points refer to all experimental heats made with or without use of inductive stirring. The diagram also shows the area of scatter for the oxygen content of the steel bath during carbon refining in the basic openhearth furnace according to results obtained in an investigation carried out by the Jernkontorets Forskningsverksamhet[6].

The oxygen contents of the steel in the arc furnace are seen to be slightly lower than in the openhearth. The rates of carbon drop in the arc furnace are, at least as far as the Surahammar heats are concerned, two or three times as high as in the openhearth furnace. Thus, the diagram illustrates the fact that the oxygen content of the steel bath is lower, when the rate of carbon drop is high. The diagram gives no indication that the stirring affects the oxygen content of the steel during carbon refining, at least not so far as higher or medium carbon contents are concerned. Nor is there any reason to expect such an effect: the carbon boil is itself a stirring movement which is so strong that the inductive stirring cannot assert itself at the same time.

However, at lower carbon contents when the carbon boil has slackened, the inductive stirring seems to exert an influence on the carbon reaction. In table IV some data have been put together giving an idea of the conditions prevailing at the end of carbon refining in the manufacture of steel with low carbon content. The data are averages from several heats and should therefore give a reliable picture of the state of things. The figures indicate that with the aid of inductive stirring it is possible to obtain a low carbon and low oxygen content simultaneously, or at least, that it is possible to approach this condition much more closely than was the case previously without stirring. At low carbon contents, the consequence of inductive stirring is that the over-saturation of oxygen in the steel is lower than normal, and therefore the carbon reaction comes closer to the equilibrium value. In commercial operation—when experimental heats are not involved—the result would be that a steel made with the induction stirrer would be lower in carbon than a steel made in the conventional way. This is also found to be the case: at Surahammar the pit carbon content of a certain grade of steel decreased from an average of 0.045 to an average of 0.037 since it was made in the new furnace with inductive stirring.

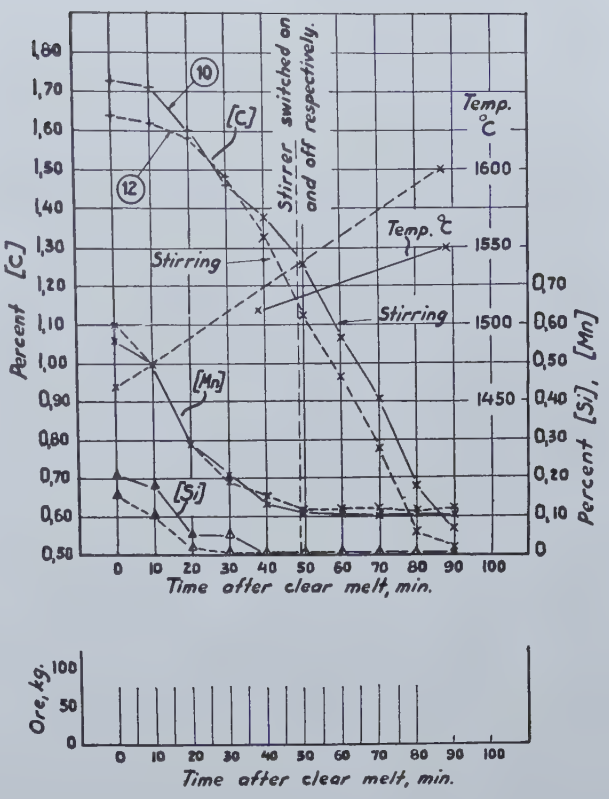

Fig 13—Decarburization curves, heats No. 10 and 12.

TABLE IV

Data From End of Carbon Refining. Low-Carbon Steels

Kind of Stirring	Number of Heats	Pct [C]	Pct [O]	[C] x [O]	(FeO)	[O] (FeO)
None	6	0.029	0.094	0.0028	46.2	0.0020
Inductive	5	0.031	0.071	0.0022	36.2	0.0020

[1] *L. Dreyfus: "Induktiv omröring i ljusbågsugnar. Elektrotekniska synpunkter". (Inductive Stirring in Arc Furnaces. Electrotechnical Aspects). Jernkontorets Annaler 133, 1949, pp. 371/383.*

[2] *F. Nilsson: "Induktiv omröring i ljusbagsugnar. Metallurgiska synpunkter". (Inductive Stirring in Arc Furnaces. Metallurgical Aspects). Jernkontorets Annaler 133, 1949, pp. 385/453.*

[3] *S. Fornander: Discussion on Inductive Stirring in Arc Furnaces, Jernkontorets Annaler 133, 1949, pp. 453/463.*

[4] *S. Fornander: Discussion on Determination of Reactive Oxygen, Journ. Iron Steel Inst. 156, 1947, pp. 526/528.*

[5] *S. Fornander: "Temperaturmätning i stålbad" (Temperature Measurements in Steel Baths), Jernkontorets Annaler 131, 1947, pp. 225/242. "Temperature Measurements on Liquid Steel", Trans. Instruments and Measurements Conference, Stockholm 1947, pp. 233/237.*

[6] *S. Fornander: "The Behaviour of Oxygen in Liquid Steel During the Refining Period in the Basic Open Hearth Furnace", Discussions of the Faraday Soc. 4, 1948, pp. 296/307.*

From table IV it is seen also, that the FeO content of the slag is lower when stirring is employed. The difference in the FeO content is considerable, 10 pct, which means that the ingot yield will be somewhat higher when the induction stirrer is used.

(3) The slag removal: It has been pointed out already that the stirrer considerably facilitates the slagging off operation, and the reason for this has been explained. Efficient removal of the oxidizing slag is of great importance in the production of large tonnage steels from impure raw materials as well as in the manufacture of quality steels.

Tests which were carried out at the Uddeholm furnace have shown that the time required for the slagging off operation is about the same whether or not the stirrer is used. The main reasons why the stirrer is advantageous are, that the deslagging will be carried out effectively, and that the work of the furnace crew will be facilitated. The larger the furnace, the more important are these considerations.

When phosphorus removal is aimed at, good deslagging is important. At Surahammar a heat was made recently with use of the stirrer. The raw material, which was uniform, contained 0.35 pct P. The phosphorus content of the finished steel was 0.020 pct. The steel was killed and it is true that it had a low carbon content. However, it is worthy of note that it was made under a white slag.

In the production of one specific grade of steel, where it is desirable to get rid of impurities as completely as possible, the following experience was gained. The steel quality in question was formerly made in an arc furnace of conventional type, the charge containing 50 pct commercial scrap. Three slagging-off operations had to be made in order to remove the oxidizable impurities effectively. The same steel quality is now made in the new furnace using the electric stirrer. The charge consists of 100 pct commercial scrap, and only one slagging-off operation is carried out. In spite of this, the oxidizable impurities are as low as or lower than previously.

Another observation, which seems to be connected with the effectiveness of slag removal, concerns the slag composition during the reducing period. At the Uddeholm furnace it was found that the CaO/SiO_2-ratio had an average value of 3.25 in the heats made with inductive stirring and an average of 2.75 in the heats made without stirring. The additions of lime and fluorspar were the same in both cases.

At Surahammar similar observations were made, see table V. For the six heats made in an older furnace without stirring coil, the average CaO/SiO_2 ratio of the reducing slag was 2.2. For the five heats made in the new furnace with stirring coil the average basicity value was 3.O. The additions of burnt lime and fluorspar were the same in both cases. The improved basicity value of the reducing slag for the latter group of heats can probably be attributed to the more effective slag removal.

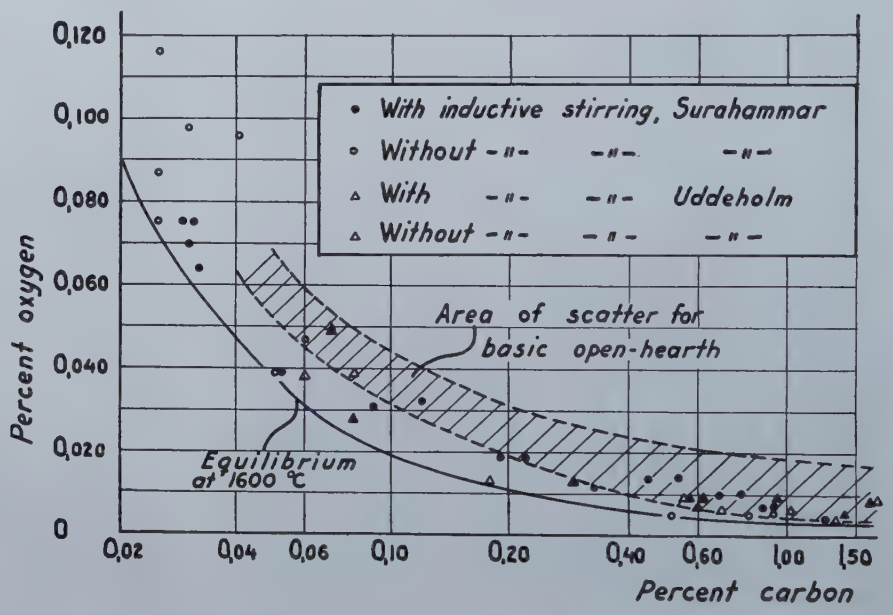

Fig 14 — Oxygen content during the oxidizing period.

TABLE V
Slag Composition During Reducing Period

Kind of Stirring at Slag-Off	Number of Heats	(CaO)	(MgO)	(FeO)	(SiO_2)	$\frac{(CaO)}{(SiO_2)}$
None	6	55.9	10.5	1.3	26.2	2.16
Inductive	5	62.3	6.0	1.1	20.7	3.03

Next month the authors will conclude this article with a description of the reducing period, effect on furnace linings and economical aspects of the inductive stirring equipment.

Effect of

Melting Practice On Hydrogen

by Sam F. Carter

In this first part of a two-part article, the author presents a number of quantitative hydrogen analyses of some electric arc-furnace steels with varied melting practices. First there is a review of the many research contributions on the causes and effects of hydrogen in steel; next a description of the procedures used in this most recent investigation and then a discussion of results for carbon steels.

Among the quality problems that have faced steelmakers through the years, some of the most mysterious and evasive have been caused by hydrogen in very small concentrations. Two thousand research contributions over the years have developed a reasonable qualitative understanding of the causes and effects of hydrogen in steel. Because of analytical and sampling problems the determination of actual hydrogen contents and the study of effects of melting practice have been made possible only in the last few years. It is the purpose of this investigation to contribute some quantitative hydrogen analyses of some electric arc-furnace steels with varied melting practices.

Sam F. Carter, Junior Member AIME, is Assistant Melding Superintendent of American Cast Iron Pipe Co., Birmingham.

This paper was presented before the Seventh Annual Electric Furnace Conference, Iron and Steel Div., AIME, Pittsburgh, Dec. 8-10.

The most obvious defect caused by hydrogen is gas porosity, recognized in the wrought industry as "bleeding ingots" and in the casting industry as "blow holes".[1, 2, 3] Some metal compositions containing considerable contents of such deoxidizing elements as Si, Cr, etc. have proven especially prone toward this hydrogen type of porosity. The more subtle effect of hydrogen is embrittlement. This mysterious loss of ductility has been experienced on certain heats over the years in such forms as: the premature failure of railroad rails,[4] "shatter cracks" and brittleness in forgings,[5] low ductility in the center of large castings,[6, 23] embrittlement of wire and sheet after pickling,[7] and low ductility welds.[8, 9, 10] Certain fracture patterns that accompany hydrogen embrittlement have been recognized and given the familiar names of "flakes", "shatter cracks", "fish eyes", etc.

A considerable volume of experimentation has finally established hydrogen as a potential cause of one type of porosity and one type of embrittlement. Both effects have been artificially reproduced by hydrogen additions. Many solubility and equilibrium relationships have been obtained on laboratory melts,[11, 12, 13] and a theory explaining the embrittlement mechanism has been fundamentally agreed upon.[6, 14, 15] Decreased solubility and the attempted escape of hydrogen from metal solution seems to cause the trouble in both cases. Escape of hydrogen out of solution during solidification produces gas holes. Precipitation later from the solid metal builds up the considerable pressures that resist deformation and cause embrittlement.

Mill operators discovered a number of years ago that this type of embrittlement could be relieved by special heat treatment. Subsequent research has verified the outward diffusion of hydrogen which takes place slowly at room temperature and at an accelerated rate at higher temperatures. Optimum treatments for hydrogen elimination have been determined as well as actual diffusion rates and the effect of composition and structural condition. The reason for more hydrogen in the center of large sections has been made apparent and a distinction made between the temporary or abnormal loss of ductility from hydrogen and the more permanent effects of

nitrogen, oxygen, inclusions, etc. The cure for hydrogen embrittlement has been developed more completely than its prevention.

The melting operation is only one of several possible sources of hydrogen but the most difficult one to study. The hydrogen content as melted may be decreased by pouring and subsequent treatment or it may be increased by further absorption from heat treating atmospheres, pickling and electrolytic baths, welding, etc. Moisture has been proven the most

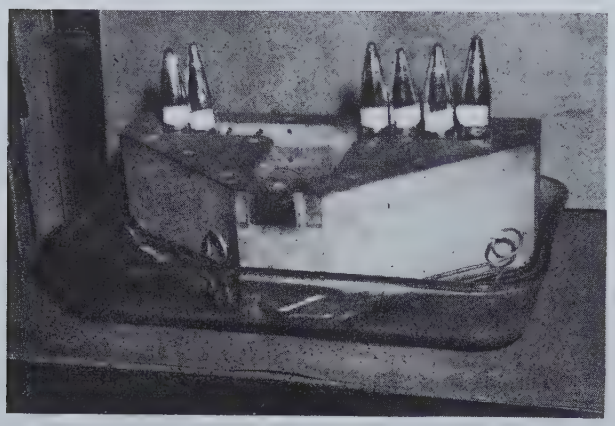

FIG 1—Wooden trough containing mercury and inverted centrifuge tubes.

potent source of hydrogen in the furnace because of its decomposition to hydrogen in the presence of molten iron.

Development of analytical methods for hydrogen and several methods of sampling molten metal have made possible several recent investigations of actual hydrogen contents of molten metal in the furnace. Although the reliability of some of the earlier analytical methods have been questioned they make a valuable contribution to quantitative knowledge even after liberal allowance for error.

In 1937 Hare and Soler reported some vacuum-fusion hydrogen analyses incidental to an oxide study of some high-carbon and Ni-Mo bearing steels.[16] Three basic openhearth heats finished with hydrogen contents of 0.52, 0.79 and 0.79 Relative Volumes* (0.00068, 0.00090 and 0.00090 pct by weight). Four basic-electric heats showed considerable hydrogen increases from "slag off" to tap under the reducing

*** All hydrogen contents reported as weight percent or cc per 100 gm converted to Relative Volumes for convenience of discussion and comparison.**

second slag, finishing with concentrations at tap ranging from 0.61 to 1.45 Relative Volumes. In the winter months of lowest humidity 24 heats averaged 0.57 R.V., whereas during the summer months with highest humidity 31 heats averaged 0.81 R.V. On two heats finished with a leak in an overhead water cooler, hydrogen concentrations were reported equivalent to 5.10 and 6.70 Relative Volumes.

In 1938 Chuiko[17] reported vacuum-fusion analyses on some Russian electric-arc steels which melted as high in hydrogen as 0.90 to 1.80 R.V. but were lowered by violent boils to 0.45 to 0.70 R.V. Highest concentrations were reported on two heats that were not boiled and one on which wet lime was used.

In the same year Kobayasi[18] reported on some Japanese steels that ran 0.35 to 0.65 R.V. at tap. A hydrogen decrease was experienced during the oxidation period on acid-openhearth heats but not on basic-openhearth or basic-electric heats. Hydrogen was found prone to increase after "killing" and after tap. An attempt was made to correlate hydrogen content with the FeO content of the steel.

In the U.S. in 1939 Schwartz[19] reported on some white cast irons melted in three types of furnaces with hydrogen contents ranging from 0.09 to 1.20 Relative Volumes. These were determined by a combustion method on drilled samples.

In 1944 Hurst[1] in England reported hydrogen results on high silicon iron from 0.11 to 0.78 R.V. Porosity was generally experienced when concentrations ran higher than 0.40 R.V.

In 1947 Wells and Barraclouch[20] made a comparative study of five methods of sampling molten metal and showed the rate of hydrogen escape at room

FIG 2 — External clamping frame used to seal glass tubes.

temperature, the increased rate of 100°C, and the retarded rate at dry-ice temperatures.

In the same year Sykes, Burton, and Gegg[2] reported some British openhearth and arc-steels to average near 0.30 R.V. on carbon steels and from 0.37 to 0.62 R.V. on low-alloy steels. On several "wild" heats hydrogen concentrations as high as 0.70 to 1.30 R.V. were determined. Poor correlation was found between hydrogen elimination and the length of the boil.

Contemporary with the British work, hydrogen studies were made at Battelle by Sims, Moore, and Williams for the Steel Founders' Society of America.[21] Their large volume of quantitative data of considerable practical value was reported at the 1947 Electric Furnace Conference.[22] This work developed a sampling method that was simple enough for plant use. A method of extraction at 1925°F was used that seemed to show improved accuracy and consistency.[24] A rather complete quantitative relationship was developed for the first time between hydrogen content and temporary loss of ductility as well as the rate of hydrogen removal and ductility restoration by various heat treatments.[23]

Hydrogen determinations also were made on seventeen commerical heats of casting steel made in four types of furnaces. Samples were taken at various stages of the melting operation. Furnace practice was recorded in very complete detail for the first time. Principal purpose was to find the average hydrogen contents of casting steel as currently produced by American Steel Foundries. Final hydrogen contents in the ladle ranged from 0.12 to 0.42 R.V. Variations in furnace practice were hardly great enough to definitely establish the effects of more than a few of the many variables involved. One definite conclusion was the appreciable hydrogen increase from newly lined or wet ladles as generally used. In spite of a few exceptions, their data seemed to indicate generally a hydrogen decrease during oxidation, a tendency to increase after deoxidation, and a general inclination to follow atmospheric moisture. Violence of the boil seemed to prove a better criterion for the effectiveness of the elimination process. A ladle hydrogen as low as 0.12 R.V. was produced by a special practice consisting of a violent and prolonged boil, short deoxidation time, thoroughly dried materials, and a used ladle. The acid-arc furnace was considered most amenable to low hydrogen and the basic openhearth most difficult to control.

Last December Speight and Cook[25] reported some hydrogen determinations on more British commercial steels. A sealed mold was used and vacuum extraction at 1380°F was claimed to be indicative after 1 hr and complete after 2½ hrs. Fourteen basic-openhearth heats of carbon and low-alloy steels melted with hydrogen contents that ranged from 0.33 to 0.79 R.V. for an average of 0.54 R.V. The same heats at tap time ranged from 0.47 to 0.93 R.V., averaging 0.63 R.V. Seven basic-electric heats averaged 0.41 R.V. 10 min after the "white slag" and 0.48 R.V. at tap. Since principal emphasis was on analytical details and no description of melting practice was given, the only conclusions possible are the increase during the heat and the high level of hydrogen content in these steels.

Wentrup, Fucke, and Rief[26] have very recently reported the averages of some German heats of carbon and low-alloy steels. Ten acid-openhearth heats averaged 0.47 R.V. at tap and 0.56 R.V. in a molten sample removed from the ingot mold. Nineteen basic-openhearth heats averaged 0.74 R.V. at tap and 0.65 R.V. from the mold. Eight basic-arc heats averaged 0.71 R.V. at tap and 0.89 R.V. in the mold. Considerable quantities of hydrogen were found in the furnace slags both as H_2 and as H_2O. The total ranged from 30 to 100 cc H_2 per 100 gm on acid slags and from 40 to 205 cc per 100 gm on basic slags. Some effect of aluminum was suggested but not very well supported.

The lack of description of melting practice and charge composition in most of these reports prevents much evaluation of furnace practice. The average steelmaker is aware of the unavoidable sources of moisture in the air and openhearth fuel and seeks to avoid the obvious additional sources of moisture such as rust and water on scrap, damp alloys and slag materials, leaking overhead coolers, and improperly dried spouts, runners, and ladles. However, laboratory care is hardly possible in the plant and certain of these moisture sources are unavoidably encountered at times. What the practical man is ultimately most interested in is not so much the one way that steel might be made lowest in hydrogen, but in how many ways steel may be produced with hydrogen low enough for acceptable quality. Certain ideal practices from the hydrogen standpoint might have disadvantages from the standpoint of chemical control, availability of materials, economics, and production schedules, in which case the steelmaker

FIG 3—External view of special shipping box.

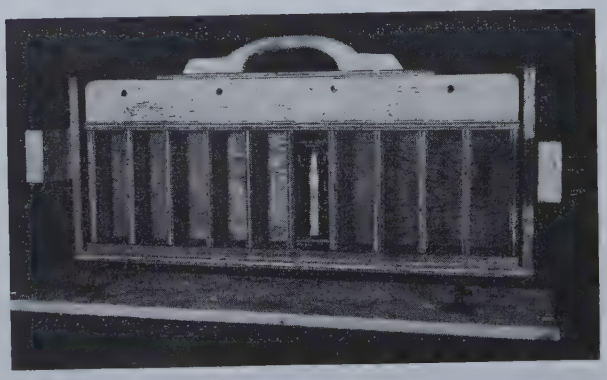

FIG 4—Inside view of shipping box.

[1] *Hurst J. E.: Address to Staffordshire Iron & Steel Institute, 1944.*

[2] *Sykes C., H. H. Burton, and C. C. Gegg: "Hydrogen in Steel Manufacture", Jrl. of Iron & Steel Inst., 156 (June 1947).*

[3] *Zapffe C. A. and C. E. Sims: "Hydrogen and Nitrogen as Causes of Gassiness in Ferrous Castings", Trans. Amer. Foundrymen's Society, 51, (1944).*

[4] *Cramer R. E. and Bast E. C.: "The Production of Flakes by Treating Molten Steel with Hydrogen and the Time of Cooling Necessary to Prevent Their Formation", Trans. Amer. Soc. Metals, 27, (1939).*

[5] *Foley F. B.: "Flakes and Cooling Cracks in Forgings", Metals and Alloys, 12 (1940).*

[6] *Zapffe C. A. and C. E. Sims: "Hydrogen Embrittlement, Internal Stress, and Defects in Steel", Trans. A.I.M.E. 145 (1941).*

[7] *Noble, N. J.: "Hydrogen Embrittlement", Iron Age, 148 (1941).*

[8] *Zapffe, C. A.: "Fish Eyes in Steel Welds Caused by Hydrogen", Metal Progress, 42 (1942).*

[9] *Reeve L.: "The Relation Between the Hydrogen Content of Weld Metal and Its Oxygen Content", Jrl. Amer. Welding Soc., 24, 194, p. 6185.*

[10] *Lefevre, M.: "Flakes in Welds", Jrl. Amer. Welding Soc., 26, (Jan. 1947).*

would like to know how far he might deviate from the best practice before experiencing trouble.

The final hydrogen of a heat is the net effect of a sequence of operations which may individually contribute or eliminate hydrogen. For simplicity these elements of furnace practice are considered (1) charge, (2) melt conditions, (3) active oxidation period, (4) deoxidation period and (5) tapping into ladle.

[11] *Sieverts, A.: "The Absorption of Gases by Metals", Z. Metallkunde, 21, (1929).*

[12] *Fontanna M. G., and J. Chipman: "Equilibrium in Reaction of Hydrogen with FeO in Liquid Iron at 1600°C", Trans. Amer. Soc. Met., 24, (1936).*

[13] *Chipman, J. and A. M. Samarin: "Effect of Temperature Upon Interaction of Gases with Liquid Steel", Trans. A.I.M.E., 125, (1937).*

[14] *Houdremont, E. and H. Shrader: "Combined Action of Hydrogen and Stresses in the Formation of Flakes", Stahl & Eisen, 61, (1941).*

[15] *Poole, S. W.: "Flaking in Alloy Steels", Iron Age, 160 No. 1, (July 17, 1947).*

[16] *Hare, W. A. and G. Soler: "Study of Iron Oxide and Gas Content of Molten Alloy Steel", Trans. Amer. Soc. Met., 25, 1937.*

[17] *Chuiko, W.: "Theory of Hydrogen Elimination During Electric Steel Making", Teoriga i Prokt, Met. (1938); Metals and Alloys (1939).*

[18] *Kobayasi, W.: "Tetsu to Hagane", Vols. 23, 24, and 25 (1937 to 1939).*

Consideration of the first of these, the furnace charge seems to have been neglected in most of the previous work. The original charge for steelmaking may vary from all molten pig iron to all cold steel scrap. A steel scrap charge could conceivably consist of all foundry returns, characterized by large sections, clean surface possibly protected with sand, and a composition highly deoxidized with Si and aluminum. On the other hand the charge might be made up entirely of low carbon plate of rimmed steel composition, containing essentially no deoxidizers, thin in sections and very rusty. On alloy heats the presence of Cr, Ni, Mo, etc. is a possibility with their effects on hydrogen absorption and elimination. In an acid-arc furnace with the charges identical, one heat might melt in such a gradual manner that the slag remains oxidizing and considerable amounts of Si, Mn, and carbon are oxidized as melting proceeds. On the other hand, the same charge might bridge in such a manner that a viscous low FeO slag, and relatively reducing condition are maintained until the addition of the oxidizing agent. Such variations could conceivably have considerable effect on hydrogen content as melted.

The oxidation period or boil has now been accepted as necessary for consistent production of quality steel. But the means of measuring the oxidation process are highly controversial. At one time or another such factors as lowest carbon after the boil, lowest Si and Mn residual, carbon drop, etc. have been proposed as the one principal criterion for an adequate boil. More recently attempts have been made by separate investigators to correlate hydrogen content with FeO of metal and slag, length of boil, and violence of boil. Because of the number of concurrent conditions that accompany the boil it has been hard to determine how much of the effect is chemical and how much mechanical. With the use of oxygen it becomes easier to produce the gas flush of the boil without the degree of oxidation ordinarily inclined to precede it. The relative effects of both should be properly recognized.

It is generally agreed that steel is more likely to absorb hydrogen after deoxidation. However, deoxidation is a relative term which requires further quantitative definition.

In order to check on hydrogen contents obtained and possibly contribute some data toward the solution of various questions on furnace practice, hydrogen determinations were made on samples from some electric-arc steels made at the American Cast Iron Pipe Co. These included nineteen carbon steels (sixteen acid and three basic) and ten high alloy Cr-Ni steels (four acid and six basic). Extreme variations in melting practice were sought and certain elements

[19] *Schwartz and Guiler: "Hydrogen in White Iron", Trans. A.F.A., 47, (1939).*

[20] *Wells, J. E. and K. C. Barraclough: "Determination of Hydrogen in Liquid Steel", Jrl. Iron and Steel Inst., 155, (Jan. 1947).*

[21] *Sims, C. E., G. A. Moore, and D. W. Williams: "Effect of Hydrogen and Nitrogen on the Ductility and Porosity of Cast Steels". S.F.S.A. Research Report No. 14, 1947.*

[22] *Sims, C. E., G. A. Moore, and D. W. Williams: "A Quantitative Experimental Investigation of Hydrogen and Nitrogen Contents of Steel During Commercial Melting", Proc. Elect. Fur. Conference of A.I.M.E. 1947.*

[23] *Sims, C. E., G. A. Moore, and D. W. Williams: "The Effect of Hydrogen on the Ductility of Cast Steels", Trans. A.I.M.E. Oct. 1948.*

[24] *Sims, C. E. and G. A. Moore: "Apparatus for the Hot-Extraction Analysis for Hydrogen in Steel", Trans. A.I.M.E. June 1948.*

[25] *Speight, G. E., and R. M. Cook: "The Determination of Hydrogen in Liquid Steel", Jrl. Iron & Steel Inst. Dec. 1948.*

[26] *Wentrup H., H. Fucke, and O. Rief: "Hydrogen Contents of Liquid Steel Melted by Different Processes", Stahl und Eisen, Feb. 17, 1949.*

[27] *Carter, S. F.: "Effect of Some Melting Variables on the Tensile Properties of Acid Electric Steel", Proc. Electric Fur. Conf. of A.I.M.E. 1947.*

[28] *Hulme P. M.: "Removing Dissolved Gases from Molten Metals", Steel, 119 No. 2, Oct. 14, 1946.*

of furnace practice were deliberately exaggerated. In several cases the charge was soaked with water and water was sprayed into the furnace throughout the heat. This was intended to eliminate any doubt about moisture availability, and make the hydrogen absorption directly indicative of the susceptibility of the steel under the chemical condition prevailing.

Indications were obtained toward a solution of only a few of these questions. The volume of data was scant and not adequately confirmed in every case. But it is hoped the experience in sampling and in the manipulation of variables of the furnace practice will help and encourage further research along these lines. Much research will be required to confirm apparent conclusions of this paper, investigate other variables of furnace practice, and study other steel composition types.

Some incidental nitgrogen analyses were determined but no attempt was made to correlate the results.

Experimental Method

The sampling system used was that developed and used by Sims and associates.[21] The analytical work was done by Battelle by the method which

has been reported in detail by them.[24] The only contribution of the author was a shop method of sealing and transporting the samples several hundred miles by commercial express. Since the method proved simple enough for plant use, it will be described again for the benefit of any group that might consider similar work.

A cylindrical $\frac{5}{8}$ x $1\frac{1}{4}$ in. sample was chill-cast in a split copper mold. Because of its thermal conductivity, density, and volumetric heat capacity pure copper produces the most drastic chill of any practical mold material. A refractory "neck down core" separated the sample from the pouring basin and facilitated the rapid sawing or breaking of the sample from the basin. This core made of silica flour and clay was baked at 2400°F and stored in a dessicator. With the mold set up by the furnace, metal was dipped from the furnace with a well slagged spoon, killed with aluminum wire, and poured into the mold. The sample was stripped, the basin removed, a weight check made for soundness, and the sample inserted into a mercury filled glass tube within 3 min. after casting. The "T" shaped wooden trough used for filling the tubes with mercury and keeping the open ends sealed under a mercury bath was made by the pattern shop.

The glass tubes used first were calibrated centrifuge tubes 5 in. long and tapered to a tip at the closed end. Rough volumetric measurements of the gas were made as it evolved from the specimen at room temperature and collected in the tip of the tube over a period of days. The volumes were only relative and not under standard conditions because of the reduced pressure of a 4 to 5-in. column of mercury. Because of considerable breakage of these tubes, it was found best to transfer the gas by inverted pouring to stronger heavy wall test tubes for shipment. No breakage was experienced on the heavier tubes used on the last 30 samples.

The principal problem was sealing the glass tubes containing mercury, metal sample, and gas to permit transporting to the laboratory without breaking the glass or permitting the escape of any gas. Some tubes were stoppered with fair success with expansion type rubber stoppers used in thermos bottles. A central shaft shortened by an external cam spreads the rubber stopper. The principal disadvantage was the air unavoidably squeezed from the stopper during its compression. Although dilution of the gas with air need not impair the accuracy of the hydrogen determination it was considered undesirable. Better success was experienced with an external clamping frame shown in fig. 2. A rubber-lined wooden pad on the open end and a concave wooden pad on the closed end were drawn together by four long bolts. Tubes were clamped in this frame before removing the open end from the mercury bath. Low permeability inner tube rubber was used. However, there remained the possibility that some hydrogen might escape through the rubber if the tubes should remain in an upside down position for several days and if pressure should be increased considerably by a temperature increase. To prevent any such possibility and to keep the gas in the closed end of the glass tube, a special shipping crate was designed. A false exterior shown in fig. 3 consisted of a rounded top, a flat bottom, sides with a calculated slope, and a low center of gravity. This made it practically impossible for the box to remain in a position that would permit the gas to contact the rubber pad. The inside consisted of ten compartments in which the tubes in the frames were packed with sponge rubber, fig. 4.

Upon arrival at Battelle the free gas that had already been evolved was collected and analyzed. The metal specimens were cleaned and weighed and placed in the vacuum-extraction equipment for the high-temperature treatment. The high-temperature fraction was also analyzed. Based on the fact that at 1925°F hydrogen evolution proceeds in the manner of a first order reaction, a correction for the residual hydrogen left in the specimen was determined and added. The total volume of hydrogen was calculated to both the weight per cent and the relative volume of the metal sample. Because of a more convenient magnitude Relative Volumes will be used throughout this discussion.

Mention might be made of some precautions found by experience to improve the accuracy of the work. Samples adequately killed with aluminum evolved hydrogen less readily at room temperature, which is in favor of better retention in the sample and generally improved accuracy. On samples with gas porosity much hydrogen would escape upon solidification with the CO evolved. Some samples whose weights indicated internal unsoundness were rejected and not sent off for analysis.

Dirty mercury was found another source of trouble. If enough film of dust and oxide is trapped inside a glass tube, air can be pulled into the tube through capillary channels in the mercury at a rate that will be mistaken for hydrogen evolution. However, this air will be indicated in the analyses. To prevent this it was found advisable to skim the mercury trough frequently, filter the mercury at occasional intervals, and fill the tubes from below the surface.

When the volume of gas in a tube was too large, the metal specimen was found to have enough freedom to bounce around and break the glass tube in shipment. It proved advisable to transfer the larger proportion of the gas to a supplementary tube for shipment.

Discussion of Results

Carbon Steels: Table I presents the essential melting data and hydrogen analyses for sixteen acid and three basic heats of carbon steel for foundry castings. None of the heats were intended to represent preferred practice or a best attempt to obtain a low hydrogen. Each one is characterized by some deviation that might be suspected of increasing hydrogen content to a critical amount. The first four are more nearly representative of normal practice which was described in detail at the 1947 Conference.[27] Briefly, this consists of a rusty charge of foundry returns, killed steel, and rimmed steel averaging a theoretical composition of 0.35 to 0.45 pct C and 0.10 to 0.30 pct Si. Following a meltdown that is at least slightly oxidizing and a 2 to 4 pct ore addition when nearly melted, a violent boil is produced that eliminates 0.08 to 0.15 pct C in 5 min and another 0.10 to 0.15 pct over a period of 10 to 20 min while the carbon is being adjusted. Left open and boiling as long as possible the heat is deoxidized with simultaneous additions of ferromanganese and ferrosilicon. Where physical quality is the primary concern, all Mn and Si is added 3 min before tap. Where chemical control is more important a mild block of 0.40 pct Mn and 0.20 pct Si is added 5 to 10 min before tap on a slightly oxidizing slag. All carbon heats in this report were deoxidized in the ladle with an

aluminum addition chosen to give a residual of 0.03 to 0.08 pct Al.

Unfortunately, on many of the earlier samples the glass tubes were cracked in shipment and a complete study of some of these heats is not possible. However, in every case either the tap or the ladle analysis is available from which the overall melting practice can be evaluated. On many of the samples on which the room temperature fraction was lost, reasonable estimates could be made on the basis of the volume of gas before shipment, the usual range of concentration of the evolved gas, the usual range of proportionate evolution at room temperature, etc. This estimated fraction plus the retained fraction that was analyzed permitted an estimation within sufficient limits for some conclusions. Such estimates are indicated by two limiting numbers in parenthesis.

Heat No. C-1 is characterized by a later boil than usual because of a "reducing" melt down. A 0.25 pct C steel was made in an acid-lined, electric-arc furnace on a fairly low-humidity day (52 grains of moisture per pound of air). The charge consisted of 70 pct killed steel (scrap shells) and 30 pct rimmed steel (plate) averaging a theoretical composition of 0.35 C and 0.15 Si. During the meltdown the charge bridged temporarily, producing a more "reduced" melt characterized by higher Si in the metal and a large volume of high SiO_2, low FeO slag. Consequently, the 2 pct ore addition was sufficient to little more than oxidize some excess Si and produce a mildly oxidizing slag. The short carbon boil obtained was later and at a higher temperature than normally encountered. Carbon was lowered only to 0.30 pct. Another 1 pct ore was added and a violent boil was obtained immediately that carried the composition to 0.18 C, 0.06 Si and 0.15 Mn. The heat was considered normal from this point on. Seven minutes before tap a block of 0.40 Mn and 0.20 Si was added on a slag that measured 4 in. in a Herty-type viscosimeter with a ¼-in. channel. The balance of the Mn and Si were added 2 min. before tap on a 3 in. slag and the heat tapped at an optical temperature of 3200°F. The tapping ladle had been used several times before. The second boil eliminated 0.12 C over a period of 9 min. for a maximum violence rate of 0.80 C per hr. The time from the first ore addition to the first deoxidizer was 35 min. and the time from block to tap was 7 min.

The only satisfactory determination on this heat was the tap sample which contained 0.13 R.V. of hydrogen. On both the boil and the ladle samples the room temperature fractions were lost from accidents in shipment. However, it seems safe to estimate the boil samples between (0.11-0.22) R.V. and the ladle sample (0.13 to 0.20) R.V. These results seem sufficient to conclude that hydrogen content of this heat was reasonably low and not seriously handicapped by this characteristic late boil.

Heat No. C-2 was a test of a wet charge and high atmospheric humidity. A charge of similar composition, but wet from rain was melted on a rainy day of high humidity. The melt down was the other extreme, very oxidizing. During melting solid scrap continued to fall into the pool keeping the temperature low and the slag oxidizing.

The 2½ pct ore addition to a bath already low in Si and Mn and high in FeO boiled the heat to an unusually oxidized level of 0.10 C, 0.03 Si and 0.10 Mn with an 8 in. slag. The electrodes were dipped to raise the carbon and clean up the slag. After that the heat was normal and was blocked with Mn and Si 6 min. before tap. The boil sample contained an estimated (0.10-0.20) R.V., the tap sample 0.21 R.V. and the ladle sample 0.15 R.V. The tap sample seems out of line with the other two. It may be debated whether the hydrogen increased from boil to tap, then decreased from tap to ladle, or whether the tap sample from a still bath might not have been as representative as samples following the mixing action of the boil or tapping.

On C-3 the melt procedure is probably most nearly average practice except for an intentionally wet charge and water sprayed into the furnace throughout the heat. A special spray cap with eight $\frac{1}{16}$ in. holes was placed on the end of a ¾ in. pipe and inserted into the furnace through a hole just below the roof ring. Water was sprayed into the center of the furnace at the rate of approximately ½ gal. per min. A rusty charge of foundry returns and killed wrought steel was melted in a moderately oxidizing manner. A 3 pct ore addition produced a boil of normal violence and average residuals. The heat was left open until all the Mn and Si was added 3 min. before tapping into a used ladle. In spite of the extreme exposure to moisture, hydrogen content of the final ladle sample was only 0.18 R.V. No pin holes were found in the castings or in a special wedge shaped specimen cast in green sand as a porosity test.

Heat No. C-4 was intended to test a short boil to a high ore-down carbon in the definite presence of moisture from the water spray. In making 0.40 pct C steel a similar wet charge was melted on a day of high humidity with water sprayed into the furnace throughout the heat. Only 1½ pct ore was added. A short, relatively mild boil produced a high ore down carbon of 0.28 pct and relatively high residuals of 0.06 Si and 0.19 Mn. Several additions of recarburizing pig iron were made producing further mild boiling. The heat was finished with no preliminary block and tapped at 3200° into a used ladle. Hydrogen content at melt was 0.19 R.V., after the boil 0.29 R.V., before the Mn and Si an estimated (0.16-0.27) R.V., and from the ladle 0.18 R.V. Among these results the melt and boil samples were hardest to reconcile. If both are representative samples then hydrogen seemed to be increased by the boil. Such an increase could conceivably have been experienced because of the mildness of the boil and the high potential hydrogen in the atmosphere. At any rate, no pin holes were encountered, and it seems safe to conclude that the overall melting procedure of this heat was sufficiently resistant to the excess moisture in the furnace atmosphere to produce a steel of average commercial quality.

All four of these heats finished with hydrogen contents between 0.15 and 0.20 R.V. From these it can be concluded that in making this type of steel from this type of charge with a vigorous boil and very short deoxidizing periods, reasonably low hydrogen contents are likely to be obtained under any deviations of furnace practice and any exposure to furnace moisture likely to be encountered in our plant.

The next four heats were produced with essentially no boil. The oxidized condition was obtained but the charged carbon was too low to generate the violent evolution of CO gas generally considered necessary for low hydrogen. Most effective phosphorus removal in the basic electric furnace requires such a gradual oxidation during melting that insufficient carbon is left for a violent boil. Because

TABLE I
CARBON STEELS

	Heat No. Lining Steel	Moisture Atmosphere	Extra Sources	Charge Composition	Melt Condition	Finish Practice	Min Resid.	Violence Boil-Max Rate C Elim.	Ratio Time Ox/Deox	Slag Cond.	No.	Sample Time	Temp.	Nitrogen, Pct	Hydrogen Rel. Vol.
C-1	37071 Acid S 1025	52 grains per lb	Dry chg.	K&R 0.35 C 0.15 Si	Bridge Clean melt.	2 pct & 1 pct Ore. Late boil Mn-Si blk.	0.18 C 0.06 Si 0.15 Mn	0.12 pct C / 9 min / 0.80 pct C / Hr	35′ / 7′	5″ / 3″	(66) (67) (68)	Boil Tap Lad U†	3100° 3200°		(0.11-0.22)* 0.13 (0.13-0.20)
C-2	37084 Acid S 1025	95 (Rain)	Damp chg.	R&K 0.30 C 0.10 Si	Oxidizing melt.	2½ pct Ore Boil to low C. Dip electrodes. Mn-Si blk.	0.10 C 0.03 Si 0.10 Mn	0.15 pct C / 10 min / 0.90 pct C / Hr	30′ / 6′	8″ / 3″	(70) (71) (72)	Boil Tap Lad U	3000° 3250°		(0.10-0.20) 0.21 0.15
C-3	36928 Acid S 1025	130	Wet chg., Spray	F&K 0.40 C 0.30 Si	Mod. oxidizing.	3 pct Ore Normal boil No block	0.15 C 0.04 Si 0.11 Mn	0.20 pct C / 12 min / 1.00 pct C / Hr	42′ / 3′	(2)**	Other samples broken (15)	Lad U		0.0054	0.18
C-4	56752 Acid S 1040	118	Wet chg., Spray	F&K 0.40 C 0.30 Si	Bridge Clean melt.	1½ pct Ore Short boil Ni C No block	0.28 C 0.06 Si 0.19 Mn	0.09 pct C / 10 min / 0.54 pct C / Hr	35′ / 3′	3 / 2½ / 1½	(21) (22) (23) (24)	Melt Boil Mn&Si Lad U	2950° 3020° 3200°	0.0028 0.0039 0.0034 0.0044	0.19 0.29 (0.16-0.27) 0.18
C-5	36889 Acid S 1025	60	Dry chg.	Rimmed 0.15 C 0.02 Si	Rusty Very oxid.	No boil No. blk. Very ox.	0.08 C 0.02 Si 0.09 Mn	0.04 pct C / 15 min / 0.16 pct C / Hr	42′ / 3′	10″ / 5″	(1) (2) (3)	Melt Tap Lad U	2950° 3200°	0.0044	0.21 (0.09-0.11) 0.12
C-6	36894 Acid S 1025	100	Wet chg. H_2O Spray	Rimmed 0.15 C 0.02 Si	Rusty Very oxid.	No boil No. blk. Very ox.	0.09 C 0.02 Si 0.09 Mn	0.04 pct C / 15 min / 0.16 pct C / Hr	50′ / 3′	6″	(4) (5)	Tap Lad U	3250°	0.0048	0.15 0.17
C-7	37027 Acid S 1025	80 (Rain)	Wet chg., Spray Green pole New Ladle I	Rimmed 0.15 C 0.02 Si	Bridge slightly oxid.	No boil No. blk. Fairly oxid.	0.12 C 0.04 Si 0.16 Mn	0.02 pct C / 20 min / 0.06 pct C / Hr	48′ / 3′	6″ / 3″	(40) (42) (43)	Melt Tap New Lad I.	2950° 3250°		0.19 0.25 0.32
C-8	56805 Basic S 1025	110	Fur. full water. Leak throughout	R+Pig 0.35 C 0.05 Si	Rusty Very ox.	Mild boils No block Very ox.	0.12 C 0.02 Si 0.16 Mn	0.08 pct C / 12 min / 0.40 pct C / Hr	50′ / 3′	Very ox. / (Oxid)	(35) (36)	Boil Ladle	3000° (3220)**		(0.19-0.37) 0.27
C-9	56832 Basic S Cast Iron	45	Dry chg.	R Steel + graphite 0.05 Si	Rusty	Dead melt Add Si 10 B.T.		0			(44) (45)	Tap Lad U	2900°		0.12 0.13
C-10	36957 Acid S Cast Iron	105	Dry chg.	R Steel + graphite 0.05-0.15 Si	Rusty	Dead melt Add Si 10 B.T.		0		(1½″)	(38)	Lad U	2900°		0.19
C-11	56873 Acid S Cast Iron	72	Dry chg.	K Steel + graphite 0.15-0.50 Si		Dead melt Add Si 10 B.T.		0		(½″)	(95)	Tap	3000°		0.21

C-12	56887 Acid S 4140	33	Leak 10 min before tap	F&R 0.35 C 0.20 Si	Mod. oxid.	3½ pct Ore. Normal boil. Recarb. Block Mn-Si.	0.15 C	0.18 pct C 10 min 0.78 pct C Hr	40′ 10′	2½″	(100)	Tap	(3200°)		0.25
C-13	56807 Basic D 1025	88	Dry chg. Dry materials	K-R + Ore 0.30 C 0.10 Si	Very oxid.	Double slag. Early blk. Red. Slag.	0.07 C 0.02 Si 0.12 Mn	0.05 pct C 15 min 0.20 pct C Hr	15′ 35′	Red.	(37)	Lad.	(3300°)		0.21
C-14	36944 Acid S 1025	120	Wet chg. Spray throughout	R&K 0.25 C 0.10 Si		2 pct Ore. Boil, very low & ox. Early Si blk. Very ox. slag.	0.06 C 0.02 Si 0.08 Mn	0.12 pct C 7 min 1.02 pct C Hr	20′ 30′	8″ 10″ 7″ 3″	(16) (17) (18) (19) (20)	Melt Boil 15′ Blk 27′ Blk Lad U	2900° 3000° 3150° 3220°	 0.0047	0.20 (0.10-0.20) 0.29 0.16 (0.19-0.30)
C-15	56788 Acid D 1025	125	Wet chg. Spray till 5 min 2nd slg.	Killed 0.45 C 0.20 Si	Clean melt.	5 pct Ore Violent boil Red 2nd slg. Reduce all 0.49 Si.	0.17 C 0.07 Si 0.14 Mn	0.23 pct C 8 min 1.72 pct C Hr	14′ 31′	2″ 1″ (½″)	(31) (33) (34)	Boil 15′ BT Lad U	3100° 3150° 3230°	0.0033 0.0037 0.0028	0.09 0.11 (0.25-0.45)
C-16	37038 Acid D 1025	60	Damp chg. Spray till 5 min 2nd slg.	K&R 0.35 C 0.10 Si	Clean melt.	1½ pct Ore Mild boil Hi C. Red 2nd slg. Reduce all 0.56 Si.	0.21 C 0.07 Si 0.18 Mn	0.10 pct C 10 min 0.60 pct C Hr	17′ 33′	2½″ ½″	(53) (55) (56)	Boil Mn Lad U	3050° 3250°	0.0036 0.0028 0.0030	0.22 0.18 0.28
C-17	56979 Acid S 1025	80	Dry. New ladle II	Killed 0.45 C 0.20 Si	Bridge Red. melt.	5 pct Ore Mild boil to hi. C. Blk Mn & Si.	0.27 C 0.07 Si 0.17 Mn	0.13 pct C 10 min 0.78 pct C Hr	16′ 10′	3″	(115) (116)	Tap Ladle N II	3300°	0.0078 0.0077	0.19 0.15
C-18	37354 Acid S 1025	88	Dry. New ladle III	Killed 0.45 C 0.20 Si	Mod. oxidizing	5 pct Ore Normal boil Av. C Blk Mn & Si.	0.15 C 0.04 Si 0.13 Mn	0.25 pct C 8 min 1.90 pct C Hr	25′ 8′	4½″	(117) (118)	Tap Ladle N III		 0.0096	0.09 0.11
C-19	56957 Acid S 1025	58 (Rain)	New fur. hearth	K&F&R 0.40 C 0.10 Si	Oxidizing melt.	2 pct Ore Normal boil low C. Blk Mn & Si.	0.10 C 0.03 Si 0.10 Mn	0.20 pct C 10 min 1.90 pct C Hr	30′ 5′	4″	(111) (113) (114)	Melt Tap Lad U		0.0069 0.0091 0.0195	0.14 0.17 0.13

Atmospheric moisture expressed as grains of moisture per lb of air.

Charge composition is theoretical composition, R = rimmed steel, K = killed steel, F = foundry returns.

Minimum residuals represented lowest C, Si, and Mn at the depth of the oxidation period.

Boil rate is rate of carbon elimination per time unit for the period of maximum violence.

Ratio of oxidizing time to deoxidizing time is time from ore to block over time from block to tap.

Slag condition is (on acid heats) fluidity measured in Herty viscosimeter with ¼-in. channel. Indicative of FeO.

Temperature determined by optical reading in spoon or tap stream with 0.4 E correction.

**Temperatures and fluidities in parenthesis on ladle samples indicate condition before tap.

*Hydrogen results in parenthesis indicate an accident to room temperature fraction. Two figures in parenthesis are limits within which result may be estimated on basis of extrapolation of graphs, limits of other samples, etc.

†"U" after ladle indicates one *used* several times previously. "N" indicates a *new* lining.

of occasional raw material situations it has been advantageous to melt charges made up almost entirely of low-carbon plate scrap. Without some carburizing addition, such charges melt too low in carbon to generate a vigorous boil. In order to evaluate such a practice from the standpoint of hydrogen, four heats of this type were studied, one dry, one with an accidental leak, and two intentionally sprayed with water.

On C-5 a dry charge of rimmed steel was melted on a day of relatively low atmospheric moisture and with no known additional source of hydrogen but possibly the rust on the scrap. With no ore added and essentially no boil an 0.08 pct carbon resulted along with very low residuals, and a very oxidizing slag. The heat remained in this extremely oxidized condition until 3 min. before tap when all the Si, Mn, and recarburizing pig was added on a slag that measured 6 in. and analyzed 29.6 pct FeO. Hydrogen content at melt was 0.21 R.V., at tap (0.09-0.11)* R.V., and from the ladle 0.12 R.V. This is one of the lowest contents reported in the literature.

** The room temperature fraction of 0.45 ml was lost after having been measured at Battelle. Had the evolved gas been 100 pct hydrogen the sample could not have exceeded 0.12 R.V. Gases evolved from a number of ladle samples ranged from 70 to 95 pct hydrogen. If within this range hydrogen concentration of the sample would be 0.09 to 0.11 R.V.*

Heat No. C-6 was intended to check such a practice against the definite presence of moisture. A wet charge was melted on a humid day with water sprayed into the furnace throughout the heat. Melting practice was identical with the previous heat, with similar low residuals and a very oxidizing slag. This heat was in a molten oxidizing condition 50 min. and in the furnace after deoxidizers only 3 min. Final slag before the Mn and Si measured 6 in. and analyzed 34.4 pct FeO. Hydrogen content at tap was 0.15 R.V. and from the ladle 0.17 R.V. No pin holes were encountered. With the exception of the difficulty of skimming the thin slag, casting quality was not adversely affected. Although 0.05 R.V. higher than the dry heat, final hydrogen was surprisingly low in view of the absence of a vigorous boil and the approximately 40 gal. of water sprayed into the furnace during the heat. For all practical purposes absorption of hydrogen from a high moisture atmosphere was prevented by some chemical condition which obviously could only be an extreme state of oxidation. This seems to be a practical application of some equilibrium studies indicating decreased hydrogen solubility with increased FeO.[12, 13] However, this oxidized condition included several things that might affect hydrogen. The high FeO and low Si and Mn residual in the metal would be expected to decrease hydrogen solubility in the metal itself. The high FeO in the slag might offer more protection from the moisture saturated atmosphere above. On the other hand, the more oxidizing atmosphere would conceivably decrease the decomposition of water to hydrogen

$$2\,H_2O \leftrightarrows 2\,H_2 + O_2$$

by increasing the concentration of one of the products and shifting the equilibrium toward the left. However, this experience might apply only when the potential source of hydrogen is in the atmosphere above the slag. Further research will be necessary to determine the effect of moisture added directly to the slag or directly to the bath beneath the slag.

On C-7 similar practice was intended on the same type charge, wet and sprayed throughout. In addition, green wooden poles were plunged into the bath at four intervals for periods of 30 sec. each to determine the effect of moisture sources exposed directly to the bath. In addition this heat was tapped into a newly lined ladle whose preheating had been followed with a pyrometer. This heat was given every exposure to moisture conceivable and every rule broken except one, the maintenance of an oxidized condition. Unfortunately, this heat was not as oxidized as planned and another variable was included. Because of a bridge in melting, the slag was lower in FeO and higher in SiO_2, and metal residuals were not as low as the two previous heats. By tap time slag fluidity was 3 in. and no more oxidizing than normal. Hydrogen content as melted was 0.19 R.V. Forty minutes later with continuous water spraying and after exposure to the green poles, hydrogen had increased to 0.25 R.V. at tap. This is a 0.06 R.V. increase over the melt and 0.10 R.V. higher than the previous heat at tap. No doubt the source of moisture under the slag supplied by the poles could have been a more readily absorbed source of hydrogen. However, a possible effect of the less oxidizing condition must be recognized. Further research will be necessary to separate these possibilities. The ladle used was lined with a rammed mixture of one-third clay and two-thirds ganister. After air drying several days, the ladle was placed on a vertical heating wall, heated slowly for 18 hr up to a temperature of 1600°F, and then increased in four more hours to a maximum temperature of 2380°F. In spite of such preheating, hydrogen was increased from 0.25 R.V. to 0.32 R.V. from the ladle. Since the lining was certainly physically dry this 0.07 R.V. increase can only be accounted for by the combined water of the clay that was not completely removed by this heating cycle.

Heat No. C-8 was a basic single slag heat run on a furnace bottom that had been filled with water over the weekend by an overhead leak. The furnace was drained, surface dried for one hour, and charged. Very early another leak developed which dripped water into the bath throughout the heat. An extremely oxidized practice similar to the three previous heats was chosen. Several mild boils occurred and more carbon was lost in melting and recarburizing, but no vigorous boil was obtained. The bath was carried to a low carbon, low residuals, and a very oxidizing slag which was maintained until the Si and Mn addition 3 min. before tap. Hydrogen content between mild boils was an estimated (0.19-0.37) R.V. and final hydrogen in the ladle was 0.27 R.V.

From these four heats some evidence seems present that the chemistry of an extremely oxidized metal-slag-atmosphere system either limits or retards hydrogen absorption. This suggests another approach to a low hydrogen with the emphasis on prevention of absorption rather than improved elimination. This method however, would require the assurance of melting low in hydrogen which has only been accomplished with a rimmed steel charge. Further research will be necessary to determine if a low enough hydrogen melt is possible with large proportions of foundry returns and more deoxidized scrap. Furthermore, this practice in all but a few cases would be less practical than the normal boil and from the limited evidence it is less effective

against high moisture atmospheres. Of the three extremely oxidized heats sprayed with water one was equal but two were higher than the two boiled heats that were sprayed.

The next three heats (C-9 to C-12) are cast irons made synthetically in the electric furnace from steel scrap. A steel charge was melted on an excess of fine graphite, a carbon content of about 3.50 pct was absorbed, and 2 pct silicon was added a few minutes before tap. This method produced a very low-phosphorus iron at a time when pig iron was scarce. On all three heats the charge and all additions were perfectly dry and the only sources of hydrogen recognized were the hydrogen of the charged steel and moisture in the air.

Heat C-9 was made in a basic lined furnace on a day of low humidity. Hydrogen content before tap was 0.12 R.V. and from the ladle 0.13 R.V. The heat was neither oxidized nor boiled. Excess carbon was present but residual silicon was very low until the addition just before tap. Since no part of the heat could be expected to eliminate hydrogen, it was presumed that the rimmed steel charge melted very low in hydrogen and little more was absorbed because of the relatively low humidity and the absence of additional sources of moisture.

For cast iron heat C-10, the same charge was melted but in an acid furnace. The principal difference was the tendency to reduce a few points of silicon toward the end of the heat. Moisture in the atmosphere was over twice as high as the previous basic heat. The ladle hydrogen of this heat was 0.19 R.V. This is considerably higher than the 0.13 R.V. of the basic heat but the higher humidity seems adequate cause.

Cast iron heat C-11 was also melted in an acid furnace. However, a charge of 0.20 pct Si killed steel was melted instead of the 0.02 Si rimmed steel of the other two heats. This charge retained a higher residual silicon throughout and reduction of more Si started earlier and proceeded further than on the previous heat. Atmospheric humidity was midway between the other two heats which would suggest a hydrogen of about 0.16 R.V. purely on the basis of the atmospheric difference. However, actual hydrogen content at tap was 0.21 R.V. This highest hydrogen of the three might be attributed to a higher content in the killed steel charge, or it could be caused by more favorable conditions for absorption due to lower FeO and higher Si throughout the heat.

The next five heats (C-12 to C-16) were directed toward a study of hydrogen pickup after deoxidation. A statistical study has indicated that on acid heats of this type of steel better ductility is obtained if the heats are not deoxidized too early or if the slag does not become too low in FeO.[27] However, in some basic processes and on some alloy types of steel certain compensating advantages can be realized from an earlier deoxidizer addition or a reducing slag. The quantitative effect of various states of deoxidation on hydrogen absorption should be better understood. Previous research has indicated that, in general, steel has more affinity for hydrogen after deoxidation and especially during the reducing period of the basic double slag heat. This completely deoxidized state includes a number of conditions that might contribute toward greater hydrogen absorption: a mechanically quiet bath, the presence of deoxidizing elements in the metal, a very low FeO in the metal, virtual absence of FeO in the slag, a reducing atmosphere above the slag, etc. However, this represents the ultimate state of deoxidation and not all these conditions are met in every steel bath that is considered deoxidized. An acid slag might be reducing to silica and yet contain over 10 pct FeO. Furthermore, small additions of deoxidizers may be added to an oxidized bath and slag, deoxidizing the bath several minutes before equilibrium forces can bring the slag to an equivalent state of deoxidation. On the other hand the slag might be made "reducing" without any deoxidizer addition to the bath. In the first case the metal bath is made to lead the slag and in the last case the slag leads the metal in the deoxidation process. The question arises, which is most conducive to hydrogen pick up, a deoxidized slag or a deoxidized bath?

C-12 is an acid heat of SAE 4140 steel (Cr and Mo) on which an overhead leak dripped water into the furnace for 10 min. after a prelimnary deoxidizer addition. The charge consisted of half foundry returns and half rimmed scrap with molybdenum added. The heat was given a vigorous boil to a normal level, recarburized with pig iron and blocked 10 min. before tap with an addition of 0.40 pct Mn and 0.20 Si to a 4-in. slag. Chromium was added 4 min. before tap and the balance of the manganese and silicon 2 min. before tap. The leak was discovered 10 min. before tap. Hydrogen content of this steel at tap time was 0.25 R.V. Heats with similar practice and no additional moisture ran 0.11 to 0.15 R.V. Heats left oxidizing and sprayed with water ran 0.17 to 0.18 R.V. indicating a 0.05 R.V. increase from the extra water on an oxidizing bath. The 0.25 R.V. of this heat with a leak on a deoxidized bath suggests a hydrogen content 0.12 R.V. higher than if no leak had developed and probably 0.07 R.V. higher than if the heat had not been blocked during the time of the leak. This theorizing ignores the possibility of some increased affinity for hydrogen produced by the alloys present.

However, no pin holes were encountered and this hydrogen content was not higher than the apparent average of openhearth steels. For acid practice this is typical of a so-called deoxidized bath, a minimum deoxidizer addition to a bath under a slightly oxidizing slag of 15 to 25 pct FeO content. More hydrogen might have been absorbed under more highly deoxidized conditions.

Heat No. C-13 is typical of a basic double slag practice with a reducing second slag. Ore and rust in the charge made this charge melt very oxidizing and low in C, Mn, and Si with no more than several mild boils. Slag was drained to remove phosphorus. A reducing slag mixture of dry lime, spar, graphite, and fine calcium-silicon was added, followed by recarburizing pig iron and a block of 0.40 pct Mn and 0.20 pct Si. The bath remained quiet and deoxidized for a total of 35 min. the last 10 min. of which the slag was definitely reducing as indicated by a carbidic slag. All additions were dry and the ladle and spout had been used several times. Only the ladle

sample was analyzed. Hydrogen content was 0.21 R.V. This is apparently equal or lower than the average for basic heats of this type. However, in view of the care exercised in keeping materials dry and the average humidity, this is rather high in comparison with the more oxidized acid heats.

C-14 is an attempt to investigate the hydrogen absorption tendencies of a supposedly deoxidized bath under an oxidizing slag. A charge of rimmed and killed wrought scrap was soaked, and melted with water sprayed throughout the heat. As intended, a 2 pct ore addition produced a boil of normal violence but ending with unusually low residuals of 0.06 C, 0.02 Si and 0.08 Mn and a very high FeO slag. A deoxidizing addition of 0.40 pct Si was made to this highly oxidized bath. Gradual oxidation of Si required replacement with several other Si additions. A total silicon addition of 0.90 pct was added to obtain the final of 0.42 pct. This condition was maintained for 30 min. with the water being sprayed. Manganese was added 3 min. before tap. Hydrogen at melt was 0.20 R.V.; after the boil an estimated (0.10-0.20) R.V., 15 min. after the block 0.29 R.V., 3 min. before tap 0.16 R.V., and from the ladle an estimated (0.19-0.30) R.V. According to these samples hydrogen jumped up and down several times during the heat. This could justify suspicion of certain samples but no basis was found for suspecting one more than others. On the other hand, some occurrences between samples might be theorized as the basis for the hydrogen change. At the time the 15 min. block sample was caught, a slight bubbling activity was observed on the bath, hardly vigorous enough to be called a boil and producing no significant carbon drop. More silicon was added to restore that lost, and the activity subsided. This very nearly happened again about 8 min. later before the next Si addition.

It seems very likely that the 0.20 R.V. melt was decreased to about 0.15 R.V. by the boil and then increased after the block to the 0.29 R.V. Then as the Si was depleted by oxidation from the metal and the FeO of the bath increased, some hydrogen could have been rejected because of decreased solubility, accounting for the drop to 0.16 R.V. If this did occur, the activity observed might have been principally a hydrogen boil rather than a carbon boil. Of course, one erroneous sample would destroy the basis of this explanation and make other theories just as likely. No conclusions should be drawn from any one heat and especially this one that was so hard to keep up with. The author would like to see this occurrence repeated with closer observation of bath activity and more samples. Also, another heat might be run in a similar way but keeping the silicon level higher and maintaining the oxidizing slag by several FeO additions.

The next two heats, C-15 and C-16, were intended to investigate the other extreme, a reducing-acid slag with no deoxidizer added to the bath. Of course, such a slag ultimately deoxidizes the metal bath and the reduction reaction supplies a Si content to the steel. It was intended to spray these heats throughout. However, an arc could not be maintained on the viscous low FeO slags, and the spray had to be removed. As a result these heats were exposed only to atmospheric moisture during the reducing period under investigation.

On C-15 a charge of killed steel was melted under a continuous water spray. Humidity was high. A 5 pct ore addition produced one of the most violent boils reaching a maximum carbon elimination rate of 1.72 pct per hr. By driving the furnace hard the carbon was carried to 0.17 C with 0.07 Si and 0.14 Mn. The slag was drained and a second reducing slag added, consisting of a mixture of sand, lime, graphite, fine ferrosilicon, and manganese oxide. A recarburizing addition of 0.08 pct C was made. Within a few minutes the slag began reducing Si with all the "puffing and blowing" associated with the process. The water spray had to be removed. The steel remained under this slag for 31 min. Manganese was added 2 min. before tap. No silicon was added; the final of 0.49 pct Si was all obtained by reduction. Hydrogen content after the boil was 0.09 R.V., midway of the second slag 0.11 R.V., and from the ladle an estimated (0.25 to 0.45) R.V. and more probably (0.30 to 0.40) R.V. In all probability this was the highest content in the carbon steels investigated.

One significant observation from this heat was the very low hydrogen obtained after the boil in spite of the water spray. This can be most readily attributed to the extreme violence of the boil. Neither the length of the boil nor the lowest carbon were excessive. A second conclusion is the obvious increase in hydrogen under the reducing slag even with liberal allowance for experimental error.

Heat No. C-16 was finished with a similar long period under a reducing acid slag. Again the water spray had to be removed before real reducing conditions had been developed. Atmospheric moisture content was less than half that of the previous heat. The principal difference in working the heat was the relatively mild boil with a maximum elimination rate of 0.60 pct C per hour. The same second slag was added and all 0.56 pct Si obtained by reduction. Hydrogen content after the boil was 0.22 R.V., 3 min. before tap 0.18 R.V., and from a used ladle 0.28 R.V.* Although the 0.28 R.V. final hydrogen was high compared to more oxidized heats, the major portion was not absorbed under the reducing slag, but retained after the boil.

** The lower middle sample is hard to explain. From a sampling standpoint this sample from a quiet bath would be more readily questioned than the boil and ladle samples that followed considerable mixing of the bath.*

This seems further confirmation that a steel bath seeks an equilibrium between its capacity for hydrogen and the external source of hydrogen. When hydrogen content is low and below this equilibrium the tendency to increase is much greater than when already high and approaching or above this equilibrium level.

The author will conclude this article next month with further data and discussion of results, as well as an analytical study of evolved gas.

The System Chromium-Carbon

The chromium-carbon system up to 20 pct carbon was reinvestigated using metallographic, X ray, and thermal analyses. The transformation temperatures pertinent to the three known carbides were examined, resulting in higher temperatures than heretofore given for some of these transformations. Many attempts were made, all unsuccessful, to form a carbide "CrC".

by David S. Bloom and N. J. Grant

THE development of high temperature, high stress alloys had proceeded with such rapidity during the war, and for a short time afterward, that our knowledge of the constitution of the alloys had become seriously inadequate. To interpret correctly alloy behavior it is not only necessary to recognize the phases present, but also to know the properties of the phases under all varieties of conditions and treatments.

Chromium in these high temperature alloys holds the unique distinction of being the only one element which must be present when an oxidizing or generally corrosive atmosphere is present and when a long life is desired in service. Carbon and nitrogen must also be considered where chromium is present. Carbon is always present, either as an impurity in the raw alloying elements, or as a deliberate addition agent to increase the strength. Nitrogen is generally picked up from the atmosphere during melting or may be added as an alloying element. The effect of nitrogen additions is not too dissimilar to that of carbon additions.

As such, chromium carbides and nitrides become of great interest since they are present in a very large number of alloys, including alloy steels, stainless steels, super alloys, and the like.

In the chromium-carbon system there are three accepted carbides: Cr_4C, Cr_7C_3, and Cr_3C_2. The existence of one more carbide, a still higher carbon form CrC, has been advanced[1]. The phase diagrams of chromium and carbon as published by Friemann and Sauerwald[2] and by Tofaute, Kuttner and Buttinghaus[3] do not extend beyond the carbide Cr_3C_2, which contains 13.3 pct carbon; but Hatsuta[1] has extended the diagram up to 20 pct carbon, and in doing so hypothesized, with the use of some questionable experimental results, the compound CrC. This carbide would contain 18.75 pct carbon, 81.25 pct chromium, by weight.

It is further known that as the chromium carbides increase in carbon the acid resistance increases but the oxidation resistance decreases[4,5]. This is of great importance in high temperature alloys where time-temperature stability, as well as oxidation resistance, is of prime importance. The possible existence of a carbide of the formula CrC thus becomes of prime importance and it was considered important to recheck the chromium-carbon binary constitutional diagram for such a compound.

In view of the wide spread of values listed for the melting point of chromium (1500° to 1850°C)[1] and 1930°C[6], it was considered that the liquidus temperatures might well be redetermined more ac-

DAVID S. BLOOM is Research Assistant, and N. J. GRANT, Junior Member AIME, is Associate Professor of Metallurgy, Mass. Inst. of Technology.

New York Meeting, Feb. 1950.

TP 2722 E. Discussion (2 copies) may be sent to Transactions *AIME before Apr. 1, 1950, and is tentatively scheduled for publication Nov. 1950.*

Manuscript received June 17, 1949; revision received Oct. 17, 1949.

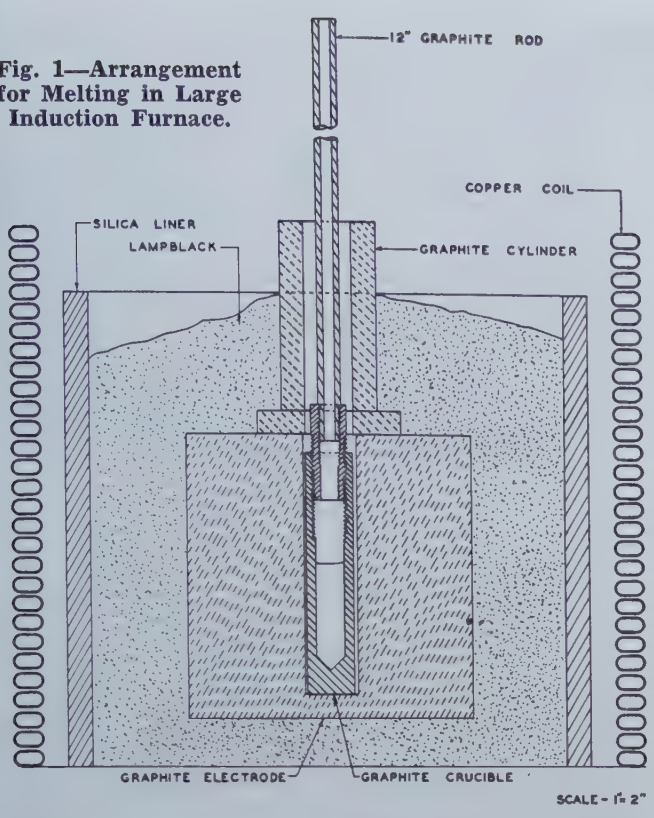

Fig. 1—Arrangement for Melting in Large Induction Furnace.

curately by working with high purity materials free of nitrogen—the most logical element to cause the low melting point in previously determined constitutional diagram. Oxygen is known to lower the melting point also, but not nearly as severely as carbon or nitrogen.

The first portion of the problem was to endeavor to produce the carbide CrC by any of the tools available to the metallurgists.

Vacuum Melting: The first method tried involved the use of vacuum of better than 10^{-5}mm of mercury pressure.

Electrolytic chromium (used throughout the experimental work) was placed in a graphite crucible and heated, the graphite crucible acting as a heating element and also supplying carbon to the melt, as well as a deoxidizing action. When melting occurred, much gas was liberated from the metal, the liberation sometimes becoming quite violent and necessitating a slow heating rate up to the melting point of Cr_4C (1518°C). The maximum temperature achieved by this method was 2250°C as determined by an optical pyrometer. The pressure in the system after melting as determined by a MacLeod gauge was about 10^{-3}mm of mercury. Considerable chromium metal was found deposited on the cooler furnace surfaces above the melt after cooling. Inasmuch as the boiling point of pure chromium is about 2480°C[6], it may be considered that there was an appreciable amount of chromium vapor above the melt; therefore, the actual temperature of the body of the melt was probably higher than 2250°C. No temperature correction was made for this chromium vapor during optical readings.

Examination of the ingot by X-ray diffraction in a Phragmen camera, and by comparing the diffraction pattern with that of known chromium carbides and carbon, showed that the resultant metal was Cr_3C_2 plus excess carbon. The total carbon content as determined by oxidation of the carbon and collection of the oxide was 16.50 pct.

The maximum temperature attained was considerably above that of the estimated melting point of CrC, as given by Hatsuta[1]; however, the resulting products did not include CrC. It was possible that CrC could exist as a high temperature phase and break down to Cr_3C_2 and carbon upon cooling; but since an examination at the elevated temperatures was not possible, the next best thing was to suppress by a very rapid cooling any transformations which might occur on slow cooling.

Melting Under a Protective Atmosphere: Therefore, the subsequent series of experiments consisted of melting the chromium in a graphite crucible which had a hole in the bottom plugged with a graphite stopper rod. After reaching the desired temperature, the chromium carbide could be poured, by pulling the graphite stopper, into a copper mold for quick cooling. The whole assembly operated in an argon atmosphere. However, the maximum temperature reached was only between 1700°-1800°C, as determined by the optical pyrometer, and this was not satisfactory.

Arc Furnace: Another attempt to achieve a high temperature followed by a rapid quench required the use of the tip of a graphite electrode in an electric arc furnace as the heating element. The chromium was inserted in a hole drilled and tapped in the tip of the electrode; the hole was then sealed with a threaded graphite plug. After heating by drawing an arc, the electrode was removed and quenched in cold water. It was found that a maxi-

Table I. Pertinent Data for Illustrations

Fig.	Heat No.	Phases Present	Analysis—by Weight				Remarks
			Carbon		Chromium	Others	
			Combined Pct	Free Pct			
2	23	$Cr_3C_2 + C$	11.3	12.6	bal.		X ray diffraction pattern
3	23	$Cr_3C_2 + C +$ $Cr_3C_2 - Cr_7C_3$ peritectic	11.3		bal.		Water quenched from 2300°C
4	28	$Cr_2A1C + C$	7.75	4.4	67.5	18.8A1	X ray diffraction pattern
5	28	$Cr_2A1C + C$ + Aluminum Carbide	2.88		bal.		Aluminum menstruum melt
7	31	$Cr_4C + \alpha$ Cr + C					As cast sample
8	31	$Cr_4C + \alpha$ Cr + C					As cast sample
9	31	$Cr_4C + \alpha$ Cr + C					Annealed 16 hr at 1350°C in vacuum
10	40	$Cr_7C_3 + Cr_4C + C$	5.50		bal.		As cast
11	40	$Cr_7C_3 + Cr_4C + C$	11.10		bal.		Annealed 16 hr at 1350°C in vacuum
12	39	$Cr_7C_3 + Cr_3C_2 + C$					Annealed 16 hr at 1350°C in vacuum
13	39	$Cr_7C_3 + Cr_3C_2 + C$					
14	41	$Cr_3C_2 + Cr_7C_3 + C$	12.78		bal.		As cast

Fig. 2—Heat 23. Total Carbon 23.9 pct.

Diffraction pattern of Cr_3C_2+ C. Phragmen camera (50.2 mm radius) with angular coverage of 28° to 57°. Chromium target.

mum temperature of about 2200°C (as measured by the optical pyrometer with the electric arc shut off) was reached. The resulting product was again Cr_3C_2 plus carbon.

64KW Motor-generator Induction Furnace: The next method tried involved the use of a much larger furnace and power supply (see fig. 1). The induction furnace coil of 28 turns of copper tubing was 12 in. in diam. Inside of the coil was placed a graphite electrode 6 in. in diam and 6 in. high containing a hole in its center. In this cavity the 1 in. diam crucible containing the chromium carbide charge was placed. With an applied power of 49 kw at 67 amp, a temperature of 2300°C was attained by the melt. The temperature was determined by

Fig. 3—Heat 23. Combined Carbon 11.3 pct.

Quenched from 2300°C. Cr_3C_2 with small amounts of Cr_7C_3-Cr_3C_2 peritectic and free graphite. Electrolytic NaOH etch. 500X. Slightly reduced in reproduction.

an optical pyrometer, and inasmuch as a greenish vapor was visible above the melt it is considered that the temperature of the melt was higher than that of the pyrometer reading. The crucible was then quickly removed and quenched in water. The result was Cr_3C_2 and carbon again, the total carbon being 23.9 pct by weight (see fig. 2 and 3). Table I lists the data for all illustrations.

Menstruum Melting: One of the methods used to make refractory carbides[7] was also used to try to produce CrC. Aluminum, iron, and other metals may be used as menstrua. Accordingly, in an effort to make CrC, an aluminum menstruum melt was made in the vacuum fusion apparatus. A tank of argon was connected to the system, so that after melting in vacuum, argon could be bled into the system and the remainder of the run made under approximately atmospheric pressure to prevent excessive loss of chromium or menstruum metal.

After the graphite crucible containing the chromium and aluminum had been at 2000°C for 20 min. and then cooled, the ingot was placed in a 1:1 HCl acid solution for two days. The residue was a dark grey, flaky substance. X ray analysis revealed that the substance was none of the chromium carbides previously encountered. However, chemical and spectroscopic analysis showed that the compound was actually Cr_2AlC (see fig. 4 and 5).

The next menstruum metal tried was nickel. The molten metal was held at 2000°C or higher for about 30 min., after which it was removed and placed in a 1:1 HCl solution for four days. An X ray diffraction pattern of the residue identified it as being Cr_3C_2.

Copper was also tried as a menstruum metal. The melt was held at 1800°C for approximately 30 min. The ingot, upon solidification, was found to consist of two layers; the lower being coppery in color and was completely dissolved in nitric acid, the upper section was metallic grey in color and suffered practically no alteration in nitric acid. X ray diffraction showed that it was Cr_3C_2.

Diffusion: Finally an attempt was made to make CrC by diffusion at high temperatures in the solid state. Cr_3C_2 with enough additional carbon to bring the carbon content up to 26 pct was ground and compressed into the form of pellets, one being pressed at 61 tons per sq in., the other at 102 tons per sq in. These two pellets were then placed in a graphite crucible, surrounded by powder of the same composition as the pellets, and held at 1800°C for 6 hr in a vacuum. Examination of the pellets showed that some chromium had diffused out of the pellets, but by X ray diffraction it was determined that only Cr_3C_2 and carbon were present.

No other means of preparing CrC presented themselves, unless the possibility of melting chromium and carbon under high pressures and temperatures could be investigated; however, it seemed conclusive that the carbide CrC did not exist in normal melting.

Phase Diagrams: Using an apparatus whereby chromium and carbon could be melted in a high purity argon atmosphere, with temperatures determined by a tungsten-molybdenum thermocouple[10], the chromium-carbon phase diagram was reinvestigated. The apparatus used is illustrated in fig. 6. The tungsten-molybdenum thermocouples (0.020 in. diam) were encased in alumina tubes cemented to beryllia protection tips which projected well into the molten carbide. The emf of the thermocouples

Fig. 4—Heat 28. Diffraction Pattern of Cr_2AlC.

Same camera as fig. 2.

Fig. 5—(left) Heat 28. Cr_2AlC Crystals in Aluminum Carbide Matrix (with Graphite).
Unetched. 100X. Slightly reduced in reproduction.

Fig. 6—(below) Apparatus for Fusion in Argon Atmosphere.

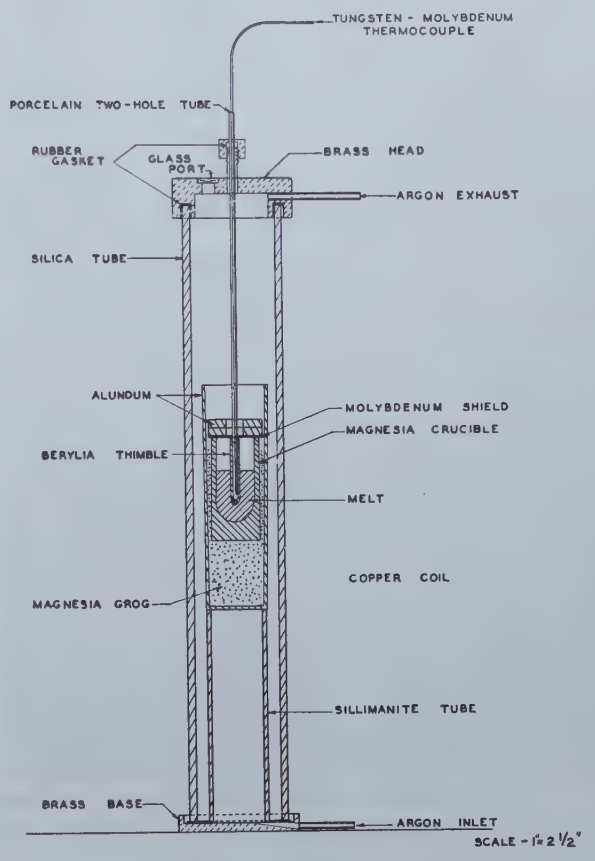

was first determined by a potentiometer, but this was replaced after a few runs by a Leeds & Northrup "Speedomax" automatic recording potentiometer. With this instrument a continuous record with practically no time lag occurring between a temperature change and its recording was obtainable.

The chromium used in this work was electrolytic chromium obtained from the U. S. Dept. of the Interior, Bureau of Mines. It contained 0.40 pct iron, 0.5 pct oxygen, 0.01 pct sulphur, and 0.004 pct carbon. Since all the alloys contained carbon the oxygen was reduced to values below 0.02 pct. Nitrogen in the final alloys, analyzed by vacuum fusion, was less than 0.01 pct. Accordingly, the alloys contained only the iron contamination which was of significant magnitude. The results of some of these heats are shown in fig. 7 through 14. Fig. 7 is a photograph of a slowly cooled portion of an ingot of Cr_4C and α chromium. Fig. 8 shows a section near the top surface of the same ingot, and the effect of the more rapid cooling is evident. Fig. 9 shows an annealed sample. Fig. 10 and 11 show Cr_7C_3 and Cr_4C, the angular crystals being Cr_7C_3 and the matrix being Cr_4C plus Cr_7C_3. Fig. 12 and 13 show some Cr_7C_3 and Cr_3C_2 plus carbon, the dark areas being graphite deposits which have been etched out. Fig. 14 shows an ingot consisting of Cr_3C_2, Cr_7C_3 and carbon, the carbon being etched out while the Cr_3C_2 is practically untouched.

In Fig. 15 is shown the chromium-carbon phase diagram which this investigation showed to be more nearly correct than those previously published. The melting points of all the carbides are indicated as being higher than those given in previous determinations, and are summarized in Table II.

Table II. Melting Points of Carbides

	Cr, °C	Cr_4C, °C	Cr_7C_3, °C	Cr_3C_2, °C
Hatsuta[1]	1760	1530	1670	1830 (Est.)
Friemann-Sauerweld[8]		1550	1665	
Tofsute, Kuttner, Buttinghaus		1550		
New Determination	1930	1520	1780	1895

The determination of the melting point of chromium, noted at 1930° ± 10°C in this work checks quite well with that given by Parks and Bens[6] which was 1950° ± 50°C. These two most recent determinations definitely place the melting point of pure chromium far above all previously reported values. Values as low as 1550°C must have been due to severely contaminated chromium metal, particularly with respect to nitrogen (also carbon) which drastically lowers the melting point of chromium—as is indicated by the chromium-carbon and chromium-nitrogen diagrams.

The selected chromium-carbon diagram is patterned after the one reported by Hatsuta[8], with the corrections and exceptions listed below. The diagram in the Metals Handbook, 1948, p. 1181, is also apparently patterned after Hatsuta; however, the source of one or two changes is not given, nor is Hatsuta's work referred to.

In the present work, most of the temperatures of transformation have been redetermined or were determined for the first time. Further, a transformation characterized by a horizontal line in $\eta + \zeta$ and in the $\zeta + \varkappa$ fields of the Hatsuta diagram has been eliminated. This apparent transformation was not found experimentally consistently; and in the two heats in which it was detected, some Cr_4C was found which was the cause of the thermal arrest. Changes in the solidification and cooling rates play an important role in detecting this thermal arrest by affecting the formation and retention of Cr_4C. This transformation, when detected, occurred at about 1520°C, which is also the solidification temperature of Cr_4C. In the heats in which carbon was already in solution in the charge, the Cr_4C solidification was not detected. Only in

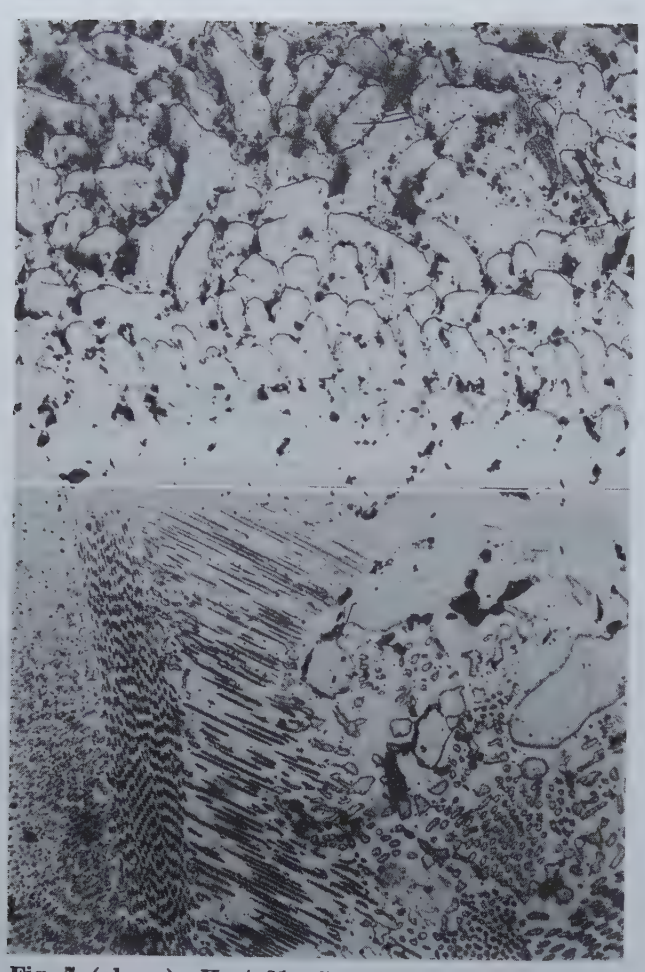

Fig. 7 (above)—Heat 31. Combined Carbon 2.88 pct.

As cast sample (slow cooled section of ingot) showing α chromium, Cr_4C and graphite. 10 pct HCl, electrolytic etch. 100X.

Fig. 8 (below)—Also Heat 31.

Rapidly cooled section of ingot showing the Cr_4C-α chromium eutectic. 75X. Both illustrations slightly reduced in reproduction.

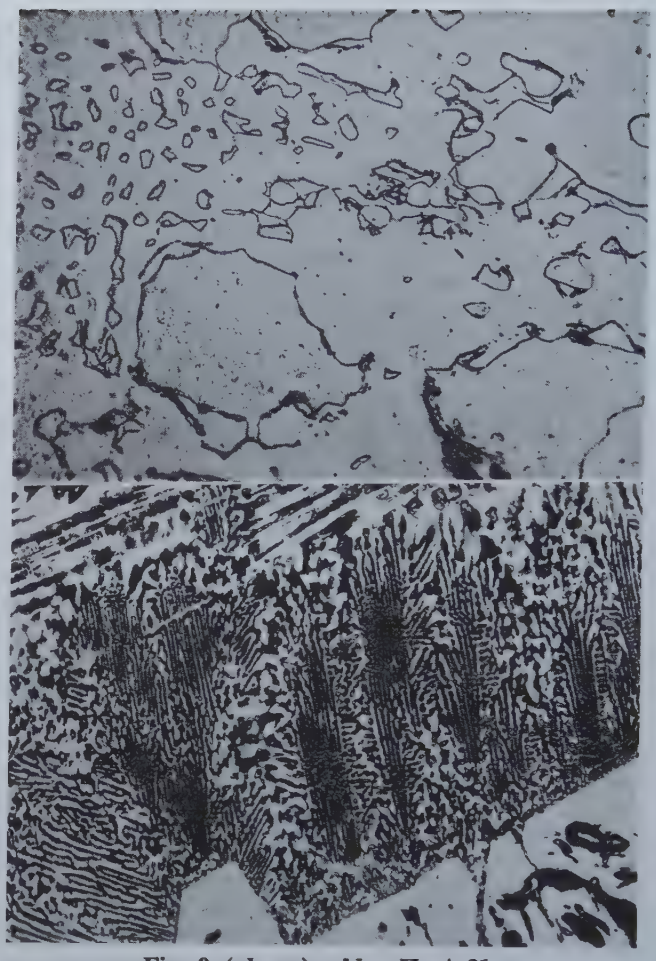

Fig. 9 (above)—Also Heat 31.

Annealed 16 hr at 1350°C. Shows α chromium matrix plus Cr_4C. Electrolytic NaOH etch. 500X.

Fig. 10 (below)—Heat 40.

Combined carbon 5.5 pct. As cast. Shows undecomposed primary Cr_7C_3 and Cr_7C_3 + Cr_4C peritectic. Electrolytic 10 pct HCl etch. 500X. Both illustrations slightly reduced in reproduction.

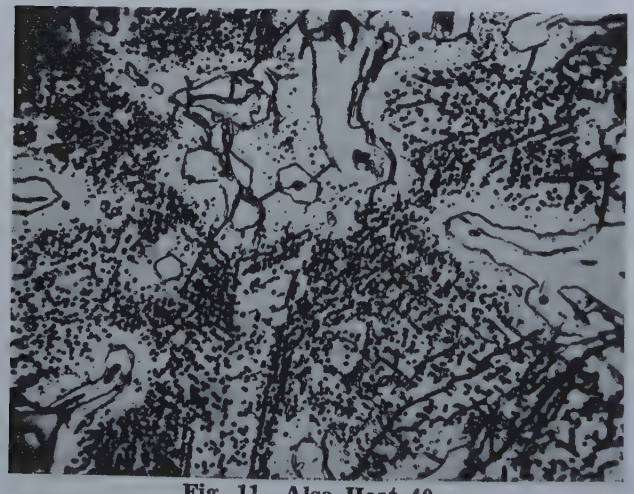

Fig. 11—Also Heat 40.

Annealed 16 hr at 1350°C. Shows same phases as fig. 10 after some decomposition. Electrolytic NaOH etch. 500X.

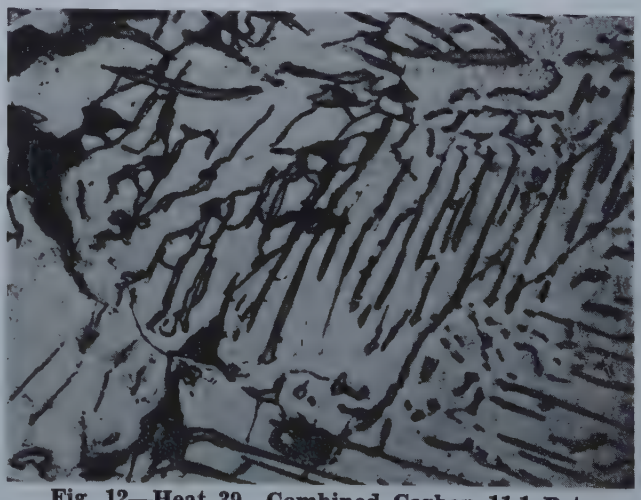

Fig. 12—Heat 39. Combined Carbon 11.1 Pct.

Annealed 16 hr at 1350°C. Cr_3C_2 matrix plus Cr_7C_3. Electrolytic NaOH etch. 750X. Both illustrations slightly reduced in reproduction.

heats in which carbon and chromium were charged was the Cr_4C transformation apparent in the Cr_7C_3 plus Cr_3C_2 field, and the heat evolution at that temperature was considered to be the solidification of a small percentage of Cr_4C in the ingot.

The existence of the carbide CrC, as indicated by Hatsuta[8] and Sykes in the Metals Handbook, was in no way indicated by any of the work reported herein. The formation of a compound possessing an X ray diffraction pattern unlike any of the known

chromium carbides can be explained if melting to form the carbides was not done under vacuum or a correct protective atmosphere. It has been shown that electrolytic chromium can absorb appreciable percentages of nitrogen from the atmosphere in only a few minutes if melted in a crucible open to the air[9]. A chromium nitride is undoubtedly formed, and a microscopic examination of a solidified chromium ingot which has been exposed to the atmosphere while molten, especially during the initial melt-down period, shows a yellow constituent, very similar to the description applied to the compound "CrC"[11].

It is considered that the phase diagram in the region of CrC and increasing carbon as shown by the dotted lines is the most probable construction. Because of the high temperatures required (in excess of 2000°C) and the presence of carbon it is difficult to find a suitable refractory for work in this field. Magnesia reacts with chromium-carbon solutions at 1900°C; zirconia is good only for a limited time. A graphite crucible seems the only possibility, and for this reason it was possible to obtain only a solidification point of Cr_3C_2. The melting point of pure chromium was obtained in a zirconia-lined dense magnesia crucible.

Acknowledgment

The authors wish to express their thanks to the Navy Department, Bureau of Ships, for support of the program, and to Mr. A. Bucklin who aided in the over-all program.

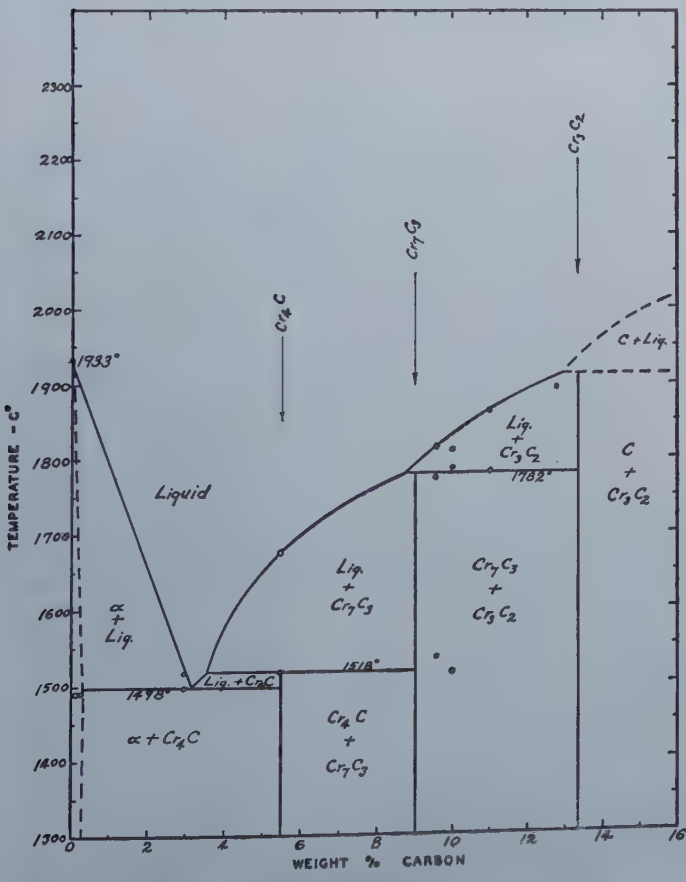

Fig. 15—Carbon-chromium Phase Diagram.

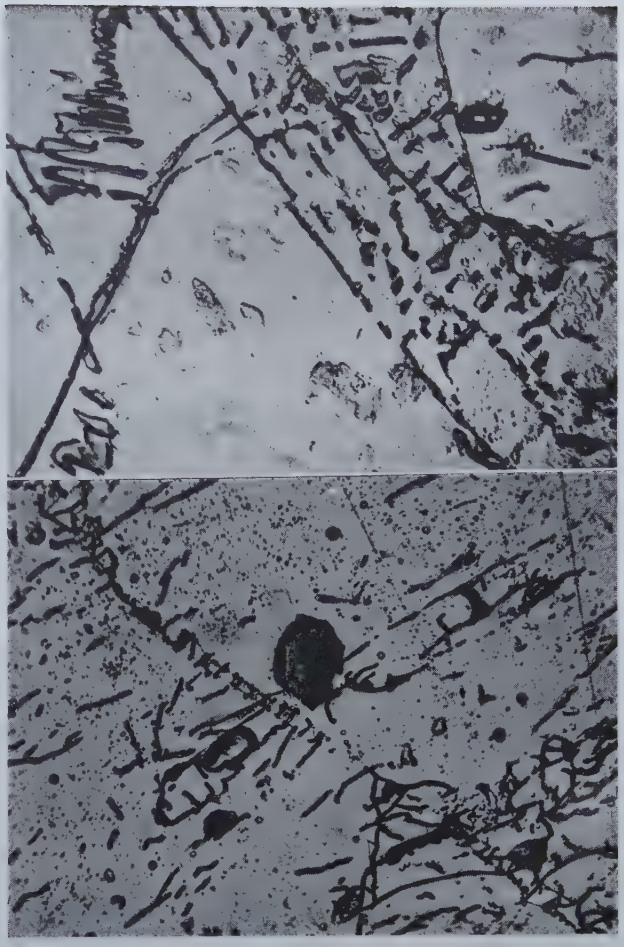

Fig. 13 (above)—Also Heat 39.

Annealed 16 hr at 1350°C. Shows primary Cr_3C_2 and $Cr_7C_3 + Cr_3C_2$ peritectic. Electrolytic NaOH etch. 750X.

Fig. 14 (below)—Heat 41.

Combined carbon 12.78 pct. As cast. Undecomposed Cr_3C_2 with long islands of Cr_7C_3 and graphite. Electrolytic NaOH etch. 500X. Both illustrations slightly reduced in reproduction.

References

[1] Kazue Hatsuta: Equilibrium Diagram for the Chromium-Carbon System. Tech. Repts., Tohoku Imp. Univ., X, No. 4 (1932).

[2] E. Friemann, F. Sauerwald: *Ztsch. anorg. Chem.* (1932), **203**. 64.

[3] W. Tofaute, C. Kuttner, A. Buttinghaus: The Iron-Chromium-Cr_7C_3-Cementite System. Brutcher Translation 1009 (1936).

[4] H. Moissan: Results of Experiments with Chromium. C. R. Acad. Sci., Paris (1894) **119**, 185; (1897) **125**, 841.

[5] K. Kelley, F. Boericke, G. Moore, E. Huffman, W. Bangert: Thermodynamic Properties of Carbides of Chromium. Bur. of Mines T.P. 662 (1944).

[6] R. Parke, F. Bens: Chromium Base Alloys. Symp. on Materials for Gas Turbines. 49th Meeting A.S.T.M. (1946).

[7] P. McKenna: Carbides of Tantalum and Like Metals and Method of Producing the Same. U. S. Pat. 2,124,509 (1935).

[8] E. Friemann, F. Sauerwald: *Ztsch. anorg. Chem.* (1932), **203**, 64.

[9] Frank Adcock: The Effect of Nitrogen on Chromium and Some Iron-Chromium Alloys. Jnl. Iron and Steel Inst. (1926), **CXIV**, 117-126.

[10] R. D. Potter and N. J. Grant: Tungsten-Molybdenum Thermocouples. *The Iron Age*, **163**, No. 13. March 31, 1949.

Electrical Resistivity and Thermoelectric Power of—Antimony-Selenium Alloys—

by B. D. Cullity, M. Telkes

and

John T. Norton

This research was initiated in an attempt to find a material for use in thermoelectric generators and although none of the antimony-selenium alloys is suitable for this purpose, the properties of Sb_2Se_3 indicate that it may have applications as a thermistor material.

THIS investigation of antimony-selenium alloys was undertaken in an attempt to find a suitable material for use in power-generating thermocouples. The chief requirements for such a material are high thermoelectric power, low electrical resistivity and low thermal conductivity[1]. Measurements of the first two properties mentioned are usually sufficient to determine whether or not a material is suitable for use in a thermoelectric generator. As a first approximation the requirements are:

1. Thermoelectric power greater than 200 microvolts per °C. 2. Electrical resistivity less than 0.002 ohm-cm. 3. Thermal conductivity less than 0.015 watt per cm per °C. These quantities are averages for the operating temperature range.

Previous Work

Experimental investigations of equilibrium in the antimony - selenium system have been summarized by Hansen[2]. These investigations extended from 1906 to 1921. In Hansen's judgment, the most accurate phase diagram is that determined by Parravano, in 1913 and this is reproduced in the upper part of fig. 1. The most notable parts of this diagram are the liquid miscilibility gap, extending from about 12 to 36 wt pct selenium, and the intermediate phase Sb_2Se_3 containing 49.3 wt pct selenium. The crystal structure of Sb_2Se_3 has not been determined.

Pelabon[3,4] made measurements of the electrical resistivity of a few antimony-selenium alloys but his investigation was not very complete. He found that the resistivity increased with the selenium content and became very large as the composition of Sb_2Se_3 was approached. For alloys containing less than 50 at. pct (39.3 wt pct) selenium, he found that the resistivity increased regularly with temperature. For alloys containing larger amounts of selenium, he found various results: in some cases, the resistivity decreased with increas-

B. D. CULLITY was Research Assistant, Dept. of Metallurgy, Mass. Inst. of Tech., Cambridge, Mass. at the time the paper was written; later Scientific Liaison Officer, Office of Naval Research, London, England; presently Asst. Professor, Dept. of Metallurgy, Univ. of Notre Dame, Notre Dame, Indiana.

M. Telkes and John T. Norton are Research Associate and Professor of Metallurgy, respectively, Mass. Inst. of Tech., Cambridge, Mass.

New York Meeting, Feb. 1950.

TP 2745 E. Discussion (2 copies) may be sent to Transactions *AIME, before Apr. 1, 1950, and is tentatively scheduled for publication Nov. 1950. Manuscript received July 1, 1948; revision received Oct. 7, 1949.*

Publication No. 25, M. I. T. Solar Energy Conversion Research Project.

ing temperature and in others it increased, passed through a maximum and then decreased as the temperature was raised.

Pelabon[5] also measured the thermoelectric power of some antimony-selenium alloys. He found that it was almost the same as that of pure antimony for alloys containing up to 50 at. pct selenium; for greater selenium contents, the thermoelectric power increased, becoming very large at the composition Sb_2Se_3.

The extensive literature concerning the resistivity and thermoelectric power of selenium has been summarized recently by Borelius and his collaborators[6,7]. Using very pure material and carefully controlled experimental arrangements, they obtained results which could be interpreted in terms of the Wilson-Fowler theory of semi-conductors.

Kozlovskii and Nasledov[8] studied the resistivity and thermoelectric power of selenium and selenium alloys containing 1 to 5 pct antimony. They found that increasing additions of antimony increased the resistivity and the thermoelectric power, the maximum effect being obtained with 4 pct antimony.

Nasledov[9] and Nasledov and Malyshev[10] found the same effect with additions of small amounts of antimony to selenium.

Experimental Methods

In the preparation of all alloys, a "special high purity" grade of selenium was used, containing more than 99.99 pct selenium and obtained from the American Smelting and Refining Co. "Lone Star" antimony from the Texas Mining and Smelting Co. was used in making most of the alloys; it contained 99.9 pct antimony, Fe, S and As being the chief impurities.

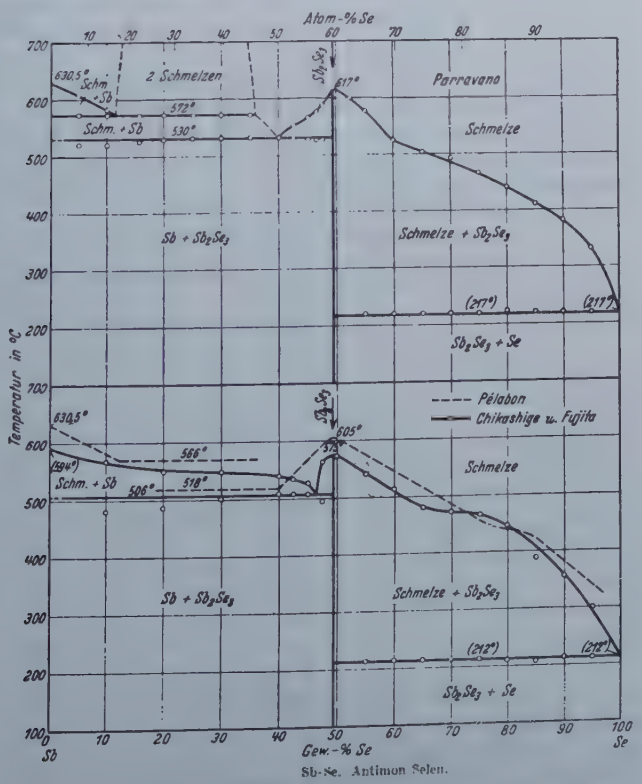

Fig. 1—Antimony-Selenium Equilibrium Diagram, from Hansen[2].

Since all the alloys investigated had relatively low melting points, it was possible to prepare them in glass tubes and for this purpose a special kind of Pyrex, known as Pyrex 172, was used. It has a softening temperature of about 925°C.

After melting in vacuo in sealed tubes, the alloys were allowed to solidify in the tubes and the resulting ingots measured 1 to 2 in. in length and about ⅜ in. in diam. All alloys were extremely brittle and had a large grain size. None of the alloys was chemically analysed: all came cleanly away from the glass tube and there was no doubt that all the metal added had entered the alloy.

Electrical resistivity was found by measuring, with a potentiometer, the potential drop along a known length of alloy when a known current was flowing. The specimen was clamped in a special fixture between two current electrodes of flat, braided cable made of tinned copper wire. The potential leads consisted of two steel needles applied to the surface of the specimen at a distance of 1 cm apart. The current used varied from about 1 amp to a few microamperes, depending on the resistance of the specimen. In a few cases of very high resistivity, where this method failed, a Wheatstone bridge or a modification of the voltmeter ammeter method was used. The temperature coefficient of resistance was measured over a range of about 15° - 100°C by immersing the specimen in a heated oil bath.

The thermoelectric power of the alloys was measured relative to copper over a temperature range of about 15° - 100°C and was taken as positive if the direction of conventional current flow was from specimen to copper at the cold junction. The specimen was clamped between two copper blocks, one heated by steam and the other cooled by a stream of water, the difference in temperature between the two blocks being indicated by a differential thermocouple. The thermal EMF was measured by means of a potentiometer connected to the copper blocks with copper lead wires.

Experimental Results

Electrical Resistivity: The electrical resistivity at 25°C of as-melted low-selenium alloys is shown in the lower part of fig. 2. The increase in resistivity when selenium is added is due mainly to solid solution of selenium in antimony. Antimony itself is to be regarded as a metal with one Brillouin zone, holding exactly 5 electrons per atom, slightly overlapping the next zone[11]. There are thus a small number of positive holes created in the inner zone and an equal number of electrons in the outer zone; the positive thermoelectric power of antimony suggests that it is the positive holes, rather than the electrons, which carry the current since the thermoelectric power has the same sign as the charge carrier. The addition of selenium, which has more valence electrons than antimony, would be expected to increase the concentration of free electrons and decrease the concentration of free holes and thus increase the resistivity. This is exactly the observed effect.

The preparation of homogeneous alloys containing 12 to 36 wt pct selenium is clearly impossible by

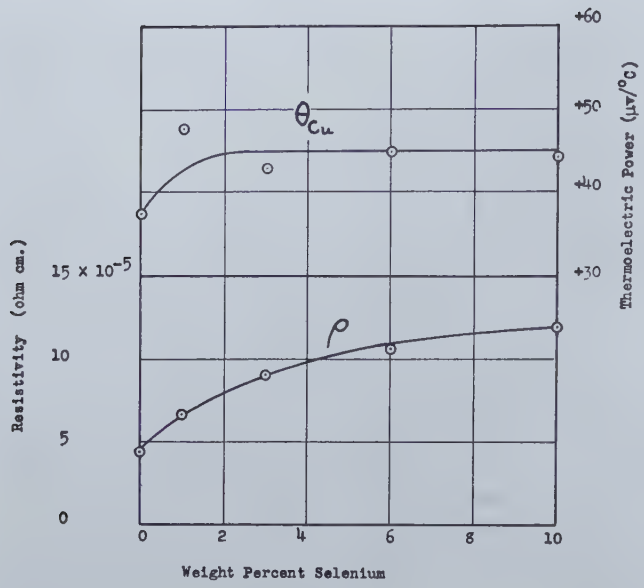

Fig. 2—Electrical Resistivity at 25°C and Thermoelectric Power (Relative to Copper) of Low-Selenium Antimony-Selenium Alloys.

the usual fusion methods because of immiscibility in the liquid state. Since investigation of the other alloys of the system showed that alloys with compositions within the miscibility gap could not have a thermoelectric power greater than +50 microvolts per °C, no alloys in this composition range were investigated.

The resistivities at 25°C of alloys whose compositions lie on the other side of the miscibility gap, namely between 36 and 100 wt pct selenium, are plotted on a logarithmic scale in fig. 3. The values reported are for as-melted alloys, if the selenium content is 49.3 wt pct selenium (Sb_2Se_3) or less, and for annealed alloys if the selenium content is larger than this amount.

Annealing greatly reduces the resistivity of the high-selenium alloys which, in the as-melted condition, have resistivities as large as many insulators. This is shown by table I.

Table I. Effect of Annealing on Resistivity

Alloy	Wt Pct Selenium	Resistivity at 25°C (ohm cm)	
		As-melted	Annealed
SS 9	60	3.0×10^5	1.3×10^5
SS 10	70	8.7	1.2
SS 11	80	140.	1.6
SS 12	90	160.	1.7
SS 13	100	Not Measurable	0.9

Selenium, either pure or existing as such in alloys as a second phase, solidifies in the amorphous form when cooled at any normal rate from the liquid state. This form has a very high resistivity and gives an X ray diffraction pattern characteristic of a liquid; in fact, it is probably best considered as a super-cooled liquid. Annealing at a temperature of about 200°C rapidly converts this form into crystalline, so-called "metallic"* selenium which has a hexagonal crystal structure and a much lower resistivity.

The most interesting portion of the curve of fig. 3 relates to alloys approaching Sb_2Se_3 in composition. It shows an extremely rapid increase in resistivity with increasing selenium content: an increase of only 0.3 wt pct selenium, from 49.0 to 49.3, increases the resistivity over 30,000 times.

The large resistivity of Sb_2Se_3 suggested that this substance might be a semiconductor. Experimentally the temperature dependence of the resistivity of Sb_2Se_3 was found to be in very good agreement with that predicted theoretically by Wilson[12, 13] for an impurity semiconductor:

$$\frac{1}{\rho} = \sigma = Ae^{-\frac{\Delta W}{2kT}} \qquad [1]$$

where ρ = resistivity (ohm cm.)
σ = conductivity (ohm^{-1} cm^{-1})
A = constant
ΔW = energy gap between the impurity levels and the top of the lower full band (electron volts)
k = Boltzmann's constant = 8.62×10^{-5} electron volt per deg.
T = temperature (Å)

The value of ΔW for Sb_2Se_3 was found to be 0.80 electron volt.

In general, the properties of semiconductors are very difficult to reproduce from specimen to specimen and Sb_2Se_3 is no exception. The resistivities of three alloys, all made up to have the compositions of Sb_2Se_3, were found to be as in table II.

The values (table II) also show effect of annealing in vacuo for 72 hr at 500°C. The reduction in resistivity so obtained is minor in comparison with that produced by the addition of impurities, as will be shown later.

An X ray diffraction powder pattern of Sb_2Se_3 showed a very large number of diffraction lines. No attempt was made to determine the structure but it appears to have less symmetry than a cubic, tetragonal or hexagonal lattice.

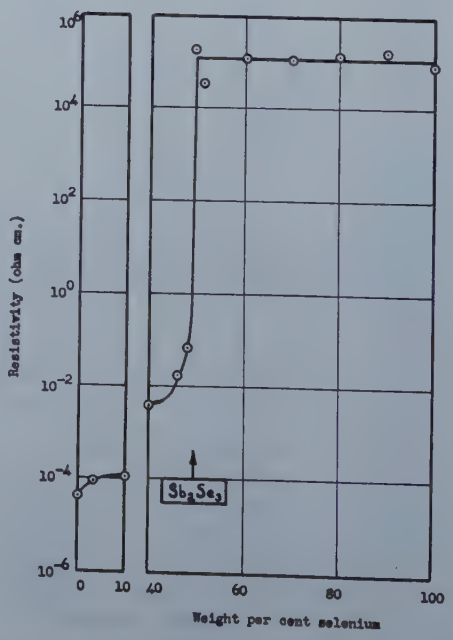

Fig. 3—Electrical Resistivity at 25°C of Antimony-Selenium Alloys.

* The term is a misnomer, since selenium has few metallic properties. Actually, it is a semiconductor.

The shape of the resistivity-composition curves of fig. 3 may be explained as follows. The practically constant resistivity of alloys containing more selenium than Sb_2Se_3 is simply due to the fact that these alloys are mixtures of two phases, both semiconductors and both having nearly the same resistivities. The rapid decrease in resistivity as antimony is added to Sb_2Se_3 is probably due to a combination of two factors:

Table II. Resistivities of Alloys

Alloy	Resistivity at 25°C (ohm cm)	
	As-Melted	Annealed
SS 8	7.1×10^4	2.5×10^4
SS 18	4.2	1.3
SS 23	47.	
	Mean 19.	

1. *Solid solution of antimony in* Sb_2Se_3. The thermoelectric power of Sb_2Se_3 relative to copper is positive, which shows that the current in Sb_2Se_3 is conducted by positive holes. This kind of conduction requires that some impurity have discrete energy levels capable of accepting electrons from the top of the filled band; the measurements of the variation of conductivity with temperature show that these levels are 0.80 electron volt above the top of the filled band.

If the observed increase in conductivity is due to the presence of antimony in solid solution, then it must be assumed that the excess antimony is acting as an "impurity" in the Sb_2Se_3 lattice. The usual theory of the effect of impurities on semiconductors is inadequate here, however; it was devised to apply to ionic solids (such as Cu_2O and ZnO) and leads to the prediction that excess metal in the lattice results in electronic conduction. Since Sb_2Se_3 exhibits positive hole conduction and, moreover, can hardly be considered as a typical ionic solid, a different approach must be used to explain the increased conductivity caused by excess antimony. The type of bonding in Sb_2Se_3 may be assumed to be largely covalent in nature, each antimony atom being bonded to three selenium atoms and each selenium atom being bonded to two antimony atoms. The resulting structure might be similar to that of pure antimony, but with selenium atoms perhaps taking up positions between the closest neighbors of the antimony lattice.

If an antimony atom is now substituted for a selenium atom, its tendency would be to take up an electron from the filled band of Sb_2Se_3, producing hole conduction, because by so doing it would have the same valence structure as the selenium atom it replaces. This line of reasoning is in agreement with the results of Scaff, Theuerer and Schumacher[14] who found that silicon containing Group III elements with one less valence electron had hole conductivity, while electron conductivity was shown by silicon containing Group V elements with one more valence electron.

2. *Addition of another phase with much lower resistivity, namely antimony.* Usually, the resistivity of two-phase alloys is approximately a linear function of the volume composition. However, other relationships are theoretically possible, depending on the mode of distribution of the two phases. At one extreme, the two constituents could occur in series with respect to the current flowing: the resistivity of the alloy is then a linear function of the volume composition. At the other extreme, the two constituents could occur in parallel; in this case, the shape of the resistivity curve depends markedly on the relative resistivities of the two phases. For example, if a small amount of a phase with low resistivity is added in parallel to a phase with high resistivity, the resistivity of the alloy will decrease very abruptly, in a manner similar to that of fig. 3. Physically, a parallel arrangement of phases means that threads or filaments of antimony must run through the alloy from one end of the specimen to the other. The phase diagram given in fig. 1 shows that an alloy containing somewhat less antimony than Sb_2Se_3 consists of crystals of Sb_2Se_3 imbedded in a eutectic matrix of antimony and Sb_2Se_3. Metallographic examination of alloys in this composition range showed that the eutectic was platelike in nature, so that an electrically parallel arrangement of phases in this alloy would demand that the plates of antimony in the eutectic be interconnected throughout the length of the specimen. It is very unlikely that this condition is completely fulfilled, but its partial fulfillment may be responsible for part of the observed rapid decrease in resistivity when antimony is added to Sb_2Se_3.

Thermoelectric Power: The thermoelectric power of as-melted low-selenium alloys is plotted in the upper part of fig. 2. As selenium is added to antimony, the thermoelectric power increases slightly at first and then remains constant.

Values of the thermoelectric power of alloys whose compositions lie on the other side of the liquid miscibility gap are plotted in fig. 4. The main feature of this curve is the abrupt and large increase in thermoelectric power at the composition of Sb_2Se_3, a change even more abrupt than the change in resistivity.

The values for the thermoelectric power of alloys containing more selenium than Sb_2Se_3 were obtained with annealed alloys. Repeated measurements on the same specimen did not agree very well and the values given are to be regarded as only approximate.

The most interesting part of fig. 4 is the abrupt change in thermoelectric power at the composition of Sb_2Se_3. The rapid decrease in thermoelectric power of Sb_2Se_3 as antimony is added is probably due to a combination of the same two effects which

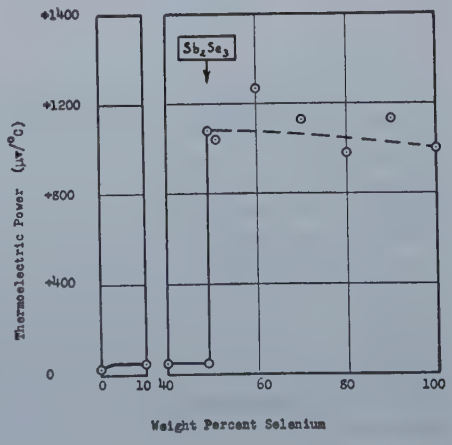

Fig. 4—Thermoelectric Power (Relative to Copper) of Antimony-Selenium Alloys.

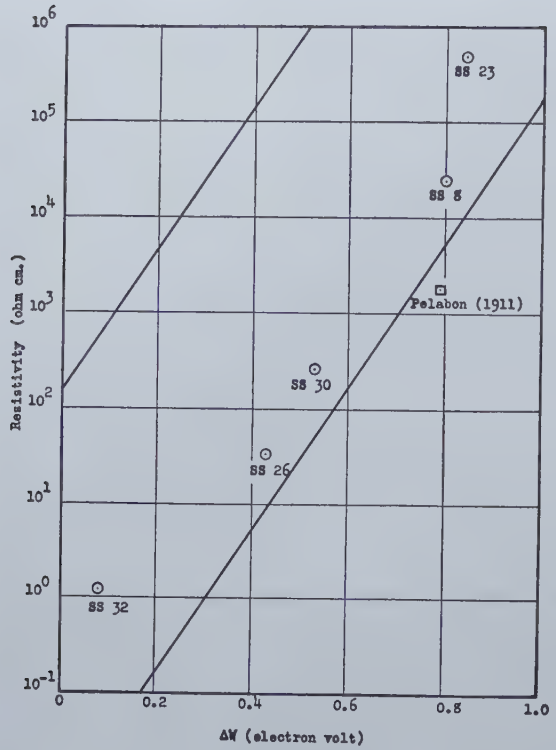

Fig. 5—(left) Values of Resistivity and Energy Gap for Various Modifications of Sb_2Se_3.

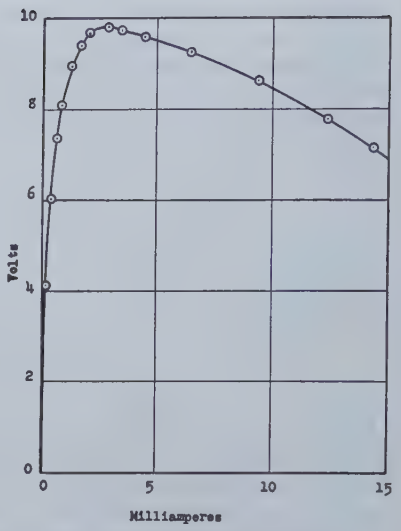

Fig. 6—(right) Direct Current - voltage Curve for a Bead Thermistor Made of Sb_2Se_3 (Alloy SS 32).

cause the rapid decrease in resistivity, namely, the formation of a solid solution and the addition of a second phase of radically different properties.

The thermoelectric power, as well as the resistivity, of Sb_2Se_3 varied from specimen to specimen and was increased somewhat by annealing 72 hr at 500°C as shown in Table III.

Table III. Effect of Annealing on Thermoelectric Power

Alloy	θ_{Cu} (microvolts per °C)	
	As-melted	Annealed
SS 8	1130	1300
SS 18	1040	1130
SS 23	1080	

Wilson's theory of semiconductors[12, 13] was applied by Bronstein[15] and Fowler[16, 17] to the thermoelectric effects in a semiconductor vs. metal circuit. Their results are practically identical. For the thermoelectric power of a hole, or defect, semiconductor relative to an ideal metal, Fowler found:

$$\theta = +\left(\frac{5}{4}\frac{k}{e} + \frac{\Delta W}{2eT}\right) = 108 \times 10^{-6} + 0.5\,\frac{\Delta W}{T} \quad [2]$$

where θ = thermoelectric power (volt per deg)
e = *absolute* value of the electronic charge (electron charge units) = | 1 |

This equation may be used to obtain an independent value of ΔW. The thermoelectric power of annealed Sb_2Se_3 is 1300 microvolts per °C, measured over the temperature range 10° - 100°C. Inserting the thermoelectric power and the median temperature of 328° abs. (55° C) into Eq 2, one obtains 0.78 ev. for ΔW, in very good agreement with the value of 0.80 ev. found from the variation of conductivity with temperature for the same specimen.

Effect of Impurities on Sb_2Se_3: Since Sb_2Se_3 is a semiconductor, its properties should be quite sensitive to changes in the impurity content. In order to investigate the effect of impurities, alloys were prepared with different grades of antimony and different additions of a small amount of a third constituent.

The properties of these alloys in the as-melted condition are given in table IV. The composition of Lone Star antimony has already been given. RMM antimony is a less pure grade, containing 99.8 pct antimony; its use decreases the resistivity of Sb_2Se_3 as one would expect, since the general rule is that the addition of impurities to semiconductors decreases their resistivity. Use of still another grade, Belmont antimony, decreases the resistivity still further. Qualitative spectrochemical analysis of this antimony showed that it contained lead in the order of 0.1-1.0 pct, together with minor amounts of silver, copper and nickel.

Table IV also shows the effect of adding 1 at. pct of various elements to Sb_2Se_3 made from Belmont antimony. Mg and Cu were found to produce a large increase in the resistivity, Bi and As a small decrease, while S, Te, Pb and Sn had no marked effect. All additions decreased the thermoelectric power. The addition of Pb and Sn even changed the method of conduction, the negative thermoelectric power of SS 28 and SS 27 indicating that the current in these alloys is carried by free electrons instead of by positive holes as in pure Sb_2Se_3.

Use of Sb_2Se_3 as a Thermistor: None of the antimony-selenium alloys, including those containing small amounts of third elements, is suitable for use in thermoelectric generators, since those alloys which have sufficiently high thermoelectric power unavoidably have a resistivity which is much too large for efficient production of power by the thermoelectric effect.

However, the properties of Sb_2Se_3 indicate that it may have useful applications as a thermistor material. Thermistors are thermally sensitive resistors made of semiconductors whose resistance changes rapidly with the temperature. Widely used today as circuit elements, particularly in the communications field, and for other special purposes, they have been fully discussed in a survey article by Becker, Green and Pearson[18].

Research on semiconductors has shown that, in general, those which have a large resistivity also have a large value of ΔW. For example, if the values

of resistivity and ΔW reported by Becker, Green and Pearson[18] for a large number of semiconductors are plotted against each other as in fig. 5, it will be found that the great majority of the plotted points will lie in a band enclosed by the two parallel lines shown. Christensen[19] remarks that the best materials for use as thermistors will have a combination of properties which lie near the lower line of fig. 5. In other words, the resistivity should be as low as possible consistent with a high temperature coefficient. (The temperature coefficient of resistance is proportional to ΔW.) When the values of resistivity and ΔW for annealed Sb_2Se_3 (alloy SS 8) were plotted on fig. 5, the point for this alloy was located near the lower line, indicating that it might make a good thermistor material.

One requirement of a thermistor is that it should

Table IV. Effect of Impurities on Sb_2Se_3

Alloy	Antimony	Added Impurity*	ρ (ohm cm at 25°C)	θ_{eu} (microvolt per °C)
SS 8	Lone Star	None	71,000.	+1130
SS 18	Lone Star	None	42,000.	+1040
SS 23	Lone Star	None	470,000.	+1080
SS 24	RMM	None	12,000.	+ 570
SS 25	Belmont	None	42.	+ 810
SS 26	Belmont	None	34.	+ 850
SS 33	Belmont	S	36.	+ 820
SS 30	Belmont	Te	260.	+ 620
SS 31	Belmont	Mg	74,000.	+ 170
SS 34	Belmont	Cu	1,460.	+ 60
SS 29	Belmont	Bi	0.64	+ 49
SS 32	Belmont	As	1.2	+ 25
SS 28	Belmont	Pb	96.	— 120
SS 27	Belmont	Sn	31.	— 160

* The amount of impurity in the alloy was one atomic percent in all cases, except for SS 31 which contains much less than one atomic percent of magnesium.

Table V. Energy Gap Values for Sb_2Se_3

Alloy	Composition	ρ (ohm cm)	ΔW (ev.) found from Temperature Coefficient	ΔW (ev.) found from Thermoelectric Power
SS 23	Lone Star Sb	470,000.	0.84	0.64
SS 8	Lone Star Sb	25,000.	0.80	0.78
Pelabon (1911)	?	1,780.	0.79	0.51
SS 30	Belmont Sb+Te	260.	0.53	0.34
SS 26	Belmont Sb	34.	0.43	0.49
SS 32	Belmont Sb+As	1.2	0.08	

be possible to vary its properties to suit specific applications. It had already been determined that the resistivity of Sb_2Se_3 could be varied considerably by changing its impurity content. In order to see if the value of ΔW could also be changed by such treatment, specimens of Sb_2Se_3 having widely different resistivities were selected and their temperature coefficients measured. The results are shown in table 5 and fig. 5.

As shown previously, it is also possible to calculate ΔW for a semiconductor from the thermoelectric power by means of Eq 2. Values of ΔW so obtained are included in table V, where they may be compared with those derived from the variation of resistivity with temperature. In general, the agreement is not very good, but one may still use the thermoelectric power to obtain a rough value of the energy gap. Eq 2 is valid only when the thermoelectric power is large, i.e. when ΔW is large compared to $2kT$.

These data show that both the resistivity and ΔW are variable over a wide range and that the plotted points lie near the lower line of fig. 5 except for very low or very high resistivities. The point representing Pelabon's[3] data of 1911 is not considered very reliable since it is based on resistivity measurements made at only three different temperatures.

Since many of the most important uses of thermistors depend on the voltage-current curve having a region of negative slope, it was decided to determine whether or not the same characteristic type of curve could be obtained with Sb_2Se_3. Alloy SS 32 was used, containing Belmont antimony and 1 at. pct arsenic, and a small bead thermistor made of this alloy gave the voltage-current curve shown in fig. 6. This resembles very closely similar curves obtained with commercially used thermistors and has the characteristic region of negative slope, where an increase in current is accompanied by a decrease in the voltage drop across the thermistor.

Acknowledgment

The writers are indebted to the Solar Energy Utilization Project at the Massachusetts Institute of Technology for the grant of funds which made this investigation possible.

References

[1] M. Telkes: The Efficiency of Thermoelectric Generators, I. *Jnl. Appl. Phys.* (1947) **18**, 1116.

[2] M. Hansen: Der Aufbau der Zweistofflegierungen. Julius Springer, Berlin (1936).

[3] H. Pelabon: Sur la Resistivite des Seleniures d'Antimoine. Acad. des Sciences, *Comptes Rendus* (1911) **152**, 1302.

[4] H. Pelabon: Sur les Proprietes des Mixtes Selenium et Antimoine. *Annales de Chimie* (1920) **13**, 121.

[5] H. Pelabon: Etude Thermo-Electrique des Mixtes Selenium-Antimoine. Acad. des Sciences, *Comptes Rendus* (1914) **158**, 1669.

[6] G. Borelius, F. Pihlstrand, J. Anderson, and K. Gullberg: Resistance of Liquid and Solidified Selenium. *Arkiv. f. Mat. Astr. Fys.* (1944) 30**A**, **14**, 1.

[7] G. Borelius, and K. Gullberg: Thermoelectric Power of Liquid and Solidified Selenium. *Arkiv. f. Mat. Astr. Fys.* (1944) 31**A**, **17**, 1.

[8] I. L. Kozlovskii, and D. N. Nasledov: *Jnl. Techn. Phys.* USSR (1943) 13 No. 11-12, 627.

[9] D. N. Nasledov: *Bull.* Acad. Sci. USSR Phys. (1941) **5**, 470.

[10] D. N. Nasledov, and E. K. Malyshev: *Jnl. Tech. Phys.* USSR (1946) **16**, 1127.

[11] N. F. Mott, and H. Jones: The Theory of the Properties of Metals and Alloys. Oxford (1936).

[12] A. H. Wilson: Theory of Electronic Semi-Conductors. *Proc.* Roy. Soc. (1931) **A. 133**, 458.

[13] A. H. Wilson: The Theory of Electronic Semiconductors, II. *Proc.* Roy. Soc. (1931) **A. 134**, 277.

[14] J. H. Scaff, H. C. Theuerer, and E. E. Schumacher: P-type and N-type Silicon and the Formation of the Photovoltaic Barrier in Silicon Ingots. AIME *Trans.* **185**, 383. *Jnl. of Metals.* Apr. 1949.

[15] M. Bronstein: On the Theory of Electronic Semiconductors. *Phys. Zeit. der Sowjetunion* (1932) **2**, 28.

[16] R. H. Fowler: An Elementary Theory of Electronic Semiconductors and Some of Their Possible Properties. *Proc.* Roy. Soc. (1933) **A. 140**, 505.

[17] R. H. Fowler: Statistical Mechanics. Second Ed. MacMillan, (1936).

[18] J. A. Becker, C. B. Green, and G. L. Pearson: Properties and Uses of Thermistors—Thermally Sensitive Resistors. *Trans.* A.I.E.E. (1946) **65**, 711.

[19] C. J. Christensen: U.S. Pat. 2, 329, 511, (1943).

Effect of Solute Elements on the

Tensile Deformation of Copper

by Rolland Sydney French

and

Walter R. Hibbard, Jr.

True stress-true strain data for copper and copper alpha solid solution alloys indicate that the strain hardening coefficient, M, is a function of the yield strength but independent of the solute element added. Approximately linear relationships were found between yield strength and atomic percent solute.

FOR tensile deformation, if the stress value is defined by the ratio of the load to the actual area, and the strain value by the natural logarithm of the ratio of the immediate length to the original gauge length of the sample, the resulting data when plotted with logarithmic coordinates result in a linear relation extending from the initial plastic yielding through the maximum load and in some cases, such as for copper and brass, to fracture[1,2]. The normal form of the curve, therefore, is a parabola, satisfying the following equation:

$$S = Ke^m \qquad [1]$$

where S and e represent true stress and strain, K is a constant, and m is a coefficient evaluating the slope of the curve and designated therefore as the strain hardening coefficient. Hollomon[2] has reported that this coefficient is a function of the yield strength as effected by grain size in alpha brass, and the carbon content and heat treatment of steel. In the case of steel, the value of the proportionality constant is a function of the carbon content. It was further shown in that paper[2] and also by Low and Prater[3] that, if the power relation between stress and strain remains valid, the strain hardening coefficient m, is equal to the strain at the maximum or necking load. Thus, an added significant feature is that this coefficient may serve as an index of the capacity for deformation prior to localized necking and subsequent fracture, e.g. drawability. The constant K may be defined as the strength of the material at unit strain. Together the K constant and the m coefficient describe an alloy's physical properties as far as strength and ductility are concerned for a particular yield strength and, in the case of steel, a particular carbon content.

The work of Lacy and Gensamer[4] gives data on alloy ferrites from which very close estimates of the strength of ternary and higher iron alloys have been made. It was the purpose of this investigation to develop similar data for commercial copper base alpha solid solution alloys.

Preparation of Specimens

Commercial binary alloys of copper with aluminum, beryllium, cadmium, nickel, silicon, tin and zinc were investigated. In addition, laboratory castings were made of a 1 pct silicon alloy and a 2 pct aluminum alloy to complete these particular series. Two types of copper were used, oxygen free OFHC and tough pitch FC. The analyses of these alloys are shown in table I.

Standard ASTM sheet tensile specimens were used to determine the usual physical properties of each alloy and to obtain stress data at strains from 0.0005 to 0.01. Small (¼ in. x 3 in. x tk.) samples

ROLLAND S. FRENCH, Junior Member AIME, is Metallurgical Engineer, Bridgeport Brass Co., Bridgeport, Conn.

WALTER R. HIBBARD, JR., Junior Member AIME, is Assistant Professor of Metallurgy, Yale University.

New York Meeting, Feb. 1950.

TP 2755 E. Discussion (2 copies) may be sent to Transactions *AIME before Apr. 1, 1950, and is scheduled for publication Nov. 1950. Manuscript received Aug. 9, 1949.*

This paper is from a report by R. S. French submitted to the School of Engineering, Yale Univ., in candidacy for the degree of Master of Engineering, May 1949.

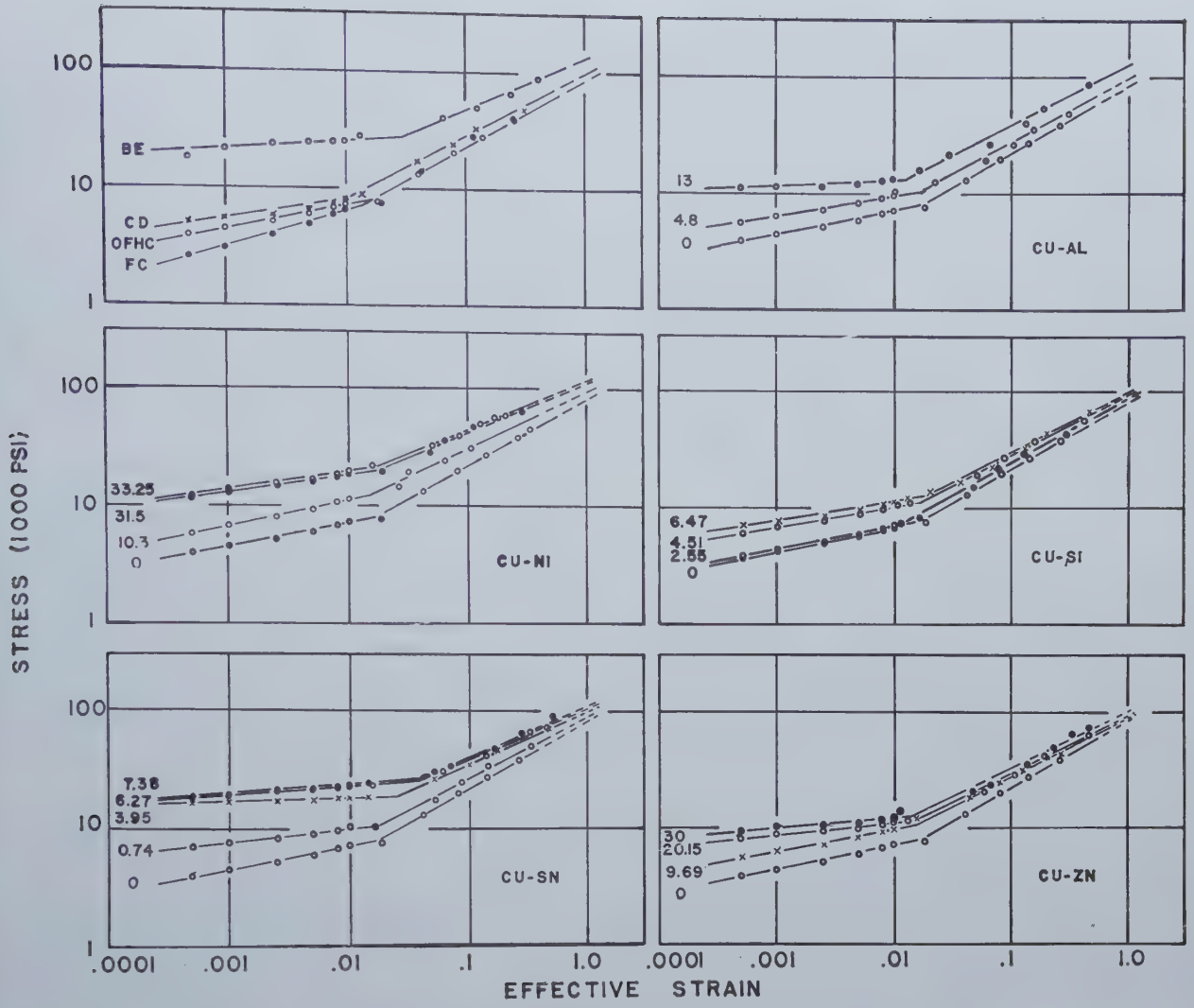

Fig. 1 (above)—True Stress-True Strain Curves.

Be indicates copper-beryllium alloy, CD indicates copper cadmium alloy, and OFHC and FC are coppers. Numbers on curves are atomic percent of solute element indicated.

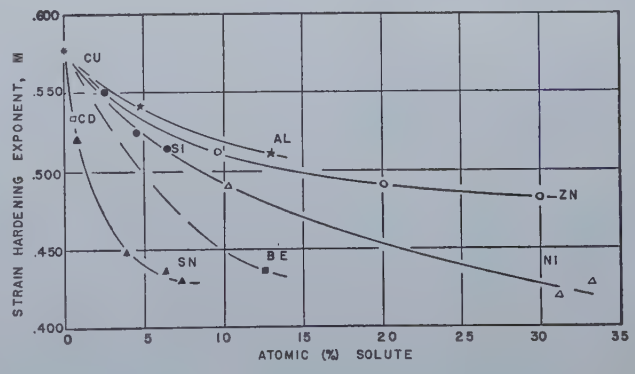

Fig. 2—Effect of Solute Concentration on the Strain Hardening Exponent, M.

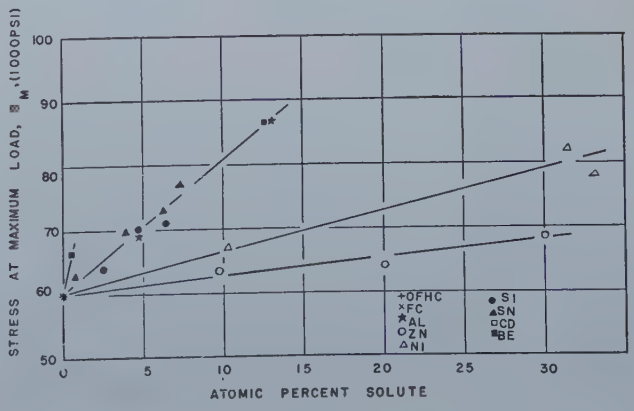

Fig. 3—Effect of Solute Concentration on the Stress at Maximum Load (S_m), where Strain equals M.

were used to obtain stress data at strains from 0.01 to near the ultimate load. After machining, the specimens were annealed under conditions indicated by preliminary tests to produce an 0.090 mm average diam grain size. The copper-cadmium alloy was packed in charcoal to avoid scale build-up during the air anneal. The copper-beryllium alloy was quenched into iced brine to preserve the alpha phase. Samples were cleaned in a 10 pct sulphuric acid pickle solution, washed and dried. It was not possible to obtain a uniform grain structure, particularly for the coppers and the aluminum and silicon alloys, where variations from 0.070 to 0.150 mm were found. An attempt was made, therefore, to keep the largest percentage of the grain size near 0.090 mm and the remainder larger, where only a small effect on the strain hardening coefficient m would be expected, based on Hollomon's data[2] for alpha brass.

Method of Test

All of the physical testing was done with load ranges having a calibrated accuracy of better than 1 pct. An autographic record of the load-elongation data through a strain range of 0-0.01 was made using a microformer strain gauge and recorder. The accuracy of the extensometer was better than ½ pct of the recorded strain over the maximum calibrated range of 0.02 in. The strain rate used was approximately 10^{-4} per sec, the load being varied as necessary.

As a true strain of 0.01 is equal to an extension of 0.0101 ipi, in the range of the small strains desired, the unit extensions from the graphs were satisfactory. To obtain the actual area of the sample at a given strain in order to find the true stress, the original area of the sample was divided by the unit extension since:

$$A = A_o l_o / 1$$

where A_o is the original area; A is the area at the specified strain; l_o is the original gauge length of 1 in.; and 1 is the final length which in these tests was equal to the unit extension. Thus, knowing the recorded load at the strain value and the true area, the true stress could be calculated. In this manner, the stresses at strains through $e = 0.01$ were obtained.

Rectangular specimens cut from strip stock were used in determining stress strain relations above this value because round stock was not available. The effective strain under the conditions of anisotropic plastic flow in rectangular specimens was shown by Fisher[5] to be given by the following equation:

$$e^2 = 2/9\ [(e_1-e_2)^2 + (e_2-e_3)^2 + (e_3-e_1)^2] \quad [2]$$

where e_1, e_2 and e_3 are the natural strains of the 3 principal coordinates. From the tensile data, load values were estimated for the small samples which were then loaded in tension to the desired value and released. The thickness and width of the specimens were measured by a micrometer and the gauge length by a microscope with a Filar eyepiece. True stress was determined from the ratio of the test load to the final area. True strain was computed by the Fisher formula from the three principal natural strains.

Results

The true stress-strain data for the alloys studied, when plotted on logarithmic coordinate paper, formed linear curves as shown in fig. 1. As noted in Hollomon's study of the properties of alpha brass[2], these curves also contain two regions of plastic flow. The first, accompanied by a low degree of strain hardening, is found in the yield strength region from very low strain values to a strain value of about 0.01. The second exists thereon through the localized or necking strain and exhibits a much more rapid rate of strain hardening. The strain hardening coefficient, m, the K value and a yield strength value at a strain of 0.01 were determined graphically on 5 in. cycle paper.

While a difference exists between the yield strength of the two coppers, their respective data form a single line above a strain of 0.01 as reported by Jackson, et al.,[6] for these metals. It will be noted that the strain hardening coefficient seems to decrease in value with increasing solute concentration, and the curves tend to approach one another.

As described previously, the strain hardening coefficient defines by its own value the maximum uniform strain that can be endured before localized necking of the sample starts. Thus, the true stress at the ultimate load, S_m, can be found at this strain

Table I. Chemical Composition of Alloys

Alloy	Pct Solute Weight	Pct Solute Atomic	Pct Weight Copper	Other Elements
OFHC			99.997	P.Mn Sb As Sn Bi Zn 0.000; Si Al Ag Cd 0.00; Pb Fe Ni 0.001
FC				Zn Al Sn 0.00; Pb Ni 0.001; Fe 0.002
Al	2.09	4.80	97.90	Pb 0.003; Fe 0.005
Al	5.96	13.00	93.66	Si 0.05; Pb 0.003; Fe 0.03; Zn 0.03; As 0.23
Be	2.26	12.60	97.23	Al 0.15; Si 0.08; Sn 0.07; Fe 0.06; Ni 0.15
Cd	0.98	0.56	99.01	Fe 0.003; Ni 0.001; Pb 0.001
Ni	9.58	10.30	89.57	Fe 0.80; Zn Mg 0.01; Pb 0.003
Ni	29.41	31.50	69.42	Mn 1.12; Fe 0.01; Pb 0.003
Ni	31.03	33.25	67.50	Mn 1.08; Fe 0.32; Zn 0.05; Mg Al 0.01
Si	1.14	2.55	98.85	Fe 0.005; Pb 0.003
Si	2.11	4.51	97.88	Ni Pb 0.001; Fe 0.01
Si	2.97	6.47	96.88	Fe Zn 0.05; Ni Sn 0.02; Pb 0.003
Sn	1.02	0.74	98.86	P 0.1; Zn 0.01; Pb 0.003; Fe 0.005
Sn	5.37	3.95	94.25	P 0.12; Zn 0.25; Pb Fe 0.004
Sn	8.44	6.27	91.25	P 0.10; Zn 0.20; Pb 0.003; Fe 0.005
Sn	9.90	7.38	89.85	P 0.15; Zn 0.04; Pb Fe 0.004
Zn	9.95	9.69	90.02	Ni 0.02; Pb 0.003; Fe 0.004
Zn	20.60	20.15	79.38	Ni 0.01; Pb 0.005; Fe 0.007
Zn	30.68	30.05	69.31	Pb 0.005; Fe 0.004

Table II. Relative Solute Effectiveness

Solute	$S_{0.01}$ per Atom pct A, psi	$S_{0.01}$ per Atom pct Zinc = 1	DPH per Atom pct[7] Zinc = 1
Zn	200	1	1
Ni	400	2	0.91
Al	500	2.5	2.45
Si	700	3.5	2.54
Mg	—	—	6.9
Cd, Be	1400	7	—
Sn	2600	13	12.7

value and the normal tensile strength calculated. Such calculations were made for these alloys and, without a correction for the effective strain, the calculated tensile strengths were within 12.7 pct of the experimentally obtained values from the ASTM type tensile specimens.

Discussion of Results

MacGregor[1] was one of the first investigators to point out the possibilities to be derived from true stress-strain data when studying deformational characteristics of a metal during cold work, and suggested that the maximum strain prior to necking was a valuable criterion for such a study. Fig. 2 shows this value, m, plotted as a function of solute

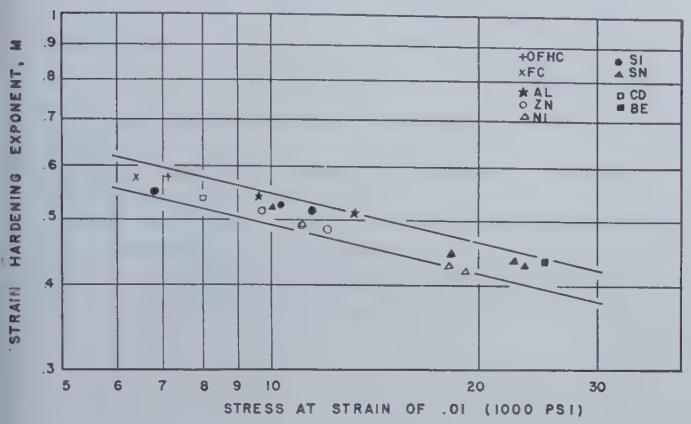

Fig. 4—Effect of Yield Strength $S_{0.01}$ on the Strain Hardening Exponent (M) Independent of Solute Element.

Fig. 5—Effect of Solute Concentration on the Yield Strength ($S_{0.01}$).

concentration for each of the alloys and these curves appear to indicate the loss in ductility experienced when these solute elements are alloyed with copper. The effect is a nonlinear one for these elements with cadmium, tin and beryllium having the greatest effect, and aluminum and zinc the least, for a given solute concentration. The maximum effect apparently occurs with small solute additions before their limit of solubility in copper is approached. Thermodynamically, both tin and beryllium are supersaturated solid solutions, and cadmium nearly so.

The true stress at the necking strain, S_m, plotted as a function of solute concentration is shown in fig. 3. In this analysis a linear relation does seem to exist and the alloys are grouped into four general classifications. On an atomic percent basis of added solute element, cadmium has the largest effect and would probably lead to some rather interesting alloys were it not so limited solubility-wise. This element is followed by aluminum, beryllium, silicon and tin to form a second group. In the last two groups, nickel and zinc have the least effect on the strength of copper, in that order. In general, zinc has been found to have a greater strengthening effect than nickel, and this is undoubtedly true for the usual commercial fine grain sizes. For an average grain size of 0.090 mm in these samples, their positions have been reversed.

It is interesting to note that, if the amount of solute element necessary to reduce the tensile ductility of copper by 10 pct from a necking strain value of $m = 0.575$ to $m = 0.518$ is obtained from fig. 2, and then the corresponding percent increase in the true strength of these alloys over copper is interpolated from fig. 3, the following approximate increases over the strength of copper are found:

	Pct
Tin and Zinc	3 1/3
Nickel	6 2/3
Beryllium	12 1/2
Silicon	20
Aluminum	35 3/4

The K constant of Eq 1 might well be defined as the modulus of plasticity since it is equal to a ratio of stress to strain. When the K values are plotted as a function of the atomic solute concentration, as were the necking stress values in fig. 3, practically identical groupings of curves result except that the

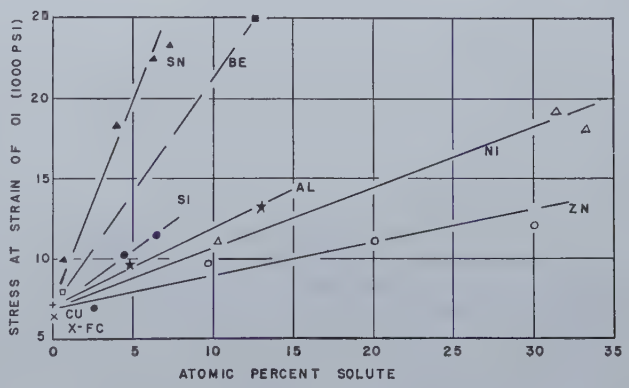

stress ordinate is magnified 1½ times and the stress origin is found at 83,000 psi, the K value for copper.

When the true stress-strain data of a prestrained sample is compared with values of a similar sample in the soft condition, its curve lies above that of the soft specimen and is found to have a seemingly lower strain hardening coefficient. By utilizing this concept, attempts were made to account for solute strengthening as a tensile prestrain in the copper lattice. While it is simple enough to determine the prestrain of copper necessary to produce an m coefficient corresponding to one of its alloys, the latter's K value is always higher by a considerable amount than the K value of the prestrained copper. Thus, it appears that if there is a strain-strengthening effect in the copper lattice due to alloying, it is not uniquely defined by tensile deformation.

It has been pointed out by Hollomon[2] that for steel samples of equal yield strength and carbon content the strain hardening coefficient is constant. It was also reported in the same paper that for cartridge brass of various grain sizes and yield strengths a

similar situation existed. If the true strength value at a strain of 0.01 is selected as the yield strength ($S_{0.01}$), then the following equation describes the relationship with the strain hardening coefficient, m:

$$m = C/(S_{0.01})^n \qquad [3]$$

where C is a constant characteristic of the base material and n is an exponential constant independent of the composition.

The strain hardening coefficients of the alloys tested in this work were plotted as a function of the yield strength as defined above, and the results are shown in fig. 4. While the data do not form a single line, they fall within a band that satisfies

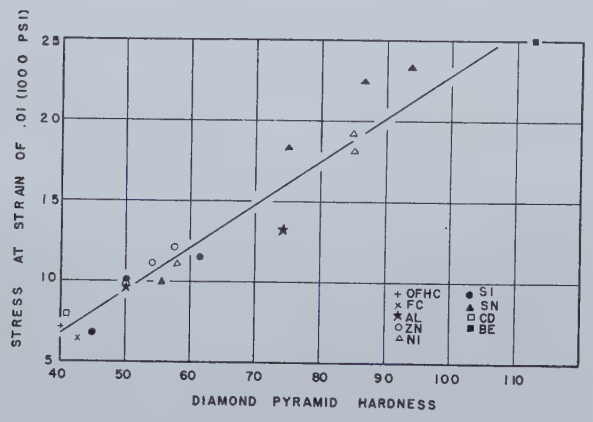

Fig. 6—Relation between Yield Strength ($S_{0.01}$) and Diamond Pyramid Hardness.

Fig. 7—Effect of Change in Lattice Parameter on the Change in Yield Strength ($S_{0.01}$)

as produced by the addition of the indicated solute elements to copper.

Eq 3. Graphical solutions of these data yield $n = 0.235$ and $C = 4.50 \pm 0.25$. The width of the band may be the result of variations in grain size. However, the slope is considerably more shallow than Hollomon's value of 0.5 for alpha brass. In general, nevertheless, the solute concentration of the various alloys in copper affects the strain hardening coefficient indirectly by changing the yield strength. Therefore, it becomes of interest to study the effect of alloying upon the yield strength of copper.

Fig. 5 shows the yield strength, $S_{0.01}$, plotted as a function of the solute concentration. The relation appears to be linear. Tin, as perhaps might be expected, has the greatest influence upon this property of copper, while cadmium and beryllium are next and, as in other studies, nickel and zinc the least. These data lead to the following equation:

$$\Delta S_{0.01} = XA$$

where $\Delta S_{0.01}$ is the increase in yield strength above that of copper, X is the atomic solute composition, and A is a constant of the solute defining the increase in yield strength for one atomic percent of the solute. These A values are shown in table II in the first column, compared to the values reduced to zinc = 1 in the second, and compared in the last column to similar results of Brick, Martin and Angier[7] obtained from *DP* hardness data.

In fig. 6 the yield strengths of the alloys investigated have been plotted as a function of the hardness of the unstrained samples. The data, while a bit scattered, is linear of the following form:

$$S_{0.01} = 270(DPH) - 4000$$

Thus, a strengthening of 270 psi is approximately equivalent to a hardening of one *DPH* number.

The increase in the yield strength for each atomic percent of solute addition is plotted against the corresponding lattice parameter change in fig. 7. An approximately linear relationship exists indicating that a change in lattice parameter of about 0.1 pct increases the yield strength by about 900 psi. As may be expected, the effect on yield strength appears to be a more basic consideration than the hardness change plotted in fig. 8. This curve is similar to that of Brick, Martin and Angier[7] except that nickel and zinc are reversed and the hardness value

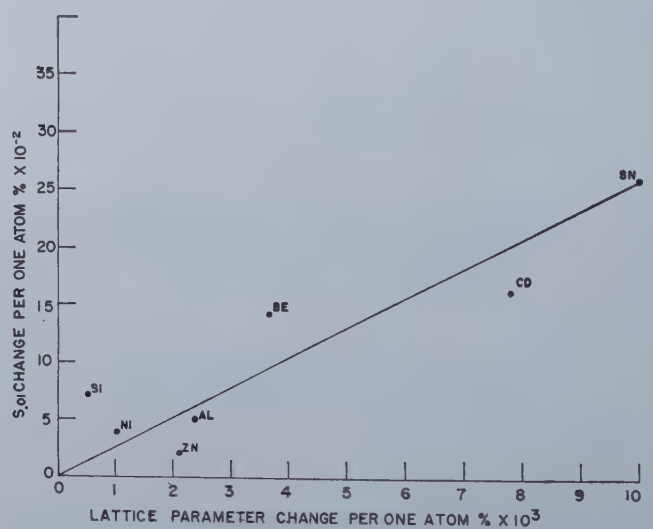

of tin is lower (e.g., the beryllium value will fit right on their curve). The noteworthy deviations from the linear curve are silicon where a small parameter change produces a marked *DPH* change, and cadmium where a marked parameter change produces a very small *DPH* change.

Summary

1. True stress-true strain data have been determined for OFHC and FC copper and alloys of copper with the following solute additions:

Al, Be, Cd, Ni, Si, Sn, Zn.

When these data are plotted on logarithmic coordinates they form linear curves which satisfy a power equation. The constants of this equation, i.e. the K value, described as the modulus of plasticity, and the m value or strain hardening coefficient, have been determined graphically together with the true

strength at a strain value of 0.01, designated as the yield strength.

2. The anomolous yielding found by Hollomon[2] in brass through strains of about 0.01 with only a slight contribution to the strength, was also found in the two coppers and in all the copper alloys studied, and appears to be characteristic of the copper base alloys.

3. The effect of various solute elements upon the necking or ultimate strength and the corresponding strain of these samples varies according to the solute present but always to increase the ultimate strength and to decrease the ability to withstand deformation prior to necking.

4. It was not possible to describe solute strengthening in terms of a tensile prestrain of copper due to alloying, for this theory does not account for the high modulus of plasticity, K values, found for the alloys.

5. As had been previously found for steel and cartridge brass, a relation exists between the strain hardening coefficient, m, and the corresponding yield strength values of these alloys. This relation is independent of the solute element employed.

6. Simple linear relations were found between the yield strength and the concentration of the various solutes indicating that of the elements studied, tin was the most effective strengthener and zinc the least. If these strength values are compared on an atomic percent basis to that found for zinc, it is found that they increase in simple multiples. These multiples compare favorably to similar values reported by Brick, Martin and Angier[7] determined from diamond pyramid hardness data.

7. A linear relation was found to exist between the *DPH* values of the coppers and the alloys and their respective yield strengths, indicating that metallic hardness as measured by this instrument is a direct function of the true yield strength.

8. Therefore, it appears that solute strengthening is caused by solute "yield strengthening" and that the yield strength controls the hardness and strain strengthening value or slope of the log stress-log strain curve through the necking values of strength and deformation, and quite likely to fracture. The yield strength, therefore, becomes the fundamental basis of comparison of the effect of solute elements.

9. The change in yield strength appears to be basically a function of the change in lattice parameter produced by the solute addition. The effect on yield strength appears to be more fundamental than the effect on hardness.

10. Based on the relations developed from the data in this paper, Eq 1 may be rewritten in terms of yield strength and solute concentration to describe the approximate relation of true stress and true strain for the copper base alloys studied.

$$S = (YS + XA)\ (e/0.01)\ \exp\ C/(YS + XA)^n$$

where S and e are the true stress and strain; YS is is the yield strength of copper at a strain of 0.01 (7200 psi); X is the atomic percent of the solute; A is a constant characteristic of the solute; and C and n are independent constants describing strain hardening in copper or copper base alloys, and equal to 4.50 ± 0.25 and 0.235, respectively.

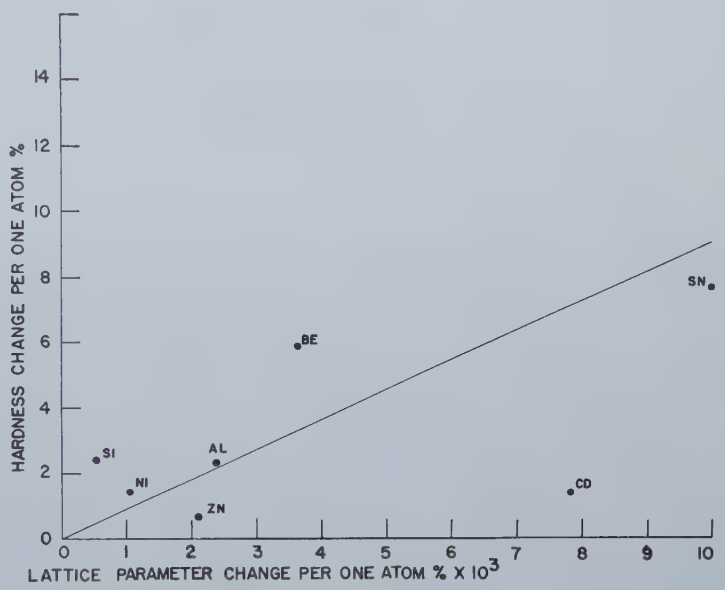

Fig. 8—Effect of Change in Lattice Parameter on the Change in Diamond Pyramid Hardness
as produced by the addition of the indicated solute elements to copper.

Acknowledgment

The authors wish to express their appreciation to Dr. Arthur Phillips for his helpful advice and encouragement; to Dr. Alan Morris and Albert Baldwin of the Bridgeport Brass Co. for the use of metallurgical laboratory facilities; and to C. L. Bulow, who supplied most of the alloys used in this work.

References

[1] C. W. MacGregor: *Trans.* AIME (1937) **124**, 208; *Jnl.* Franklin Inst. (8-1944) **238**, 111.

[2] J. H. Hollomon: *Trans.* AIME (1945) **162**, 268.

[3] J. R. Low, Jr., and T. A. Prater: OSRD Rpt. No. 4052 (1944).

[4] C. E. Lacy and M. Gensamer: *Trans.* ASM (1944) **32**, 88.

[5] J. C. Fisher: MIT Doctor's Thesis and "Anisotropic Plastic Flow", Conf. on Plasticity, Brown Univ., Feb. 1948.

[6] L. R. Jackson, A. M. Hall and A. D. Schwope: *Trans.* AIME **175**. *Metals Tech*, Sept. 1947, TP 2274.

[7] R. M. Brick, D. L. Martin and R. P. Angier: *Trans.* ASM (1943) **31**, 675.

A Preliminary Investigation of the

Zirconium-Beryllium System

By Powder Metallurgy Methods

by Henry H. Hausner

and

Herbert S. Kalish

The powder metallurgical approach was used to study the system Be-Zr since the metals beryllium and zirconium are particularly amenable to powder metallurgy methods and have received wide interest of late. Condition of the specimens after sintering, metallographic examination, and X ray diffraction studies revealed enough information to enable the authors to construct a preliminary phase diagram after only three weeks of experimental work.

IN recent years zirconium and beryllium have become of great interest because of their special properties. Zirconium is known for its remarkable ability to absorb the gases oxygen, nitrogen and hydrogen, has extensive use as a getter in electron tubes and has indeed become the primary metal in the manufacture of photoflash bulbs. Beryllium is of interest because it is light metal and as such could supplement aluminum and magnesium in light metal applications.

The late development of zirconium ductile at room temperature produced by both the iodide and calcium reduction methods has stimulated frequent articles on this metal in the recent literature. Beryllium is so closely akin to zirconium crystallographically that some investigators[1, 2] are of the opinion that beryllium should be ductile at room temperature if it were pure enough.

The crystallographic relationship of beryllium and zirconium, the interest created in Be-Zr alloys where the zirconium is believed to function as a remover of solid solution gas in beryllium and thus increase the ductility of the beryllium rich alloy, and the amenability of these metals to powder metallurgy methods stimulated this approach to an investigation of the system Be-Zr.

Preliminary work showed that a zirconium compact melted when pressed in contact with a beryllium compact and sintered at 1250°C, without any apparent final bond between the two.

A search of the literature revealed nothing pertinent about the Zr-Be system or about any zirconium - beryllium alloys. In 1936 Misch[3] vaguely identified the compound $ZrBe_2$ and reported that it has a deformed cubic structure. Two patents,[4, 5] were issued to Machlett Laboratories in 1943 and in 1946 regarding the addition of small amounts of zirconium to beryllium in order to improve the ductility of beryllium so that it may better be used for X ray windows. In considering the alloy formation of beryllium with other metals Raynor[6] thought it unlikely that zirconium would have any solid solubility in beryllium. From this indefinite information nothing could be ascertained about the possible use of Zr-Be alloys or the use of these metals intimately.

A brief preliminary study of the system Zr-Be by powder metallurgy methods was undertaken to provide regions for more intense studies of Zr-Be alloys and as a guide to a formal phase diagram determination. The investigation described in the following pages was completed in less than three weeks.

The usefulness of this rapid method to facilitate phase diagram studies and new alloy investigations will be shown.

Materials and Procedure

Zirconium powder was produced from crystal bar stock of high purity supplied by Foote Mineral Co. The crystal bar was converted to hydride at 730°C, crushed, and the hydride decomposed in purified argon at 850°C. 60 pct of the powder passed through a 325 mesh screen, 40 pct of the powder was —140 mesh, +325 mesh and the average particle size of the total was 8 to 12 microns.

The beryllium powder was used as re-

HENRY H. HAUSNER is Section Head, and HERBERT S. KALISH is Senior Engineer, Special Products Sect., Metallurgical Laboratories, Sylvania Electric Products Inc., Bayside, N. Y.

New York Meeting, Feb. 1950.

TP 2753 E. Discussion may be sent to Trans. *AIME before Apr. 1, 1950, and is scheduled for publication Nov. 1950. Manuscript received Oct. 17, 1949.*

The work described was done for the Atomic Energy Commission in the laboratories of Sylvania Electric Products Inc. This report is published with permission of the Commission.

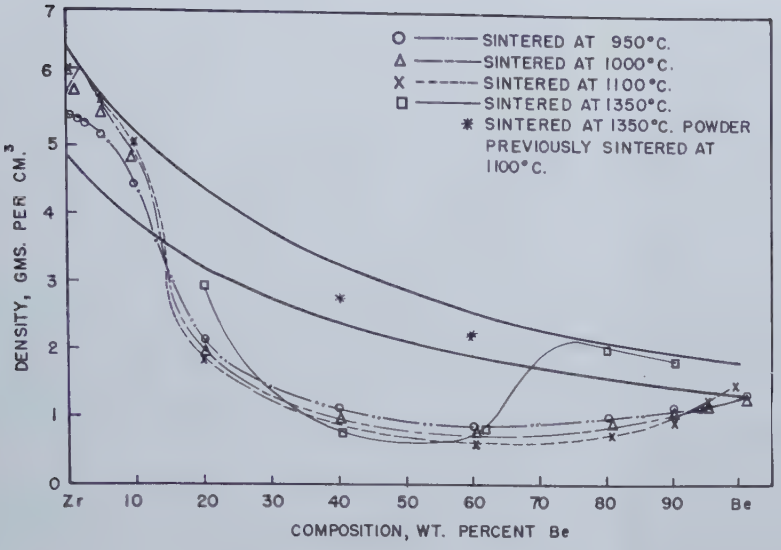

Fig. 1—The Effect of Composition on the Density of Zr - Be Mixtures.

Table I.

Effect of Sintering Zirconium-Beryllium Mixtures at Various Temperatures for 2 hours in Vacuum (0.15μ)

Composition Wt. Pct Zr/Be	Sintering Temp. °C	Sample No.	Density g per cm³			Volume Change on Sintering Percent	Appearance After Sintering
			Theoretical	Pressed at 40 tsi	Sintered		
100/0	950	ZB-2	6.5	4.87	5.43	—10.9	Normal bright
100/0	1000	ZB-1	6.5	4.87	5.7	—15.2	Normal bright
100/0	1100	ZB-3	6.5	4.87	6.12	—21.7	Normal bright
98/2	950	ZB-6	6.18	4.63	5.42	—16.4	Some signs of slight melting
98/2	1000	ZB-5	6.18	4.63	6.11	—24.8	Melted
98/2	1100	ZB-7	6.18	4.63	6.10	—23.6	Melted
95/5	950	ZB-10	5.78	4.33	5.18	—17.6	Some signs of slight melting
95/5	1000	ZB-9	5.78	4.33	5.58	—23.0	Melted
95/5	1100	ZB-11	5.78	4.33	5.69	—23.6	Melted
90/10	950	ZB-14	5.21	3.91	4.37	—12.0	Some signs of slight melting
90/10	1000	ZB-13	5.21	3.91	4.87	—21.1	Some signs of slight melting
90/10	1100	ZB-15	5.21	3.91	4.92	—22.2	Slightly melted
80/20	950	ZB-18	4.33	3.24	2.03	+57.2	Friable
80/20	1000	ZB-17	4.33	3.24	1.97	+61.4	Friable
80/20	1100	ZB-19	4.33	3.24	1.91	+68.3	Friable
80/20	1350†	ZB-20	4.33	3.24	2.94	—9.2	Slightly melted*
60/40	950	ZB-22	3.24	2.43	1.098	+113.2	Very friable
60/40	1000	ZB-21	3.24	2.43	0.98	+131.7	Very friable
60/40	1100	ZB-23	3.24	2.43	1.01	+135.0	Very friable
60/40	1350†	ZB-24	3.24	2.43	0.84	+171.0	Very friable
40/60	950	ZB-26	2.60	1.95	0.88	+112.0	Very friable
40/60	1000	ZB-25	2.60	1.95	0.75	+135.0	Extremely friable
40/60	1100	ZB-27	2.60	1.95	0.64	+187.5	Extremely friable
40/60	1350†	ZB-28	2.60	1.95	0.76	+109	Very friable
20/80	950	ZB-30	2.16	1.62	1.00	+57.0	Friable
20/80	1000	ZB-29	2.16	1.62	0.88	+78.1	Friable
20/80	1100	ZB-31	2.16	1.62	0.73	+115.0	Friable
20/80	1350†	ZB-32	2.16	1.62	2.11	—35.6	Just above solidus, dense
10/90	950	ZB-34	2.00	1.50	1.18	+32.7	Friable
10/90	1000	ZB-33	2.00	1.50	1.10	+33.1	Friable
10/90	1100	ZB-35	2.00	1.50	1.02	+40.3	Friable
10/90	1350†	ZB-36	2.00	1.50	1.87	—30.00	Melted*
5/95	950	ZB-38	1.92	1.44	1.21	+16.1	Somewhat friable
5/95	1000	ZB-37	1.92	1.44	1.18	+19.4	Somewhat friable
5/95	1100	ZB-39	1.92	1.44	1.27	+10.1	Somewhat friable
5/95	1350†	ZB-49	1.92	1.44	—	—	Formed bubble

* Dense except for gas bubble.
† Specimens at 1350°C sintered for 4 hr.

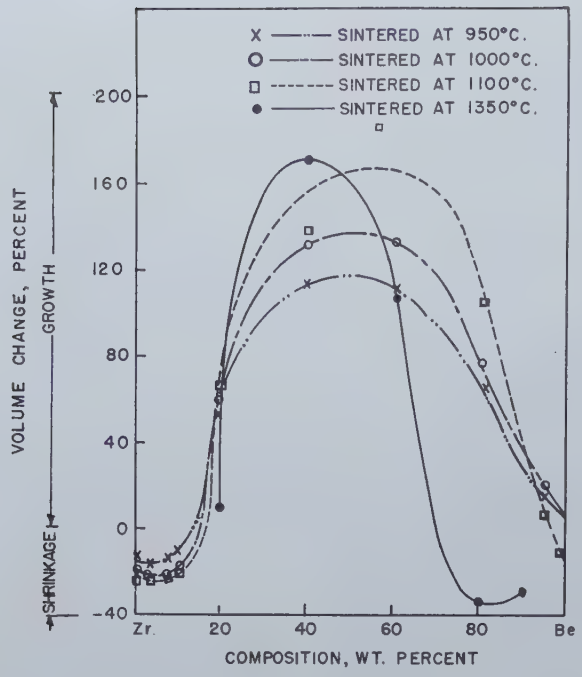

Fig. 2—The Effect of Composition and Sintering Temperature on the Volume Change of Zr-Be Mixtures.

ceived from Brush Beryllium Co. It was all —200 mesh, 17 micron average particle size, and is of the highest purity available.

The beryllium and zirconium were mixed in argon for 2 hr to produce the following compositions: 2, 5, 10, 20, 40, 60, 80, 90 and 95 pct Be. After mixing, the powders were stored in argon until ready for use. Pressing was done in air at 40 tsi to make compacts 0.803 in. in diam, 0.200 in. thick.

The compacts were packed in beryllia powder in a beryllia boat and sintered in vacuum at 950, 1000, and 1100°C, for 2 hr and 1350°C for 4 hr. The vacuum reached 1.5 x 10^{-4} mm Hg or better at the sintering temperature in all runs. It took from 3½ to 5 hr to reach the desired temperature and about 20 hr to cool the specimens in the furnace to below 100°C.

Results of Sintering

The appearance of the samples after sintering, the dimensional changes, and the densities at each temperature indicate the type of alloying which occurs in the Zr-Be system. From table I it can readily be seen that some slight melting occurs between 2 and 10 pct Be at 950°C. At 1000°C the 2 and 5 pct Be mixtures appeared completely molten. It is likely, therefore, that the liquidus line at these compositions is slightly below 1000°C. It may be concluded, from even this cursory examination, that

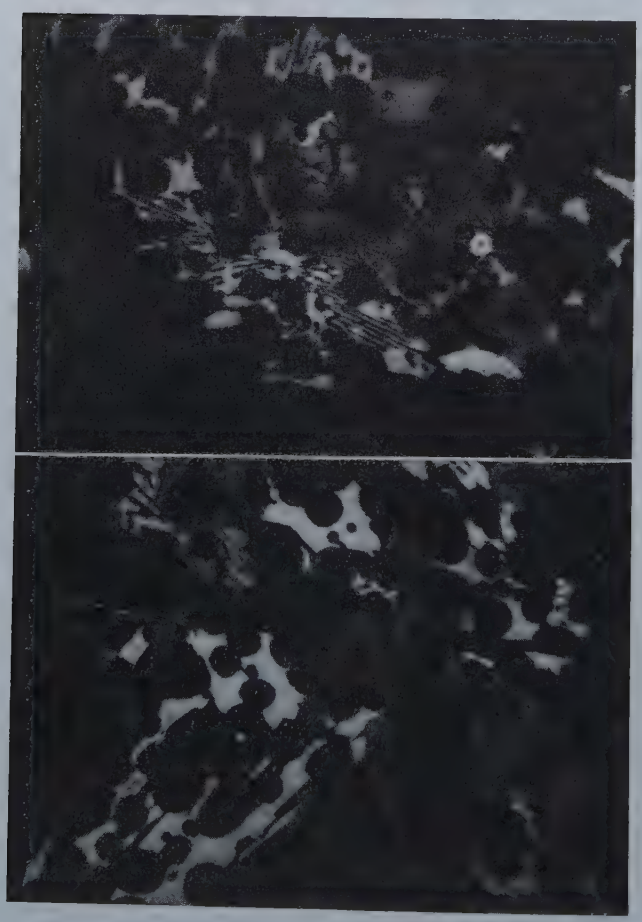

Fig. 3 and 4—Sintered Zirconium-Beryllium Mixtures.

Pressed at 40 tsi. Sintered in vacuum (0.15μ) at 1100°C for 2 hr. 250X. Polarized light. Unetched. Fig. 3 (above)—98 pct Zr—2 pct Be. Top regions of sample. Fig. 4 (below)—98 pct Zr—2 pct Be. Bottom regions of sample. Both micrographs slightly reduced in reproduction.

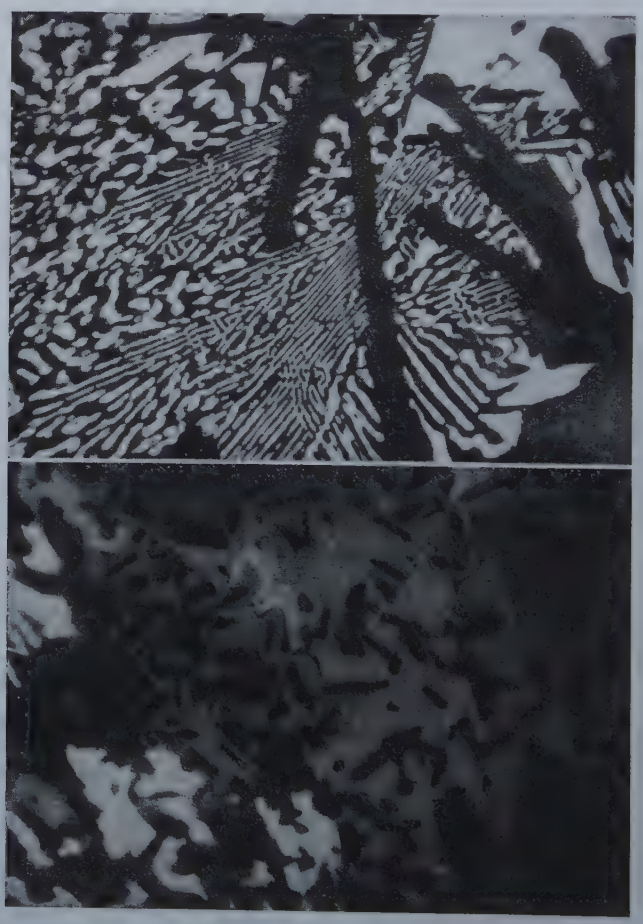

Fig. 5 and 6—Sintered Zirconium-Beryllium Mixtures.

Pressed at 40 tsi. Sintered in vacuum (0.15μ) at 1100°C for 2 hr. 250X. Polarized light. Unetched. Fig. 5 (above)—95 pct Zr—5 pct Be. Top regions of sample. Fig. 6 (below)—95 pct Zr—5 pct Be. Bottom regions of sample. Both micrographs slightly reduced in reproduction.

a eutectic exists somewhere between 2 and 10 pct Be and that the melting point of the eutectic is somewhat less than 950°C.

The slight amount of melting which occurs after 4 hr at 1350°C indicates that the 20 pct Be alloy is above the solidus at this temperature. The very friable product from sintering the 40 and 60 pct Be alloys at 1350°C implies that the melting point of these compositions is quite high. Melting occurred in the high beryllium alloys, i.e. 80 pct Be and higher, at 1350°C, but 1100°C appeared to be well below the melting point of these alloys. There is, then, no suggestion of eutectic melting of the beryllium rich alloys.

To substantiate these ideas the data of table I, viz. densities and volume change, have been plotted as functions of composition at the four sintering temperatures. Fig. 1 clearly shows the approach of the 2 and 5 pct alloys, particularly 2 pct Be, to the theoretical density even at 1000°C indicating the completeness of the degree of melting. Beyond this composition the mixtures demonstrate a greater deviation from theoretical density until there is as much as 80 pct Be present when the density again approaches theoretical, but only at 1350°C. From 20 to 60 pct Be the mixtures have final densities less than the as-pressed condition inferring growth on sintering, the amount of growth increasing with

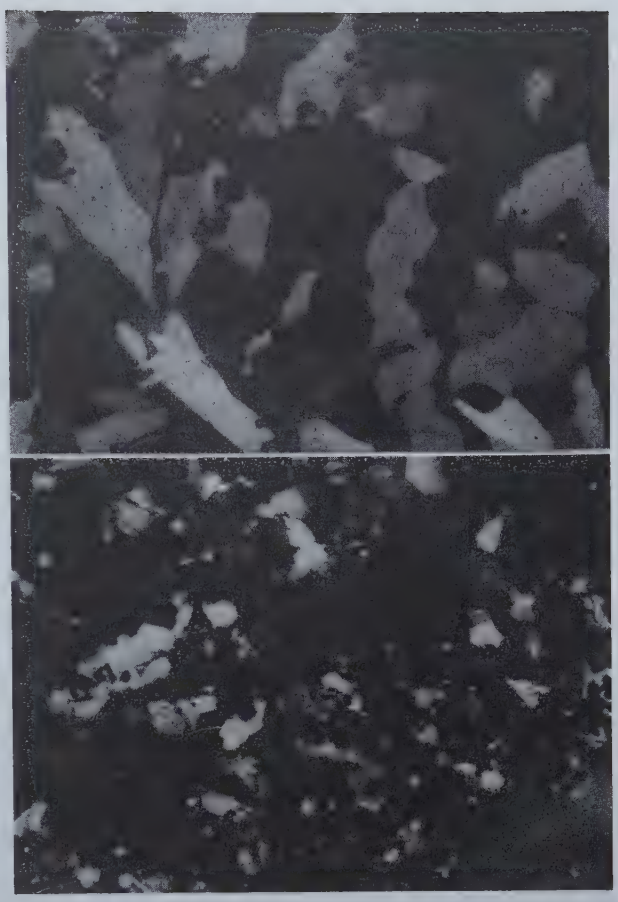

Fig. 7 and 8—Sintered Zirconium-Beryllium Mixtures.

Pressed at 40 tsi. Sintered in vacuum (0.15μ) at 1100°C for 2 hr. 250X. Polarized light. Unetched. Fig. 7 (above)—90 pct Zr—10 pct Be. Fig. 8 (below)—80 pct Zr—20 pct Be. Slightly reduced in reproduction.

higher sintering temperature. This is clarified further in fig. 2 where the amount of growth and shrinkage can be readily observed.

The remarkable growth of the alloys in the vicinity of 40 to 60 pct Be indicates the formation of a high melting point phase probably accompanied by a considerable change in volume due to a large alteration of the crystal structure from that of the original components. Even at 1350°C no indications of sintering have been observed. If some of the powder from the friable sintered compact is repressed and sintered at 1350°C it will result in a fairly well sintered alloy as shown in fig. 1 for the 40 and 60 pct Be compositions.

Metallographic Examination

The structure of the Zr-Be alloys is well revealed in the as-polished condition in polarized light. Fig. 3 shows the eutectic structure present in a 2 pct alloy. This eutectic appears to be a mixture of Zr rich solid solution, α, and a second phase which will be called γ. The α phase polarizes and is brown in appearance. The Zr without Be in solid solution in sufficient amounts does not polarize. This shows up frequently as dark areas in the center of the α phase grains demonstrating that equilibrium had not been attained. The bottom regions of the speci-

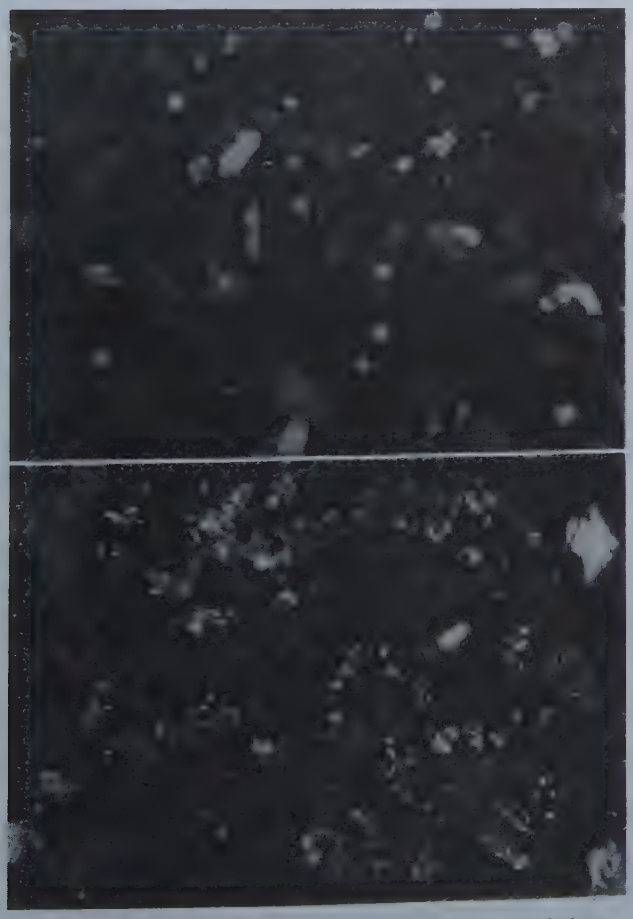

Fig. 9 and 10—Sintered Zirconium-Beryllium Mixtures.

Pressed at 40 tsi. Sintered in vacuum (0.15μ) at 1100°C for 2 hr. 250X. Polarized light. Fig. 9 (above)—100 pct Zr. Etched. Fig. 10 (below)—5 pct Zr—95 pct Be. Unetched. Both micrographs slightly reduced in reproduction.

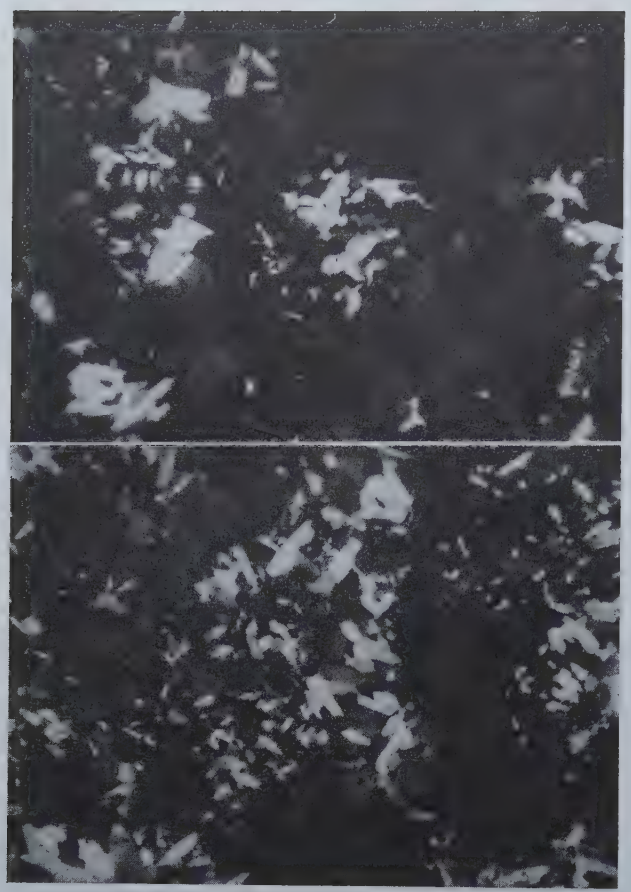

Fig. 11 and 12—Sintered Zirconium-Beryllium Mixtures.

Pressed at 40 tsi. Sintered in vacuum (0.15μ) at 950°C for 2 hr. 250X. Polarized light. Unetched. Fig. 11 (above)—98 pct Zr—2 pct Be. Fig. 12 (below)—95 pct Zr—5 pct Be. Both micrographs slightly reduced in reproduction.

men, fig. 4, did not reveal as much lamellae as the top portions, fig. 3. Undoubtedly the specimen was well in the mushy state so that the less dense beryllium rich liquid ascended to the top of the sample bringing it closer to the eutectic composition. At the bottom of the compact the molten phase solidified in between the solid grains of α phase and formed very little lamellar structure. Actually the amount of γ phase in the bottom portion of the specimen is only slightly less than the amount of this phase in the top regions as indicated by the white to grey appearance of the γ phase as compared to the brown color of the α phase.

The 5 pct Be alloy had large amounts of eutectic present after sintering at 1100°C, fig. 5. Again the bottom regions of the sample, fig. 6, did not reveal the lamellar structure and the explanation is quite the same as given above for the 2 pct alloy. It is difficult to ascertain whether any proeutectic γ phase is present even in the 10 pct Be alloy, fig. 7, but from the degree of melting as observed in table I it appears reasonable to conclude that the eutectic composition is in the vicinity of 5 pct or perhaps less Be. The lack of lamellae in the 10 pct alloy can be attributed to the fact that this alloy melted only slightly.

Examination of the structure after sintering at 950°C, fig. 11 to 14, reveals the presence of amounts of γ phase characteristic of the mixtures after sintering at 1100°C. No lamellae were present, however, after sintering at the lower temperatures.

A friable expanded compact resulted from sintering the 20 pct Be mixture at 950, 1000, and 1100°C. Thus the large number of voids present in fig. 8 and 14 makes the structure difficult to interpret. It would appear that the structure is a single phase affair composed entirely of γ phase. After sintering for 4 hr at 1350°C, however, two phases can definitely be distinguished with some evidence of a third phase as shown in fig. 15. The matrix phase is the light polarizing one identified as γ phase. The darker polarizing grains in the matrix are referred to as δ phase. The third phase in question is that composed of the very small angular grains within the matrix. At times these grains have an excellent parallelogram configuration. It is likely that this is also δ phase which crystallizes out of the γ rich liquid. The polarizing characteristics and color of these crystallites is very similar to that of the δ phase.

Sintering 40 and 60 pct Be mixtures at 1350°C resulted in a very friable compact which could not be examined metallographically. The powder produced by heating these mixtures at 1100°C was pressed and sintered at 1350°C to produce a speci-

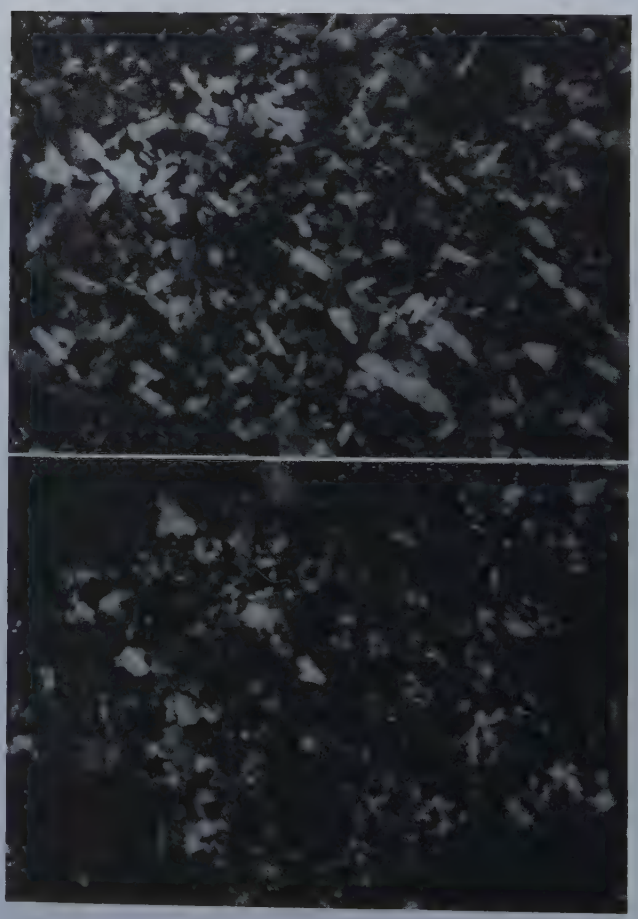

Fig. 13 and 14—Sintered Zirconium-Beryllium Mixtures.

Pressed at 40 tsi. Sintered in vacuum (0.15μ) at 950°C for 2 hr. 250X. Polarized light. Unetched. Fig. 13 (above)—90 pct Zr—10 pct Be. Fig. 14 (below) 80 pct Zr—20 pct Be. Both micrographs slightly reduced in reproduction.

men which had appreciable shrinkage on sintering and was not friable. Fig. 16 through 19 show the microstructure of these specimens. In fig. 16 a single phase polarizing structure is present which cannot definitely be distinguished from the δ phase, but which appears to have stronger polarizing characteristics. X ray evidence which will be presented later proves that this is indeed a single phase structure different from the δ phase and which will be called the ϵ phase. Notice the large number of voids and cracks shown in fig. 17 indicating that even at 1350°C the alloy was far below the melting point or a suitable temperature for sintering.

When 60 pct Be is present sintering is somewhat better, fig. 19, but a large number of voids and cracks are still present. The phase present at this composition is entirely new. It is nonpolarizing and appears black under polarized light, fig. 18, except for the presence of cracks and voids. This shall be called η phase. The large rectangular grain in the upper left of fig. 18 and 19 is unusual as to size only. The sharp angular configuration of the grains is a typical characteristic of η phase.

At 80 pct Be, fig. 20, a matrix of Be or Be-rich solid solution is produced which shall be referred to as θ phase, containing the angular grains of η phase. This matrix is identical in appearance to pure Be. It is composed of very large grains. A θ-θ phase grain boundary is shown in fig. 20. The 90 and 95 pct Be compositions are identical to the 80 pct mixture except that there are fewer grains of η phase present with increasing Be content.

X Ray Diffraction Studies

X ray analysis of all the compositions studied revealed the presence of six different phases (at room temperature) across the Zr-Be system. Table II shows the results of X ray diffraction work on several compositions which had been sintered at 1100°C and other compositions sintered at 1350°C. Where X ray data are available at both sintering temperatures the higher is the most significant since a longer time at temperature was used and the higher temperature in conjunction with slow cooling should give a good approach to an equilibrium structure.

The α phase is merely Zr or Zr containing Be in solid solution. The θ phase is Be or Be-rich solid solution. These two phases are hexagonal close packed. Of the other four phases only one has been identified structurally. It is the η phase which is simple cubic and may be an intermetallic compound or the product of a peritectic or monotectic reaction.

No attempt was made to determine the exact composition or formation temperature of these phases because of the preliminary nature of this work. In addition where the crystal structure appeared to be complex it was not ascertained.

To better show the location of the various phases a hypothetical phase diagram, fig. 24, was made on the basis of condition of specimens after sintering, microstructure, and X ray data. No point on this diagram is meant to be definite except within very broad limits.

The eutectic reaction at the Zr-rich end of the diagram is quite apparent from the low temperature melting and appearance of the microstructure in this range. The reactions for formation of the γ, δ ϵ, and η phases are uncertain, but their location

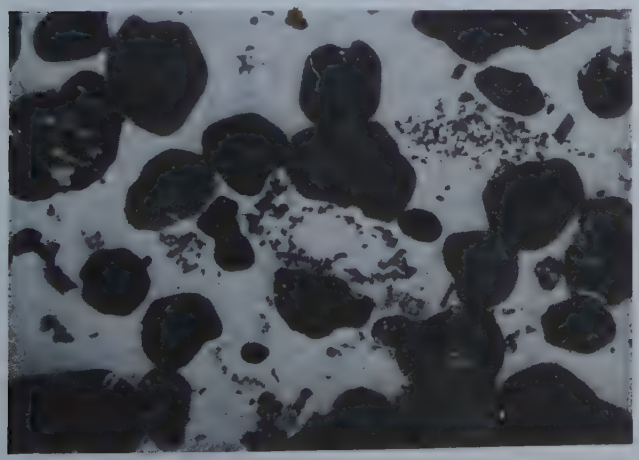

Fig. 15—Sintered Zirconium-Beryllium Mixtures.

Pressed at 40 tsi. Sintered in vacuum (0.15μ) at 1350°C for 4 hr. 250X. Polarized light. Unetched. 80 pct Zr—20 pct Be. Slightly reduced in reproduction.

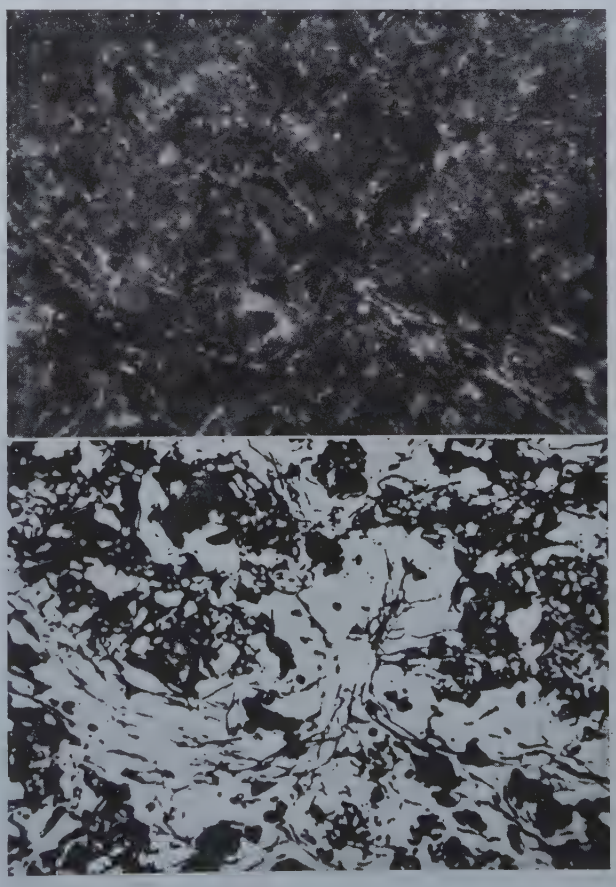

Fig. 16 and 17—Sintered Zirconium-Beryllium Mixtures.

Pressed at 40 tsi. Sintered in vacuum at 1100°C. Friable compact powdered, repressed, and sintered in vacuum (0.10μ) at 1350°C for 4 hr. 250X. Unetched. Fig. 16 (above)—60 pct Zr—40 pct Be. Polarized light. Fig. 17 (below)—60 pct Zr—40 pct Be. Bright field. Same field as Fig. 16. Both micrographs slightly reduced in reproduction.

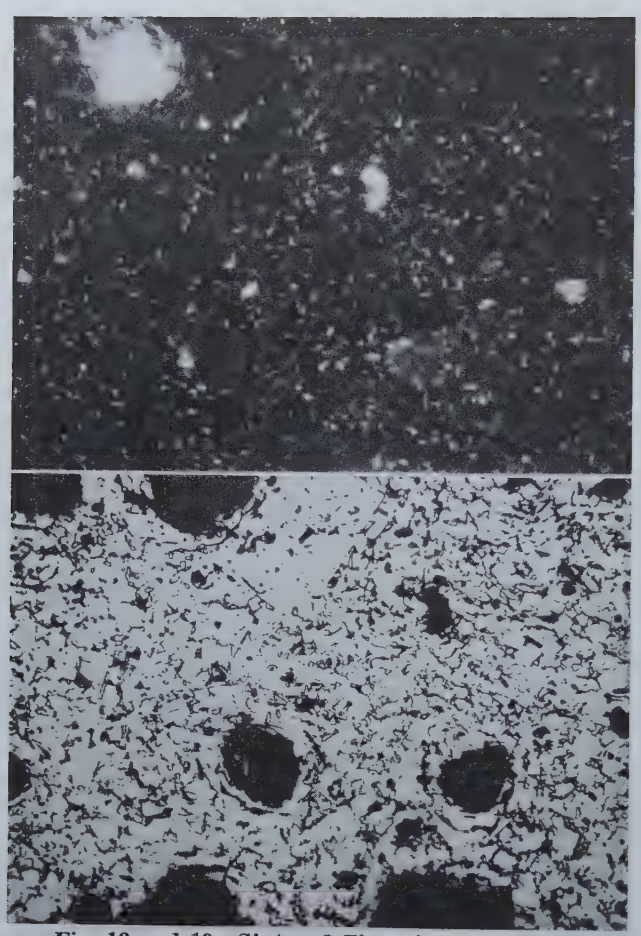

Fig. 18 and 19—Sintered Zirconium-Beryllium Mixtures.

Pressed at 40 tsi. Sintered in vacuum at 1100°C. Friable compact powdered, repressed and sintered in vacuum (0.10μ) at 1350°C for 4 hr. 250X. Unetched. Fig. 18 (above)—40 pct Zr—60 pct Be. Polarized light. Fig. 19 (below)—same field. Bright field. Both micrographs slightly reduced in reproduction.

with regard to composition has been approximately determined from X ray study and microstructure. It appears certain from the microstructures and decrease in melting point with increasing Be content from 60 to 100 pct that no important eutectic reaction occurs at the Be-rich end of the phase diagram. Probably a eutectic or peritectic occurs very close to 100 pct beryllium, but this cannot be decided until an exact determination of the invariant line between the $\eta + L$ and $\eta + \theta$ fields is made. Tentatively the invariant line is placed slightly below the melting point of Be and a eutectic is indicated in fig. 24.

Similarly there is no proof for the peritectic reaction $\beta + L \rightarrow \alpha$, but only this or a eutectic reaction could occur to accompany the α to β transformation in zirconium. It seems more logical to assume tentatively a peritectic reaction since it would tend to indicate a larger α solid solution field. The existence of a rather extensive solid solubility is inferred by the quite obvious alteration in amount of Be from the outside to the center of α grains in fig. 3 and 4.

The γ phase can be very nicely located to coincide with the $ZrBe_2$ intermetallic compound reported by Misch[3]. More X ray data are needed to substantiate this premise, however.

Conclusions

From preliminary study of the Zr-Be system there are indications that some interesting alloys can be developed. The system contains a relatively low melting point eutectic and several high melting point phases. The influence of small amounts of zirconium in beryllium could be most important in the powder metallurgy of beryllium rich alloys since the zirconium would increase the melting point while the solidus line remained at approximately 1280°C. Furthermore the presence of η phase might influence the ductility of beryllium rich alloys.

As yet virtually nothing is known about the properties of these alloys. Their physical and mechanical properties should be determined. To precede or coincide with this a more intensive study of the Zr-Be phase diagram is indicated so that proper fabrication methods can be ascertained.

It has been shown that a provisional phase diagram, useful in the study of new alloy systems, can be determined rapidly by powder metallurgy methods.

Table II. X Ray Analysis of Zirconium-Beryllium Mixtures Sintered for 2 hours at 1100°C and 4 hours at 1350°C in Vacuum (0.15μ)

Composition Wt. Pct Zr per Pct Be	Sinter Temp. °C	α Phase HCP Normal Zr Pattern	γ Phase	δ Phase	ϵ Phase	η Phase Simple Cubic	θ Phase HCP Normal Be Pattern	BeO	Unknown
100/0	1100	*vs* (pure Zr)							
98/2	1100	*vs*	*m*					*w*	
90/10	1100	*m*	*vs*						
80/20	1100		*vs*	*m*					
80/20	1350		*vs*	*m*					
60/40	1100		*m*(?)	*s*	*vs*				
60/40	1350				*vs*				
60/40	1350*				*vs*				
40/60	1100					*vs*			
40/60	1350				*m*	*vs*			
40/60	1350*					*vs*			
20/80	1350					*vs*	*w*+		*vw*
10/90	1350					*vs*	*m*		*vw*
5/95	1100					*vs*	*s*		
5/95	1350					*vs*	*m*		

* Sintered at 1100°C, powder from friable compact pressed and sintered at 1350°C.
η phase has a simple cubic structure. The structure γ, δ, and ϵ phase has not been determined.

vs — very strong
s — strong
m — medium
w — weak
vw — very weak

Acknowledgments

We wish to thank H. W. Woods for his preparation of metallographic specimens and micrographs, G. A. Davis and V. M. Hannaford for the X ray diffraction studies, and B. H. Alexander and I. N. Zavarine for discussing and assisting in the interpretation of these data.

We are particularly indebted to W. E. Kingston for numerous valuable discussions and suggestions regarding this work.

Fig. 22 and 23—Sintered Zirconium-Beryllium Mixtures.

Pressed at 40 tsi. Sintered in vacuum (0.10μ) at 1350°C for 4 hr. Fig. 22 (above)—5 pct Zr—95 pct Be. Polarized light. Unetched. Fig. 23 (below)—5 pct Zr—95 pct Be. Bright field. Etched. Both micrographs slightly reduced in reproduction.

Fig. 20 and 21 (left)—Sintered Zirconium-Beryllium Mixtures.

Pressed at 40 tsi. Sintered in vacuum (0.10μ) at 1350°C for 4 hr. 250X. Polarized light. Unetched. Fig. 20 (above)—20 pct Zr—80 pct Be. Fig. 21 (below)—10 pct Zr—90 pct Be. Both micrographs slightly reduced in reproduction.

Fig. 24—A Hypothetical Zr-Be Phase Diagram.

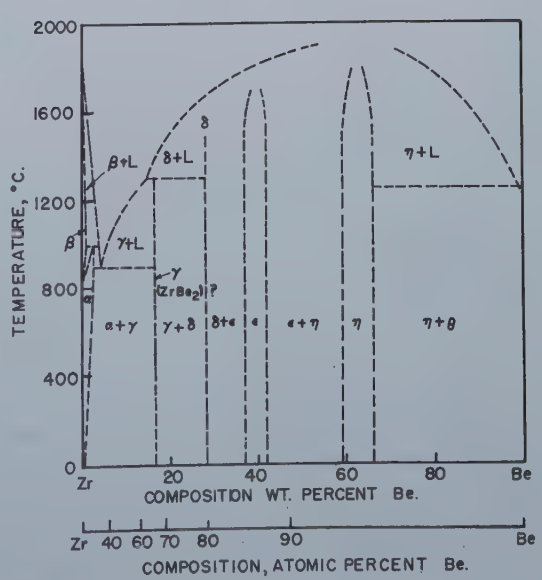

References

[1]H. A. Sloman: Researches on Beryllium. *Jnl.* Inst. Metals (1932) **44**, 365-391.

[2]G. E. Claussen and J. W. Skehan: Malleable Beryllium. *Metals and Alloys,* Apr. 1942, pp. 599-603.

[3]L. Misch: Crystal Structure Examination of Some Alloys. *Metallwirtschaft* (1936) **15**, 163-166.

[4]G. E. Claussen: Beryllium Alloys Suitable for Rolled Vacuum-tight X ray Windows. Patent issued to Machlett Labs., U.S. 2,306,592, Dec. 29, 1943.

[5]G. E. Claussen: Structure Comprising Be Windows for X-ray Tubes. Patent issued to Machlett Labs., U.S. 2,394,984, Feb. 19, 1946.

[6]G. V. Raynor: Beryllium, Beryllium Alloys and the Theoretical Principles Affecting Alloy Formation with Beryllium. *Jnl.* Roy. Aeronaut. Soc. (1946) **50**, 390-415.

Fundamental and Practical Factors in

Ammonia Leaching of Nickel and Cobalt Ores

by M. H. Caron

As indicated in the title, this article gives brief statements of investigations of various fundamental and practical factors of the ammonia leaching process for nickel and cobalt ores.

The process was in large scale operation at Nicaro, Cuba, as an emergency measure in World War II.

Descriptions of this plant and its operation have been published but these descriptions mainly covered installation and working scale results, and the present article gives a considerable amount of hitherto unpublished data on various phases of the method, including conditions for ore reduction, leaching, distillation, etc.

Possibilities as to further development and results of tests on ores other than the Cuban laterites are also included.

BASIC U. S. Patent 1,487,145 on ammonia leaching of nickel ores was issued to the author on March 18, 1924. Equivalent patents in other countries were obtained later.

The Dutch Syndicate Brikcarbo became interested in the process in 1935; and a couple of years later the late Dr. H. Foster Bain sent samples of Surigao laterite iron ore to Delft and witnessed tests made there on this material for the Philippines Commonwealth. As a result, the author was asked in April 1940 by Dr. Bain to go to the Philippines to erect and take charge of a pilot plant for the process. The World War prevented carrying out this proposal. The Dorr Co. also became interested in the process at about the same period.

The investigations by the Freeport Sulphur Co. on the process as applied to the Cuban nickeliferous laterites, which resulted in the Nicaro enterprise, and the results of this operation have been well described elsewhere.[1, 2, 3, 4, 5] This Nicaro plant was in operation for almost two years, and during this period produced about 10 pct of the world nickel production from laterites containing 1.35 pct nickel. This plant and its operation were war measures and, in view of this, activities were suspended in April 1947.

The results obtained fully demonstrated the technical feasibility of the process and its economical aspects on a commercial scale. In this respect, it should be understood that it is probable that improvements may be made by further development, and that there are possibilities for advantageous application of the process to garnierite and similar ores with higher values in nickel than the laterite iron ores at Nicaro.

While the articles cited above have given a certain amount of information, no general article containing all the important process data has been published. Since the process is of more than local interest, a fuller knowledge of the fundamental and practical factors of the method may be welcome to those interested in this new field of metals technology. The author, accordingly, takes pleasure in submitting this article to the AIME as it represents in a condensed form the results of many years of research. The brief outlines of the fundamental and other factors and the explanation of observed phenomena are presented with as little discussion of details as possible, consistent with clarity. It is a special satisfaction to the author to make some contribution of his own in return for the benefits of the many valuable publications issued by the Institute during his thirty years of membership.

Ores Adapted for Ammonia Leaching: All nickel and cobalt ores which originate from weathering of peridotites or similar basic rocks having sufficient values are suitable for treatment by the ammonia leaching process after a preliminary reduction under proper conditions.

The formation of these deposits was probably as follows:

In the course of time the basic rocks were attacked by atmospheric agencies; MgO and SiO_2 were gradually leached out, and secondary nickel minerals formed, such as garnierite, a hydrated silicate of nickel and magnesia. These secondary products are, however, not stable. They decompose in a further stage of weathering and ultimately only a relatively small residue of insoluble oxides remains, known as laterite iron ore with a small nickel content and very little cobalt. Under these mantles of laterite, richer nickel values may be found, usually indicated by the occurrence of garnierite. The more the ore is disintegrated by nature, the higher the iron content and the better the nickel extractions that may be expected therefrom.

Table I shows extractions that may be expected from different types of ores, assuming treatment of -200 mesh products and that all precautions have been taken for obtaining maximum extractions.

As for the distribution of the various nickel minerals and compounds that may be present, great variations may occur from locality to locality as well as vertically in a deposit. From such "run of

M. H. CARON, Member AIME, is Professor of Metallurgy, Delft Univ., Delft, Holland; and Metallurgical Adviser, Billiton Co.

AIME New York Meeting, Feb. 1950.

TP 2739 D. Discussion (2 copies) may be sent to Transactions *AIME before Apr. 1, 1950, and is tentatively scheduled for publication Nov. 1950. Manuscript received Sept. 20, 1949.*

mine" ore, normally quite disintegrated, nickel extractions well over 90 pct may be expected with proper treatment.

Table I. Extractions from Ores

Type of Ore	Nickel Extraction, Pct
Massive dark green pure serpentine, Ni up to 6 pct or more	80 or somewhat more
Chrysoprase	85-90
Garnierite	90 and more
Glassy type of chocolate ore	95-98
Earthy type of chocolate ore	98
Variegated clay (laterite)	98-99
Asbolan (a manganese-cobalt-nickel ore)	Nickel 99, cobalt 95-97

Physical Nature and Chemical Composition of the Ore: It has been pointed out above that the grade and chemical composition of the ore as found in garnierite deposits may show great variations.

Garnierite itself may be: (1) of a high siliceous type, (2) of the normal type, or (3) it may have a high magnesia content. Analyses of these different types are shown as follows:

GARNIERITE TYPES

	High silica, Pct	Normal	High magnesia
Ni	4.56	5.03	4.62
Fe	2.44	4.90	9.76
SiO_2	83.6	58.82	44.6
MgO	3.41	17.0	24.54

The following screen analyses were made from a sample of selected garnierite ore from Celebes:

Mesh	Pct of total weight	Ni	Fe	MgO
— 2 in. + 5 mesh	42.1	6.18	7.12	16.73
— 5 mesh + 20 mesh	27.6	6.77	7.58	15.84
— 20 mesh + 100 mesh	15.8	6.79	10.92	12.38
—100 mesh (fine sand)	5.5	6.10	18.05	9.47
—100 mesh (slimes)	9.0	5.93	22.08	8.09

The above indicates that the finest products show the highest iron and lowest magnesia content, and hence represent the most advanced state of weathering.

In addition to ores that may be selected from their green color, lower grade brown-colored ores not adapted to selection may be abundantly present. They are rather disintegrated and are made up of a mixture of soft lumps and earthy material. The porous nature of the lumps results in light weight and gives an indication of medium nickel values. Hard boulders of little decomposed, valueless, basic rock, may also be present; however, by simply rejecting these boulders a reasonably fair grade of ore containing approximately 3 pct nickel may be mined in bulk. This type is represented in Table II.

The —60 mesh product had a grainy appearance. A settling test at 20°C, ratio 1:2.5 indicated that it behaved as free settling material, settling at a rate of 10 cm per hr.

In contrast, the same product ground in a ratio 1:2.5 in a pebble mill took up considerably more water and gained colloidal properties. At ratio 1:2.5 the finely ground pulp was near the compression point and the filter cake obtained from this product on a suction filter had not less than 46 pct moisture. It should be realized that wet milling of such ores would require very large filter areas per unit of ore. The porous lumps can absorb as much as 16 pct moisture, and after grinding also become colloidal in nature. The —2 mm +20 mesh fraction of the ore could take up 44 pct moisture and the —20 mesh +60 mesh fraction 47 pct. It is often assumed that the average moisture content of the ore will be about 25 pct, but it must be remembered that laterite holds more moisture during the rainy season. Even though overburdens of laterites are normally not considered as nickel ore, their value

Table II. Screen Analysis

Mesh	Pct of weight of total sample	Ni Pct	Fe Pct	Insoluble Pct
+ 20 mm lumps	31.4	2.38	7.66	55.8
—20 mm + 10 mm pieces	16.6	2.89	8.74	55.4
—10 mm + 2 mm product	23.8	2.99	10.47	52.6
— 2 mm product	28.9	3.34	17.58	44.7
The —2 mm product was divided into further fractions.				
— 2 mm + 20 mesh	4.65			
—20 mm + 60 mesh	10.86			
— 60 mesh	12.69	3.41	22.68	39.2

may sometimes warrant mining together with the more valuable ores underneath. Sometimes laterites may hold as much as 0.2 pct Co, and, since the cobalt may be extracted simultaneously the value of the clays may be increased greatly. Laterite may be represented by the following analysis: MgO 1.09 pct, SiO_2 17.28 pct, Fe 38.92 pct, Ni 1.15 pct, Co 0.2 pct.

The transition zone underlying laterites is usually lighter in color, disintegrated, and more or less earthy in character and shows often small fragments of garnierite.

The chemical composition is characterized by a considerable increase of magnesia and silica, and a material decrease of iron oxide. The following analysis represents this type of ore taken from the transition zone:

MgO 11.67 pct, SiO_2 35.12 pct, Fe 21.8 pct, Ni 1.91 pct, Co 0.02 pct.

If conditions favor mining such overburdens separately from the more valuable underlying ore, it should be borne in mind that the soft earthy ore of the top layers does not require the same treatment prior to reduction. The former may be reduced immediately while the more valuable garnierite ore should be finely ground preceding reduction. Laterite may hold lumps of valueless chalcedony, but such lumps should be rejected by screening.

Medium Grade Common Nickel Ores: This grade of ore is usually characterized by its brown color and the practically complete absence of true garnierite. The cobalt content is low, probably somewhere between 0.05 to 0.1 pct, and the ore as present in the deposits consists largely of light weight porous lumps that crumble easily and are in a transition stage of disintegration. The silica content is rather high, the iron content medium, and the light weight of the lumps may serve as an indication of medium nickel content.

The following results may be given as an example of such ore:

ANALYSIS

Sample as mined fractions	Pct of weight of total sample	Ni-content in Pct	Fe-content in Pct	Insoluble matter in Pct
+ 20 mm lumps	31.4	2.38	7.66	55.8
— 20 mm + 10 mm pieces	16.6	2.89	8.74	55.4
— 10 mm + 2 mm product	23.8	2.99	10.57	52.6
— 2 mm product	28.2	3.34	17.58	44.7

The products of increased weathering and disintegration correspond with higher iron content as well as with higher nickel content.

The fractions of the above sample were dry ground and were first reduced at 900°C, agitated for 3 hr at room temperature and thereafter the temperature was raised to 60°C and agitation continued for 1 hr in the ratio 1:8. Strength of leach liquor used was 7 pct NH_3, 5.1 pct CO_2. No additions were made to the ore.

The fractions were dry ground to the following size	Pct	Ni-extraction
I + 100 mesh	45.75	79.6
II + 100 mesh	43.75	80.6
III + 100 mesh	42.0	81.1
IV + 100 mesh	37.0	89.5

After the addition of about 1 pct of pyrite to the ore and wet milling to —200 mesh product, extractions between 91 and 94 pct were obtained on all the fractions. For commercial operation this type of ore should be properly ground previous to reduction, and a small amount of pyrite should be added. The beneficial effect of pyrite addition is most pronounced in the case of true garnierite ore, that is for hydrated nickel silicates. The more the weathering and disintegration have advanced, the higher the iron content of the ore will be. A greater part of the nickel becomes less bound to its compounds with increased iron content, and the total effect is that extraction of the reduced ore improves. It is therefore obvious that the beneficial effect of addition of pyrite decreases with increase in iron content. This is the reason that after due comminution the final results of all the fractions showed little variations in extraction.

Special Manganese Dioxide Containing Ore: Although this type of ore, occurring in Celebes, may have no commercial significance, it may be of general interest to have an idea of its feasibility for ammonia leaching.

The ore is characterized by its high manganese dioxide content, its moderate nickel content and its rather varying though limited Co-content. Cobalt content may run between 0.2 and 0.5 pct, and is seldom higher. Nickel content may be as high as 4 to 5 pct, but is normally lower. The following sample served for the investigation: MnO_2 26 pct, insoluble about 3 pct, Ni 2.95 pct, Co 0.24 pct, remainder limonite.

This true oxide ore requires a reduction temperature of 800°C for maximum extraction. Manganese dioxide is converted to monoxide, and a Ni-Co-Fe alloy probably containing a small content of manganese is formed. Four percent high volatile coal was added to the ore, which was ground to a —100 mesh product, 34 pct remaining on 200 mesh. With fresh liquor containing 7 pct NH_3 and 5.1 pct CO_2 the reduced ore was leached at room temperature in the ratio 1:5.

Manganese monoxide is slightly soluble in leach liquor. The bulk is quickly converted into insoluble basic-manganese-carbonate. In this way a certain amount of CO_2 is withdrawn from the leachliquor.

The manganese is, however, readily precipitated from the liquor by oxidation as black MnO_2·aq and at the end of agitation the solution is almost free from this impurity. In fact the iron content of the solution is comparatively higher than the manganese content.

The rate of settling of this tailing at 20°C in the ratio 1:5 was 15 mm per hr and at a temperature of 65°C, 35 mm per hr. Increase of temperature of the tailing has a beneficial effect upon the settling rate, as was observed for all the types of ore discussed.

With the addition of 1 pct sodium chloride as solution to the ore, reduction temperature should be lowered from 800° to 725°C. From both nickel and cobalt high extractions may be obtained. Extraction time may no doubt be shortened by a finer grinding.

	Reduced at 800°C, no addition to ore.		Reduced at 725°C, 1 Pct NaCl added to ore.		Reduced at 725°C, no addition to ore.	
	Ni extr.	Co extr.	Ni extr.	Co extr.	Ni extr.	Co extr.
6 hr agitation	88.1		88.8		81.3	
12 hr agitation	97.5	95.4	98.3	98.3	83.4	94.1

Asbolan: This type of mineral may be found in red lateritic iron ores as concretions of various sizes and as a more earthy product. The mineral has a high manganese dioxide content, and cobalt and nickel are both present as oxides. Cobalt is usually in excess of nickel.

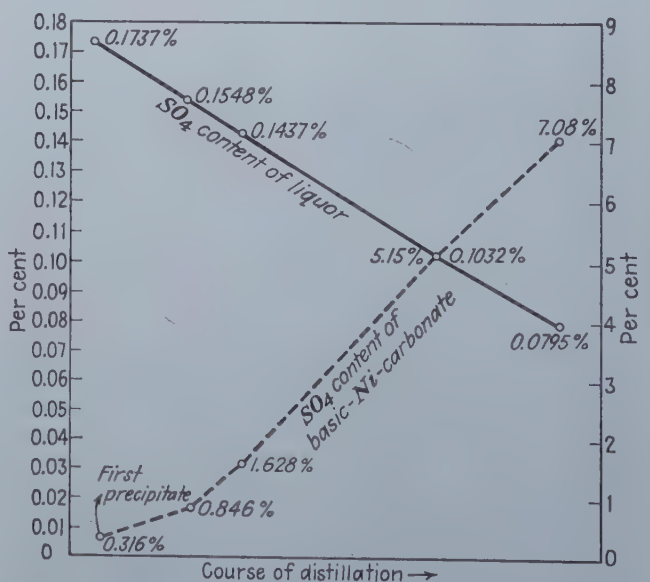

Fig. 1—Change of SO_4 Content of Liquor and Precipitate during the Course of Distillation.

After being ground sufficiently fine, the ore should be reduced at a temperature of about 800°C for maximum extraction. The reduced ore has little tendency to become pyrophoric after being cooled to room-temperature and exposed to the air, as was also observed for the manganese dioxide ore from Celebes. The sample of asbolan was ground to a

—140 mesh product prior to reduction. In the reduced state it was agitated with fresh leach liquor at room temperature for 8 hr in a ratio 1:20.

Analysis of the ore: Ni 3.85 pct, Co 8.80 pct.

Strength of leach liquor NH_3 7 pct, CO_2 5.1 pct.

Another asbolan sample with somewhat lower values was agitated in the reduced state in a ratio 1:5 with fresh leach liquor containing 7 pct NH_3 and 5.1 pct CO_2.

The metal value of the liquor after agitation was 0.80 pct Ni and 1.25 pct cobalt.

Pregnant liquors of such metal values may be obtained by treating high grade ores under countercurrent leaching conditions. It should be realized that the metal values indicated above are fairly high and the liquor may be considered as a pregnant liquor that should be distilled. In such a case 5 tons of pregnant liquor would be distilled for each ton of high grade asbolan ore treated.

Other Types of Oxide Ores: It is hardly necessary to say that the ammonia leaching process may also prove feasible for other types of oxide ores, e.g., the cobalt-containing magnetites, as found in Cornwall, Pa., or the more complex manganese dioxide ores of the Gibellini type containing nickel, cobalt, copper, zinc, molybdenum and vanadium. The first three metals of the complex ore may probably be extracted simultaneously. As yet no tests have been made on these ores by the author, but it is likely that results will indicate the feasibility of ammonia leaching.

Following are brief statements of various fundamental factors connected with reduction, the first main step of the process:

Reducibility of Hydrated Silicates of Nickel and Magnesia: Metal oxides if combined with silica as waterfree silicates do not behave as free oxides, as can be gathered from the fact that the reduction therefrom in the solid state is far more difficult to accomplish.

Experimentally it has been found that such hydrated silicates if heated in a current of reducing gas are readily reduced, although not quite as easily as the free oxide of nickel. The first reduction to metal takes place at a temperature of about 450°C and further reduction will proceed gradually with rise of temperature.

In addition it was observed that effective reduction could be accomplished with gases very lean in reducing constituents. The nickel oxide in these compounds no doubt is rather loosely bound to silica and magnesia. On heating hydrated silicates, the bulk of combined water is expelled below 650°C, and at 950°C a waterfree silicate may be obtained.

After such a heat treatment without simultaneous reduction, experiments showed that most of the nickel reached a state that could not be further reduced even in a current of hydrogen gas at 950°C, as illustrated by the results listed below.

Two —140 mesh garnierite samples were both subjected to the following treatments: 1. Samples were gradually heated right from the start in a hydrogen current up to 950°C. 2. They were first gradually heated in a CO_2 current up to 950°C prior to reduction. At 950°C a hydrogen current was passed over the ore for some time.

Both samples were cooled in a hydrogen current to room temperature (20°C).

RESULTS

No.	Reduced at 800°C, no addition to ore		Reduced at 800°C, 2 Pct FeS_2 added to ore		Reduced at 700°C, 1 Pct NaCl added to ore		Reduced at 700°C, no addition to ore	
	Ni-extr.	Co-extr.	Ni-extr.	Co-extr.	Ni-extr.	Co-extr.	Ni-extr.	Co-extr.
Hr Agitation	99.2	95.9*	99.9	97.0	98.7	96.1	94.7	94.7

* 0.027 pct manganese was present in the leach liquor after 8 hr agitation. This amount could have been further depressed by increasing the temperature of the pulp and addition of pyrite to the ore prior to reduction.

Extractions obtained by using strong leach liquors:

Sample	Mineral	Nickel extraction Pct		Chemical composition	
		Condition(1)	Condition(2)	MgO pct	Ni pct
I	pure garnierite	83.9	20.9	20.4	10.52
II	pure garnierite	80.1	28.5	12.81	7.52

The detrimental effect of preheating the samples without simultaneous reduction is evident from the above figures. Among the hydrated nickel silicates, a mineral that is almost free from magnesia has been found in Saxony known as "Rothisiet". It was of interest to learn how this mineral would behave under similar conditions.

A —140 mesh pure "Rothisiet" sample was therefore reduced under conditions (1) and (2), with the following result:

Mineral	Nickel extraction		Chemical composition	
	Condition(1)	Condition(2)	MgO pct	Ni pct
pure "Rothisiet"	87.1	85	1.45	19.16

This result differs entirely from the previous results, which were obtained with normal garnierite samples containing quite some magnesia. In the almost magnesia-free "Rothisiet" sample, obviously nickel oxide was combined only with silica.

As nickel oxide is a very weak base, it is no doubt loosely bound to silica and will remain reducible in this combination, even after being subjected to a preliminary heat treatment as indicated under (2). However, whenever strongly basic magnesia is present as in normal garnierite samples, the effect of a heat treatment as indicated under (2) will be such that the strong as well as the weak base will become strongly combined with silica and the NiO will be-

come largely unreducible. The result is consequently a very low extraction of nickel.

In order to avoid formation of unreducible compounds of nickel, it is of importance to know to what temperature the ore may be heated without becoming sensitive to this detrimental effect. If garnierite has been preheated prior to reduction to 650°C, only a slight decrease in extraction has been observed. At 750°C the nickel-extraction decreases somewhat but further increase in temperature reduces nickel-extraction even more. At the same time it was found experimentally that the solubility of magnesia in the leach liquor decreases rapidly above 750°C. Indications are therefore that both MgO and NiO rapidly become more tightly bound to silica with temperature increase. The following results are indicative:

	Straight reduction with rise of temperature to 950°C	Preheated prior to reduction in CO_2 current			
		to 650°C	to 750°C	to 850°C	to 950°C
Ni extraction	82.8	80.4	76.1	44.—	19.8

These results were obtained from a —140 mesh garnierite sample (Ni 9.03 pct) reduced by a current of hydrogen under conditions as indicated above. Extractions were obtained with lukewarm strong ammonia liquor. Obviously reduction of hydrated silicates of nickel present as normal garnierite, etc., should be started at low temperatures to obtain high nickel-extraction.

Penetration Effect of Reducing Gases in Lumps of Garnierite: Experimental observations have shown that in a relatively short time large pieces of garnierite may be reduced to the core, for they appear completely black on fracture; however, if such reduced samples were ground thereafter to a —200 mesh product, it was seen that the extractions fell short in comparison with samples of the same type of ore reduced in a finely divided state.

The great difference in extraction may be explained by assuming that the reduction inside the ore pieces did not proceed fast enough to avoid formation of some unreducible nickel. The author is of the opinion that this is the actual cause. By very slow increase of temperature during the reduction, the nickel-extraction may be improved; however, from an economical point of view, the reduction of hydrated silicates should be effected in a finely-divided state to get satisfactory nickel extractions.

The Size of Reduced Ore Particles in Connection with Their Leachability: Microscopic examination of leached ore particles may show a dark core if the particles are not sufficiently fine. In such a case the leach liquor has failed to dissolve the nickel in the core.

Silicates such as serpentine, chrysoprase and garnierite, which are respectively macro-, and micro- and cryptocrystalline, will show satisfactory extraction if ground to a —200 mesh product prior to reduction. Nickel-extraction will drop rapidly with decreasing fineness of silicate ores simply because the leach liquor has little penetration power and leaves the nickel in the cores of the particles undissolved. The following results illustrate the effect of size of particles upon nickel extraction:

Fraction	*Ni-extraction, pct*
2-1 m per m particles	15
1-0.5 m per m particles	30
0.5-0.25 m per m particles	50

A garnierite-chrysoprase mixture 15 pct Ni was screened and after reduction each fraction was treated with strong leach liquor.

On the other hand it has been found that true oxide products which are the ultimate result of weathering are very porous. Variegated clays, for instance, need no grinding before reduction, and high extractions can be obtained from such reduced ores without any comminution after reduction.

General Aspect of Gas Adsorption by Reduced Nickel Ores: The crystalline nature of some of the nickel-minerals, such as serpentine, garnierite and chrysoprase makes it evident that NiO is part of the crystal structure together with MgO, SiO_2 and H_2O.

As all these compounds may vary within wide limits in these secondarily formed minerals, one can hardly expect that the position of NiO in the space lattice of the crystal will invariably be the same. Different orientations will probably also affect reducibility.

Be that as it may, experimentally it has been observed that the reduction to metal starts at a temperature somewhere near 450°C for all hydrated nickel silicates. In the early stage of reduction the metallic particles probably are extremely small and, as they are enclosed in the space lattice of the crystal, their further growth will be hampered. With rise in temperature some migration and segregation will take place, with gradual increase in size of metallic particles.

There are, however, certain indications, that the particles remain in a state of high subdivision even at a temperature of 950°C.

An unusual phenomenon is that garnierite reduced in a current of gas will hold at that temperature quite an amount of adsorbed gas. It is this particular behavior of the hydrated silicates of nickel and magnesia after reduction that may affect the nickel-extraction unfavorably. Fortunately, as will be discussed later, a remedy may be found to secure satisfactory extractions for this class of ore as well.

The Amount of Gas Adsorbed by Reduced Nickel Ore in Connection with the Nickel-extraction: Three samples of pure hydrated silicates were selected for investigation, two of the normal garnierite type and one almost free of magnesia (Rothisiet).

Samples of 7.5 g of ore were reduced in a quartz tube and evacuated thereafter in the same tube. This tube was connected to the evacuation apparatus with ground joints. The samples were first heated to 950°C while a hydrogen current passed over the ore; thereafter they were cooled in hydrogen to 20°C. At room temperature the tube was evacuated. The temperature was then raised to 650°C and the tube again evacuated. Gases that were given off were collected in a calibrated buret for analysis. The amount of adsorbed gases was estimated in this manner for all results discussed in this publication. The results do not represent absolute figures of course, since by increasing the temperature in

the tube to 800°C and evacuating the tube at that temperature, somewhat more gas could have been collected compared with the amount evacuated at 650°C. However, general conclusions based on these results were not hereby affected.

To reach a definite conclusion regarding the effect of gas adsorption upon nickel extraction from the three different samples, the amount of adsorbed gases after reduction has been estimated in the manner described. Parallel samples, reduced in exactly the same way, but not evacuated after reduction, were leached with weak leach-liquors, since they are more sensitive than strong liquors to changes in the physical nature of the metal after reduction. Enhanced effects upon extraction may be expected from weak leach liquors, and low temperatures of leach liquors increase the difference even more. Because of this fact, most extractions were made at room temperature.

The weak leach liquor used (denominated further WL) contained 1.29 pct NH_3 and 1.738 pct CO_2 and extractions were obtained by vigorous agitation for 20 hr in contact with air.

In order to keep the dissolving power of the leach liquor nearly constant during the period of agitation, a very high ratio of liquid to solids was used for all samples. To take care of small evaporation losses after extraction, glass bulb and content were brought to the original weight by adding fresh leach liquor. The extractions were calculated from the dissolved values in the clear leach liquor.

Gas Adsorption as a Result of Reduction and Extractions by W.L. at 20°C, from —140 mesh samples of 7.5 g, reduced at 950°C:

Sample	Chemical analysis, pct				Evacuated at 650°C m.l. H_2 at 20°C and 760 per mm Hg pressure	Evacuated m.l H_2 per g of nickel	Ni extraction without evacuation
	Ni	Fe	SiO_2	MgO			
Garnierite Silesia	9.03	0.41	74.96	6.46	3.85	5.7	19.8
Rothisiet Saxony	20.71	0.39	53.7	1.45	1.70	1.1	82.6
Garnierite Celebes	20.73	3.54	47.97	9.9	8.4	5.4	6.5

The low magnesia "Rothisiet" sample had a low gas adsorption and a high nickel extraction, while the true garnierite ore samples containing considerably more magnesia showed high gas adsorption and low nickel extractions. This may indicate that a certain connection exists between low gas adsorption and high nickel extraction and vice versa and that the presence of magnesia is likely to favor high gas adsorption.

One may expect that after formation the tiny nickel particles are kept apart more effectively by the presence of magnesia in the crystal lattice than without it. In the plain silica crystal lattice the nickel particles will have more freedom to migrate with rising temperature and hence will increase faster in size and lose chemically adsorbed gases more quickly. This may be the explanation for the results observed.

The Effect of Watervapor upon Hydrogen Adsorption and the Corresponding Ni-extraction: If garnierite is reduced in gas mixtures containing both watervapor and hydrogen any increase of watervapor in the gas mixture will cause the reduced ore to adsorb less hydrogen.

Reduction gas-mixture	Hydrogen evacuated cc at 20°C and 760 m per m Hg	Remarks
Dry hydrogen	5.95 cc	
88 pct H_2 and 12 pct H_2O	5.7 cc	Below 200°C the samples were cooled to room-temperature in dry hydrogen
10 pct H_2O and 90 pct H_2O	3.27 cc	

As is evident from the following data: Samples of 7.5 g of a —140 mesh garnierite product from Celebes, No. 4 were reduced in gas mixtures while raising the temperature to 950°C. The samples contained 9.5 pct Ni, 0.93 pct Fe, 71.15 pct SiO_2 and 8.84 pct MgO.

A —140 mesh garnierite sample from Silesia was used to estimate the extractions after a normal reduction at 950°C. Below 200°C the reduced samples were cooled to —15°C in a current of dry hydrogen and immediately transferred to the weak leach liquor. This sample contained 6.71 pct Ni, 2.61 pct Fe, 49.50 pct SiO_2 and 8.29 pct MgO.

Reduction gas mixture	Ni-extraction in W. L., pct	Remarks
Dry hydrogen	59	
88 pct H_2 and 12 pct H_2O	79.3	Samples were of course not evacuated.
62 pct H_2 and 38 pct H_2O	82.0	
10 pct H_2 and 90 pct H_2O	90.2	

It is evident that increased nickel extraction runs parallel with decreased hydrogen adsorption.

Gas Adsorption as Obtained from CO and CO_2 Mixtures, etc.: As a result of further research along this particular line of investigation, it was found that nickel extraction was greatly affected by the physical state or surface condition of the metal after reduction. It became evident that high extractions could be easily obtained from reduced ore if the metal was free from adsorbed gases, but it was also observed that under certain conditions reduced garnierite may show a gas adsorption of unknown magnitude corresponding with low nickel extraction. By depressing such gas adsorption in a particular way extractions improve materially. The means of doing so have been patented by the author (c.f. Dutch patent No. 44768. Klasse 40 a. 43., granted Dec. 16, 1938; and French patent No. 837609 May 6, 1936).

As claimed, improvements are made by restriction of the reducing power of gas within certain limits, by the addition of small amounts of a sulphur compound to the ore prior to reduction, or by the use of reducing gases having a small sulphur content.

Complete elimination of adsorbed gases may be obtained by passing watervapor or CO_2 gas over red hot reduced ore for a short time avoiding, however, reoxidation.

These means may be combined advantageously by controlling the reduction of ore judiciously, by adding a small amount of finely ground pyrite to the ore, and by cooling the hot reduced ore in an atmosphere free from oxygen containing much watervapor or CO_2 gas, or a combination of both.

The results of this investigation may be summarized as follows: 1. Hydrogen and carbon monoxide may be adsorbed by reduced garnierite to a considerable extent, even if the temperature of reduction is raised up to 950°C. On the other hand the nickel metal or alloy of nickel and iron has little tendency to adsorb CO_2.

2. At a lower reduction temperature extraordinarily high gas adsorption has been observed. A garnierite sample reduced at 750°C adsorbed as much as 15.6 atoms of hydrogen per 100 atoms of nickel. This result compared with results of nickel catalysts on support, indicates an astonishingly great adsorption power of reduced garnierite, and an extremely fine division of the metal in such a product. Such a physical condition of the metal charged with gas results in low extraction. Gas adsorption diminishes with rise of temperature and for practical purposes a reduction temperature of 900°C will give satisfactory extractions and may be recommended for garnierite ores.

3. Garnierite, after reduction at 950°C and cooling to room temperature in reducing gas, will adsorb quite some oxygen when exposed to the air, indicating the presence of a very large metal surface. By raising the temperature to 100°C the oxygen adsorption increases considerably. At about 150°C absorption started and very slowly more and more oxygen was taken up by the metal. In this state the metal becomes largely passive, with a detrimental effect upon extraction.

4. The addition of small amounts of finely divided pyrite to the garnierite prior to reduction will depress the hydrogen adsorption to a certain extent, with a resulting material increase in extraction. As this addition probably also affects the potential of the metal favorably, it would seem that a combined effect is responsible for the great improvement observed.

5. When a current of water vapor or CO_2 gas is passed over red hot reduced ore, it will have the effect of eliminating quickly and completely all adsorbed reducing gas. In addition such metal will lose more or less its tendency to adsorb oxygen if exposed to the air at room temperature or temperature up to 100°C. The metal thus obtained is almost in a gas-free state prior to the extraction. This physical state favors fast dissolution of the metal, and the beneficial effect upon the extraction is very marked.

6. The extraction of reduced garnierite charged with gas may be considerably improved by the use of strong lukewarm liquors. From gas-free metal, however, high extractions may be obtained by using weak leach liquors at room temperature.

7. Nickel ores of the true oxide class, such as earthy chocolate ores, show very little tendency to adsorb gases during reduction and high extraction may be obtained therefrom even when using weak liquors at room temperature.

8. Hydrogen is a more powerful reducing agent than carbon monoxide at a temperature of 900°C. For normal ores, reduction with gas mixtures containing 90 pct H_2O and 10 pct H_2 will result in the desired high extraction of nickel. The same result may be obtained with gases containing proportionately about 75 pct CO to 25 pct carbon monoxide.

9. Below 200°C the ores shcuild be cooled in gases containing very little carbon monoxide to avoid formation of nickel carbonyl or low temperature CO adsorption which may affect the extraction unfavorably. For the exact figures of the results obtained the reader may consult the corresponding tables.

Amount of Gases Adsorbed During Reduction: Celebes. Garnierite sample No. 4. —140 mesh 10 g. Reduced at 950°C. Ni 9.15 pct, Fe 0.93 pct, SiO_2 71.15 pct, MgO 8.84 pct.

Gas mixture used for reduction		Gas evacuated at 650°C m.l. at 20°C and 760 m per m Hg pressure	
CO_2 CO	55 pct 45 pct	CO_2 CO H_2	0.95 m.l. 12.80 m.l.* 3.93 m.l.

* As combined water is gradually expelled up to 950°C, it is likely that some H_2O has been decomposed by the metallic nickel and the hydrogen formed retained by the metal.

CO_2 CO H	78.5 pct 6.1 pct 15.4 pct	CO_2 CO H_2	2.6 m.l. 1.2 m.l. 6 m.l.†

† In this case hydrogen has been absorbed in preference to carbon monoxide.

Effect of Gas Adsorption on Extraction: Celebes garnierite —200 mesh Ni 5.03 pct, Fe 4.90 pct, SiO_2 58.82 pct, MgO 17.0 pct. Reduced in hydrogen current and cooled to room temperature. Above 750°C hydrogen adsorption decreased.

Temperature of reduction, °C	750	800	850	900
Ni extr. W.L.* at 20°C	33.4	54.3	63.4	65.2
Ni extr. M.L.* at 60°C	54.3	80.3	88.4	90.1

* W.L. = weak liquor 1.29 pct NH_3 and 1.738 pct CO (agitated for 20 hr).
M.L. = medium liquor 2.9 pct NH_3 (agitated for 3 hr)

Depressing Hydrogen Adsorption by the Addition of a Sulphur Compound: Celebes garnierite sample No. 4. Ni 9.15 pct —140 mesh from 10 g ore reduced in hydrogen current at 950°C, evacuated at 650°C. m.l. hydrogen collected:

Addition to ore	H_2 adsorption m.l.
None	5.95 m.l.
0.5 pct FeS_2	3.1 m.l.

Effect of Small Addition of Pyrite on Ni-extraction: Celebes garnierite No. 28. Ni 17.28 pct, Fe 1.295 pct, SiO_2 52.7 pct and MgO 10.61 pct. Reduced in current of 90 pct H_2O and 10 pct H_2. —140 mesh sample. Cooled below 200°C in dry H_2 to 20°C extracted in weak liquor at 20°C.

Pct FeS_2 added to sample	Ni-extraction
None	48.7
0.02	60.–
0.05	68.6
0.1	72.8
0.25	74.1

Combined Effect of Gas Elimination and Sulphur Addition: Celebes garnierite ore. Ni 5.03 pct, Fe_2O_3

8.32 pct, SiO_2 58.82 pct, MgO 17 pct. —200 mesh. Reduced in hydrogen current at 800°C and cooled to 20°C before being exposed to the air.

The highest extraction and lowest tendency to passivity was found for the gas ratio 90 pct H_2O — 10 pct H_2. See column 4.

Gas mixture used for reduction	100 pct H_2	88 pct H_2 12 pct H_2	62 pct H_2 38 pct H_2O	10 pct H_2 90 pct H_2O	3.4 pct H_2 6.6 pct N_2 90 pct H_2O
Ni-extraction sample exposed to the air at −15°C	59 pct	79.3 pct	82 pct	90.2 pct	74.1 pct
Ni-extraction sample exposed to the air at 100°C	55.1 pct	35.5 pct	41.1 pct	87.2 pct	65.4 pct

	Ni-extraction		
	I reduced and cooled in hydrogen	II for 2 min. CO_2 current passed at 800°C over reduced ore and cooled in CO_2	III to ore added 0.2 pct FeS_2 further same as II
Weak liquor at 20°C 20 hr agit.	54.3	70.2	84.7
Medium liquor at 60°C 3 hr agit.	80.3	87.1	90.1

Physical condition of metal for I. Highly charged with adsorbed hydrogen. Physical condition of metal for II. Free from adsorbed hydrogen. Physical condition of metal for III. Same as II, in addition probably decreased potential as a result of the sulphur taken up by the metal. Condition III favors highest extraction and shows little difference in outcome between extraction with weak liquor (1.29 pct NH_3) at room temperature and medium strong liquor (2.9 pct NH_3) at 60°C. Nickel has been brought to the easiest soluble state in this way.

Oxygen Adsorption: Celebes garnierite sample No. 4. Ni 9.15 pct —140 mesh from 7.5 g. Reduced in hydrogen current.

	Adsorbed at 20°C M.L.	Ni-extraction in W. L. at 20°C without evacuation	Ni-extraction in W.L. at 20°C after evacuation at 650°C
Reduced at 750°C	4.0 m.l.	16.5	4.6
Reduced at 950°C	4.05 m.l. adsorbed at 100°C	30.–	4.4*
Reduced at 950°C	6.2 m.l.		

* Increased oxygen adsorption, as a result of evacuation causes diminished extraction.

For one minute a current of CO_2 passed over the reduced ore at 950°C and thereafter the sample was quickly cooled in CO_2 atmosphere.

Adsorbed at 20°C	1.3 m.l. O_2
Adsorbed at 100°C	1.8 m.l. O_2

New Caledonian earthy chocolate ore 22a, Ni 16.12 pct, Fe 23.61 pct 7.5 g were reduced in a current of 77.2 pct CO_2 and 22.8 pct CO at 950°C evacuated at 650°C and cooled to 20°C, adsorbed at 20°C, 5.4 m.l. O_2.

While the adsorption of reducing gas for this sample was very low, only 0.85 m.l. CO, the oxygen adsorption on the other hand was on the high side indicating the tendency of nickel-iron solid solutions to have great oxygen adsorption.

Effect of Reducing Power of Gas upon the Extraction and Corresponding Susceptibility of the Ore for Passivity: —140 mesh garnierite sample from Silesia. Ni 6.71 pct, Fe 2.61 pct, SiO_2 49.5 pct, MgO 8.29 pct. Reduced at 950°C and extracted in weak liquor at 20°C.

Effect of Temperature of Leach Liquor upon the Extraction: Reduced in a current of dry hydrogen at 950°C. Garnierite charged with adsorbed hydrogen. Celebes garnierite No. 28. Ni 17.28 pct — 140 mesh. Extraction in weak liquor (NH_3 1.29 pct).

Temperature of leach liquor, °C	21	40	60
Ni-extraction, pct	26.4	53.1	61.2

Passivity Caused by Increased Oxygen Adsorption: Ore reduced in hydrogen current at 950°C being exposed to the air between 150° and —15°C. Extracted in W.L. at 20°C.

Chemical composition of the —140 mesh ore specimen:

	Ni Pct	Fe Pct	SiO_2 Pct	MgO Pct
Saxony 12a. Rothisiet	20.71	0.39	53.7	1.45
New Caledonia 23. Glassy Chocolate ore	17.84	7.74	34.6	13.7
New Caledonia 22. Earthy Chocolate ore	14.88	22.41	23.4	2.5
Celebes No. 8 mixed high Silicious ore	3.68	7.11	70.–	5.4

Samples transferred after reduction through the air at	Ni-extraction					
	150°C	100°C	50°C	20°C	0°C	−15°C
12 a iron free	62	70	80			82.5
23 medium iron	16.9	23.8	40.8	70		80.5
22 high iron	0.04*	5.4	14.3	45.5		66.6
8 mixed	6.8	9.2	14.9		60.6	65.2

* This sample was pyrophoric.

Effect of Elimination of Adsorbed Reducing Gas by CO_2 upon the Extraction. Samples reduced in hydrogen current at 960°C, at which temperature a slow current of CO_2 was passed over the ore for 5 min., cooling the ore thereafter quickly in CO_2. This effects simultaneously a very low tendency for oxygen adsorption. Extraction in weak liquor at 20°C.

Exposed to the air after reduction at	Ni-extraction		
	150°C	100°C	−15°C
−140 mesh sample 23	84.2	85.7	85.8
−140 mesh sample 12a	81.8	87.6	87.6
−140 mesh sample 22	76.8	84.7	86.7
−140 mesh sample 8	43.2	62.5	62.5

Between 100° and —15°C there was no difference in extraction, indicating the absence of passivity. At the temperatures indicated, the samples were quickly transferred to the leach liquor.

Gas Adsorption of Earthy Chocolate Ore: 7.5 g, —140 mesh, sample 22. Reduced at 950°C in gas mixture containing 77.2 pct CO_2 and 22.8 pct CO. Cooled below 200°C in dry CO_2 gas.

Evacuated at 650°C gave 0.85 ml. CO, 0.65 ml. H_2 and 1.9 ml. CO_2.

This very low gas adsorption coincides with high nickel extractions in weak liquor at 20°C.

Passivity of Iron-rich Nickel Ores: Evidence has been given of the presence of nickel-iron solid solutions in reduced nickel ores and that such alloys will favor the adsorption of oxygen if exposed to the air after being cooled to room temperature. This oxygen adsorption will cause some temperature rise of the ore, and this increase in turn will promote the adsorption of more oxygen.

Under certain conditions, such as the combined effect of moist air, low temperature of reduction (about 800°C) and dumping of reduced ore on heaps, the ore may become even pyrophoric.

Ores such as laterites, high in iron but low in nickel content, will have only a very moderate NiFe alloy content after reduction. Such ores exposed to the air in piles nevertheless will become lukewarm. This is a fair indication of more or less passivity. The following example may show such an effect:

Laterite was reduced in an internally-fired laboratory rotary kiln, which had a capacity of 0.5 ton of reduced ore per 24 hr. The reduced ore was properly cooled to room temperature and dumped from the container on the floor where it soon became lukewarm by contact with the air. In the reduced state it contained 1.6 pct nickel. The reduced ore was agitated in a ratio 1:4 with leach liquor at room temperature containing about 3.5 pct NH_3. After 6 hr agitation a very poor result was obtained, as only 10 pct of the nickel had been extracted and

Table III. Results of Extraction after Reduction in H_2O-H and CO_2-CO Gas Mixtures at 950° Cooling the Reduced Ore Below 200°C in Dry Hydrogen or CO_2

N. C. Earthy Chocolate Ore Sample 22

Gas mixtures for reduction	Ni-extraction W.L. at 20°C Pct	Ni-extraction by $CuSO_4$ solution Pct	Fe-extraction by $CuSO_4$ solution Pct	Ratio Ni to Fe in alloy	Gas mixture for reduction	Ni-extraction W.L. at 20°C Pct
Dry hydrogen	66.6				dry CO*	17.2
H_2 88 pct H_2O 12 pct	18.5					
H_2 62 pct H_2O 38 pct	22.8				CO .43 pct CO_2 57 pct	48.2
H_2 45 pct H_2O 55 pct	97.2	98.6	98.5	0.672		
H_2 30 pct H_2O 70 pct	95.—	98.1	90.4	0.730		
H_2 20 pct H_2O 80 pct	95.4	97.—	69.3	0.937	CO 15 pct CO_2 85 pct	82.—
H_2 10 pct H_2O 90 pct	95.7	97.9	70.7	0.928		
H_2 6.3 N_2 2.7 pct H_2O 90 pct	95.9	97.5	70.4	0.928	CO 8.7 pct CO_2 91.3 pct	66.1
H_2 2.3 pct N_2 7.7 pct H_2O 90 pct	75.3	82.4	38.3	1.37		

* Samples reduced by CO or CO-CO_2 mixtures were cooled below 200°C to 20°C in a current of dry CO_2.

Note: It will be noted, that under conditions for high nickel reduction, the co-reduction of iron is almost stationary between certain limits of the gas components (H_2+H_2O). Below the lower limit the reduction of nickel will drop fast, that of iron still faster. Above the upper limit the gain in nickel reduction is very small. The increase of iron reduction on the other hand may be considerable. These equilibrium reactions are governed by the law for solid solutions of oxides. This law implies that the reductibility of oxides, which are difficult to reduce, may be greatly improved through intimate contact with easily reducible oxides. For nickel-iron oxides solid-solutions, in which iron oxide predominates, it can be stated that for high nickel reduction, the condition will be such that at least an equivalent amount of iron is simultaneously reduced. The results given in table III are indicative. The real equilibrium nature of the reduction may be further demonstrated by the following example: A sample of the earthy type of chocolate ore from New Caledonia was reduced in a gas mixture at 900°C, consisting of H_2 and CO_2, the latter component of the gas being quite in excess. The mixture nevertheless was sufficiently rich to produce over-reduction of the iron. Two parallel tests were run. After reduction at 900°C the ore was first cooled to only 600°C and at that temperature a CO_2 current was passed over the ore, respectively for 5 and 30 min: thereafter the ore was cooled to room temperature in CO_2. The ore contained 18.44 pct Ni and 25.48 pct Fe before reduction. Extractions were made by a 10 pct $CuSO_4$.5aq solution, outside access of oxygen and also by a strong ammonia liquor at room temperature in contact with air.

Results of $CuSO_4$ leach.

Treatment of the ore at 600°C 5 min CO_2 current over the ore					Treatment of the ore at 600°C 30 min CO_2 current over the ore				
Pct Fe dissolved	Fe extraction	Pct Ni dissolved	Ni extraction	Ratio of Fe:Ni in solid solution	Pct Fe dissolved	Fe extraction	Pct Ni dissolved	Ni extraction	Ratio of Fe:Ni in solid solution
21.755	85.4	18.40	99.8	1.18:1	18.709	73.4	18.35	99.5	1.02 : 1

Ammoniacal extraction:

Ni dissolved	Ni extraction	Ni dissolved	Ni extraction
17.91	97.12	17.56	95.23

A nickel extraction of about 95 pct as obtained by ammoniacal leaching corresponds with the co-reduction of iron in a ratio of roughly 1 to Ni. This result matches closely with the previous results obtained by direct reduction under proper gas-mixture control. This proves that the same result can be approached from opposite directions.

this result still could not be improved after 24 hr agitation.

A fresh amount of the same reduced ore was submerged in the leach liquor ratio 1:4, for about 16 hr prior to agitation. This time after 6 hr agitation, over 90 pct nickel was extracted. What may have caused this remarkable effect? The explanation is rather simple. A thin blanket of $Fe(OH)_3$ was noticed on the surface of the submerged ore. Part of the iron from the alloy that was still passive entered into solution as ferrous iron. Further oxidation caused precipitation of ferric hydroxide. Dissolved oxygen was thus removed from the liquor in the settled pulp as well as from the Ni-Fe-alloy, in which manner the metal became depolarized and a good extraction was reestablished.

In the first-mentioned case of poor extraction ore and leach liquor were strongly agitated directly and the leach liquor remained more or less saturated with dissolved oxygen throughout the period of agitation. This, no doubt, prevented a change in the passive state of the alloy and was responsible for the poor result. The very great dissolution pressure of iron in ammoniacal solution makes the metal so useful in depolarizing the passive alloy under conditions contemplated.

The new way of depolarization has been effectively used in most of the larger scale laboratory leaching tests, when 10 or more kg of ore were agitated.

The Effect of Sulphur upon Iron-rich Reduced Ore: Earlier evidence has been given that small amounts of sulphur dissolved as sulphide in leach liquor have a beneficial effect upon the nickel extraction of pure reduced garnierite ore.

The following results show a reverse effect for iron-rich nickel ores. A glassy and an earthy type of chocolate ore from New Caledonia as well as an iron-rich mixed garnierite sample from Celebes were reduced in a current of 10 pct H_2 and 90 pct H_2O at 950°C. Below 200°C the samples were cooled to —15°C in dry hydrogen. The samples were quickly transferred to the leach liquor and at once agitated at 20°C in weak leach liquor: *a*) containing some dissolved sulphide and *b*) free of sulphide. In addition, extractions were made in a neutral coppersulphate solution containing 10 pct $CuSO_4$ 5aq.

Table IV. Ni-extractions

—140 mesh	Ni	Fe	W.L. at 20°C	W.L. containing 0.51 Pct S at 20°C	Neutral CuSO solution at 20°C, Pct
Glassy chocolate ore (N.C.)	17.84	7.74	83.7	43.1	90
Earthy type of chocolate ore (N.C.)	15.03	22.41	95.7	23.5	97.5
Mixed Celebes ore (8)	3.68	7.11	65.2	40.7	66.8

In the neutral coppersulphate solution both nickel and iron from the alloy were dissolved respectively as nickel sulphate and ferrous sulphate, and no interference could be expected from precipitated ferric hydroxide.

Furthermore, extractions in weak ammoniacal liquor were in more or less close agreement with extractions from the copper sulphate solution.

To understand clearly the conditions under which nickel extractions were obtained from the ammoniacal liquor it should be remembered that the ratio of liquor to ore was very great, which was normal for all small scale tests. While the samples were being strongly agitated, dissolution took place and the oxygen content of the leach liquor must have been nearly saturated. Iron is thus readily precipitated in a flocculent form as $Fe(OH)_3$.

In the case where sulphide-containing liquor was used the oxygen content must have been very low during the early stage of agitation owing to the sulphide, which also was responsible for the greatly depressed dissolution of iron.

Then there were very low concentrations of iron and oxygen, not flocculent ferric hydroxide, but thin tenacious adhering films were formed on the surface of the alloy. Such films of a hydrophobic nature may have protected the underlying alloy very effectively from further dissolution and may have caused the low extractions. It should be noted that the sulphide in the liquor gradually oxidized to sulphur and sulphate resulting in an increase in oxygen and a decrease in sulphide during the course of agitation. There was, however, not a sufficient lack of oxygen during the course of agitation to have been responsible for the low extractions.

In the case of the sulphide-free leach liquor the flocculent $Fe(OH)_3$ formed evidently does not interfere with extraction.

Evidence that tough films of $Fe(OH)_3$ may be formed was found in the glass surface of the agitator. They adhered perfectly to the glass and were often so thin that they showed interference light colors. To investigate the supposition just made and to look into this matter from another point of view a few samples were reduced with hydrogen sulphide in order to get metal sulphides instead of an alloy. As such sulphides dissolve slowly in ammoniacal liquor by using a great excess of leach liquor and strong agitation it is likely that the liquor will hold sufficient oxygen to precipitate the iron in the flocculent harmless form. If this supposition is correct, nickel extractions from sulphides of nickel and iron should be reasonably good, in contrast with results obtained from normal reduction, extracting the alloy thereafter in sulphide-containing liquors. This was borne out experimentally.

Table V. Ores Reduced with H_2S at 950°C

—140 mesh	Ni	Fe	S content of sample after reduction, Pct	Ni-extraction in W.L. at 20°C
Glassy type of chocolate ore (N.C.)	17.84	7.74	15.18	64
Earthy type of chocolate ore (N.C.)	15.03	22.41	25.58	68.8
Pure garnierite from Celebes	11.7	trace	6.01	74.9
Pimielit Silesia	9.03	0.41	5.08	82.1

The complex nickel-iron sulphides under the given conditions are somewhat less soluble than plain nickel sulphide. Part of the sulphide was oxidized to sulphur and part to sulphate. The extractions are considerably better than obtained after normal reduction and the use of weak sulphide containing leach liquor to dissolve the alloy.

Considering these facts, it is logical to add the sulphur as pyrite to complex, iron containing garnierite ores prior to reduction in order to improve the extraction, or as a constituent of the reducing gas. Both means are effective and patented, c.f. Dutch patent, Dec. 16, 1938, No. 44768 klasse 40a.43. French patent, May 6, 1936, No. 837.609.

Carbonyl Formation or CO-adsorption below 180°C and Its Influence upon Extraction: The finely-divided state of the nickel or nickel-iron alloy as formed by the reduction of garnierite ore will no doubt favor carbonyl formation.

As has been pointed out earlier, the extraction of reduced garnierite may be unfavorably affected by the adsorption of reducing gas, and it was therefore worth while to investigate the effect of low temperature CO-adsorption.

For this investigation two pure garnierite samples were selected as well as a normal garnierite sample containing iron and two samples chocolate ore, one of the glassy and one of the earthy type. They were reduced in a current of CO at 950°C and cooled below 200°C; (*a*) in a stationary atmosphere of CO to —15°C; (*b*) in a nitrogen current to —15°C.

Afterwards they were quickly transferred to the leach liquor. Besides the reduction with CO, one of the samples,—the earthy type of chocolate ore—was also reduced in a current of 20 pct H_2 and 80 pct H_2O at 950°C and cooled below 200°C, (*a*) in dry hydrogen, (*b*) in a stationary atmosphere of CO and (*c*) in a slow current of CO, however in such a way, that the loss of nickel by volatilization was negligible for (*c*).

Table VI. Results of Ni-extraction in W.L. at 20°C after CO-reduction

Samples	Ni Pct	Fe Pct	Ni-extraction: Cooled below 200°C in stationary CO	Ni-extraction: Cooled below 200°C in nitrogen current	Remarks
Pure garnierite from Celebes No. 14	5.58	0.95	17.5	57.7	extraction of iron-free samples much affected
Pure pimielit Silesia No. 11	9.03	0.41	23.1	55.7	
Normal garnierite from Celebes	4.42	8.48	26.2	26.2	extraction of iron-rich samples not affected
Glassy chocolate ore (N.C.)	17.84	7.74	66.3	66.8	
Earthy type chocolate ore (N.C.)	15.03	22.41	15.8	17.1	

Earthy type of chocolate ore reduced in a current of 20 pct H_2 and 80 pct H_2O at 950° C.

	Cooled below 200°C in dry H_2	Cooled below 200°C in stationary CO	Cooled below 200°C in slow CO current
Nickel extraction	96.5 pct	90.7 pct	82.4 pct

It may be pointed out that: 1. The ores reduced in a current of CO have taken up a small amount of carbon above 900°C in solid solution, because in the course of reduction the very finely divided metal has served as a catalyst for the Boudouard reaction $2\ CO \rightleftarrows C + CO_2$ and quite some amorphous carbon has been precipitated on the ore, as was confirmed by analyses. 2. After reduction the samples must have passed the range of nickel carbide formation while cooling from 420° to 200°C. As the rate of cooling was very fast, however, it is not likely that carbide formation of any importance took place. Above 900°C the nickel-iron alloy may have dissolved only a very small amount of carbon, since nickel has the tendency to depress the solubility of carbon in iron materially in the austenitic phase. Nevertheless it may have had some effect upon the extraction, for it is significant that the samples reduced by CO showed no difference in extraction as a result of CO contact below 180°C, whereas the samples reduced by hydrogen were somewhat affected, particularly by a slow current of CO. At any rate it would seem advisable in commercial operation to cool the ore below 200°C for example in a stationary atmosphere containing very little CO, which may be obtained by almost complete combustion of the reducing gases. The atmosphere should be relatively rich in CO_2 but free from oxygen. Under such conditions there is no need to fear decreased extraction or loss of nickel by volatilization.

Required Concentration of Reducing Components in Gas for Effective Reduction of Nickel Ores: We are aware of the fact that it is difficult to reduce Fe_2O_3 to metallic iron by CO-CO_2 and H_2-H_2O gas mixtures and that high concentrations of CO or H_2 are required. NiO, on the other hand, is very readily reduced to metallic nickel under quite low concentrations of CO or H_2 in the gas mixture.

From the equilibrium curves as plotted by Eastman and others it is evident that at about 735°C the reducing power of CO and H_2 for the reduction of Fe_2O_3 is equal, but at higher temperatures hydrogen becomes a more powerful reducing agent for iron oxide. In run-of-mine garnierite ore nickel oxide may be present in combined form as garnierite, or may occur as free oxide, intimately mixed with iron oxide.

Between these extreme members of this mineral family quite a number of intermediate products may exist, such as chocolate ore, chrysoprase and even serpentine, the member closest related to the virgin basic rock, may be present. All such products behave differently when reduced by hydrogen and/or carbon monoxide.

It has been noted earlier: (1) that NiO in the combined form as garnierite is not quite so easily reduced as the free oxide; and (2) that true oxides of nickel and iron free from silica, though rather easily reduced, require a certain minimum reducing power of the gas mixture which obviously should be greater than for true silicate ores with high nickel content. As all these compounds are normally present in run-of-mine garnierite ore, an investigation was made to determine the required reducing power of the gas mixture for several types of minerals.

Sample 12*a*, a hydrated silicate of nickel almost free from magnesia, represented the most easily reducible type, while sample 22, a homogeneous earthy type of chocolate ore high in iron oxide,

would require no doubt a greater reducing power of the gas used for reduction.

The nickel extractions were made in weak leach liquor at 20°C. (Table VII.)

Table VII. Required Reducing Power of Gas Mixture

Gas mixture for reduction at 950°C	Sample 12a Ni 20.71 pct Fe 0.39 pct SiO_2 55.1 pct MgO 1.45 pct	Sample 22 Ni 15.03 pct Fe 22.41 pct SiO_2 23.4 pct MgO 2.5 pct
(1) H_2	82.6	66.6
(2) H_2 88 pct H_2O 12 pct	70.9	18.5
(3) H_2 62 pct H_2O 38 pct	67.6	22.8
(4) H_2 10 pct H_2O 90 pct	77.4	95.3
(5) H_2 2.5 pct N_2 7.5 pct H_2O 90 pct	83.9	81.6
(6) CO	70.9	17.1
(7) CO 43 pct CO_2 57 pct	74.4	48.2
(8) CO 15 pct CO_2 85 pct	85.7	82.–
(9) CO 8.7 pct CO_2 91.3 pct	88.9	66.1

Reduction under (5) was more successful and gave higher extraction, as can be seen by comparing results of the hydrogen reduction for that iron-rich sample and the carbon monoxide reduction under (9). Hydrogen, as could be expected, is therefore a stronger reducing agent than carbon monoxide at a temperature of 950°C.

A better illustration was obtained from the glassy type of chocolate ore (Table IX). All three samples were reduced simultaneously under exactly the same conditions.

Table IX. Required Reducing Power of Gas Mixture

Gas mixture for reduction at 950°C	Sample 23 Ni 17.84 pct Fe 7.74 pct SiO_2 34.6 MgO 13.7 Ni-extr. W.L. at 20°C
H_2	80.5
H_2 88 pct H_2O 12 pct	64.4
H_2 62 pct H_2O 38 pct	70.6
H_2 10 pct H_2O 90 pct	83.7
H_2 2.5 pct N_2 71.5 pct H_2O 90 pct	81.8
CO	66.8
CO 43 pct CO_2 57 pct	83.2
CO 15 pct CO_2 85 pct	73.3
CO 8.7 pct CO_2 91.3 pct	56.9

From the foregoing results it may be concluded that the gas-mixtures required to obtain high nickel extractions need to have only a moderate concentration of CO and H_2. These gases can be easily produced, for example by incomplete combustion of solid or liquid fuels or of high grade gas. Thus two aims may be combined, internal-firing and simultaneous reduction with the products of partial combustion.

Results of Reduction with Gas Mixtures as Obtained by Partial Combustion of High Volatile Coal: The analyses of the gases are given on a waterfree basis. A normal garnierite —200 mesh sample from Celebes was reduced at 875°C and cooled below 200° to 20°C in a CO_2 current. Analysis of the ore Ni 5.03 pct, Fe 4.90 pct, SiO_2 58.2 pct, MgO 17.0 pct. The influence of the sulphur content of the reducing gas is plainly shown by the extractions obtained.

Table X. Analysis of Gas Used for Reduction

		I Pct	II Pct
	CO_2	13.75	11.6
	CO	12.70	13.6
	SO_2	0.5	0.1
	N_2	73.0	75.3
Ni-extraction in M.L. at	60°C	92	87.7

Solubility of Magnesia as Present in Reduced Ore in Leach Liquor: For this investigation the same normal garnierite sample from Celebes, Ni 5.03 pct and MgO 17.— pct was used, with the addition of 0.2 pct finely ground pyrite. After reduction in a hydrogen current at 950°C, a current of CO_2 was passed over the ore for 2 min. and the ore was quickly cooled in CO_2 to 20°C. In view of the fact that the solubility of MgO is rather limited in ammoniacal leach liquor, 40 parts of leach liquor to 1 part of solids were taken in order to get reliable figures for the amount of MgO entering the solution.

Table XI. Solubility of Magnesia

Temperature of reduction, °C	MgO dissolved in pct of ore weight by W.L. at 60°C, pct	MgO dissolved in pct of ore weight by M.L. at 60°C, pct	Nickel-extraction W.L. at 60° C	Nickel-extraction M.L. at 60°C
750	1.11	1.47	70.8	75
800	0.30	0.44	84.7	90.1
850	0.15	0.22	89.5	93.2
900	0.11	0.13		
950	0.06	0.09		

The solubility of magnesia decreases rapidly with increase of reduction temperature over 750°C. As soon as solutions become supersaturated with MgO some of it will crystallize out as an ammonium compound $(NH_4)_2CO_3.MgCO_3$ 4aq. (Magnesia Alba) and NH_3, releasing this ammonia.

Since undesirable ammonia losses in the tailing result from the fact that ammonia magnesia compounds may crystallize out under certain conditions, appropriate measures for the prevention of such losses should be taken to prevent this happening in the agitators or in the washing circuit of the plant. Fortunately conditions are generally favorable in countercurrent leaching and washing circuits, and losses of this nature are not likely to occur if due precautions have been taken. In the event that tailings should be steamed, obviously such compounds will be broken up and NH_3 will be recovered.

Saturation Point of Leach Liquors for Nickel and Cobalt: Very little nickel can be dissolved in pure ammonia liquors free from carbon dioxide. Even though the solubility of Ni in a pure ammonium-carbonate solution with a weight percent ratio, NH_3: CO_2 of about 1:2.2 is considerably better, liquors that are most suited for the dissolution of nickel and cobalt should have a ratio NH_3 : CO_2 by weight of 2:3 or vice versa. Such liquors can hold considerable nickel and cobalt in solution. The best ratio, however, should be NH_3 somewhat in excess

of CO_2. In the dissolved state, e.g. in pregnant solution, nickel and cobalt will be to a large extent present as complex compounds with NH_3 and CO_2, and to a smaller extent dissociated as complexes. Distillation of a nickel liquor will result in a saturated solution directly upon precipitation of basic carbonate of nickel. After cooling to room temperature such liquors do not remain entirely saturated. The ratio of $Ni:NH_3$ and $Co:NH_3$ found from such a cooled solution gives an indication however of the amount of NH_3 combined with these metals.

While calculating the amount of NH_3 combined to nickel it should be remembered that the liquor always contains some magnesia which also combines with NH_3.

From a nickel solution as pure as possible, saturated at boiling temperature, the following analysis was obtained after cooling:

Ni 3.43 pct, NH_3 5.0 pct, CO_2 4.58 pct

The mol ratio in this case was $Ni:NH_3 = 1:4.17$

It is thus likely that in pure saturated and concentrated liquors 1 mol nickel will combine with 4 mol NH_3. By analysis of a very pure cobalt solution practically free from nickel and other impurities, saturated at boiling temperature, the following results were obtained:

Pct Co	Pct NH_3	Pct CO_2	Ratio $Co:NH_3$
0.724	1.28	1.10	1 : 6.1
0.235	0.41		1 : 6.–

One mol of cobalt seems to combine with 6 mol NH_3 under these conditions. These results do not necessarily mean that the metals will combine with NH_3 in the ratios found when NH_3 is present in great excess in the leach liquor, but they may give a basis for calculation of the lowest amount of NH_3 necessary to keep these metals in solution. From such a calculation we may also get an idea of the amount of free NH_3 present in the liquor. This is of importance as commercial liquors must have a reasonable amount of NH_3 and CO_2 in excess to keep the liquor sufficiently active. For instance a liquor containing 2 pct Ni will contain at least 2.3 pct combined NH_3, and with 2 pct cobalt this would be 3.5 pct NH_3. It is advisable, however,—under countercurrent leaching conditions—to use liquors with about 6 pct NH_3 to obtain pregnant solutions with 2 pct nickel. In the case of cobalt extraction, the strength of NH_3 should be at least 7 to 8 pct.

Normal leach liquors, containing small amounts of magnesia and ammonium sulphate (the latter resulting from the presence of added sulphides to the ore) were boiled till precipitation of basic nickel carbonate started. After cooling, the liquors were analyzed. (Table XII)

Table XII. Results of Analyses

Ni	NH_3	CO_2	Ratio $Ni : NH_3$
4.6	6.65	5.75	1 : 5
3.35	5.00	4.50	1 : 5.2
2.5	4.15	3.53	1 : 5.75
1.7	3.04	2.57	1 : 6.2
0.7	1.51	0.66	1 : 7.45

Liquors with decreasing Ni-content will require comparatively more NH_3 to keep the nickel in solution. For practical purposes it appears advisable to calculate the free ammonia content of the pregnant liquors on the basis of 1 mol of nickel combined with 6 mol NH_3, in order to be able to measure the remaining dissolving power of the liquor.

Partial Combustion of Fuels by Air: Partial combustion of powdered low grade high volatile coal from the Netherlands East Indies:

The results discussed below were obtained by operating a full size Fuller burner and cutting off the secondary air.

Analysis of coal	Combined water	5.45 pct
	Ash	24.61 pct
	Volatile matter	36.4 pct
	Calorific value	5328 cal per kg

By complete combustion of 1 kg of coal, 0.941 kg of water was formed. Gas analyses as obtained during the test follow. (Percentages by volume are given on waterfree basis.)

Gas composition

	CO_2	CO	H_2	N_2
(a)	9.8	13.1		remainder
(b)	10.0	12.5		remainder
(c)	10.0	13.2		remainder

The gas temperature was measured at about 1300°C after the kiln had reached a constant temperature. These analyses do not represent the actual composition of the gas at high temperature, but a simple calculation will give the following:

CO_2 8.7 pct, CO 11.2 pct, H_2 trace, H_2O 11.3 pct, N_2 68.8 pct

Partial Combustion of City Gas: The laboratory rotary kiln was internally heated by incomplete combustion of city gas, which made it possible to reduce ore at a temperature of about 900°C. From several runs gas samples inside the kiln were taken and analyzed. (Table XIII)

Table XIII. Analysis of Gas Samples

	Analysis of city gas, Pct	Gas from partial combustion on water free basis, Pct
CO_2	4.5	7.0
O_2	1.0	
CO	17.5	10.5
CH_4	4.6	
H_2	69.6	3.5
N_2	3.8	79.0

The actual composition of the gas at high temperature after partial combustion, is found by calculation to be as follows:

CO_2 4.1 pct, CO 6.1 pct, H_2 2.1 pct, H_2O 41.4 pct, N_2 46.5 pct

It is obvious that hydrogen is preferentially first oxidized when city gas is burned by an amount of air insufficient for complete combustion.

By diminishing the air supply somewhat more hydrogen may be obtained in the gas mixture. The

following analyses on a waterfree basis were obtained from three different runs of the kiln:

	a	b	c
CO_2	4.1	3.9	4.0
CO	12.1	11.1	11.2
CH_4	absent	4.6	2.6
H_2	15.9	13.1	15.4
N_2	67.9	67.3	66.8

Under these conditions hydrogen no doubt affected most of the reduction. On the other hand, with powdered coal the reduction of ore can be affected only by carbon monoxide, as hydrogen is almost absent in the reducing gas.

The following are practical factors of the process:

Ore Treatment in the Rotary Kiln: The rotary kiln by virtue of its qualities has found extensive application, and it may be used to advantage in reducing nickel ores, under certain conditions. It is well known that this sort of ore contains a considerable percentage of combined water which will be gradually expelled with rise in temperature. Finely ground ore of this nature when charged dry to the kiln will flow as a result of the fact that the water vapor that is driven out cannot escape fast enough and the reducing gas moreover does not come in contact with the ore. The combined effect is detrimental for proper reduction. However, if properly wetted the colloidal nature of the finely ground ore may be used advantageously to overcome this difficulty. The addition of 15 to 20 pct water to ore, for instance, will make the ore more or less sticky and the rolling action of the kiln will cause the formation of small soft pea-size lumps. Water vapor can escape easily through this loose charge and the ore bed will roll normally through the kiln. In this way a good gas-solid contact is obtained and there is no more tendency for flowing of the ore.

Results were obtained in a rotary laboratory kiln with a 9 in. id having a capacity of 0.5 ton of reduced ore per day. A commercial size unit will probably give the same results. In order to secure an early reduction within the ore bed, 3 to 4 pct of high volatile powdered coal was thoroughly mixed with the feed.

In the kiln internally heated by partial combustion of city gas, the ore was not retained for a longer period than 15 min., and the temperature was gradually raised to about 900°C at the discharge end.

Soft earthy ores of the transition zone may be treated in a like manner and need no comminution prior to reduction. It is quite possible that in commercial operation, a limited amount of high grade garnierite ore must be treated simultaneously with low grade ores of the earthy type in which case it may be advantageous to give the garnierite a wet milling and add it as a slurry to the earthy type of ore. This will give a proper mixture and desired physical condition of the feed for the rotary kiln, as was the case in successful experimental runs in the laboratory rotary kiln. Three percent of high volatile powdered coal was mixed with the feed. A normal transport of the charge through the kiln was observed, small soft lumps were formed and a good reduction and extraction were obtained.

True garnierite ores in the proper sense should be reduced in a finely ground state, and such products having a moisture content of 15 to 20 pct may be readily treated in the rotary kiln after addition of a small amount of finely ground pyrite to improve the extraction.

In the laboratory rotary kiln runs were made with laterites and soft ores from the transition zone. To this earthy type of ore no pyrite was added. The reduced ore was cooled to room temperature in a CO_2 atmosphere and then dumped on the floor from the container. After being crushed to a —40 mesh product the ore was left undisturbed for several hours submerged in the leach liquor prior to agitation for most of the tests.

A measured volume of air was blown through the pulp, causing oxidation accompanied by a rise in temperature.

Treatment of Laterite: Ores of this type, including garnierite deposits, usually contain over 30 pct iron. A sample from Celebes containing 33 pct iron was reduced in the laboratory rotary kiln at a temperature of about 900°C. To the air-dry ore 15 pct water was added and 3 pct high volatile powdered coal. After reduction the ore contained 1.725 pct Ni, and in a neutral copper sulphate solution free from contact with the air, nickel and iron were dissolved in the ratio 2:3, indicating that the alloy formed had probably this composition. The carbon content of the reduced ore was 1.08 pct, equivalent to about 1.3 pct coke. As the coal had 45 pct volatile matter, only a small amount of coke was consumed for reduction. Reduction, therefore, was affected mainly by gases from partial combustion of city gas, and by the gas evolved from the coal. The partial combustion served for internal heating as well as for reduction.

Part of the reduced ore was ground to 33.6 pct on 200 mesh. The part that was not ground consisted of soft lumps and some fine material. Both samples were treated under the same conditions. They were agitated at a ratio of 1 kg of ore to 6 liters of fresh leach liquor. The liquor contained 5.67 pct NH_3 and 4.5 pct CO_2 and the temperature of the pulp was raised to about 37°C. A controlled amount of air was introduced below the level of the pulp, and a strong agitation by a propeller was maintained in the closed asbestos-jacketed aluminum agitator which effectively prevented any settling of the ore treated. (Table XIV)

Table XIV. Results

Time of agitation	Ground after reduction to 33.6 pct on 200 mesh Ni-extraction	Not ground after reduction soft lumps Ni-extraction
15 min.	54.6	44.5
30 min.	62.4	54.3
1 hr	70.5	62.5
2 hr	81.5	74.3
3 hr	85.2	78.7
4 hr	85.8	81.1
5 hr	86.4	82.3
6 hr	87.—	83.8

From these results it may be concluded that the leach liquor had ready access to the metal present in the reduced ore, as well as in the sample that was not ground.

Ratio of Ore to Leach Liquor: Although in commercial operation it is likely that countercurrent leaching will be adopted, batch leaching tests were preferred for the laboratory test. Even though not entirely comparable with countercurrent leaching tests, they nevertheless give a sufficiently clear picture of the factors of importance in commercial operation. The dissolution of nickel-iron alloy formed by reduction proceeds rapidly in the beginning, gradually slowing down towards the end. The iron after dissolution is readily precipitated as ferric hydroxide, which is almost insoluble in the leach liquor. During the early stage of batch leaching much iron enters into the solution and it is likely that the oxygen content of the leach liquor may be very low, even almost depleted during this period. In countercurrent leaching since the ore is continuously fed to the agitator, the leach liquor will not lose its oxygen content so easily, and it is probable that in the early stage of dissolution extraction may proceed even faster. This is one point of difference between batch treatment and continuous countercurrent leaching.

Batch tests were made to investigate the course of dissolution. The fresh leach liquor used contained 3.78 pct NH_3 and 3.00 pct CO_2 and the max. temperature of the pulp was 37°C.

Table XV. Results on Reduced Laterite Ni 1.725 Pct

Time of agitation	Ratio 1 : 1.5		Ratio 1 : 3	
	Fe content of liquor, pct	Ni-extraction, pct	Fe content of liquor, pct	Ni-extraction, pct
15 min.	0.056	35.7	0.0157	53.3
30 min.	0.047	38.9	0.0023	62.9
1 hr	0.032	42.7	0.0021	72.3
2 hr	0.021	49.8	0.0019	79.5
3 hr	0.009	55.4	0.0016	81.9
4 hr	0.0032	60.6	0.00145	82.6
5 hr	0.0021	65.2	0.00145	82.6
6 hr	0.0021	67.5	0.00145	82.6
15 hr		78.5		

Leached in the ratio 1:6, 84.9 pct of the nickel was dissolved. It is evident that a low ratio of liquor to ore is not favorable for high extraction. Conditions in the early stage of dissolution probably cause the formation of hydrophobic ferric hydroxide films, which may affect extraction more or less. In addition it should be realized that the nickel content of the liquor for the 1:1.5 ratio extraction test was 0.897 pct at the end of the dissolution and only 0.479 pct for the 1:3 ratio. The dissolution power of the latter liquor therefore remained stronger, having some effect upon extraction.

The Iron Content of Pregnant Liquors: The CO_2 content of the leach liquor may result in the dissolution of more or less iron as the following results indicate. The same sample of laterite (Ni 1.725 pct) was agitated in the ratio 1:6. At the start of agitation the temperature of the pulp was 22°C.

Composition Fresh leach liquor NH_3 pct	CO_2	Fe content of leach liquor		Ni extraction after 6 hr agitation
		after 15 min. agitation	after 30 min. agitation	
3.50	2.49	0.017	0.008	84.6
3.68	5.71	0.057	0.030	82.2

The results indicate the CO_2 is the constituent that controls the rate of dissolution of iron and also affects the final iron content of the liquor after due agitation.

This is evident from the figures in Table XVI. Under the same condition the sample of laterite was treated in the ratio 1:6 Ni 1.725 pct. The maximum temperature of the pulp did not rise above 37°C.

Table XVI

Fresh leach liquor composition		Iron content of liquor after agitation		
Pct NH_3	Pct CO_2	15 min. Pct Fe	30 min. Pct Fe	6 hr Pct Fe
3.68	5.71	0.057	0.030	0.0041
3.78	3.00	0.033	0.020	0.0015
3.50	2.49	0.017	0.008	0.0006

Although the iron content of the liquor may seem rather unimportant, it nevertheless affects the purity of the basic nickel carbonate obtained from the liquor by distillation. The iron content of the liquor can be still further depressed by increasing the temperature of the pulp to 50° or 60°C and by introducing sulphur ions in the solution, resulting from the addition of a small amount of pyrite to the ore prior to reduction. Sulphides present in the reduced ore will give sulphur ions in the liquor. The combined effect of lukewarm liquors and sulphur ions reduces the iron content materially, but it is impossible to remove all the iron from the liquor.

The Nickel Content of the Liquor and Its Influence upon the Nickel Extraction: Evidence has been given, that a mol ratio of 1:4 of nickel and NH_3 may be present in pure concentrated saturated liquors. If this basis is accepted for the following solution containing 1.39 pct Ni, 5.43 pct NH_3 and 4.67 pct CO_2, the content of free NH_3 and CO_2 should be respectively 3.79 pct and 3.33 pct.

Extraction with this solution was compared with that of a fresh liquor containing 3.78 pct NH_3 and 3.00 pct CO_2. The same sample of reduced laterite, with 1.725 pct Ni, was treated in a ratio of 1 to 6 but the maximum temperature of the pulp was only 37°C. (Table XVII)

Table XVII. Results

Time of agitation	I Ni rich liquor Ni 1.39 pct NH_3 5.43 pct, CO_2 4.67 pct		II Fresh liquor NH_3 3.78, CO_2 3.00	
	Fe in solution, pct	Ni-extraction	Fe in solution	Ni-extraction
15 min.	0.0445	48.5	0.033	47.3
30 min.	0.0201	58.3	0.020	52.5
1 hr	0.0048	65.7		61.8
2 hr	0.0031	77.4		70.5
3 hr	0.0021	78.6		78.4
4 hr	0.0017	80.4		82.6
5 hr	0.0015	80.8		84.–
6 hr	0.0014	81.2		84.9

Leach liquor I has a nickel content of 1.63 pct and II, 0.24 pct at the end of extraction.

The dissolution pressure of a metal according to Nernst's conception, will be counteracted by the metal ions present in the solution. This being the case, the cause of decreased extraction is understandable in the case of the nickel rich liquor.

Implications are that liquors with low nickel concentrations favor high nickel extractions; hence it is obvious that countercurrent leaching is most effective. Furthermore as was found experimentally, 4 to 4.5 pct free ammonia, e.g. not combined to nickel, should be present for effective extraction. For instance, in a pregnant solution containing 2 pct nickel at least 2.3 pct NH_3 will be combined with the nickel, whereas for countercurrent operation such liquors should contain about 7 pct total NH_3. Such a solution is still active, an important factor for fast dissolution of nickel in the early stage of extraction and desirable for a favorable effect on the outcome.

So far all results were obtained from samples agitated directly after the ore was added to the leach liquor. The following tests differ only in that the samples remained undisturbed in the leach liquors for several hours prior to agitation. This precaution was taken to avoid erratic results from possible passivity.

The Effect of Strong Liquors upon the Extraction: Another sample of laterite from Celebes was reduced in the rotary kiln at about 900°C. The reduced ore contained 1.60 pct Ni, was rather coarsely ground, like the previous sample, and was agitated in a 1:3 ratio with a resulting rise in the pulp temperature from 22° to 37°C. As in the previous tests, the CO_2 content of the liquor was lower than the NH_3 content. (Table XVIII)

Table XVIII. Results of the Nickel Extraction

	AGITATION							
Leach Liquor NH_3 pct	1 hr	2 hr	3 hr	4 hr	5 hr	6 hr	7 hr	8 hr
4.32	43.4	62.9	73.8	77.7	78.8	80.9	82.8	83.5
6.52	53.–	72.3	80.1	86.1	90.5	91.5	92.5	93.5

For this grade of ore this was the lowest pulp ratio for effective extraction. A ratio of 1:4 requiring only 6 hr agitation would have been better. 10 pct more extraction was obtained with the stronger liquor. After agitation the first liquor had a nickel content of 0.445 pct and the second 0.499 pct. It should be noted that the use of stronger leach liquor was the only cause of a material increase in extraction and the use of strong leach liquors therefore should not be overlooked. A strength of 6-7 pct NH_3 should be normal.

Velocity of Extraction: Strong lukewarm leach liquors, together with ample amounts of liquid, strong agitation, and adequate supply of oxygen (air) will cause rapid solution of nickel.

The velocity of dissolution of the nickel-iron alloy is largely controlled by the supply of oxygen. By increasing the ratio of solution to ore more oxygen can be dissolved and the time required for complete extraction is thus greatly reduced. It is of prime importance to supply oxygen rapidly, since the capacity of the liquor to absorb oxygen largely controls the velocity with which the alloy dissolves under strong agitation. In the first stage of dissolution, when much alloy must be dissolved, provision should be made for adequate agitation and air supply.

If countercurrent agitation is used the air supply for each set of agitators should be properly adjusted since the amount required gradually diminishes and becomes very small in the last stage.

It should also be borne in mind that in order to leach high grade nickel ores rapidly more solution per unit of dry solids is required than for lower grade ores. For the treatment of 4 pct nickel ores a 1:5 ratio may be recommended to obtain the desired high extraction within a reasonable length of time, say within 6 hr of agitation. Laboratory tests even indicated that 3 to 4 hr of agitation may be sufficient if a ratio 1:8 is used.

Temperature Rise of the Pulp as a Result of Dissolving Nickel-alloy: As stated before, the leaching of laterite in a ratio 1:3 caused a temperature rise of the pulp of about 15°C. Oxidation of 1 kg iron to the ferric state liberates 7746 cal and for the oxidation of 1 kg nickel to NiO this figure amounts to 1051 cal.

Assuming for the sake of simplicity that the specific heat of the solution is 1, and that of the ore is 0.25, we find the mean specific heat of the pulp in the ratio 4:1 to be 4.25:5=0.85. Assuming further that 4 pct nickel and 4 pct iron have to be dissolved from reduced garnierite ore we find by a simple calculation that dissolving the amount of nickel present in 100 kg of ore will liberate $4(1{,}051 + 1{,}746) = 11{,}188$ cal. This amount of heat would raise the temperature of 500 kg of pulp by $(11{,}188)\ 425 = 26$°C, if no heat is lost. Assuming that the reduction has been overdone to such an extent, that in dissolving 4 pct nickel, 8 pct iron would also have to be oxidized, then the temperature of the pulp would be raised by $4(1{,}051 + 3{,}492)\ 425 = 43$°C. Under tropical conditions, with an original pulp temperature of 30°C, the final temperature in the first case would have reached 56°C, and in the second case of over reduction 73°C. That such over reduction is not very desirable needs no further comment. A temperature of 56°C may not be objectionable as far as the extraction is concerned and the increase in pulp temperature will favorably affect the settling rate of the pulp.

Air Requirements for Dissolving Nickel Alloy: Earlier evidence has been given that when reducing a certain class of chocolate ore 10 parts of iron were reduced simultaneously with 9 parts of nickel when nickel extraction is high. This does not mean that for other types of ore the same ratio will hold true: e.g., the ratio for laterite may be 3:2.

The amount of iron reduced will affect the amount of air required. The following results were found by laboratory tests, but they do not necessarily apply to commercial operation. It was found that when treating laterite, with 1.725 pct Ni in a ratio 1:3 with fresh leach liquor containing 3.78 pct NH_3 and 3.00 pct CO_2, during agitation for 6 hr, 333 liters of air per kg of ore passed through the agitator, and 4.2 kg of NH_3 and 3.4 kg of CO_2 per ton of ore were carried off by the exhaust air still rich in oxygen. Pulp temperature did not exceed 37°C. Assuming that 1.6 pct Ni and 2.4 pct Fe were dissolved, the theoretical amount of air required would have been approximately 100 liters per kg of ore. Under laboratory conditions a large excess was used as found by analyzing the exhaust air, which showed

an oxygen content of 10 to 15 pct. In commercial operation a better efficiency of air consumption can probably be achieved.

Analysis of Exhaust Air from the Agitator: A sample of laterite was agitated in a ratio 1:2.5 with a leach liquor containing 2.16 pct Ni, 5.63 pct NH_3 and 7.06 pct CO_2. The temperature of the pulp was gradually raised during the course of agitation and the exhaust air was analyzed at frequent intervals. (Table XIX)

Table XIX. Analysis of Exhaust Air

Pulp temperature, °C	Corresponding analysis of exhaust air on dry basis by volume	
	NH_3	CO_2 Pct
45	0.2	2.8
48	0.6	3.8
53	1.05	5.05
57	2.6	7.4
65	6.4	13.8
70	12.3	14.9

Leach liquor analyzed at end of agitation: NH_3 5.34 pct, CO_2 5.80 pct. By distilling pregnant liquors the ratio CO_2 : NH_3 as found in the distillate will always be lower than unity although the CO_2 content of the pregnant liquor may greatly exceed the NH_3 content. During the first stage of distillation most of the CO_2 escapes through the condenser as a gas. Fortunately the ratio of CO_2 : NH_3 in the recovered distillate allows this liquor to be used as makeup for fresh leach liquor as needed to dissolve ore values. If the extraction is carried out at high pulp temperature, it may be advisable to feed the exhaust air to the last washing circuit repulper, so that prior to stripping the last amounts in a scrubber the NH_3 and CO_2 values may be reduced.

Effect of Over Reduction upon Settling: The settling rate of pulp, as well as the ratio of solids to liquid in the settled pulp, are of great importance in the successful application of countercurrent leaching and washing. Over reduction results in increased iron content of nickel-iron alloy which requires more air for dissolving, the net effect being that more heat will be generated in the pulp, and more ferric hydroxide will be precipitated from the liquor. Even though greater increase of temperature may counteract this undesired effect to a certain extent the voluminous iron product will retard the settling of the pulp. Pulp temperature should not rise beyond a certain limit. Quite a rise in temperature will occur in treating medium grade ores containing 3 to 4 pct nickel, as was explained earlier. It is obvious that under such conditions over reduction is objectionable. It was observed while watching the settling of tailings containing much secondarily formed $Fe(OH)_3$ that although the bulk of the ore settles fairly well the $Fe(OH)_3$ lags and settles very slowly.

Furthermore such pulp will hold more liquor in the compression state which also affects the countercurrent process unfavorably.

Samples of laterite were reduced under various conditions, the aim being to demonstrate the effect of over reduction. One half per cent of NaCl was added to the ore, the use of which was patented in the original basic Dutch patent, granted to the author March 16, 1925, No. 12975 Klasse 40a, Groep 43.

In order to prevent a reverse effect on extraction the temperature of reduction should be decreased when adding small amounts of sodium chloride to the ore. It should be borne in mind that even the slightest sintering is detrimental to extraction.

The various samples after reduction were leached at room-temperature, ratio 1:8, by 6 hr agitation. The fresh liquor contained 7 pct NH_3 and 5.1 pct CO_2. (Table XX)

Table XX. Results of Leaching at Room Temperature

	I Normal reduction at 900°C, no addition Ni-extraction	Normal reduction at 850°C 0.5 pct NaCl added Ni-extraction	Normal reduction at 900°C 0.5 pct $CaCl_2$ added Ni-extraction
6 hr agitation Color tailing	93.7 pct black	98.1 black	98.— slightly brown from $Fe(OH)_3$
Ratio solids to liquor in pulp in state of compression	100:98	100:103	100:127
Ratio of Co to (Ni + Co) in leach liquor	11.9	11.6	11.6
Comparative rate of settling with each other	94	162	80

Sample II settled about twice as fast as III. The addition of a small amount of NaCl solution to the ore prior to reduction improved the rate of settling quite materially, as can be seen by comparing with I. Extraction is also increased. Reduction of sample III was pushed too far and as a result it settled badly since the pulp contained too much $Fe(OH)_3$.

Addition of $CaCl_2$ increases extraction, but does not affect the temperature of reduction, as experiments showed. Over reduction is objectionable, since it requires more air, generates more heat in the pulp while dissolving the alloy and requires more and larger thickeners in the washing circuit.

Dissolving Cobalt: Although silicate ores of the garnierite type usually contain very little cobalt this metal may be present in a more concentrated form in the ultimate products of weathering from peridotite.

In addition to nickel laterites may contain 0.15 to 0.2 pct cobalt and the red earthy iron oxide deposits from peridotites also may contain greater concentrations of cobalt. The form of occurrence of cobalt in a sample of laterite was therefore investigated. About half the amount of cobalt present could be concentrated by gravity as tiny rather heavy grains, the particles consisting mainly of manganese dioxide. At any rate, it appeared that mechanical concentration procedures could not give a reasonable recovery.

The occurrence of cobalt as very fine mineral particles or combined with iron oxide, probably as a coprecipitate makes it probable that cobalt will be dissolved with nickel when reduced ore is leached with an ammonium carbonate solution, since cobalt, like nickel, forms complex compounds with ammonia. Cobalt being of more basic character than nickel, the oxide is not so readily reduced as nickel oxide. When it is present in the ore, however,

it is reduced simultaneously with the nickel, and no doubt will be present after reduction as a complex alloy of nickel-cobalt and iron, probably with a small content of manganese. Manganese oxide is difficult to reduce, but the presence of nickel and cobalt may facilitate reduction just as iron reduction is facilitated by the presence of nickel.

Leaching tests made on reduced laterite indicated that cobalt can be extracted, but strong leach liquors are essential for high extraction, as may be observed from results given in the next table. The ore was leached in a ratio 1:4, agitating the pulp for 6 hr at room temperature. (Table XXI)

The effect of the temperature of the liquor upon the cobalt extraction was next investigated. For this purpose the same sample of laterite was used, (Ni 1.60 pct) after reduction. The reduced ore was agitated in a ratio 1:8 respectively at 65°, 20°, and 0°C for 4 hr. (Table XXII)

The unfavorable effect of too high temperature of the pulp is evident from the results of tests 1 and 2, and too low temperatures are certainly also not desirable for both nickel and cobalt. A further investigation revealed that the formation of $Fe(OH)_3$ causes a reprecipitation—at least partially—of dissolved cobalt. The effect is more pronounced with increase of temperature but is counteracted by the use of strong liquors, with high NH_3 content. Evidence that Co is reprecipitated by $Fe(OH)_3$ was experimentally proved in the following way.

To a liquor containing 0.22 pct Ni, 0.0324 pct Co and 2.63 pct NH_3, hence to a relatively weak solution, there was added 5 pct of a ferrous sulphate solution containing 1 pct Fe. The liquor was agitated at room temperature for ¾ hr, after which nearly all the iron was precipitated as $Fe(OH)_3$. Therefore, about 0.05 pct Fe was precipitated as $Fe(OH)_3$ from the liquor. By analysis it was found, calculated on the original volume, that the liquor contained after this treatment 0.0259 pct Co, and hence about 16 pct of the cobalt present was precipitated.

By repeating the test, but agitating for 18 hr, the cobalt content proved to be 0.0269 pct, indicating a decrease of 12.8 pct Co. Under these conditions of low NH_3 content of the liquor, cobalt that has been precipitated by $Fe(OH)_3$ is not easily redissolved. This will explain the low cobalt extraction when using weak solutions, that is, liquors with low NH_3 content.

Redissolution of precipitated cobalt is quite evident from the following tests. These tests were done on a bigger scale, allowing samples to be drawn periodically from the agitator (Table XXIII). The same sample of laterite was used for the tests (Ni 1.60 pct). The reduced ore was agitated in the ratio 1:3.

The iron content of the liquor became very low after 4 hr agitation and we see thereafter that the cobalt content increases very regularly.

In the first period of agitation, during the first 2 hr, most of the cobalt has been dissolved, but part of it has been precipitated by $Fe(OH)_3$. Precipitation continues as long as $Fe(OH)_3$ is precipitated from the liquor, during the next 2 hr agitation, and as the cobalt has been dissolved already earlier, the net outcome is, that the cobalt content of the liquor decreases.

On further agitation, the precipitated cobalt is redissolved to quite some extent. Since the nickel extraction increases very regularly, there is no evidence that nickel will also be precipitated by $Fe(OH)_3$, at least not to any appreciable extent.

By treating a liquor almost free from iron with leached ore no effect upon the cobalt content was observed after 6 hr agitation to over 40°C. There is accordingly no evidence that cobalt will be precipitated from the liquor by the ore itself.

Hydrolysis of Pregnant Liquors: Countercurrent washing has proved to be effective for many leaching processes, provided that hydrolysis (from dilution) does not interfere. For this reason, it was of prime importance to investigate carefully the possibility of such interference for this process. This was done for the following pregnant liquors of varying composition: Liquors containing normal, high

Table XXI. Results of Leaching Tests

Fresh leach liquor as used for extraction		Ni extraction	Cobalt extraction
Pct NH_3	Pct CO_2	Pct	Grams per ton of ore
4.32	3.2	80.9	650.–
6.66	5.0	94.4	1452 –
10.85	8.42	94.5	2044.–
13.78	11.10	98.2	2159.–

Table XXII. Effect of Temperature of Leach Liquors

No.	Temperature of liquor °C	NH_3 content of liquor after agitation, Pct	Ni extraction, Pct	Co extraction grams per ton of ore
1	65	6.26	95	1508
2	20	6.91	96	1813
3	0	6.33	85.8	1269

Table XXIII. Redissolution of Precipitated Cobalt

		NH_3 6.6 pct			NH_3 4.3 pct	
Agitation, hr	Temp. of pulp	Ni extr.	Co extr. grams per ton of ore	Temp. of pulp °C	Ni extr. pct	Co extr. grams p/t
Start	14			17¼		
1	20*	52.7	883	23¾	43.4	870
2	24½	72.7	1203	27¾	62.9	1138
3	27	80.9	1000	29½	73.8	870
4	28¾	86.–	740	31	77.7	604
5	28½	92.5	1260	30½	78.8	1111
6	26½	94.4	1470	28½	80.9	1293
7	43†	94.7	1571	27	82.8	
8	37.5	95.5	1577	26	83.3	1361

* Natural increase of temperature, due to the oxidation of the metal dissolved.
† Agitator heated from the outside.

Table XXIV. Analyses of Liquors

	CO_2 Pct	NH_3 Pct	Ni Pct	
I	6.72	4.06	2.31	diluted with distilled water
II	2.84	4.06	2.31	
III	2.58	5.71	2.10	
IV	2.37	7.01	1.92[5]	diluted with 2 pct NaCl dissolved in distilled water
V*	2.84	4.06	2.31	

* Same as II

and low CO_2 content. Analyses of these liquors are given in Table XXIV.

After dilution the liquors remained in closed flasks for 72 hr and were analyzed thereafter. (Table XXV)

These results give the general impression that liquors with corresponding NH_3 and CO_2 content, as given in the examples, but with less nickel content, will not show hydrolysis until a greater dilution has been reached.

Conclusions that may be drawn from these results may be summarized as follows:

1. The critical dilution ratio for hydrolysis, will increase with decreasing carbon dioxide and increasing NH_3 content of the pregnant liquor.

2. From the pregnant liquors investigated, it was evident that liquors with high carbon dioxide content will precipitate basic nickel carbonate at a moderate dilution ratio and liquors with a low carbon dioxide content at a rather high dilution ratio. The first liquors will precipitate nickel more slowly and less completely than the latter liquors on further dilution.

3. The presence of NaCl in the liquors has only little effect upon hydrolysis.

When treating garnierite ores under conditions of countercurrent leaching and washing, there is no need to fear hydrolysis with proper operation, as will be explained below.

Distillation of Pregnant Liquors: In the course of distillation during which the temperature of the liquor is gradually raised, the excess of NH_3 and CO_2 will be expelled first before nickel is precipitated as basic carbonate. Near the point of nickel saturation some of the impurities, e.g. iron, are already partially precipitated, and it may be useful to filter the saturated liquor to improve the quality of the final precipitate obtained after complete distillation.

The following results are indicative of what happens during the first stage of distillation up to the point of nickel precipitation. The pregnant liquor used for this investigation contained: Ni 2.336 pct, NH_3 6.68 pct, CO_2 6.07 pct.

At frequent intervals fractions of the distillate were analyzed. The average NH_3 content of the liquor during the corresponding interval is given. The temperature of the condenser was 8½ °C, the still being heated from the outside. The first fraction of the distillate came off at 75°C and the last at 90°C. (Table XXVI)

From these results we may conclude that the lower the NH_3 content of the liquor, the higher the ratio of concentration in the corresponding fraction of the distillate.

The ratio of CO_2:NH_3 gradually drops in the successive fractions of the distillate up to the point of

Table XXV. Results after Dilution

Nickel precipitated by hydrolysis in pct of the original amount in liquor.

	Ratio of dilution											
	1:5	1:7	1:8	1:9	1:10	1:13	1:15	1:18	1:20	1:30	1:40	1:50
I	be-	8.2 pct					26 pct		37.2	50.6	58.8	61.2
II	gin		be-	6.4	12.6		34.4 pct		51.8	69.7	81.75	86.5
III			gin			be-						
IV						gin		be-	24.—	50.3	65.5	75.5
V	(same liquor as II)							gin	7.8	35.1	53.2	66.4
									49.8	68.2	78.3	82.6

Table XXVI. Values Found

Fraction	Ni pct in liquor	Corresponding average NH_3 content of liquor	Distillate		Ratio of concentration of NH_3 in distillate	Ratio of CO_2:NH_3 in distillate
			Pct NH_3	Pct CO_2		
1st	2.40	6.60	20.83	25.35	3.16	1.22
2nd	2.43	6.35	20.06	25.90	3.16	1.29
3rd	2.30	5.90	19.36	23.91	3.29	1.23
4th	2.59	5.25	17.72	18.79	3.38	1.06
5th	2.67	4.60	15.98	14.66	3.48	0.92
6th	2.75	4.00	13.96	11.27	3.50	0.84
7th	2.786*	3.55	13.26	10.28	3.74	0.775

* Beginning point of precipitation of basic nickel carbonate.

Table XXVII. Pregnant Liquor I

	Precipitated from the liquor 30 pct of the nickel content. Analysis of air-dried basic-nickel-carbonate	Precipitated from the liquor the remainder of the nickel (70 pct). Analysis of air-dried basic-nickel-carbonate
Ni	39.93	36.6
SiO_2	0.073	0.053
Fe_2O_3	0.080	0.023
S	0.065	0.43
Co	0.005	0.01
MgO	0.39	0.045

Pregnant Liquor II

	Precipitated 75 pct of the nickel. Analysis air-dried basic nickel carbonate	Precipitated remainder of nickel (25 pct). Analysis air-dried basic nickel carbonate
	Impurities	
SiO_2	0.060	0.020
Fe_2O_3	0.094	0.021
S	0.065	1.762
MgO	0.371	0.086

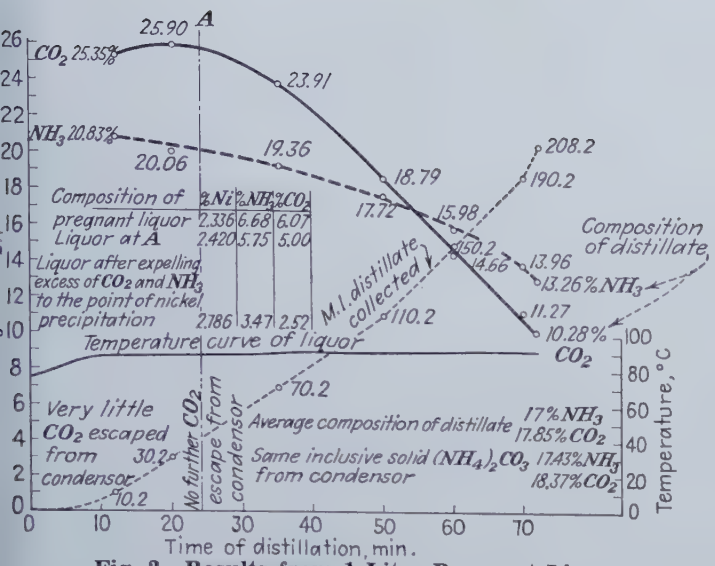

Fig. 2—Results from 1 Liter Pregnant Liquor.
Course of distillation under atmospheric pressure change of composition of distillate. Temperature of condenser 8½°C.

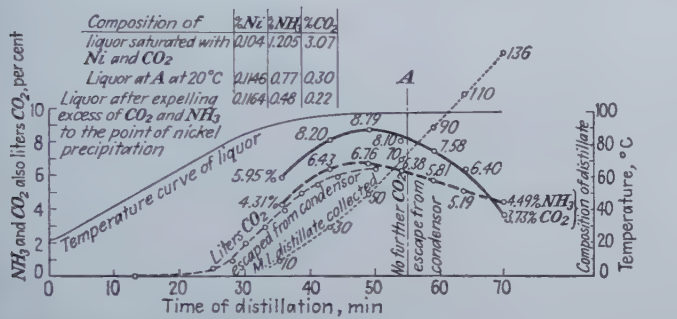

Fig. 3—Results from 1 Liter Weak Liquor.
Course of distillation under atmospheric pressure change of composition of distillate. Temperature of condenser 9°C.

saturation of nickel in the liquor. It may be noted that ammonium carbonate was crystallized out to a certain extent in the first and second fraction of the distillate, and under commercial operation due precautions should be taken in order to prevent trouble of this nature. (fig. 2) (See also figs. 3, 4, and 5.)

Impurities in the Pregnant Liquor: Normally pregnant liquors will be saturated, or nearly saturated, with magnesia, iron, manganese and silica. In addition the liquor will contain sulphur mostly as sulphate. Although the amounts of the first-mentioned impurities may be rather small, they nevertheless contaminate the precipitate of basic-nickel-carbonate obtained by distillation, for these impurities will also precipitate simultaneously with the nickel.

At room temperature magnesium will crystallize from supersaturated solutions as $(NH_4)_2CO_3.MgCO_3$ .4aq. This compound will decompose in boiling water into magnesia alba ($4MgO.3CO_2.4aq$) and NH_3. In the distillation of pregnant liquors most of the magnesia alba will gradually precipitate in the same early stage of precipitation as basic-nickel-carbonate. The same will hold for ferric hydroxide, manganese hydroxide and silica. Sulphur, on the other hand, will precipitate probably as basic sulphate of nickel, increasing gradually in amounts with advance of nickel precipitation. This may be seen from curves given in fig. 1.

Some examples may confirm the statements made with reference to iron, silica and magnesia impurities. (Table XXVII)

Decomposition of Basic Nickel Carbonate by Heat: The basic nickel carbonate obtained by distillation from pure nickel liquors has a beautiful bright light green color. After being air-dried this compound will have the composition $3Ni(OH)_2.2NiCO_3.4aq$. Heating to 100°C will cause a loss of weight of about 12 pct equivalent to 4 aq. At 250°C it will begin to turn black and will become entirely black at 275°C, when it is transformed to a black oxide containing some Ni_2O_3.

This black oxide is changed to NiO at about 800°C when it shows a light olive green color that becomes more pronounced after being heated to 1200°C. Small amounts of cobalt affect the green color of nickel oxide by giving it a brownish shade.

A sample of basic nickel carbonate, after being dried over concentrated H_2SO_4, contained 48.038 pct Ni and 0.3342 pct sulphur largely as sulphate. After being quickly heated to 900°C the nickel oxide had a nickel content of 75.6 pct with only a trace of sulphur.

Dry Versus Wet Grinding: The different types of ore as they are found in deposits from the surface downwards may be classified as: (1) laterite (top layer), (2) a transition zone of soft, entirely disintegrated ore and (3) moderate grade brown colored garnierite ore, almost free of green garnierite. This is partially disintegrated, the bulk consisting of light weight characteristic lumps. These lumps are porous, have little strength, and can be readily crushed.

When these three types are present in distinct layers, it would seem possible under certain favorable conditions to mine each of the layers separately, or to strip the overburden from the more valuable underlying ore. The upper layers overlying the moderate-grade garnierite ore need no comminution prior to reduction; however, it may be advisable to reject pieces of chalcedony if they are present. There is usually a high moisture content of probably not less than 30 pct, but to avoid improper heat balance conditions for a one diameter reduction kiln, the feed should not contain over 15 to 20 pct moisture. Ores containing an excess of moisture should, therefore, be dried till they contain about 15 to 20 pct moisture prior to reduction. The predrier may also serve in mixing a certain amount of powdered coal with the ore.

The (3)-type ore should be finely ground, and the question is whether wet or dry grinding is preferable. In wet milling the ore acquires colloidal properties requiring large thickener area and large filter capacity per unit of ore. The filter cake will contain finally not less than 46-50 pct moisture. Even though wet milling gives a finer product which may increase nickel extraction somewhat, this (3)-type ore already gives satisfactory extractions when ground to a —100 mesh product and dry grinding would probably be more economical. If such is the case a rotary drier should be installed ahead of the mill to expel the 25 to 30 pct moisture that may be expected in this class of ore. After fine comminution, 15 to 20 pct water should be added to the fine ore to give it the characteristics desired for charging to the rotary reduction kiln. The desired amount of coal and pyrite can be added to the

mill feed. When treating this class of ore, about 600 kg of moisture has to be evaporated from each ton of 1000 kg of dry ore, while about 430 kg of moisture would have to be evaporated from types (1) and (2), assuming 30 pct moisture is present.

The real high grade nickel ores, consisting mostly of hydrated silicates of nickel of the true green garnierite type, probably warrant wet grinding, since this class of ore needs to be very finely ground prior to reduction to secure high extractions. When such ore is mined separately, it may be wet ground, some pyrite may be added, and it may be added in right proportion as a slurry to the ore products of types (1), (2) and (3) to give the final mixture the right moisture content for the rotary reducing kiln. If treated separately, the required amount of powdered coal should be added to the filter cake, and after predrying this product to about 15 to 20 pct moisture content it can be fed to the rotary kiln.

Economical considerations in conjunction with the amounts of high grade ore available will naturally determine the flow sheet; obviously, however, the larger tonnages of medium or lower grades of ore will favor the reduction and treatment of mixtures of different types of ore. A mixture of 10 pct high grade garnierite ore ground to a slurry was added to mixed ores of types (1) and (2), as mined, and this final mixture with the desired moisture content was charged to the rotary laboratory kiln with great success. If the different types of ore (2) and (3) or (1), (2) and (3) are rather mixed in the deposits, it will be difficult to make a separation. Run of mine ore should be dried and ground

Table XXVIII. Analysis of Garnierite Ores

	Chemical analyses Pct				Moisture content of pulp in the state of final compression at room temperature, pct	Size of sample
	Ni	Fe	SiO_2	MgO		
I	4.56	1.7	83.6	3.41	36	1.2 pct on 200 mesh
II	2.89	13.53	48.7	6.97	43.2	31.5 pct on 200 mesh
III	4.35	5.32	60.3	15.96	51.2	1.5 pct on 200 mesh
IV	3.17	5.25	43.4	25.12	61.3	33 pct on 200 mesh from which 9 pct on 140 mesh
V	4.62	6.8	44.6	24.54	70.–	1.5 pct on 200 mesh

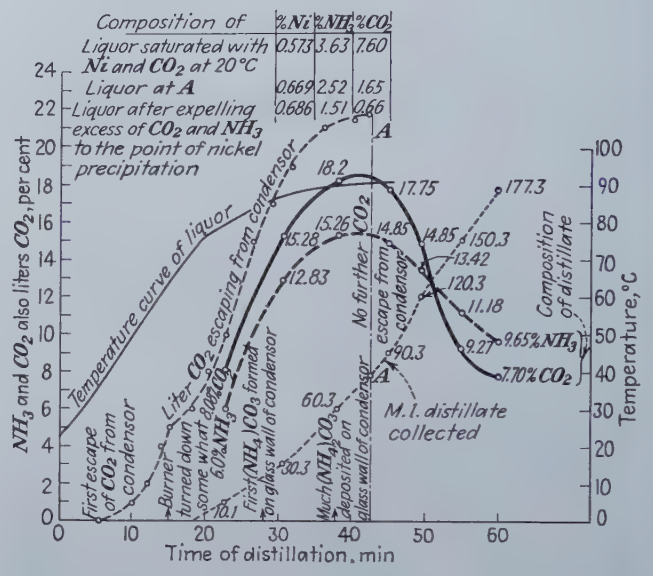

Fig. 5 (Above)—Results from 1 Liter Liquor.

Course of distillation under atmospheric pressure change of composition of distillate at fast rate of distillation. Temperature of condenser 10°C.

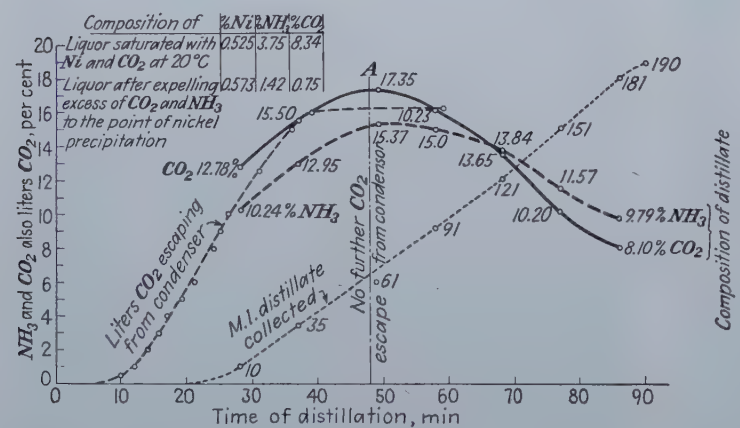

Fig. 4 (Left)—Results from 1 Liter Liquor.

Course of distillation under atmospheric pressure change of composition of distillate at slow rate of distillation. Temperature of condenser 10°C.

entirely ahead of reduction. After dry comminution it is always necessary to add 15 to 20 pct moisture to the ore to give the feed the desired physical properties to prevent flowing in the rotary kiln. For high extractions such mixtures always require pyrite addition and a certain amount of powdered coal. In case types (1) and (2) ores are reduced without preliminary comminution, the reduced ore should be ground with ammonia liquor in a ball mill to the desired degree of fineness in order that a part of the ore will not settle too fast in agitators and thickeners. For the same reason it may be necessary also to pulp up properly the soft porous small-sized lumps obtained from ground ore.

The chemical analysis and the physical nature of garnierite ores may vary considerably, as will be evident from the results in Table XXVIII.

The conclusion that may be drawn from these results is that ores with increasing MgO content and decreasing SiO_2 content will become more colloidal in nature after fine grinding. Above the virgin rock there is usually a transition zone consisting of green appearing boulders that are heavy and dark brown on a fresh fracture. The outside is coated with thin films of garnierite, hence the green color. The boulders consist of nickel containing serpentine, usually having moderate to low nickel content. This material with high MgO content is very colloidal following fine wet grinding after which it can be added as a slurry to dry ground ore to give the latter the desired moisture content.

The Rotary Kiln for Reduction of Oxide Nickel Ores: The rotary kiln has found considerable application because of its simplicity, rather low cost

and high efficiency. On a commercial basis it has been used for reduction of refractory manganese silver ores in Sumatra with highly satisfactory results. Manganese dioxide ores containing about 19 pct moisture and 20 pct manganese dioxide were reduced at about 750°C. Internal heating and simultaneous reduction were obtained by partial combustion of producer gas. 1.3 tons of moist run of mine ore, gave one ton of 1000 kg of reduced ore. This required 577,000 cal using producer gas of 115 Btu per cubic foot. The efficiency of the kiln may be judged from the waste gases leaving the kiln, which normally contained 20-21 pct CO_2 and were almost free from CO and oxygen. These results are encouraging when considered in connection with the commercial application of the rotary kiln for the reduction of nickel ores. If these ores are present in a finely ground state they should never be charged dry, since then they will flow through the kiln. If they are, however, wetted with 15 to 20 pct moisture, soft lumps will be formed and they will roll normally through the kiln. As has been pointed out earlier, a laboratory rotary kiln, internally heated by partial combustion of city gas, gave highly satisfactory results. A few calculations may give a general idea of the dimensions required for commercial units with regard to capacity, etc. We have to assume of course the ore composition, the calorific value of the powdered coal used, the temperature of the gases leaving the kiln, etc.

Partial combustion of low grade high volatile coal from the N.E.I. was investigated experimentally by the author. A full-size Fuller burner was used and the secondary air cut off. Composition of the ore (assumed): Fe_2O_3 28.6 pct, NiO 2.55 pct, combined water 14.85 pct, MgO SiO_2 54 pct. Temperature of waste gases leaving the kiln 300°C.

The one diameter kiln may be divided in three parts: the zone in which the moisture of the feed is evaporated; the preheating zone with a neutral atmosphere outside the actual ore bed, in which early reduction is obtained by powdered high volatile coal present in the charge and where most of the combined water is expelled; the reduction zone, in which the space outside the ore-bed consists of reducing gas obtained by partial combustion of powdered coal.

Experimentally it was found that such gases would contain 10 pct CO_2 and 13 pct CO on a water free basis and that the corresponding gas temperature would be about 1300°C.

Assume the following composition of the coal: C 70 pct, H_2 5 pct, N_2 0.5 pct, O_2 11.5 pct, combined water 5 pct, ash 8 pct. The calorific value of the coal would be per ton (1000 kg) of coal 5,780,000 kg cal. 1000 kg of ore will need 363,000 kg cal for heating to 900°C. If the air dry ore is wetted with 150 kg of water, this amount will leave the kiln as watervapor of 300°C carrying off 113,000 kg cal. All waste gas resulting from complete combustion of powdered coal, in the preheating zone will leave the kiln at 300°C. Per ton of coal the amount of heat thus leaving the kiln will be 1,140,000 kg cal. With good Sil-O-Cel insulation we assume 15 pct loss by conduction and convection of the available heat in the kiln.

5,780,000 — 1,140,000 = 4,640,000 kg cal. Loss of 15 pct would leave actually available per 1000 kg of coal 3,940,000 cal or 68 pct of the total calorific value.

	Cal
1000 kg of ore required for heating to 900°C	363,000
150 kg of watervapor for heating to 300°C	113,000
Total	476,000

1 ton of coal should be sufficient to expel the moisture from and reduce 3,940,000 (476,000) = 8.30 × (1000 kg air dry ore plus 150 kg water). The reduced ore is discharged at 900°C. Per 1000 kg of air dry ore 120 kg coal will be required. If 4 pct powdered coal is added to the ore, 16 pct would be necessary.

It is assumed that in the preheating zone at about 700°C the remainder of the CO will be completely burned by admission of secondary air, which may be easily introduced at the required point.

Assuming a 1.5 meter id kiln, the surface of the lining will be 4.7 m^2 per meter kiln length. Gas volume produced per 1000 kg of coal computed at 0°C and 760 mm Hg will be 6500 m^3.

Per ton of dry ore, there will be used 12 pct coal = 780 m^3 gas at 0°C. If 3 tons of dry ore should be reduced per hr this would require 2340 m^3 gas at 0°C or at 1300°C, 13500 m^3, or per sec 3.74 m^3.

As the cross section will be 1.755 m^2, the velocity of the gas at 1300°C will be 2.12 meters, and at 700°C, 1.31 meter per sec, and the average velocity in the active reduction zone will be 1.72 meters per sec. A gas temperature of 700°C will correspond approximatively with an ore bed temperature of 400°C.

Assuming that all heat is first transferred from the gas to the lining, and that the lining will transfer this heat to the rolling charge and that in the reduction zone the difference between the gas temperature and the lining will be about 350°C, then we will find by applying the formula: $0.000028 (2 + \sqrt{V172} \times 350)$ that 1.48 kg cal per m^2 per sec will be transferred from the hot gas to the lining. Per hr per m 5.300 kg cal.

The required amount of heat in the reduction zone will be 3 × 185,000 cal = 555,000 cal plus 15 pct for convection losses = total 638,000 cal. To take up this amount of heat by the lining would require 638,000 / 5,300 = 120 m^2 / 4.75 = 25.5 meters kiln length. In the first part of the kiln heat is also transferred by radiation. It would be difficult to calculate the actual amount, but it is quite likely that the required amount is taken up by the lining of the kiln in the first 12 meters. The remaining CO in the gas mixture will have to be burned at a temperature of about 700°C in such a way that a neutral atmosphere will result. This procedure will divide the kiln in two zones, one with a prevailing reducing atmosphere, and one with a neutral atmosphere in which the ore is preheated to about 400°C. In the latter, heat transfer by radiation will be of no importance. The heat available in the neutral gas mixture will be transferred to the lining of the kiln and from there to the ore bed. This will require 956,000/8,200 = 120 m^2 lining surface equivalent to 26 meters kiln length, making the total length of the kiln 38 meters for treating 72,000 kg of dry ore, charged with 15 parts of water to 100 parts of dry ore. Increased diameter of the kiln shortens the length for the same capacity. A

kiln of 3 meters id and 38 meters length will have roughly a capacity of 150 tons of ore on the dry basis. It is, however, charged with an additional 15 pct moisture. A feed traveling normally remains in the kiln for 90 min. at an inclination of 1:20 with 1.8 rpm, or at an inclination of 1:15 with 1.35 rpm, giving entirely satisfactory reduction. The ore will be discharged as small soft lumps. The ore bed in the kiln is very porous having approximately a specific gravity of 1.06, as found experimentally in the laboratory rotary kiln. This would give a maximum depth of the ore bed of about 17 to 18 cm for a 150 tons kiln. In the different zones of the one-diameter rotary kiln the heat obtained from the hot gases passing through the kiln is very nicely in balance with the amounts of heat required under the conditions contemplated in each of the zones.

It is well known that in cement kilns the feed may be charged as a slurry containing about 38-40 pct moisture; however, it should be remembered that the clinker formation requires a temperature of about 1500°C and considerably more fuel is required per unit of dry material. As a result there is a large increase of gas volume, greater velocity of gases, greater capacity thereof to evaporate the larger moisture content, and increases in temperature of exhaust gases due to the greater velocity.

It is out of the question therefore, for nickel ores to be fed to the kiln as a slurry and reduced at 900°C, as this would entirely upset the proper conditions required for the reduction. Any moisture in excess of 15 or 20 pct should be evaporated in a rotary drier ahead of the rotary reduction kiln.

Because of their colloidal character and the moisture content of the feed, nickel ores of the sort contemplated when properly wetted, will cause little dusting. The lining of the kiln should be smooth, as an irregular and badly worn out lining causes increased dusting.

According to calculations made, one ton of dry ore, charged with an additional 15 pct moisture, requires 693,700 cal for reduction at 900°C. As the weight of reduced ore may be roughly 15 pct less than that of dry ore, the amount of heat required per ton of reduced ore will be correspondingly higher.

This calculated figure for nickel ores seems very reasonable in comparison with results obtained on a commercial basis in Sumatra, where refractory manganese dioxide containing silver ores were reduced at a temperature of about 750°C. 577,000 cal were required per ton of reduced ore, obtained from 1.3 tons of moist run of mine ore. Treatment of medium grade nickel ores will involve the evaporation of 600 kg of water per 1000 kg of dry solids, as has been pointed out earlier. Roughly 9 pct coal is required to evaporate 450 kg water, bringing the total amount of coal required to dry and reduce the ore at 900°C on a dry solid basis to about 25 pct.

Countercurrent Leaching and Washing: Because of its efficiency this process has found many applications and it will no doubt be feasible for extraction of reduced nickel ores. The following calculations for medium grade reduced nickel ores show the possible effectiveness of such a treatment.

Assuming the following conditions and values: Nickel content of reduced ore 4.4 pct from which 4 pct will be extracted, using a leach liquor containing 7 pct NH_3 and 5 to 7 pct CO_2. A circuit consisting of three groups of agitators with connecting thickeners (A, B and C), and a washing circuit consisting of three thickeners X, Y and Z with an Oliver filter at the end of the circuit (fig. 9) is assumed. The 1st group of agitators will dissolve 80 pct of the nickel values. The 2nd group of agitators will dissolve 10 pct of the nickel values. The 3rd group of agitators will dissolve 2½ pct of the nickel values.

The tailing from the Oliver filter will contain 0.7 ton of solution for each ton of dry solids.

The pregnant liquor will contain 2 pct Ni; hence for each ton of ore treated 2 tons of pregnant liquor will be withdrawn from the circuit to be distilled. The strong fresh distillate will contain 20 pct NH_3, and 0.7 ton of strong fresh liquor will be added to the 3rd group of agitators to make up for the amount withdrawn as pregnant liquor. The pulp will leave the thickeners in a ratio 1:1, whereas the ore will be agitated in a ratio 1:4. For the sake of convenience and simplicity, it may be accepted that all values will be returned by the Oliver filter, as 2 tons of washwater may be used for each ton of dry solids in the tailing. With a displacement factor of 90 pct, 99 pct will be returned, and with a factor of 80 pct, 96 pct. On the basis that all values are returned, the following simplified equation can be made:

$$4B = A + 3C + (1/5\,A)$$
$$4C = B + 2.3X + (1/20\,A)$$
$$3.3X = C + 2.3Y$$
$$3.3Y = X + 2.3Z$$

$$3.3Z = Y + Z \qquad Z = \frac{Y}{2.3} \qquad Y = \frac{X}{2.3} \qquad X = \frac{C}{2.3}$$

$$4C = B + C + 1/20\,A \qquad 3C = B + 1/2\,A$$

$$4B = A + B + 1/20\,A + 1/5\,A \qquad B = \frac{26}{60}A$$

$$\text{or } B = \frac{26}{60} \times 2 \text{ pct Ni} = \frac{52}{60} \text{ pct Ni.}$$

$$3C = \frac{52}{60} \text{ pct Ni} + 0.1 \text{ pct Ni} = \frac{58}{60} \text{ pct Ni}$$

$$C = \frac{58}{60} \text{ pct Ni} : 3 = \text{about } 0.3 \text{ pct Ni}$$

$$Z = \frac{Y}{2.3} = \frac{X}{(2.3)_2} = \frac{C}{(2.3)_3} \qquad Z = \frac{C}{12.167} =$$

about 1/12 C

or $1/12 \times 0.3$ pct Ni = 0.025 pct Ni

$Z = 1/12 \times 7$ pct NH_3 = 0.58 pct or about 0.6 pct NH_3

These are the values in solution in the pulp leaving the thickener Z.

Next comes the reduction of the values by the Oliver-filter.

On the basis of 90 pct displacement we may expect the following losses per ton of dry tailing:

Nickel loss $0.00025 \times 0.7 = 1.75$ g Ni per ton of dry tailing.

NH_3 loss $0.0058 \times 0.7 = 40$ g NH_3 per ton of dry tailing.

On the basis of 80 pct displacement these figures will be respectively for nickel 7 g per ton dry tailing and for NH_3, 160 g per ton of dry tailing and

on the basis of 70 pct displacement the losses will be 15.75 g Ni and 360 g NH_3.

The amount of nickel in the liquor of the pulp leaving thickener C, the lowest value of the circuit, was found by calculation to be 0.025 pct with a corresponding NH_3 value of 0.6 pct. Under these conditions the dissolved nickel values are far from the hydrolysis point, as is evident from the experimental results given for hydrolysis. There need be also little concern for hydrolysis for the displacement of the remaining nickel values in the Oliver-filter cake.

In treating nickel ores with 3 pct soluble nickel and distilling pregnant liquors containing 1.5 pct Ni, almost corresponding conditions may be expected. This also holds for 2 pct soluble nickel pregnant liquors of 1 pct nickel. Generally speaking as far as tailing is concerned the losses of dissolved nickel values will be negligible and those of NH_3 very reasonable. From the pregnant liquors containing 7 pct NH_3 fresh distillates may be obtained with approximately 14 to 20 pct NH_3 values depending upon the conditions of distillation. Should the fresh distillate contain about 14 pct NH_3, then in the 3rd group of agitators 1 ton of 14 pct NH_3 should be added to make up for the amount withdrawn by 2 tons of pregnant liquor of 7 pct NH_3. In this case the amount of washwater will be reduced from 2 to 1.7 tons. Since this amount is still sufficient to wash out the Oliver-filter cake, it has little effect on the outcome, as pointed out earlier. This means that the operation is very flexible and changes in the NH_3 strength of the distillate may be easily corrected by proper control. As basic nickel carbonate is precipitated by distillation, carbon dioxide will be withdrawn from the circuit, and an equivalent amount should be added to the fresh distillate by passing CO_2 through the liquor. Counter-current leaching has a slight disadvantage for nickel ores, in that the pregnant liquor will contain a comparatively large amount of iron. This may however be corrected by aerating the pregnant liquor and separating the precipitated ferric hydroxide by filtration prior to distillation. Concurrent leaching, on the other hand, favors a pregnant liquor of very low iron content which may be distilled directly. When leach liquors have high nickel values extraction is unfavorable, and concurrent leaching is at a disadvantage. If the nickel values in leach liquors are limited to 1 pct, when using leach liquors containing 7 pct NH_3, the difference in yield between concurrent and countercurrent is not of much importance. Under such conditions, however, 4 tons of pregnant liquor will have to be distilled for each ton of ore. Concurrent leaching will increase the ratios between nickel and NH_3 in the countercurrent washing circuit, but hydrolysis may still be avoided by proper operation.

The treatment of low grade lateritic nickelliferous ores is likely to result in a deficiency of washwater when distilling pregnant liquors with at least 1 pct Ni and as a result ammonia losses may be increased to such an extent that steaming of the tailing will be economically justified.

Besides the NH_3 losses contemplated above there may also be losses of NH_3 in the tailing of another sort.

Under certain conditions, for instance, $(NH_4)_2CO_3 \cdot MgCO_3 \cdot 4aq$ may crystalize out when cooling pregnant liquors saturated with magnesia. If such a compound is present in the tailing, it is evident that some NH_3 is lost in a nonsoluble form. The presence of ferric hydroxide in the tailing may also cause losses of adsorbed NH_3. To investigate the magnitude of these combined losses, a sample of laterite was leached in a ratio 1:3 with a solution containing 3.78 pct NH_3 and 3.00 pct CO_2. For some weeks the sample remained in a closed flask at room temperature. The washed tailing was then treated with NaOH and by distillation it was found that the losses of NH_3 amounted to 0.65 kg per ton of dry ore. This does not mean that under commercial conditions losses of NH_3 from this source will be of the same magnitude, for $(NH_4)_2CO_3 \cdot MgO_3 \cdot 4$ aq crystallizes very slowly out from supersaturated liquors. Under countercurrent washing conditions probably NH_3 losses of this nature will be of little importance, if they occur at all.

From the preceding data one may conclude that there will not be much variation in flowsheets for the ores contemplated. It may be expected that the values of the pregnant liquors may vary between 1 and 2 pct (Ni + Co). The NH_3 content will be somewhere near 6-7 pct with a corresponding CO_2 content of 5 to 6 pct. The ratio of solids to liquor in the pulp may vary between 1 to 3 and 1 to 6 according to the metal value of the ore. More or less heat will be generated while the reduced ore is dissolved depending upon the amount of alloy, with a resulting rise in pulp temperature. Increased temperature causes a better settling of the pulp, but the settling rate will remain low for most of the ore pulps to be treated. To a certain extent improvement may be made by adding small amounts of an ammoniacal starch solution, even so the thickener surface required per unit of ore will be rather great. If a general figure could be given, it would be probably about 5 to 6 sq ft thickener area per 24 hr per 1000 kg of dry solids. On the other hand the large amount of washwater available when treating medium grade nickel ores limits the number of washing thickeners required. Dissolving of metals proceeds rather fast, e.g. from 4 to 8 hr agitation will give good yields. Strong agitation and adequate air supply are essential. The agitator capacity required will be reasonable as will be the NH_3 losses in the waste air.

Everything taken into consideration, the ammonia leaching process properly controlled is promising and flexible and permits daily fluctuations of the grade of ore to be treated.

References

[1] *Fortune.* July 1945

[2] *Mining and Metallurgy.* Aug. 1945

[3] *Chem. News.* Oct. 1945

[4] Rev. of the Nicaro Nickel Project, Plancor 690 (Distributed by the office of the Publication Board, Dept. of Commerce, Wash., D. C.)

[5] *De Ingenieur.* Royal Inst. of Eng., The Hague, Holland

54. - 15 - 29 - 1939 (No. 13)
58. - 37 - 40 - 1946 (No. 22)
59. - 21 - 22 - 1947 (No. 24)
59. - 31 - 41 - 1947 (No. 32)

Separation of

Nickel and Cobalt

by M. H. Caron

This article describes several chemical methods for separating nickel and cobalt as obtained by ammonia leaching.

An electrolytic method for separating alloys of the two metals is also described.

THE most outstanding property of ammonia liquors, used in the ammonia leaching process is their very limited ability to dissolve all compounds present in reduced ore except nickel and cobalt. Although they do have such a high degree of purity, even the smallest amounts of impurities contaminate the precipitate of basic nickel carbonate that may be obtained from pregnant liquors by straight distillation. Figures have been given in a separate paper regarding the extent of such contamination. The product of straight distillation is likely to contain small amounts of Fe, Mn, MgO and SiO_2 as well as some sulphate and sulphide.

The sulphur can be readily eliminated by calcination of the product at the proper temperature and MgO and SiO_2 by reduction and melting of the metal with a suitable flux. After such treatment the metal is relatively pure, and the iron and manganese content will be very small. The cobalt content, however, may vary considerably, depending upon the ore treated. The metal obtained from pure true garnierite ores usually has only a small cobalt content of less than 1 pct. Metal obtained from medium grade iron-rich nickel ores may show cobalt values from 2 to 3 pct, and the alloy obtained from laterite is likely to contain as much as 10 pct cobalt. By proper treatment a good deal of cobalt may be recovered from lateritic nickeliferous iron ores, and cobalt will become the major constituent of the pregnant liquor if asbolan ores or similar products are treated. The pregnant liquor of "run of mine" nickel ores may have a pinkish shade, indicating the presence of cobalt. It is evident that from such liquors the metals should be recovered separately. Even if cobalt is present in only very small amounts, it would probably be economically justifiable to recover both metals as pure as possible if a suitable process could be devised. The author has made investigations along this line and has patented some processes adapted to the treatment of this type of solutions.

Selective Dissolution of Nickel from Basic Nickel Carbonate Containing Some Cobalt: Basic nickel carbonate obtained from true garnierite ores by straight distillation of the pregnant liquors, always contains some cobalt as well as the normal impurities. In order to improve the quality of the nickel product and to recover most of the cobalt, the following process has been devised. By using liquors with a low CO_2 to NH_3 ratio, nickel can be redissolved preferentially to cobalt. It is not a sharp and clean separation but a selective one, for the bulk of the nickel may be redissolved with a small amount of cobalt, and a small residue may hold the bulk of the cobalt. The greatly increased cobalt content of the residue is indicated by a pronounced olive green color, in contrast with the light green color of pure basic nickel carbonate. The following example is given from Dutch patent No. 52788, Klasse 40a. 43 granted June 17, 1942: The original precipitate contained about 0.55 pct cobalt calculated on total nickel + cobalt. Eight hundred and fifty grams of the basic nickel carbonate were redissolved in leach liquor containing 7.12 pct NH_3 and 2.12 pct CO_2. The weight of the dry residue was about 3.5 pct of the original weight. By analysis it was found that the residue contained: Fe 1.93 pct, Co 6.01 pct, Ni 34.87 pct and also a certain amount of silica. The clear filtered blue liquor was distilled and the precipitate of basic nickel carbonate from this analyzed: Fe 0.008 pct, Co 0.0146 pct, Ni 42.37 pct.

It is obvious that this product is considerably more pure, since calculation shows that about 94 pct of the original cobalt remained in the residue.

Cobalt and nickel can be recovered by further

M. H. CARON, Member AIME, is Professor of Metallurgy, Delft Univ., Delft, Holland; and Metallurgical Adviser, Billiton Co.

New York Meeting, Feb. 1950.

TP 2740 D. Discussion (2 copies) may be sent to Transactions *AIME before Apr. 1, 1950, and is tentatively scheduled for publication Nov. 1950. Manuscript received Sept. 20, 1949.*

treatment of the residue. One unfavorable result of this simple process is that the residue is rather slimy and filters very badly in contrast with the original product. This is no doubt partially due to the silica content, which, although small in the basic nickel carbonate originally, accumulated in the residue.

Selective Precipitation of Basic Nickel Carbonate from Pregnant Liquors by Interrupted Distillation: To avoid the filtration difficulties of the slimy residues obtained by selective dissolution another process not having this inconvenience has been devised and patented. (Dutch patent No. 52607 granted May 16, 1942, and U.S.A. patent No. 2,290,-313, granted July 21, 1942.)

The following example is given in these patents: Starting from a pregnant solution containing in proportion 1.1 pct cobalt to (Ni + Co), by selective precipitation it was found possible to precipitate first the bulk of the nickel with very little cobalt, then by further distillation of the clear filtrate thereof, the bulk of the cobalt was collected in a relatively small final precipitate. Both products filter excellently. Earlier it was pointed out that most of the iron, manganese, magnesia and silica impurities will come down during the first stage of distillation, whereas most of the sulphur will be precipitated towards the end of distillation. It is obvious therefore that the bulk of the nickel precipitated first collects the greater part of the impurities and that the cobalt-rich final product holds comparatively few impurities but considerably more sulphur. The following results are quoted from the U.S.A. patent: "A nickeliferous and cobaltiferous ammoniacal solution of ammonium carbonate was subjected to four stage distillation, and the four precipitates so formed were isolated, the result being:

	Amount in mg of		Proportion of cobalt Pct
	Ni	Co	
In first precipitate	563.1	0.60	0.107
In second precipitate	5623.1	6.24	0.111
In third precipitate	281.0	17.62	5.9
In fourth precipitate	134.7	48.1	26.3

Thus more than 90 pct of the total amount of cobalt present in the ammoniacal liquor was concentrated in the last two precipitates, and these contained only 6.3 pct of the total amount of nickel. The first two precipitates contained 93.7 pct of the nickel, the proportion of cobalt thereof being lower than that of electrolytic nickel." The amount of Co in the nickel-precipitate is about 0.11 pct of (Ni + Co), or 1/10 of the original proportion as present in the pregnant liquor.

Vacuum distillation will proceed at lower temperature, and experimentally it has been found that the precipitate of basic nickel carbonate thus obtained will hold somewhat less cobalt. The same was observed by passing CO_2 through the liquor during the course of distillation in order to accelerate the distillation. As NH_3 will be expelled faster from the liquor by this procedure, the greater part of the precipitate was formed at a somewhat lower temperature, hence the better result. Both processes, selective dissolving and selective precipitation of basic nickel carbonate, may under certain conditions give similar results as far as the concentration of cobalt is concerned. The final nickel product of the first process, however, will contain fewer impurities than the product obtained by selective precipitation. The latter process, on the other hand, is more simple and economical and excellent filtering products will be obtained from it.

Precipitation of Basic Nickel Carbonate of High Purity from Pregnant Liquors. General Aspects: Although the results so far obtained by the processes discussed, were rather satisfactory from the point of view of cobalt concentration in a small residue, yet they have not given full satisfaction with regard to the elimination of impurities from the main product. Sulphur, for instance, should be eliminated from the improved nickel product by calcination at high temperature, and even though this operation may not be considered a problem, it will be an economical improvement if it can be avoided. The author has devised a process for the almost complete elimination of all impurities, including sulphur, from the main nickel product. This process consists of one single and simple treatment. (See Dutch patent No. 55376 40a.43, granted Sept. 16, 1943, and French patent No. 931,765, granted Aug. 2, 1946.)

Earlier evidence was given that it is the CO_2 content of the leach liquor that is mainly responsible for holding impurities such as Fe, Mn and silica in solution. These impurities will be precipitated during the course of distillation while the CO_2 is being expelled from the solution. It has also been pointed out that ammonium carbonate solutions having a ratio NH_3 to CO_2 as 1 to 2.2 have but a limited solubility for nickel. The CO_2 content of solutions may be increased materially by saturation of the solution with gaseous CO_2 at room temperature. Under such conditions solutions may be obtained which hold three times as much CO_2 as NH_3, and such solutions are indeed very poor solvents for nickel. On the other hand if the ratio NH_3:CO_2 is 1:1, they are good solvents for nickel and can hold a maximum amount of nickel in solution. Such liquors saturated with nickel may be easily obtained by partial distillation of pregnant liquors only to the point when nickel begins to precipitate. After cooling to room temperature, such solutions can be readily saturated by CO_2, causing the bulk of nickel to precipitate from the supersaturated liquor. Under such conditions, however, the solubility of the liquor for Fe, Mn, SiO_2 and MgO does not diminish and will even increase. Hence it is obvious that the impurities will remain in solution while basic nickel carbonate is precipitated, which also holds true for the sulphate present in the liquor. These fundamental factors will give the product the high purity desired. Last, but not least, the primary aim of keeping the cobalt in solution is nearly fulfilled, for very little cobalt will come down with the basic nickel carbonate. Separation of nickel from cobalt is thus more effective with the low temperature precipitation process than with the two processes previously mentioned. (Table I).

Total amount of Ni precipitated from liquor 79.3 pct. The percent cobalt, (pct Co in Ni + Co) as present in the precipitate is 0.125 pct or 1/40 of the

original ratio as present in the pregnant liquor. This result gives a fair idea of the effective elimination of impurities and how small the tendency is for cobalt to contaminate the nickel precipitate. The process opens the possibility for double treatment. As most of the nickel precipitates from the liquor, there is an excess of NH_3 in the filtrate that can be expelled again by partial distillation, and the cycle can be repeated. (Table II).

Relationship Between the Amount of CO_2 Absorbed by the Pregnant Liquor and the Amount of Ni precipitated: The lower the temperature of the liquor, the more CO_2 that can be taken up and the larger the precipitate of basic nickel carbonate. (Table III).

It is also interesting to note that a considerable increase in nickel precipitated can be gained by dilution of the nickel-saturated liquor prior to saturation with CO_2.

A pregnant liquor containing not less than 3 pct nickel was saturated at room temperature with CO_2.

Table I. Results

Analysis of pregnant liquor saturated with nickel		Analysis filtrate after CO_2 saturation on original volume	Analysis washed and dried basic-nickel-carbonate	
	Pct	Pct		Pct
Ni	0.701	0.145	Ni	39.62
NH_3	1.27	1.18	Co	0.05
CO_2	1.38	3.82	Fe	trace
SO_4	0.136	0.135	MgO	0.006
Pct Co of Co (Ni + Co)	0.036	0.036	SiO_2	0.004
	5	20	SO_4	0.005

The fall of basic nickel carbonate was very bulky and 62.4 pct of the nickel was precipitated. The filtrate was diluted with water to twice the volume, whereupon it could take up a good deal of CO_2 again. The total effect was that 89 pct of the nickel was precipitated, a material increase making a double treatment superfluous. It should be realized that

Table II. Example

	Pct NH_3	Pct CO_2	Pct Ni	Pct Co	Pct Co in (Ni + Co)	Precipitate Pct Co in (Ni + Co)
Pregnant liquor	1.27	1.38	0.701	0.367	5	
1st filtrate	1.18	3.82	0.145	0.364	20	0.125
2nd filtrate	0.39	0.92	0.077	0.363	32	0.36

Table III. Example

	Pregnant liquor	Filtrate after saturation with CO_2 at 20°C	Filtrate after saturation with CO_2 at 0°C
Ni	1.71	0.396	0.28
NH_3	3.04	2.87	2.94
CO_2	2.57	6.12	6.89
Pct nickel precipitated from liquor		76.8 pct	83.6 pct

in this case twice as much solution should be distilled to recover the remaining Ni (and Co) from the mother liquor. It is advisable to expel with wet live steam the excess NH_3 and CO_2 from the pregnant liquor, thus increasing naturally the volume of the liquor. A single treatment makes a much

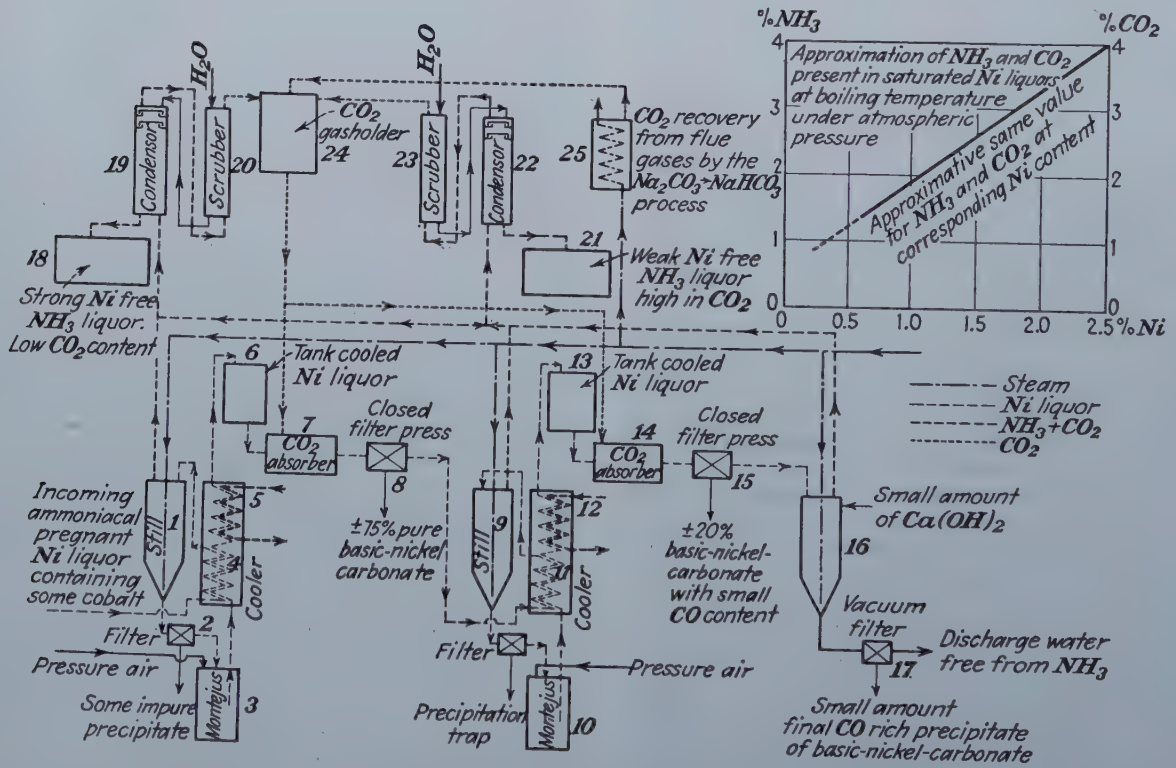

Fig. 1—Flow Sheet

for the recovery of very pure basic nickel-carbonate and a small intermediate product materially enriched with cobalt.

simpler flowsheet and should be given preference whenever possible.

As has been outlined above, a dilution of the liquor with H_2O to twice its volume, will materially increase the amount of nickel that can be precipitated by CO_2 saturation of the liquor. This increase, however, does not continue to any extent by further dilution. This was borne out by experiment. A liquor saturated at boiling temperature with nickel, as indicated by a visible turbidity and cooled thereafter to room temperature contained 2.8529 pct Ni and 4.35 pct NH_3.

The saturation with CO_2, at room temperature, was affected in a closed agitator under a constant pressure of 780 mm Hg. Under these conditions, the NH_3 content of the liquor remained unchanged during the saturation, and the temperature of the liquor was measured immediately after saturation.

heating has some advantage in that it will give little dusting, because of the small gas volumes passing through the cylinder. A more dense metal sponge can also be obtained in a rotary kiln internally heated by partial combustion of sulphur free gas, and it would be an easy matter to produce Ni-sponge at 900°C or 1000°C. Cyclones will, of course, be required because of the greater dusting. The sponge obtained at 700°C is still very light but can be easily compressed to "rondelles"; the sponge produced at 1000°C is somewhat more dense. If the nickel is to be used in the production of nickel plate, or in the normal dense form, it must be melted. Because of the high purity of the sponge, it should be borne in mind that every additional treatment is apt to introduce impurities into the metal.

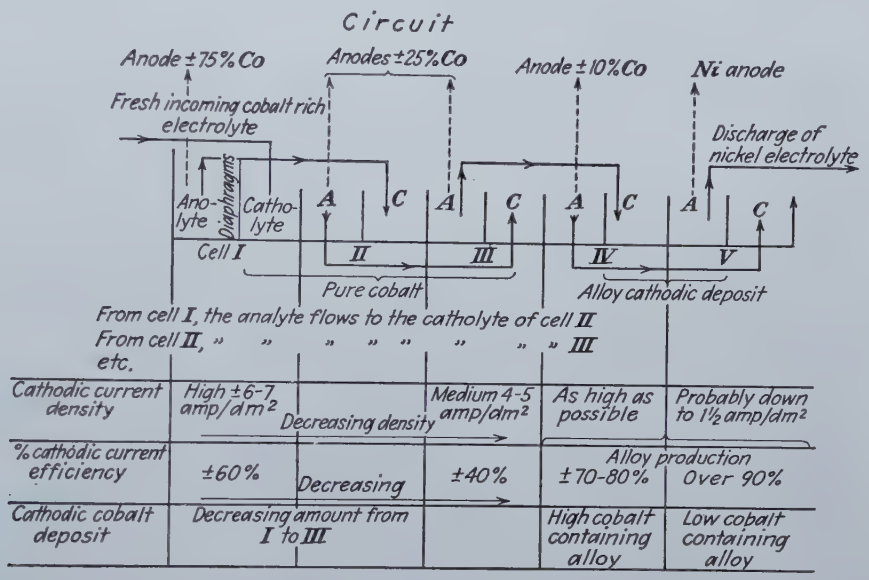

Fig. 2—Circuit of Cells.

Parts of the original liquor were also diluted with one, two and three times their volumes with water. Thus the corresponding values of nickel and NH_3 of those samples were respectively 1/2, 1/3 and 1/4 of that of the original sample. (Table IV).

Under vacuum the precipitate of basic nickel carbonate filtered excellently. No cracks were noticed in the filter-cake.

The Significance of Very Pure Basic Nickel Carbonate: The process as described has many advantages in producing nickel oxide or nickel of a very high degree of purity as compared with other processes.

A simple calcination at about 300°C gives black oxide, containing some Ni_2O_3, a voluminous product quite different from the heavy dense green product, NiO, obtained by calcination at 1000-1200°C. It is questionable if the black oxide can find a market but if it can, production is very simple. All that should be required is a rotary steel cylinder, externally heated to recover simultaneously the CO_2 expelled from the basic carbonate. To obtain very pure sponge metal, calcination and reduction with a sulphur free gas can be readily accomplished by external heating at 700°C in a rotary steel cylinder of heat resisting steel. In this special case external

Nature of the Basic Nickel Carbonate as Obtained by Saturation of Solutions at 20°C with CO_2. Analysis of Product Air-dried at Room Temperature: *Analysis:* Ni 35.36 pct, H_2O 33.78 pct, CO_3 28.94 pct. By calculation it was found that 5 mol Ni has combined with 3.975 mol CO_2 or more likely it will be 5 with 4. Hence the product probably has the following chemical structure.

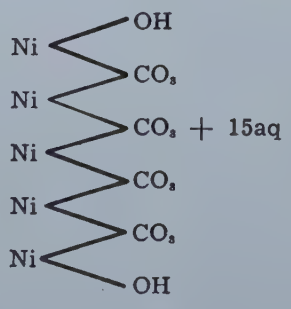

The amount of H_2O present in the compound depends upon the formation temperature of the basic nickel carbonate.

	Ratio NiO:H_2O	
Distilled at 93°C	5.9	all samples dried at room temperature
Vacuum distillation at 78°C	4.8	
Vacuum distillation at 73°C	4.35	
Saturation with CO_2 at 22°C	2.09	
Saturation at about 0°C	1.6	

It was also found that the CO_2 content of the basic carbonate, precipitated by saturation with CO_2, increased with decrease of temperature of the solution. The CO_2 content of the solution increased at the same time. No doubt there is a close relationship between the CO_2 content of the basic nickel carbonate and the CO_2 content of the solution. The CO_2 is loosely bound in compounds obtained at low temperature as was observed in a product obtained at 0°C by saturation of the solution with CO_2. While being washed with hot water it spontaneously lost part of its CO_2 content. The product is voluminous but nevertheless it filters very well.

Table IV. Results

Dilution with H_2O	Saturated with CO_2 at °C	Remaining Ni in solution computed to original volume	Pct Ni precipitated from liquor as basic Ni-carbonate	Remarks
None	24	0.6084	78.7	Fluidity of the suspension good
1 x vol	23.5	0.3291	87.8	Very fluid, CO_2 was taken up fast
2 x vol	22.5	0.3265	88.9	Idem
3 x vol	23.0	0.3352	88.6	Idem

Nature of Cobalt Present in Small Amounts in Basic Nickel Carbonate: Some information has been obtained from solutions free from nickel and impurities, containing only Co, NH_3 and CO_2. By distilling such pure cobalt solutions, $Co(OH)_3$ will be precipitated after the excess of NH_3 and CO_2 has been expelled.

If only part of the Co is precipitated by distillation, no precipitate is formed when the dark red filtrate is cooled to room temperature and saturated with CO_2. The high CO_2 content of the liquor does not diminish the solubility of cobalt. Products obtained by distillation may contain more or less $Co(OH)_3$. There is no indication, however, that basic nickel carbonate, formed by CO_2 saturation of the liquor at room temperature, would contain such a compound or any other Co compound.

It was observed that cobalt present in such products will color the washwater, even after repeated washings. If the filtrate at last becomes colorless a rose-colored filtrate may appear again after the addition of hot water. The cobalt content of such products depends not only on the amount of washwater used but also upon the temperature of the washwater. Indications are that physical sorption is partially responsible for the cobalt content of basic nickel carbonate, since the product only loses its cobalt content gradually with prolonged washing. The same phenomenon was observed while washing products obtained by straight distillation. For such products there are possibly two causes for the presence of cobalt: (1) precipitation of some $Co(OH)_3$; (2) physical sorption by the basic nickel carbonate.

It was further proved that nickel products obtained from vacuum distillation contain somewhat less cobalt than products from normal distillation, and products obtained by CO_2 saturation at low temperature show the smallest amounts of cobalt.

The conclusion may therefore be drawn, that the nickel products should be thoroughly washed with ample hot washwater.

Heat of Neutralization: When carbon dioxide combines with dilute ammonia solutions, heat will be liberated according to the equation:

$$H_2O + 2NH_3 + CO_2 = (NH_4)_2CO_3 + 10.7 \text{ cal.}$$

The result is that for each 4.1 pct CO_2 taken up by the ammonia solution its temperature will rise 10°C if the specific heat of the solution is assumed to be one. Liquors saturated with about 2 pct nickel may rise 15°C or more in temperature by complete saturation with CO_2, if no heat is lost by conduction or other means. It is therefore essential either to cool the liquors sufficiently prior to saturation with CO_2, or during the saturation.

Solubility of Nickel in Washwater: If basic nickel carbonate is washed with hot water on a suction filter, the washwater may contain about 0.01 pct Ni. Agitating basic nickel carbonate with distilled water at room-temperature and in the meantime saturating the water with CO_2 results in the appearance of pale green liquor containing about 0.1 pct Ni. Obviously the solubility of basic nickel carbonate in water increases with increasing CO_2 content.

By adding a small amount of a clear solution of $Ca(OH)_2$ to the washwater, nickel ceases to be soluble, as is the case when very small amounts of

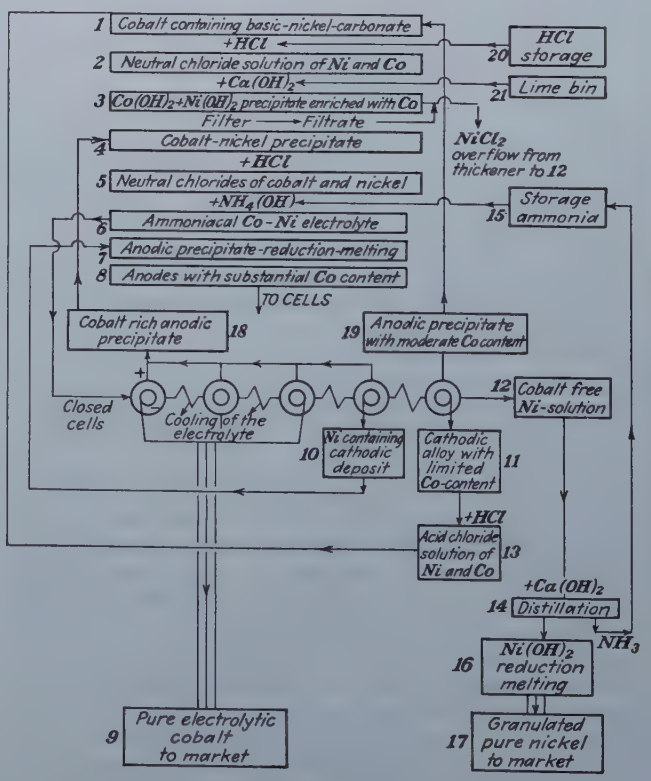

Fig. 3—Flow Sheet.

Electrolytic separation of cobalt and nickel.

ammonia are added. It is merely a question of bringing the pH of the washwater somewhat above 7.

When basic nickel carbonate is washed with water or wet steam, the washwater will contain small amounts of nickel and cobalt. By adding a small amount of $Ca(OH)_2$, nickel will be quantitatively precipitated as the hydroxide almost free from cobalt, while cobalt may be precipitated by adding Na_2S to the clear colored filtrate. Losses can be thus prevented, but it would be more practical simply to return the washwater to the pregnant solution prior to its saturation with CO_2, since a dilution of the solution is in this case desirable.

Distillation of Liquors Saturated with CO_2: It is characteristic that when solutions saturated with CO_2 are distilled, the bulk of CO_2 will come off in the early stage of distillation before the NH_3, and most of the CO_2 simply passes through the condensor as a gas. NH_3 and CO_2 are found in about equal amounts in the condensate and in exactly the desired ratio for making up fresh leach liquor. The recovery of both gases in the condensate is almost complete in the case of solutions containing less CO_2 than NH_3.

Recovery of basic nickel carbonate from the pregnant solutions will withdraw an equivalent amount of CO_2 from the ammonia circuit, and CO_2 must therefore be introduced in the strong fresh ammonia liquor to make up for the loss. Assuming that basic carbonate of nickel will be calcined in such a way that the CO_2 expelled from the compound can be recovered by passing through the fresh strong condensate, it is obvious that except for inevitable losses, the CO_2 cycle is fully closed. No doubt the process outlined will prove to be quite feasible and attractive since it gives very pure products. The progress of distillation of four different types of solutions has been plotted on curves. They are comprehensive and need no further comment (see TP2739D, page 67, this issue).

Flowsheet (fig. 1). Although a single operation seems preferable, a double stage treatment may be required to get a sufficient concentration of cobalt in the final product. For this reason a two-stage flowsheet has been drawn to clarify the required steps. To secure a final complete recovery of all the values, it is necessary to add a small amount of $Ca(OH)_2$ to the still to break up small amounts of $(NH_4)_2SO_4$ that may be present and may hold some nickel, cobalt, and ammonia in solution. In the right upper corner of the flowsheet a straight line has been plotted, indicating roughly the corresponding NH_3-CO_2 values of solutions in the presence of more or less nickel. These solutions are distilled until the first precipitate of basic nickel carbonate appears. As has been pointed out earlier, the NH_3 and CO_2 contents are not exactly equal in such solutions but for a rough orientation this line may serve the purpose.

Electrolytic Separation Methods

General Features of the Process. The three processes discussed so far aimed at the recovery of a primary nickel product containing very little cobalt and the concentration of cobalt in a relatively small amount of secondary product. From this secondary product both nickel and cobalt should be recovered in a pure state if possible. This problem has been solved by the author in two different ways. On the electrolytic process, patents have been granted in the Netherlands No. 61227, Klasse 40c. 8, May 16, 1948, and in France No. 936,742, granted Aug. 9, 1946.

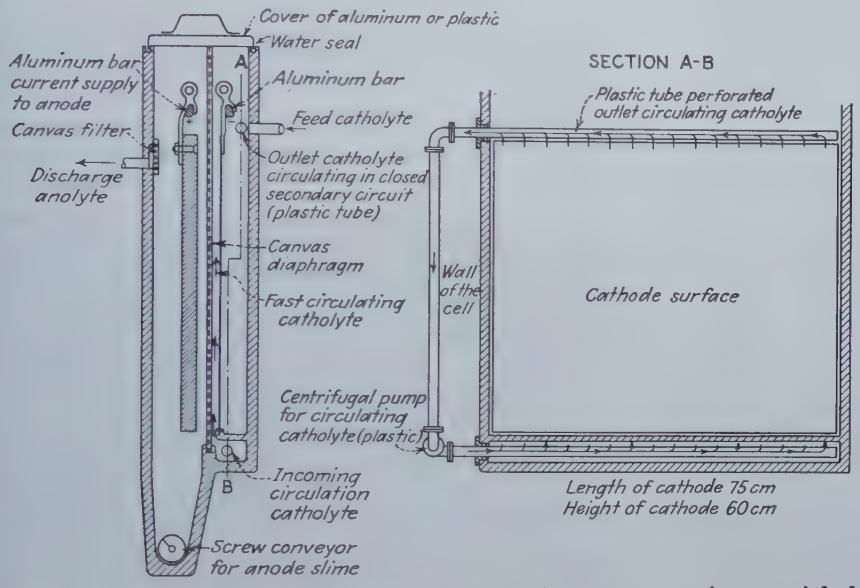

Fig. 4—Sketch of Proposed Construction for Cell.

The general features of this process will be discussed in the following pages, but it is first of interest to refer to an article that appeared in "Transactions of the American Electrochemical Society" Vol. LVIII (1930), (see p. 377, and the corresponding curve on p. 375). The article discusses the electrolytic deposition of nickel and cobalt from acid sulphate and chloride solutions, both metals occurring as simple ions. Experimentally it was found that cobalt was deposited in preference to nickel. From electrolytes containing both metals in equal proportions it was observed that pure cobalt was deposited, and as a result the cobalt content of the electrolyte decreased and nickel began to precipitate. As the ratio Co:Ni dropped to 3:97, an alloy was plated on the cathode containing both metals in equal proportions. Using an alloy con-

taining 50 pct each of nickel and cobalt as anode, in a closed circuit an equilibrium will be established when the ratio Co to Ni in the electrolyte is 3:97. From that moment the alloy dissolved at the anode will be simply transferred to the cathode, assuming that the current efficiencies for anode and cathode are the same.

Under white electroplating conditions this actually takes place.

An analysis of the electrolyte, however, would reveal a much lower Co:Ni ratio than present in the anode. It is generally accepted that the separation of nickel and cobalt by electrolysis is not easy.

Characteristics of the method devised by the author may be summarized as follows:

1. The use of ammoniacal electrolytes free from impurities.
2. The use of soluble anodes of Co-Ni alloys.
3. The use of electrolytes of compositions that will show the strongest possible tendency of cobalt to be plated free from nickel.
4. The adoption of an open circuit, passing the electrolyte through a number of cells in series, producing continuously pure cathodic cobalt in the upper part of the circuit, and discharging a cobalt-free high nickel electrolyte at the lower end of the cells.
5. Securing a strong circulation of the catholyte along the cathode, and keeping the anolyte separated from the catholyte, e.g. by a canvas diaphragm.
6. Using closed cells.

The process is further characterized by a great difference in cathode and anode current efficiency, which in conjunction with the tendency to form insoluble basic cobalt nickel compounds with highly increased cobalt content at the anode, has greatly helped to solve the problem. The basic compounds with a high cobalt content can be dissolved readily and may be returned as electrolyte to enrich the cobalt content of the electrolyte in the upper cells, thus facilitating the deposition of pure cobalt. At the lower end an almost cobalt-free high nickel containing electrolyte is discharged. By distilling this solution after the addition of $Ca(OH)_2$ or NaOH, nickel will be recovered as hydroxide and ammonia will be returned to the process. The ammonia circuit is therefore entirely closed. Having now outlined the main features, it will be necessary to discuss the process more in detail.

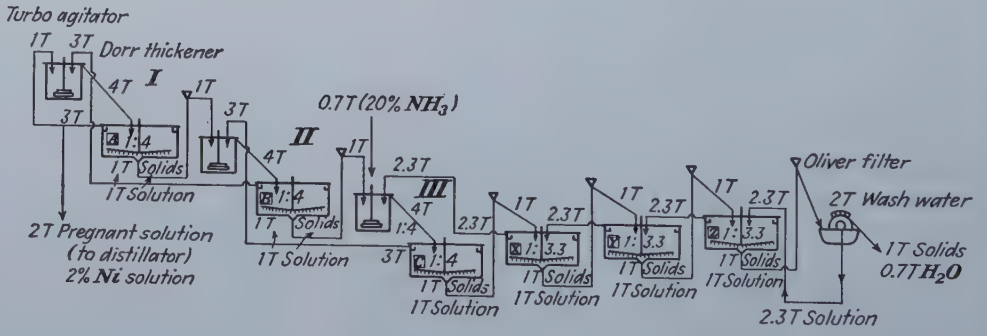

Fig. 5—Flow Sheet for Celebes Reduced Nickel Ore.

Amount of solution per ton of ore.

Chemistry of the Process: From basic nickel carbonate enriched with cobalt, neutral chloride solutions may be obtained readily by dissolving an excess of the product in hydrochloric acid. This reaction will proceed with the liberation of CO_2 and the evolution of a good deal of heat. In such solutions both metals will be present in the bivalent state. Instead of hydrochloric acid, other acids such as sulphuric acid, acetic acid, etc. may be used to produce neutral liquors. By adding sufficient ammonia to such solutions, soluble complex compounds will be formed. There is, however, a difference in behavior between nickel and cobalt. Nickel, the more noble metal, will remain in the bivalent state, whereas cobalt, having a more basic character, will be changed readily to the trivalent state in ammoniacal liquors that are in contact with the air. The freshly prepared liquor has a brown color, and as it comes in contact with the air the color becomes gradually darker, becoming finally a dark red as a result of oxidation.

The cobalt is changed to the trivalent state, and the solution is clear if sufficient NH_4Cl is present. This oxidation result may be obtained instantaneously by adding hydrogen peroxide.

In the absence of NH_4Cl, oxidation of cobalt will proceed just the same, but the result will be somewhat different, as is evident from the following equation:

$$3CoCl_2 + H_2O + 1/2O_2 + 10NH_3 = 2Co(NH_3)_5Cl_3 + Co(OH)_2.$$

In the absence of chlorine one third of the cobalt will precipitate as $Co(OH)_2$, and will be gradually oxidized to the brown colored $Co(OH)_3$, while the clear filtrate will be dark red colored. In this ammoniacal chloride solution cobalt will be present as $Co(NH_3)_5Cl_3$. This compound may crystallize out if the ammonia content of the solution is insufficient or if the concentration of cobalt is too high.

On adding ammonia to chloride solutions $CoCl_2(NH_4)Cl$ will be formed as an intermediate compound that will readily change to $Co(NH_3)_5Cl_3$ on further addition of ammonia. And if there is sufficient chlorine as free HCl or NH_4Cl present in the liquor there is no reason that $Co(OH)_3$ should be formed. In the absence of excess acid it is obvious that no NH_4Cl will be formed, assuming that no dissociation of $Co(NH_3)_5Cl_3$ takes place. Cobalt is thus present in the solution as $Co(NH_3)_5Cl_3$ when the simple ammonium salt (NH_4Cl) is not present.

As nickel will remain in the bivalent state while being converted to the ammoniacal complex compound $NiCl_2.6NH_3$ a clear ammoniacal solution will be obtained from a neutral nickel chloride solution without the formation of any precipitate when sufficient ammonia has been added. The ammoniacal solutions that may be obtained from basic nickel carbonate enriched with cobalt may therefore be divided into two distinct classes: *a.* Solutions con-

taining both metals, nickel and cobalt, as ammoniacal complex compounds free from simple ammoniacal salts such as $(NH_4)Cl$, $(NH_4)_2SO_4$ etc.; and *b*. solutions that do contain a certain amount of simple ammoniacal salts such as $(NH_4)Cl$, etc. in addition to the complex compounds of nickel and cobalt. The last class may be obtained by purposely adding simple ammonia salts to the class mentioned under (*a*), or by starting with solutions containing a certain amount of free acid.

Cathodic Reactions: If an electric current is passed through an ammoniacal solution containing both metals, cobalt is not at once precipitated, but it takes some time before the first deposit is formed. Under certain conditions of relatively low current density no cobalt will be deposited at all if the electrolyte is free from nickel, because cobalt will be present in the trivalent state. The first reaction at the cathode will be:

(1) $Co^{+++} + e^- = Co^{++}$ (a reduction from the trivalent to the bivalent state).

In contact with the air, oxidation may offset this reduction,

(2) Co^{++} + oxidation by air = Co^{+++}.

Both reactions may be in equilibrium at a certain current density, etc., and under such conditions cobalt will not be deposited at the cathode. At least this will hold true if we assume that cobalt can be plated only from the bivalent state, and there is no reason for another conception. The mechanism of the cathodic reactions as discussed readily explains the very low cathodic current efficiencies observed experimentally under low current densities.

As soon as reaction (1) predominates, cobalt is plated out,

(3) $Co^{++} + 2e^- = Co$

but not until a certain current density is reached. All cathodic current efficiencies to be discussed have been calculated on the basis that cobalt was plated from the bivalent state, implying that theoretically about 1100 mgr Co will be deposited per amp hr. It is interesting to note that similar phenomena have been observed in chromic chloride solutions subjected to electrolysis, in which case the current must pass through the electrolyte for some time before chromium will be deposited. This may have been caused by similar reactions.

(1) $Cr^{+++} + e^- = Cr^{++}$
(2) $Cr^{++} + 2e^- = Cr$.

In solutions of ammoniacal complex compounds of cobalt the following reaction takes place at the cathode:

$$Co(NH_3)_5^{++} + 5H_2O + 2e^- = Co + 5(NH_4)OH.$$

This reaction will proceed without the evolution of hydrogen, but there are also NH_4 ions present, which may also give off their charge:

$$NH_4^+ + e^- + H_2O = (NH_4)OH + H.$$

Such a reaction seems to be of little importance if the electrolyte is free from simple ammonia compounds such as $(NH_4)Cl$, $(NH_4)_2SO_4$, etc.; however, if increased amounts of simple ammonium compounds are present, hydrogen evolution at the cathode is likely to occur. With the use of electrolytes of correct composition hydrogen pitting on the cathode deposit has never been observed.

Assuming that the efficiency of anodic oxidation of cobalt will be 100 pct and that no hydrogen will be liberated at the cathode, it is evident that the most favorable cathodic current efficiency will not be more than 2/3 of the theoretical value for the sole reason that 1/3 of the current is required for the reaction $Co^{+++} + e^- = Co^{++}$.

The current efficiencies for nickel will naturally be very high, since nickel remains in the bivalent state in the ammoniacal electrolyte. Experimentally it was also found that nickel can be plated at low current density.

It was observed that the cathodic current efficiency of cobalt is greatly affected by decreasing current density, in contrast to that of nickel. The difference in behavior of both metals is plainly exhibited by the figures in Table V.

Table V. Difference in Behavior of Metals

Pure ammoniacal Ni-liquor		Ammoniacal cobalt-nickel-liquor			
Dynamic potential	Current efficiency	Dynamic potential	Current density per dm^2	Current efficiency	Remarks
Volt		Volt	Amperes		Deposit
1.95	87.7	1.85	3.55	27.6	Pure cobalt
2.53	95.4	2.18	6.—	46.—	Pure cobalt
3.48	98.—	2.40	8.05	64.—	Pure cobalt
		2.78	11.7*	73.5	8.8 pct Ni in alloy

* The current density of 11.7 amp per dm^2 is far too high to secure a good separation; hence some nickel is found in the deposit of cobalt. The nickel has been calculated as cobalt for the estimation of the current efficiency, thus explaining the value above the possible theoretical one.

Ionization and Anodic Reactions: The ammoniacal complex compounds of nickel and cobalt are only slightly ionized, whereas simple compounds such as NH_4Cl to an electrolyte of composition *a* will cause a drop in dynamic potential, while the cathodic current density will remain the same. This results also in a somewhat lower cathodic current efficiency. On the other hand, it may be stated that the anodic dissolution of the metal may vary somewhere between 102 pct to 105 pct for chloride containing electrolytes, while it is almost independent of cathodic current density. What will be the effect of this behavior on the electrolyte, etc.? It is clear that if cobalt is deposited in a pure form free from nickel, e.g. at a current efficiency of 60 pct, an amount of chlorine equivalent to the composition $Co(NH_3)_5Cl_3$ will become available at the anode. With a 100 pct anode current efficiency the amount of Co and Ni dissolved will be considerably greater than the amount of cobalt deposited at the cathode, so the chlorine content will be too low to keep up for the amount of Ni and Co oxidized at the anode in solution as $NiCl_2.6NH_3$ and $Co(NH_3)_5Cl_3$. In addition we must realize that the OH-ion concentration at the anode will be high, the combined effect being that basic compounds will be formed at the anode.

$$(1)\quad Ni < \begin{matrix} Cl \\ OH \end{matrix} \qquad Co > \begin{matrix} Cl \\ OH \end{matrix}$$

$$(2)\quad Co^{++} + 2(OH)^- = Co(OH)_2$$
$$Ni^{++} + 2(OH)^- = Ni(OH)_2$$

The more basic character of cobalt causes it to be precipitated in preference to nickel; hence the basic compounds formed at the anode will contain a larger percentage of cobalt than present in the anode.

Increase in cathodic current efficiency will cause more chlorine to be liberated at the anode thus depressing the amount of basic compounds formed.

With the addition of NH_4Cl to the electrolyte of type *a* more chlorine ions will be liberated at the anode. The result is that NH_4Cl will be broken up, $(NH_4)OH$ will be formed at the cathode, less basic compounds will be formed at the anode, more metal will enter into solution, and there will be an increased tendency for hydrogen to be liberated at the cathode.

Discussion of Results: Cylindrical anodes (short tubes) of Ni-Co alloys were cast for this investigation. Cylindrical cathodes were used, rotating at a speed of 135 rpm within the anodes. The internal diameter of the anodes was 37 mm, with corresponding cathodes of 20 mm diam and 0.2 dm^2 surface. Cells were of the open type. In only one case was it found that the cobalt deposit was visibly pitted because of hydrogen bubbles adhering tenaciously to the surface. This occurred when 3 pct NH_4Cl was added to the electrolyte of composition *a*. This undesirable effect was not noticed with less than 2 pct NH_4Cl.

Selectivity of the Electrolyte

Experimentally it was found that the amounts of NH_3 and NH_4Cl in the ammoniacal liquor have a good deal of influence on its properties as an electrolyte. The following results show that certain requirements must be met to give the electrolyte the desired qualities. The anode consisted of 75 pct Co and the rest Ni. The electrolyte had the composition of type *a*, and did not contain NH_4Cl as a simple ammonium compound. (Table VI).

Table VI. Selectivity of the Electrolyte

Temperature of electrolyte	Dynamic potential	Cathodic current density amperes per dm^2	Cathode current efficiency	Ni in cathode deposit pct Ni of (Ni+Co)	KWH consumed per Kg cobalt deposited	Ratio total metal content to NH_3 content of electrolyte
Chloride Electrolyte (1) Co 1.468 pct, Ni 0.488 pct, NH_3 5.3 pct						
(1) 20°C	1.72	2.5	43	11.4 pct	3.6	1:2.7
Electrolyte (2) Co 1.101 pct, Ni 0.666 pct, NH_3 6.30 pct						
(2) 26°C	2.20	4.2	69.2	2.4 pct	3.2	1:3.6
Electrolyte (3) Co 0.758 pct, Ni 0.613 pct, NH_3 7.37 pct						
(3) 25°C	2.35	3.9	58.8	0.0 pct	3.6	1:5.4
From these experiments the following conclusions may be drawn: A sufficiently high ratio of metal to NH_3 is essential for obtaining good selectivity. The result is probably due to a change of ionization such that the ratio between the available cobalt and nickel ions increases in favor of cobalt. To a sulphate liquor of the type *a* containing no $(NH_4)_2SO_4$, 1 pct NH_4Cl was added.						
Electrolyte (4) Co 0.602 pct, Ni 0.704 pct, NH_3 4.78 pct $(NH_4)Cl$* 1 pct						
(4) 23°C	2.20	2.5	41.5	0.0 pct	4.8	1:3.7

* Added to prevent passivity of the anode.

It is evident from these results, that electrolytes with great selectivity should contain a substantial excess of ammonia and a certain amount of a simple ammonia compound.

Attention was focused upon the deposition of pure cobalt in the upper part of the circuit. At the lower end the electrolyte has to be discharged as a solution containing most of the nickel and almost no cobalt.

Electrolyte (3) seems promising for producing pure cobalt in the upper cells of the series, and the addition of a small amount of NH_4Cl will probably improve the quality still further. Electrolyte (4) also gave satisfactory results. The amount of NH_4Cl to be added should not be too great as was shown by the following results: To an electrolyte of type *a* 1 pct and 3 pct NH_4Cl were added. (Table VII).

Table VII. Results

Electrolyte of the type *a* added	Dynamic potential	Cathodic current density	Cathodic current efficiency	KWH consumption per kg of Co deposited	Temperature of electrolyte
1 pct NH_4Cl	2.10	5.6	61.7	3.09	26°C*
3 pct NH_4Cl	2.14	9.0	64.5	3.01	27°C†

* The cathode deposit was very smooth.
† The cathode deposit was pitted as a result of hydrogen bubbles.

The following experiments were made to get a clear picture of the conditions at the lower end of the circuit, aiming at the discharge of a cobalt-free nickel solution.

The cathodic current density was kept constant for all three experiments at 1 2/3 amp per dm^2 surface and the temperature was held between 17-22°C; composition of anode: Ni 88.27 pct, Co 11 pct, Fe 0.5 pct, Si 0.23 pct.

Pct Co of (Ni + Co) = about 11.2 pct.

Composition of electrolytes:

(1) 6 pct NH_3 and in addition 2 pct NH_4Cl free from nickel.

(2) 6 pct NH_3 and in addition 2 pct NH_4Cl containing 1.89 pct nickel.

(3) 6 pct NH_3 without NH_4Cl containing 1.893 pct nickel.

A low current density is required since the alloy deposited on the cathode contains chiefly nickel. (Table VIII).

It was to be expected that electrolyte No. 3, containing no NH_4Cl would not only produce the greatest amount of basic compounds, but the cobalt content thereof was higher than with electrolytes No. 1 and 2, both of which contained NH_4Cl. The low cobalt content of the cathodic deposit of electrolyte 3 is fully explained by the fact that 30 pct of the cobalt is withdrawn from the electrolyte as an insoluble basic compound.

Electrolyte No. 2 with 2 pct NH_4Cl showed a very high selectivity for depositing cobalt first, as the ratio of the Co content of the deposit to the Co content of the electrolyte proved to be not less than 85 while with electrolyte No. 3 containing no NH_4Cl this ratio was only 30.

The presence of NH_4Cl in the electrolyte is therefore no doubt indispensable. It is also evident from the results that the application of an anode of pure nickel in the last cell of the series will cause a com-

plete removal of remaining cobalt in the electrolyte; thus a cobalt-free nickel electrolyte can be discharged at the lower end of the open circuit.

The Amount of Basic Chloride Formed at High Cathode Current Density at the Anode: The production of pure cobalt at high current density will minimize the amount of basic chloride formed at the anode and will simultaneously result in a reasonable current efficiency, as has been explained earlier. In order to achieve this it is desirable to use anodes and electrolytes with a reasonably high cobalt content in the upper cells of the series, and it is of importance to know the amount of basic compounds that will be formed under such conditions. The following experiment was therefore made. (Table IX). The results were obtained by using an anode containing 75 pct Co and 25 pct nickel. Electrolysis was at room temperature.

Under these conditions 1/3 of the cobalt content of the anode will be reprecipitated at the anode as a basic chloride with enriched cobalt content, which product can be returned to the process in the form of an electrolyte with a high ratio of cobalt to nickel. (Table X).

Table VIII. Results

	Electrolyte 1	Electrolyte 2	Electrolyte 3	Remarks
Dynamic potential in volts	2.30	1.90	2.02	
Current efficiency in pct	93	96	97	High current efficiency due to high nickel content of alloy plated
Co in cathode deposit	10.9	10.3	6.02	
Co redeposit on anode as a basic compound	9	12.6	30	Pct of total Co dissolved from anode
Co in basic compound from (Co+Ni+Fe) present	25.6	24.4	30	
Pct nickel	58.8	68.6	62.7	
Pct Fe	15.6	7.–	3.6	
Composition electrolyte at finish of test	Ni 0.246 Co very little	Ni 1.992 Co 0.00475	Ni 1.986 Co 0.00815	
Ratio pct Co to (Ni+Co) in electrolyte		0.24 pct	0.41 pct	
Average ratio during the test		0.12 pct	0.20 pct	
Ratio Co content of cathode deposit to Co content of electrolyte		85.–	30.–	
Pct Ni redeposit on anode as a basic compound		3.8 pct	6.9 pct	Pct of total Ni dissolved from anode

Table IX. Production of Basic Chloride at High Current Density

	Amount cobalt	Calculated on the basis of 1000 mg Co deposit on the cathode	Roughly in round figures per unit of cobalt deposited at the cathode
Deposit at anode			
Cobalt as basic chloride	307 mg Co	333 mg	1/3
Dissolved cobalt from anode in total	892 mg Co	967 mg	1
Cobalt entered into the electrolyte	585 mg Co	634 mg	2/3
Pure cobalt deposited on the cathode	922 mg Co	1000 mg	1
Hence decrease of cobalt content of electrolyte	337 mg Co	365 mg	1/3

Table X. Composition of the Basic Compounds

Pct Co of anode	Pct Co of (Ni+Co) in basic compounds	Analysis of basic compound: Pct Co	Pct Ni	Pct Cl	Color
11.2	25.6				green
25.8	68.5	33.98	15.66	14.85	dark green*†
75.–	91.85	42.–	3.73		pinkish‡
* Values of another test		32.28	19.5	14.68	
† From ammoniacal sulphate electrolyte containing 1 pct NH_4Cl		26.7	17.1	SO_4 20.3	
‡ Values of another test		45.7	4.21		

The great relative increase in cobalt content in the basic compounds is evident. The basic compounds adhere more or less to the surface of the anode, and are porous, not voluminous. Their presence on the surface of the anode does not seem to effect the anode current efficiency or cause anodic polarization.

Ammonium Chloride Consumption During Electrolysis: The following figures give a fair picture of what may be expected by applying different cathodic current densities. (Table XI.) Operating on a technical scale with a cathodic current density of 5-6 amp per dm^2 surface it is likely that from 1 to 1½ kg of NH_4Cl will be consumed per kg of Co deposited. This does not mean that the ammonia in NH_4Cl has been destroyed but only that the chlorine content thereof has been consumed in the formation of cobalt and nickel compounds whereas NH_3 has been set free thereby increasing the free ammonia content of the electrolyte. The experiments have plainly demonstrated that with increase of current density, or better with increase of cathodic current efficiency, less NH_4Cl will be consumed.

All in all, the presence of NH_4Cl in the electrolyte has proved to be desirable, and it is obvious that the amount consumed during electrolysis should be replaced.

Energy Consumption: The electrolyte contained 2 pct NH_4Cl, 5.90 pct total NH_3, 0.319 pct Ni, 1.538 pct Co; pct Ni from (Ni + Co) at start 17.18 pct. (Table XII).

Under plant conditions a certain amount of cobalt will be deposited in the lower cells as an alloy high in cobalt that must be returned to the process in the form of anodes. Since part of the cobalt will thus have to be deposited twice, we will have to count on a higher energy consumption of probably not less than 5-6 kwh per kg of pure cobalt obtained.

Physical Condition of the Cobalt Deposit: Cobalt may be deposited from ammoniacal electrolytes in a smooth and mat condition even at such high cur-

rent densities as 8 amp per dm^2. Nickel, on the other hand, gives bright, very hard and flaking deposits even below 1 amp per dm^2. This is probably due to the absorption of hydrogen by the nickel metal. Fortunately it is not necessary to recover nickel from the spent electrolyte by electrolysis, as the cobalt-free electrolyte must be distilled with lime to recover the NH_3 and nickel will be recovered simultaneously as hydroxide.

Dark colored cobalt deposits are sometimes obtained from electrolytes of type *a* that do not contain NH_4Cl, but by adding 1-2 pct NH_4Cl the deposits will become bright and light colored. The deposits adhere quite well to Pt cathodes at medium current densities. Above 8 amp per dm^2 current density the deposits are likely to hold a small amount of nickel. They will become hard, indicating internal tension of the metal, and are liable to crack.

The physical properties were investigated in the following manner:

Platinum foil, 1/10 mm thick, bent into a half-cylinder was used as a rotating cathode. The cathode surface was 0.2 dm^2 and the diameter of the half cylinder as measured between the opposite edges of the cathode was 20 mm at the start of each test. If there was any tension in the deposited metal, the half cylinder was deformed increasing the distance between the edges of the cathode. The amount of deformation gave rapid and reliable evidence of internal tension of the metal deposit. Hydrogen absorption by the metal is probably the cause of internal tension, hardness, and cracks at high current densities, since these were usually accompanied by pitting of the deposit. To diminish the tendency to hydrogen evolution at the cathode, 0.02 pct NO_3 as ammonium nitrate, was added to the electrolyte with successful results. The deposits became very smooth and mat, and no signs of cracks or internal tension were observed. The surface of the deposit, however, became tarnished. The same beneficial effect probably may also be obtained by passing air or oxygen through the catholyte, but it has not yet been investigated because of lack of proper equipment. The quality of the deposit is further improved because trivalent cobalt will oxidize hydrogen that may be set free at the cathode.

The conditions for depositing nickel are quite different. Nickel will remain in the bivalent state and hydrogen will be set free readily at the cathode even at low current densities. The nickel deposits from ammoniacal electrolytes are always hard, brittle, and flaky as a result of hydrogen absorption by the metal.

Table XII. Energy Consumption

Ampere hour consumed	Cathodic current density amp per dm^2	Dynamic potential volts	Cathodic current efficiency	Anodic current efficiency	KWH consumption per kg of Co	Average temperature of electrolyte, °C
0.71	3.55	1.85	27.6	102.2	6.08	25
1.61	8.05	2.40	64.–	107.6	3.74	26

The physical condition of the surface of the cathode may also have some influence upon the purity of the cobalt deposit, as may be illustrated by the following experiments. Mat and glossy platinum gauze cylinders in every other respect identical were used as rotating cathodes for these experiments, which were carried out under exactly the same conditions. The cylinders were rotated at 135 rpm. The anode consisted of a cast short tube containing 25.88 pct Ni, 70.21 pct Co, and 3.91 pct Si. (Table XIII).

Table XIII. Results

Character of Cathode surface	Electrolyte		Ratio Ni:Co	Pct NH_3 total	Dynamic potential volts	Cathode deposit Pct Ni from (Ni+Co)
	Pct Ni	Pct Co				
Glossy gauze Pt	0.196	1.144	1:5.8	7.5	2.00	35.5
Mat gauze Pt	0.2094	1.1766	1:5.6	7.5	2.02	1

This remarkable result no doubt is due to the difference in surface conditions of the cathode. Possibly a mat surface causes better agitation of the liquid directly adjacent to the cathode, thus supplying more quickly the required Co ions. Although no exact figures can be given about the current density, probably it was high, which would have contributed to the great difference in the results observed. At any rate it was found essential to keep the current density well within proper limits, and to move the electrolyte along the cathode surface fast. Deposits obtained under such conditions are always smooth and mat, and the physical surface condition probably favors the deposition of pure cobalt.

Metals Adapted for Sheet Cathodes: It was found experimentally that cobalt adheres very well on a fresh smooth aluminum surface but the aluminum will be attacked more or less inside the open rotary cathode.

Although this corrosion is not severe, it is sufficient to cause the formation of a rose-colored col-

Table XI. Ammonium Chloride Consumption

No.	Cathodic current density amp per dm^2	Co deposited at the cathode, mg	Loss of weight of anode in mg	Liberated chlorine at anode calculated from cobalt deposited at cathode mg	Chlorine present in anodic basic compounds, mg	Dissolved Co + Ni from anode, mg	Chlorine linked to Ni and Co dissolved from anode, calculated mg	Chlorine withdrawn from $(NH_4)Cl$, mg	Equivalent consumption of NH_4Cl per kg of Co deposited in kg
1	3.55	216	799	260	113.81*	502	604	458	2.12
2	8.05	1030.7	1910	1241	216.6 †	1312	1579	554	0.537

* This sample of basic chloride contained 18.6 pct Cl weight 612 mg.
† This sample of basic chloride contained 16.06 pct Cl weight 1282 mg.

loidal floculent precipitate in the electrolyte, which proved to be aluminum hydrate having a rather high cobalt content. If aluminum is used as cathode, due precautions should be taken to cover the inactive part of the cathode surface with a protective coat.

It was also found that cobalt adhered well on 18-8 chromium nickel steel, and will probably do so on other stainless steels. Which metals will serve the purpose best is difficult to say, but even thin sheets of cobalt may be used if desirable.

Electrolytes Containing Other Acid Radicals: Ammoniacal sulphate electrolytes that are free from Cl-ions will make the anode passive immediately. The dynamic potential will rise above 4 volt, oxygen will be evolved at the anode, and the alloy will be oxidized at its surface. By the addition of 1 pct NH_4Cl to the sulphate electrolyte, for instance, passivity will disappear at once, and the voltage will become normal. The anode current efficiency will rise to slightly above 100 pct under such conditions and the cathodic current efficiency may be raised somewhere near 60 pct under proper operation conditions. The selectivity for separation of cobalt from nickel is also very good.

A disadvantage is that the solubility of complex sulphate compounds of Ni and Co is considerably less than that of complex chloride compounds. The concentration of Co and Ni in the electrolyte will have to be kept rather low to avoid crystallization of such compounds on the walls of the cells.

Ammoniacal acetate electrolytes will not give anodic passivity, but their selectivity appears to be not so good as that of the previous electrolytes. This solvent is therefore not to be preferred. Formate and citrate ammoniacal electrolytes were also investigated. Unfortunately formic acid cannot be considered as a solvent for basic nickel carbonate, and the plated metal from ammoniacal citrate electrolytes contains carbon. Probably a certain amount of carbides is deposited with the metal. Plated metals free of carbon were obtained from ammoniacal electrolytes obtained from acids containing only carboxyl (CO OH) groups such as formic acid, acetic acid and oxalic acid.

Of all the ammoniacal electrolytes investigated, the ammoniacal chloride electrolytes are probably most adaptable and should be preferred for the application of this process. The process may also prove feasible for the separation of nickel and cobalt from alloys containing Co-Ni-Fe and some silicon. Chloride solutions may be obtained by dissolving the granulated alloy in hydrochloric acid. A great deal of iron is of course, objectionable, since the ferric hydroxide precipitated by the addition of ammonia is bulky and makes filtration a problem.

Procedure for Making Up the Electrolyte: The wet Oliver-filter cake of basic nickel carbonate greatly enriched with cobalt is treated with strong hydrochloric acid. By adding an excess of basic nickel carbonate to the hydrochloric acid, a neutral chloride solution will result and CO_2 may be recovered and returned to the process. This reaction proceeds with the evolution of much heat. Assuming that the filter cake will hold 50 pct moisture and the temperature at the start of reaction of both ingredients will be about 30°C, the temperature of the solution may rise to 70°C. The neutral or only slightly acid chloride solution will contain roughly 16 pct Cl and 13 pct nickel plus cobalt. A certain amount of free acid should be added to this neutral chloride solution so that the final electrolyte obtained will contain 1 to 2 pct NH_4Cl. To each part of this solution should be added 2.5 parts of strong NH_4OH of about 20 pct NH_3 content. The chloride solution should be added slowly to the well-stirred ammonia solution, to dissolve both metals completely as complex compounds. The rather concentrated solution should be diluted with water to seven times the original volume of the neutral chloride solution. The small precipitate of $Fe(OH)_3$ and silica gel that will appear should be filtered off. The iron-free solution will contain about 2 pct combined nickel and cobalt, 3.5 pct Cl and about 7 pct NH_3. No $Co(NH_3)_5Cl_3$ nor $NiCl_2.6NH_3$ will crystallize out from the electrolyte if prepared in this way.

Cobalt Enrichment of the Electrolyte Countercurrently in the Cells in Series: It is logical to dissolve the anodic cobalt-rich basic compounds and to move the high cobalt values upwards as fresh electrolyte in the upper part of the circuit. In so doing the electrolyte of the upper cells will be supplied with the highest Co values and it will be easy to produce pure cobalt in that part of the circuit.

Systematically the circuit of the cells may be represented by the diagram, fig. 2.

This diagram is given only as an example to elucidate the suggested application. The number of cells may vary and so may the details. If we assume that the incoming electrolyte will contain 2 pct (Ni+Co), of which 30 pct is cobalt, and that the electrolyte while passing through the three upper cells will dissolve an amount of cobalt from the anodes equivalent to the amount present in the incoming electrolyte, then in total 12 g of cobalt would be available per liter electrolyte to be deposited. Accepting that 2/3 will be deposited as pure cobalt, then the remainder should be stripped from the electrolyte in the lower part of the circuit. Assuming further that for each 8 g of cobalt deposited, 12 g of solid NH_4Cl have to be added to the electrolyte to meet the amount consumed, then it is obvious that the spent electrolyte will contain about 0.4 pct more total NH_3 than the incoming electrolyte. By adding NH_4Cl as a solution there will be very little change in the NH_3 content of the electrolyte while passing through the cells. Such an open circuit gives a very flexible operation, for the amount of intermediary products may vary considerably without affecting the final outcome.

A comprehensive picture of all the steps required may be found in the flow-sheet fig. 3, and after the previous discussion of the fundamental factors, further comment is superfluous, with one exception, viz, step 3. This step aims at a further concentration of cobalt. Cobalt may be precipitated from the solution almost quantitatively as $Co(OH)_2$ by the addition of lime, but in doing so much nickel will be precipitated simultaneously as hydroxide, and it is difficult to get the remaining neutral nickel chloride solution free from cobalt. A certain concentration of the cobalt in the precipitate may, however, be obtained in this way, but it is far less effective than the concentration obtained by the carbon dioxide saturation process discussed earlier.

In the case that the cobalt content of the basic nickel carbonate is on the low side, the logical procedure would be to redissolve the basic nickel carbonate in ammonium carbonate solution and to repeat the separation of the cobalt from the nickel by the carbon dioxide saturation process. In case of emergency, (if stills fall out, and the distilling capacity be inadequate) step 3 may prove to be useful. Normally the neutral chloride solution from step 2 will be treated directly with ammonia. A sketch of a closed-type unit cell is given to illustrate the case. (Fig. 4.) Anolyte and catholyte are separated by a canvas diaphragm, and the catholyte is strongly circulated in a closed secondary circuit, an essential condition for producing cobalt free from nickel. It will be further noted that the anodes can be easily lifted out of the cell in order to remove adhering basic compounds, and the product that has settled at the bottom of the anode department can be transported out of the cell from time to time by a screw conveyor.

The Precipitation of Cobalt from Ammoniacal Liquors: Cobalt may be precipitated from ammoniacal solutions by agitating the liquors with freshly prepared nickel sulphide.

For an effective treatment an excess of nickel sulphide should be added in order that the reaction: $NiS + Co(NH_3)_6^{++} = Ni(NH_3)_4^{++} + CoS + NH_3$ may proceed sufficiently fast. Next the mixed sulphides may be separated from the liquor by filtration. This product needs a further treatment to recover both metals separately. It is this more complicated treatment that will make this method less attractive than the simpler methods discussed above.

By adding a controlled amount of hydrogen sulphide to the ammoniacal cobalt containing liquor, cobalt may be precipitated almost completely, but quite some nickel will be precipitated simultaneously in this way and there is no special gain in such a treatment. (Table XIV).

Cobalt Ores: A class of ore occurring in New Caledonia may be represented, for instance, by the following analysis:

NiO 1.25 pct, CoO 3.00 pct, Mn_2O_3 18.00 pct, Fe_2O_3 30.00 pct
CaO 8.00 pct, Al_2O_3 5.00 pct, MgO 1.00 pct, SiO_2 8.00 pct

These ores, or ores of a similar type, are well adapted for the ammonia leaching process since very high extractions of these metals may be expected. The pregnant solutions obtained are dark red because of their high cobalt content and for such solutions the author has devised a very effective and simple process to recover pure cobalt. Application for patent has been made in the Netherlands and more information regarding this process will be given as soon as the patent has been granted. The process also can be applied advantageously to Co enriched precipitates as obtained by the processes discussed earlier. (See fig. 5.)

Table XIV. Results

Values in leach liquor		Values after H_2S treatment		Values precipitated by H_2S	
Ni pct	Co pct	Ni pct	Co pct	Ni pct	Co pct
0.49	0.0088	0.4625	0.00009	5.5	almost complete

Acknowledgment

The investigations of the main features of the various processes involved in the ammonia leaching process for the recovery of nickel and cobalt from oxide and hydrated silicate ores required considerable time. During the years 1930-1934 Miss M. E. van de Kleine-Mulder and from 1934 to 1943 Miss A. C. W. C. Bot, both Chemical Engineers from Delft connected with the Metallurgical Department of the Technical University of Delft, have made many analyses for the author. It is therefore a great pleasure to acknowledge with gratitude their much appreciated assistance.

Method for Studying

by Philip R. Sperry

Grain Boundary Migration in Aluminum

A METHOD was recently devised to indicate two or more successive stages of the migration of grain boundaries in aluminum, and to record the direction of the migration. This technique was used for the study of the various types of boundary migration occurring in high purity aluminum.[1]

The method employs alternate annealing and electrolytic etching treatments, repeated as many times as desired. All successive sets of grain boundary positions revealed by the various etches appear superimposed on each other. The last etch is designed to leave an oxide film on the surface which is optically anisotropic. The orientation of the oxide film at each point is determined by the orientation of the underlying aluminum grain. When viewed with polarized light using crossed nicols and a Biot-Klein quartz plate, grains with differing orientations appear in different colors, as described by Hone and Pearson.[2] The last boundary positions are revealed by these color differences.

The first step of the process is to obtain a desired starting grain size by annealing, for example, if high

PHILIP R. SPERRY is Metallographer, Dept. of Metallurgy, Univ. of Notre Dame, Ind.

Technical Note No. 32 E. Manuscript received Nov. 1, 1949.

purity aluminum is used, at 600°C for 5 min. If cold working is desired, it is best accomplished by rolling or compressing since these methods produce a surface which is flat and suitable for electrolytic polishing.

The technique employed for electrolytic polishing and etching was that of Hone and Pearson, with slight modifications. The electrolyte composition, used with a Buehler-Waisman electrolytic polisher, was as follows:

	pct by volume
Orthophosphoric acid (85 pct)	53
Distilled water	26
Diethylene glycol monoethyl ether ("Carbitol")	20
Hydrofluoric acid (48 pct)	1

A high initial potential, approximately 80 v, was required to warm the specimen sufficiently during polishing. When polishing starts, the current instantaneously reaches a high value and then decays. As the specimen becomes warm the current increases again. When the current density reaches 60 amp per sq dm, the voltage should be decreased to about 40 v. Caution must be exercised to prevent overheating but, if the current density is not high enough, an oxide film forms on the specimen surface and prevents further polishing. A large quantity of electrolyte and effective agitation of the bath are required. The polishing time is 2 to 3 min.

Etching is accomplished with the same electrolyte. With the specimen at room temperature and 40 v applied, the ammeter registers < 0.1 amp. An etching time of 1.5 to 2 min was found sufficient for the purpose described in this paper. This etching procedure reveals the microstructure in three ways: (1) step-down effect at grain boundaries due to difference in rate of attack of different grains depending on orientation, (2) roughening of the surface of cold worked grains,[3] and (3) the color effect shown in polarized light of the oxide film formed during etching. It was found that several alternate annealing and etching treatments can be applied without substantially altering the first two effects produced by previous etches. The third effect, however, produces very confusing results if the oxide film from a previous etch is not completely removed before the next etch is applied. The film can be removed by immersion of the specimen for 1 or 2 min at 100°C into a solution of 35 ml of orthophosphoric acid (85 pct) and 20 g of chromium trioxide per liter of aqueous solution.

Following the first etch and the oxide removal, an annealing treatment such as 400°C for 1 min is given to produce boundary migration. It is desirable to immerse the specimen in the oxide-removing solution before etching to remove the oxide film which may have formed during annealing. The specimen is then etched and examined microscopically using crossed nicols and a Biot-Klein quartz plate. Further stages of boundary migration may be shown by repeating the process of oxide removal, anneal, and etch. Previous boundary positions will appear only as black lines while the boundaries formed during the last anneal are also marked by color differences, indicative of the orientation differences of the adjacent grains.

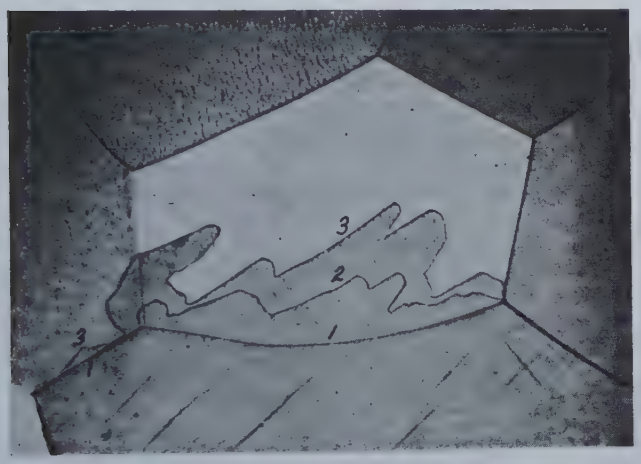

Fig. 1—Two stages of strain induced boundary migration in high purity aluminum.

The specimen was annealed at 600°C for 90 min, reduced 7.5 pct by rolling (boundaries numbered 1), annealed 500°C for 5 sec (boundary numbered 2), and annealed 500°C for 20 sec (boundaries numbered 3). 75X. Crossed nicols and quartz plate. Reduced approximately one half in reproduction.

An example illustrating the use of this technique is shown in fig. 1. The colors of the individual grains are reproduced as varying shades of gray. Two anneals were used after cold working; as a result, the original boundaries (1) moved to their final positions (3).

This work was supported by the Office of Naval Research, U. S. Navy, Contract No: N6 ori-165, T.O. 1.

References

[1] Paul A. Beck and Philip R. Sperry: Strain Induced Grain Boundary Migration in High Purity Aluminum. *Jnl.* Appl. Phys., Feb., 1950.

[2] Andre Hone and E. C. Pearson: Grain Orientation in Aluminum Revealed by Anodic Film. *Metal Progress* (1948) **53**, 363.

[3] Paul Lacombe and Louis Beaujard: Etude Micrographique de l'ecrouissage et de la recristallisation de l'aluminium extra-pur. *Rev.* de *Met.* (1947) **44**, 71.

Reflections on the

Electrolytic Cells

Used in the

Production of Aluminum

by Bruno B. A. Luzzatto

The electrolytic furnace as used in extraction of aluminum from alumina. Starting with an analysis of the electrochemical and thermal aspects of the process, the necessity of striving for a reduction of heat losses, especially those through the upper surface, is emphasized. This can be achieved by the use of improved self-baking electrodes as a substitute not only for the multiple prebaked electrodes, but also for the conventional self-baking electrodes now in use.

ALUMINUM is today the most widely used of the nonferrous metals. The technical literature on the aluminum smelting process is, nevertheless, very meager, so that anyone interested in the subject cannot rely on more than a couple of dozen publications.[2] The patent literature is equally scarce; most patents refer to the production of alumina from aluminum-bearing ores, while not more than a few score significant patents deal with the electrolytic reduction of alumina, which is the real core of the aluminum smelting industry.

The "reduction phase" is, from a technical and a scientific point of view, much more interesting than the "alumina phase", which, in effect, is only a combination of such well-known chemical operations as dissolving, precipitating, filtering, drying, and calcining. The electrolytic reduction of alumina, on the other hand, has features which do not appear in any other metal smelting operation. Some of them are of great technical and scientific interest even for those not directly engaged in the production of aluminum.

BRUNO B. A. LUZZATTO is a Consulting Engineer at Washington, D. C.

San Francisco Meeting, Feb. 1949.

TP 2650 D. Discussion (2 copies) may be sent to Transactions *AIME before March 1, 1950. Manuscript received Nov. 15, 1948; revision received Aug. 29, 1949.*

The purpose of this paper is to describe in some detail the basic facts and developments of the reduction phase of aluminum smelting.

Two Aspects of the Electrolytic Process

The raw material for the reduction process is alumina (Al_2O_3). Its purity in general runs as high as 99.50 pct or more. Small differences in the chemical composition generally do not affect the reduction process.* Of more importance are the physical properties of the alumina, since they affect not only its rate of solution in the molten bath but also its heat insulating power.† In the following pages, unless otherwise stated, it is assumed that a standard "Bayer" alumina is used.

* However, an unusually high phosphorus content endangers the electrolysis; a high potassium content (as in the alumina obtained from leucite and alunite) may also cause difficulties, such as damage to the carbon lining.

† The importance of the physical structure becomes evident when alumina obtained by an electric fusion process, such as "Haglund Alumina", is used.

The reduction process, by which alumina is broken down into its components, may be roughly defined as its electrolysis in molten cryolite. The oxygen separates at the anode, and the aluminum at the cathode, which forms the bottom of the electrolytic cell.

The electrolytic cell (or pot) where the process is carried out is a strongly reinforced steel box. The

inside lining of baked carbon blocks is connected by steel bars with the negative pole of a source of dc current and acts as the cathode. One or more carbon blocks, prebaked or self-baking, suspended over the cathode and connected to the positive pole of the same source of dc, act as the anodes. Many cells are connected in series to a generator. The overall arrangement of the various parts of the conventional modern cell does not differ substantially from the one adopted by its inventors Hall (U.S.A., 1889) and Heroult (France, 1889), as may be seen by the few sketches and pictures showing respectively a cell installed by Heroult at La Praz, France, in 1893 (fig. 1), a standard cell still being used in most French plants in 1947 (fig. 2), and a German cell used since 1926 (fig. 3).* However, behind the apparent simplicity of structure there are many problems, as we shall see in the following pages.

* (PB7003C).

Electrochemical Aspects

Fundamental Reaction: The theory of the electrolysis has not yet been fully developed. The simplest reaction, still currently used as a basis for technical and practical considerations assumes that the alumina, dissolved in an amount of less than 10 pct in molten cryolite [$3(NaF)AlF_3$], kept at a temperature of around 950° C, is decomposed by the electric current as follows:

$$2Al_2O_3 = 6\ O + 4\ Al$$

I. $6\ O + 3\ C = 3\ CO_2$

II. $6\ O + 6\ C = 6\ CO$

The occurrence of reactions I and II between the oxygen, which is the primary product of the electrolysis, and the carbon composing the anodes, depends upon the prevailing temperature and other factors. Practical experiments have shown that CO_2 seldom represents less than 70 pct of the gases that develop during the electrolysis. (See below.)

The above reaction admittedly gives an oversimplified picture of what happens in the cell, and various hypotheses have been proposed as to the real nature of the electrolytic reactions.

A widely accepted theory, backed by conductivity measurements and theoretical considerations, assumes that alumina is the solvent and sodium fluoride, one of the components of cryolite, is the substance undergoing electrolytic decomposition according to the following reactions:

$$12\ Na\ F = 12\ Na + 12\ F$$
$$12\ Na + 4\ Al\ F_3 = 12\ Na\ F + 4\ Al$$
$$12\ F + 2\ Al_2O_3 = 4\ Al\ F_3 + 6\ O$$

The net result is still:

$$2\ Al_2O_3 = 4\ Al + 6\ O$$

The cryolite is either a passive solvent, or else it is continually being decomposed and reformed; in either case, no cryolite is directly consumed in the process. Some losses do occur—roughly 5 pct of the weight of the aluminum produced—due to thermal decomposition, volatilization, or mechanical losses. There is, however, a theory which ascribes the cryolite losses to its decomposition according to the second reaction shown above.

A new attractive theory has recently been suggested by R. Gadeau.[4] This theory states that the primary electrolysis is that of Na_2O, which is always present in small amounts in the molten bath. The reaction would be as follows:

$$6\ Na_2O = 12\ Na + 6\ O$$
$$12\ Na + 4\ Al\ F_3 = 12\ Na\ F + 4\ Al$$
$$6\ O + 3\ C = 3\ C\ O_2$$
$$12\ Na\ F + 2\ Al_2O_3 = 4\ Al\ F_3 + 6\ Na_2O$$

Feed

The primary product of the electrolysis is Na, of which the largest portion (80-90 pct) reacts with $Al\ F_3$ as shown above. A small part vaporizes, rises through the molten bath, and meets CO_2 at the anodes, with which it reacts as follows:

$$2\ Na + CO_2 = Na_2O + CO$$

Only a small amount of gas develops from this reaction, causing yellow flames (visible only in hot pots). This theory will be mentioned again later when we discuss the current efficiency of the process.

Voltage Relationships: The basic equation for the electrolytic process is:

$$V = E + I\,R$$

where E = decomposition voltage, I = current and R = cell resistance.

The decomposition voltage* may be calculated theoretically on the basis of assumptions as to temperature, concentration, heat of formation of alumina, etc. Depending on the assumptions made as to the anodic depolarization and other circumstances, the theoretical decomposition voltage ranges between 0.97 and 1.28 V.[5]

* Actually, in the following remarks, the decomposition voltage also includes (somewhat improperly) the polarization voltage. (Standard Handbook for Elec. Eng. (1941), pp. 1918 ff.)

More interesting for practical and technical purposes is the decomposition voltage as determined in operating pots by a method suggested by Edwards and Frary. This method consists of rapidly changand I and reading the corresponding values of V, on the assumption that these rapid changes do not affect R. The various values of V and I allow an easy calculation of E. Edwards and Frary's value, E = 1.70 volts, has been repeatedly confirmed by the writer in 12,500 amp and 25,000 amp multiple anode cells.*

* Data obtained in 1937 on 91 cells: V = 1.69; on 85 cells, V = 1.65; on 90 cells, V = 1.78; average: 1.70 volts.

More recent experiments made in German factories give a value of $E = 1.60 \pm 0.02$ volts as the result of a long series of determinations.[6] This value is reported to be independent of current efficiency and temperature.

The difference between this value of 1.60 ± 0.02 volts and the theoretical decomposition voltage at 950°C, (1.15 volts) is explained, in part, as follows:

1. Incomplete depolarization, i.e., reduced electrochemical effect of the reaction $6\ O + 3\ C = 3\ CO_2$, which accounts for 0.18 volt.
2. Incomplete saturation of the solution of Al_2O_3 in cryolite, which accounts for 0.02 volt.

This leaves a gap of 0.25 volt due to reversible pro-

cesses at the anode and cathode not clearly understood.†

† Other experiments with large self-baking electrodes have shown decomposition voltages of 1.5 to 1.55 volts.

A recent paper (Ferrand)[7] reports various experiments during which the decomposition voltage was found to be only 1.27. The same author, by extrapolating the voltages corresponding to various currents, arrives at a voltage of 1.75—in striking agreement with the previously reported experiments. Accordingly, Ferrand concludes that the decomposition voltage to be used in industrial calculations is around 1.75.

Knowledge of the practical decomposition voltage is very important because it affects the interpretation of the heat balance of the aluminum cell, and the proportioning of its various parts at the planning stage.*

* It is known that experiments in this field are under way to reduce the decomposition voltage by more efficient use of the anodic depolarization.

Faraday's Law and Current Efficiency: The electrolysis of molten substances differs considerably from the electrolysis of aqueous solutions.[8] The intricacies of this type of electrolysis appear clearly when one considers how Faraday's law applies to it. According to this law, each ampere-hour should separate 0.336 g of aluminum at the cathode; actually, only about 80 to 85 pct of the theoretical amount is ever obtained. Many aqueous electrolyses reach a current efficiency of close to 100 pct.

The reason for this low efficiency is the very nature of this electrolysis, and particularly the fact that the aluminum which accumulates at the bottom of the cell has a density only slightly higher than the density of the molten bath and a temperature some 300° C, above its melting point.

The theory of the electrolysis of molten substances shows that losses of the cathodic product which account for the low current efficiency of the process may be due to one or more of the following causes:[8] (1) Mechanical loss on account of imperfect separation of the metal from the bath. This cause affects laboratory experiments rather than industrial operations. (2) Losses caused by combination with the cathode (same remark as above). (3) Losses by vaporization (may apply to sodium but not to aluminum. The Gadeau theory however considers this the most important cause of the low current efficiency). (4) Losses by the formation of salts of higher valence at the anode and their reduction at the cathode. (Apparently not relevant for the aluminum electrolysis). (5) Loss by the cathodic production of a salt of lower valence which diffuses to the anode and is reoxidized. (Same remark as (4) though with less certainty). (6) Loss by the formation of metal fog. (7) Recombination of the anodic and cathodic products, which are brought together by stirring and diffusion. This may be due to a metal fog or to a solution of the metal in the bath.

According to the prevailing views, (6) and (7) affect the aluminum electrolysis to the greatest extent, while the other causes may contribute to a lesser degree. Theory and practice agree that:

1. The formation and reoxidation of cathodic metal fogs of aluminum[9] are more active the higher the temperature of the metal and the bath; and the efficiency is correspondingly lower. The highest efficiency is favored by the lowest possible temperature of the molten bath consistent with other requirements, such as the solubility of alumina in it and general workability of the cell. Experience shows that even a slight increase of the temperature above the maximum causes an abrupt decline of current efficiency, so much so that a good potroom superintendent must be able to judge the temperature of the bath in the cells by noting the color, fluidity, etc., in order to intervene whenever the temperature is out of line. Extensive measurements made in this field in Italian and German plants since 1939[10] have shown that the temperature varies between 922 and 990° C, the latter being already too high for a good power consumption. The temperature increases by some 25° from the time when alumina is stirred into the molten bath until the next anode effect takes place; this is detrimental to the current efficiency. The shape of the temperature curve gives a good hint of how the cell is operating and of its characteristics.

2. The rate of reoxidation of the cathodic metal fog (or compounds, or whatever it is) is, generally speaking, inversely proportional to the anode-cathode distance, i.e., that between the carbon anode and the molten aluminum. For small cells and low amperages (12,000-13,000 amp) using a high current density, this distance may be as small as 3 cm; but with larger anodes the distance is usually 5 cm or more. Self-baking electrodes of large dimensions require, as we shall see later, an anode-cathode distance of 6 to 7 cm. This distance is one of the parameters of any calculations of a new cell, and a correct balance must be sought between it and the current density, the type of electrodes, etc. When many electrodes operate in a single cell, as is usually the case when pre-baked electrodes are used, keeping them at an even distance from the cathode is one of the principal operational problems.

3. The reoxidation is further speeded up by movements which develop in the bath either as a result of electrodynamic phenomena or from local overheating or cooling due to uneven current distribution or to local dumping of alumina into the bath. An energetic agitation of the bath may, nevertheless, be required to dissolve the alumina if it is introduced by breaking the bath-crust manually or mechanically.

If Na is the primary product[11] of the electrolysis, a very simple explanation of the low current efficiency is possible. The primary electrolysis of Na_2O has an efficiency of close to 100 pct, but when Na appears in the molten bath, its temperature is much above its boiling point. Some of it cannot react with Al F_3, and it reaches the anodic zone, where it reacts with the CO_2. With lower current density, the concentration of Na decreases, the reaction between Na and Al F_3 can take place more fully, and the current efficiency increases. This theory does not seem to contradict the preceding one, since sodium and aluminum fogs probably coexist in the bath.

Whatever causes a reduced current efficiency also causes local or general overheating of the bath,

which in turn unfavorably affects the current efficiency. Although the conductivity of the bath increases with the temperature thereby counteracting the effect of the reduced current efficiency, there seems to be no automatic equilibrium for a furnace which is out of order,* this constitutes one of the difficult problems in the pot-room's operations.

* The current efficiency is also reduced by direct conduction, i.e., by portions of the total current which do not actually go through the molten bath but are carried by chains of carbon particles. This partial short circuit of the cell occurs either between the electrodes and the metal or between the electrodes and the sides of the cell. High carbon dust content in the molten bath is detrimental to the operation.

Anode Effect: The average voltage of a cell operating under normal conditions is about 4 to 6 volts.

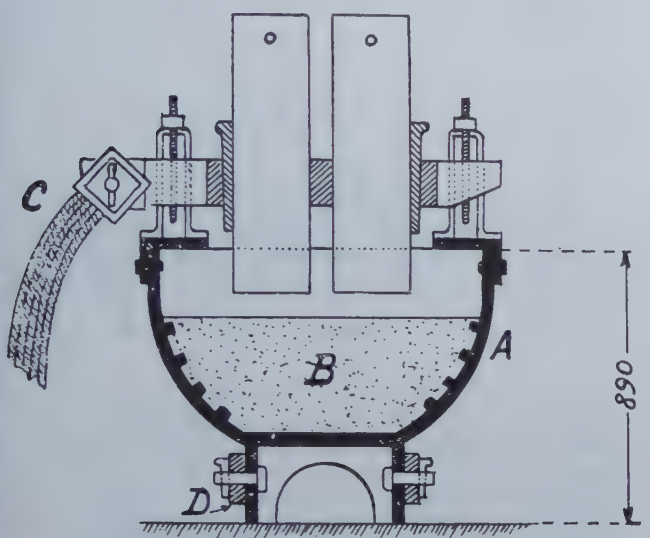

Fig. 1—Cell by Heroult. 1892. La Praz, France. Source: Ferrand, Soc. des Ingenieurs civils. Jan.-Feb. 1935.

At regular intervals it increases suddenly to 50 or 60 volts, i.e., ten times the normal value. This occurrence is called the "anode effect" and occurs in the electrolysis of many molten salts. A complete and satisfactory theory of this phenomenon has not yet been developed, but the following simplified explanation is satisfactory from all practical purposes. The voltage increase is due to the formation of a very thin layer of anodic gas which surrounds the anodes when the alumina concentration in the bath has sunk below a certain value, so that the molten bath does not "wet" the anodes. The electric current passes from the anode to the bath by means of innumerable small electric arcs, which cause the continuous and characteristic scintillation which is noticed at its surfaces; this requires some 30 to 40 volts. Marked local overheating of the bath is the result of this phenomenon, which also causes volatilization or decomposition of cryolite. Since it occurs when the alumina content in the bath is low, the phenomenon is used to indicate that a new charge of alumina should be added to the bath.

When the anode effect occurs, an electric lamp connected in parallel with the cell lights up and calls the attention of the furnace attendant. Fresh alumina is stirred into the molten bath, the phenomenon disappears, the voltage returns to normal, and a new cycle begins. The occurrence of the anode effect at regular intervals is a sign of proper behavior of the cells, but efforts are constantly made, to make these intervals as long as possible or even to suppress the anode effect. At present, the length of the intervals is from 6 to 8 hr. The alumina content of the bath falls from a maximum of 6 to 7 pct (rarely 10 pct) to a minimum of about 1.5 pct.[3]

Electrolytic Gases: The combination of the anodic oxygen with the carbon anodes results in the production of a certain amount of carbon dioxide (CO_2) and carbon monoxide (CO). There is no more agreement on which is the primary gaseous product of the electrolysis than there is on the electrolytic reaction itself. The writer, in extensive industrial experiments (1933), found that generally there is about 70 pct CO_2 in the gases developed by an electrolytic cell in normal operation. The experiments were made with 12,500 amp cells with 10 prebaked anodes. During the anode effect, the percentage of CO increases considerably, and the proportion is actually reversed. The question of the equilibrium between CO, CO_2, and C is a complicated one, since not only the temperature but also the concentration of the primary gas (CO_2) under the anode, and the impregnation of the anode with molten cryolite play important roles. Cadariu[7] has recently shown that the concentration of CO_2 declines from 42 pct to 14 pct if the cell current is reduced from 55,800 to 13,800 amp. This is explained by the fact that CO_2 has more time to react with C, and temperature becomes the determining factor affecting the composition of the electrolytic gases. A similar remark was made previously by Drossbach (*Ztsch. f. Elektrochemie* (1936)).

If the gases are withdrawn by aspiration, as shown by Grünert[9, 13] so that the time of contact with the carbon is reduced, the CO_2 content may be as high as 94 pct. According to Gadeau, there is no doubt that CO_2 is the primary product; the presence of CO is due to reaction between CO_2 and the metal fog (especially Na) and to a lesser extent to the reaction between CO_2 and the carbon anode. Gas analyses made at the plant of the AFC (*Alais,*

Fig. 2—Standard cell used in French plants since 1930. Source: Personal files.

Froges et Camargue) show the following composition:

	Pct	Pct
Prebaked multiple anodes:	68 CO_2	32 CO
Söderberg anodes:	45 CO_2	55 CO

The Söderberg anodes operate with a lower current density, are more reactive, and the temperature is generally higher.

The fluorine content of the gases is due mostly to the volatilization of cryolite at the high temperature and to its decomposition during the anode effect. The decomposition of the cryolite may be due, in part, also to the moisture which is contained either in the cryolite itself or in the alumina which sometimes is not fully dehydrated and to the moisture in the air. It is believed that these causes have a minor importance compared to the other causes of decomposition of the molten bath.

If self-baking electrodes are used, the gases contain sizeable amounts of tar compounds and soot, resulting from the distillation and cracking of the coal tar pitch which is the binder of the carbon mixture of which the electrodes are made.

Thermal Aspect

Energy Balance: From the technical point of view, thermal considerations have the greatest importance because they determine the size, the design and the operational conditions of the cell. The wellknown basic voltage equation, $V = E + I\,R$, is converted into a power equation:

$$W = V\,I = I\,E + I^2R$$

in which:

W is the power required by the cell to operate.

$I\,E$ is the portion of the total power required for the electrolysis itself, i.e., for the decomposition of the alumina. (See above.)

$I^2\,R$ is the power transformed into heat in the various parts of the cell. It corresponds to:

$\Sigma r_n\,I^2$, where r_n are the various resistances in the cell.

Only $I\,E$ corresponds to useful work, while the rest is loss. In fact, if it were possible to eliminate all resistances, it would be possible to produce aluminum by applying to the cell the voltage E which would cause the current I to pass through.

The power efficiency* of an aluminum cell, i.e., the percentage of the applied power used for the actual electrolysis, is therefore measured by the equation:

$$\frac{IE}{IE + I^2R} \times 100 = \frac{E}{V} \times 100$$

This has not changed very much during the past twenty years. In 1926, a 12,500 amp cell operated with a voltage of 6.50. Assuming that $E = 1.70$, only about 26 pct of the total power absorbed by the cell was doing useful work.[14] Many cells of this type are still in operation.†

In some of the recent cells voltages of 5.5 or less have been obtained.* The energy efficiency would thus reach 35 pct, but it is still very low compared with that of the arc furnaces used in electrothermic processes (carbide, etc.), which is about 60 to 70 pct.

Where the Heat Develops: In a cell operating at constant temperature, all the heat generated is dissipated, but the generation and dissipation do not necessarily occur in the same part of the cell. The cell is, from the electric* point of view, a series of resistors, each one having a resistance r_n; for each, the voltage drop v_n caused by current I is Ir_n. For the sake of simplicity, the following example instead of showing r_n shows v_n, which simplifies the later discussion.[14]

Voltage measurements were made by the writer in 1931 on a typical 12,500 amp cell similar to that shown on fig. 6 (but without covers). Table I gives results.

* Power efficiency and energy efficiency are synonymous since the time factor is eliminated when percentages are used.

† The 12,500 amp cells, to which many of the experiments given in the text refer, are very similar to that shown in fig. 3. See also fig. 6.

* The many discrepancies among voltage data are due also to the fact that in some cases the voltage of the individual cell is given, disregarding the increases due to the anode effects. The important factor is the average voltage of all cells of a given type, including all the increases due to the anode effect.

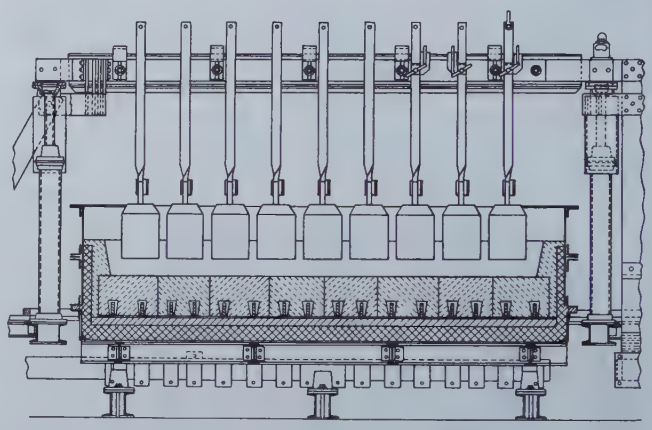

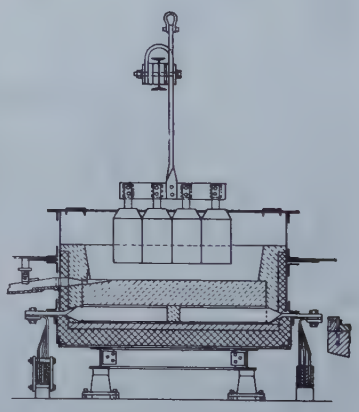

Fig. 3—Cross section and details of installation of a 30,000 amp multiple prebaked anodes cell. German design, Lautawerk, Germany, 1939. Source: German documents PB 70030, Frame 6676.

Table I. Voltage Drops, Energy Absorption, and Heat Generation in a 12,500 Amp Aluminum Cell

	Volts	KW (Energy Absorption)
V TOTAL	6.50	81.00
E	1.70	21.22
V_a Overvoltage due to anode effect, daily average	0.30	3.75
V_b Carbon lining	0.50	6.25
V_c Conductors, connections, external	0.50	6.25
V_d Anodes	0.30	3.75
V_e Molten bath	3.20	39.78

The heat generated per hour corresponds to 59.78 kwh, i.e., 81.00 less 21.22.

Of the above "losses", V_c, which occurs outside of the cell, is controlled by the usual economic considerations, relating the cost of the installation to the cost per kwh, taking into account structural circumstances, etc. The remaining "losses" will be analyzed later. The above measurements refer to an outmoded cell, but they are typical of most open cells with prebaked electrodes.

Where Heat Is Dissipated: Measurements of voltage drops are relatively easy to take. Much more difficult is the determination of how and where the heat thus generated is dissipated.

The writer has made an extensive series of temperature measurements on several operating cells of the type mentioned above (fig. 6), from which the heat dissipated from the various parts of the cell has been calculated. (Table II).

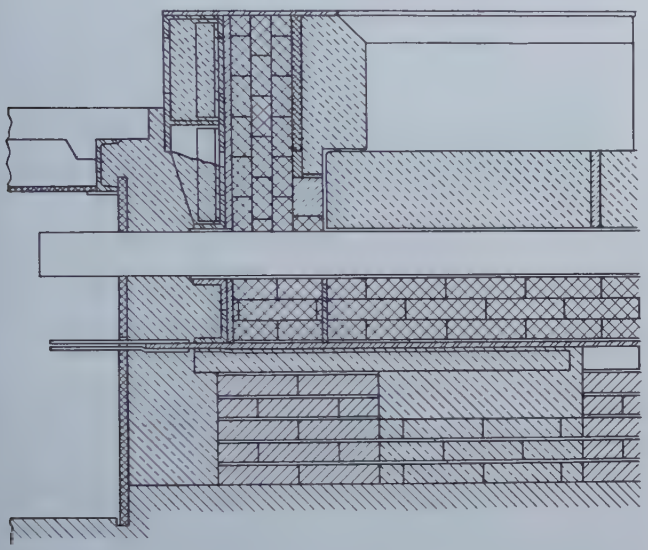

Fig. 4—Bottom lining and insulation of a 30,000 amp German cell, 1938, Töging, Germany. Source: German documents PB 70030.

These measurements and calculations cannot be very precise and are characteristic only of a given type of cell, a given type of alumina, and a given method of operation. However, the order of magnitude of the dissipation from the various parts of

Table II. Heat Dissipation in an Aluminum Cell (12,500 amp)

	KWH	Pct
External connections	6.24	10.50
Walls and bottom of cell	16.00	26.70
Metal tapped (heat content)	1.00	1.68
Gas developed (CO_2, CO)	1.75	2.92
Upper surface	27.29	45.70
Operations and misc.	7.50	12.50
TOTAL	59.78	100.00

a cell does not differ very much from one open cell to another. In fact the dissipation through the upper surface and that due to normal operation for this particular case, account for 58.20 pct of the total; Ferrand (*op. cit.*[14]), who experimented with a different type of cell, reports a loss of 61.5 pct. Furthermore, Drossbach (*op. cit.*[14]) indicates 38 pct as his appraisal of the dissipation through the upper surface excluding operational losses, while our measurements indicate 45.8 pct.

Reduction of Heat Generation: The breakdown of the total heat generated in a cell (table I) shows that roughly 2/3 of that heat is generated in the bath. This heat generation, and the voltage drop to which it corresponds and by which it can be measured, may be expressed by $V_e = IR_e$, where R_e is the resistance of the electrolyte. If we indicate the current density by $d = \frac{I}{a}$, i.e., the number of amperes per cm² that flow through an ideal cross section a (the average between the anodic and cathodic surfaces), the above expression may be written as follows:

$$V_e = IR_e = \frac{\rho l}{a} I = \rho l d,$$

in which ρ is the specific resistivity of the molten bath and l the anode-cathode distance.

Theoretically, all of the above factors are variable, but practically, ρ must be considered constant, since temperature, (which to a considerable extent determines the resistivity*) cannot be increased for the purpose of reducing ρ.

* It is theoretically possible to consider a molten bath of lower resistivity, since even a reduction of the alumina content from, say, 15 to 5 pct would reduce the resistivity by 10 pct. But this field has not been fully explored so far. (Arndt-Kalass. *Ztsch. f. Electrochemie*).

The anode-cathode distance l may be increased, but generally not decreased, so that a reduction of V generally cannot be achieved by changing it. The cells on which the measurements were made generally had $l = 3.5$ cm, very exactly controlled, and a reduction below this limit is not convenient for reasons explained above (see p. 107).

We are thus left with one factor, d, which can be subjected to relatively considerable variation. The current density d thus becomes the basic characteristic of every cell and a reduction of current density is the means used for reducing the heat generated in a cell.†

† In general, reference is made to anode density, which differs from d, which is average density. The ratio anode density/average density is assumed to be a constant. It corresponds to the coverage factor, i.e., the factor which indicates what proportion of the bath surface is occupied by the electrodes. It differs for the two types of electrodes, the multiple prebaked and the self-baking. The latter, naturally, have a better coverage factor.

Table III gives the anodic current density of various cells.

Table III. Anodic Current Density of Cells with Prebaked Electrodes*

Type	Year	Anodes		Amp	Density amp per cm²
		No.	Size, cm		
Heroult (France)	1890	1	25 x 25	4,000	6.40
Hall (U.S.A.)	1890	32	46 cm²	6,000	4.05
La Praz (France)	1893	6	22 x 25	5,000	1.50
Argentiere (France)	1925	12	43 x 43	20,000	0.90
Lautawerk (Germany)	1925	10	32 x 25 (?)	12,500	1.55
Mori (Italy)	1928	16	40 x 28	25,000	1.40
Argentiere (France)	1934	20	35 x 65	45,000	1.00
Lautawerk (Germany)	1939	36	25 x 32	30,000	1.05

* Ferrand, op. cit.; PB 70020; PB 60889.

There has been a noticeable tendency toward lower current densities, but with prebaked electrodes, it does not seem advisable to go much below 1 amp per cm^2. There is also an ultimate limit in this reduction in open cells, since the heat losses are proportional to the size of the cell and especially, as we have seen, to its upper surface. This is especially true for cells using prebaked electrodes.

The other voltage drops, adding up to 1/3 of the total, are less important but some of them are significant. A great deal of work has been done and is being done to reduce the voltage drop in the bottom.[16] Again and again metallic cathodes have been tried and rejected, so that currently prebaked pressed carbon blocks are generally used. This voltage loss in the bottom cannot be reduced much below a minimum of, say 0.25 or 0.30 in cells having a low cathodic current density and a carefully constructed carbon lining. As for the external voltage drop in the conductors and in the anodes, it is sufficient to state that all of the contacts between carbon and metal conductors are a perennial problem in the production of aluminum.[17]

The overvoltage and the corresponding generation of heat resulting from the anodic effect have attracted much attention since the earliest days of aluminum production, due to the necessity of breaking the bath crust, stirring the bath, etc., all of which also cause increased heat losses. Several aluminum plants have experimented and are experimenting on the suppression of the anodic effect, and it is likely that a rational solution to this problem will eventually be found. The mechanical "picking" of the aluminum cells, now used in some plants, seems to be a transitory device.

Reduction of Heat Dissipation: A reduction of the heat losses through the walls and the bottom is easily achieved by adding successive layers of heat insulating bricks around and under the carbon lining.*

* The efficiency of such insulating layers decreases as the thickness increases since each successive layer increases the outer surface, but the limit has not yet been reached in most cases.

However, a serious problem arises when it comes to insulating the sidewalls: preventing the destruction of the carbon lining by the molten bath. For this reason it is preferable not to exceed, at the inner surface of the carbon lining, a temperature some 10° lower than the temperature of the molten bath, so that a thin coat of frozen bath protects the lining from attack. It is also advisable, in order to avoid short circuits, to maintain a sufficient distance between the anodes and the walls. Then the appropriate insulation can be provided on the outside.[18]

The 12,500 amp cell, to which the data of tables I and II refer, and most German furnaces built before 1939 (fig. 3) were not insulated along the walls, but the trend in medium cells (fig. 4) has been toward more insulation of outer walls.

It is mechanically very easy to insulate the bottoms, and since the early days of the aluminum industry most bottoms have been insulated. But there is always a certain danger in overinsulating, since the metal becomes hotter, thus unfavorably affecting the current efficiency. Leakages of metal are likely to occur and the life of the carbon lining may be shortened. Practical applications of these concepts are exemplified in fig. 3 and 4.[18]

Fig. 3 is a vertical cross section of a 30,000 amp multiple prebaked electrode cell used at Lautawerk, Germany, in 1934. Similar types with a different electrode arrangement had been installed there in 1927.* Cells for 25,000, 30,000, and 40,000 amp have also been built based on this design. These cells have no heat insulation along the walls and little at the bottom; furthermore, they are installed above the ground floor, so that the heat losses are increased through ventilation.† Fig. 4 is a German version (Töging, Germany, 1938) of a type which has found more general acceptance in aluminum plants all over the world. It is provided with substantial heat insulation along the walls and is abundantly insulated at the bottom. It is installed in the ground, so that heat losses through ventilation are minimized. The French cell shown in fig. 2 and the American cell shown in fig. 5 are other examples of this type of construction. By insulating the walls and the bottom of the electrolytic cells, the proportion of heat lost through them (which was about 25 pct in the small scarcely insulated 12,500 amp cell tested at Mori) may be reduced to about 15-18 pct. This is a reduction of 1/3 of the total included under this heading, but only about 8-10 pct of the total heat losses.

* The Mori 12,500 amp cell, to which the experiments in tables I and II refer, is a smaller version of the same cell and was built on the basis of the original Lautawerk drawings (1927).

† The purpose of this type of installation is to allow a speedy change of the bottom when the lining is worn out or damaged.

Reduction of Dissipation Through the Upper Surface. Experiments With Closed Cells. The losses through the upper surface, which account for about 50 pct of the total losses in the conventional open cell, are obviously the key to the problem of reducing the energy consumption of the aluminum cell. This fact, while not overlooked during the early phase of the development of the aluminum industry, was not given its due importance, and the insulation of the upper surface was and still is left to the alumina blanket which is spread over the frozen bath crust. This heat-insulating function of the alumina blanket is a predominant factor in the heat balance of the conventional aluminum cell with multiple prebaked electrodes.‡

‡ Accordingly, if instead of an alumina which is dry, light, and fluffy, as is the standard Bayer alumina, an alumina quality with higher bulk density, with coarser grains, is used, such as Haglund alumina, the resulting changes in the behavior of the cell may be dramatic. Several years ago (1932-3), the writer was witness and actor in a large-scale experiment which consisted of changing from Bayer-type to Haglund-type alumina in several pot-lines in an Italian plant. The desperate effort to maintain the same voltage and the same general operating conditions in spite of the physical differences between the two aluminas resulted in a disrupted electrolytic process due to cold acid bath, incrustation of the bottoms, etc. Other causes, such as the lower solubility of the alumina, were also a factor, but the main reason for the troubles was the disruption of the heat balance due to increased heat loss through the upper surface.

The heat losses are particularly high when the alumina is stirred into the bath after the anode effect. In most plants this is still a manual operation, and too often heat losses occurring during these operations, repeated up to six times a day, are not taken into account when the overall results of a cell are evaluated.

The protection against heat losses afforded by the alumina blanket is reduced by the thermal short

circuit caused by the electrode (anode) heads projecting above the alumina blanket (fig. 2—5). Covering the anode heads with alumina probably results in a reduction of the heat loss, but it increases their temperature and, accordingly, their burning loss.*

* German experiments (see PB 70021) carried out as recently as June, 1943, shortly before the collapse of Germany, brought production to a virtual standstill and confirm this point on a large scale.

To counteract the oxidation, anodes are now often

Fig. 5——Upper view of a multiple prebaked anodes cell in a U. S. plant. Source: Courtesy of the Aluminum Co. of America.

protected by an aluminum casing, which, however, hardly reduces the heat losses through the electrode heads.

Some attempts to enclose aluminum cells were made in the early days of the aluminum industry, but the necessity of supervising cell operation and of not overheating the anodes was why the experiments never reached an industrial scale.

It is believed that the first large-scale use of enclosed cells was made at the Italian plant at Mori in 1931. The immediate reason for the experiment was to find a means of counteracting the increased energy consumption due to the use of Haglund alumina (see above) by reducing the heat loss through the upper surface. Several 12,500 amp cells, which were the standard equipment of the Mori plant, were fitted with light removable hoods of various designs, of which the most typical is shown in fig. 6. These hoods, as might have been foreseen, did not compensate for the effect of the Haglund alumina since they were not air-tight, were often opened, and were not heat insulated. They would have been added to the long list of unsuccessful experiments if, shortly afterwards, the "fluoric gases incident" had not occurred.

This started when the population of a poor farming village located some three miles downstream of the factory, under the impression that the gases of the factory were damaging to their cattle and silkworms, started clamoring for payment of damages. Very soon, in a strange medieval setting, all the diseases in that poverty-stricken community were being attributed to "the factory." The Italian Government ordered the immediate stoppage of the operation of the electrolytic cells until proper measures had been taken to prevent the dispersion of fluorine compounds in the atmosphere. Two measures were decided upon. One was the installation of some enclosed Söderberg electrode cells (see below); the other was to provide all the existing furnaces with hoods similar to those previously tested for a different purpose, connected with a system of exhaust pipes (fig. 7) through which the gases were conveyed to scrubbing towers.

From the point of view of cell operation, these hoods had many disadvantages. Since they were not airtight and dispersion of the gases had to be avoided as much as possible, the amount of air sucked from each cell was considerable. This prevented overheating and burning of the anodes but reduced to nil the already negligible heat insulating effect. The frequent inspections, the charging of alumina and the ladling of the metal were causes for opening the lids, with resulting dispersion of gases when their concentration was at its maximum. The hooded cells are still operating in Italy at Mori and Bolzano in the 12,500 amp and 25,000 amp sizes, but this type was not adopted anywhere else since its use in the Italian plant was dictated exclusively by the legal imposition to prevent the dispersion of fluoride-bearing gases. The recovery of cryolite and other fluorine compounds from the scrubbing plant is not a paying proposition with this type of cell, as the dilution is such as to require enormous installations.

In 1934, Louis Ferrand (Paris) proposed an enclosed furnace* which presented some unusual

* U.S. pat. 2,061,146. Nov. 17, 1936.

features. Its main purpose, to avoid the heat losses through the upper surface, was achieved by means of a complicated heat-insulated hood. Other features of the invention were the oscillating prebaked anodes, movable around horizontal shafts. To the writer's knowledge, the only attempt to operate this cell on an industrial scale was made in Rumania during World War II, with good results in terms of energy consumption. It is, however, doubtful that such a complicated apparatus could compete with modern types of cells with self-baking electrodes, which will be described below.

The Modern Electrolytic Cell with Prebaked Electrodes

The main features of the modern electrolytic cell with prebaked electrodes have often been referred to in the preceding pages, but it is interesting to examine in greater details the structural lay-out of a modern cell of this type and consider its performance.

A good example is the German 30,000 amp cell shown in fig. 3 (PB 70030). The drawing is detailed enough so that the various parts may be clearly distinguished. The anodes are grouped four by four in nine rows; their size is 32 x 25 cm. Each group is attached to a common rod suspended from the anode bus, and the anode-cathode distance for each group can thus be regulated independently. All of the main elements of the anode assembly are very similar to those of the French cell (fig. 2), the American cell (fig. 5), and the Italian cell, built on a German prototype (fig. 6). This type has been used with few modifications in German plants and in some of the Italian plants since 1926. Some instal-

lations were made in 1939. An interesting improvement was tried at Mattigwerk, Germany, probably with success, since it resulted in the installation (1943) of a complete potline, which, however, never actually operated. Instead of the usual anodes, eight large 37 x 127 cm blocks were used, thus lowering the anode current density to 0.79 amp per cm^2.*

* A similar arrangement is being tested at present by other European aluminum plants, in high powered furnaces, with good results.

It is difficult to strike a balance between the advantages and disadvantages of the prebaked electrodes at this point. Only a few basic points will be summarized here:

1. Heat insulation of the upper surface is difficult; it conflicts with the reduction of anode consumption and with the necessity of changing the anodes.
2. The recovery of the fluorine compounds is also difficult and uneconomical; in fact, only two plants are equipped to do so.
3. The periodic withdrawal of electrode stubs and the introduction of new electrodes, necessarily by hand, results in a detrimental discontinuity in cell operation. Attempts to develop continuous prebaked anodes have so far failed.*

* The writer, among others, once took out a patent for a continuous anode made of prebaked blocks, but he did not even dare test it since it was obviously inferior to the self-baking continuous anode. PB 74586 records a test made at Lautawerk in 1941 of a 30,000 amp cell which used two large electrodes made of prebaked blocks. The experiment was not successful and was discontinued.

4. On the other hand, cells with multiple prebaked anodes are simple and less expensive than other more advanced types and their operating results satisfactory. The fact that some of the largest potlines built in the United States during World War II were equipped with prebaked electrode cells clearly emphasizes the uncertainty which still exists of the relative advantages of the various types of aluminum cells.

Table IV, compiled mostly from German documents, gives consumption figures for prebaked electrode cells. The French consumption figures are known to be similar to the German ones;† those of the U.S., it is believed, show slightly better results.

† Some recent experimental cells seem to have yielded better results.

Table IV. Consumption Data for Pre-baked Multiple Electrode Cells§

Plant	Lautawerk VAW*	Lautawerk VAW*	Bolzano INA†	Pt. Marghera AIAG‡	Russian Plant
Year	1943	1943	1941	—	1940
Amperes, avg.	13,000	26,000	11,766	32,000	35,000
Volts per cell	6.38	5.65	6.47	4.8–5.4	—
KWH/100 kg. of Al	2,227	2,066	2,212	1,750	1,820
Current efficiency, pct	87.0	83.50	86.76	—	86.2
Alumina, kg./100 kg. of Al	—	—	195.40	—	—
Cryolite, kg./100 kg. of Al	—	—	4.81	—	—
Electrodes, kg./100 kg. of Al	—	—	54.85	—	—

§ Source: PB 70025. The Porto Marghera, Italy, and the Russian consumption data are second-hand reports.
* Vereinigte Aluminum Werke. † Industria Nazionale Alluminio. ‡ Aluminium Industrie A.G.

The Electrolytic Cell with Self-baking Electrodes

The self-baking electrode was developed during the first World War by a Norwegian engineer, C. W. Söderberg.[20] It was originally applied to the manufacture of calcium carbide and ferroalloys. Its basic principle is to use part of the heat generated during the operation of the electric furnace for the baking *in situ* of a semifluid electrode paste, which is fed from the upper part of the electrode while being progressively used up at the lower end.

Very early experiments had indicated that it was possible to use the same principle in the electrolytic cells producing aluminum, and large-scale experiments were carried out in the United States, in France, and Spain* with slightly modified Söderberg electrodes. A first change from the "carbide type," where the electric contact was carried out by means of clamps, occurred when the electrode was suspended by means of ribs attached to an aluminum sheet casing, (fig. 8).† This system, however, did not meet with favor, and its application was not extensive. The first real improvement came about 1925, when steel contacts introduced laterally were used to lead the electric current into the baked carbon paste. These contacts were extracted when (as a result of the progressive use of the electrode) they were about to touch the molten bath (fig. 9 and 10).‡ This system of steel studs is still in use.

* The first patent related to aluminum production, was granted to Söderberg on May 15, 1928 (U. S. Pat. 1670042, applied for in Norway, July 25, 1923).

Fig. 6—Hooded 12,500 experimental electrolytic cell at Mori, Italy, 1933. Source: Personal files.

† Some early types did continue to use steel sheets, but the iron spoiled the aluminum.

‡ Westly. U.S. Pat. 1757695, May 6, 1930, filed in Norway, Sept. 30, 1925. Fig. 12 and 13.

Up to 1930, the self-baking electrodes for aluminum cells were round and could carry up to 30,000 amp; for several reasons, such as quality of the paste, limitation in size, and some imponderable factors which always make difficult the success of a new device, they were only a moderate success.[21]

The turning point for the self-baking electrode

applied to the production of aluminum occurred in 1931, when the first test cell came into being at the aluminum plant of Riouperoux, France, with large rectangular electrodes.§ The success of the first experiment was followed by the installation of a series of these cells, and in 1932-3, technical experts convened in Riouperoux to study the new system,* which presented the following advantages:

§ U.S. Pat. 1958328, P. Torchet, May 8, 1934; applied for in France, Oct. 21, 1931. U.S. Pat. 2073356, P. Torchet, March 9, 1937; applied for in the United States, April 18, 1933.

* The Riouperoux system as it was presented was much more than a new form of electrode: it was also the "know-how" in the manufacture of the electrode paste, the operation of the cell, the design of the cell itself, etc.

Fig. 7 — Covered cell potline and exhaust system, Mori, Italy, 1933. Source: Personal files.

1. One or more large sized electrodes of rectangular form could be used in a high-ampere cell. The consumption data were remarkably lower than those of the self-baking electrode cells up to that time.

2. They could be enclosed in a box from which the fluoride-bearing gases and tar gases could be withdrawn by a fan and forced through a washing plant in which the fluorides were recovered. (Fig. 11).

Cells of the Riouperoux type were very soon installed in Switzerland, Germany (by the AIAG), England, France, and Mori (Italy), where they seemed to be the solution of the serious gas problem.

Other plants adopted the Riouperoux type between 1935 and 1940, and many more cells of similar type were installed during World War II in the United States, Canada, France, Italy, Germany, Japan, Switzerland, the United Kingdom, etc. These cells were derived from basic designs supplied by the firm "Elektrokemisk," Oslo, Norway, which was and is the owner of most of the Söderberg and derived patents.[20] The Riouperoux version, which used two electrodes per cell (fig. 11 and 12) was modified after 1940, when the trend progressively shifted to a "single-electrode" cell. This proved to be more rational, cheaper in construction, and avoided the problem of the burning by the air of the two adjoining electrode surfaces. A typical single-electrode cell is shown in fig. 13. They can still be considered as typical of today's practice.

The main characteristic of the cells with self-baking electrodes, as it is for those with prebaked anodes, is the anode current density. The fact that the self-baking anode is a compact block with no space wasted (except the area between the two electrodes, if the now outmoded version is used) allows a lower current density without requiring an increase in the size of the bottom.*

* On the other hand, it is necessary to adopt a greater anode-cathode distance in order to prevent short circuits, when very long electrodes are used.

The original Riouperoux experiments seemed to indicate that the width of an electrode could not exceed 110 cm. This limitation resulted in the necessity of using either very long electrodes, as the total amperage increased, or putting two or more electrodes in a cell. Both solutions were unfavorable both to thermal balance and to smooth and economical operation. Accordingly, most cells, up to the beginning of World War II, were built for not more than 22,000 to 30,000 amp. However, later experiments[28] were carried out with larger electrodes, and it became apparent that the limitation in width was not really significant, and electrodes up to 150-160 cm wide could be used without disadvantage. The dreaded disturbances due to the accumulation of gas bubbles under the electrode, while theoretically probable, did not affect the operation. Consequently, single large electrodes with low current density in high ampere cells entered the field of practical application.

As shown in table V, the current density is consistently lower than for the prebaked electrodes, and modern furnaces show a trend toward even lower figures. However, the lower the current density, the slower is the lowering of the electrode and the higher is its burning above the bath level if it is not protected; and this increases the electrode consumption. Furthermore, the time during which electrolytic CO_2 (in the reaction $CO_2 + C = 2CO$), is in contact with the electrode increases, and more CO can be produced, thus further increasing the electrode consumption.

Fig. 8—Early self-baking electrode in a 11,000 amp cell, Riouperoux, France, 1929. Source: Personal files.

The self-baking electrodes (following the Riouperoux example) are very often enclosed, not only

allowing the recovery of fluorine compounds, but also preventing the dispersion into the pot-room of the tar gases, which develop during the baking of the electrode. The effectiveness of this removal is questionable, however, so that there is very seldom an economic justification for building large installations to recover the fluorine compounds. In any case, the workers are still exposed to tar gases during the various operations such as the extraction of the lateral contacts, the crushing of the crust and the feeding of alumina into the cell, the removal of the metal, etc., since all of these operations involve opening the enclosures. During these operations, the fluoride gases are freely dispersed into the atmosphere—even when there is a scrubbing and recovering plant.

Consumption figures of various cells with Söderberg electrodes are given in table VI. The kwh per kg of aluminum are of the same order of magnitude as those shown on table IV for the prebaked electrode cells. The same is true for the current efficiency.

Table V. Dimensions of Electrodes and Current Density in Various Self-Baking Electrodes

Plant	Year	No. anodes	Size cm	Amp	Intensity amp per cm^2
Mori, Italy*	1931	1 round	ϕ 125	12,500	1.02
Clavaux, France†	1930?)	1 round	ϕ 150	14,000	0.80
Riouperoux, France*	1932	2 rect.	100 x 135	22,000	0.81
Mori, Italy*	1933	2 rect.	100 x 135	25,000	0.93
Sabart, France*	1940	1 rect.	100 x 375	33,000	0.88
Mattigwerk, Germany‡	1940	1 rect.	155 x 265	30,000	0.73
Mattigwerk, Germany‡	1940	2 rect.	110 x 170	30,000	0.80
Lautawerk, Germany‡	1942?)	1 rect.	120 x 320	30,000	0.78
Kitakata, Japan§	1943	1 rect.	150 x 330	40,000	0.81
Russian‡	1942?)	1 rect.	161.6 x 316.8	?	?

Sources: * Personal files, † Guillet, *Les metaux legers*, (1935), ‡ Various German documents of the PB series. § Aluminum Metallurgy in the Japanese Empire, U.S. Dept. of Commerce, Oct., 1947.

The New Enclosed Cells

In 1931, even before the Riouperoux experiment had been disclosed, the writer had an opportunity to work with Söderberg electrodes when two 12,500 amp single round electrode cells were installed at Mori, Italy. Both cells had round electrodes (125 cm diam) with lateral contacts of the Westly type (fig. 9 and 10). Among the various measurements taken by the writer on those furnaces, those of temperature had a prominent place as the writer was interested in comparing the heat balance of this type of cell with that of the cell with prebaked electrode cells which he had previously tested. The results (table VII) showed that a 12,500 amp furnace dissipated as much as 21 out of 64.5 kw (32 pct) through the upper surface and 17.3 kw (26.7 pct) through the electrode. In other words, about 60 pct of all heat losses occurred through the upper part of the furnace. In striving to achieve a reduction of these heat losses, the writer reached the conclusion that:

1. The structure of the conventional aluminum-cell with self-baking electrodes would have to be redesigned so as to transform it into a real electric cell, resembling furnaces used in other electrometallurgical operations (steelmaking).
2. This transformation would require the elimination of the lateral contact stubs near the bath level, which would have prevented the use of insulated covers.
3. The electrode, if enclosed under an insulated cover should be protected against corrosion, since the temperature in an insulated enclosure would necessarily be high and infiltration of air could not be entirely avoided.

These ideas crystallized in December, 1931, in a concrete proposal to replace the lateral contacts with vertical ones, which, cutting through the unbaked upper portion of the electrode paste, would reach into the lower baked portion. These contacts were made with a specially shaped thread, were to be progressively extracted by simple rotation, and were also to serve as suspension for the electrode. The electrode, thus freed of the lateral contacts and of all the related accessories could be enclosed in an airtight permanent steel casing that

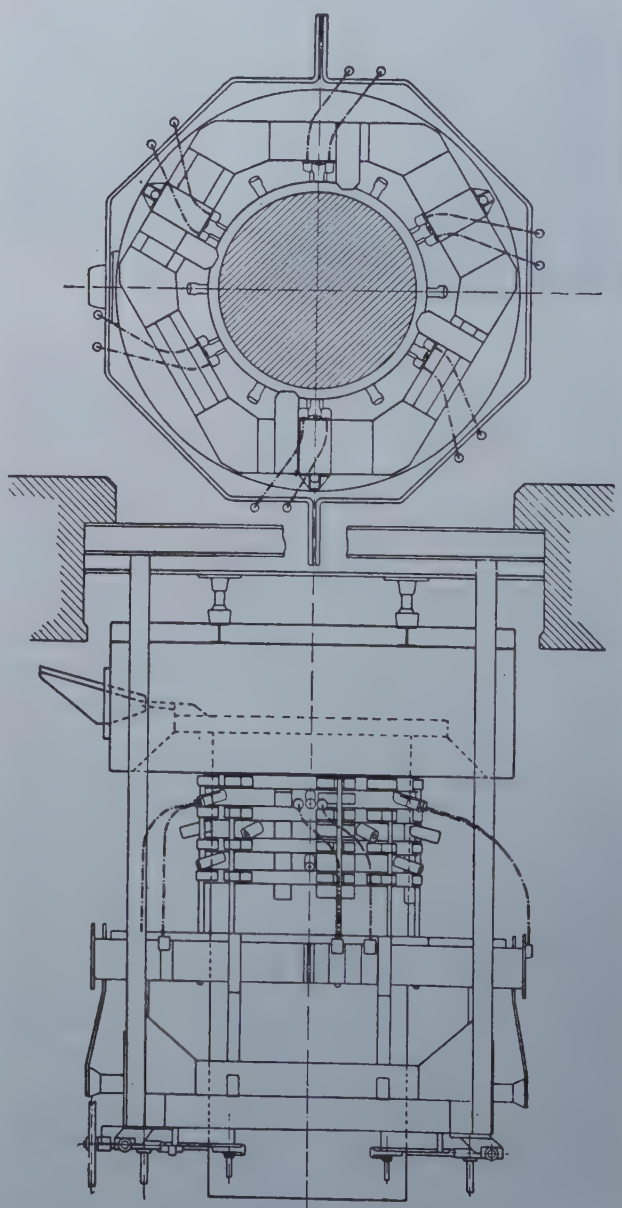

Fig. 9—Self-baking electrode cell, 12,500 amp, Mori, Italy, 1931. Source: "Elettrotecnica" and personal files.

Table VI. Consumption Data for Cells with Self-Baking Electrodes

Plant	Lautawerk	Lippe	Lippe	Lippe	Mattig	Kitakata
Year	1943	1944	1943	1943	1943	1945
No. electrodes			2	1	1	1
Amp, avg.	29,384	30,156	30,022	29,990	30,131	36,086
Volts per cell	5.00	5.29	5.31	4.47	4.96	—
Kwh per 100 kg of Al	1,801	1,854	1,895	1,820	1,746	1,980
Current efficiency, pct	82.7	85.7	83.6	81.5	84.8	90
Alumina per 100 kg of Al	192.2	190.6	194.5	192.8	192.74	
Cryolite per 100 kg of Al	4.16	6.67				
Electrode paste per 100 kw of Al	55.9	57.64	57.90	57.31	56.94	60
Source	PB 70025	PB 70032	PB 70032	PB 70022	PB 70022	U.S. Dept. of Commerce

would protect its lower portion and thus allow its enclosure under insulated covers. These basic concepts are embodied in the cell shown on fig. 14 (which was used in filing the patent for the new cell, U.S. 2100927).* The writer accordingly modified one of the 12,500 amp Söderberg furnaces at Mori (without, however, installing the alumina bins, which were left for later experimentation), and in the fall of 1933 the first test furnace was started. All the relevant details of this experiment are shown clearly in fig. 15 and 16. In particular, fig. 16 shows the airtight steel casing which protects the electrode underneath the covers. The covers were not heat-insulated but were made of two metallic sheets with asbestos filling between them. All the procedures connected with the operation of the cell were simplified, and a remarkable smoothness of operation was achieved.

The writer undertook the same measurements on this modified furnace that he had made before on the conventional type with lateral contacts.

From the data collected and from the practical experience, the following main conclusions were drawn:

1. The covering of the cell with a lightly insulated cover, made possible by the adoption of vertical contacts, resulted in a reduction of power consumption from 25 to 22.80 kwh per kg Al, or roughly 10 pct.

2. Most losses, 22.7 kw out of 57.3 (or about 40 pct) occurred through the air and gases aspirated from the enclosed cell. The problem of insulating the upper surface was thus reduced, transformed into the simpler problem of building a tight and better insulated cover, and reducing the amount of air which was aspirated with the gases.

3. The electrode was perfectly protected by the steel casing, and even when the bath was overheated no corrosion appeared. Furthermore, the aluminum casing used in the conventional Riou-

* Reference is made in a recent paper[20] to the fact that the Elektrokemisk had tested vertical screws as current carrier since 1919. These experiments, of which no one knew at that time, were probably not backed by a sufficient understanding of the heat balance of the aluminum cell and of the importance of enclosing the electrode. They were soon forgotten because they were not properly interpreted.

Fig. 11—Enclosed 22,000 amp furnaces with self-baking (Söderberg) electrodes, Riouperoux, France, 1932. Two 100 x 135 cm electrodes. Source: "Elektrokemisk Bulletin".

Fig. 10—Photo of the cell in Fig. 9. Source: Personal files.

Table VII. Consumption Data and Breakdown of Energy Losses in Experimental Söderberg Cells

		Standard Söderberg type Fig. 9 and 10	Mod. B.L. cover cell Fig. 15 and 16
Current	amp	12,500	12,400
Voltage	volts	6.90	6.50
Current efficiency	pct	82	83
Power consumption	kwh per kg Al	25	22.80
Power per cell	kw	85.5	78.3
of which (*a*) used	kw	21	21
(*b*) dissipated	kw	64.5	57.3
Breakdown of Energy Losses, in kw			
Losses through the bottom		11.20	11.20
Upper surface (covers)		21	3.80
Electrode		17.30	3.90
Contacts (external)		6.20	6.20
Operation		6	6
Electrolytic gases		1.80	0
Metal		1.00	1.00
Opening of covers		0	2.50
Gases plus air		0	22.70

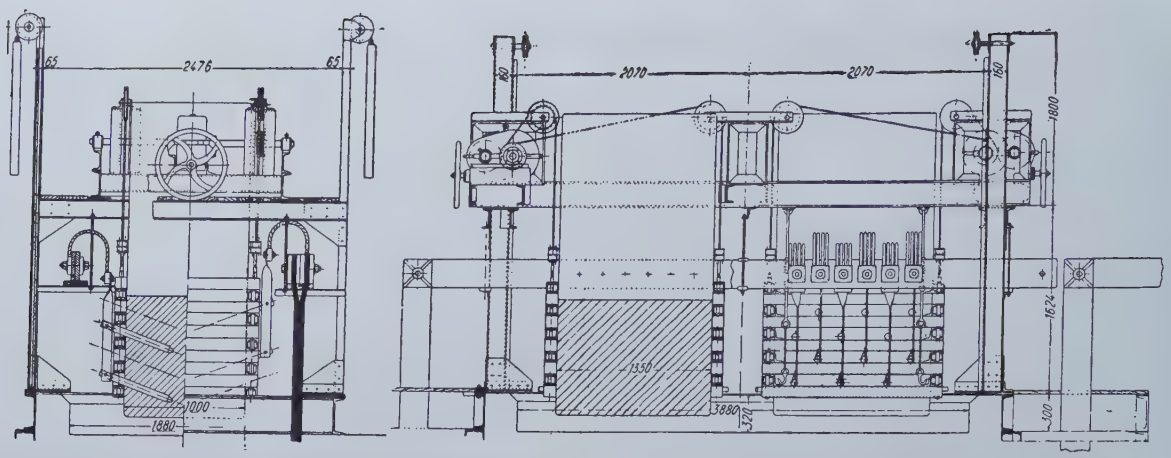

Fig. 12—Enclosed 25,000 amp furnace, Mori, Italy, 1934. Source: "Elettrotecnica" and personal files.

peroux type became superfluous, as the electrode slid easily in the fixed casing.

The promising results achieved with the first test furnace prompted further experimentation. To this end, a standard bottom for a 25,000 amp multiple prebaked electrode cell was fitted (fig. 17) with two self-baking electrodes, and the resultant cell was installed in a 12,500 amp potline. The anode current density on the two electrodes (100 cm x 90 cm) was very low (0.70 amp per cm^2), the lowest on record at that time. The bottom was exceedingly large and hence its heat losses were relatively high, but the over-all extremely favorable results of the first cell were fully confirmed. (See table VIII, Experiment 1).

The interesting features of this cell were: 1. Carefully insulated covers which pivoted on horizontal hinges. 2. A very neat external appearance which made the cell look like a real electric furnace, an impression which had been missing from the aluminum cells up to that time. 3. Gas and air suction was reduced to a minimum.

Preliminary calculations had shown that if the 25,000 amp bottom with multiple prebaked electrodes had been connected to a 12,500 amp potline, it would have required 110 kw, corresponding to approximately 9 volts; otherwise the bath would have frozen as a result of the excessive heat losses. The experimental cell with insulated covers required only 92.50 kw, or about 7.40 volts (average current 12,500 amp) (see table VIII). If the covers were left open, the cell could not operate at less than 8.50 volts, and even then the operation was very troublesome. The cell was, however, oversized, and conclusions as to the power consumption could not have been drawn from that experiment. Another experiment was therefore made by equipping the same cell with two 100 x 120 electrodes and installing it in a 25,000 amp potline. Table VIII, Experiment 2, shows the results of this test. The

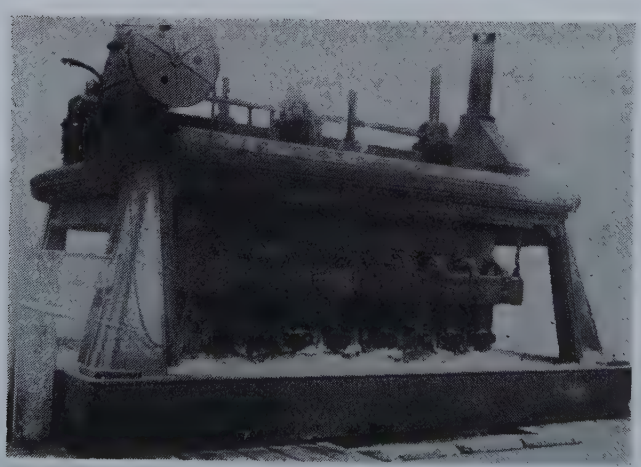

Fig. 13—(above) Single-electrode cell.

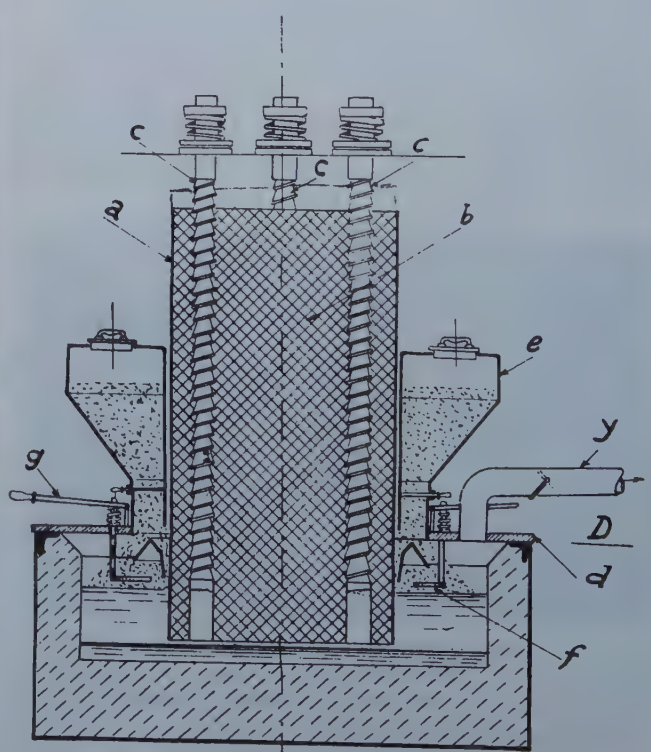

Fig. 14 — (below) Self-baking electrode with vertical threaded contacts. Enclosed cell. Original patent drawing. Source: Personal files.

Fig. 15 — Closed electrolytic cell, self-baking electrode with vertical threaded contacts. Type BL I. Mori, Italy, 1933.

energy consumption was remarkably low in spite of the unfavorable operating conditions (due also to the anode current density, which was far too high for the self-baking electrodes). This experiment finally proved that the vertical contacts with permanent tight casing and with insulated covers opened new perspectives for the aluminum cell.*

* The writer in 1935 started a two-electrode 100 x 140 cm, 24,000 amp cell at Chippis (Switzerland), and in 1940 he installed a single-electrode 120 x 375 cm, 33,000 amp cell at Sabart (France). (Anode current density in each case less than 0.75 amp per cm^2.) The Chippis experiment was finally discontinued in 1938 because the screws had a too pronounced conicity and tended to break the electrode, thus creating uneven distribution of current, short circuits, etc. During the Sabart experiments, the above difficulty was overcome, but a severe corrosion of the screws by the sulphur contained in small proportion in the petroleum coke (raw material for the electrode paste) forced the discontinuance of the experiment. The screws were made of ordinary carbon steel; a proper alloy might have resolved this problem also, but the circumstances under which the test was made (1941, France) were not the most favorable.

While these vertical screw contacts were still undergoing tests, an intermediate solution was tried at Mori in 1939. It consisted, briefly, in lengthening the normal contact studs and inserting them vertically in the unbaked paste. (Fig. 18). Otherwise, the cell looked very much like the test cells with threaded vertical contacts mentioned above.

Table VIII. Consumption Data of Two-electrode Experimental Cells (1935-6)

		Experiment 1	Experiment 2
Number of electrodes		2	2
Size	cm	100 x 90	100 x 120
Anode current density	amp per cm^2	0.70	1.04
Actual amperage		12,400	25,000
Voltage		7.40	5.50
Current efficiency	pct	81	84
Power consumption, kwh per kg Al		27	19.5
Power per cell	kw	92.5	137
of which a) used	kw	21.0	42
b) dissipated	kw	71.5	95
Breakdown of Energy Losses, in kw			
Through bottom		26	26
Upper surface (covers)		6	7
Electrodes		6	7
External contacts		5	12
Operations		6	8
Metal		1	2
Opening of covers		2.5	5
Gas and air aspirated		19	28

The first tests were highly successful, and in 1940, several potlines were installed at Bolzano, Italy (fig. 19 and 20). Unfortunately (as often happens in the industrial application of pilot plant improvements), while the anodic part, i.e., electrode, was a decided improvement over previous types, the cathodic part, i.e., the bottom of the cell itself, was too narrow and not rationally heat-insulated, so that not all the advantages of the new approach to cell construction could be fully exploited. Even so, the cells in themselves and the installation as a whole are very impressive, though quite expensive.

The cell (fig. 19) has a single elongated electrode with rounded ends (it could with but slight impropriety be described as an oval electrode). The bottom follows the same shape. The anodic surface is about 33,000 cm^2; the theoretical amperage is 28,000; the corresponding current density, 0.85, is too high for a modern cell. The operating results have been marred by a high electrode consumption due, in part, to poor paste. The electrical data are, nevertheless, remarkable:

Amperes	26,858
Volts	4.86
Kwh per kg of Al	17.70
Current efficiency	81.5 pct

Source: PB 70023

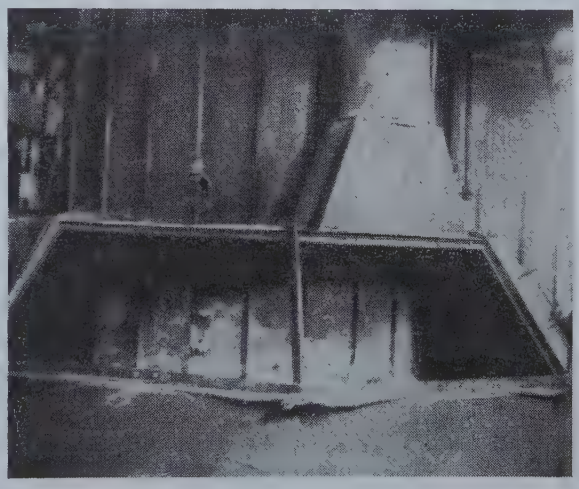

Fig. 16—View of same cell with two covers open. Source: Personal files.

The example of the Bolzano plant was followed by the French (La Praz), who adopted a somewhat simplified and cheaper structure (1942). Other experimental furnaces of this type are now operating in other countries.

The Electrolytic Furnace of Tomorrow

From what has been said of the various types of electrolytic furnaces equipped with prebaked electrodes, and of the developments of the self-baking electrode up to the "Vertical contacts-permanent casing-heat insulated covers" type, it seems logical to conclude that the latter opens up a new field of progress which is likely at last to make the electrolytic cell more of an electric furnace and less of a hand-operated pot.

The writer, though recognizing the danger of extrapolations in this field, ventures the following

forecasts of the impending developments in the design of electrolytic cells for the production of aluminum:*

* Patents are pending covering some of the points mentioned in the following paragraphs. This explains a certain vagueness of expression. As soon as convenient, an addendum will bring the matter up to date.

Capacity: The tendency toward larger cells will continue and, while today a 40,000 amp cell is classified as large, this description will apply in the future to cells of 100,000 amp. The use of vertical contacts with steel casing will allow the reconsideration of the use of two or more electrodes

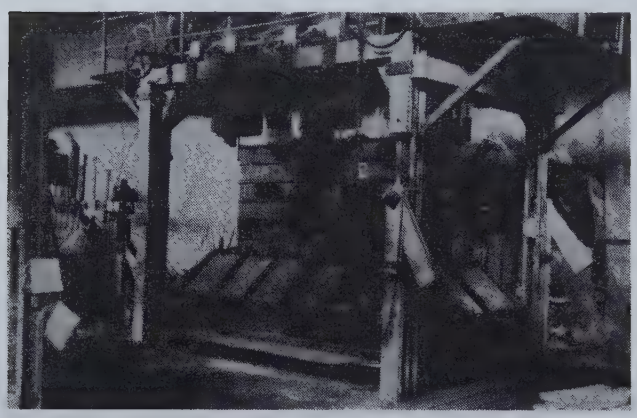

Fig. 17—Closed electrolytic cell with two self-baking electrodes. Type BL II. Mori, Italy, 1935.

separately or jointly regulated. A rectangular 100,000 amp cell with two self-baking electrodes 200 x 350 cm, having an anode current density of only 0.7 amp per cm^2, could be built today. Its electrodes, thoroughly protected from burning by gas-tight casings, would operate under insulated covers. Also, a single 200 x 700 cm electrode for 100,000 amp could be used. The use of 100,000 amp cells cannot become general since only a very few large plants have a sufficiently large power supply.* Moreover, any interruption of the current supply to a 100,000 amp cell (a possibility that must always be reckoned with) causes very serious trouble.

* A 180-cell potline would require some 80,000 kw and would produce 45 tons of aluminum per day, or some 16,000 tons per year.

Shape: The latest technique justifies consideration of the advantages of the round cell, which has been left aside, always regretfully, since the Riouperoux developments promoted the rectangular electrode.

Thus, one can imagine a 40,000 amp cell having one electrode with diam about 270 cm which would match the performance of much larger cells. Its structure would be much simpler than that of a 100,000 amp cell, and the heat losses would be reduced to a minimum since the round electrode and the round cell could be more easily insulated than the corresponding parts of a 100,000 amp cell. A power consumption of 14 kwh per kg could easily be attained even in this medium-size cell and would probably be bettered. Other forms of electrodes will probably be used in particular circumstances. Oval electrodes have already been mentioned, but all sorts of shapes of electrodes will be possible when the improved electrode techniques are used. Some experiments made now in this direction.

Recovery of Fluoride Compounds: The use of airtight covers and other devices would allow a drastic reduction in the amount of air and gases which must be sucked from above each cell. The higher concentration of fluorides in the gases to be scrubbed would enable an effective recovery of the fluorides with small, inexpensive scrubbers. The precipitation of tar particles could be accomplished electrostaticly, and many other improvements would become possible owing to the small amount of gas to be handled.[24] A recent patent (Luzzatto. Norw. Pat. 72332, July 14, 1947) which is the result of the writer's earlier experiments with vertical contacts and enclosed cells, promises to offer not only a more comprehensive solution of the problem of catching and utilizing the fluorides, but also the possibility of other important advantages.

This invention consists of a narrow collecting channel surrounding the electrode casing at its lower end. The electrolytic gases and the tar gases are collected in this annular chamber which is made air-tight by an alumina seal[20]. The gases thus captured are highly concentrated and it is easy to eliminate them or to use them without expensive installations.

Large scale experiments are being made in Norway, France and Italy. The results achieved so far justify the expectation of further important advantages in the following directions: reduction of the power consumption, mechanization of the principal operations, reduction of operating costs.

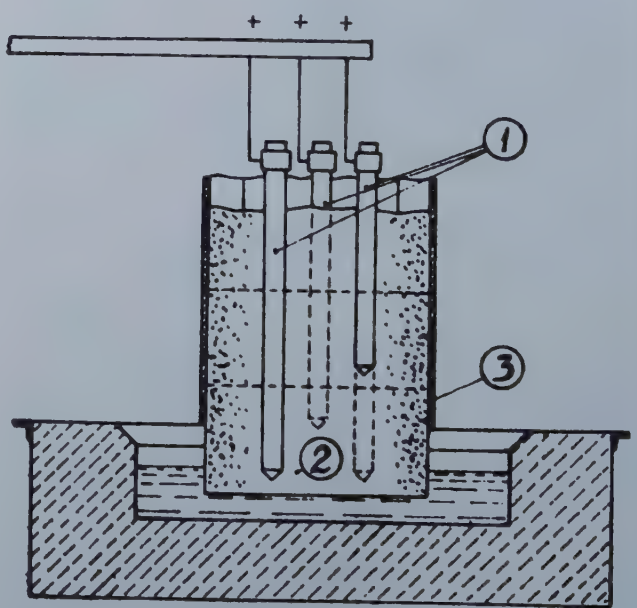

Fig. 18—Sketch of a self-baking electrode with vertical contacts, U. S. Patent 2,224,739. Source: Elektrokemisk, Oslo, Norway, Report to the licensees, Sept. 9, 1941. PB 70028.

Mechanization: Manpower requirements will be reduced to a minimum by the use of mechanical contact extractors, as in the Bolzano installation.

The feeding of the alumina will also be mechanized, as will be the removal of the molten metal.

Consumption: Power consumption will be about 14-15 kwh per kg of alumina, i.e., 2/3 of the consumption of most installations of today's aluminum plants. Consumption of electrode paste depends as much upon the quality of the paste as on the design of the cell, but the elimination of the burning of the electrodes by the air and the improved conditions under which the baking takes place will certainly result in a sizable reduction of electrode consumption to, say, 48-50 lb per 100 lb of aluminum.

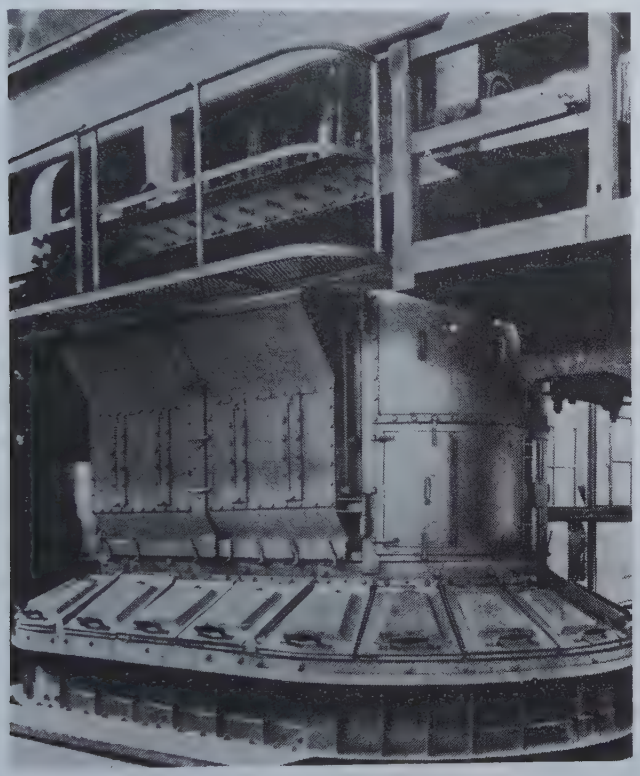

Fig. 19—Electrolytic cell at Bolzano, Italy, 28,000 amp, single electrode, vertical contacts. Source: Elektrokemisk and PB 70028.

The effective recovery of the fluorides from the electrolytic gases will reduce the net consumption of cryolite and other fluorides in the pots to small percentages of the present consumption.

Summary: The electrolytic aluminum cell of tomorrow will be round and equipped with self-baking electrodes with vertical contacts. It will have heat-insulated covers, mechanical devices for feeding alumina, removing the metal, and shifting the contacts. The atmosphere of the pot-room will be clear, as a consequence of the careful and economically profitable aspiration and scrubbing of the electrolytic gases. Man-power requirements will be reduced. The capacity of the furnaces will not need to be larger than 50,000 amps, although in particularly favorable circumstances larger furnaces could possibly be installed.

It is hoped that the aluminum industry will be able to take advantage of these improved techniques when the new expansion of aluminum production gets under way.

References

[1] Engle, Gregory and Mossé; *Aluminum, a Marketing Appraisal.* Richard D. Irwin, Inc., Chicago, 1945.

[2] A number of German documents have been made available by the Office of Technical Services, U. S. Dept. of Commerce, on microfilm or in mimeographed form. Some of them include original material and original drawings from the files of German factories, particularly those of the Vereinigte Aluminum-Werke. These documents have been used to supplement materials collected by the writer during his twenty years of activity and interest in the aluminum industry. Sources are referred to by their PB number, which identifies them in their OTS and Library of Congress files.

[3] PB 70021 includes a thorough report on the physical properties of alumina. "Zur frage der physikalischen Beschaffenheit der Tonerde in Besonders der Verstäubung," Lautawerk, Germany, Dec., 1943.

[4] R. Gadeau's report to the Societé Française des Electriciens, May 22, 1947.

[5] A. Vayna: Tensione di decomposizione dell'allumina e meccanismo della elettrolisi nei forni industriali. *Alluminio* (1949) 147. It analyzes the theories suggested by Cadariu and Ferrand and refers to the experimental work being done at Mori, Italy, on the various factors affecting the electrolysis.

[6] Dr. Moritz: Polarization Erscheinungen nach der Abbildungsmethode über die Polarizationspannung technischer Aluminium Elektrolyseöfen. Lautawerk, Germany, March 8, 1944. PB 70023 and PB 70021, Lautawerk, July, 1942.

[7] Cadariau: Sur la tension electrolytique de decomposition d'alumina. Soc. Française des Electriciens, Nov., 1947. Comments by L. Ferrand.

[8] R. Lorenz: Die Elektrolyse geschmolzener Salze. 1906. R. Lorenz: Die Pyrosole. P. Drossbach: Die

Elektrochemie geschmolzener Salze. 1938. De Kay Thompson: Theoretical and Applied Electrochemistry (1939) 183.

[9] According to Grünert: Beitrage zur Kentniss der Theorie der Technischen Aluminium Elektrolyse. *Ztsch. f. Electrochem.*, Aug., 1942, PB 70026, aluminum fog does not exist, since Al reacts with the molten bath, thus liberating Na.

[10] PB 70023. Lünen, Germany, July 1941. Töging, Germany, June 1942 and Jan. 1943.

[22] Det Norske Aktieselskab. For Elektrokemisk Industri, Oslo, Norway, PB 70028. Report to the Licensees, May 1943. Several photos and patent drawings show the developments at that time.

[23] See also PB 70020. Experiments at Mattigwerk, Aug. 10, 1943.

[24] PB 70023. The rate of suction of air + electrolytic gases + electrode gases was almost 0.6 to 0.8 m^3 per sec. for the 30,000 amp conventional Söderberg cells installed at Töging, but only 0.4 m^3 per sec. for the vertical contact cells of the same capacity installed at Bolzano, Italy. New developments indicate that much lower rates are possible today and with less heat dissipation.

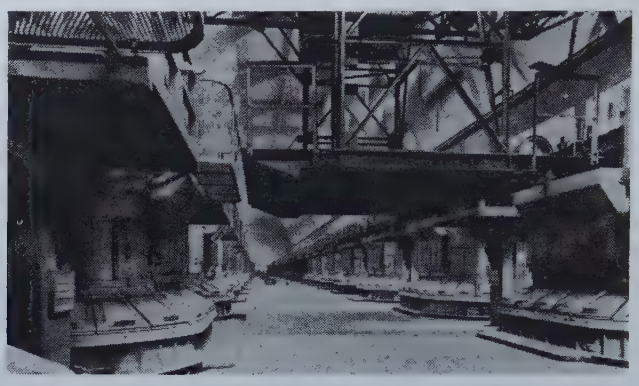

Fig. 20 — Potline of the cells shown above. Source: PB 70028, Frame 5692.

[11] See Gadeau, op. cit., and Grunert, op. cit.

[12] Tandowsky: *Jnl. of Appl. Chem.* (Russian), 1932, found that the CO_2 content is as high as 90 pct or as low as 48 pct. CO is as low as 9.4 pct or as high as 47.3 pct. During the anode effect the CO_2 goes down to 29.8 or even to 10.4 pct, while CO goes up to 64.6 and 86 pct.

[13] Ibid. and PB 70032, "Anodengaserscheinungen," Lautawerk, Jan. 1937. "The quality of the electrodes affects the gas composition, resulting in, with good electrodes, CO_2 74-85 pct; CO 22-12 pct; with low grade electrodes, CO_2 58-69, CO 39-31 pct. During the anode effect, with good electrodes, CO_2 26 pct, CO 35 pct, residual 38 pct; with bad electrodes, CO_2 10.4 pct, CO 71.2 pct, residual 18.2 pct."

[14] Drossbach, *Ztsch. Electrochem.* (1936) 744: efficiency 25 pct. Tafel: *Metal und Erz* (1939) **36**, 516: heat losses 70 pct. Ferrand: Soc. des Ingenieurs Civils de France, *Bulletin*, Jan.-Feb. 1935; efficiency 31 pct.

[15] L. Ferrand: Le controle et la prevision des conditions de fonctionnement des electrolyseurs à aluminium, Soc. Franç. des Ingenieurs, Jan. 1945. The author amplifies considerations presented in a previous article.

[16] Several PB microfilms contain interesting German studies on this subject, e.g., PB 70027.

[17] The German documents are full of reports on this subject, e.g., PB 70027, 70021, etc.

[18] PB 70023. Frames 481-506. Experiments in German plants indicated that a distance of 550 mm between anodes and wall was better than one of 400 mm.

[19] German documents PB 70030.

[20] M. Sem, J. Sejersted, O. Bockman: Twenty five years development of the Söderberg system in aluminum furnaces. *Jnl.* of the Electrochem. Soc. **94**, No. 5, Nov. 1948. The same article explains why the idea which was conceived by the writer in 1939 was patented in Norway only in 1947. It explains also why in some countries the patent application (in France and some others) had been made in 1944 in the name of R. Jouannet of the Cie. Alais, Froges and Camargue.

[21] Jean Billiter: Technische Elektrochemie. Smelzflusselektrolyse (1932).

DISCUSSION

A. C. LOONAM*. In the first place it must be said that the electrolytic process for the production of aluminum is pretty good, as it has dominated the field for about 60 years without any serious competition. An interesting development in this connection is that the first contact rectifier† to be installed in this country is going into operation this week at the plant of the Buffalo Electro-Chemical Co. at Tonawanda, N. Y.

During the war the Germans did a lot of work on the electric smelting of aluminum and developed a lower halide process for refining the crude metal so obtained. Has anybody done any work on this process or heard any details about the reactions that take place? There have been some rather startling reports of its efficacy. In one case, for example, aluminum of 99.85 pct purity was produced from an electric furnace silicon-aluminum alloy containing less than 58 pct aluminum, while in another, a scrap alloy containing about 97.3 pct Al was refined to a purity of 99.98 pct.

J. D. SULLIVAN‡: I cannot discuss the halide process although I know that there has been work done in this country on that and a patent issued to Alcoa. I think that patent was limited to the fluoride.

A. C. LOONAM. There is a recent article by Klemm and his coworkers§ which gives considerable qualitative thermodynamic data on the lower aluminum halides.

J. D. SULLIVAN: The thermal itself is O.K. under certain conditions of temperature.

* Deutsch & Loonam, New York City.

† Otto Jensen: *Trans.* Electrochem. Soc. (1946), 90, 93.

‡ Bettelle Memorial Inst., Columbus, O.

§ W. Klemm, E. Voss, and K. Geiersberger: *Ztsch.* anorg. Chem. (1948) 256, 15.

Textures in

Cold Rolled Copper and 70-30 Alpha Brass

by Walter R. Hibbard, Jr.

IT has been proposed[1] on the basis of slip and flow that the ideal deformation texture of cold rolled face-centered cubic metals is (110) [112]. As pointed out recently by Brick,[2] this theory does not account for the difference between the pole figures for cold rolled copper and 70-30 alpha brass, which develop strikingly different spreads from the ideal orientations. It does suggest that the pole figures might be similar for these two metals if they are rolled sufficiently. This has been found to be the case for cold drawn wire.[3]

WALTER R. HIBBARD, JR., Member AIME, is Assistant Professor of Metallurgy at Yale University, New Haven, Conn.

Technical Note No. 33 E. Manuscript received Oct. 26, 1949.

Experimental Procedure: Four inch sections of cast cakes of copper and 70-30 alpha brass were obtained through the courtesy of the Bridgeport Brass Co. Pieces from these cakes were cold straight rolled 99.993 pct reduction in thickness with the assistance of the Remington Arms Co., Bridgeport, Conn., and by the use of pack rolling. Pole figures were made using the X ray camera and techniques described by Brick.[4] These pole figures were not significantly different from those previously published for the same materials rolled 98 pct.[5] Eight thicknesses of this strip were then pack rolled. This material failed completely and extensively in tension as shown in fig. 1, developing wavy transverse fractures and bulges. No further work could be done on these samples.

Summary: Within the range of this experiment, no attainable amount of cold rolling would cause the pole figures of cold rolled copper and 70-30 brass to become similar, in spite of the fact that such a similarity is predicted by theory.[1]

References

[1] W. R. Hibbard, Jr. and M. K. Yen: *Trans.* AIME (1948) **175**, 126. *Met. Tech.* Feb. 1948. TP 2334.

[2] R. M. Brick: *Trans.* ASM (1949) **41A**, 99.

[3] W. R. Hibbard, Jr.: *Trans.* AIME (1949) **185**, 598. *Jnl. of Metals*, Sept. 1949.

[4] R. M. Brick: *Trans.* AIME (1940) **137**, 193.

[5] R. M. Brick, D. L. Martin and R. P. Angier: *Trans.* ASM (1943) **31**, 675.

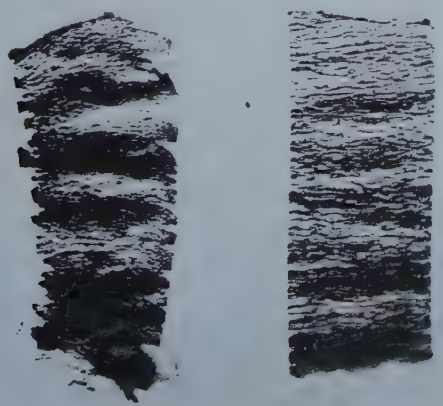

Fig. 1—Copper and 70-30 alpha brass cold rolled more than 99.993 pct reduction in thickness. (Actual size).

Faults in the Structure of

Copper-Silicon Alloys

by Charles S. Barrett

Disorders (faults) in the stacking of atomic planes in Cu-Si alloys were detected and analyzed by X ray diffraction, and the conditions for generating faults were determined. They were found in alloys of 4.0-5.4 pct Si after deformation, when supersaturated.

THE crystal imperfections known as faults in stacking (stacking disorder) are of importance to both fundamental and applied science and are receiving increasing attention. On the theoretical side there have been recent advances in the analysis of diffraction patterns in terms of stacking faults, and on the experimental side it has been found that certain metals develop a faulted structure on cooling through a phase transformation. Beyond this, little is known of what may be called the physical and mechanical metallurgy of faulting, although there has been no lack of discussion and conjecture as to the presence of faults in metals and the effect of faults on mechanical properties and microstructures.

In the close-packed metals the nature of faults can be described very simply. Face-centered cubic (FCC) crystals consist of close-packed layers of atoms, (111) planes, stacked above each other in a definite manner. If one layer is designated as the A layer, the next must be a B or a C layer; that is, every atom of the second layer lies not above the atoms of the A layer, but nestles in the hollows between these, using the hollows designated as the B positions, or the equivalent hollows designated as C. If the sequence of layers is ABCABC . . . ., so that layers three spacings apart are directly over each other, the crystal is FCC; if CBACBA . . . it is an FCC crystal that is a twin of the former; if ABAB . . . . . or BCBC . . it is hexagonal close-packed (HCP). A fault is a break in the sequence, such as ABCABABC . . . which has the effect of inserting an HCP lamella into an FCC crystal. Regularly spaced faults spaced two layers apart would convert an FCC crystal entirely to HCP, or an HCP to FCC. A fault in an FCC crystal is also equivalent to creating an FCC twin of minimum thickness; in fact, the entire crystal would be converted to its twin if faults were introduced regularly. (In HCP crystals, however, twinning does not occur on the basal plane and a fault on this plane is not identical with a thin twin).

Faults are one of the possible causes for annealing twins,[1] for the strain markings that are brought out by etching deformed metal,[2,3] for the altered X ray reflecting power of metal at slip bands that is revealed in X ray reflection micrographs,[4] for the extinction of Kikuchi lines in electron diffraction patterns,[5] and for the hardening of latent slip planes.[5] Since other explanations of these effects are also available,[6] there has been no direct proof of faults from deformation; yet it has appeared likely that they would occur.[7] Faults resulting from phase transformations in metals, however, have been clearly revealed by diffraction in cobalt[8, 9] and lithium.[10, 11]

It is to be expected that the faulting tendency is greatest

CHARLES S. BARRETT, Member AIME, is Professor, Institute for the Study of Metals, Univ. of Chicago.

AIME New York Meeting, Feb. 1950.

TP 2754 E. Discussion (2 copies) may be sent to Transactions *AIME before Apr. 1, 1950, and is scheduled for publication Nov. 1950. Manuscript received Sept. 30, 1949.*

This research has been supported in part by the Office of Naval Research, U. S. N., Contract No. N-6 ori-20-IV, NR 019 302.

under conditions such that the interface energy caused by a fault is least. The copper-silicon alloys provide a variety of conditions with which this point of view can be tested, and offer unique advantages for the study of faulting and its effects.

The alpha phase (FCC) in the copper-rich alloys can be made to precipitate kappa (HCP) or vice versa, as will be evident from the phase diagram, fig. 1, and the closely similar atomic radii in alpha and kappa permit these phases to fit together on interfaces that have almost no interface energy or strain energy, as Cyril Smith[12] has pointed out. Furthermore, each of these structures can be transformed to the other by glide on the close-packed planes that are the slip planes. Below the eutectoid temperature (552°C) there is an opportunity to decompose the hexagonal phase into alpha plus another cubic structure, of the beta-manganese type, the gamma phase. It is also possible to precipitate gamma from alpha.

The Lattice Dimensions of the Phases: The random substitutional FCC solid solution of Si in Cu extends to 4.65 pct Si (9.95 at. pct) at the eutectoid, 552°C, and to a maximum of 5.3 pct (12.45 at. pct) at 842°C, according to Smith.[12] The two phase region, alpha plus kappa, extends from the alpha phase limit to 5.2 pct (11.05 at. pct) and to 5.9 pct (12.45 at. pct) at 552°C and 842°C, respectively. The alpha plus gamma region extends to 8.35 pct (17.15 at. pct) at 552°C, according to Smith.[12] Andersen's diagram[13] is in satisfactory agreement with Smith's.

According to precision X ray determinations by Andersen,[13] Si expands the lattice of Cu according to the linear relation $a_0 = 3.6077 \pm 0.00065C$ kx-units, where C is atomic per cent silicon; at the solubility limit for 560°C, $a_0 = 3.61395$; and at 750°C, 3.61462 ± 0.0002 kx; the HCP kappa phase in equilibrium with alpha at these two temperatures, respectively, has $a = 2.5539$, $c = 4.1765$, $c/a = 1.6353$ and $a = 2.5566$, $c = 4.1737$, $c/a = 1.6325$, in kx units, all values being measurements made at room temperatures.

The distances between the atoms of the hexagonal array on the (111) alpha plane and the (00·1) kappa plane for alloys in the two-phase region are very nearly identical. According to Andersen's measurements, which were made on alloys quenched to room temperature after long anneals, they differ by only 0.05 to 0.08 pct, and the spacings of these planes differ by only 0.025 to 0.08 pct. These differences are too small to be recorded as splitting of lines in powder patterns of two-phase alloys and are only obtained by computations from measurements of several lines. It appears likely that the interatomic distances are actually identical at the elevated temperatures, as Smith has suggested;[14] at any rate, there is much reason to expect this in most laboratory experiments where one phase is precipitated from the other in the absence of recrystallization of the parent phase, and where coherency between the lattices is, therefore, almost certain to occur.

During the present work it was confirmed that the structures of the two phases are of the types mentioned, that the atomic radii are identical or substantially so, and that the axial ratio of kappa is 1.633 within the accuracy of the patterns, which are somewhat less precise than Andersen's.

When the (111) and (00·1) planes of alpha and kappa form the interface between the two phases, with close-packed rows of atoms parallel in the two and with equal or nearly equal atom spacings in the two, the interface must be of exceedingly low energy, which accounts for the observation that the banded kappa plus alpha structures resist spheroidization almost indefinitely during annealing.[12] This orientation, predicted earlier,[12] was confirmed in the present investigation.

The gamma phase, according to Arrhenius and Westgren[15] and to Sautner,[16] has the beta manganese structure, cubic, with 20 atoms per cell, and with $a_0 = 6.210$ kx. There are marked similarities in the atom pattern of (111) gamma and (111) alpha,

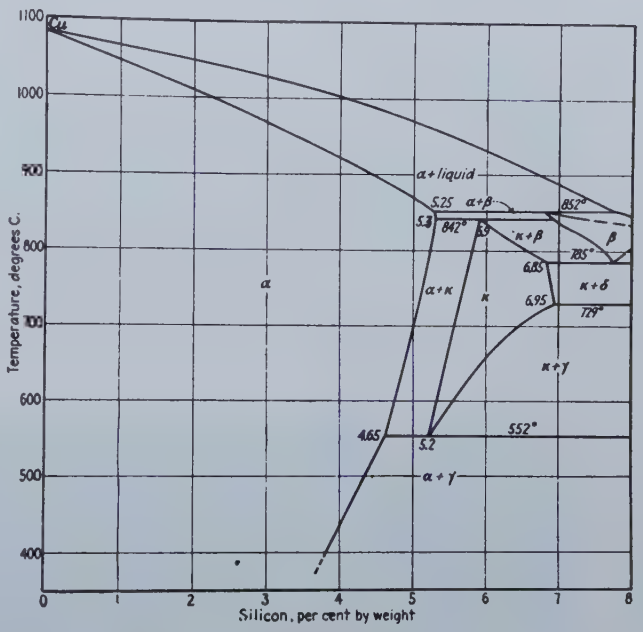

Fig. 1—Equilibrium diagram for Cu-Si alloys, according to Smith[12].

some atoms of the alpha matching the gamma within 0.08 pct.

Materials and Methods: The specimens were taken from the hot rolled homogenized alloys used in Smith's investigation,[12] supplemented by a melt that analyzed 5.50 ± 0.04 pct silicon, which was hot rolled and annealed 40 hr at 800°C for homogenization. Heat treatments were carried out in air, with small samples, usually wrapped in copper foil. The samples were introduced into a furnace that was controlled at the annealing temperature; some were subsequently cooled in air by gradually withdrawing them from the furnace, reaching 100°C in 3 to 5 min; others (unprotected by copper foil) were quenched in water. The specimens were deeply etched to remove surface layers that may have been depleted in silicon.

Oscillating crystal pictures of these specimens have spotty Debye rings that prove to be convenient for studying the structures. A series of pictures was made on a small Debye camera using circular 1 mm

diam pin holes and nickel-filtered copper K radiation. The samples were oscillated 3° to 6° or occasionally more, the range being chosen to give a convenient number of spots. The samples averaged 2x3x10 mm in size and were placed in the camera with one surface at an angle of about 10° to the beam.

The Streaks on Diffraction Patterns: It is found that the X ray diffraction patterns very frequently contain details that cannot be accounted for by normal FCC and HCP phases. In addition to sharp spots from one or both of these phases, and Laue streaks from the general radiation component of the incident radiation (Laue spots elongated into streaks by the specimen oscillation), there are streaks at angles very divergent from the Laue streaks. The Laue streaks, which are radial near the equator of the films and are always at predictable angles, are ignored in the analysis to follow and reference is made only to the other streaks, which are made by the monochromatic filtered (characteristic) radiation.

Typical films are reproduced in fig. 2 for a quenched alpha phase alloy, (4.91 pct Si) deeply etched, and in fig. 3 for an alpha alloy (4.16 pct Si) that had been slowly cooled (fig. 3*a*) and one that had been lightly hammered under liquid nitrogen and deeply etched (fig. 3*b*). The prominent streaks lie in definite preferred directions, from which can be deduced the directions of the corresponding rods in the reciprocal lattice.

When the angle of oscillation of the specimen in the X ray camera is restricted to a few degrees, or

It is found that the streaks from both alpha and alpha plus kappa Cu-Si alloys are oriented as in fig. 4, with the rods parallel to the hexagonal c axis or [111] cubic directions. The FCC alpha crystals can also be indexed in the rhombohedral system with hexagonal axes, with the [111] direction becoming the c axis (see the indices followed by letter R, fig. 4).

The orientation of the streaks is such as would be caused by an imperfection in the manner of stacking the close-packed (111) planes of the cubic phase (or the close-packed basal planes of the hexagonal phase) for the effect of disorders in stacking is to elongate reciprocal lattice points in the direction normal to the planes that are faultily stacked. This effect has been studied in metallic crystals after transformation, for example in cobalt[8, 9] and lithium[10, 11] and is observed in many nonmetallic substances.

Before concluding that the streaks are caused by stacking disorders, however, it is necessary to prove that they are not due to thin plates of a phase, or merely thin isolated layers having a composition different from the surrounding material, for these could serve as two dimensional gratings and produce streaks much like the observed ones.

Cause of the Streaks: Experimental proof that the streaks result from stacking disorders, rather than thin plates or silicon-enriched planes, rests on the appearance of spots on the FCC (220) ring on films made with a small angle of oscillation of the specimen. The spots on this ring from the FCC phase have rhombohedral-hexagonal indices 11·0 and 10·4.

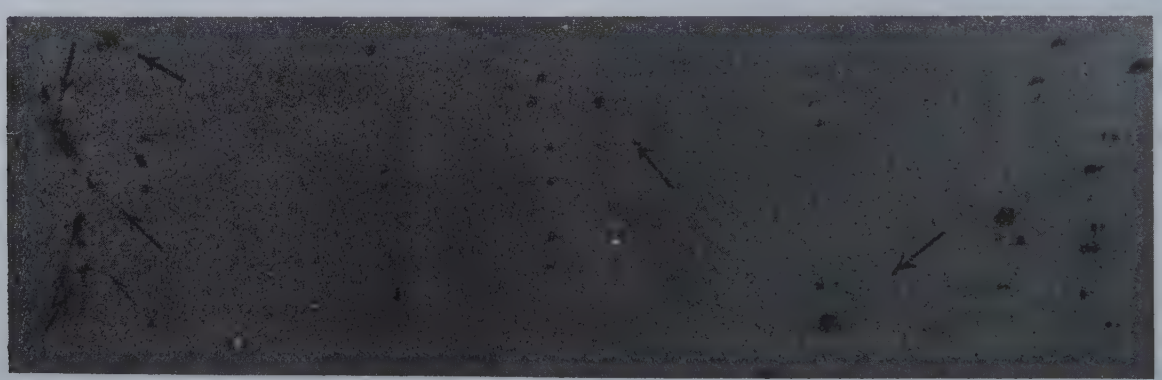

Fig. 2—X ray diffraction pattern of alpha phase alloy (Cu+4.91 pct Si) quenched after recrystallization at 820°C.

Non-Laue streaks indicated. All patterns made with small oscillation (usually 3° to 6°) of polycrystalline specimen in Ni-filtered Cu radiation.

when the specimen is stationary, there are *long* streaks only if reciprocal lattice rods are tangent to the reflection sphere. If streaks are tangent to a certain Debye ring it follows from geometrical considerations that planes reflecting to make spots on that ring are planes of a zone having an axis in the direction of the rods. This is true whether the Debye ring is real or merely corresponds to planes having zero reflecting power.*

It has been shown theoretically and experimentally[9, 17, 18] that 11·0 spots are not widened into streaks when stacking disorders are present since they belong to the class $h\text{-}k=3n$ where n is any integer, including zero. This is because faulting leaves these planes undisturbed. But the 11·0 spots would be widened by thin plate effects if these existed, and the direction of widening would be tangential to this Debye ring, since the rods in reciprocal space

* The relation may be visualized by referring to fig. 4, which is a sketch of a rod parallel to the c axis in reciprocal space with points indexed with hexagonal indices (marked R in fig. 4), the rod orientation having been deduced from patterns like fig. 2 and 3. Consider a particular grain that is oriented as in this drawing, and let the incident beam be perpendicular to the rod. Since the reflection sphere has the incident beam as a diameter and one end of the diameter is at 000 in the reciprocal lattice, it is seen that the beam may be oriented with respect to the grain so that the rod is tangent to the sphere at the point X, which would have indices 10.0 and would belong to the zone [00.1], and the long streak will be at the angle $\phi_1 = 90°$ to the (invisible) 10.0 Debye ring. The angle ϕ_1, and the other angles ϕ_2, ϕ_3....for long streaks at other Debye rings will be found in the equatorial region of cylindrical oscillating crystal films as the angle between the ring radii and the streaks.

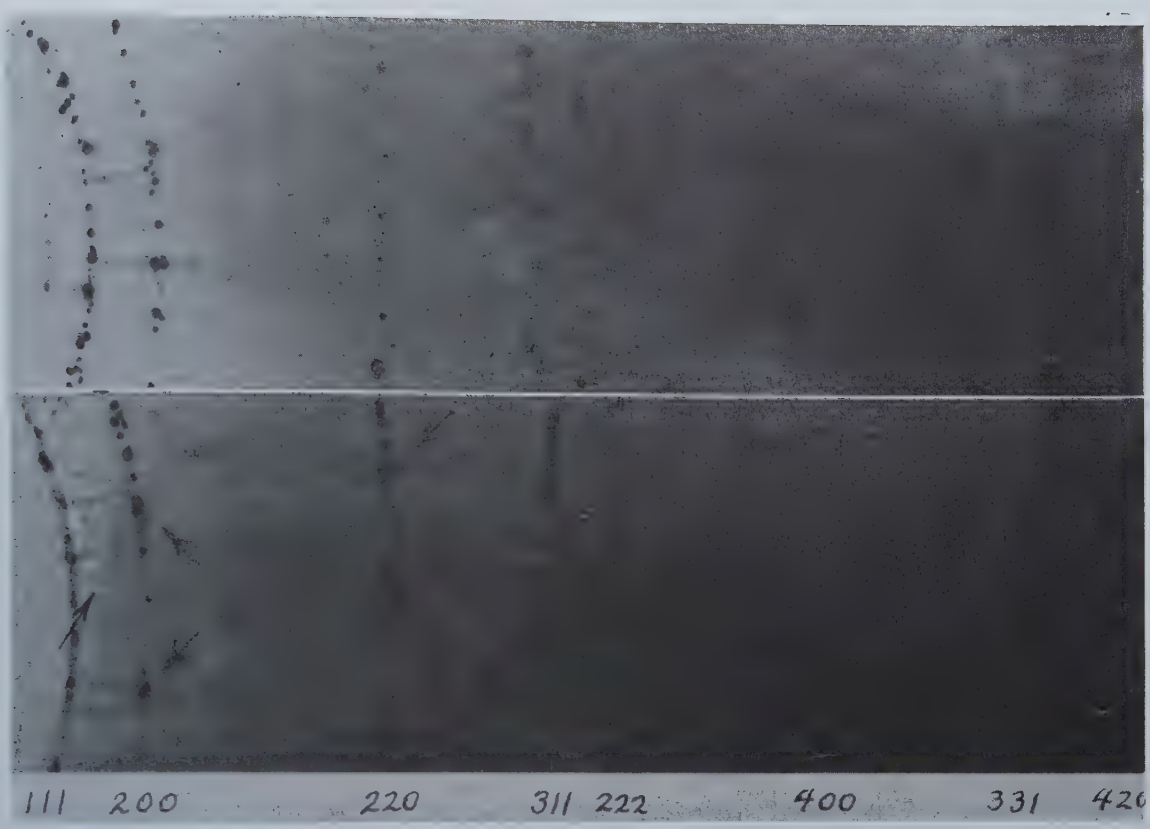

Fig. 3—Pattern of alpha (Cu+4.17 pct Si) recrystallized at 820°C.
(*a*) slowly cooled, (*b*) hammered slightly at liquid nitrogen temperature. Shows non-Laue streaks from the hammering.

would necessarily be parallel to the [00·1] direction of the rhombohedral-hexagonal cell, like the rod in fig. 4. On the other hand, the 10·4 spots would lie on streaks having a preferred direction at an angle to the ring. Now on all films showing streaks there are always spots on this ring that are unwidened and unassociated with streaks, and there are no tangential streaks through any spots on the ring. It therefore follows that stacking faults, not isolated thin plates or enriched planes of atoms, are responsible for the streaks. The possibility is not excluded, of course, that faulted regions may tend to develop a concentration different from that in the unfaulted surroundings, becoming a more conventional precipitate. The streaks could not be due to thermal vibrations of the atoms during the X ray exposure because the streaks are absent after certain heat treatments (see fig. 3*a*).

Intensity Distribution Along the Streaks in Alpha Alloys: In the patterns of alloys containing only the alpha phase, the streaks have more or less pronounced broad maxima at the diffraction angles of the alpha phase, as in fig. 2 and 3. This would be expected if the cause of the streaks is an imperfection of stacking in the FCC phase.

Zachariasen has derived relations for the intensity distribution along a streak in terms of the relative displacements of identical, parallel, and equidistant atom layers with respect to each other.[17] These may be applied to stacking disorders in the FCC structure by choosing x and y axes, at 120° to each other, parallel to the close-packed rows of the (00·1) plane of the rhombohedral-hexagonal structure — the (111) plane referred to cubic axes—and the z axis normal to this plane. The degree of stacking disorder is expressed in terms of the probability p_1 that a layer will be in the close-packed position such that an atom is at the coordinate position x, y equal to 1/3, —1/3 with respect to an atom in the adjacent layer at the position 0,0. There are two close-packed positions, and since every layer is assumed to be in one or the other of these, it follows that if p_2 is the probability of being in the other, i.e., at x, y equal to —1/3,1/3, then $p_1 + p_2 = 1$. In a perfect FCC single crystal, $p_1 = 1.0$; the condition $p_1 = 0$ represents a twin of the crystal for which $p_1 = 1.0$; when the layers are stacked at random $p_1 = 0.5$. The analysis assumes that faults are distributed statistically at random so that the stacking in any pack of layers chosen at an arbitrary position in the structure is representative of the whole crystal, or

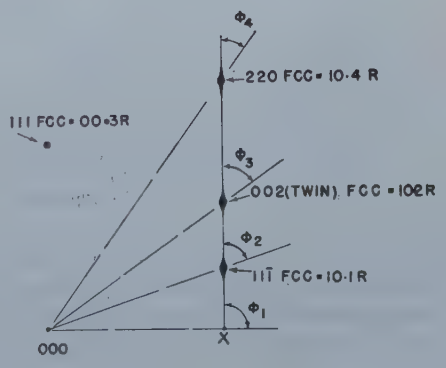

Fig. 4 — Portion of reciprocal lattice for patterns such as fig. 2 and 3.

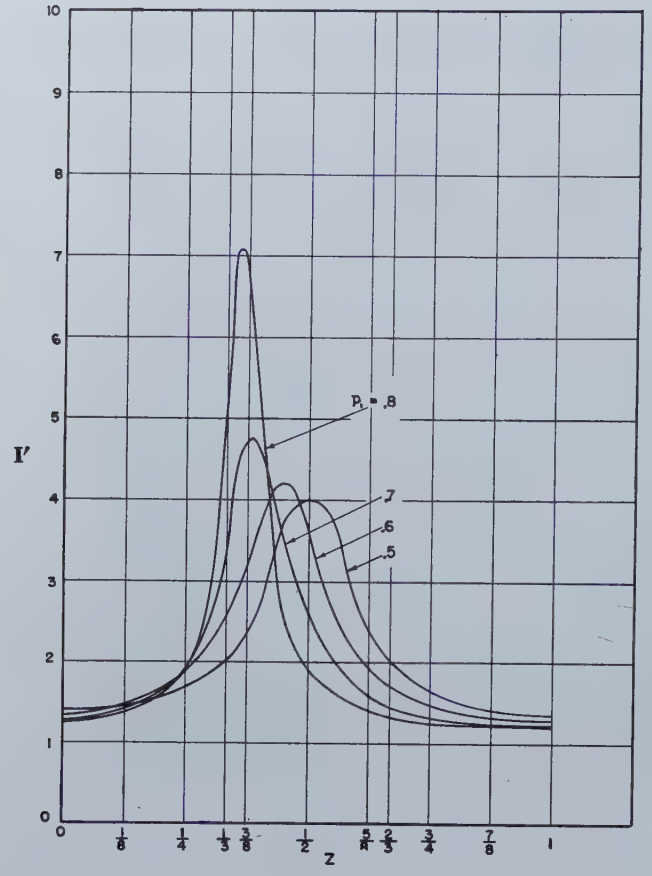

Fig. 5—(left) Distribution of intensity factor I' along row of reciprocal lattice for stacking disorders p_1 in a FCC crystal for h - k = 3n + 1 (hexagonal axes).

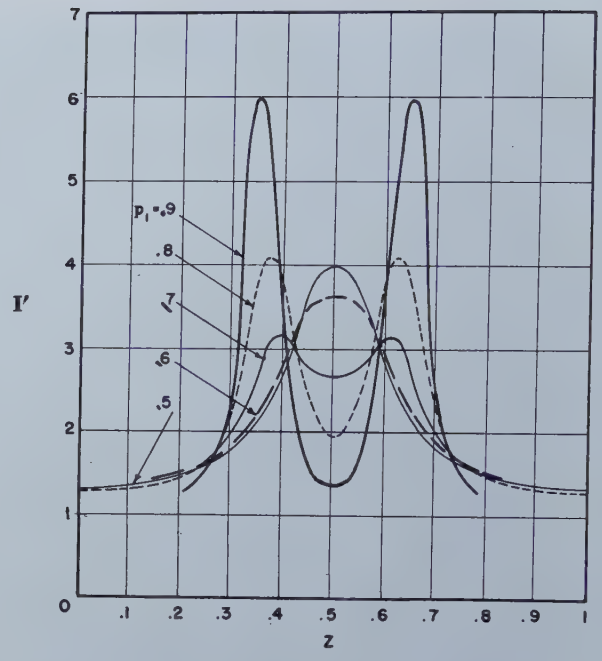

Fig. 6—(above) Intensity factor I' when h-k = 3n + 1 is averaged with h - k = 3n - 1, as in twinned FCC grains.

of that portion of it to which the analysis is applied.

These probabilities determine the probabilities of relative displacements of layers M spacings apart. If the probabilities that the Mth layer will have positions 0,0 or 1/3,—1/3 or —1/3,1/3 with respect to the atom at the origin are $P_{M\circ}$, P_{M+} and P_{M-} respectively, then all close-packed arrangements require $P_{M\circ}+P_{M+}+P_{M-}=1$. Simple computation shows that these values are related to p_1 and p_2 as stated in table I. (Small terms are omitted in the last two rows). These probabilities in turn determine Fourier coefficients $W_{hk}{}^M$ from which may be computed the contribution of the pairs of layers M spacings apart to the intensity of X ray scattering.

Table I. Probabilities for Positions of Planes M Layers Apart in Terms of p_1 and p_2

M	$P_{M\circ}$	P_{M+}	P_{M-}
0	1	0	0
1	0	p_1	p_2
2	$2p_1p_2$	$p_2{}^2$	$p_1{}^2$
3	$p_1{}^3+p_2{}^3$	$3p_1{}^2p_2$	$3p_1p_2{}^2$
4	$6p_1{}^2p_2{}^2$	$p_1{}^4+4p_1p_2{}^3$	$p_2{}^4+4p_1{}^3p_2$
5	$5p_1p_2{}^4+5p_1{}^4p_2$	$10p_1{}^3p_2{}^2+p_2{}^5$	$10p_1{}^2p_2{}^3+p_1{}^5$
6	$p_2{}^6+20p_1{}^3p_2{}^3+p_1{}^6$	$15p_1{}^2p_2{}^4+6p_1{}^5p_2$	$15p_1{}^4p_2{}^2+6p_1p_2{}^5$
7	$21p_1{}^2p_2{}^5+21p_1{}^5p_2{}^2$	$7p_1p_2{}^6+35p_1{}^4p_2{}^3+p_1{}^7$	$p_1{}^7+35p_1{}^3p_2{}^4+7p_1{}^6p_2$
8	$8p_1{}^7p_2+70p_1{}^4p_2{}^4+8p_1p_2{}^7$	$p_2{}^8+56p_1{}^3p_2{}^5+28p_1{}^6p_2{}^2$	$p_1{}^8+56p_1{}^5p_2{}^3+28p_1{}^2p_2{}^6$
9	$p_1{}^9+84p_1{}^6p_2{}^3+\ldots$	$9p_1{}^8p_2+\ldots\ldots$	$36p_1{}^7p_2{}^2+\ldots\ldots$
10	$45p_1{}^8p_2{}^2+\ldots\ldots$	$p_1{}^{10}+120p_1{}^7p_2{}^3\ldots$	$10p_1{}^9p_2+\ldots\ldots$

In the FCC case the Fourier coefficients have the value

$$W_{hk}{}^M = P_{M\circ} + P_{M+}\, e^{i2\pi(h-k)/3} + P_{M-}\, e^{i2\pi(h-k)/3}$$

and these predict the intensity I_{hkz} along the rows of points in reciprocal space through the relation

$$I_{hkz} = K\, \Psi_{hk}{}^2\, \Sigma_M W^M{}_{hk}\; e^{i2\pi Mz}$$

where K is a constant, Ψ_{hk} is the structure factor for the layer, h and k are the Miller indices of the row, and the coordinate z may have any integral or nonintegral value. From this equation it follows that there are no rods along the reciprocal lattice rows of points for which $h - k = 3n$, where n is any integer, but when $h - k = 3n \pm 1$ there are rods parallel to z in the reciprocal lattice with intensities along the rods given by

$$I_{hkz} = K\, \Psi_{hk}{}^2\, \Sigma_M\, (3P_{M\circ}-1)\cos 2\pi Mz \pm \sqrt{3}\, \Sigma_M\, (P_{M+}-P_{M-})\sin 2\pi Mz = K\, \Psi_{hk}{}^2 I'.$$

Fig. 5 is a plot of the function I' with different values of the probability p_1 for $h - k = 3n + 1$, and with z extending throughout one unit cell of the reciprocal lattice, e.g., from 10·0 to 10·2 in an HCP cell or from 10·0 to 10·3 in a three-layer cell ("R"). As p_1 approaches 1.0 from the value for random stacking, the peak at $z = \frac{1}{2}$ moves toward $z = 1/3$ and increases in sharpness and intensity; on an X ray pattern this corresponds to an intensity maximum along a streak moving from a position at a Debye

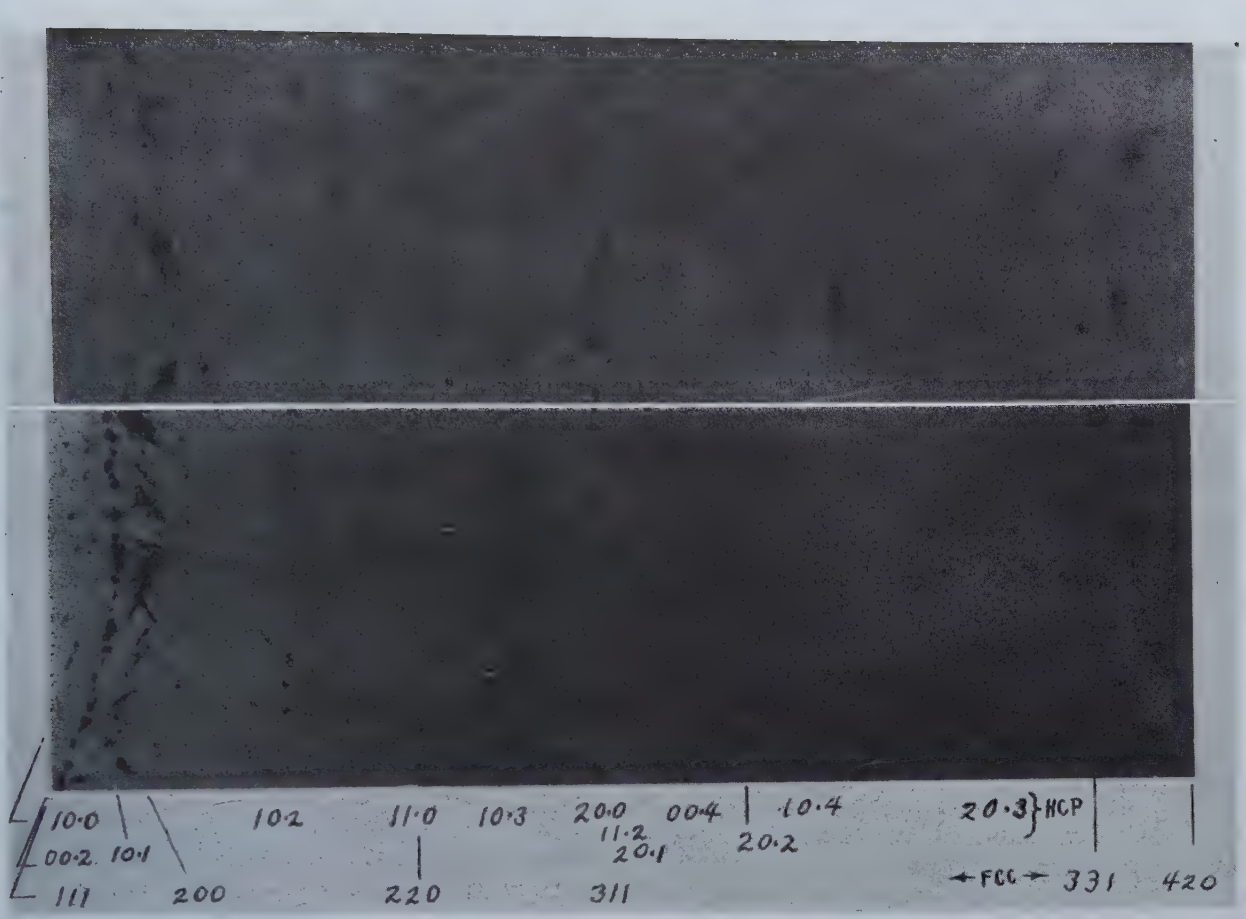

Fig. 7—(above) Pattern of alpha + kappa (Cu-5.12 pct Si) quenched and abraded after recrystallization at 820°C.
Long non-Laue streaks with non-FCC maxima.

Fig. 8—Pattern of Cu+5.39 pct Si alloy.
Recrystallized as kappa at 600°C, heated 1 hour at 750°C (alpha + kappa), quenched and abraded. Streaks and gamma maxima.

ring for HCP packing to a position at a ring for FCC packing. The curves for $h - k = 3n - 1$ are identical with those plotted in fig. 5 if the z coordinates are reversed, running from 1 on the left to 0 on the right.

If in each grain there are twins so that there are about as many regions with p_2 having a certain value as there are with p_1 having that value, the scattering from the grain as a whole is the average of $h - k = 3n - 1$ and $h - k = 3n + 1$, giving the curves of fig. 6. As the grain becomes more perfect the intensity maximum splits into two peaks which sharpen as they approach $z = 1/3$ and $2/3$, which are FCC reflections having hexagonal indices 01·1, 10·2, 20·1, 02·2, 01·4, 20·4, 10·5, 02·5, etc. in the rhombohedral cell, three layers high, that is identical with the FCC cell.

In the patterns of alpha-phase alloys the streaks appear about as expected from this theory with p_1 having a value in the neighborhood of 0·8 to 0·9 in some portions of the grains, thus indicating one or two faults per 10 atom layers in the faulted regions, but with other regions apparently remaining perfect FCC and superimposing strong sharp spots on the streaks.

The X ray technique used in this study permits qualitative and semiquantitative studies of faulting to be made conveniently, but not precision quantitative measurements such as are needed for Zachariasen's Fourier analysis of disorder,[17] or for comparison with Wilson's computations.[18]

The Streaks in Alloys Containing Kappa and Alpha: Many streaks in the diffraction patterns of alloys that contain both alpha and kappa phases are different from those discussed in the previous section. (These alloys are subject to a very sluggish eutectoid decomposition below 552°C). The streaks, instead of being short spikes extending out in one or more directions from alpha spots, are very long, as, for example, in fig. 7, and are either nearly uniform in intensity throughout their length or have diffuse maxima on them at diffraction angles corresponding to neither the FCC nor the HCP phase. They pass through one or more of the spots 10·1, 10·2, 10·3, 10·4, and 20·3 of the HCP phase, but have a diffuse minimum of intensity at these spots rather than a maximum; they also pass through FCC spots but show neither a pronounced maximum nor a minimum near these spots. The streaks extend in the same directions as the shorter streaks discussed earlier, suggesting stacking errors on (111) FCC planes as the cause. Fig. 7 was prepared from a quenched sample containing 5.12 pct Si that was polished mechanically and etched. Still more pronounced maxima on the streaks were obtained when

a quenched 5.39 pct Si alloy was polished and etched (fig. 8).

The distribution of intensity in reciprocal space is indicated roughly in fig. 9. It appears impossible to account for the position of the pronounced maxima on the streaks with any curve of the family plotted in fig. 6. The maxima more closely agree with the reflection positions for the gamma phase than either the alpha or kappa phases, but the exceptionally strong lines that are listed for gamma[16] lie ½° to 2° from the intensity maxima on the streaks. It is very likely that the phase causing these maxima is a transition structure rather than the equilibrium gamma; it will be referred to as gamma′.

The position and diffraction angles of the gamma′ maxima show that this phase is related in orientation and structure to both kappa and gamma. The directions of the streaks and their alignment with the alpha and kappa spots imply that the gamma′ phase has important atom layers parallel to (00·1) of kappa and (111) of alpha, and that they are coherent with these planes, matching them in atomic array or in a multiple of the array. Presumably these layers are arranged with frequent stacking errors which cause the streaks. It is evident that the gamma′ is accurately oriented with respect to the kappa, for the streaks from the gamma′ are invariably aligned with spots on the kappa Debye rings; the streaks also pass through alpha spots. In fig. 8 each 10·1 kappa spot ($\theta = 23.3°$) lies on a streak containing maxima at 22.5° and 24.1°. Equilibrium gamma has the three strongest reflections at 21.8°, 23.0° and 24.3° with ($h^2 + k^2 + l^2$) values equal to 9, 10 and 11 respectively.[16] There are similar pairs of maxima connected with kappa 10·3, 20·3 and 12·1 spots.*

* The pattern resembles somewhat the spots with ghosts (wings) that were obtained by Daniel and Lipson[19] in the alloy Cu₂FeNi₃ as a result of periodic variation of the lattice spacing, the period increasing with the length of annealing in the range where the FCC matrix decomposes into two FCC phases of different lattice dimensions. The diffuse maxima in the present alloys, however, are spaced at different distances from the matrix spots of the different HCP Debye rings, being particularly widely spaced and diffuse around 10.2; therefore, they cannot be accounted for by assuming either periodic variations in spacing or in composition; furthermore, the intensities of the diffuse maxima do not vary with order as expected by periodic disturbance theories.

Much more complete data would be necessary for a rigorous analysis of the structure of gamma′, but the present experiments lead to the conclusion that (1) it is a metastable phase that does not form with spontaneous eutectoid decomposition during long annealing; (2) it is produced by straining alpha plus kappa alloys, as is discussed later, presumably by the gliding of close-packed layers parallel to themselves; (3) it exists in coherence with alpha and kappa, with atomic matching at the interface and with exact orientation with respect to these phases; (4) it produces diffraction effects of the general type to be expected of a phase with frequent stacking errors, and (5) when initially formed by plastic straining its composition must be essentially that of the matrix from which it forms, not of equilibrium gamma, since there has been opportunity for negligible diffusion.

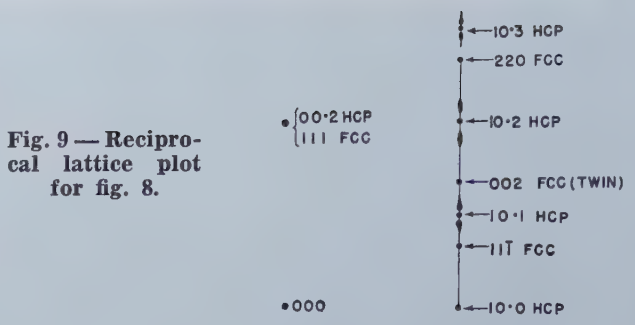

Fig. 9 — Reciprocal lattice plot for fig. 8.

Production of Faults: A large number of experiments were conducted to determine the factors that control the production of faults in the Cu-Si alloys, using the presence of streaks on the oscillating sample patterns as the criterion for the presence of faults.

Quenching. Quenching in water from 820°C produces abundant faults in 5.39, 5.12, and 4.91 pct Si alloys, very few in the 4.17 pct Si alloy, and none in the 2.94 and 0.96 pct Si alloys. The faults are detected by X raying the samples not only after light etching, but also after etching until the quenched samples are reduced 40 to 50 pct in thickness. Fig. 2 illustrates the streaks that are typical of the quenched alloys. The FCC spots frequently have more than one streak radiating from them, indicating that a single alpha grain has faults on more than one set of the {111} planes. This would be expected from the microstructure of faulted alpha or of alpha plus kappa alloys, which show markings or bands on various {111} planes in nearly every alpha grain.

Several experiments on samples consisting purely of kappa (5.5 pct silicon) failed to produce faults. Strain markings in the microstructure are also absent or very rare in these. All alpha alloys that show streaks on the X ray films were supersaturated with silicon when quenched to room temperature (see fig. 1).

In control experiments with cold rolled samples annealed at 820°C and cooled in air, no streaks are found with alloys of 0.96, 2.94, 3.77, 4.17, 4.59 and 4.91 pct Si. Only occasional streaks are found in 5.39 pct Si alloys; these may be residual from earlier conditions in the samples. Cooling faultfree samples of 4.17 pct silicon to —195°C without straining them produces no streaks; this indicates that the production of faults cannot be ascribed to a spontaneous precipitation or a martensitic transformation.

Since quenching is known to cause plastic flow in polycrystalline samples it was suspected that the role of quenching was merely that of introducing plastic deformation in the samples while in the supersaturated condition, so a number of tests were made on the effect of deformation on slowly cooled

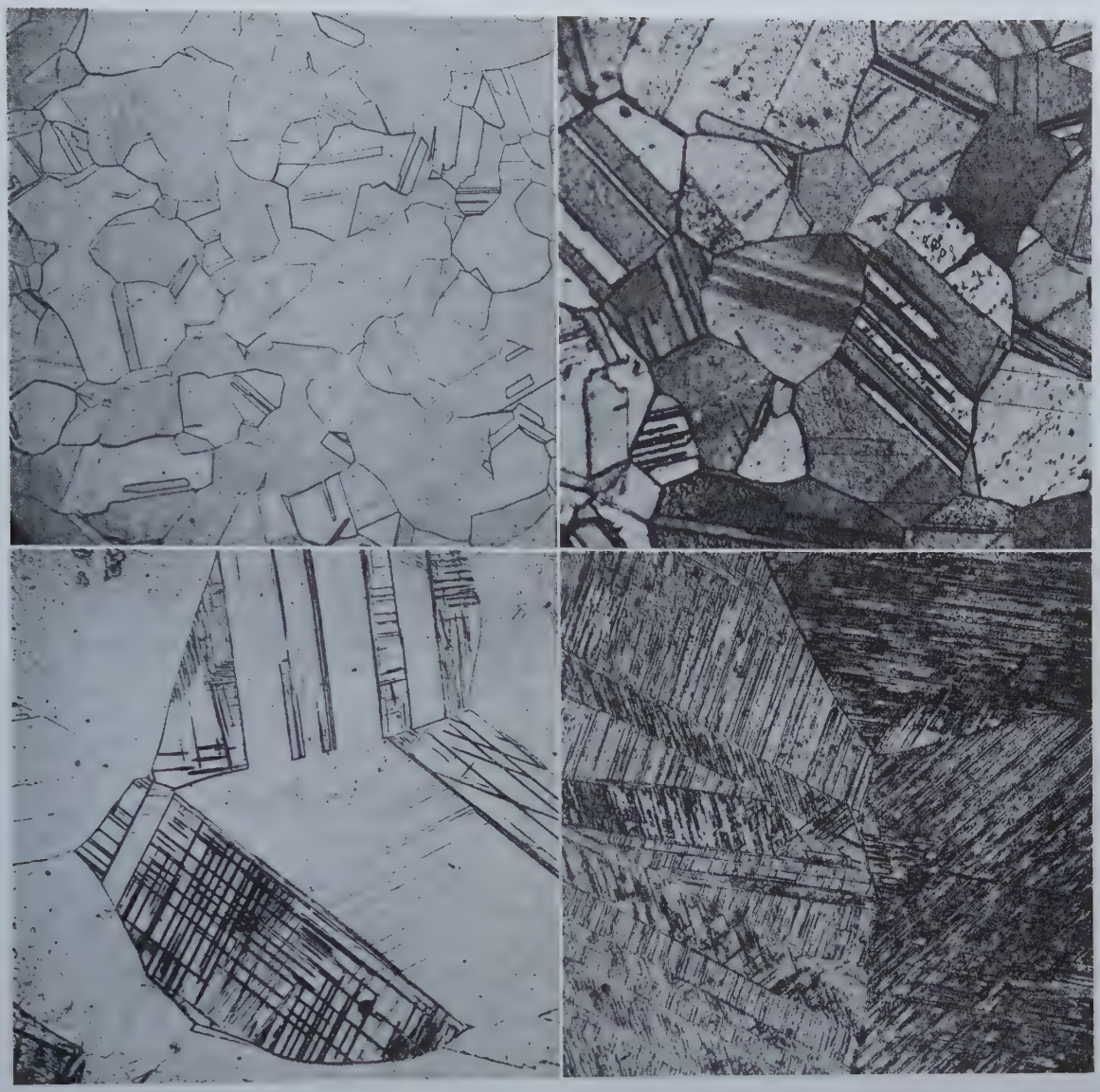

Fig. 10—Strain markings in Cu-Si alpha alloys quenched from 820°C after recrystallization.

Electropolished after mechanical polishing, etched with hydrogen peroxide—potassium hydroxide—ammonium hydroxide reagent.[12] (*a*) 0.96 pct Si x 150; (*b*) 4.17 pct Si x 200; (*c*) 4.91 pct Si x 200; (*d*) 5.12 pct Si x 250. Reduced one fourth in reproduction.

samples. The results reported in the following section confirm this view of the role of quenching.*

* Another possible theory was also considered but disproved; namely, that faults are spontaneously induced by thermal agitation, the number increasing as the annealing temperature is raised, many being retained when the specimens are quenched but most being lost by diffusing out during slow cooling. The following experiments disprove this theory. Samples containing 4.91 pct Si were first cold rolled, then recrystallized by annealing at 820°C for 15 min. A sample quenched in water after this annealing was found to contain many faults, and a sample cooled in still air was free of faults. Yet when a quenched sample, containing faults, was reheated to 850°C, annealed for 5 min., and cooled at approximately half the rate used for the air cooled sample, it was found to contain faults in quantities closely resembling the quenched sample, proving that faults are not lost during cooling. A similar experiment on a 5.39 pct Si sample gave the same result.

Plastic Deformation. A clear proof that faults are introduced by plastic flow was obtained in an experiment illustrated by fig. 3. A sample containing 4.17 pct silicon that was recrystallized and slowly cooled was found to be fault-free, showing no streaks other than the Laue streaks from general radiation (fig. 3*a*). This sample was lightly hammered while immersed in liquid nitrogen, and though the plastic deformation thus introduced caused only slight blurring of the spots, moderately intense streaks were then found on the patterns (fig. 3*b*). The streaks radiated out from the alpha-phase spots, usually in several directions, indicating faulting on more than one set of {111} planes. A subsidiary experiment showed that immersion in liquid nitrogen in the absence of cold work did not generate faults.

Very prominent streaks, indicating profuse faulting, are obtained not only by hammering at low temperatures, but also at room temperature, and in some alloys also hammering at elevated temperatures—provided the alpha phase is supersaturated. In the 4.17 pct alloy of fig. 3 it was also found that straining by impact is not necessary, for faults were introduced when a sample was reduced 3 pct in thickness by slow compression at room temperature, and when samples were slowly compressed 5 and 18 pct.

Profuse faulting is obtained also by abrasion on

emery paper and by mechanical polishing. This is illustrated by fig. 7 and 8, which show the streaks obtained in 5.61 and 5.39 pct silicon alloys after quenching, then rubbing on emery paper, and lightly etching. Quenching alone does not produce streaks as intense as these.

The variation of faulting tendency with composition and with deformation temperature was studied in a series of tests in which deformation was carried out by hammering samples at different temperatures. No precision can be claimed for this series, since the number of spots with low indices was not large, the grains were not uniform in their reaction to the stress, the strains were not uniform, and some grains may have recrystallized into a fault-free state during cooling even when cooling commenced immediately after straining. It was possible, nevertheless, to evaluate the general faulting tendency by discarding films in which the spots indicated that the sample had received either too little or too much deformation for proper visibility of the streaks, or had apparently recrystallized, or was of unusually small grain size.

The tendency to faulting is strongly dependent on composition. No X ray evidence of faults was obtained in any experiments on alloys containing less than 4 pct silicon. Alloys of 0.95, 2.94 and 3.77 pct silicon showed none, but faults were observed with alloys of 4.17, 4.91, 5.12 and 5.39 pct silicon. As the silicon content increased above 4 pct the faulting became more prominent in the single phase alpha alloys. The two phase alpha plus kappa alloys showed prominent faulting, but pure kappa showed none. The range of silicon content of alloys susceptible to faulting as judged by the X ray tests lies between about 4.0 and 5.4 pct.

The susceptibility of the alloys to faulting roughly parallels an important feature in their microstructure, namely, the number of straight lines, "strain markings," that are visible in the microstructure. Fig. 10 illustrates the progressive change in microstructure as alpha-phase alloys increase in silicon content; low silicon alloys are relatively free from internal lines in the grains except for the usual broad annealing twins, but the number of lines increases as the alloys become richer than 4 pct and reaches a maximum in the richest alpha compositions. The lines are similar in appearance to the bands in the banded alpha plus kappa structure, and to thin deformation twins, and lie on the close-packed {111} planes of the face-centered cubic solid solution. Because of this and the fact that they can be produced by deformation it is safe to conclude that they represent a modification of the normal stacking of matrix planes, for this would be true either if they were clusters of faults, lamellae of kappa, transition precipitate, twins, or locally distorted metal along slip planes. (Since the number per grain is orders of magnitude smaller than the number of faults necessary to cause the streaks that are seen in diffraction patterns it is clear that they are not *individual* faults). It can be concluded that when the matrix readily tolerates a rearrangement that produces these lines it also tolerates rearrangement in the form of stacking faults; the matrix stacking sequence can be modified without appreciably increasing either interface energy or internal energy.

The tendency to faulting as a function of the temperature at which various samples were deformed may be judged from the results plotted in fig. 11. No X ray evidence of faults is found when alloys are deformed within the stability range of the alpha solid solution; some degree of supersaturation seems to be required. For example, 4.17 pct silicon samples show no fault-streaks on X ray patterns when hammered at 550°C or 350°C but show many when deformed at 20° or —195°C. This composition becomes supersaturated below about 475°C. The alpha phase of all two-phase alloys was probably slightly supersaturated during deformation, since the wrapped samples dropped a few degrees in temperature during hammering outside of the furnace.

The streaks on the films are short spikes running out from alpha spots for alloys having less than about 5.0 pct silicon; long streaks make their appearance in the richer alloys, often together with short streaks. Long streaks are obtained with samples that contain alpha plus kappa, which are samples that would undergo eutectoid decomposition at a slow rate. None of the treatments produced faults in the pure kappa alloy of 5.5 pct silicon even though this, too, contained a suppressed eutectoid transformation at many of the deforma-

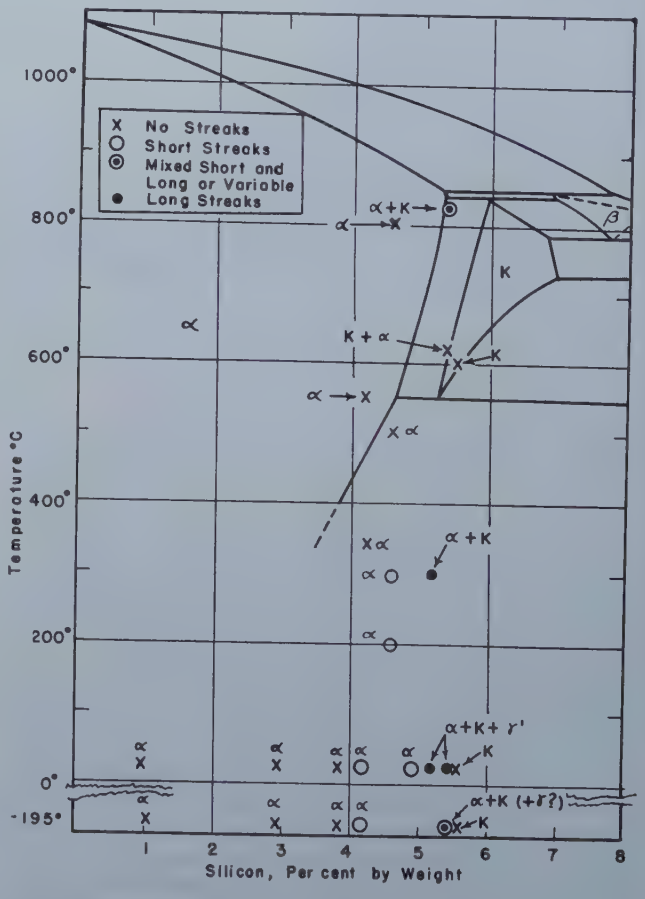

Fig. 11—Summary of type of X ray diffraction streaks obtained when various alloys are deformed by hammering at the temperatures indicated.

Short streaks are ascribed to faulted alpha, long ones to faulted gamma'. The phases present in the samples when deformed are indicated.

tion temperatures used; repeated tests were made with deformation at 600°, 20° and —195°C. The absence or near-absence of strain markings in this alloy again points to the close relation between X ray evidence of faulting and strain markings in the microstructure.

The Removal of Faults: There are many experiments in this series which prove that recrystallization removes faults from alpha-phase alloys. Regardless of the prior thermal or mechanical history of a specimen, if it has been cold worked, recrystallized, and slowly cooled within the alpha phase range it is found to be free or nearly free from X ray evidence of faults. On the other hand, some annealing treatments did not result in fault-free material. These included some annealing treatments in the two-phase regions of the phase diagram (see the following section). Another example was the annealing of a 4.91 pct silicon sample that contained faults from quenching; these persisted throughout a 1½ hr anneal in the alpha phase range at 750°C and slow cooling from this temperature. It is suggested that the mechanism for fault removal is the sweeping of grain boundaries across the faulted grains, and that in the absence of grain growth or recrystallization there is no fault removal.

The Effect of Annealing for Segregation: Since the introduction of a fault into the alpha phase transforms a thin layer either to kappa or to gamma′, it might be anticipated that there would be a tendency for diffusion to alter the composition of the fault with respect to the surrounding matrix. It appears possible to test this by annealing faulted material, allowing segregation to occur without permitting recrystallization or appreciable grain growth. The experiment is possible owing to the lack of coalescence of faults and the lack of spontaneous generation of faults during annealing. If segregation does occur, it would be expected to increase the intensity of the streaks on the X ray films.

An apparent confirmation of this theory was obtained with an alloy of 5.39 pct silicon, for streaks that were very weak were obtained after a sample was recrystallized, then quenched from 750°C, and finally reheated to 750° for 5 min and slow cooled (fig. 12) but after the same sample had been further annealed at 750°C for 3 hr the streaks were intense (fig. 13) and were visible at nearly every alpha spot, though the relative proportions of the phases and the grain size appeared to remain substantially unaltered. This result was confirmed with another specimen, which after quenching from 750°C yielded negligible streaks, but after a subsequent annealing for 8 hr at 750°C produced moderately intense streaks.

When an alpha phase alloy of 4.91 pct silicon was quenched from 820°C to produce faults, subsequent annealing of 1½ hr at 750°C did not increase the intensity of the streaks. This indicates that annealing within the alpha solid solution range does not lead to segregation on the faults.

Segregation appeared also to intensify the long streaks that occurred with alpha plus gamma alloys; faulted samples that had been aged one week at room temperature or 82 hr at 500°C yielded streaks that were perhaps the most intense of any obtained in these tests.

Spontaneous eutectoid decomposition produced no evidence of faulting. For example, faults were not detected in a 5.5 pct silicon alloy that had been slowly cooled from above the eutectoid and annealed 4 days at 525°C so as to be decomposed to alpha plus gamma, and they were absent also in a 5.39 pct silicon alloy that was annealed at 525°C for two weeks, also fully decomposed. Shorter heat treatments of this type also gave negative results (370°C for 20 hr, 500°C for 17 and for 48 hr, with the 5.39 pct alloy) but it is possible that some critical treatment might give positive results.

Precipitation of Alpha from Kappa: It was expected that faults would be numerous if the kappa phase was heated so as to precipitate alpha with the characteristic banded microstructure. This, however, was found not to be the case; precipitation produced negligible faulting compared with quenching or deforming, as judged by the following experiments.

Samples from the 5.39 pct Si alloy were cold rolled to a reduction of thickness of 25 to 35 pct, annealed 1 hr at 590°C, and cooled in air. In this condition they consisted almost entirely of kappa, with only a trace of alpha, and exhibited almost no streaks from faults when X ray patterns were prepared. There continued to be no more than occasional faint streaks on the patterns when these samples were introduced into a furnace controlled at a temperature in the range of alpha precipitation, held at 750°C for 1, 5, 15, 75, and 180 min, and air cooled in copper foil. After these precipitation treatments the alloys consisted of alpha and kappa in roughly equal proportions. A sample of this series introduced into a furnace at 820°C, brought to temperature, and immediately air cooled also yielded no streaks, though even this short time of heating transformed roughly a third of the sample from kappa to alpha (fig. 14). Had an appreciable amount of faulting occurred early in the precipitation process all of the specimens just mentioned should have yielded patterns with prominent streaks, for supplementary experiments show that faults can survive annealing for hours at 750°C, and micrographic studies[12] have shown that banded alpha plus kappa structures persist for hundreds of hours at this temperature.

Precipitation of Kappa from Alpha: A negligible amount of faulting was found after precipitation of kappa from alpha during air cooling. Specimens containing 5.39 pct Si were cold worked and annealed at 820°C, which made them preponderantly alpha, then slowly withdrawn from the furnace and air cooled, the cooling time to 100°C being about 5 min. One of these showed no definite streaks from faulting; the other showed a few very weak streaks associated with about one out of ten of the well exposed spots on the inner diffraction rings (fig. 15). (One may credit the traces of faulting to a failure to cool slowly enough to avoid faulting from quenching or to residual faults not removed by annealing prior to the cooling.) That the heat treatment actually caused a substantial amount of precipitation was made clear by comparing the patterns from these specimens with the pattern of a speci-

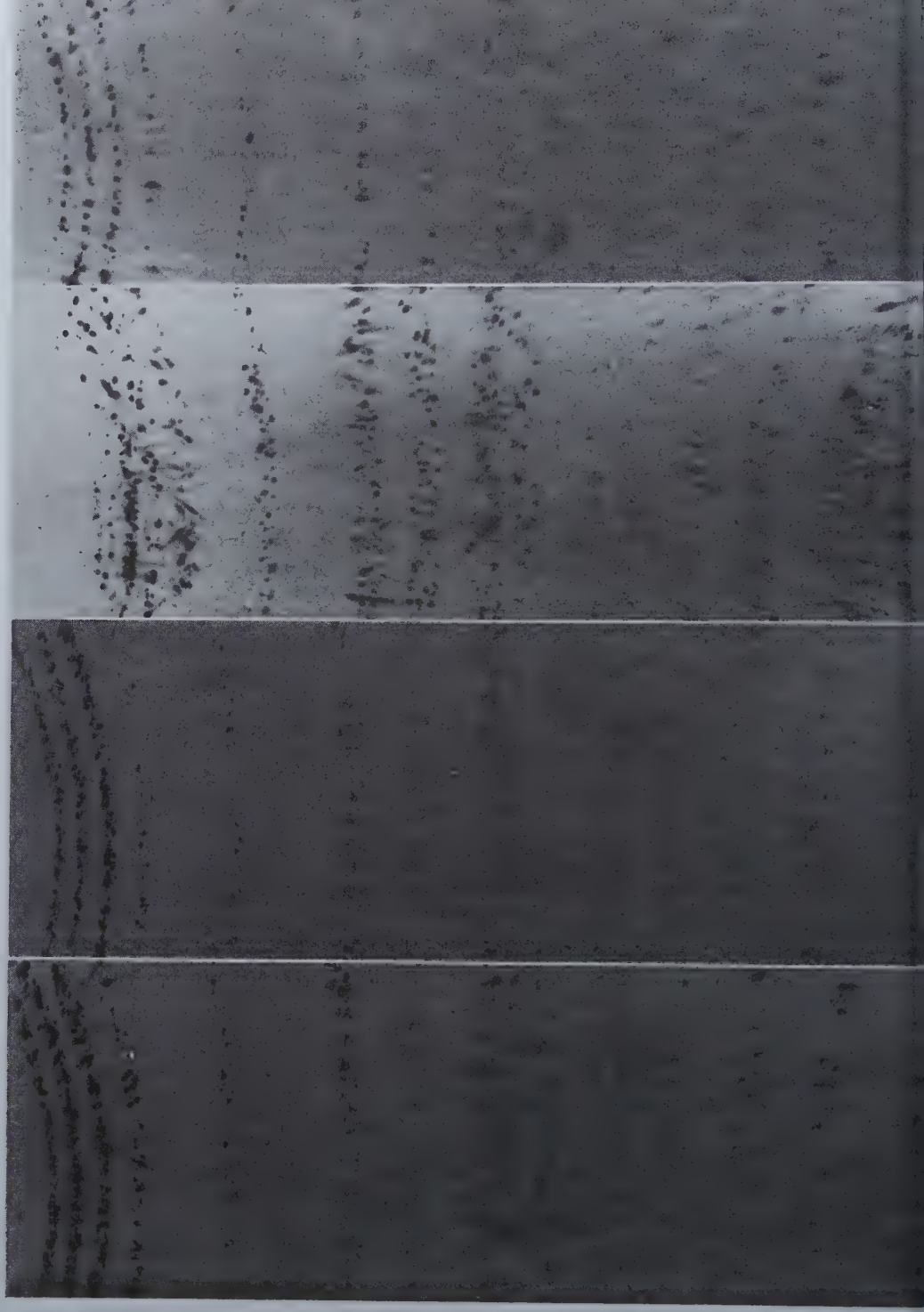

Fig. 12— Pattern of Cu+5.39 pct Si. Recrystallized at 600°C, quenched 1 hr 750°C, quenched 5 min. 750°C, air cooled.

Fig. 13 — Sample of fig. 12 after additional 3 hour anneal at 750° and air cooling.

Fig. 14— Kappa alloy. 5.39 pct Si recrystallized at 600°C and fault-free, heated for alpha precipitation to 820°C and slowly cooled.

Fig. 15— Alpha alloy. 5.39 pct Si recrystallized at 820°C, slowly cooled for precipitation of kappa.

men of the same composition that had been quenched from the same annealing temperature. The slow cooling had increased the amount of kappa from a trace to about 2/3 of the volume of the sample.

Discussion of Results

The present experiments provide what is believed to be the first direct evidence of stacking disorders generated during plastic deformation of metal crystals. There has previously been only indirect evidence, such as that furnished, for example, by electron diffraction, that tapping an aluminum crystal destroyed Kikuchi lines without producing visible slip planes,[6] and other observations, mentioned early in the paper, that admit of other interpretations.

Fault Spacings: Metallographic data would not indicate that faults would occur in the great numbers and the close spacing that is necessary to produce visible X ray diffraction streaks. Even if one assumes that faults are left on an appreciable fraction of the active slip planes[7] and uses the electron microscope data for the closest spaced slip planes that have been measured, namely, 200 Å, as observed in aluminum by Heidenreich and Shockley,[5] the faults would be an order of magnitude farther apart than those found in the present research, where faults every 5 to 10 layers are common. The discrepancy between the spacings of faults in the present research and the spacings of slip lines that have been observed in copper and brass is even greater. If the interpretation of the Cu-Si X ray

films is correct, the individual faults could not be seen metallographically, and strain markings are to be accounted for by clusters of faults, by some distortion, or by precipitation along slip planes.

Since sharp spots are located on the streaks in the diffraction films it is concluded that there are portions of each grain that are relatively perfect, and that the distribution of faults is very uneven. This applies to faults of the type found below 5.0 pct silicon, and also to the type found between 5.0 and 5.4 pct silicon (the gamma′ type), and suggests again that the strain markings involve *clusters* of faults. In the discussion of the two types of streaks observed with alloys of varying silicon content it was pointed out that with alloys richer in silicon than 5.0 pct the intensity distribution along the streaks is not as predicted by the computations based on table I. As the computations should apply only to crystals in which each layer is influenced as to position by nearest neighboring layers and layers two spacings distant, it may be concluded that more distant layers interact and influence the distribution of faults in the 5.0-5.4 pct silicon range.

Faulting vs. Stress for Flow: Perhaps the production of faults accounts for strain hardening being so marked in Cu-Si alloys, especially in the higher silicon alloys, when compared with Cu-Ni, Cu-Zn, and Cu-Al alloys on an equal atomic per cent basis,[20] fig. 16; and the fact that the indentation hardness increase per one atomic per cent dissolved silicon is greater than the increase in these alloys even though the change in lattice parameter per atomic per cent added element is *less* in silicon than in any of these.[21] The unusually rapid strain hardening of Cu-Si alloys is also apparent in stress-strain curves of material that has been rolled to various reductions.[22]

The stress at which the stress-strain curves deviate from a straight line is unusually low when compared with Cu-Zn and Cu-Sn alloys, though all these require about the same stress for 0.002 pct permanent set.[23] This is ascribed to the ease of glide into the faulted position that would be anticipated when the faulting tendency is high.

Faults and the Hardening of Latent Slip Planes: Recent research on alpha brass crystals by Maddin, Mathewson and Hibbard[24] shows that strain hardening and X ray evidence of lattice distortion are absent when slip is confined to a single set of parallel slip planes, or to two nonparallel sets of planes that use a common slip direction, whereas both strain hardening and distortion become marked as soon as slip commences on planes having a different slip direction. Thus when glide has to cut through previously slipped regions in directions different from the slip direction previously used, the resulting disruption of the structure is severe. This may be understood in terms of faults left at the sites of the active slip planes, for faults in the FCC lattice that result from slip in one slip direction should not interfere with slip on parallel planes, but would leave atoms at positions that one would expect would interfere with slip on planes cutting across these.[5] The low strain hardening characteristics of hexagonal single crystals compared with face-centered cubic single crystals can be explained in the same way, for faults that result from slip on a basal plane should have little if any effect on slip on other basal planes.

The differing tendency in different alloys to harden latent slip planes seems likely to be caused by the differing faulting tendency. If so, this latent slip plane hardening should be a maximum in crystals of Cu-Si near the maximum solubility limit.

Faults and Annealing Twins: For over twenty years the question of whether FCC metals twin during deformation has been discussed.[1-3, 6, 7, 24-28] Mathewson and his coworkers have shown the attractiveness of the concept and have used it to explain various metallographic and texture observations. There has been objection on the basis that no mechanism is obvious by which a thick deformation twin can form,[7] but the objection does not apply to faults, which have been regarded as very probable. Recent experiments of Kronberg and Wilson[25] and the recent contributions from Yale University[26, 27] lend additional indirect support to the concept that deformation leaves faults and to the conclusion that faults are intimately associated with the origin of annealing twins. Kronberg and Wilson find, for example, that twin-free cubically aligned grains when lightly cold worked will recrystallize into grains containing many twins. (This experiment has been repeated and confirmed by the author.) And it is found that annealing twins have composition planes parallel to the slip planes that have been active during deformation,[27] as if conditions in a slip band were appropriate to nucleating an annealing twin. The present results seem to leave no more room for doubt that deformation can introduce faults into at least some alloys.

Evidence is increasing that annealing twins can

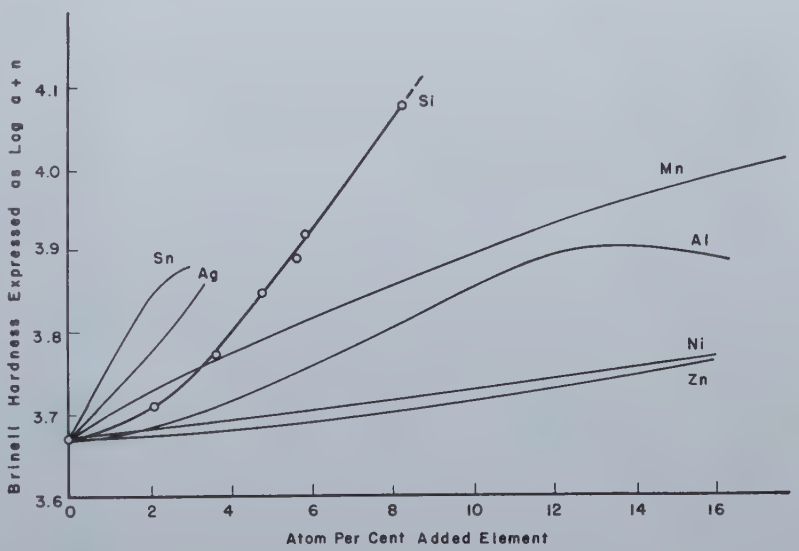

Fig. 16—Brinell hardness of copper-base alloys, after Norbury.
Hardness expressed as log $a + n$ from the expression $L = a\ d^n$ where L is applied load producing indent of diameter d.

originate when a growing grain encounters material in twin or near-twin relationship to the orientation of the growing grain. The author has observed the reluctance of such material to be absorbed into growing single crystals of iron;[28] in recent experiments in this laboratory J. E. Burke has noted that annealing twins appear to originate in this way in copper, and J. B. Hess has noted that in gold, copper and Fe-Ni austenite, after grain growth there are large areas that are subdivided by twin boundaries, further evidence that grains in twin relationship are stable during growth. The list of observations could be extended. It therefore seems probable that annealing twins can originate when a moving grain boundary encounters a properly oriented fault or fault cluster, as well as a properly oriented grain. This point of view would account for the fact that the number of annealing twins in alpha Cu-Si alloys increases with silicon content because the number of faults increases.

Summary

Stacking disorders in Cu-Si alloys were detected and analyzed by diffraction patterns made with polycrystalline samples oscillating through small angles by noting the direction, length, and intensity of non-Laue streaks.

Quenching or cold working supersaturated Cu-Si alloys in the range 4.0 to 5.4 pct Si introduces numerous faults in stacking, the faults occurring at intervals that reach a minimum of between five and ten atomic layers of the face-centered alpha solid solution. The faults are on the close-packed (111) planes of the lattice. This is believed to be the first direct proof of mechanically induced faulting of metals. The quenching is effective in fault production merely because it causes plastic strains.

In two-phase alpha plus kappa Cu-Si alloys the faults are parallel to the basal planes of the kappa (hexagonal close-packed) as well as the (111) planes of alpha, because of the mutual orientation of the two. Straining alloys with silicon in the range 5.0 to 5.4 pct produces a faulted phase (gamma') which is metastable and different from equilibrium gamma; this phase is accurately oriented with respect to alpha and kappa and is probably coherent with alpha or kappa. The kappa phase has a negligible tendency to faulting.

The spontaneous precipitation of alpha from kappa or of kappa from alpha produces little or no faulting. Thermal agitation during annealing near the solidus, cooling to —195°C and spontaneous eutectoid decomposition are also ineffective in generating faults.

Specimens can be made substantially fault-free by recrystallizing and cooling slowly. But faulted material does not lose its faults during long annealing unless recrystallization or grain growth occurs, just as the banded kappa plus alpha microstructure resists coalescence indefinitely owing to the low interface energy.

The anomalously high strain hardening of solid solutions of Si in Cu may result from the faults and the abnormally frequent annealing twins in these alloys probably originate in the faults. It is suggested that the relative hardening of latent slip planes may correlate with faulting tendency. The frequency of strain markings in micrographs correlates with the faulting tendency, though the faults are orders of magnitude closer to each other than are the visible strain markings.

Acknowledgments

The author is indebted to Cyril S. Smith, W. H. Zachariasen and J. B. Hess for helpful discussions of the work, and to the American Brass Co. for the alloys used.

References

[1] C. H. Mathewson and A. Phillips: *Trans.* AIME (1916) **54**, 608.

[2] C. H. Mathewson: *Trans.* Am. Soc. Metals (1944) **32**, 38-87.

[3] Discussion by C. H. Mathewson to the paper of ref. 6.

[4] C. S. Barrett: *Trans.* AIME (1945) **161**, 15-64.

[5] R. D. Heidenreich and W. Shockley: Rep't. of Conf. on Strength of Solids. Phys. Soc., 57-75, (London, 1948).

[6] J. E. Burke and C. S. Barrett: *Trans.* AIME (1948) **175**. *Metals Tech.*, Feb. 1948, TP 2327.

[7] C. S. Barrett: The Crystallographic Mechanism of Translation, Twinning, and Banding. A.S.M. Symp. on the Cold Working of Metals, (Phila., Oct., 1948). (In press).

[8] O. S. Edwards and H. Lipson: *Jnl.* Inst. Metals (1943) **69**, 177.

[9] O. S. Edwards and H. Lipson: *Proc.* Roy. Soc. (1942) **180**, 268-277.

[10] C. S. Barrett: *Trans.* AIME (1948) **175**. *Metals Tech.* Aug. 1948, TP 2449. (Author's reply to disc. of C. S. Barrett and O. R. Trautz, *Met. Tech.* Feb. 1948, TP 2338).

[11] C. S. Barrett: Transformations in Pure Metals. N.R.C. Symp. of Phase Transformations in Solids. Cornell, (1948). (To be published).

[12] Cyril S. Smith: *Trans.* AIME (1940) **137**, 313-333.

[13] A. G. H. Andersen: *Trans.* AIME (1940) **137**, 334-350.

[14] Cyril S. Smith: (Disc.) *Trans.* AIME (1940) **137**, 351-352.

[15] S. Arrhenius and A. Westgren: *Ztsch. Phys. Chem.* (1931) **B14**, 66-79.

[16] K. Sautner: Forschungs Arbeiten Uber Metallkunde und Rontgenmetallographie. (1933) **9**, 1-31.

[17] W. H. Zachariasen: *Phys. Rev.* (1947) **71**, 715-717; *Acta Cryst.* (1948) **1**, 277-281.

[18] A. J. C. Wilson: *Proc.* Roy. Soc. (1942) **A-180**, 277-285; "X-ray Optics." Methuen & Co., London, 1949.

[19] V. Daniel and H. Lipson: *Proc.* Roy. Soc. (1943) **181A**, 368-378; (1944) **182A**, 378-387.

[20] A. L. Norbury; *Jnl.* Inst. Met. (1923) **29**, 423.

[21] R. M. Brick, D. L. Martin and R. P. Angier: Preprint 37, ASM, (1942).

[22] R. A. Wilkins and E. S. Bunn: Copper and Copper Base Alloys. McGraw-Hill, (1942).

[23] C. S. Smith: *Proc.* ASTM (1941) **41**, 1-21.

[24] R. Maddin, C. H. Mathewson and W. R. Hibbard, Jr.: *Trans.* AIME (1949) **185**, 527; *Jnl. of Metals*, Aug. 1949. TP 2658.

[25] M. L. Kronberg and F. H. Wilson: *Trans.* AIME (1949) **185**, 501; *Jnl. of Metals*, Aug. 1949.

[26] W. R. Hibbard, Y. C. Liu, and S. F. Reiter: *Trans.* AIME (1949) **185**, 635; *Jnl. of Metals*, Sept. 1949.

[27] R. Maddin, C. H. Mathewson and W. R. Hibbard: *Trans.* AIME (1949) **185**, 655; *Jnl. of Metals*, Sept. 1949.

[28] C. S. Barrett: (Disc. to paper by S. E. Maddigan and A. I. Blank). *Trans.* AIME (1940) **137**, 190.

Undercooling of Minor Liquid Phases in Binary Alloys

by Chih-Chung Wang
and
Cyril Stanley Smith

TURNBULL and his collaborators[1, 2] have developed the theory of homogeneous nucleation as applied, *inter alia*, to solidification of liquid metals. Vonnegut[3] and Turnbull[4] have shown that if a liquid metal is subdivided into small droplets a vast majority of them will undercool very considerably before solidification, generally to as low as about 0.8 of the freezing temperature on the absolute scale. The nuclei effective at small degrees of supercooling in bulk metal seem to be internal or surface heterogeneities, relatively small in number. If the metal is subdivided, those droplets that happen to contain such nuclei will solidify at a temperature not greatly below the true freezing point, but only a small part of the whole volume will be affected and the majority of the drops will undercool to the much lower temperature at which homogeneous nucleation occurs as a result of fluctuations.

CHIH-CHUNG WANG, Student Associate, is on the staff and CYRIL STANLEY SMITH, Member AIME, is Director, Institute for the Study of Metals, Univ. of Chicago.

AIME New York Meeting, Feb. 1950.
TP 2756 E. Discussion (2 copies) may be sent to Transactions *AIME before Apr. 1, 1950, and will be published Nov. 1950. Manuscript received Oct. 4, 1949.*

It occurred to one of the authors that an appropriate subdivision to give effective freedom from random nuclei is produced during the solidification of many alloys that contain a minor amount of a phase of low melting point, and that one might then expect marked undercooling of the distributed phase.

Experimental: The alloys selected for initial study were copper with minor amounts of lead and bismuth, and aluminum with tin. In all these alloys, the major component freezes at a temperature not much below that of the pure metal, and there is little further change in constitution on cooling until the lower melting point constituent freezes in an almost pure state.

Cooling curves were taken using the controlled heat flow method[5] permitting approximate specific heats to be obtained. Chromel-alumel thermocouples were used, with the standard emf tables, since extreme precision was not needed. The crucible (¾ in. id, 5/16 in. wall) was made of B & W K-20 insulating brick. It held about 10 cc of the alloy being investigated. The cooling rate was 2.5° to 2.9°C per min under a controlled temperature difference of 20°. Approximate specific heats were computed from the inverse rate curves together with data from a blank run and from a standard run with a copper cylinder of known heat capacity.

The alloys for investigation were made from high-purity metals (99.99+pct) and cast into graphite molds. The castings were machined to fit the crucible and to provide a hole for the inner thermocouple. Cooling curves were taken after heating to a temperature about 50° above the melting point of the minor, lower melting-point, constituent.

Results

The lead phase in an alloy of copper with 5 pct lead did not undercool more than 3° below the melting point of lead (327°C) either as cast or after annealing to produce a new dispersion of the liquid phase. A copper-zinc-lead alloy with 23.75 pct zinc and 5 pct lead undercooled more but showed no thermal effect below 319°C. A cast alloy of copper with 5 pct bismuth undercooled to 249°C (M.P. bismuth 271°C), but once solidification started it was completed at the same temperature. This was anticipated, since the bismuth forms a nearly continuous phase between the grains of copper, and a solid crystal nucleated anywhere would rapidly* consume the entire network of liquid, unless the physical continuity of the liquid were broken through volume changes, inadequate fluidity, or gas evolution. Similar arguments apply in the case of copper-lead alloys, where the lead-rich liquid forms a network along grain edges, though not grain faces. In both cases there would be a few isolated particles

* The rate of growth of the solid will be greater than in massive undercooled metal because the thermal diffusivity of the matrix is much higher in relation to the amount solidifying and there will be little temperature rise due to latent heat.

The tin in an aluminum-tin alloy with 10 pct tin solidifies over a temperature range as high as 100°C. The tin is partly distributed in isolated droplets and the amount of undercooling depends on the chance presence of nuclei effective at various temperatures in drops of varying sizes. Heat treatment affects the size distribution and modifies the cooling curve. Similar behavior is to be expected in any alloy where the liquid is physically discontinuous and where solidification is not nucleated by a previously solidified constituent. It is probably the cause of some spurious arrests that have been observed in cooling curves of simple alloys.

of liquid which would undercool unless their solidification were nucleated by the copper grains in which they are embedded, and it is assumed that this actually occurred.

Aluminum-tin alloys with 10 and 20 wt pct tin did show the predicted behavior.

An alloy with 10 pct tin (2.5 at. pct; 4.0 vol. pct) was cast, rapidly reheated to 285°C and cooled, giving the specific heat curve shown in fig. 1. A sharp arrest corresponding to the solidification of about two-thirds of the tin occurs at 221°C, which corresponds to undercooling of 8°C below the eutectic at 229°C. Smaller, less sharp peaks appeared at 199° and 167°C, and solidification was not complete until 159°C. After the alloy had been given a prolonged anneal (8 hr at 480°C and furnace cooled) the highest temperature peak in the specific heat curve was greatly decreased in area, while the lower ones increased, and a third much smaller one appeared at 151°C (fig. 2). The total integrated heat due to the tin was about the same in all samples and corresponded to a latent heat of 15.4 to 16.3 cal per g of tin.

The cooling curve for a given sample was reproducible on subsequent reheating and cooling, but different samples gave curves differing in detail but alike in general features. The greatest degree of undercooling observed in any sample was 99°C (to 130°C), compared with 110°, the maximum obtained by Vonnegut.

The details of these curves depend upon the presence of nuclei of varying effectiveness (a function of their particular size, shape, and surface structure) and the actual distribution of these nuclei among particles of tin of various sizes, which determines how much tin will be solidified by a given nucleus. The character of the nuclei is more or less beyond control, but the distribution of the tin is strongly influenced by thermal history. The difference in behavior of the alloy after annealing is easily understood from its microstructure (fig. 3 and 4). In the casting the liquid tin exists largely in the form of a continuous interdendritic network, while on annealing it collects under the influence of sur-

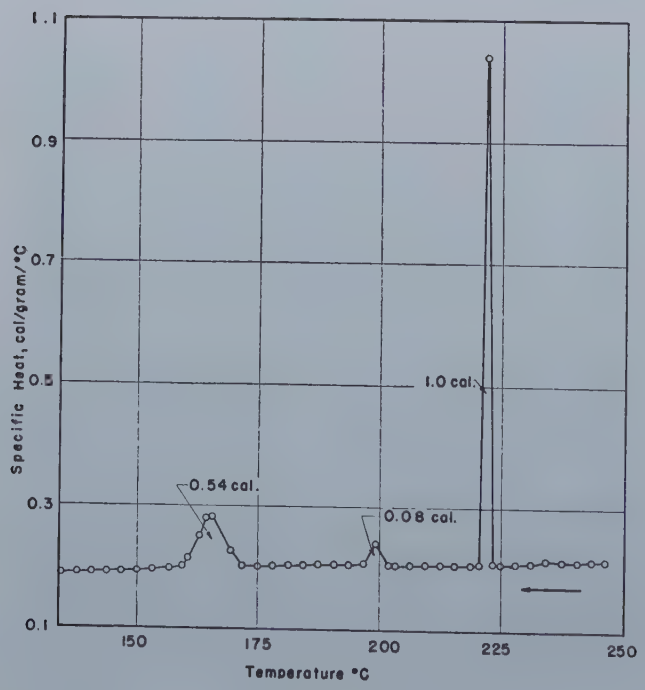

Fig. 1—(left) Apparent specific heat derived from cooling curve of cast 90-10 Al-Sn alloy.

Total heat evolution due to tin solidification 16.3 cal per g of tin present in the alloy.

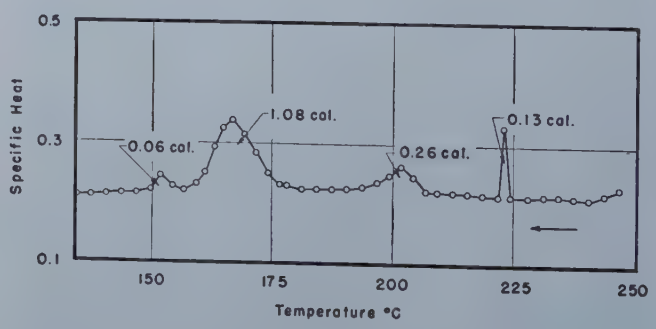

Fig. 2—Specific heat of same alloy as fig. 1, cooled after annealing 8 hours at 480°C.

Total latent heat 15.4 cal per g.

Fig. 3 (left)—Microstructure of cast 90-10 Al-Sn alloy. X150. Fig. 4 (right)—Same as fig. 3, after annealing 8 hours at 480°C. X150.

face tension into isolated droplets, with a relatively small amount retained in the continuous network along grain edges.

For comparison with these alloys, an additional sample of the same shape, weight, and average composition was made synthetically by symmetrically drilling three 3/16 in. holes in a cylinder of pure aluminum, and setting therein three separate pieces of pure tin of appropriate weight. The resulting cooling curve, shown in fig. 5, clearly shows arrests corresponding to each of the three pieces, which by chance had tramp nuclei effective at different temperatures. The curve was duplicated on remelting and again cooling. It is easy to see how, with increased subdivision of the tin, the arrests integrate, as in fig. 2, into a small increase of specific heat spread over a large range of temperature.

These experiments suggest that the solidification of castings of alloys may be greatly extended, perhaps occasionally with unpleasant practical results. They provide a possible explanation for the spurious and multiple arrests in cooling curves that have been puzzling in the past, particularly the drop in eutectic or peritectic temperature often observed in cooling curves of alloys as the amount of liquid present at the solidus temperature decreases. Without a mechanism similar to the one proposed, the duration of the arrest should decrease, but not the temperature at which it occurs.

Undercooling will not occur to an abnormal extent when the liquid is a major part of the alloy or when the details of solidification mechanism cause the liquid to be retained as a continuous network, neither can it occur when one of the previously solid constituents of the alloy serves as a nucleus for final solidification of the residual liquid.

It is possible that solid phases may behave similarly and fail to transform at normal temperatures when distributed in fine particles. For example, iron can be partially retained in the austenitic condition on quenching a two-phase copper-rich alloy of copper and iron. Generally, however, the interface between two solid phases will itself serve to nucleate any possible transformation in either, and statistical volume-dependent nucleation is rarely involved.

Summary

The tin in an aluminum-tin alloy with 10 pct tin solidifies over a temperature range as high as 100°C. The tin is partly distributed in isolated droplets and the amount of undercooling depends on the chance presence of nuclei effective at various temperatures in drops of varying sizes. Heat treatment affects the size distribution and modifies the cooling curve. Similar behavior is to be expected in any alloy where the liquid is physically discontinuous and where solidification is not nucleated by a previously solidified constituent. It is probably the cause of some spurious arrests that have been observed in cooling curves of simple alloys.

Acknowledgment

This research has been supported in part by the Office of Naval Research, U.S.N. (Contract No. N-6ori-20-IV, NR 019 302).

References

[1] J. C. Fisher, J. H. Hollomon, and D. Turnbull: Nucleation. *Jnl. Appl. Phys.* (1948) **19**, 775-784.

[2] D. Turnbull and J. C. Fisher: Rate of Nucleation in Condensed Systems. *Jnl. Chem. Phys.* (1949) **17**, 71-73.

[3] B. Vonnegut: Variation .... of Nucleation Rate .... *Jnl. Colloid Science* (1948) **3**, 563-570.

[4] D. Turnbull: Subcooling of Liquid Metals. *Jnl. Appl. Phys.* (1949) **20**, 817.

[5] C. S. Smith: Method of Thermal Analysis .... *Trans.* AIME, (1940) **137**, 236-244.

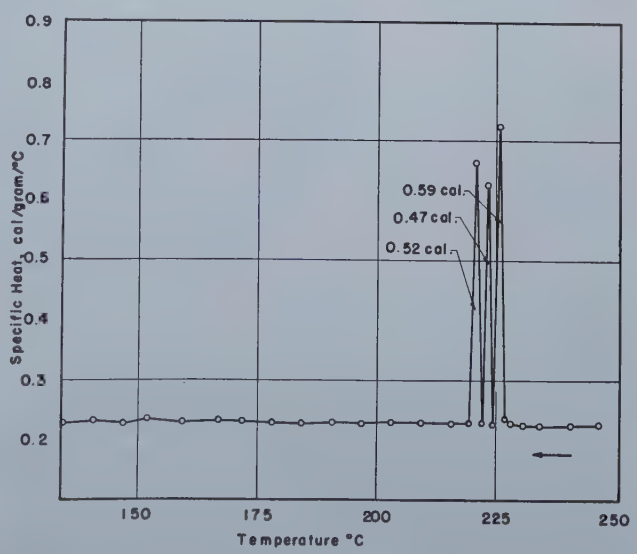

Fig. 5—Apparent specific heat curve obtained from composite specimen.

Cylinder of aluminum with three lumps of tin, having same average composition as alloy in fig. 1. Total latent heat 15.8 cal per g of tin.

Aging Behavior of a Zinc Alloy

Containing 25 pct Manganese, 15 pct Copper, 0.1 pct Aluminum

by P. W. Ramsey
and
G. L. Werley

Describes aging changes in Zn-25 pct Mn-15 pct Cu-0.1 pct Al experimental die casting alloy in temperature range 60-185°C. The exponential increase of aging rate with temperature is used in predicting lower temperature behavior, and the analogy between aging and diffusion behavior is noted. Q values derived from aging rate curves show some agreement, ranging from 18,400 to 21,200 cal per g atom for the various property changes studied.

THERE have been numerous examples in recent years of the similarity between aging behavior and diffusion behavior, where a plot of the logarithm of the aging rate versus the reciprocal of the absolute temperature yields an approximate straight line, analogous to a similar plot of the diffusion coefficient D (log D vs. $1/T$).

Austin and Rickett[1] have pointed out that this linear relationship holds empirically for the decomposition of austenite into pearlite and bainite in carbon steels, and Robertson[2] has shown similar trends in the aging of 24S-type aluminum alloys. Jenkins and Bucknall[3] have also demonstrated the association between aging and diffusion rates for nickel-silicon-copper alloys. Jetter and Mehl,[4] however, have shown that the maximum rate of dilation of a series of aluminum-silicon alloys does not show this linear relation and Mehl[5] has pointed out that careful study of available knowledge indicates that "aging rates increase with temperature approximately exponentially, whereas D increases precisely exponentially." He further notes that "the rate of aging at a given temperature is the greater the lower the melting point of the alloy, which is also true for D."

This paper describes the aging changes occurring in a zinc-25 pct manganese-15 pct copper-0.1 pct aluminum die casting alloy.[6] It was found that this alloy does show this linear relationship and use was made of this relationship to estimate aging rates at low temperatures from data acquired at elevated temperatures. It should be noted that the aging reaction is being studied only indirectly, using changes in certain properties as criteria of the progress of the phenomenon. This alloy is purely an experimental one and is not available commercially.

Zinc-Manganese-Copper System: The zinc-rich portion of the zinc-manganese-copper diagram which is of significance in the present work is quite uncertain. X ray examination of the alloy as die cast shows a phase similar to the epsilon phase (hexagonal close packed) of the copper-zinc system. All of the data accumulated indicate that the epsilon phase of the zinc-manganese-copper alloy is stable at high temperatures; that is, 500°C or above. Below this temperature a new phase is precipitated on annealing, and a decrease in specific volume occurs. At elevated temperatures this phase change occurs quite rapidly, while at room temperature the alloy has shown no change after several years. According to X ray data, this precipitated phase resembles the gamma phase (cubic) of the copper-zinc system, a hard and brittle structure. From examination of the microstructure and from X ray examination of the alloys annealed at

P. W. RAMSEY, Member AIME, and G. L. WERLEY are Investigators, Technical Dept., The New Jersey Zinc Co. (of Pa.), Palmerton, Pa.

AIME New York Meeting, Feb. 1950.

TP 2766 E. Discussion (2 copies) may be sent to Transactions *AIME before Apr. 1, 1950, and is scheduled for publication Nov. 1950. Manuscript received Oct. 17, 1949.*

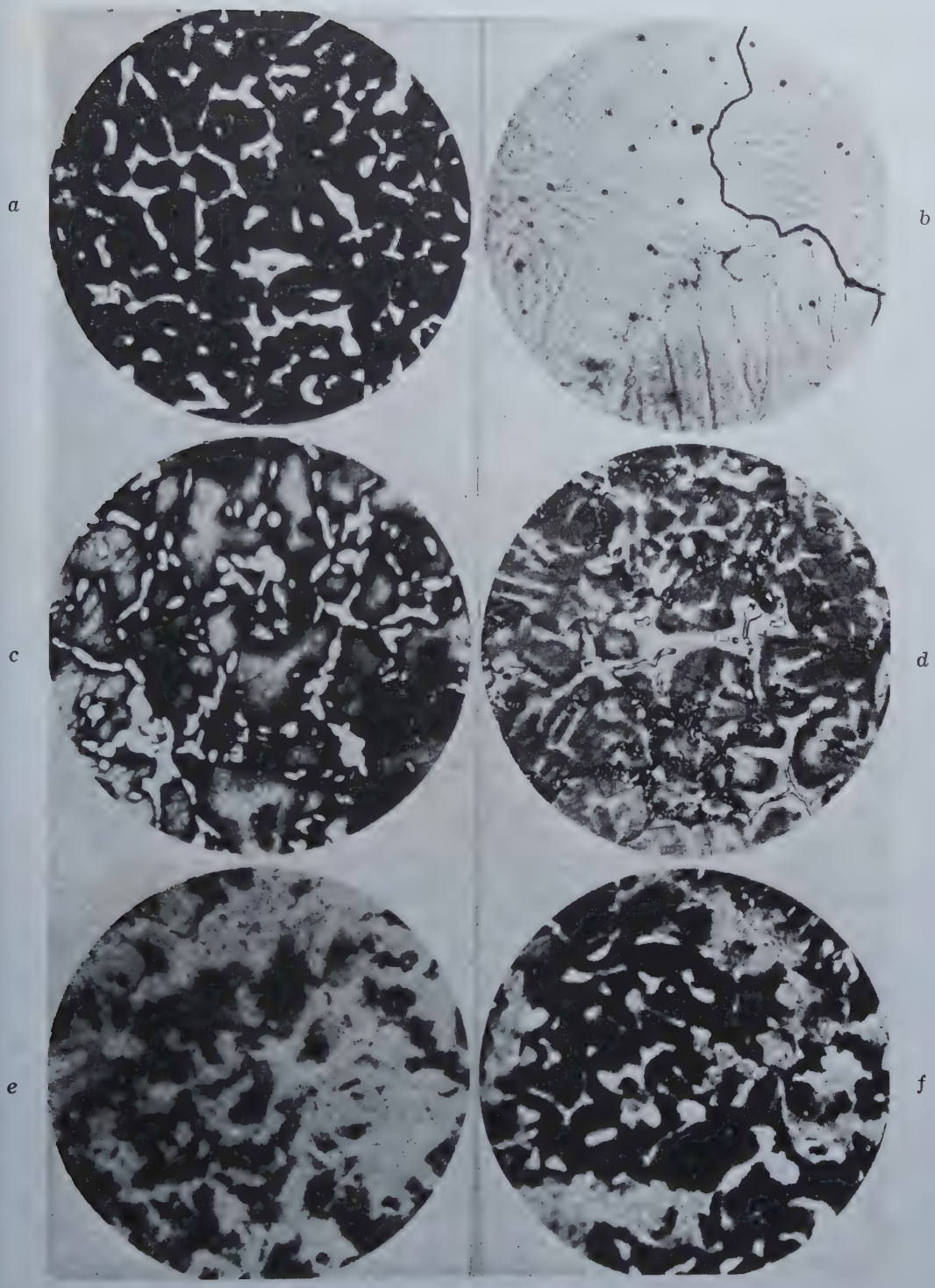

Fig. 1 — Microstructure of a zinc alloy containing 25 pct Mn-15 pct Cu-0.1 pct Al.

Aged at various temperatures. a. As die cast. X1000. Principally cored ϵ, small patches of γ in center of some of the white ϵ. b. Annealed 16 hr at 500°C. X1000. Single ϵ phase, slightly cored. c. Annealed 16 hr at 400°C. X1000. Cored ϵ with precipitate of γ phase. d. Annealed 16 hr at 300°C. X1000. Cored ϵ with γ precipitate partly in eutectoidal structure. e. Annealed 16 hr at 200°C. X1000. White ϵ with beadlike γ eutectoidal precipitate. f. Annealed 6 mo. at 100°C. X1000. Cored ϵ with fine beadlike γ eutectoidal precipitate. Etch: 10 pct $(NH_4)_2S_2O_8$.

100°C, it appears that the gamma constituent is deposited at the grain boundaries.

The microstructures of specimens annealed at 300°C and below seem to indicate that at these temperatures an additional phase is codeposited with the gamma phase from the original epsilon phase, the precipitated structure having the appearance of a eutectoid.

The microstructures, as cast and after annealing at various temperatures, are shown in fig. 1.

Material and Preparation of the Alloy: The alloy was prepared from special high grade zinc, electrolytic manganese, electrolytic copper and primary aluminum, melted (m.p. 775°C) in an alumina lined crucible without a flux cover. Care was taken to prevent flue gases from contacting the melt. The alloy was pigged, remelted in an induction furnace in an alumina lined crucible, and die cast into tensile and impact bars in an experimental cold chamber type machine. Table I shows an

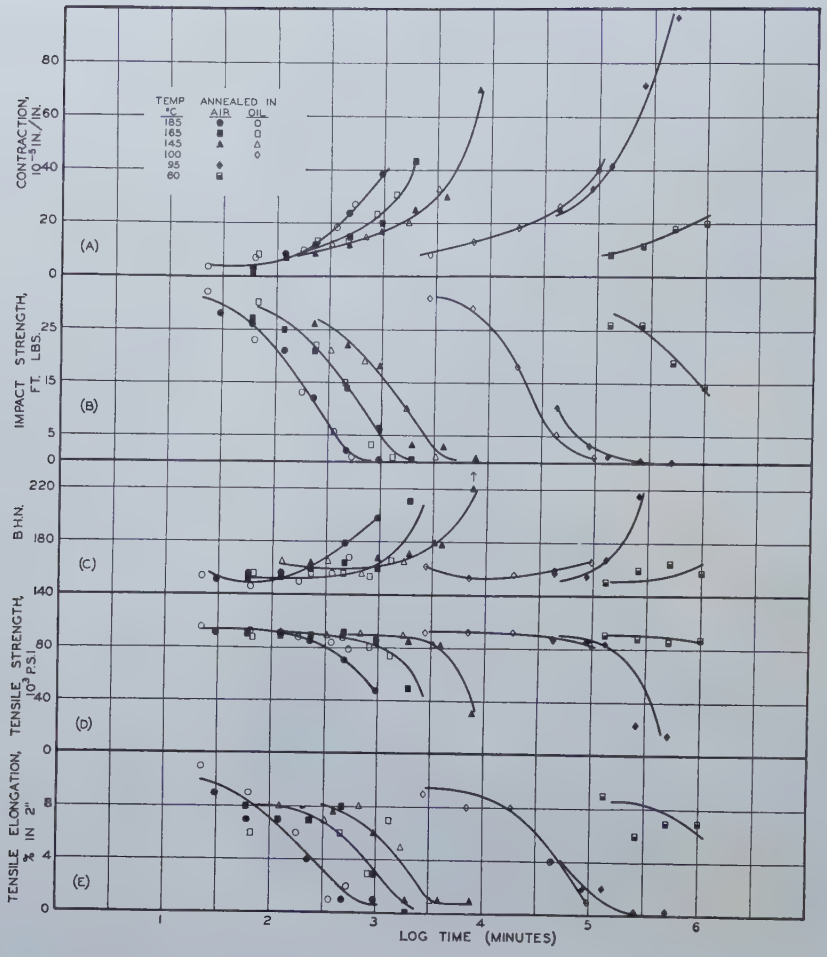

Fig. 2—The effect of aging on properties of a zinc alloy containing 25 pct Mn-15 pct Cu-0.1 pct Al.

Annealed at various temperatures. Log Time vs. Property. (A) Contraction. (B) Impact Strength. (C) Brinell Hardness. (D) Tensile Strength. (E) Tensile Elongation.

analysis of the die cast test bars. The alloy has a specific gravity of 7.47.

Table I. Composition of the Zinc-Manganese-Copper-Aluminum Alloy

Alloy No.	Analysis—Weight Per Cent			
	Mn	Cu	Al	Zn (by difference)
N217	24.7	14.2	0.14	60.96

Experimental Procedure and Results: Die cast test bars were aged in an oil bath at 185°, 165°, 145° and 100°C, and in air at 185°, 165°, 145°, 95° and 60°C. In the former series, groups of two tensile and five impact specimens were tested after various aging times, and in the latter series groups of five tensile and ten impact specimens were similarly tested.

The contraction occurring during aging was measured on 6-in. impact specimens, having machined ends, using a micrometer of sensitivity 1x 10^{-4} in. In addition tensile properties, impact strength (Charpy), and hardness were obtained. Values shown represent the averages of five determinations, except for impact strength where ten bars were tested.

Property-time curves were obtained for contraction, impact strength, hardness, tensile strength and tensile elongation at aging temperatures of 185°, 165°, 145°, 100°, 95° and 60°C. These curves are shown in fig. 2.

A few data were also obtained on bars solution-annealed 24 hr at 500°C prior to aging, and a typical curve for impact strength is shown in fig. 4.

The mechanical properties of the alloy as cast are shown in table II.

Table II. Mechanical Properties of the Zinc-Manganese-Copper-Aluminum Alloy, As Cast (Alloy No. N217)

Tensile Strength, psi	90,800
Tensile Elongation, pct in 2 in.	8
*Impact Strength (Charpy), ft-lb	29
Brinell Hardness	145
Rockwell "B" Hardness	87

* ¼x¼x3 in. unnotched specimens.

Discussion of Results: The linear relationship between the logarithm of the time for given property changes and the reciprocal of the aging temperature is demonstrated for several properties in fig. 3. These curves have been useful in estimating service life for the alloy at various temperatures. For example, a drop in impact strength to 15 ft-lb occurs after aging a few hours at 185°C, about 2 yr at 60°C, and by extrapolation, about 70 yr at room temperatures. Other increments of change in impact strength, if plotted similarly, yield parallel and straight lines.

The effect of solution annealing for 24 hr at 500°C prior to aging at 185°C is shown in fig. 4.

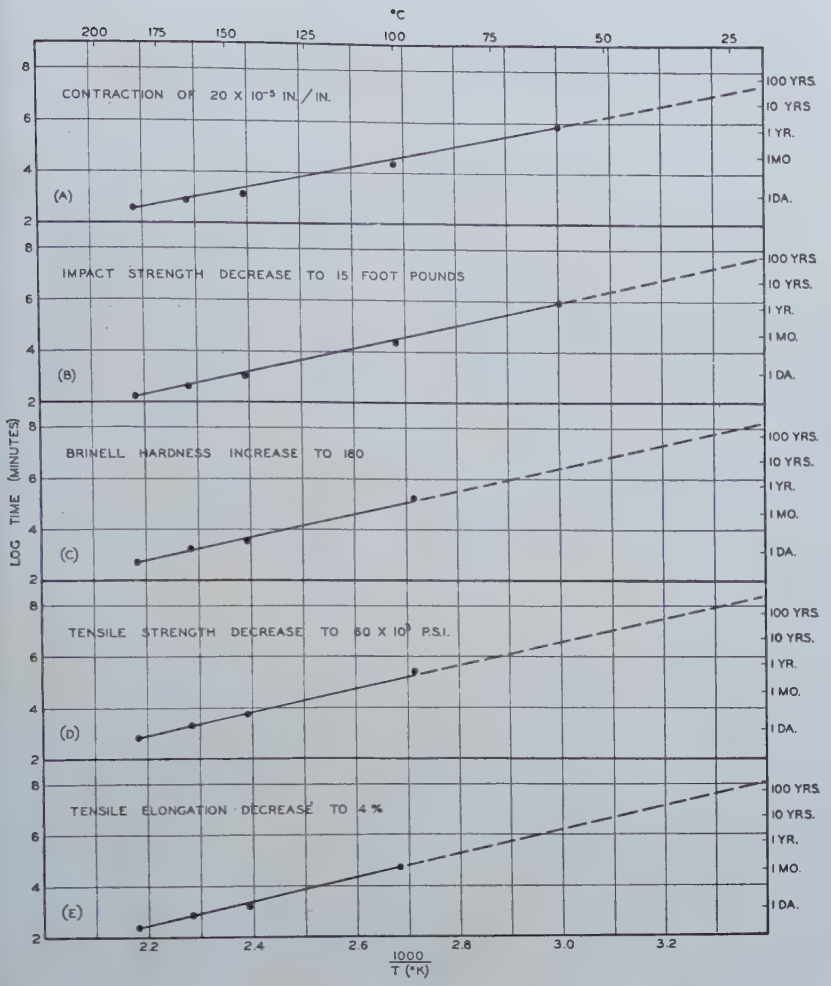

Fig. 3—Effect of aging temperature on time required for various changes in properties in as cast bars.

Log time vs. 1/T plots. Points derived from fig. 2. (A) Contraction, (B) Impact Strength, (C) Brinell Hardness, (D) Tensile Strength, (E) Tensile Elongation.

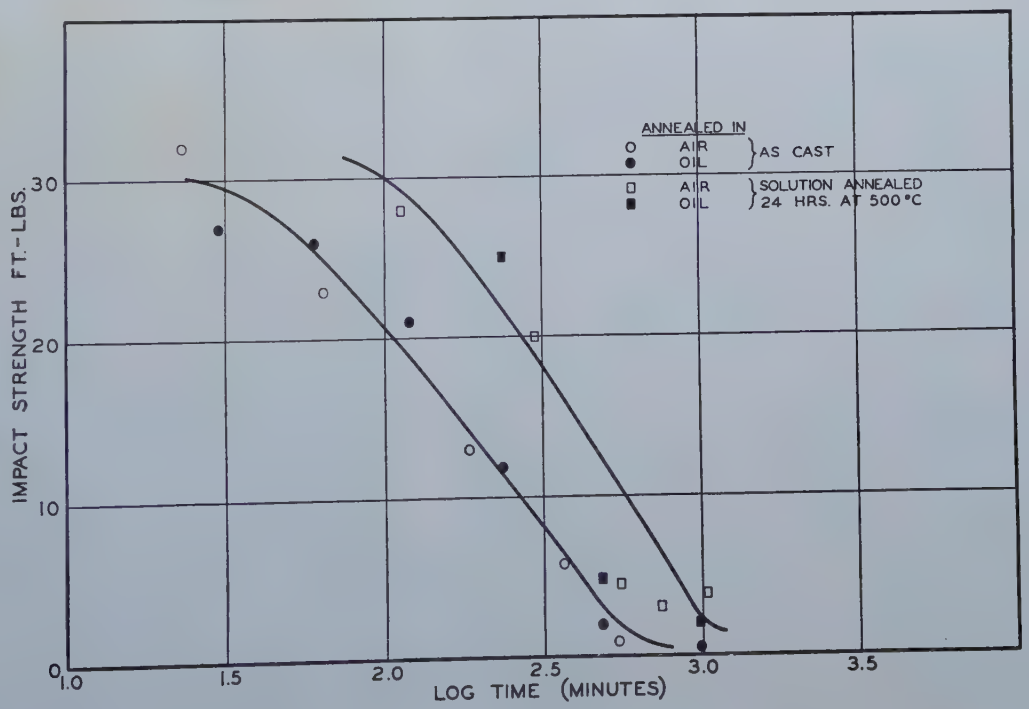

Fig. 4 — Aging curves for a zinc alloy containing 25 pct Mn-15 pct Cu-0.1 pct Al, annealed at 185°C.

Showing the effect of solution heat treatment at 500°C on impact strength.

This displacement of the property curve to the right is also found for other aging temperatures. Fig. 5 shows a comparison of time-temperature relationships of solution annealed and as cast bars for an impact strength drop to 15 ft-lb plotted as log t vs. $1/T$, and illustrates the stabilizing effect of solution annealing. Assuming these curves are parallel, and extrapolating to 25°C, the estimated times for a drop in impact strength to 15 ft-lb are about 70 yr for as cast bars and 140 yr for solution

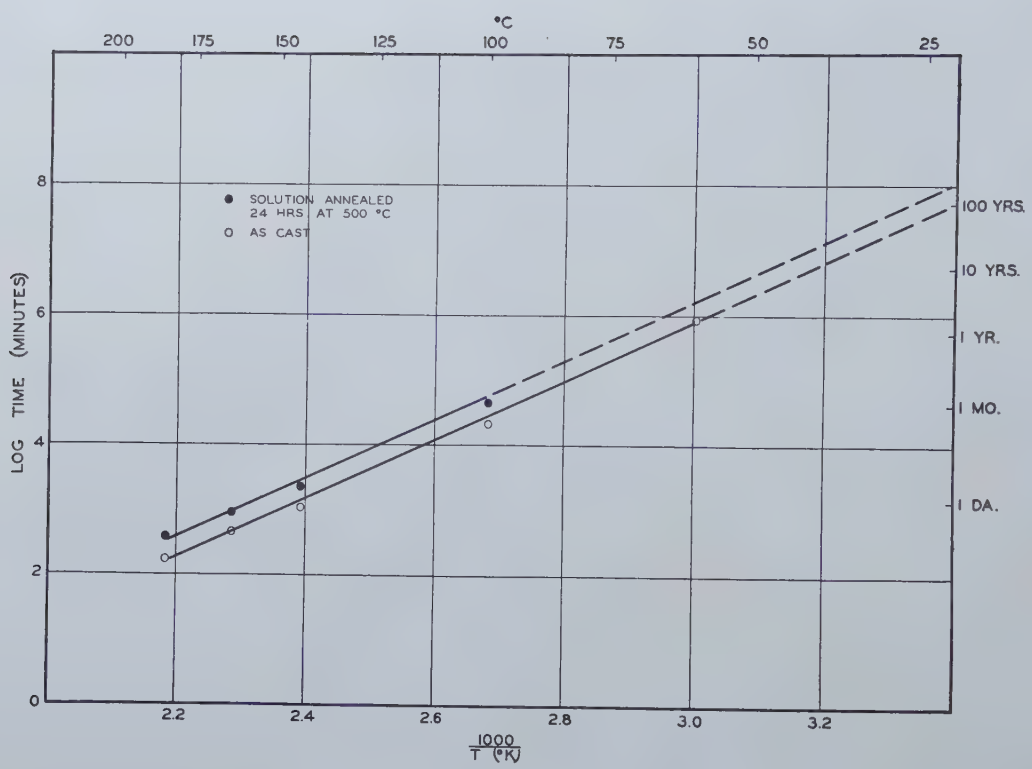

Fig. 5 — Effect of aging temperature on time required for impact strength to drop to 15 ft-lb, for as cast and solution annealed bars.

Log time vs. 1/T plot.

annealed bars, the solution anneal in effect doubling the expected service life.

The experimental data fit reasonably well the equation of Jenkins and Bucknall[3]:

$$t = K \cdot 10^{m/T} \qquad [1]$$

or in more convenient form,

$$\log t = \frac{m}{T} + \log K \qquad [2]$$

for the time required to attain maximum hardness and tensile strength in the aging of nickel-silicon-copper alloys, where t is the time required for a certain property change at temperature T (absolute), and m and K are constants. This, as others have observed, is analogous to the equation for the variation of the diffusion coefficient D with temperature,

$$D = A \cdot e^{-\frac{Q}{RT}} \qquad [3]$$

where Q is the activation heat of diffusion; T, the absolute temperature; R, the gas constant; and A, a constant.

As a matter of interest the derived Q values from the analogous diffusion equation were calculated from the curves in fig. 3 and are given in table III. This quantity has been identified as Q', heat of precipitation. No significance is attached to those values except insofar as they are an indication of a general mechanism involving diffusion by which the changes occurred, and are interrelated.

Table III. Comparison of Q′ Values, "Heats of Precipitation", Derived from Curves in fig. 3

Property Change Plotted	Heat of Precipitation, Q′, Cal per g Atom
Tensile strength decrease to 60,000 psi	20,800
Tensile elongation decrease to 4 pct	21,200
Impact strength decrease to 15 ft-lb	20,900
Brinell hardness increase to 180 Bhn	20,700
Contraction of 20x10^{-5} in. per in.	18,400

As indicated by the Q' values the slopes of these curves are quite similar, lending confidence that such property changes give a reliable measure of the aging rate.

This analysis while useful in predicting aging rates does not aid in understanding the mechanism of the aging process, and the data do not permit calculation of nucleation or growth rates.

Summary

In the aging of a zinc alloy containing 25 pct manganese, 15 pct copper and 0.1 pct aluminum the effect of time and temperature on changes of impact strength, hardness, tensile strength, tensile elongation and contraction can be expressed as:

$$\log t = \frac{m}{T} + \log K$$

which gives essentially linear plots of log t vs. $1/T$. This relationship has been useful in estimating the aging rates of the alloy at temperatures below those of the range investigated (60°-185°C).

The analogy between aging behavior and diffusion has been noted, and Q values derived from aging rate curves show some agreement, ranging from 18,400 to 21,200 for the various property changes studied.

Acknowledgment

The authors wish to express their appreciation for the assistance of other members of the Technical Department of The New Jersey Zinc Co. (of Pa.) in carrying out the experimental work.

References

[1] J. B. Austin and R. L. Rickett: *Trans.* AIME (1939) **135**, 396.
[2] W. D. Robertson: *Trans.* AIME (1946) **166**, 216.
[3] C. H. Jenkins and E. H. Bucknall: *Jnl. Inst. Met.* (1935) **57**, 141.
[4] L. K. Jetter and R. F. Mehl: *Trans.* AIME (1943) **152**, 166.
[5] R. F. Mehl: *Trans.* AIME (1944), **156**, 325.
[6] U. S. Pat. 2,272,390, Feb. 10, 1942.

Self-diffusion in Alpha and Gamma Iron

by C. E. Birchenall and R. F. Mehl

The self-diffusion coefficients for alpha and gamma iron have been measured from 720 to 1357°C. The data approximately obey $D\alpha = 2.3 \times 10^3 e^{-73200/RT}$ and $D\gamma = 5.8 e^{-71200/RT}$, although there is evidence for curvature of the log D vs. 1/T plot for alpha iron. An appreciable grain size effect was noted.

SINCE Maxwell[1] first considered the self-diffusion process in 1872 its importance in the kinetic theory of matter has been recognized. Until the discovery of isotopes in 1913, a direct measurement of this quantity seemed impossible. The only information that could be gathered indirectly was for gaseous systems for which the kinetic theory was well developed. When methods of direct observation became available, investigations on self-diffusion were carried out in condensed phases. In metals these data are presumably of potential importance in the study of recovery, recrystallization, creep, sintering, and related phenomena.

C. E. BIRCHENALL is a Member of Staff, Metals Research Laboratory, Carnegie Inst. of Technology, Pittsburgh, Pa.

R. F. MEHL, Member AIME, is Director, Metals Research Laboratory, Head, Dept. of Metallurgical Engineering, Carnegie Inst. of Technology.

AIME New York Meeting, Feb. 1950.

TP 2752 E. Discussion (2 copies) may be sent to Transactions *AIME before Apr. 1, 1950, and will be published Nov. 1950. Manuscript received Oct. 17, 1949.*

Following the pioneer work of Von Hevesy[2] and his collaborators, who determined the rate of self-diffusion in lead with the naturally occurring thorium B isotope, several metals have been investigated. Pb, Ag[3], Au[4, 5], and Cu[6, 7, 8, 9] are examples of isotropic crystals existing in only one phase modification. Anisotropy of diffusion has been demonstrated in Bi[10] and Zn[11]. This paper is a study of a single metal in two allotropic forms and also of self-diffusion in a body-centered cubic lattice.

Despite the fact that the measurements in each of the papers cited on self-diffusion in copper seem to be internally consistent to about 10 to 15 pct, the curves reported by different authors differ by factors of 2 to 4 at the same temperatures. This uncertainty may account, in part, for the failure to establish a successful correlation between the self-diffusion rates and other physical characteristics of the metals. No satisfactory theory of metallic self-diffusion has as yet been proposed to account for all the existing data and to permit estimation in other metals.

Experimental Part: Two units of radioactive iron were used in these experiments, each a mixture of Fe^{55} and Fe^{59} [12]. Fe^{55} decays by K electron capture and the emission of an X ray with a half life of about 4 years. Fe^{59} emits two beta spectra, one with a maximum energy of 0.26 Mev, the other 0.46 Mev, and gamma rays of 1.1 and 1.3 Mev, with a half life of about 44 days. They were present in nearly equal concentration initially. The composite half life started at about 50 days and increased as the Fe^{59} decayed, leaving Fe^{55} relatively more abundant. After aging a year, the half life was too long to measure significant decay in a month. The absorption properties also changed with time. Because of the importance of the absorption coefficient in the diffusion calculations, it was necessary to determine this quantity frequently over the period during which these experiments were carried out. This correction was unsuspected at the time of publication of notes[13] on this work and accounts for the discrepancy in alpha iron and for part of the discrepancy in gamma iron.*

* The data in the present paper supersede those given in the notes entirely. In one note the scale of log D was inadvertently reversed. In addition to the correction for the drift in absorption coefficient, the D values for gamma iron at low temperatures were high owing to insufficient correction for diffusion occurring during heating and cooling through the high temperature part of the alpha range at a rate much slower than that employed in the runs reported here. The high temperature alpha rates are much higher than the low temperature gamma rates and correspond to large equivalent times at these temperatures. These experiments were discarded and new measurements taken.

Independent experiments with the same activity units indicated a radioactive contaminant in the iron, but exhaustive attempts to isolate and identify it chemically failed. These experiments† indicate that the contaminant represented only a trace of little importance in the diffusion results.

† These experiments will be discussed in a later publication from this laboratory.

The active iron was plated from an iron chloride solution. Enough of the solution was dropped on a 1½ in. square of filter paper to wet it thoroughly.

The paper was then placed on a platinum sheet anode and a circular iron disk of 1 in. diam and ¼ in. thickness placed on the paper. Active iron was plated upon the iron surface by passing a current through this assembly. The thickness of the plate, based on the measured activity, was of the order of 0.02 microns or less. This could be considered an infinitely thin layer, since average diffusion distances were about 50 microns.

The iron disks used in most of these experiments were machined from a 1 in. square forged bar of electrolytic iron melted under hydrogen ("Westinghouse puron"), containing oxygen as principal impurity and no other contaminants in more than trace amounts. The faces were ground parallel and one face of each disk was polished to 4-0 emery paper before plating. The plated disks were counted for surface activity using a bell-type, thin mica window beta counter in a scale of sixty-four counting circuit. At first, points were taken over a period of two weeks or more to establish the decay line with considerable certainty, the samples counting at a rate between 1000-5000 counts per min above background. Later it became possible to decrease the number of counts taken. Concurrent control samples were counted to determine the change in half life with time.

Two disks of nearly the same surface activity were placed face to face without added pressure in a porcelain tube furnace to minimize vaporization losses. While the furnace was heating, it was alternately evacuated to about 10^{-5} cm and flushed with purified hydrogen. A charge of hydrogen (usually the third) at slightly greater than one atmosphere pressure was allowed to remain in the furnace tube during the diffusion heat treatment. The furnace was cooled to room temperature before the samples were removed, except in one or two runs where hot samples were quenched in methanol.

For good results on gamma diffusion, samples had to be introduced into a furnace at temperature and quenched out at the end of the run to avoid large additional diffusion, (see footnote, p. 144), in the heating and cooling through the alpha range. During this process the grains of the specimens frequently grew to diameters of 1 to 2 mm and were easily visible to the naked eye. If the samples had not oxidized during the heat treatment they could be separated with no difficulty. If appreciable oxidation had occurred, separation could be accomplished only by force. These latter samples were discarded. Oxide films were readily visible when present.

After diffusion, the samples were again counted for a period to establish the decay line, counts now falling in the range 350 to 3000 counts per min above background. A plot of logarithm of activity versus time was made and the decay lines before and after diffusion were extrapolated to some intermediate time. Values read directly from these curves gave the fraction of activity detectable at the surface after diffusion. Each point represents an average for the two disks.

Steigman, Shockley, and Nix[6] have given a mathematical analysis relating the decrease in surface activity to the diffusion coefficient, D, and the absorption coefficient, μ, for the radiation in the metal. If the disk is thick compared to the depth of penetration of the diffusing atoms, the fraction, F, of activity observed at the surface after diffusion is given to a very good approximation by

$$F = e^{z} \left[1 - \theta \left(\sqrt{Z} \right) \right] \qquad [1]$$

where θ is the Gauss error integral and

$$Z = \mu^2 Dt \qquad [2]$$

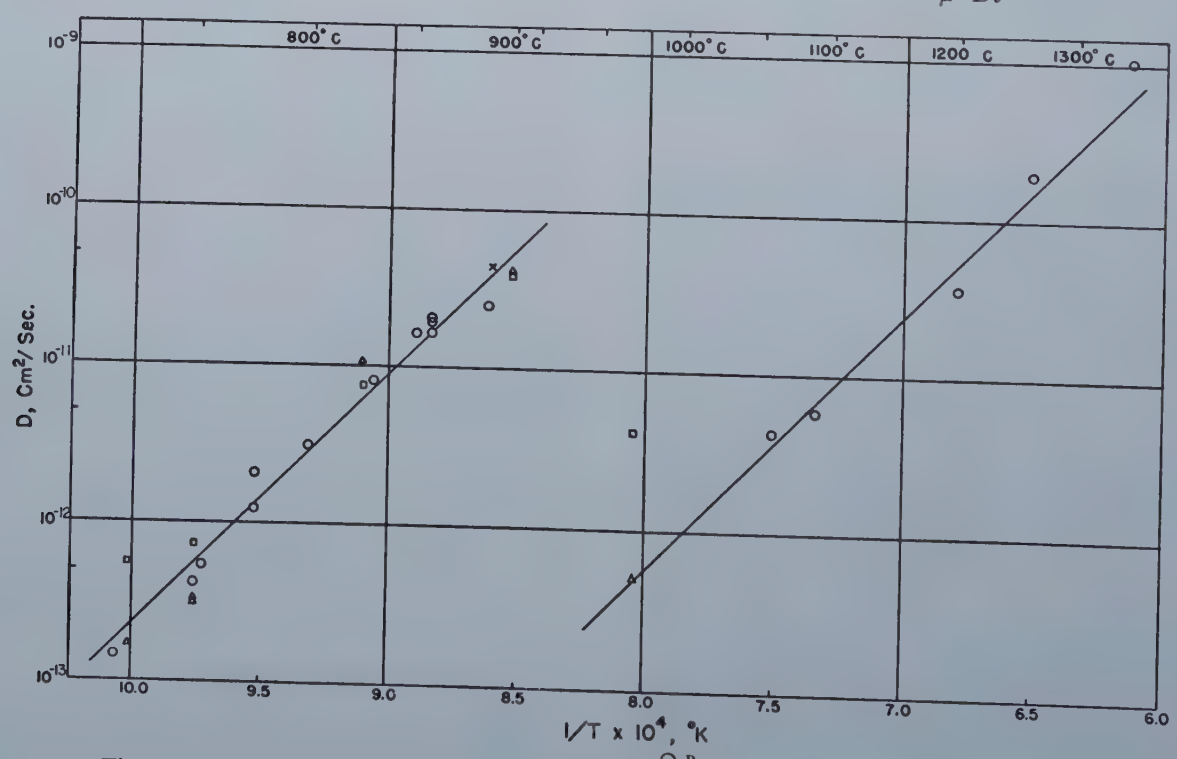

Fig. 1—Self-diffusion in alpha iron.

where t is the time for which the sample was held at the diffusion temperature. It is convenient to make a table of F versus Z; from this, when F is determined, Z may be read off.

The use of Eq 1 and 2 requires that the measured activity decrease exponentially with absorber thickness at least to the depth where contributions to the measured activity after diffusion from the penetration curve will be relatively small. This will depend to some extent upon the counting equipment and geometry. The absorption curves measured here were found to satisfy these conditions.

The absorption coefficients were measured for aluminum, the effective coefficient indicating the proportion of betas and X rays being counted at a given time. The mass absorption coefficient for betas is nearly the same for aluminum and iron. However, it differs for X rays. This contribution was calculated for iron and an effective absorption coefficient for iron was obtained by combining this with the beta contribution.

Although μ was determined frequently, great precision cannot be claimed for the factor, and the error in μ^2 (and D) from this source may be of the order of 15 to 20 pct for individual points. The values for μ^2 are higher and more precise than the lower ones since they involve a greater number of measurements. Also the beta activity had become very small, and the X rays remaining obey the conditions for the use of Eq 1 and 2 precisely.

Temperature control of the furnaces was maintained with automatic controllers operating on platinum, platinum-rhodium thermocouples inserted in the heating coil. The sample temperatures were measured with chromel-alumel couples for low temperature runs and Pt, Pt-Rh for the highest temperatures, sheathed in silica tubes, inserted to a point in the heating chamber directly above the sample. This procedure was established after chromel-alumel couples used in early runs in contact with furnace atmosphere showed rapid deterioration.

Uncertainties in temperature measurement and control for most runs are probably of the order of 3°C although a few runs involve somewhat greater uncertainty, especially in the upper gamma range. Counting errors, including the statistical errors, reproducibility of geometry, etc., probably aggregate to about 3 pct. The precision in the measurement of time greatly exceeds that for the other factors. An estimated overall uncertainty cannot be based upon these factors alone since the plated surfaces showed extreme susceptibility to oxidation and were easily damaged in handling. In addition, it should be noted that excellent internal consistency was attained by the observers of the self-diffusion coefficients of copper though they disagreed markedly between themselves. These discrepancies do not seem to depend upon the method of observation, that is, whether the decrease in surface activity was measured or whether the sample was sectioned by machining layers to determine the penetration curve, since there seems to be little correlation of the relative values with method used. The purity factor seems to have little effect in copper according to both Maier and Nelson[8] and Steigman, Shockley, and Nix.[6] Maier and Nelson found grain size effects to be very small and in the direction opposite to the expectation of faster intergranular diffusion, while Steigman, Shockley, and Nix detected no trend at all. Nor does it seem likely that all of the discrepancy can be ascribed to errors in determining absorption coefficients. Two of the series[7, 8] were determined by sectioning methods which would be insensitive to this factor. The other two may suffer from this source of error. Further, Seith and Keil[14] found no grain size effect in lead self-diffusion. Until

Table I. Self-diffusion in Alpha Iron

No.		T °C	t (sec.)	F	Z	μ^2	D	$1/T$	Material
1		720	11.2×10^5	0.782	0.055	3.32×10^5	1.48×10^{-13}	10.07	Puron*
2		755	6.91	0.689	0.137	3.71	5.33	9.73	Puron
3		800	5.20	0.510	0.550	3.42	31.0	9.32	Puron
4		830	3.60	0.417	1.08	3.73	80.3	9.07	Puron
5		850	3.84	0.325	2.18	3.45	164	8.90	Puron
6		887	1.476	0.389	1.33	3.64	247	8.61	Puron
7	a	725	9.88	0.609	0.263	4.77	5.59	10.02	Commercial†
	b			0.746	0.0805	4.77	1.71		Carbonyl‡
8	a	825	0.612	0.852	0.022	4.77	75.7	9.11	Commercial
	b			0.828	0.031	4.77	107		Carbonyl
9	a	900	0.072	0.693	0.132	4.77	384	8.53	Commercial
	b			0.684	0.143	4.77	416		Carbonyl
10	a	751	15.6	0.508	0.558	5.00	7.18	9.76	Commercial
	b			0.582	0.324	5.00	4.15		Puron
	c			0.618	0.246	5.00	3.16		Carbonyl
	d			0.614	0.253	5.00	3.26		Carbonyl
11	a	858	0.26	0.614	0.253	5.00	194	8.84	Annealed puron
	b			0.610	0.262	5.00	202	8.84	Cold worked puron
	c			0.634	0.217	5.00	168	8.84	
12	a	776	2.91	0.592	0.300	5.00	20.6	9.53	Annealed puron
	b			0.658	0.178	5.00	12.2	9.53	Cold worked puron

* Puron—Electrolytic iron melted under hydrogen and forged into a 1 in. square bar by Westinghouse Electric Co. Contains about 0.04 pct oxygen, 0.005 pct carbon, 0.004 pct nitrogen, 0.003 pct sulphur, 0.0015 pct nickel and no other impurities exceeding 0.001 pct. Iron by difference, 99.95 pct.

† Commercial iron sheet—20 ga sheet of Carnegie-Illinois special killed steel. Contains 0.30 pct manganese, 0.067 pct carbon, 0.03 pct chromium and sulphur, 0.02 pct nickel and copper, 0.009 pct silicon and 0.005 pct phosphorus.

‡ Carbonyl iron—Reduced in hydrogen for 750 hr at 1200°C. A similar sample gave: 0.01 pct carbon, 0.04 pct nickel, 0.006 pct copper, 0.003 pct oxygen, less than 0.001 pct nitrogen and 0.0004 pct hydrogen. Chromium, tin and molybdenum aggregated less than 0.005 pct. No manganese, silicon, phosphorus, or sulphur was detected.

Table II. Self-diffusion in Gamma Iron.

No.		T °C	t (sec.)	F	Z	μ^2	D	$1/T$
1		1357	0.398×10^4	0.321	2.27	5.10×10^5	1120×10^{-12}	6.13×10^{-4}
2		1260	0.840	0.453	0.831	5.10	194	6.51
3		1200	2.85	0.518	0.519	5.10	35.6	6.78
4		1090	1.92	0.817	0.0362	3.22	5.87	7.33
5		1058	41.3	0.441	0.908	5.10	4.32	7.51
6	a*	970	30.0	0.756	0.0726	4.77	0.51	8.04
	b†	970	19 8	0.556	0.394	4.77	4.16	8.04

* Carbonyl iron.

† Commercial sheet.

the reason for these large discrepancies has been ascertained it appears idle to ascribe great accuracy to any set of self-diffusion measurements. The average uncertainty in the individual points given here is estimated to be about ± 25 pct, based upon the known sources of error. The log D vs. $1/T$ line should be much more precise than this.

Data: Table I records the data for alpha iron, the first six items representing pairs of puron disks, the following groups representing two or more pairs of samples run simultaneously to investigate the dependence of the diffusion coefficient on the source of iron or the effect of cold work prior to diffusion. The cold work studies will be discussed by Ruder.[15] The table has columns in the following order: a number to identify the run, the temperature in degrees centigrade, the time in seconds, the fraction of initial activity observed after diffusion, Z calculated from F by Eq 1, the square of the absorption coefficient at the time of the run, the diffusion coefficient calculated from Eq 2, the reciprocal of the absolute temperature, and identification of the material used in the run. In addition to these samples, one welded couple was also run. The sections cut parallel to the weld interface were counted in the form Fe_2O_3. The resulting point is given in fig. 1; the data are plotted in fig. 2 for comparison with the penetration curve calculated for $D = 4.4 \times 10^{-11}$ cm^2 per sec.

Table II gives the same record for gamma iron. All of these samples were puron except pairs 6*a* and 6*b*; these were run simultaneously in order to be as closely comparable as possible. The difference in time given for 6*a* and 6*b* arises from the correction for heating and cooling through the alpha range. An equivalent time was calculated on the basis of the alpha curve to give the same penetration at temperature. Had the two sets shown the same diffusion coefficient at temperature the time corrections would have been the same. As mentioned earlier, this correction was minimized on all other gamma samples by introducing them into a furnace at temperature and quenching at the end of the run.

All data from the tables are plotted in fig. 1 as log D against the reciprocal of the absolute temperature, corresponding to the Arrhenius equation

$$D = D_0 e^{-Q/RT} \qquad [3]$$

where Q is called the activation energy, D_0 the frequency factor, R the gas constant, and T the absolute temperature.

Inserting the values from the curves in fig. 1 leads to the following equations in the above form:

Alpha iron: $D\alpha = 2.3 \times 10^3 e^{-73200/RT}$

Gamma iron: $D\gamma = 5.8 e^{-74200/RT}$

Discussion of Results

Fig. 1 shows that at high temperatures in α Fe self-diffusion data in the three sources of iron are in good agreement. However, as the temperature declines the divergence becomes quite large. The hydrogen reduced carbonyl iron, which is the purest and the largest in grain size, gives the lowest self-diffusion rates. Puron, intermediate in grain size and purity, falls above this. The highest rates were observed in the fine grained commercial steel.

Two pairs of disks, 6*a* and 6*b*, were run at 970°C in the gamma range; 6*a* was of carbonyl iron, 6*b* of commercial sheet. The carbonyl iron point seems to be in excellent agreement with the puron samples run at higher temperatures, falling on the extrapolated curve for puron, but the commercial iron gave a much higher value. Since the heating and cooling correction was large, the agreement for 6*a* and the puron samples may be fortuitous. It was also observed that the initial large grains of carbonyl iron (6*a*) recrystallized during the cycle to produce much finer grains. There was no way to decide whether either of these corresponded to the grain size at temperature, so no further studies of this kind were attempted in the gamma range.

On the alpha iron curve four sets of points are of interest. At 900°, 825°, and 725°C runs were carried out using a pair of carbonyl iron samples and a pair of commercial steel disks. At the highest temperature the two sets gave nearly identical results; at the intermediate temperature the separation was greater but of the order of the experimental scatter observed, the carbonyl iron giving the higher result. At the lowest temperature the difference seemed too great to be experimental error, and the carbonyl iron, with the largest grain size, was much the lower.

To check this last point a group of four pairs of samples was run at 750°C in the alpha range. One pair was puron (10*b*), another commercial iron (10*a*), and the remaining two sets of carbonyl iron had different grain sizes. One of the carbonyl iron sets had grains of an average diameter of 5 mm (10*c*), but the other set (10*d*), had recrystallized when heated into the gamma range in an earlier experiment to produce surface grains of about one tenth this diameter. The surfaces were machined to remove the radio-iron, repolished and replated with active iron. After diffusion the radioactive layers were again machined off, the faces polished to 4/0 paper and etched with 3 pct nital. The 10*d* faces showed chiefly large grains like the other set although a few were broken into fine grains. The back faces were all fine grained with diameters averaging about 0.5 mm. At this point the whole sample was about 1/16 in. thick. It is not certain whether diffusion in this set of samples was in the fine grained or large grained part, so great weight cannot be given to this.

The results for the two sets of carbonyl iron disks (10*c*, *d*) were indistinguishable, the puron (10*b*) was higher and the commercial iron (10*a*) was much higher. This leaves little doubt that in the lower part of the alpha range (and probably in the lower part of the gamma range) where the volume diffusion coefficient is very low, a large part of the diffusion may occur in grain boundaries.

It has been mentioned that in lead and copper self-diffusion, no grain boundary diffusion effect has been observed. In carbonyl iron a possible ten fold decrease in grain diameter produced no difference. But in puron and a commercial iron a marked in-

crease was noted. There are two possible contributing factors which vary from one iron to the other: grain size and purity. The two are not unrelated for it would be a major feat to grow 5 mm grains in the commercial sheet.

The lack of grain size effects in very pure metals (carbonyl iron, lead, copper) and their presence in less pure metals and many alloys may possibly be explained in the following way: A grain boundary in a very pure metal must be very similar to intragranular regions, offering little increase in mobility to the atoms in its vicinity. However, it may act as a site for the accumulation of dissolved impurities whose presence modifies its properties out of proportion to their overall concentration. Inspection of the diffusion literature arouses the suspicion that some of its inconsistencies arise in this manner.

This is not a new idea, nor is it without parallel support. Measurements on anelasticity[16] show that grain boundary relaxation sometimes has an activation energy very near that for volume diffusion, indicating that the grain boundary may not differ markedly from the bulk material with respect to the mobility of atoms. It would be desirable to know, however, which impurities are surface active, i.e., reduce the surface tension of the metal, and which are the converse. The technique used for pure copper by Udin, Shaler, and Wulff[17] might be useful for this. A direct measurement of concentration in grain boundaries might be obtainable in extreme cases by autoradiography using radioactive impurities.

Rhines and Mehl[18] have suggested that the diffusion rates in dilute alpha solid solutions of copper approximate the copper self-diffusion rate. Further support for this principle and a discussion of its limitations have been given by Thomas and Birchenall.[19] It is interesting and informative to compare the self-diffusion rates for iron with the rates of diffusion of molybdenum,[20] manganese,[21] and nickel[22] in iron when the solute is dilute or when the concentration dependence curves are extrapolated to very dilute solution. Such a comparison is available in fig. 3. In all these cases except molybdenum in gamma iron solubility is appreciable. This exception represents the largest displacement from the self-diffusion curve. The manganese and nickel curves lie very close to that for gamma self-diffusion except for a lower activation energy. The alpha iron self-diffusion curve agrees well with molybdenum diffusion by extrapolating to common intermediate temperatures. This overall agreement must be regarded as good support for the absolute values of the sets of diffusion data involved.

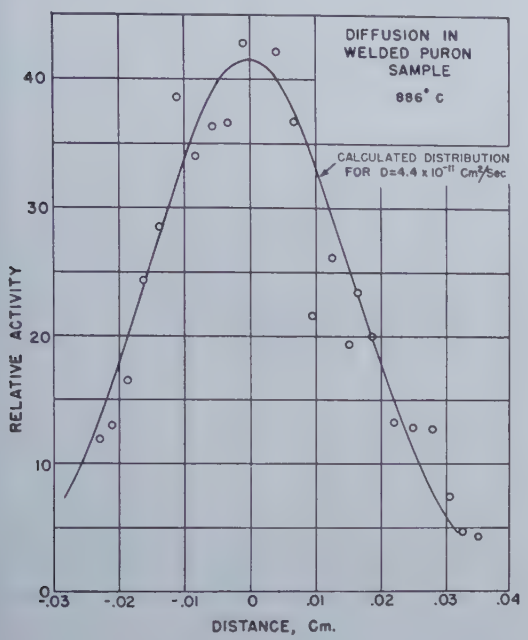

Fig. 2—Penetration Curve for welded puron sample.

The solid line is calculated for $D = 4.4 \times 10^{-11}$ cm² per sec. The points are experimentally determined.

At the transformation temperature, 910°C, the self-diffusion coefficient of alpha iron is about 660 times as large as that for gamma iron. For molybdenum the rate is about 100 times faster, while Stanley finds that for carbon the factor is about 400. Though of the same order of magnitude the differences are appreciable. No explanation can be given at this time to account for the size of the factor or its variation with composition, but it seems reasonable to expect higher rates in the less closely packed system.

Within the experimental error the activation energies in the two phases are in agreement, although the difference is of about the same magnitude and direction as that reported by Ham for molybdenum diffusion. Inspection of the data for alpha iron, both self-diffusion and molybdenum diffusion, and the higher activation energy obtained by Kê[16] for grain boundary relaxation in iron at 490°C suggests that log D may not be a linear function of the reciprocal of the temperature over a wide range of temperatures. Such a curve is necessary to fit all of the self-diffusion data for lead.

The tentative equations of Cohen,[32] Bakalar, and Buffington fall within the range of the data given

here although the slopes of the curves differ considerably.

Summary

1. Self-diffusion coefficients have been measured for alpha and gamma iron over the temperature range 720° to 1357°C.
2. At the transformation temperature the rate is about 660 times faster in alpha iron than in gamma iron.
3 The activation energies were found to be 73 k cal per mol for alpha iron and 74 k cal per mol for gamma iron. This difference is probably less than the experimental uncertainty.
4. A grain size effect was noted at the lower temperatures studies in the alpha range (and perhaps at the lowest temperature in the gamma). This effect may be related to the purity of the material used.
5. The data agree well with the rates of diffusion of molybdenum, manganese and nickel in dilute solution in iron.

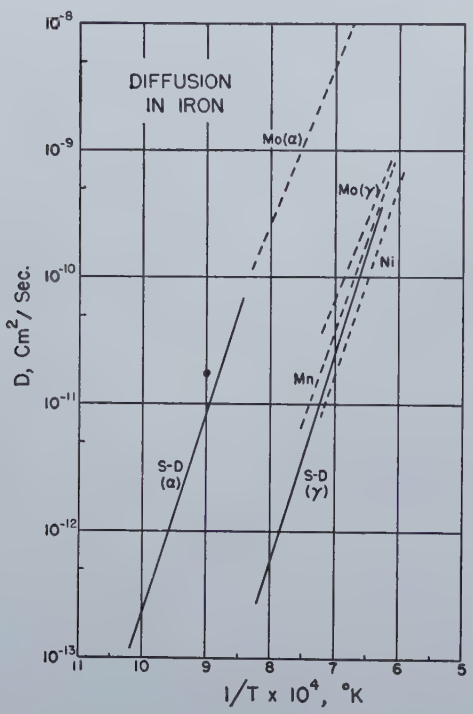

Fig. 3—Diffusion in dilute solution in iron compared with self diffusion.

Mo, ref. 20. Mn, ref. 21. Ni, ref. 22.

Acknowledgments

The authors are grateful to the Office of Naval Research for their support of this work. The radioactive iron used in this investigation was obtained from the Isotopes Division, U. S. Atomic Energy Commission.

The counting was carried out by a staff first under the direction of Dr. C. Schwob and later under L. F. Gronholz. Assistance in making several runs was provided by W. Batz, R. C. Ruder, and Miss Helen Burgess. The authors gratefully acknowledge this help. Special thanks are due to Dr. Morris Cohen, M.I.T., for discovering an error in the absorption coefficients used in calculating the results given in the original manuscript.

References

[1] C. Maxwell: Theory of Heat. (1872). Longmans, Green (1921).

[2] G. von Hevesy: *Trans.* Farad. Soc. (1938) **34**, 841.

[3] W. A. Johnson: *Trans.* AIME (1941) **143**, 107.

[4] A. M. Sagrubskii: *Phys. Ztsch. Sowjetunion* (1937) **12**, 118. *Bull.* Acad. Sci. U.S.S.R., Classe sci. math. nat., Ser. phys. (1937), No. 6, 903.

[5] H. A. C. McKay: *Trans.* Farad. Soc. (1938) **34**, 845.

[6] J. Steigman, W. Shockley and F. C. Nix: *Phys. Rev.* (1939) **56**, 13.

[7] B. V. Rollin: *Phys. Rev.* (1939) **55**, 231.

[8] M. S. Maier and H. R. Nelson: *Trans.* AIME (1942) **147**, 39.

[9] C. L. Raynor, L. Thomassen, and L. J. Rouse: *Trans.* A.S.M. (1942) **30**, 313.

[10] W. Seith: *Ztsch. Elektrochem.* (1933) **39**, 538.

[11] P. Miller and F. Banks: *Phys. Rev.* (1942) **61**, 648.

[12] U. S. Atomic Energy Commission, Isotopes Branch: Catalog and Price List No. 2. Revised Sept. 1947.

[13] C. E. Birchenall and R. F. Mehl: *Jnl. Appl. Phys.* (1948); *Mining and Metallurgy* (1947).

[14] W. Seith and A. Keil: *Ztsch. Metallkunde* (1933) **5**, 104.

[15] R. E. Ruder: To be published.

[16] T. S. Ke: *Jnl. Appl. Phys.* (1949) **20**, 274.

[17] H. Udin, A. J. Shaler, and J. Wulff: *Trans.* AIME (1949) **185**, 186. *Jnl. of Metals,* Feb. 1949.

[18] F. N. Rhines and R. F. Mehl: *Trans.* AIME (1938) **128**, 185.

[19] D. E. Thomas and C. E. Birchenall: To be published.

[20] J. L. Ham: *Trans.* A.S.M. (1945) **35**, 331.

[21] C. Wells and R. F. Mehl: *Trans.* AIME (1941) **145**, 315.

[22] C. Wells and R. F. Mehl: *Trans.* AIME (1941) **145**, 329.

[23] M. Cohen, D. Bakalar and F. S. Buffington: Reported by F. V. Lenel: *Metal Progress* (1949) **56**, 576.

Plastic Deformation

in the Rolling Process

by B. L. Averbach

The distribution of principal strains within a bar after a 20 pct rolling reduction was determined by radiographing a lead grid imbedded in a cast tin bar. Axial and vertical principal strains of about the same magnitude and direction as those reported by others at the surface of a bar were observed in the interior. The lateral principal strain, however, changed from tension at the center of the bar to compression midway between the center and the outside in a section perpendicular to the roll axis.

THE rolling process may be considered as a case of a nonhomogeneous plastic flow. In such a heterogeneous deformation there is no direct general solution, and the plastic deformation varies from point to point as a function of the coordinates. It is practicable to determine these plastic strains only at the conclusion of the rolling process, and the local strains can be studied by observing the deformations produced in a suitably placed grid system.

B. L. AVERBACH is Asst. Professor, Dept. of Metallurgy, Mass. Inst. of Technology, Cambridge, Mass.

AIME New York Meeting, Feb. 1950.

TP 2761 E. Discussion may be sent to Transactions *AIME before Apr. 1, 1950, and is scheduled for publication Nov. 1950. Manuscript received Sept. 30, 1949.*

Strains at the surface of a bar after rolling have been reported by MacGregor and Coffin,[1] but the strain distributions within the bar have not been previously observed. Siebel[2] has investigated the plastic deformations resulting from wire-drawing by splitting the wire along its axis, milling a grid coordinate system on the inner plane surfaces, and binding the wire together so that it would pull through a die as a single unit. This method was possible because of the rotational symmetry of the die. In the rolling process, however, such a system was not readily applicable. This paper describes another method of including a grid system, and reports some preliminary data on the plastic rolling strains within a square bar.

Experimental Procedure

A network grid containing squares approximately 2.1 mm wide (144 network squares per sq in.) was punched from a thin lead sheet with a steel die and supported in a brass mold by thin copper wires. Pure tin was then poured around the grid to form a solid bar, with the network securely imbedded at a given position. This bar was then machined to a square 15.2 mm (0.60 in.) wide, and then radiographed.

The lead grid was quite adherent and sufficiently ductile to follow the deformation of the bar faithfully. The network lines also remained sharp enough to maintain a high radiographic contrast, and the tin bar, with the grid included, could withstand considerable deformation at room temperature without splitting at the interface. In order to fill the mold, it was necessary to cast the tin at 260-280°C and during pouring the lead grid was supported at short intervals to prevent warping. Some shrinkage cavities were encountered, but only bars which were free of shrinkage in the network region were used. This method is similar to the one employed by Steinberg[3] in an investigation of the strain distribution in a tensile specimen.

Before rolling, the machined bars were radiographed in two directions to obtain accurate initial dimensions of each square and to observe whether the grid was straight and correctly positioned. The rolling was performed in a small hand mill with 2 in. diam rolls at room temperature, and a 20 pct reduction based on the original height was employed. The rolls were clean and no lubricant was used. Halfway through the bar, at the center of the network, the rolls were reversed and the bar extracted. These bars were then radiographed again

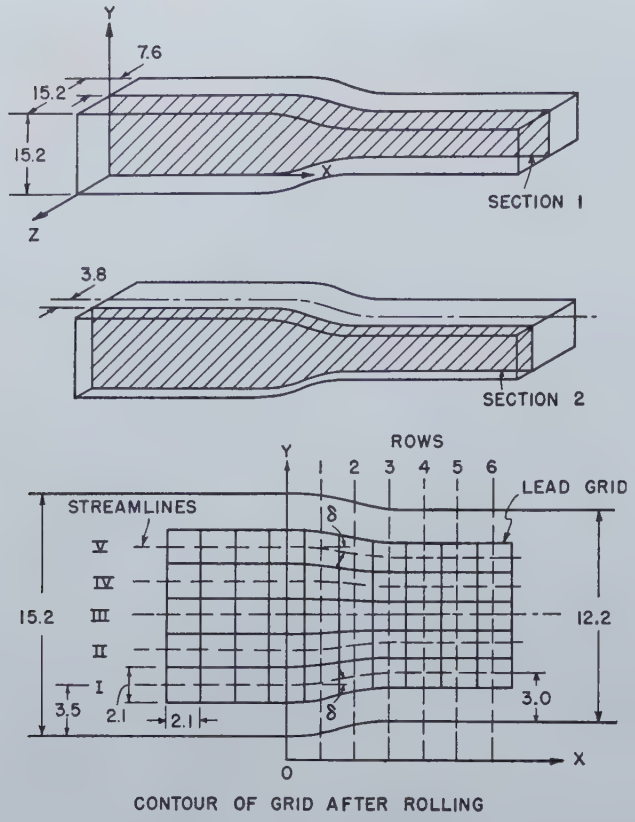

Fig. 1—Positions of lead grid and measuring positions in tin bar after rolling.
All dimensions in mm.

in both directions to detect any warping, and the final dimensions of each grid square after deformation were obtained. Fine-grained X ray film was employed, and the radiographs were enlarged by a factor of four for measurement.

Bars were rolled at the same setting with grids in four different positions. If we define the *X* direction as the longitudinal axial direction of the bar, the *Y* direction as the vertical height, and the *Z*

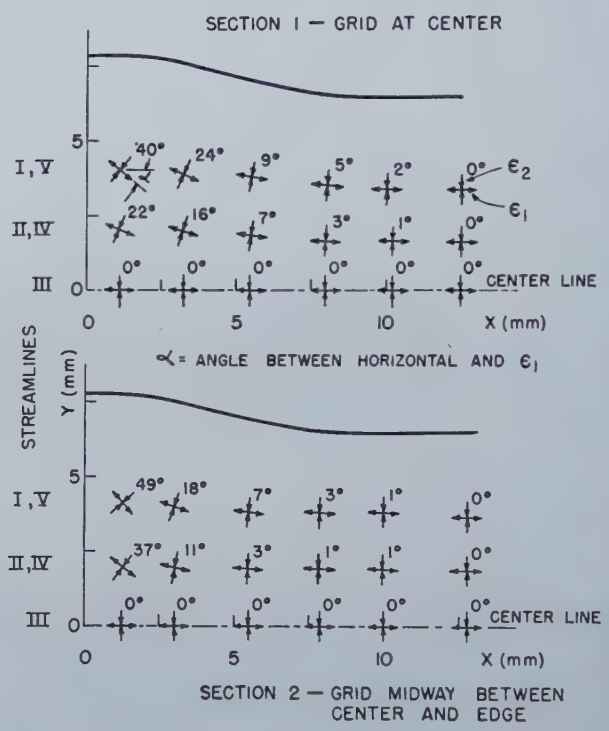

Fig. 2 (above)—Directions of principal strains ϵ_1, ϵ_2.

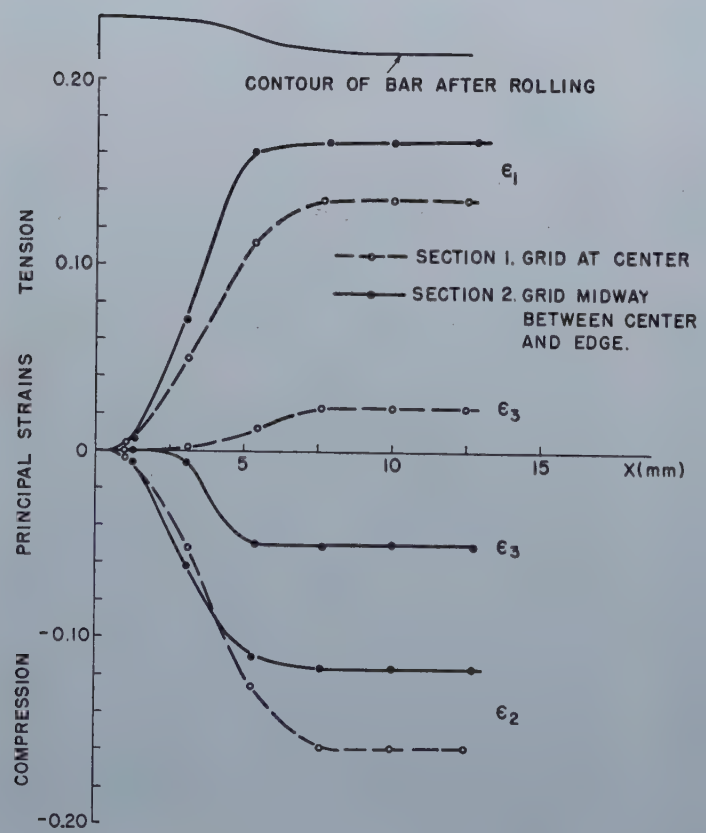

Fig. 3 (left)—Principal strains. Streamline III.

direction as the lateral width, the positions of the grids may be described as follows:

Section 1. *XY* plane at the center of bar, i.e., perpendicular to the roll axis.

Section 2. *XY* plane, 7.6 mm (0.15 in.) from the center line, i.e., midway between the center and the side.

Section 3. *XZ* plane at the center of the bar, i.e., parallel to the roll axis.

Section 4. *XZ* plane, 7.6 mm above the center line, i.e., midway between the center and the top surface.

The lateral strains obtained from Sections 3 and 4 were too small for accurate measurement and all of the computations which follow were taken from Sections 1 and 2. Fig. 1 illustrates the positions of the lead screens, and shows the coordinate system which was used to describe the positions of the deformed network squares. The streamlines were defined as the loci of the centers of consecutive longitudinal squares, and vertical positioning lines were used to define the loci of consecutive vertical rows of squares. The origin for all measurements was taken as the first row of squares which showed no deformation. The longitudinal and vertical strains ϵ_x and ϵ_y were evaluated directly from the radiographs, and the lateral strains ϵ_z were computed on the assumption that the volume does not change as a result of plastic deformation. This is the usual assumption of plastic flow theories, and the strain formulas which were used are listed in the appendix.

The following measurements were made on each network: 1. The initial dimensions of each square of the grid before deformation. 2. The dimensions of each parallelogram after deformation. The bases and heights were measured separately and averaged for each parallelogram. Corresponding parallelograms on each side of the center line were also averaged. 3. The angular distortion or shear angle, δ, was measured for each parallelogram. Since the vertical lines in fig. 1 remained essentially perpendicular to the longitudinal axis after rolling, this angle was taken as the one between the horizontal axis and the deformed axial side of the network squares. 4. The vertical distance of the center of each distorted grid square from the central axis of the bar. 5. The distance of the center of each distorted square along the longitudinal axis of the bar. The origin was taken as the first square without plastic deformation.

Results

None of the grids was warped as a result of rolling and this may be taken to indicate that the lateral principal strain, ϵ_3, is perpendicular to the *XY* plane, i.e., parallel to the roll axis. The natural strains, ϵ_x, ϵ_y, ϵ_z, were calculated from the expressions given in the appendix. The shear strain was then computed for each square from the measured angular distortions, and the angle, α, between the principal strain axis and the horizontal axis was calculated from Eq 5 in the appendix. Mohr's circle was solved for each position, and the principal strains were thus obtained.

Fig. 2 shows the directions of the principal strains ϵ_1 and ϵ_2 at various positions in the bar and the values for the angle α agree quite well with those obtained by MacGregor and Coffin under somewhat different conditions. The values for the principal strains are plotted in fig. 3-5 and the values for ϵ_1 and ϵ_2 are also quite similar to those obtained by MacGregor and Coffin. The values of ϵ_3, however,

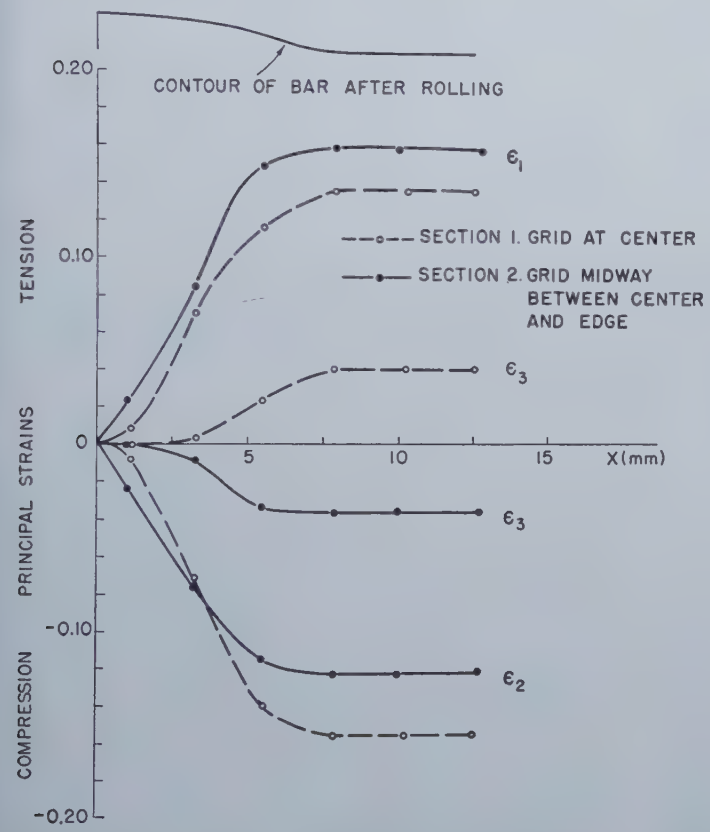

Fig. 4—Principal strains. Streamlines II, IV.

showed an unexpected peculiarity. These strains are, of course, quite small in magnitude since there is very little increase in width as a result of rolling. At the center of the bar (Section 1) there was a small tensional lateral strain, as would be expected. Midway between the center and the side, however, (Section 2) the lateral strain was one of compression although still quite small. The presence of this compressional strain was observed on each of the streamlines and it seems as if the effect must be real. The lateral strains were calculated on the basis that $\epsilon_1+\epsilon_2+\epsilon_3=0$. This relationship would have to be in error by 50 pct to account for the observed compressional lateral strains, and deviations of this magnitude have not been observed. The values for the lateral strains are also well beyond the experimental error. It is to be emphasized, however, that these grids were comparatively large and that a more precise survey with a final grid system would be in order.

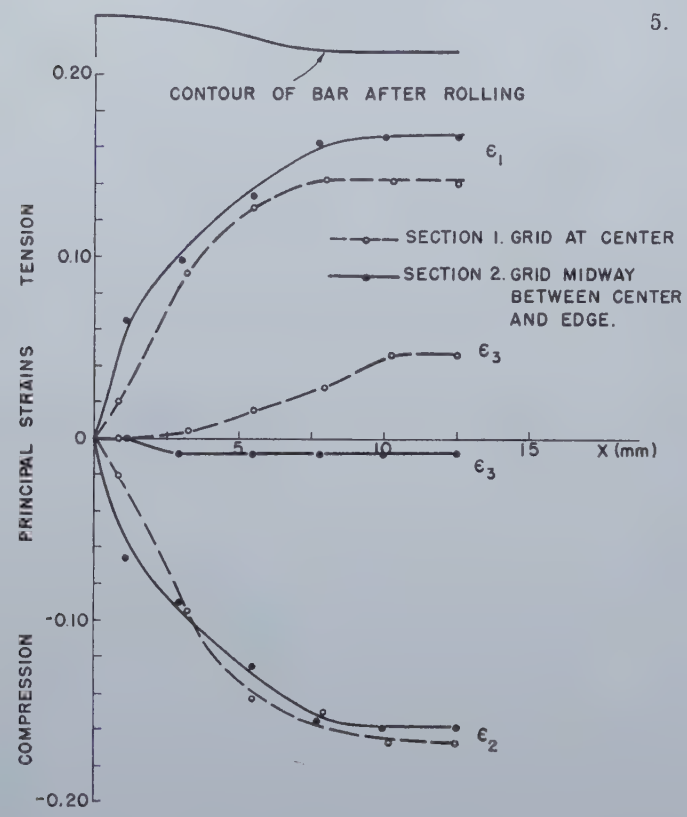

Fig. 5—Principal strains. Streamlines I, V.

Conclusions

The distribution of principal strains within a bar as a result of a 20 pct rolling reduction was determined as a function of the coordinates. The axial and vertical principal strains have about the same magnitudes and directions as those previously determined by others[1] at the surface of a bar. The lateral principal strain, however, changes from tension at the center of the bar to compression midway between the center and the outside in a section perpendicular to the roll axis.

Acknowledgments

The author would like to acknowledge the assistance of Professor C. W. MacGregor and Morris Steinberg during the course of this investigation.

References

[1] C. W. MacGregor and L. F. Coffin, Jr.: *Trans.* ASME **10** (AB-20).

[2] E. Siebel: *Steel* **94** (Apr. 9 and Mar. 19, 1934).

[3] M. Steinberg: ScD Thesis, Dept. of Metallurgy, MIT (1948).

Appendix

In the calculation of principal strains the following formulas were used:

1. $\epsilon_x = ln\frac{1_x}{1_0}$
2. $\epsilon_y = ln\frac{1_y}{1_0}$
3. $\epsilon_z = -\epsilon_x-\epsilon_y$
4. $\gamma_{xy} = \tan\delta$
5. $\tan 2\alpha = \frac{\tan\delta}{\epsilon_x-\epsilon_y}$

ϵ_x = axial strain
ϵ_y = vertical strain
ϵ_z = lateral strain
1_x = final length of grid in x direction
1_0 = original length of grid
1_y = final length of grid in y direction
γ_{xy} = shear strain

6. $\epsilon_1 = \frac{\epsilon_x+\epsilon_y}{2} + \sqrt{\left(\frac{\epsilon_x-\epsilon_y}{2}\right)^2+\left(\frac{\gamma}{2}\right)^2}$

δ = observed angle between horizontal axis and deformed side of network square.
α = angle between principal strain ϵ_1 and horizontal axis.

7. $\epsilon_2 = \frac{\epsilon_x+\epsilon_y}{2} - \sqrt{\left(\frac{\epsilon_x-\epsilon_y}{2}\right)^2+\left(\frac{\gamma}{2}\right)^2}$

$\epsilon_1, \epsilon_2, \epsilon_3$ = true principal strains in axial, vertical and lateral directions. Solved graphically by Mohr's circle.

8. $\epsilon_1+\epsilon_2+\epsilon_3=0$

The Effects of Nitrogen, Iron, or Nickel Upon the Alpha-Beta Transformation and Gamma Precipitation in Cobalt-Chromium Alloys

by A. R. Elsea and C. C. McBride

This paper describes a metallographic investigation of the influence of nitrogen, iron, or nickel additions upon the transformation and precipitation reactions occurring in cobalt-rich cobalt-chromium alloys. It is shown that nitrogen, iron, or nickel additions lower the alpha-beta transformation temperature range and tend to promote the formation of gamma phase.

HIGH-TEMPERATURE alloys, that is, alloys that are strong at high temperatures, have become increasingly important with the development of modern aircraft engines. Many alloys of this type are available. However, metallurgists do not have a clear understanding of the phases or structures which are responsible for these high-temperature properties. If these basic factors were understood, it might be possible to make better or cheaper alloys for service at high temperatures.

For this reason, an investigation of the fundamental factors promoting high-temperature strength in alloys was started at Battelle Memorial Institute. This was to have included a study of the relationship between the structure and properties of cobalt-chromium base alloys of the vitallium type. It soon became clear that the structure of vitallium is quite complex and that the equilibrium diagrams which should explain these structures were unreliable. As a result, the cobalt-chromium binary diagram was determined as the first phase of this investigation[1]. This diagram is shown in fig. 1.

During the study of the cobalt-chromium binary system, it was learned that these alloys may pick up considerable nitrogen when melted and heat treated in air. The extent to which nitrogen affects the various reactions in cobalt-chromium base alloys was not known, but there were indications that this impurity might be responsible for some of the erratic test results obtained for vitallium. Consequently, nitrogen was the first ternary addition studied. Thereafter the work was extended to ternary additions of iron and of nickel.

This paper describes the investigation of the effects of nitrogen, iron, and nickel upon the reactions in cobalt-chromium alloys with 80:20 and 68:32 cobalt-chromium ratios.

Experimental Work

Alloy Preparation: A series of cobalt-chromium base alloys containing various amounts of the third element being studied were made for both the 80:20 and the 68:32 cobalt-chromium ratios.

Electrolytic chromium, cobalt, and iron, and reagent-grade nickel powder were used as melting stock. Table I contains the chemical analyses of these materials. The charges were melted in alundum thimble crucibles which absorbed chromium oxide and effectively deoxidized the melts. These crucibles were supported by close-fitting graphite sleeves so that if they cracked during melting the metal would not be lost. Carbon increases, during

A. R. ELSEA, Member AIME, and C. C. McBRIDE are Assistant Supervisor and Research Engineer of Metallurgical Engineering, respectively, Battelle Memorial Institute.

This work was done under the sponsorship of the Office of Naval Research, U. S. Navy, Contract N5ori-111.

AIME New York Meeting, Feb. 1950.

TP 2757 E. Discussion (2 copies) may be sent to Transactions *AIME before Apr. 1, 1950, and is scheduled for publication Nov. 1950. Manuscript received Oct. 13, 1949.*

melting, ranged from 0.08 to 0.1 pct; however, during subsequent homogenization, the carbon was reduced to within the limits of 0.01 to 0.05 pct which was considered satisfactory.

The melting furnace consisted of a vertical porcelain tube heated by a tubular Globar element and was designed for either vacuum or controlled-atmosphere melting. Nitrogen atmospheres were obtained by passing tank nitrogen through a drying tower containing magnesium perchlorate and then through the furnace. When argon atmospheres were used, tank argon (99.87 pct argon) was passed through magnesium perchlorate to remove the moisture and then through a container of titanium metal granules heated to 750°C for removal of nitrogen and oxygen.

The melts were briefly stirred prior to casting and then centrifugally cast into precision investment molds yielding 3/16 by ¼-in. rectangular

Table I. Analyses of Melting Stock

Element	Per Cent			
	Electrolytic Cobalt	Electrolytic Chromium	Electrolytic Iron	Nickel Metal Powder
C	0.06	0.02	0.005	0.080
Si	0.01	0.08	0.003	0.090
Fe	0.05	0.048	Balance	0.490
Ni	0.32		0.008	Balance
S	0.008		0.004	
Cu				< 0.05
Sn				< 0.005
Pb				< 0.005
Mg				< 0.001
Mo				< 0.001
Co	Balance			< 0.1
Cr		Balance		
O_2	0.15	0.5		
N_2		0.004		
Mn			0.002	
P			0.001	

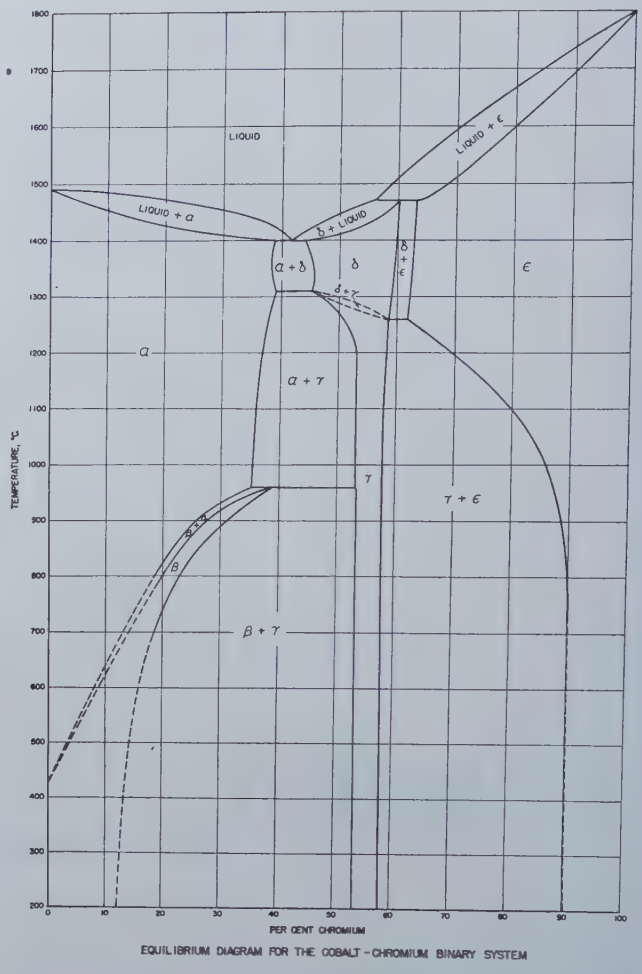

EQUILIBRIUM DIAGRAM FOR THE COBALT-CHROMIUM BINARY SYSTEM

Table II. Chemical Analyses and Melting and Homogenizing Data for Cobalt-Chromium-Nitrogen Alloys

Alloy	Melting Atmosphere	Analysis, Per Cent, As Cast			Homogenizing Atmosphere	Analysis, Per Cent, After Homogenizing		
		Cr	N_2*	C		Cr	N_2*	C
T-71-B(Top)	N_2	19.5	0.063		A	19.5	0.006	
(Bottom)		19.6	0.071					
T-1-A	A	19.6	0.084	0.03	A	19.6	0.006	
T-1-B	A	19.2	0.011		A	19.2	0.007	
T-1-C(Top)	A	19.7	0.016		A	19.5	0.010	
(Bottom)		19.8	0.015					
T-71-F(Top)	N_2				A	20.3	0.012	0.02
(Bottom)						20.4		0.02
T-71-A	N_2	19.9	0.085		A	19.8	0.019	
T-1-B	A	19.2	0.011		N_2	19.2	0.046	
T-1-C(Top)	A	19.7	0.016		N_2	19.5	0.051	
(Bottom)		19.8	0.015					
T-1-F(Top)	A				N_2	20.0	0.052	0.03
(Bottom)						21.6		0.03
T-71-B	N_2	19.5	0.063		N_2	19.5	0.060	
T-71-A	N_2	19.9	0.085		N_2	19.8	0.067	
T-71-G	N_2				N_2	20.4	0.070	0.01
T-4-G	A				A	31.6	0.014	
T-4-A	A	31.9	0.017	0.03	A	32.0	0.024	
T-70	N_2	28.5	0.274		A(Melted)	28.5	0.027	
T-4-F(Top)	A			0.10	A	32.6	0.034	0.05
(Bottom)						32.2		0.04
T-5	N_2	30.9	0.281		A(Melted)	30.9	0.062	
T-4-B(Top)	A	31.7	0.108		A	31.4	0.066	
(Bottom)		31.7	0.107					
T-70-B(Top)	N_2	32.0	0.368		A	31.6	0.100	
(Bottom)		32.0	0.359					
T-70E-(Top)	N_2				A	31.9	0.115	0.05
(Bottom)						31.7		0.05
T-4-I	A				48A—>48N_2	32.1	0.262	0.02
					50 More A	32.1	0.141	
T-70-A	N_2	31.2	0.35		A	31.0	0.142	
T-70-C	N_2				N_2	31.6	0.404	
T-70-D	N_2				N_2	31.5	0.367	

* By wet-chemical method.

Fig. 1—(above) Equilibrium diagram for the cobalt-chromium binary system.

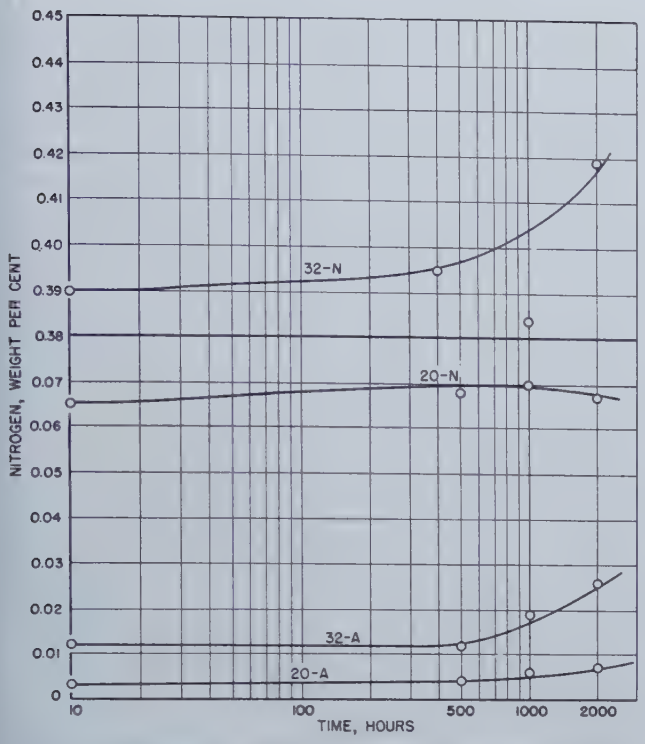

Fig. 2—Nitrogen pickup in cobalt-chromium alloys heated in air at 900°C (1650°F).

bars about 5 in. long. In the early stages of the investigation, chemical analyses were obtained for the tops and bottoms of the as-cast bars to determine melting losses and uniformity.

Heat Treatment: Two types of furnaces were used in the heat-treating operations. Both types were combustion tube furnaces which could be supplied with either purified argon or dry nitrogen atmospheres. The furnaces used for heat treatment at temperatures above 1050°C were heated by pin-type Globar elements and could be controlled to within ±5°C. Heat treatments at temperatures below 1050°C were conducted in chromel resistance wound furnaces, designed to maintain the desired temperature to within ±2°C.

The cast bar stock was homogenized for 50 hr at 1260°C and water quenched. Metallographic examination of the homogenized stock showed that it was free from microsegregation. Chips were obtained from the tops and bottoms of the homogenized bars for chemical analyses.

Specimens of the homogenized alloys were heat treated for 50 hr at temperatures in the range of 625 to 1025°C and water quenched to room temperature. In general, temperatures at 25°C intervals within the above-mentioned temperature range were selected for the heat treatments. The specimens were then subjected to metallographic examination to determine the phases present. The phases were identified, using the procedure described in an earlier paper.[1] Results of this examination, plotted as a function of temperature and composition, showed the effects of the third element

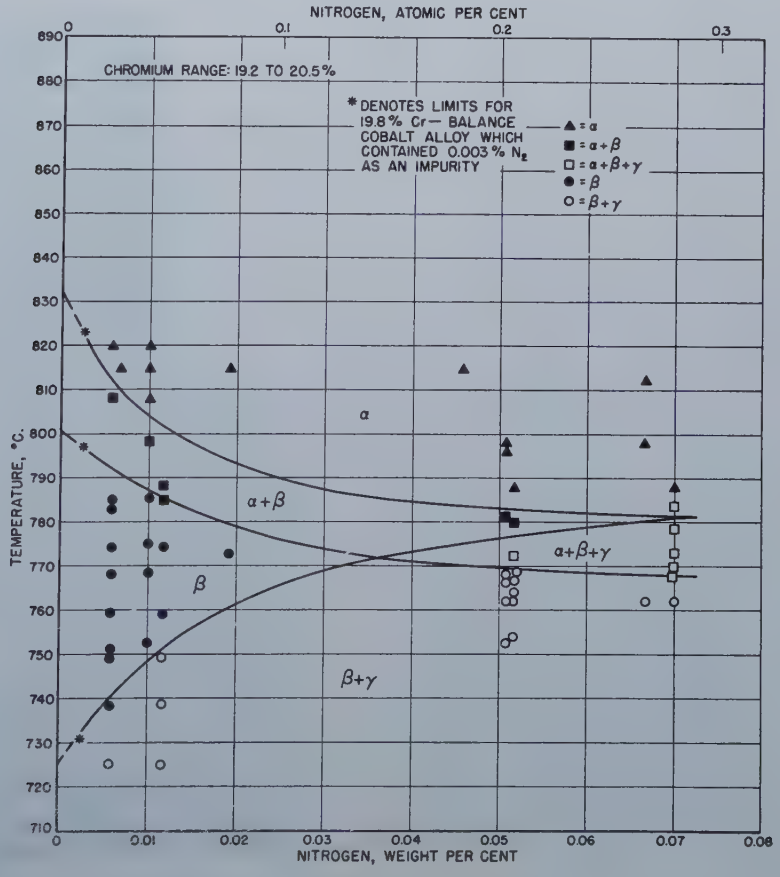

Fig. 3—Alpha plus beta temperature range and gamma precipitation

as a function of nitrogen content for cobalt-chromium-nitrogen alloys containing 19.2 to 20.5 pct chromium.

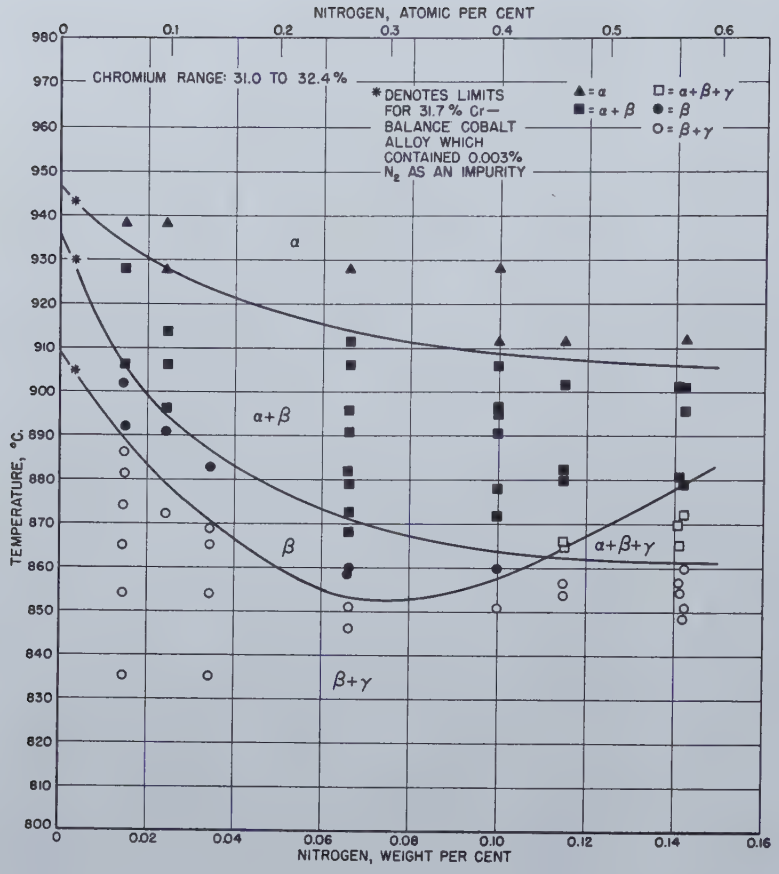

Fig. 4 — Alpha plus beta temperature range and gamma precipitation

as a function of nitrogen content for cobalt-chromium-nitrogen alloys containing 31.0 to 32.4 pct chromium.

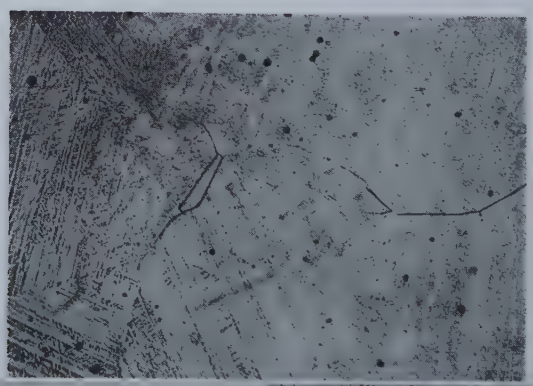

Fig. 5—Alpha plus trace beta

(0.006 pct N_2. Heat treated for 100 hr at 808°C).

Fig. 6—(left) Beta

(0.006 pct N_2. Heat treated for 100 hr at 784°C).

Fig. 7—(right) Alpha plus 2 pct beta

(0.051 pct N_2. Heat treated for 100 hr at 781°C).

Note: The above micrographs at 250X (reduced one third in reproduction) show the effect of nitrogen additions upon the alpha-beta transformation temperature range of cobalt-chromium alloys containing approximately 20 pct chromium. Fig. 5 and 6 illustrate specimens containing 0.006 pct nitrogen after heat treatment for 100 hr at 808° and 784°C, respectively. The specimen shown in fig. 7 contained 0.051 pct nitrogen and was heat treated for 100 hr at 781°C; this shows about the same amount of alpha as that observed in fig. 5. Thus an increase of 0.045 pct nitrogen lowered the alpha-beta transformation about 27°C.

upon the alpha-beta transformation temperature range and the precipitation of gamma.

The transformations in these alloys are very sluggish; consequently, the results obtained from some of the tests show only trends. Later in this report, a description is given of an experimental technique used to determine more accurately the limits of the reactions in certain of the alloys. However, in most cases, the results obtained from the tests described above were considered to be sufficiently accurate.

The Effect of Nitrogen Additions on the Alpha-Beta Transformation Temperature Range and the Precipitation of Gamma in Cobalt-Chromium Base Alloys: Table II gives the chemical compositions and melting and homogenizing data for the cobalt-chromium-nitrogen alloys.

Alloy T-4-G represents the lowest nitrogen content that was obtained in the alloys containing approximately 32 pct chromium. Alloy T-5 was made with the same melting stock as that used for Alloy T-4-G, the only difference being that Alloy T-5 was melted in an atmosphere of dry nitrogen. The method of preparing Alloy T-70 was similar to that for Alloy T-5, except that the chromium melting stock for Alloy T-70 was previously treated for 4½ hr at 1300°C in an atmosphere of dry nitrogen, after which it contained 11.1 pct nitrogen. Alloy T-70 was expected to contain the maximum nitrogen content for alloys of this chromium content. The chemical analyses indicated, however, that, regardless of whether ordinary or high-nitrogen chromium was used as melting stock, melting under a dry nitrogen atmosphere resulted in a nitrogen content of approximately 0.28 pct. However, alloys which were desired to be high in nitrogen had 0.3 pct nitrogen added to the charge in the form of high-nitrogen chromium (containing 11.1 pct nitrogen), to insure an excess of nitrogen during melting. Further variations in nitrogen contents were obtained by homogenizing in either dry nitrogen or purified argon.

The general procedure used for controlling the nitrogen content was as follows: Melting and homogenizing in purified argon produced alloys with the lowest nitrogen contents. Melting in nitrogen and homogenizing in argon produced alloys with slightly higher nitrogen contents. Melting in argon and homogenizing in nitrogen produced alloys with still higher nitrogen contents. Melting and homogenizing in nitrogen produced alloys with the highest nitrogen contents. These results show that during homogenization, the nitrogen contents of cobalt-chromium alloys can be varied over quite a range, depending upon the amount of nitrogen present in the homogenizing atmosphere.

From the data in table II, the solubility of nitrogen in cobalt-chromium alloys containing approximately 20 pct chromium, at 1260°C and a pressure of 1 atm, can be estimated. Alloys which were relatively low in nitrogen, as cast, (T-1-B with 0.011 pct nitrogen and T-1-C with 0.016 pct nitrogen) picked up nitrogen when homogenized in dry nitrogen at a temperature of 1260°C (after treatment, 0.046 pct nitrogen and 0.051 pct nitrogen, respectively). Alloys which were initially high in nitrogen (T-71-A with 0.085 pct nitrogen and T-71-B with 0.063 pct nitrogen) lost nitrogen when homogenized in dry nitrogen (after treatment, 0.067 and 0.060 pct nitrogen, respectively). These data indicate that, in alloys containing approximately 20 pct chromium, between 0.051 and 0.060 pct nitrogen is in equilibrium at 1260°C with gaseous nitrogen at 1 atm pressure. Although similar data are not available for the alloys containing 32 pct chromium, it is apparent that under a given set of conditions, these alloys contain more nitrogen than do the 20 pct chromium alloys.

Since high-temperature alloys are often in contact with air for extended periods of time at elevated temperatures, it was of interest to learn whether changes occur in the nitrogen contents of cobalt-chromium alloys treated in air at normal operating temperatures. Samples of 20 and 32 pct chromium alloys with both low and high nitrogen contents were heated at 900°C (1650°F) for 500, 1000, and 2000 hr in air and the changes in nitrogen content determined. The results of these tests, listed in table III and plotted in fig. 2, show comparatively small changes in nitrogen content under these conditions.

As previously described under *Heat Treatment,* specimens of homogenized stock were heat treated for 50 hr at 25°C temperature intervals and examined metallographically to determine the approximate effects of nitrogen additions upon the alpha plus beta field. The tests showed that nitrogen additions lower the temperature range of the alpha-beta transformation. Since the transformations in this system are quite sluggish, it was not known whether the lowering of the transformation was real or whether it was an apparent effect resulting from increased sluggishness of the transformation. To eliminate the factor of sluggishness, specimens of both the high-temperature phase, alpha, and the low-temperature phase, beta, were isothermally treated at various temperatures in the range of the transformation. The specimens were then examined metallographically to determine the phases formed.

These tests were conducted as follows: Specimens of each alloy were heat treated at temperatures determined from the blocking-in tests, to obtain structures which were predominately beta phase. A specimen of the homogenized stock was pretreated at 1200°C for 3 hr to insure a structure which was all alpha phase and then transferred hot, along with one of the cold beta specimens, to the heat-treating furnace. They were held at temperature in the furnace for 100 hr and water quenched. Metallographic examination of these specimens yielded the results which are summarized in fig. 3 and 4. These show the effect of nitrogen additions upon the alpha-beta transformation temperature range for alloys containing approximately 20 and 32 pct chromium.

Fig. 3 shows a lowering of the transformation temperatures with the width of the field remaining fairly constant. Fig. 4 shows a lowering of the alpha-beta transformation temperatures with the width of the field increasing as the nitrogen content increases. Additional tests were made for 375 hr in order to spot check the curves. The results of these tests were in agreement with fig. 3 and 4.

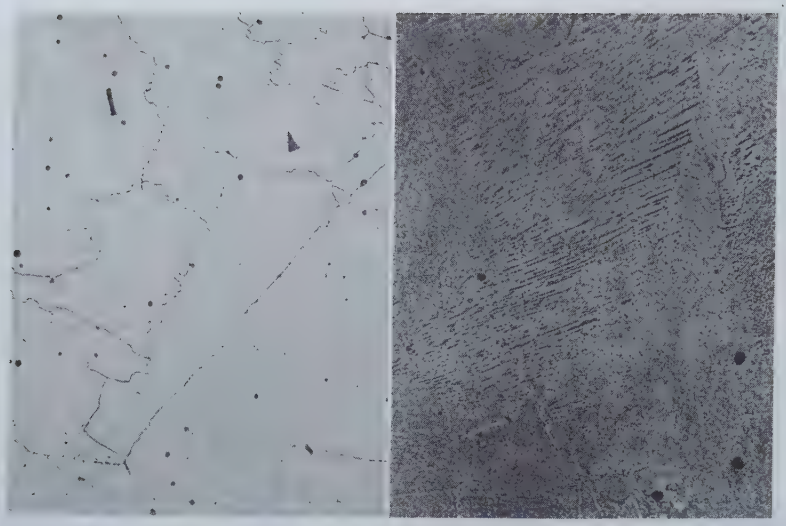

Fig. 8—(left) Beta

(0.006 pct N_2. Heat treated for 100 hr at 751°C).

Fig. 9—(right) Beta plus gamma precipitate.

(0.70 pct N_2. Heat treated for 100 hr at 762°C).

Note: The above micrographs at 500X (reduced one third in reproduction) show the effect of nitrogen additions upon the precipitation of gamma in cobalt-chromium alloys containing approximately 20 pct chromium. fig. 8 and 9 are micrographs of specimens heat treated for 100 hr at 751° and 762°, respectively, and show that the precipitation of gamma increases as the nitrogen content increases.

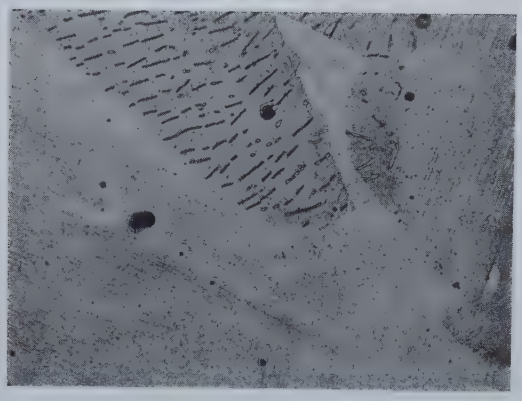

Fig. 10—Alpha plus beta plus gamma precipitate.

(0.141 pct N_2, 32.1 pct Cr, heat treated for 100 hr at 870°C). This micrograph at 500X (reduced one third in reproduction) is typical of the alpha plus beta plus gamma structure observed in cobalt-chromium alloys containing 20 and 32 pct chromium.

Table III. Changes in Nitrogen Analyses of Cobalt-Chromium Alloys after Exposure to Air at 900°C (1650°F) for 500, 1000, and 2000 Hr

Alloy	Analysis, Per Cent							
	Before Test		500 Hr at 900°C in Air		1000 Hr at 900°C in Air		2000 Hr at 900°C in Air	
	Cr	N_2	N_2	Change in N_2	N_2	Change in N_2	N_2	Change in N_2
20-A	18.4	0.003	0.004	+0.001	0.006	+0.003	0.007	+0.004
20-N	19.7	0.065	0.068	+0.003	0.070	+0.005	0.067	+0.002
32-A	31.9	0.012	0.012	0.000	0.019	+0.007	0.026	+0.014
32-N	31.6	0.390	0.395	+0.005	0.384	−0.006	0.419	+0.029

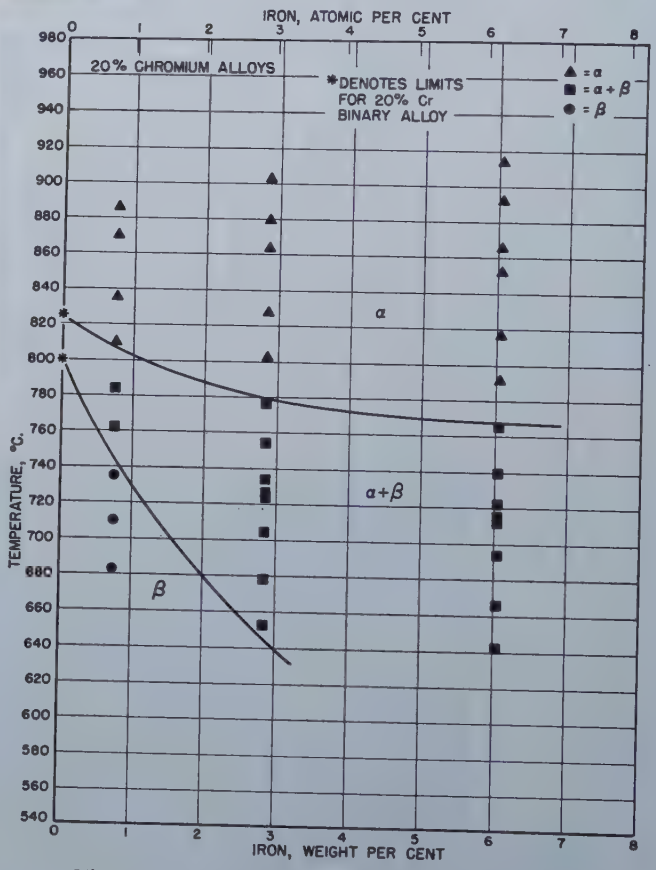

Fig. 11—Alpha plus beta temperature range

as a function of iron content for cobalt-chromium-iron alloys containing 20 pct chromium.

Determinations of the temperatures at which gamma starts to precipitate were conducted as follows: A 2½-in. section of bar stock of each alloy was pretreated for 3 hr at 1200°C to insure complete solution of gamma. The specimens were then transferred hot to aging furnaces operating at temperatures which would transform them to beta phase. After 100 hr at temperature, the specimens were water quenched and a sample procured for metallographic examination. The specimens were then aged for 50 hr at progressively lower temperatures (the samples were examined metallographically after each treatment) until gamma precipitate was observed. From the results of these tests and the structures observed in the isothermally treated specimens, it was possible to estimate the temperatures at which gamma starts to precipitate. These estimated values are also plotted in fig. 3 and 4. They show that, at a constant temperature, the amount of gamma precipitate increases as the nitrogen content increases.

The micrographs in fig. 5 to 10 show typical structures that were observed in this study.

The Effect of Iron Additions on the Alpha-Beta Transformation Temperature Range and the Pre-

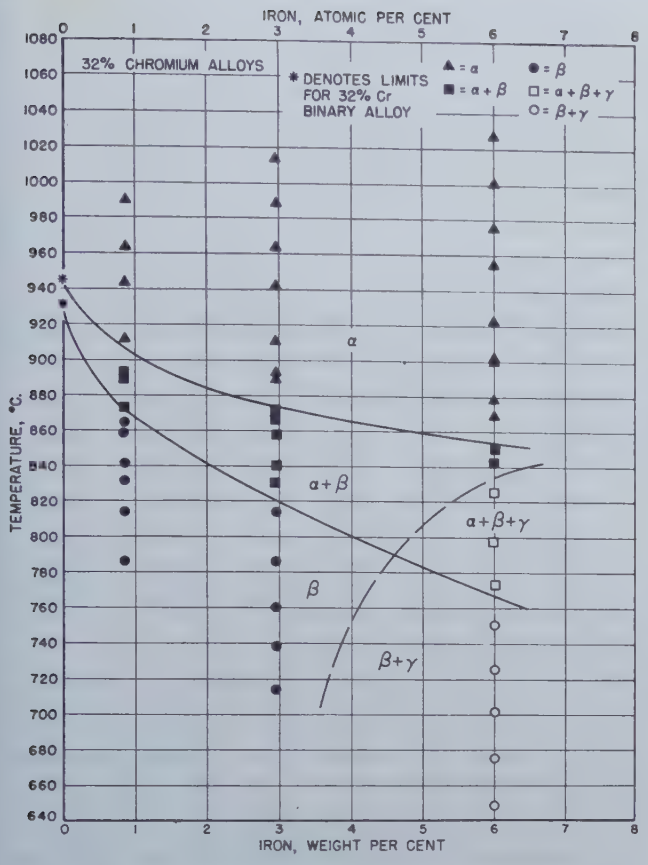

Fig. 12—Alpha plus beta temperature range
as a function of iron content for cobalt-chromium-iron alloys containing 32 pct chromium.

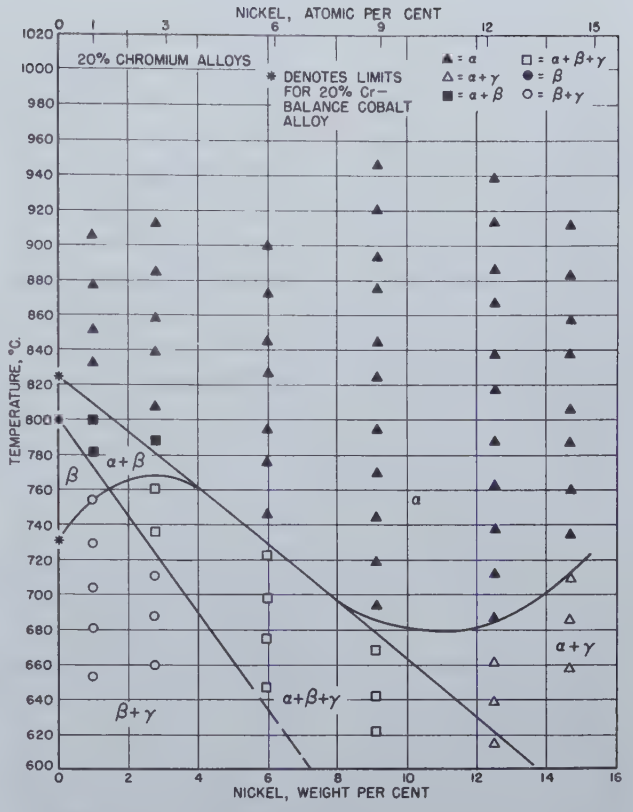

Fig. 13—Alpha plus beta temperature range and gamma precipitation
as a function of nickel content for cobalt-chromium-nickel alloys containing 20 pct chromium.

cipitation of Gamma in Cobalt-Chromium Base Alloys: The alloys used in this study were melted and heat treated in a purified argon atmosphere in order to hold the nitrogen content to a minimum. The chemical analyses of these alloys are contained in table IV.

As described earlier in this paper, specimens of the homogenized alloys were heat treated for 50 hr at predetermined temperatures, and examined metallographically to determine the phases present. The results of this examination are shown graphically in fig. 11 and 12.

It was intended that the study would be conducted on alloys with $\frac{Cr}{Co + Cr} \times 100 = 20$ and 32. As shown in table IV, the alloys did not exactly meet these composition requirements. Consequently, corrections were applied to the data before they were plotted in fig. 11 and 12. These corrections were determined as follows: The value of $\frac{Cr}{Co + Cr} \times 100$ was calculated for each alloy (these values are given in table IV). Then by reference to the cobalt-chromium binary diagram (shown in fig. 1), the respective transformation temperatures for alloys with those chromium contents were noted. The difference between each of these temperatures and the transformation temperature for the 20 and 32 pct chromium alloy, as the case might be, was taken as the correction factor. For example, the limits of the alpha plus beta field for Alloy T-46, which has a value of $\frac{Cr}{Co + Cr} \times 100 = 19.4$, are 10°C lower than the limits for the binary alloy containing 20 pct chromium. Thus, 10°C was added to each testing temperature when the data for this alloy were plotted.

Table IV. Chemical Analyses of Cobalt-Chromium-Iron Alloys

Alloy	Analysis, Per Cent				
	Cr	Fe	Co*	N_2	$\frac{Cr \times 100}{Co + Cr}$
T-46(Top)	19.20	0.75	80.02	0.003	19.4
(Bottom)	19.25	0.75			
T-47-A(Top)	19.20	2.9	77.87	0.005	19.8
(Bottom)	19.25	2.8			
T-48(Top)	19.25	5.9	74.68	0.003	20.51
(Bottom)	19.30	6.2			
T-55(Top)	32.5	0.90	65.65	0.003	33.79
(Bottom)	34.5	0.80			
T-56(Top)	31.4	2.9	64.0	0.005	34.05
(Bottom)	34.7	3.0			
T-57(Top)	30.0	6.0	64.0	0.004	31.91
(Bottom)	30.0	6.0			

* Obtained by difference.

The curves in fig. 11 and 12 show that additions of iron lower the transformation temperature and/or increase the sluggishness of the transformation. In

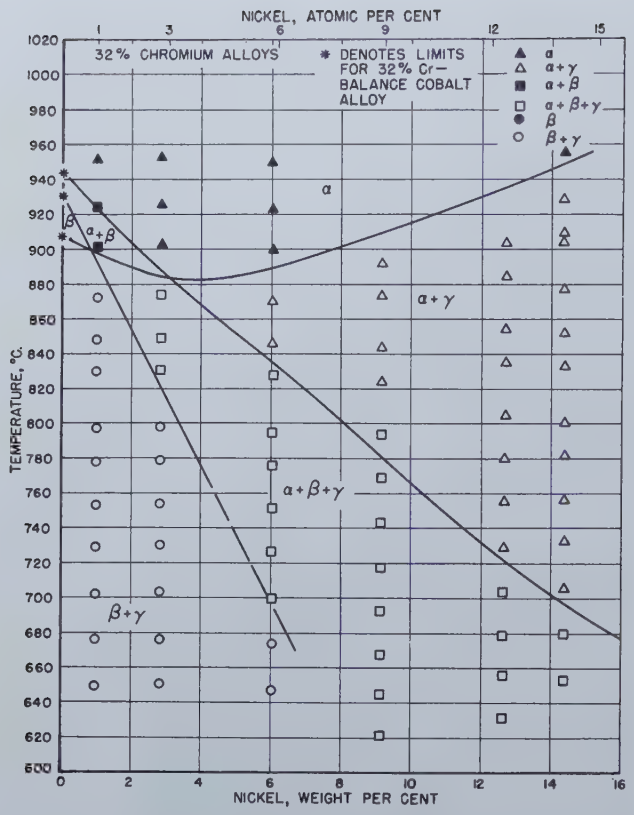

Fig. 14—Alpha plus beta temperature range and gamma precipitation

as a function of nickel content for cobalt-chromium-nickel alloys containing 32 pct chromium.

order to determine whether the apparent lowering of the transformation was real or whether it was a result of increased sluggishness, several tests were made using 32 pct chromium alloys in which pairs of specimens with all alpha and all beta prior structures were heat treated at temperatures in the range of the transformation. By considering only the phases which were forming at a particular temperature, the factor of sluggishness was eliminated.

These tests substantiate the results of the previous tests and show that the lowering of the transformation temperature range is real and not the result of increased sluggishness.

Gamma precipitate was observed in only one of the cobalt-chromium-iron alloys; the one with $\frac{Cr \times 100}{Co + Cr} = 32$ containing 6 pct iron. In cobalt-chromium binary alloys, the precipitation of gamma from beta phase is a very sluggish reaction. Apparently, the addition of iron to the system increases the sluggishness of the reaction, so that under the conditions of testing, gamma did not precipitate.

The Effect of Nickel Additions Upon the Alpha-Beta Transformation Temperature Range and the Precipitation of Gamma in Cobalt-Chromium Base Alloys: The alloys used in this study were melted and heat treated in an atmosphere of purified argon in order to hold the nitrogen content to a minimum. Chemical analyses of the homogenized alloys are contained in table V.

Results obtained from the metallographic examination of the cobalt-chromium-nickel specimens, heat treated for 50 hr at 25°C intervals, are shown graphically in fig. 13 and 14. As in the case of the cobalt-chromium-iron alloys, temperature correction factors were applied to the heat-treating temperatures when plotting fig. 13 and 14, to adjust for variations in composition. Fig. 13 and 14 show a lowering of the alpha-beta transformation temperature range and a widening of the field.

Table V. Chemical Analyses of Cobalt-Chromium-Nickel Alloys

Alloy	Cr	Ni	Co*	N_2	$\frac{Cr \times 100}{Cr + Co}$
T-22(Top)	19.4	1.02	79.62	0.010	19.59
(Bottom)	19.4	0.94			
T-23(Top)	18.8	2.68	78.54	0.001	19.23
(Bottom)	18.6	2.83			
T-24(Top)	18.7	5.91	75.23	0.004	19.99
(Bottom)	18.9	6.02			
T-82	18.4	9.10	72.5	0.001	20.24
T-83	18.1	12.50	69.4	0.002	20.70
T-76(Top)	16.5	14.5	68.85	0.003	19.33
(Bottom)	16.5	14.8			
T-31(Top)	31.4	1.01	67.57	0.004	31.76
(Bottom)	31.5	0.95			
T-32(Top)	30.6	2.77	66.41	0.013	31.65
(Bottom)	30.9	2.91			
T-33(Top)	30.2	6.07	63.84	0.012	32.04
(Bottom)	30.0	6.04			
T-84	30.0	9.14	60.86	0.032	33.02
T-85	27.4	12.60	60.00	0.018	31.35
T-77(Top)	26.4	14.4	59.15	0.020	30.94
(Bottom)	26.6	14.3			

* Obtained by difference.

As shown by fig. 13 and 14, increasing amounts of nickel raise the gamma precipitation temperature until gamma and alpha coexist. This may indicate that nickel additions broaden the alpha plus gamma field (see fig. 1) and extend it to lower chromium contents.

Since in the cobalt-chromium-nickel alloys it was not possible to obtain beta phase free from gamma, no attempts were made to determine more accurately the temperature limits of the transformation using the technique described earlier in this paper. Consequently, these curves show only trends and may be influenced by increased sluggishness resulting from the nickel additions.

Summary

Results of this investigation show that nitrogen, nickel, or iron additions to cobalt-chromium alloys lower the alpha-beta transformation temperature range and promote the formation of gamma. The effect of nitrogen upon the alpha-beta transformation was determined accurately. But the remaining studies were not equilibrium studies and, hence, show only the trend of the effects.

Acknowledgment

The authors wish to express their appreciation to the sponsoring agency, Materials Section, Office of Naval Research, U. S. Navy Department, for permission to publish these results. They also wish to thank the various members of the Battelle staff for their assistance during the course of this investigation, especially Dr. H. W. Russell and G. K. Manning, under whose supervision this research was conducted.

Reference

A. R. Elsea, A. B. Westerman, and G. K. Manning: The Cobalt-Chromium Binary System. *Trans.* AIME (1948) **180**. *Metals Tech.*, June, 1948, TP 2393.

The Growth of Austenite As Related to Prior Structure

by A. E. Nehrenberg

New austenite is restricted in its growth by the grain boundaries in the prior structure, and initially assumes the size and shape of the prior grains. The new austenite is equiaxed when the prior structure is the result of a high temperature transformation, and is acicular in shape when the initial structure is bainite or martensite.

THE mechanism by which austenite forms in steels has received a great deal of attention in the literature in past years.[1-24] Our present knowledge concerning this mechanism has been recently summarized quite concisely by Bain and Vilella,[1] while a few years ago the literature was carefully reviewed by Roberts and Mehl.[2] The consensus is that any ferrite-carbide interface is a potential site for the nucleation of austenite during heating above the A_{c1} temperature, and that the new austenite generally grows freely to produce approximately equiaxed grains, whether the carbides are initially present in the lamellar or the spheroidal form. In the case of eutectoid steels, growth of the new grains of austenite continues until contact is established with other grains. Then growth stops and an initial austenite grain size is established which does not change until the heating is continued to some high temperature at which grain coarsening begins. In the case of pearlitic steels which are not of eutectoid composition, the proeutectoid ferrite or carbide may interfere with the growth of the austenite if the temperature is not above that designated the A_{c3} or the A_{cm}, respectively.

Although a large amount of work has been done to establish the mechanism of austenite formation in steels, it became clear to the present author while he was studying the transformation characteristics of a new 0.25 C Mn-Si-Ni-Mo hypoeutectoid steel[25] that the manner in which austenite grows in steels depends upon some factor, or factors, not previously considered. This was indicated by the fact that when this steel in the spheroidized condition was heated above the A_{c1} temperature the new austenite which was formed did not envelop the carbides and grow in an equiaxed manner as described by Bain[3] for spheroidized steels. Instead, in this steel, the austenite was observed to grow much more readily in certain directions than in others with the result that at temperatures within the A_{c1}-Ac^3 transformation range the austenite grains were acicular in shape. The excess ferrite was also found to be acicular with the distribution of these phases being such that a lamellar pattern was developed. This unusual directional growth of austenite in this new steel initially in the spheroidized condition is illustrated by fig. 1.

A search of the literature revealed that this type of growth was not necessarily peculiar to this steel for similar microstructures had been observed by other investigators.[4-8] However, the full significance of these microstructures does not appear to have been appreciated, and no work has been done to determine the conditions responsible for this directional growth of austenite or to arrive at an understanding of it. It was for this purpose that the work described in the present paper was carried out.

Material: During the course of this investigation a total of 15 steels was studied. They consisted of hypoeutectoid, eutectoid and hypereutectoid carbon steels, and hypoeutectoid and hypereutectoid alloy steels, all of which were obtained in the annealed condition from commercial warehouse stock. As received, the carbon and alloy hypereutectoid steels had microstructures which consisted of spheroidal carbides in ferrite, whereas the eutectoid steel and the hypoeutectoid steels were pearlitic.

The grades of steel represented were 1050, 1080, 10110, 3310, 4140, 4340, 4615, 6145, 8620, 9260, 9442,

A. E. NEHRENBERG is Supervisor, Research Laboratory, Crucible Steel Co. of America, Harrison, N. J.

New York Meeting, Feb. 1950.

TP 2762 E. Discussion (2 copies) may be sent to Transactions *AIME before Apr. 1, 1950, and is scheduled for publication Nov. 1950. Manuscript received Apr. 29, 1949.*

2pctCr-Mo, 5pctCr-Mo, the new Mn-Si-Ni-Mo steel, and a 0.9C-1.3Mn-0.5Cr-0.5W oil hardening tool steel. It does not seem necessary to tabulate the actual analyses of the steels used because they did not differ significantly from the nominal compositions for these grades, and because the relation found to exist between prior structure and the manner in which austenite forms in steels is independent of variations in composition within the limits studied.

Procedure: The initial work carried out in this investigation was confined to the hypoeutectoid steels, and consisted of a study of the microstructures produced by heating steels in the following prior conditions to various temperatures within the A_{c1}-A_{c3} transformation range: 1. Lamellar pearlite plus ferrite. 2. Spheroidal carbides plus ferrite obtained by tempering martensite at 1200°F for 225 hr. 3. Spheroidal carbides plus ferrite obtained by a high temperature transformation. 4. Martensite.

For prior condition 1 the steels were used as received from warehouse stock. For conditions 2 and 4 a 1700°F austenitizing and a water quench were employed. Condition 3 was obtained by austenitizing the steel in question at about its A_{c3} temperature followed by a high temperature transformation.

Samples about ⅛ in. thick were prepared from bars in each of the above prior conditions. These specimens were heated in lead for 1 hr at temperatures within the A_{c1}-A_{c3} range and were water quenched. After being tempered for 30 min at 400°F to darken the areas of martensite that resulted from quenching the austenite formed on heating, the specimens were prepared for microscopic examination.

The picral-zephiran chloride etching reagent described by Grange and his associates[26] was used for developing the details of the various structures.

Later, a carbon steel of approximately eutectoid content, and hypereutectoid carbon and alloy steels were studied to determine whether the observations made in the case of the hypoeutectoid steels applied to such steels as well. For this part of the investigation a number of ⅛ in. thick samples with a pearlitic prior structure, and with a spheroidized structure produced by tempering martensite for 100 hr at 1300°F, were placed in a lead bath at 1300°F, and were held for ½ hr. At the end of this soaking period the samples were heated in the lead bath at the rate of 60°F per hr. When 1325°F was reached samples representing each of the prior conditions were quenched in water. This procedure was repeated for each 5°F interval up to 1450°F. Before they were prepared for microscopic examination all of the specimens were tempered at 400°F for 30 min to darken the areas of martensite that resulted from quenching the austenite formed on heating.

In the final part of this investigation a study was made of the mechanism by which austenite forms in various prior structures. For this work the 4140 steel was selected. It was heated at 2250°F for 16 hr for homogenization so that there would be a minimum of chemical segregation present. This heating also served to develop prior structures which were

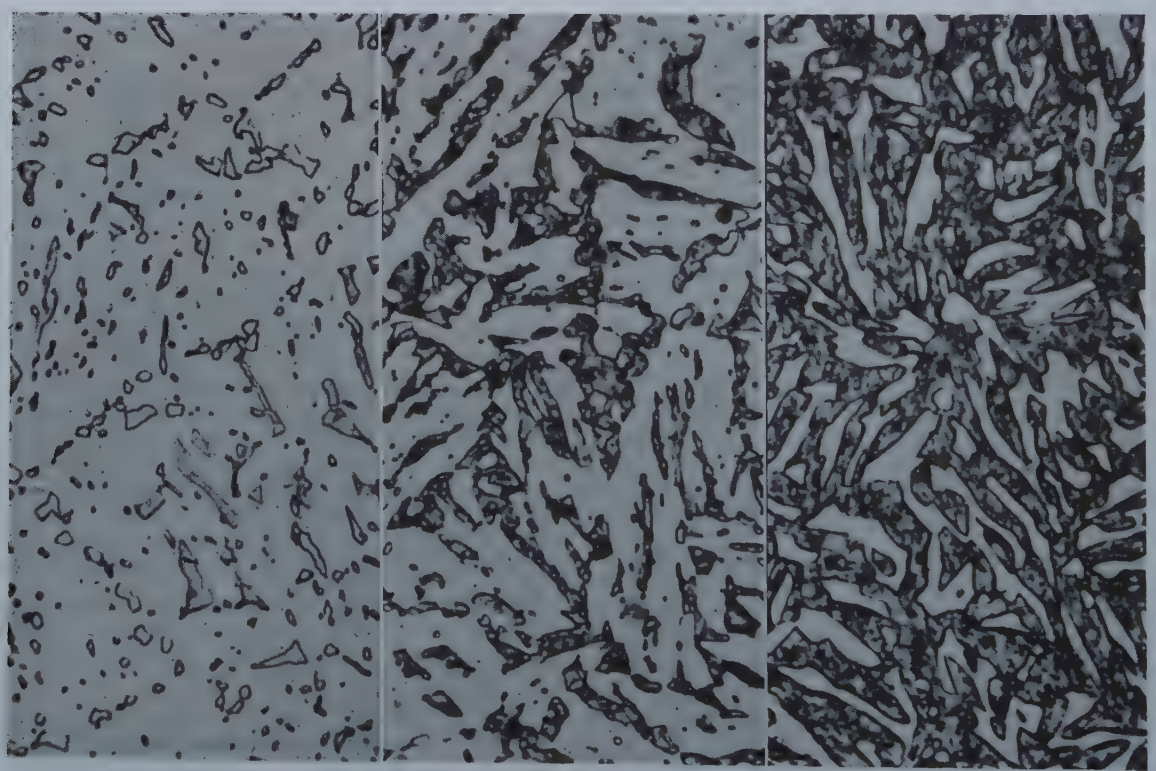

a. **1320°F. ½ hr. R_c 19.** *b.* **1340°F. ½ hr. R_c 27.5.** *c.* **1420°F. ½ hr. R_c 44.5.**

Fig. 1—Acicular growth of austenite grains in a spheroidal structure

in the new 0.25 C Mn-Si-Ni-Mo steel during heating to various temperatures within the A_{c1}-A_{c3} transformation range. Water quenched from the indicated temperature and tempered ½ hr at 600°F. Dark etching structure (tempered martensite) was austenite at time of quench. The indicated hardnesses were obtained before the temper. X2000. Etched in picral-zephiran chloride reagent.

coarse and in which, therefore, the changes which occurred during subsequent heating could be more readily observed.

The four prior structures mentioned previously were produced by the heat treatments shown in table I. Specimens ⅛ in. thick in each of these conditions were soaked ½ hr at 1300°F, heated at the rate of 60°F per hr and quenched at 5°F intervals in the manner described for the eutectoid and hypereutectoid steels. A 30 min temper at 400°F was again employed to darken the martensite present in the quenched samples.

Table I. Summary of Heat Treatments Employed to Produce Various Prior Structures in SAE 4140

STEEL	HEAT TREATMENT	RESULTING MICROSTRUCTURE
4140	2250°F 16 hr, water quench	Martensite
	2250°F 16 hr, water quench plus 1300°F, 100 hr	Tempered Martensite
	2250°F 16 hr, transferred to furnace at 1325°F, held for 16 hr, then air cooled	Ferrite and Pearlite
	2250°F 16 hr, water quench. Reheated at 1325°F for 6 hr, then at 1450°F for 1 hr, and finally transformed at 1325°F for 16 hr, cooled 10°F per hr to 1250°F	Spheroidal Carbides in Ferrite

A new etching reagent developed by A. Allten, an associate of the author, for use in connection with microstructural studies of stainless steels was found to be quite useful in this study of the mechanism of austenite formation. Its utility will be demonstrated later on. The Allten reagent is used electrolytically at 6 volts potential and consists of hydrochloric, lactic and tartaric acids dissolved in ethyl alcohol in the following proportions:

ethyl alcohol	225cc
lactic acid	225cc
tartaric acid	35g
hydrochloric acid (conc)	20cc

The optimum etching time for the steels used in this investigation was about 15 sec.

Formation of Austenite in Pearlitic Structures: There are many micrographs in the literature which illustrate the nucleation and growth of austenite in pearlitic structures. However, it seems desirable to include a set of such micrographs in this paper to serve as a basis for evaluating the effect of the other prior structures investigated. Fig. 2 shows that when austenite is formed in pearlitic structures growth occurs quite freely in every direction, resulting in grains which are approximately equiaxed while the last ferrite to be transformed is blocky. It is well known that this type of growth occurs in pearlitic structures, whether the steel is hypoeutectoid, eutectoid, or hypereutectoid in composition, so no further comments on this prior condition are required at this time.

Formation of Austenite in Spheroidized Structures: Spheroidized microstructures are generally produced in either of two ways:* (1) by the high temperature transformation of inhomogeneous austenite, or (2) by the tempering of martensite. It evidently has not been recognized by other investigators that there is a fundamental difference between the spheroidized structures which result from the use of these two different procedures. In the most recent publication[2] on the mechanism of austenite formation, the view is expressed that since carbide is precipitated and somewhat spheroidized during the heating of martensitic structures for austenitizing, such structures should austenitize in a similar manner to spheroidized structures, but at a different rate.

Fig. 3 shows, however, that the manner in which austenite grows in spheroidized structures depends upon how these prior structures were produced. When the spheroidization is the result of a high temperature transformation the austenite which forms during heating above the A_{c1} temperature appears to grow more or less freely in every direction, and equiaxed grains are developed. On the other hand, when the spheroidization is the result of tempering of martensite, the austenite exhibits an unexpected marked directional growth with the result that acicular grains are formed, and the excess ferrite also has an acicular, rather than a blocky shape.

That this acicular growth of austenite is by no means peculiar to only this hypoeutectoid alloy steel is illustrated by fig. 4 which shows the result of partially austenitizing a hypereutectoid carbon steel and a hypereutectoid alloy tool steel spheroidized by tempering. Both steels are shown to exhibit the same general mechanism, the only differences being that the excess ferrite and the austenite grains are more acicular in the case of the alloy steel, and that some equiaxed austenite grains formed in the carbon steel along with the acicular grains, whereas none was observed in the alloy steel.

The black areas in the microstructures shown in fig. 4 for the carbon steel consist of very fine pearlite, and have been observed before by other investigators.[2, 5, 9, 10, 13, 17, 19] Such areas were not observed in any of the alloy steels studied. Their presence denotes that the austenite that formerly occupied those regions was so low in hardenability as a result of its low carbon content that the pearlite reaction could not be avoided during the quench.[3, 15]

In martensitic structures which are not tempered before being heated above the A_{c1} temperature the austenite grows in the same manner as it was shown to grow in thoroughly tempered martensite. This is illustrated by fig. 5.

Composition is not a factor in this behavior because the acicular growth of austenite in martensitic structures occurred in each of the 15 steels studied which covered a wide range of composition. These steels consisted of plain carbon hypoeutectoid, eutectoid and hypereutectoid steels, and alloy hypo- and hyper-eutectoid steels. An explanation for this acicular growth of austenite from martensitic structures will be offered in a subsequent part of this paper.

Isothermal Formation of Austenite in a Spheroidized Hypereutectoid Carbon Steel: It should now be clear that the mechanism described by Bain[3] for

* Spheroidization may sometimes also be accomplished by tempering pearlite at a temperature just below the A_1. It is probable that austenite would grow in such a structure in the same manner as it grows in pearlite.

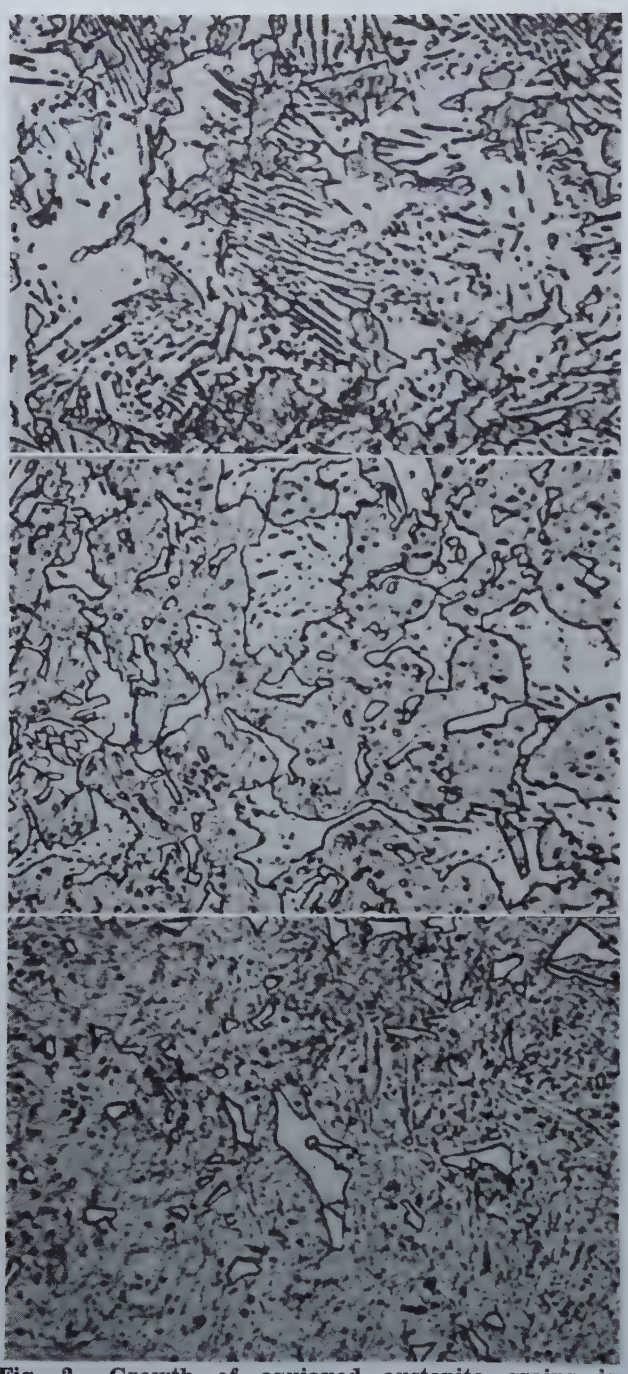

Fig. 2 — Growth of equiaxed austenite grains in pearlitic 4340

during heating to various temperatures within the A_{c1}-A_{c3} temperature region. Water quenched from the indicated temperature and tempered ½ hr at 400°F. Dark etching structure (tempered martensite) was austenite at time of quench. X2000. Etched in picral-zephiran chloride reagent. *a*. Pearlite heated to 1325°F 1 hr. *b*. Pearlite heated to 1350°F 1 hr. *c*. Pearlite heated to 1375°F 1 hr. (Slightly reduced in reproduction.)

the formation of austenite from spheroidized structures does not apply when the spheroidization is accomplished by tempering. Even in the case of spheroidized structures produced by a high temperature transformation it did not appear in the early stages of the formation of austenite that the growth was occurring in a symmetrical manner around carbide particles in the manner to be expected on the basis of Bain's work. In some cases there were no carbides visible in the first austenite that formed. When there were carbides present they did not necessarily appear at the center of a tiny austenite grain, but might be located at a corner of the grain.

This difference in the observations made by Bain and the present author required some additional consideration since Bain's concept of the symmetrical growth of austenite around spheroidized carbides has become so firmly established. In the present work steels with normal carbide size were austenitized in a conventional manner during continuous heating, whereas in Bain's work very coarsely spheroidized steels were austenitized isothermally. It seemed that the difference in the observations might be attributed to the techniques used, and that the best way to proceed would be to attempt to duplicate the conditions that prevailed in Bain's experiments. Accordingly, the hypereutectoid plain carbon steel was subjected to treatments involving either cold working followed by subcritical annealing, or multiple full annealing with the objective of producing extremely coarse carbides. Unfortunately, carbides as coarse as those in Bain's hypereutectoid pure iron carbon alloy were not obtained in the commercial steel, but the treatments employed did produce carbides considerably coarser than those usually encountered in practice.

The result of forming austenite isothermally at 1400°F in this coarsely spheroidized steel is shown in fig. 6. It will be noted that in this commercial steel it is the exception, rather than the rule, for austenite to envelop a single carbide in the early stages of its growth. Nucleation evidently occurs at a carbide-ferrite interface but the subsequent growth bears no relation to the shape or distribution of the carbides. Instead, it is indicated in fig. 6*a* and 6*b* that the austenite does not readily grow across the existing ferrite grain boundaries, and hence, that its growth is probably confined at first within the ferrite grain in which the growth starts. Further evidence that the ferrite boundaries offer a restraining influence on the growth of austenite will be presented later in this paper.

It was disappointing to the present author to be unable to duplicate the mechanism described by Bain for the formation of austenite in coarsely spheroidized steels, for this would have served to define the conditions for which this mechanism would apply. As a result of the present author's work the conclusion seems justified that the idealized symmetrical growth of austenite around coarse, spheroidized carbides occurs rarely in commercial steels austenitized in the conventional manner by continuous heating.

Formation of Austenite from Bainite: It can be taken as established, therefore, that in steels with prior structures of martensite or tempered martensite, austenite shows marked preferential growth in certain directions, and a lamellar distribution of austenite and acicular ferrite exists within the transformation range. When the prior structure is pearlite, or spheroidite produced by a high temperature transformation, this marked direction growth does not occur, the austenite is more nearly equiaxed, and the residual ferrite is blocky.

It was natural to determine at this point how austenite grows in prior structures which were formed at intermediate temperatures, that is, in

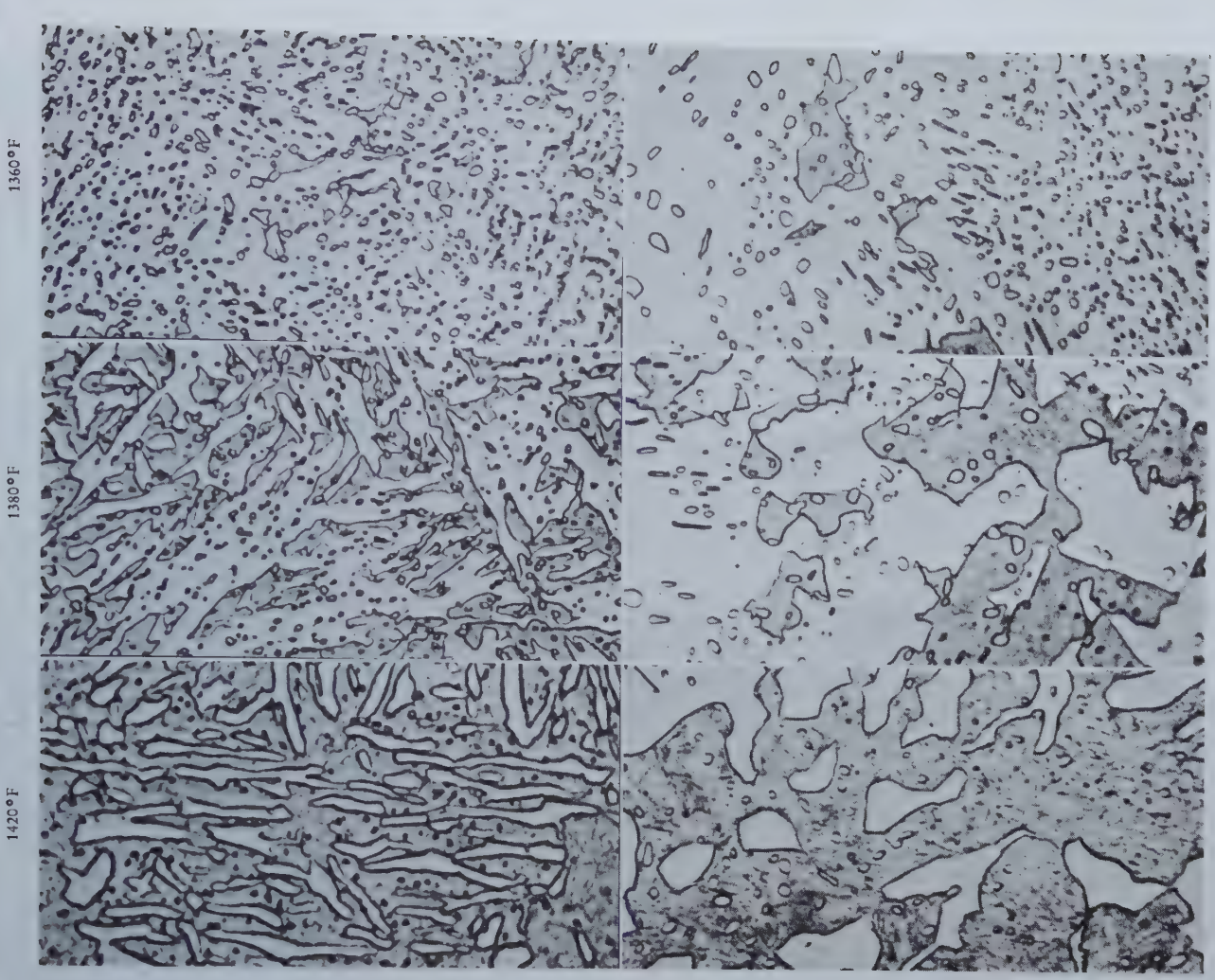

Fig. 3—Growth of austenite in spheroidal structures in 4140

produced by a. (left) tempering martensite 225 hr at 1200°F and b. (right) by a high temperature transformation. Water quenched from the indicated temperature and tempered ½ hr at 400°F. Dark etching structure (tempered martensite) was austenite at time of quench. X2000. Etched in picral-zephiran chloride reagent. (Slightly reduced in reproduction.) Top 1360°F. Center 1380°F. Bottom 1420°F.

bainite. In some work that need not be reproduced here it was found that the same directional growth of austenite occurs in bainitic structures that was described for martensitic structures, whereas the equiaxed growth of austenite occurs only in the case of prior structures resulting from a transformation in the pearlite region.

The Structure of Martensite: Before the observations which were made to establish the mechanism by which the acicular growth of austenite occurs in martensitic structures are described and discussed, some attention should be given to the structure of martensite. It will be shown subsequently that it is this structure that exerts the controlling influence on the growth of the new austenite.

The fact that martensite has an acicular or needle-like structure is well known, and there are many excellent micrographs[27–29] in the literature which illustrate this constituent of hardened steels. Many individual needles of martensite result from the transformation of a single grain of austenite, and Greninger and Troiano[30] have shown that each of these needles is a single crystal of martensite. Baeyertz[29] has suggested, on the basis of the similarity in shape of the ferrite grains produced by tempering martensite, that each needle of martensite becomes a single ferrite grain on tempering.

The martensite needles form parallel to a given crystallographic plane of the parent austenite lattice. In the case of the medium carbon steels Greninger and Troiano[29] have ascertained that martensite delineates the {4 4 10} planes of the austenite. This orientation habit is a function of the carbon content, and is independent of the temperature of formation of the martensite, as these authors have pointed out. There is also known to be a definite relationship between the lattice of martensite and that of the parent austenite. Greninger and Troiano[30] have accurately determined this relationship for a 0.8 pct carbon, 22 pct nickel alloy.

As a consequence of the orientation relationships between martensite and the parent austenite it is possible to develop an indication of the prior austenite grain size of hardened steel by the use of suitable etching procedures.[1] An example of this is shown in fig. 7*a*. The darker portions of fig. 7*a* when examined at high magnification consist of needles which vary in color from black to almost white. This is illustrated by fig. 7*b*. In the lighter portions of fig. 7*a* it is not possible to develop very much

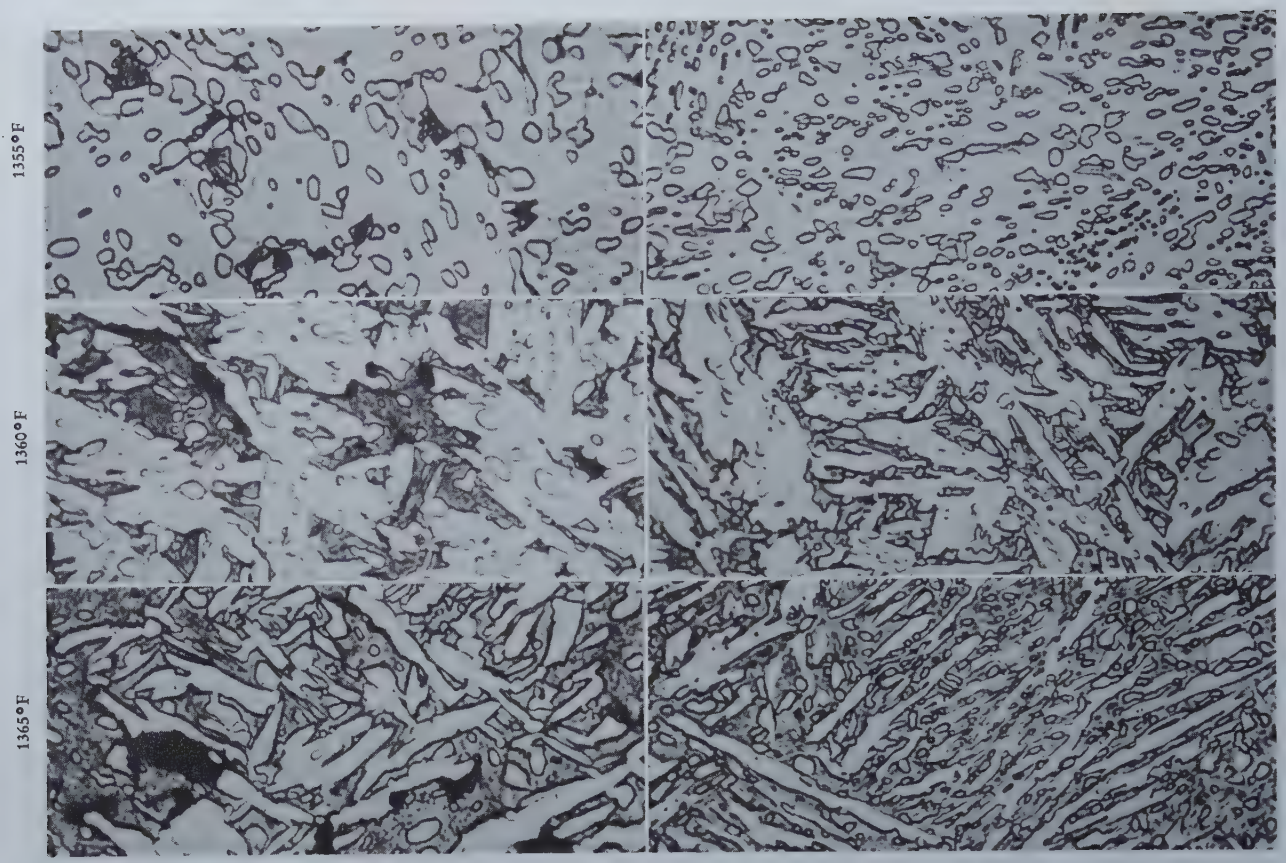

Fig. 4—Acicular growth of austenite in a hypereutectoid carbon steel and in a hypereutectoid alloy tool steel

spheroidized by tempering 100 hr at 1300F. a. (left) 1.10 pct carbon plain carbon steel. b. (right) 0.90 pct C—1.30 Mn—0.5 Cr—0.5W steel. Specimens were heated at the rate of 60°F per hr and were quenched when the indicated temperatures were reached. Tempered ½ hr at 400°F. Dark etching areas were austenite at time of quench. X2000. (Slightly reduced in reproduction.) Etched in picral-zephiran chloride reagent.

contrast between the various needles of martensite as fig. 7c shows. All three of the micrographs in fig. 7 were obtained from a hardened, untempered sample of 4140 steel given a single etch.

During the tempering of martensite the tetragonal crystal structure becomes cubic and there are a precipitation and agglomeration of carbides. The resulting ferrite retains the orientation and acicular shape of the martensite needles from which it forms. This is illustrated by fig. 8 which contains three micrographs for 4140 hardened to martensite, and tempered at 1300°F for 100 hr. It will be noted that these micrographs are similar to those shown in fig. 7 for untempered martensite. The prior austenite grain size is still indicated as fig. 8*a* shows. Also in the darker portions of fig. 8*a* good contrast can be developed between the ferrite grains (fig. 8*b*) but not in the lighter portions (fig. 8*c*).

Observations similar to these were made about 25 yr ago by Hanemann and Schrader[28] and formed the basis for their epsilon-eta hypothesis. In brief, these authors believed that martensite consists of two metastable phases of different carbon contents. As a result of the microscopic examination of tempered samples it was concluded that the epsilon crystals after tempering consisted of ferrite with a small amount of precipitated carbide whereas the eta crystals consisted of ferrite with a great deal of carbide. Furthermore, that the ferrite resulting from the decomposition of the epsilon phase etched differently from that obtained from the eta phase.

However, later work has shown that in steels[31, 32, 33] and other alloys[34, 35] the martensite transformation involves no diffusion. A more reasonable explanation for the differences in etching behavior of the individual martensite grains, and of the ferrite grains which result from them on tempering, is that this is attributable to differences in their lattice orientations, particularly since a great deal of contrast can be developed in certain fields with little contrast in other fields in the same microsection.

Since it has not been previously recognized in this country that etching differences exist in the ferrite of tempered martensite, it would perhaps be well to record a few observations on the effect of etching time with the new etching reagent, and on the effect of using different standard reagents. Fig. 9 shows the effect of a 5 and a 15 sec electrolytic etch in Allten's reagent, and of a 15 sec immersion etch in the picral-zephiran chloride reagent on the appearance of a single field in a sample of 4140 steel quenched to form martensite, and thoroughly tempered by a 100 hr heating at 1300°F. The specimen was repolished lightly after each etch.*

* Different inclusions appear in the micrographs but this is because the inclusions were not large enough to persist through the repolishing operations.

It will be seen in fig. 9 that alternate acicular ferrite grains are etched in 5 sec in the Allten reagent whereas the intervening grains are only barely attacked. A 15 sec etch in this reagent fully develops the carbides in the more resistant ferrite,

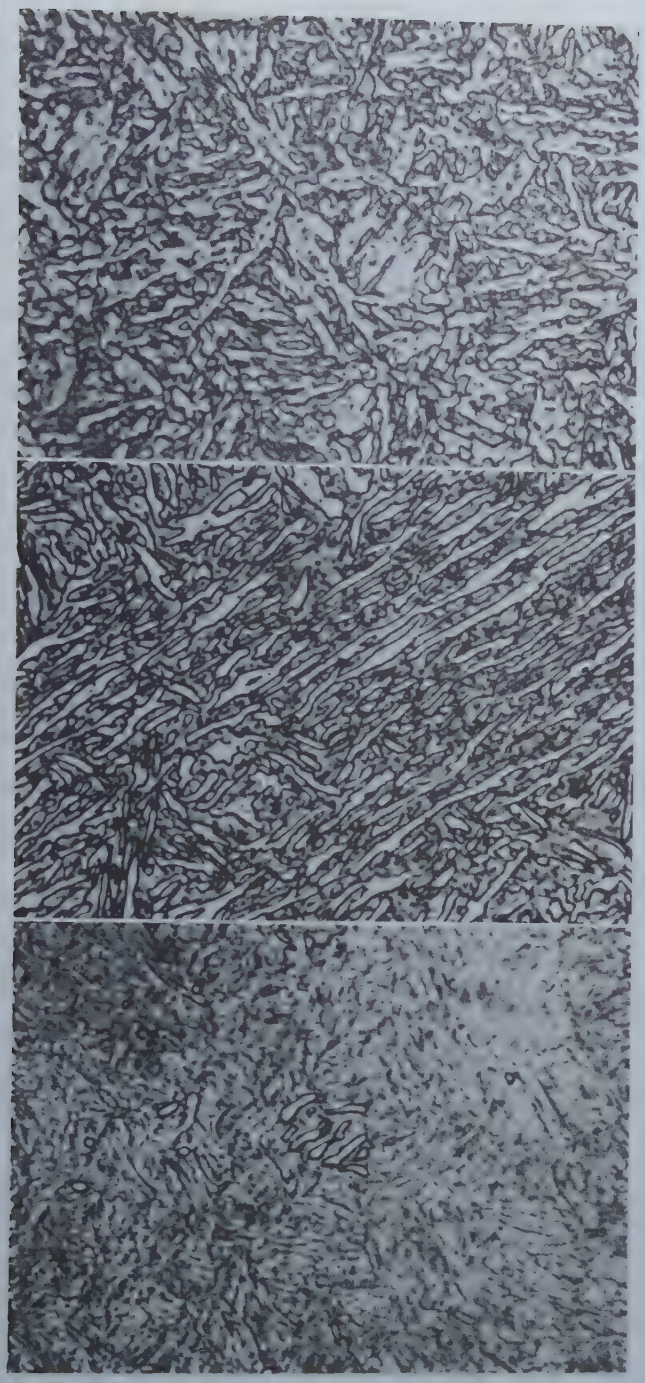

Fig. 5—Acicular growth of austenite in martensite of the 4340 steel

heated within the Ac_1-Ac_3 temperature region. Water quenched from the indicated temperature and tempered ½ hr at 400°F. Dark etching structure (tempered martensite) was austenite at time of quench. *a*. (top) Martensite heated to 1325°F 1 hr. *b*. (center) Martensite heated to 1350°F 1 hr. *c*. (bottom) Martensite heated to 1375°F 1 hr. X2000. Etched in picral-zephiran chloride reagent. Slightly reduced in reproduction.

but begins to overetch the readily etched ferrite. The use of a longer etching time, as in fig. 8*b* which was discussed previously, results in a considerable amount of roughening of the readily etched ferrite.

Results similar to those shown in fig. 9*a* and 9*b* can be obtained by using nital, but this reagent does not delineate the carbides as satisfactorily as the Allten reagent. When picral is used, on the other hand, the differences in etching behavior of adjacent acicular ferrite grains are no longer apparent as fig. 9*c* shows.

The Mechanism of the Formation of Austenite in Martensite or Tempered Martensite: Since some tempering must occur during the heating of martensite up to and above A_{c1} temperature, the real difference between the initial conditions termed martensite and tempered martensite in this paper is in the extent of the tempering, that is, in the degree of agglomeration of the carbides. In the case of the martensitic prior condition little time was available for this agglomeration, whereas an unusually long time was allowed for the tempered condition.

The rate of austenite formation was affected by the degree of tempering, but the mechanism of the formation of austenite from either martensite or tempered martensite must be fundamentally the same because similar microstructures were produced by partially austenitizing samples in either condition. The only difference that could be detected was that the width of the elongated grains of austenite and residual ferrite appeared to be slightly greater in the samples which had been previously tempered at 1300°F for 100 hr. The reason for this will become known later in this paper.

Micrographs which illustrate the mechanism of the formation of austenite in martensite which had been tempered by a 100 hr heating at 1300°F prior to being heated above the A_{c1} temperature are contained in fig. 10. In these micrographs the slightly dark etching structure (tempered martensite) denotes areas that were austenite when the specimens were quenched.

The exact locations at which the new austenite shown in fig. 10*a* and 10*b* was nucleated could not be observed because the smallest areas of new austenite contain the sites of both ferrite-ferrite and ferrite-carbide interfaces. Since it is commonly accepted that the work involved in the formation of a nucleus of a new phase is a minimum at grain boundaries, and since all of the smallest new austenite grains which were observed throughout the course of this investigation contained ferrite-ferrite interfaces, it appears reasonable to conclude that the nuclei formed in these boundaries, probably at points where carbides are located.

In the case of areas in which it was possible to develop good contrast between adjacent acicular ferrite grains, it appeared that the early growth was confined within the grains most resistant to etching. Examples of this are shown in fig. 10. It will be noted that there is a sharp grain boundary between the new austenite and the ferrite in which it is growing only at the sites of the former ferrite boundaries. The growth seems to occur from opposite sides of a ferrite grain toward the center until that grain is completely transformed. Then, the intervening ferrite grains are transformed by growth from the former sites of the ferrite grains most resistant to etching.

Why the early growth of austenite should appear to be confined to the one type of ferrite is difficult to understand. Since the difference in the ferrite is believed to be one of orientation, the implication is that one orientation of ferrite is more favorable for the growth of austenite than another. Whether this is true or not, it seems clear that the growing

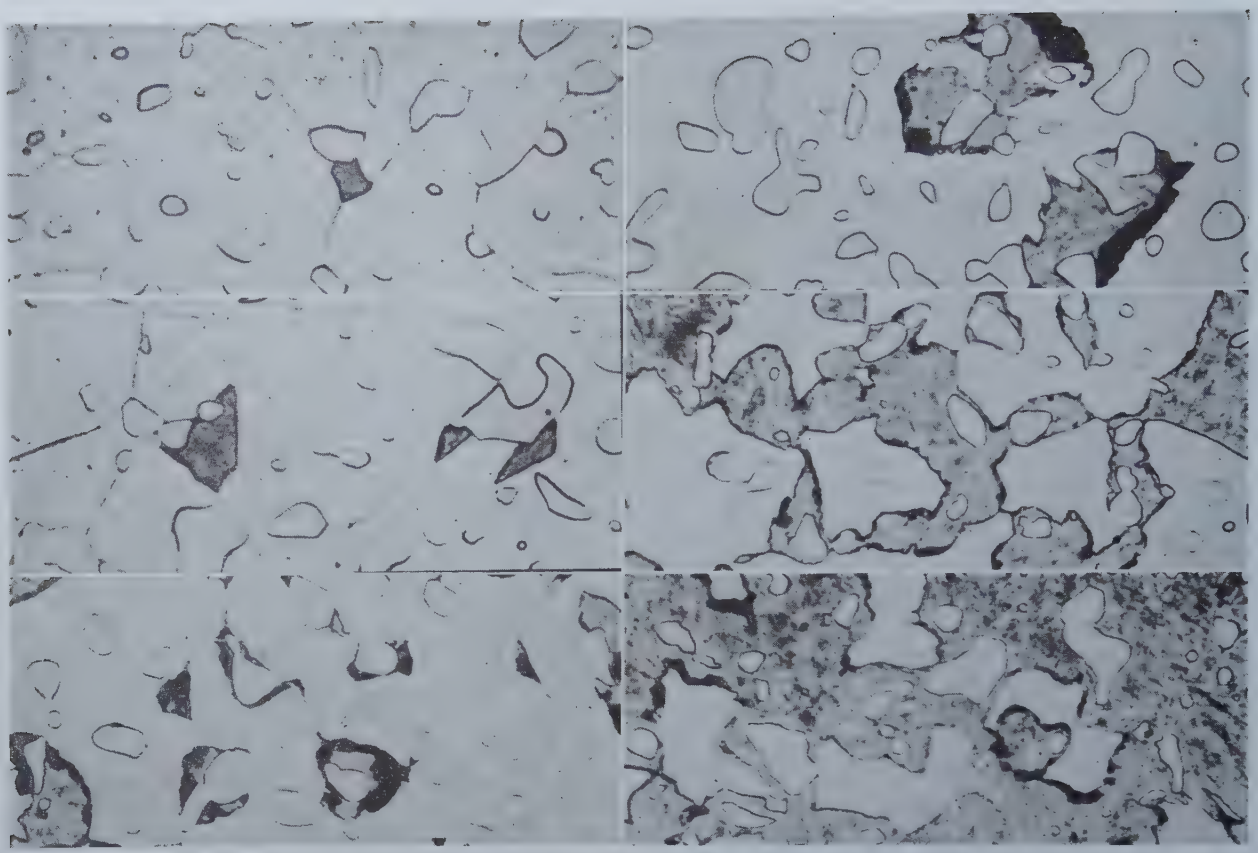

Fig. 6—Isothermal growth of austenite in a 1.10 pct carbon, plain carbon steel coarsely spheroidized by multiple full annealing.

Samples ⅛ in. thick were heated in lead at 1400°F for the indicated times and quenched. Tempered at 400°F for ½ hr. Dark areas were austenite at time of quench. *a.* 25 sec. *b.* 30 sec. *c.* 40 sec. *d.* 60 sec. *e.* 100 sec. *f.* 120 sec. X2000. Etched in picral-zephiran chloride reagent.

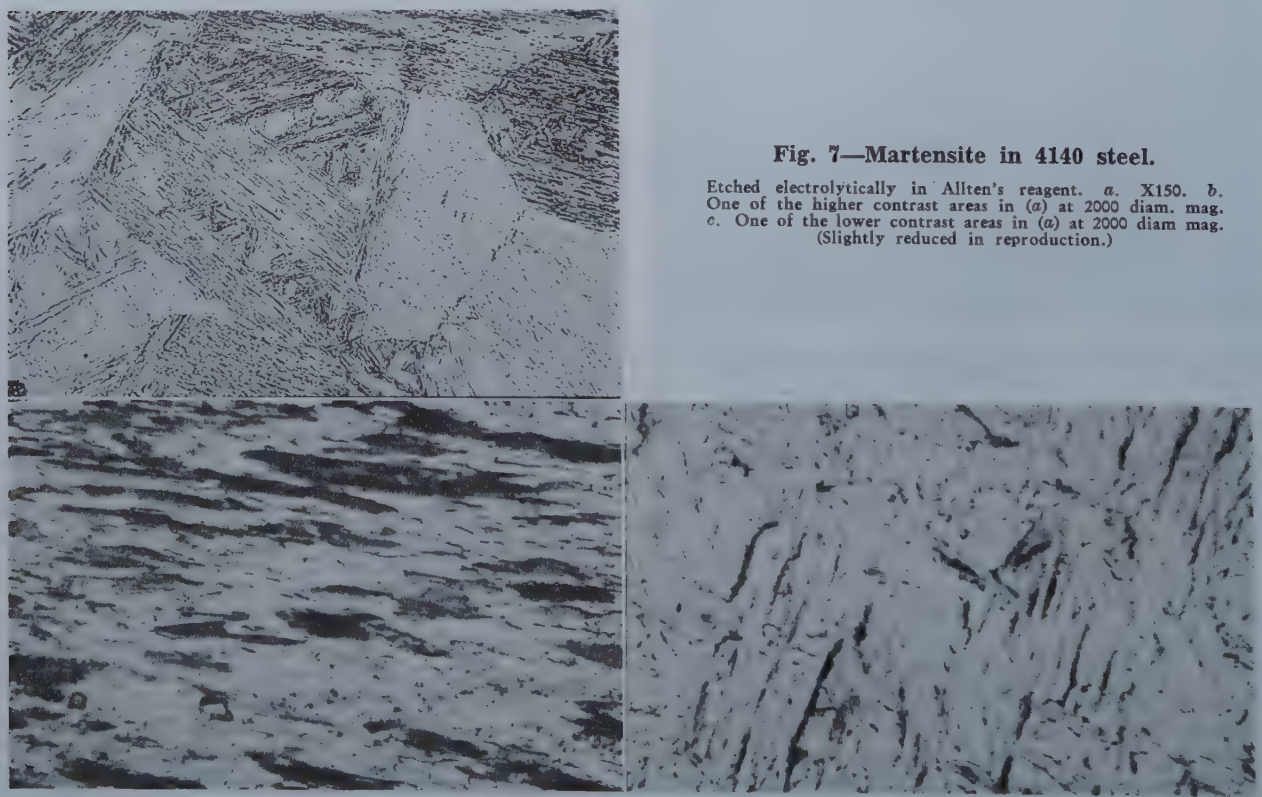

Fig. 7—Martensite in 4140 steel.

Etched electrolytically in Allten's reagent. *a.* X150. *b.* One of the higher contrast areas in (*a*) at 2000 diam. mag. *c.* One of the lower contrast areas in (*a*) at 2000 diam mag. (Slightly reduced in reproduction.)

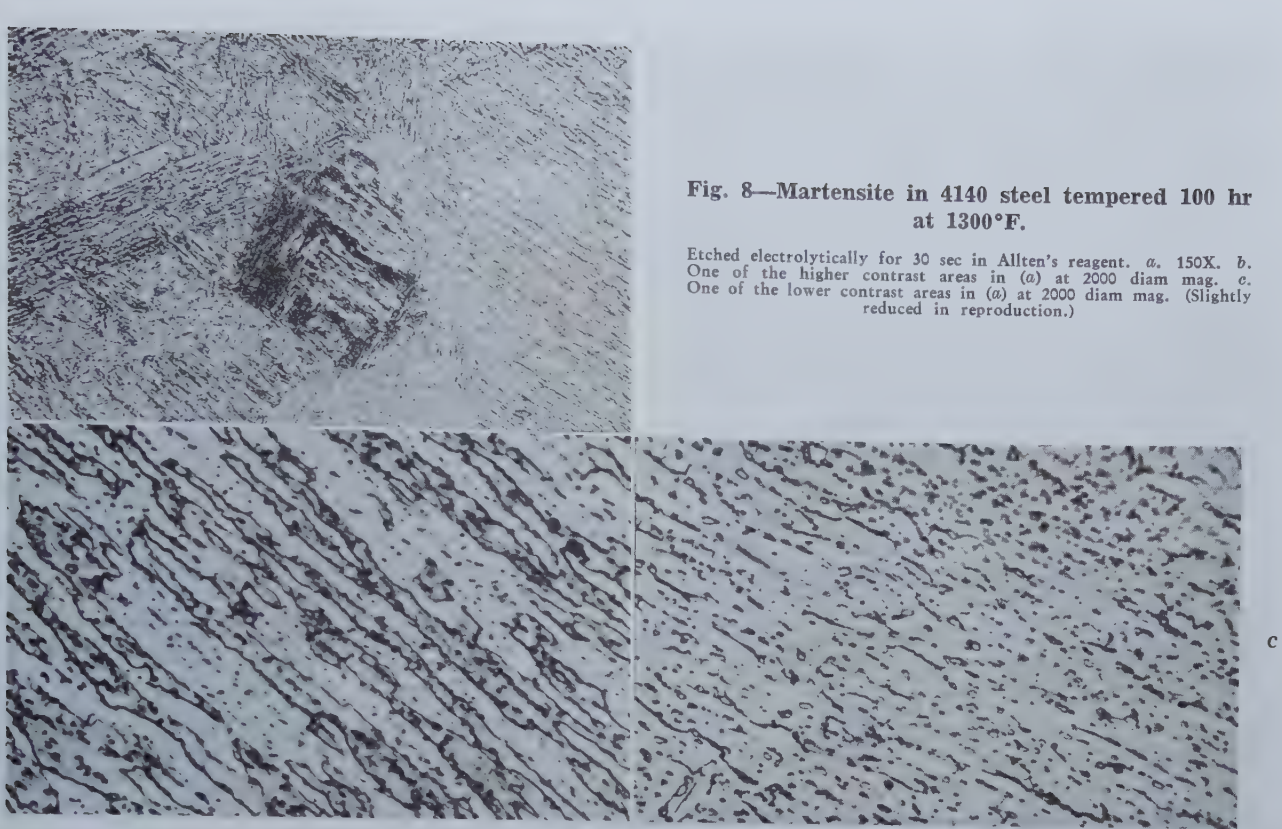

Fig. 8—Martensite in 4140 steel tempered 100 hr at 1300°F.

Etched electrolytically for 30 sec in Allten's reagent. *a*. 150X. *b*. One of the higher contrast areas in (*a*) at 2000 diam mag. *c*. One of the lower contrast areas in (*a*) at 2000 diam mag. (Slightly reduced in reproduction.)

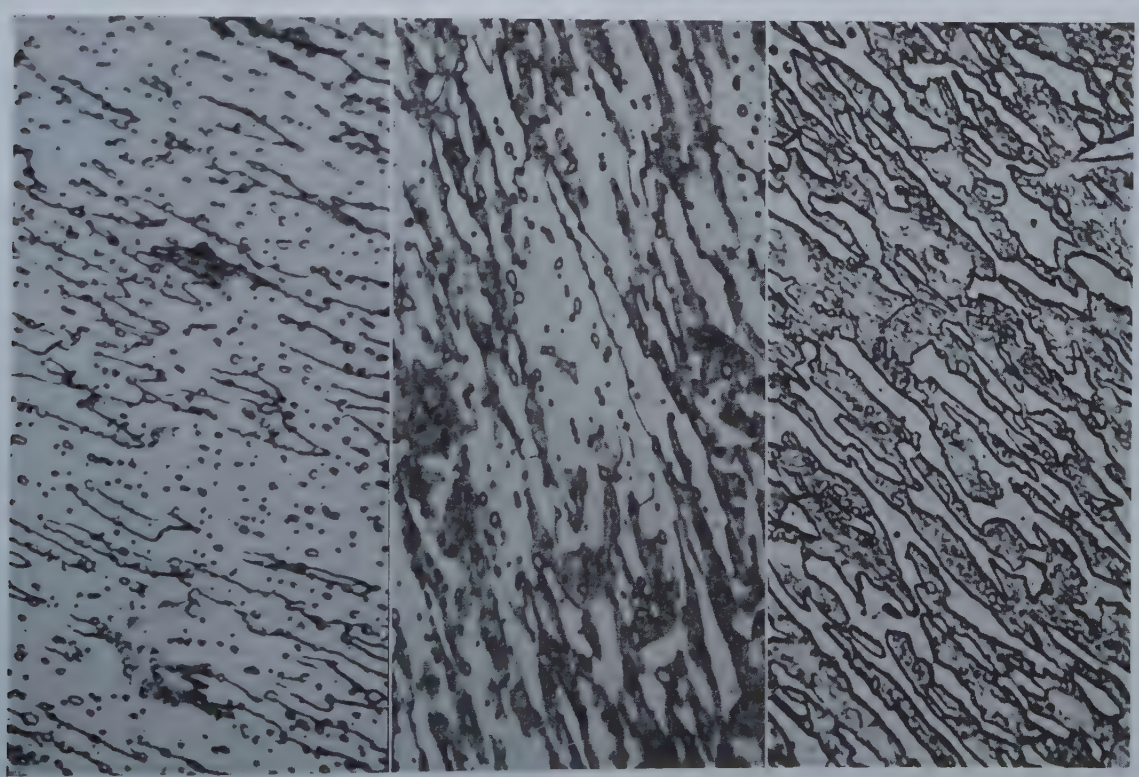

Fig. 10—Nucleation and growth of austenite in martensite

in 4140 steel which had been tempered by a 100 hr heating at 1300°F prior to being heated above the Ac_1 temperature. Specimens were heated continuously at the rate 60°F per hr, quenched from the temperatures indicated, and tempered ½ hr at 400°F as follows. Dark etching areas were austenite at time of quench. X2000. Etched electrolytically in Allten's reagent. *a*. 1400°F. *b*. 1410°F. *c*. 1450°F.

austenite does not readily cross ferrite boundaries, particularly when the adjacent grains have considerably different lattice orientations, and the new austenite therefore assumes the shape of the acicular ferrite grains in which it begins its growth.

Mechanism of the Formation of Austenite in

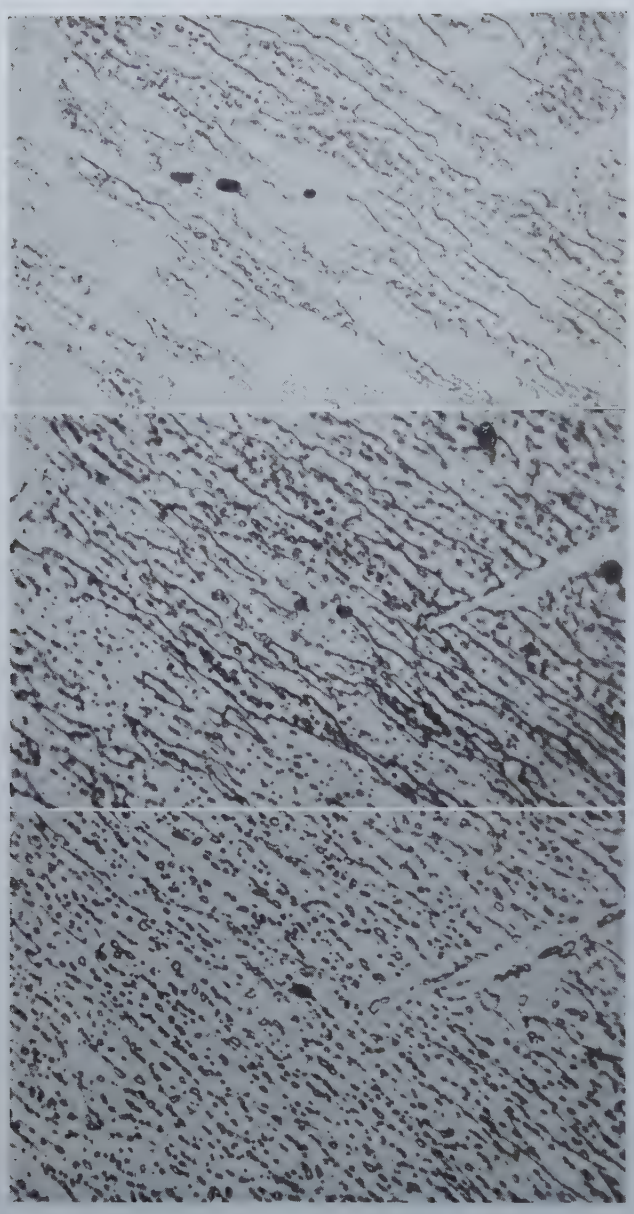

Fig. 9—Effect of different etching reagents on the microstructure of tempered martensite in 4140 steel.

All three photographs are of the same field. The specimen was repolished to remove the previous etch before being re-etched. X2000. (Slightly reduced in reproduction.) *a*. (top) 5 sec electrolytic etch in Allten's reagent. *b*. (center) 15 sec electrolytic etch in Allten's reagent. *c*. (bottom) 15 sec immersion in picral-zephiran chloride reagent.

Fig. 11—Nucleation and growth of austenite in spheroidite

in 4140 steel produced by a high temperature transformation. a. (top) 1390°F. b. (bottom) 1450°F. Specimens were heated continuously at the rate of 60°F per hr, quenched from the indicated temperature, and tempered ½ hr at 400°F. Darker etching areas were austenite at time of quench. X2000. Etched electrolytically in Allten's reagent. (Slightly reduced in reproduction.)

Spheroidal Structures Produced by a High Temperature Transformation: Fig. 11 shows that the mechanism of the formation of austenite in spheroidal structures produced by a high temperature transformation is similar to that just discussed for spheroidized structures produced by tempering martensite. That is, nucleation appears to have occurred in ferrite boundaries, and the growth is confined within the ferrite grain in which the austenite started to grow with the result that it assumes the shape of the prior ferrite grain. The differences in the shape of the austenite grains produced in prior structures spheroidized by a temper, and in those produced by a high temperature transformation, are attributable to the fact that the ferritic matrix consists of acicular grains in the former case and equiaxed grains in the latter.

It is further indicated by fig. 11 that it is possible to develop by means of a suitable etching procedure differences in the adjacent ferrite grains in a high temperature transformation product which are comparable to those previously described for the ferrite resulting from the tempering of martensite. In fig. 11*a* there are three distinctly different orientations of the ferrite grains. Some of them are roughened (darkened) as a result of being slightly overetched, others are properly etched and appear to be white and contain well defined carbide particles, and still others are underetched, that is, have not been etched sufficiently to develop the carbides clearly. Now, it seems even more likely that the differences in the etching characteristics of the ferrites in tempered martensite are attributable to differences in orientation because it is hard to believe that there could be any other factor that could cause these similar differences in a ferritic matrix resulting from a high temperature transformation.

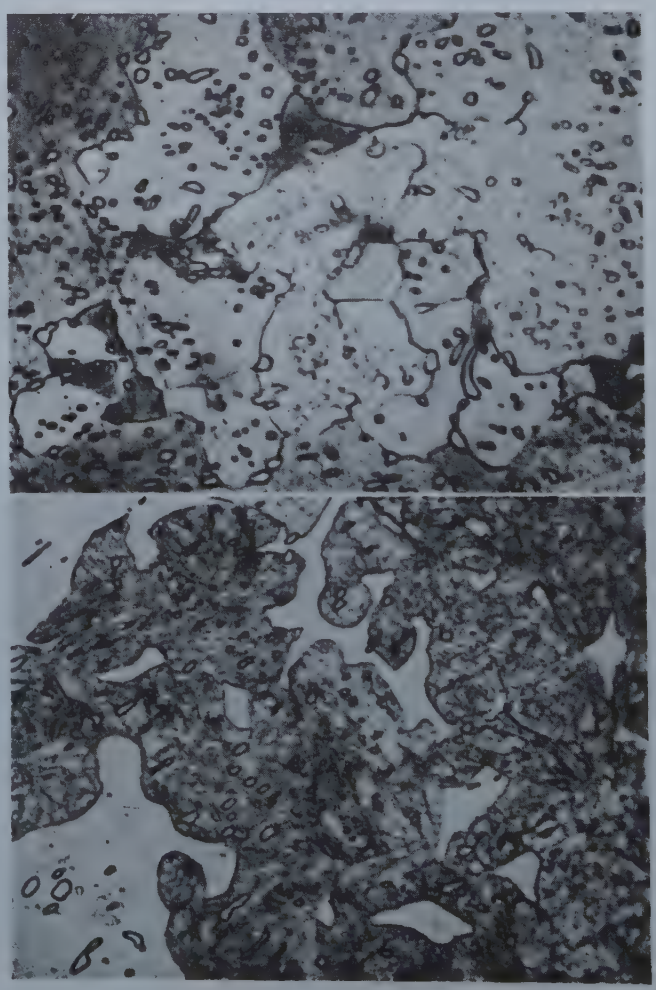

Fig. 12—Stability of acicular ferrite

in new 0.25 C Mn-Si-Ni-Mo steel held at 1350°F for *a*. (above)—1 hr, *b*. (below) 136 hr. Water quenched and tempered ½ hr at 600°F. Prior condition as rolled. (Bainite plus martensite.) X2000. (Slightly reduced in reproduction.) Picral-zephiran chloride etch.

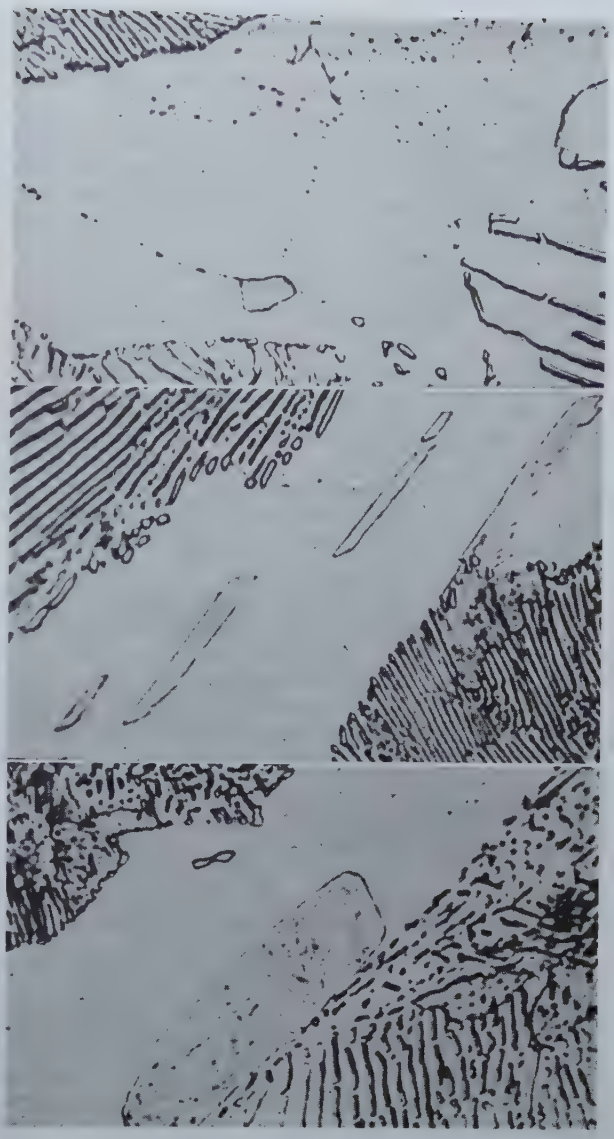

Fig. 13—Early stages in nucleation and growth of austenite in lamellar pearlite and ferrite in SAE 4140.

Specimens were heated continuously at rate of 60°F per hr, quenched from indicated temperature, and tempered ½ hr at 400°F to darken the martensite formed from the austenite present at time of quench. *a*. (top) 1380°F. *b*. (center) 1390F. *c*. (bottom) 1390°F. X2000. Etched in picral-zephiran chloride reagent.

Finally, it is clear from fig. 11*a* that the orientation of the ferrite is not a factor in the growth of austenite in this prior structure, for it can be seen that growth is occurring simultaneously in three ferrite grains of three different orientations. It may very well be, then, that the observation that austenite appeared to grow preferentially in the etch resistant ferrite in the case of tempered martensitic structures may not have been entirely reliable. In fig. 11*a* it can be seen that the most readily etched ferrite grains are about as dark as the areas which were austenitic at the time of quenching. It would therefore be extremely difficult to ascertain whether or not the readily etched ferrite areas in tempered martensite contained austenite when quenched from above the A_{c1} temperature.

Stability of Acicular Ferrite at High Temperatures: Since equiaxed ferrite grains can be formed by the transformation of austenite at temperatures as low as 1000°F, it seemed somewhat surprising to observe in this investigation that the acicular ferrite resulting from the tempering of martensite, or from the bainite reaction, does not become equiaxed when heated above the A_{c1} temperature. In order to find out how long the acicular ferrite could retain its shape in a hypoeutectoid steel at temperatures within the A_{c1}-Ac_3 region samples of the new Mn-Si-Ni-Mo steel were heated for various periods of time ranging from 1 to 136 hr at 1350°F, and were examined to ascertain the distribution of the austenite and ferrite in each sample. The temperature used is about 50°F above the A_{c1} temperature for this steel which was selected for this experiment because it has a wide spread between the A_{c1} and A_{c3} temperatures.

Fig. 12 shows that the ferrite and austenite tend to become less acicular with time, but that this change takes place very slowly. Evidently, the acicular shape is very persistent even though the steel is heated for long periods of time at temperatures as much as 300°F higher than that at which equiaxed ferrite grains form from austenite by isother-

mal transformation. Fig. 12*b* indicates that even at the end of 136 hr at 1350°F the austenite and ferrite are still far from assuming the equiaxed, or equilibrium shape.

Formation of Austenite from Lamellar Pearlite plus Proeutectoid Ferrite in 4140 Steel: In the course of this investigation some observations were made in connection with the formation of austenite in the 4140 steel in the pearlitic condition which have not been described in the literature, and therefore seem worth recording here. The annealing cycle which was used to produce lamellar pearlite in this steel resulted in the separation of the proeutectoid ferrite in the grain boundaries of the prior austenite. The very first austenite to form during subsequent heating was located in this ferrite. Many areas similar to the one shown in fig. 13*a* were observed while there were relatively few instances in which the directional growth like that shown in fig. 13*b* was seen. Ordinarily it is considered that in hypoeutectoid steels nucleation of austenite first occurs in pearlite areas.[9, 11–18] In fig. 13*c* the growth of austenite in ferrite areas is farther advanced than it is in the adjacent pearlite areas.

Another interesting observation is that most of the last ferrite to transform to austenite actually did not exist as such in the initial structure. Instead, this last ferrite came from pearlite colonies from which the carbon diffused as the heating progressed. This is illustrated by fig. 14. Fig. 14*a* illustrates the initial structure which consisted of proeutectoid ferrite at the prior austenite grain boundaries with a number of different pearlite colonies within the grain. Fig. 14*b* shows the effect of heating this structure to 1425°F at the rate of 60°F per hr. It will be noted that the transformation to austenite has occurred at a greater rate in the vicinity of the prior austenite grain boundary than it has within the grain, and that much of the proeutectoid ferrite has been transformed. By the time 1450°F is reached most of the prior proeutectoid ferrite has been transformed and there are now ferrite areas within the prior austenite grain where there were only pearlite colonies before.

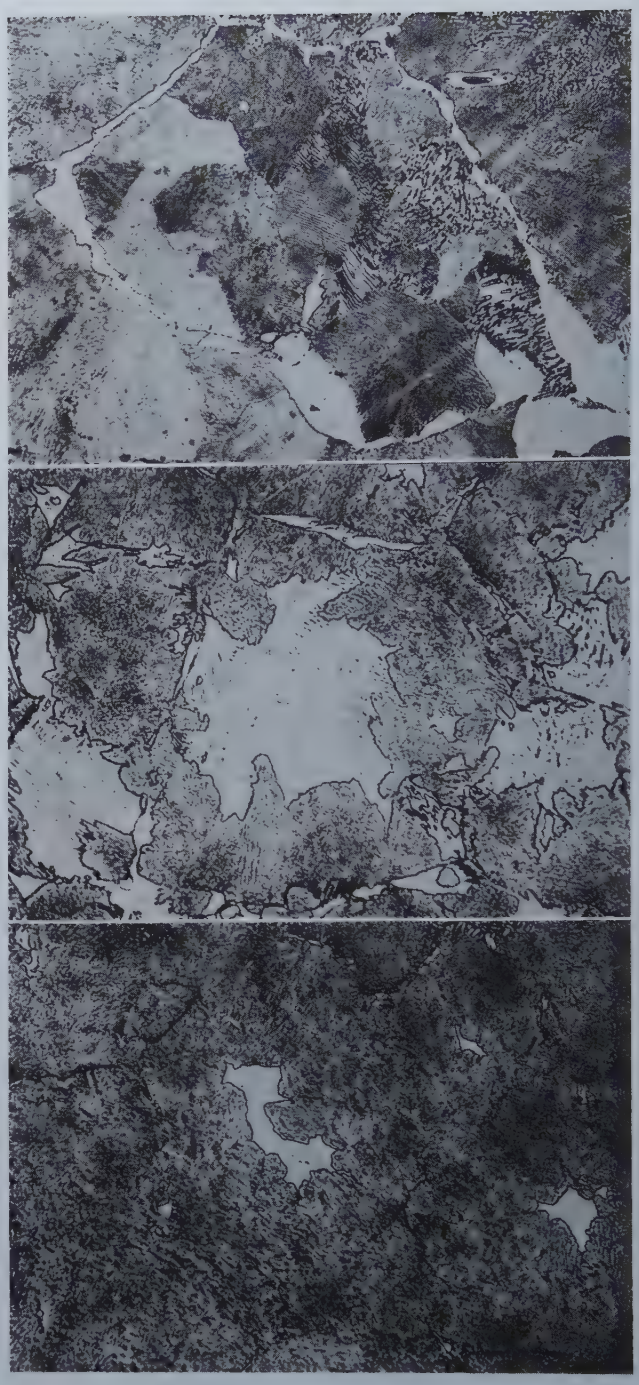

Fig. 14—Evidence of diffusion of carbon in SAE 4140 from pearlite colonies during transformation.

Note in (c) that most of the last ferrite to be transformed is located within the prior austenite grains in areas formerly occupied by pearlite, and that only small amounts of the proeutectoid ferrite at the prior austenite grain boundaries are untransformed. Temperatures indicated are those reached on continuous heating at the rate of 60°F per hr. Quenched specimens were tempered ½ hr at 400°F to darken the martensite formed during the quench. X250. Picral-zephiran chloride etch. (Slightly reduced in reproduction.) *a*. (above) Initial structure. *b*. (center) 1425°F. *c*. (bottom) 1450°F.

Summary

In this investigation it was shown that a relation exists between prior structure and the manner in which austenite grows during heating above the A_{c1} temperature. In steels partially transformed to austenite when the prior structure is pearlite, or spheroidite produced by a high temperature transformation, the austenite that forms grows in an equiaxed manner and the excess ferrite is blocky. When the prior structure is martensite, tempered martensite, or bainite, on the other hand, the austenite and ferrite grains are acicular in shape and lamellar microstructures consisting of these alternate acicular grains of austenite and ferrite are developed. This relation was found to hold for hypoeutectoid, eutectoid and hypereutectoid carbon steels and for hypoeutectoid and hypereutectoid alloy steels, that is, for steels in general.

In order to arrive at an understanding of this relation between prior structure and the mode of austenite formation a study was made of the mechanism by which austenite forms in steels. It was found that the new austenite does not grow freely in the manner assumed by previous investigators, but is confined in the early stages of its growth within the boundaries of the ferrite grain in which it happens to start its growth. It therefore assumes the shape of that ferrite grain. When the ferritic

matrix is equiaxed as a result of a high temperature transformation the austenite grains are equiaxed, and when the ferrite grains are acicular as they are in tempered martensite or bainite, the initial austenite grains are also acicular.

Certain similarities between the microstructures of untempered and tempered martensite were mentioned. It was shown that in tempered martensite there are regions in which adjacent acicular ferrite grains are attacked at different rates by certain etching reagents, and that there are corresponding areas in untempered martensite in which adjacent needles are also etched differently. It was suggested that these differences are the result of differences in the lattice orientations of the martensite needles and of the acicular ferrite grains which result from the tempering of martensite. The prior austenite grain size was shown to be delineated in thoroughly tempered as well as in untempered martensite which indicates that the orientation relationships between the parent austenite and the martensite are not changed by the tempering operation. In other words, during the tempering of martensite there is a collapsing of the tetragonal lattice and a precipitation and agglomeration of carbides without a change in the lattice orientation of the ferrite.

Acknowledgment

The author gratefully acknowledges the assistance given him by F. Baureis, A. Simon, and G. Stefanelli of the Research Laboratory Staff of Crucible Steel Co. of America in obtaining the data which have been presented. The helpful suggestions and criticisms made by Lo-ching Chang, J. Gilman and other members of the Research Laboratory staff with whom the data were reviewed and discussed are greatly appreciated.

The author is particularly indebted to P. Payson, Assistant Director of Research, for his interest and encouragement in this work.

References

[1] E. C. Bain and J. R. Vilella: Austenitic Grain Size in Steel. A.S.M. Handbook, 1948 ed., p. 399-406.

[2] G. A. Roberts and R. F. Mehl: The Mechanism and the Rate of Formation of Austenite from Ferrite-Cementite Aggregates. *Trans.* A.S.M. (1943) **31**, 613-650.

[3] E. C. Bain: Functions of the Alloying Elements in Steel. A.S.M. (1939) p. 101-112.

[4] J. M. Robertson: The Transformation of Austenite Below the Critical Range. Carnegie Scholarship Memoirs (1931) p. 1-64.

[5] C. L. Shapiro: The Effect of Heat Treatment, Aging and Working Upon the Condition of Carbon in Steel. Carnegie Scholarship Memoirs (1936) p. 141-196.

[6] J. H. Andrew and H. A. Dickie: The A_{c1} Range in Special Steels. *Jnl.* Iron and Steel Inst. (1927) **115**. No. 1, 647-684.

[7] J. A. Jones: The A_{c1} Range in Alloy Steels. *Jnl.* Iron and Steel Inst. (1923) **107**, No. 1, 439-454.

[8] C. C. Hodgson and H. G. Baron: Large Crystal Grain Size in Silicon-Chromium Valve Steel. *Jnl.* Iron and Steel Inst. (1949) **161**, No. 2, 81-85.

[9] M. Baeyertz: Effects of Initial Structure on Austenite Grain Formation and Coarsening. *Trans.* A.S.M. (1942) **30**, 458-490.

[10] T. G. Digges and S. J. Rosenberg: A Metallographic Study of the Formation of Austenite from Aggregates of Ferrite and Cementite in an Iron-Carbon Alloy of 0.5 per cent Carbon. *Trans.* A.S.M. (1943) **31**, 753-776.

[11] H. C. H. Carpenter and J. M. Robertson: Structural Changes in Hypoeutectoid Steels on Heating. *Jnl.* Iron and Steel Inst. (1933) **127**, No. 1, 259-300.

[12] H. C. H. Carpenter and J. M. Robertson: The Austenite-Pearlite Inversion. *Jnl.* Iron and Steel Inst. (1932) **125**, No. 1, 309-338.

[13] H. C. H. Carpenter and J. M. Robertson: *Metals.* **2**, 914-923. Oxford Univ. Press, 1939 ed.

[14] M. A. Grossmann: Grain Size in Metals, with Special References to Grain Growth in Austenite. *Trans.* A.S.M. (1934) **22**, 861-878.

[15] M. A. Grossmann: On Grain Size and Grain Growth. *Trans.* Amer. Soc. for Steel Treaters (1933) **21**, 1079-1111.

[16] M. A. Grossmann: Principles of Heat Treatment. A.S.M. (1940) 1-43.

[17] E. Walldow: The Mechanism of the Solution of Cementite in Carbon Steel and the Influence of Heterogeneity. *Jnl.* Iron and Steel Inst. (1930) **122**, No. 2, 301-341.

[18] J. O. Arnold and A. McWilliams: The Thermal Transformations of Carbon Steels, *Jnl.* Iron and Steel Inst. (1905) **68**, No. 2, 27-55.

[19] A. Hultgren: The A_{c1} Range of Carbon Steel and Related Phenomena. *Trans.* Amer. Soc. for Steel Treaters. (1929) **16**, 227-256.

[20] J. H. Whiteley: The Formation of Globular Pearlite. *Jnl.* Iron and Steel Inst. (1922) **105**, No. 1, 339-357.

[21] J. H. Whiteley: The Growth of Austenite Above A_{c1} in Plain Carbon Steels. *Jnl.* Iron and Steel Inst. (1932) **126**, No. 2, 289-300.

[22] H. Jungbluth: The Retarded Solution of Granular Pearlite at the Transformation Point. *Stahl und Eisen,* (1925) **45**, 1918.

[23] A. Portevin and V. Bernard: Influence of Coalescence on the Mechanical Properties of Steel and on Alloys. *Jnl.* Iron and Steel Inst. (1914) **90**, 204.

[24] J. H. Andrew, J. E. Rippon, C. P. Miller and A. Wragg: The Effect of Initial Temperature Upon the Physical Properties of Steel. *Jnl.* Iron and Steel Inst. (1920) **101**, No. 1, 527-612.

[25] P. Payson and A. E. Nehrenberg: New Steel Features High Strength and High Toughness. *The Iron Age,* **162**, No. 17, Oct. 21, 1948, p. 64-71 and No. 18, Oct. 28, 1948, p. 75-80, 152, 154.

[26] R. A. Grange, W. S. Holt and E. T. Tkac: Transformation of Austenite in an Aluminum-Chromium-Molybdenum Steel. *Trans.* AIME (1947) **172**, 452-466.

[27] F. Lucas: The Microstructure of Austenite and Martensite. *Trans.* ASST (1924) **6**, 669-691.

[28] H. Hanemann and A. Schrader: On Martensite. *Trans.* ASST (1926) **9**, 169-239.

[29] A. B. Greninger and A. R. Troiano: Crystallography of Austenite Decomposition. *Trans.* AIME (1940) **140**, 307-336.

[30] A. B. Greninger and A. R. Troiano: Mechanism of Martensite Formation. *Trans.* AIME (1941) **145**, 289-291. *Jnl. of Metals,* Sept. 1949, 590.

[31] E. Ohman: X-Ray Investigations on the Crystal Structure of Hardened Steel. *Jnl.* Iron and Steel Inst. (1931) **123**, No. 1, 445-463.

[32] K. Honda and Z. Nishiyama: On the Nature of the Tetragonal and Cubic Martensites. Sci. Rep. Sendai (1932) **21**, 299.

[33] G. Hagg: X-Ray Investigation on the Structure and Decomposition of Martensite. *Jnl.* Iron and Steel Inst. (1934) **130**, No. 2, 439-451.

[34] W. Schmidt: Rontgenographische Untersuchen uber das System Eisen-Mangan. *Arch. Eisenhuttenw.* (1929) **3**, 293.

[35] M. Hansen: Der Aufbau der Zweistofflegierungen. Julius Springer, Berlin, 1936, p. 696.

The Elastic Coefficients of

Single Crystals of Alpha Brass

by Raymond W. Fenn, Jr., Walter R. Hibbard, Jr., and Henry A. Lepper, Jr.

From tension and torsion experiments on single crystals of alpha brass, the following values were obtained for elastic coefficients: (Unit: 10^{-13} cm² per dyne)

		71.2 pct Copper	77.4 pct Copper
	S_{11}	18.82	17.10
	S_{12}	—9.45	—8.23
	S_{44}	15.55	14.90
Elastic anisotropy	$S_{44} - 2(S_{11} - S_{12})$	—40.99	—35.7
Poisson's ratio	$-S_{12}/S_{11}$	0.502	0.482

THIS paper reports the results of static tension and torsion tests made on single crystals of alpha brass for the purpose of determining its elastic coefficients. 70-30 alpha brass was chosen because it has been used extensively in the study of the plastic deformation and because it has the following desirable characteristics: (1) face-centered cubic structure, (2) marked elastic anistropy, (3) low elastic modulus.

In 1928 Masima and Sachs[1] using static methods reported the following values for the elastic coefficients of 72-28 pct alpha brass:

$$S_{11} = 19.4 \times 10^{-13} \text{ cm}^2 \text{ per dyne}$$
$$S_{12} = -8.35 \times 10^{-13} \text{ cm}^2 \text{ per dyne}$$
$$S_{44} = 13.9 \times 10^{-13} \text{ cm}^2 \text{ per dyne}$$

These values were obtained from the measurements shown in fig. 1. The experimental points for both tension and torsion lie consistently below the lines drawn to represent them. Fig. 2 shows the stress-strain curves for their specimens. Only a few points in the elastic range of these curves were available to obtain their values for Young's modulus. Therefore, it was considered that a re-evaluation of these data was desirable.

In addition a variation of from 1.13 to 1.485 kg per mm² was found in the values of the critical resolved shear stress for 70-30 alpha brass reported by Burghoff,[2] Treuting and Brick,[3] Martin,[4] Maddin, Mathewson and Hibbard[5, 6] and von Göler and Sachs.[7] Therefore, it was desired to evaluate the conclusion of Boas and Schmid[8] that a constant resolved shear stress and not a constant elastic shear initiates plastic deformation.

Theoretical Considerations*: The elastic deformation of cubic crystals may be defined by three elastic coefficients (S_{11}, S_{12}, S_{44}) or three elastic parameters (C_{11}, C_{12}, C_{44}). These coefficients or parameters are sufficient to define the stress and strain relations for cubic crystals in the generalized form of Hooke's law referred to Cartesian coordinates.

Elastic parameters and coefficients in the cubic system are related by the expressions:

$$C_{11} = \frac{S_{11} + S_{12}}{(S_{11} - S_{12})(S_{11} + 2S_{12})} \quad [1]$$

$$C_{12} = \frac{-S_{12}}{(S_{11} - S_{12})(S_{11} + 2S_{12})} \quad [2]$$

$$C_{44} = 1/S_{44} \quad [3]$$

It is possible to determine all the elastic coefficients for a cubic metal by measuring two of the three elastic constants: Young's modulus (E), torsion modulus (G), or compressibility (S). The following relations exist between crystallographic orientation and E, G and S for cylindrical crystals of the cubic system:

$$\frac{1}{E} = S_{11} - 2\left[(S_{11} - S_{12}) - \frac{1}{2}S_{44}\right](\gamma_1^2\gamma_2^2 + \gamma_2^2\gamma_3^2 + \gamma_3^2\gamma_1^2) \quad [4]$$

* For a recent comprehensive review, see Ref. 9.

R. W. FENN, JR., Student Associate AIME, is affiliated with the Magnesium Division, The Dow Chemical Co., Midland, Mich. W. R. HIBBARD, JR., Member AIME, and H. A. LEPPER, JR., are Assistant Professor of Metallurgy and Associate Professor of Civil Engineering, respectively, Yale University, New Haven, Conn.

From a dissertation by Raymond W. Fenn, Jr. presented to the Faculty of the School of Engineering, Yale University, in candidacy for the degree of Doctor of Engineering, May 1949.

AIME New York Meeting, Feb. 1950.

TP 2751 E. Discussion (2 copies) may be sent to Transactions *AIME before Apr. 1, 1950, and is scheduled for publication Nov. 1950. Manuscript received Oct. 17, 1949.*

$$\frac{1}{G} = S_{44} + 4\left[(S_{11} - S_{12}) - \frac{1}{2}S_{44}\right](\gamma_1^2\gamma_2^2 + \gamma_2^2\gamma_3^2 + \gamma_3^2\gamma_1^2) \quad [5]$$

$$S = S_{11} + 2S_{12} \quad [6]$$

where: γ_1, γ_2, γ_3 represent the cosines of the angles between the stress axis and the respective cube poles.

Young's modulus, E, is determined by the slope of the elastic portion of the load-strain curve for the tension test. The torsion modulus, G, is calculated by the usual formulas of mechanics of materials from the slope of the elastic part of the torque-twist curve.

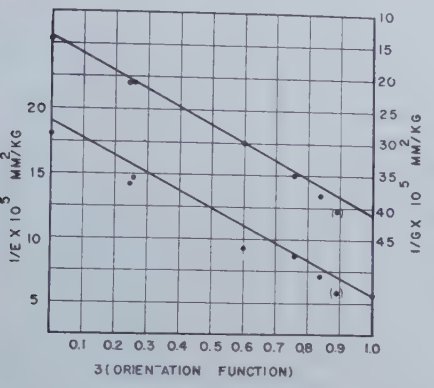

Fig. 1 — Effect of orientation on reciprocal elastic modulus for tension and torsion.
(Masima and Sachs)

The reciprocal values of Young's modulus and the torsion modulus calculated from the experimental results may be plotted against a function of orientation (direction cosines, $\gamma_1^2\gamma_2^2 + \gamma_2^2\gamma_3^2 + \gamma_3^2\gamma_1^2$). Since Eq 4 and 5 express a linear relationship between these quantities, extrapolation of the reciprocal moduli to a zero value of direction cosines evaluates the coefficients S_{11} and S_{44} from the tension and torsion data respectively. Eq 4 and 5 may then be solved simultaneously to obtain a value for the coefficient S_{12}.

The elastic anisotropy[10] can then be evaluated by the expression

$$S_{44} - 2(S_{11} - S_{12}) \quad [7]$$

and Poisson's ratio[10] becomes

$$\mu = \frac{-S_{12}}{S_{11}} \quad [8]$$

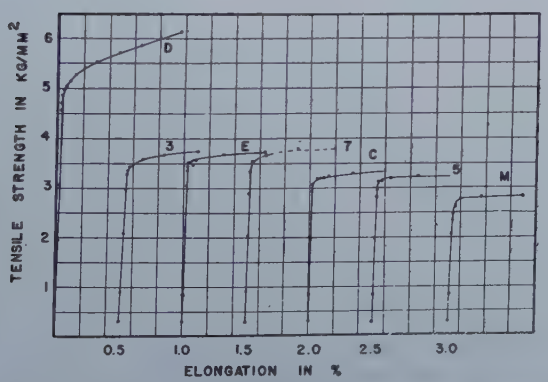

Fig. 2—Tensile stress-strain curves for single crystals of alpha brass.
(Masima and Sachs)

The expression for the resolved shear stress[10] is:

$$s = \frac{P}{A}\sin\chi\cos\lambda \quad [9]$$

where: s = resolved shear stress
P = load
A = cross sectional area
χ = angle between the axis of the specimen and the operating glide plane
λ = angle between the specimen axis and the slip direction

At the initial onset of extensive plastic yielding, this above expression becomes the critical resolved shear stress.

Resolved shear[10] is obtained using the following relationship:

$$t = \frac{1}{\sin\chi_0}\left[\sqrt{d^2 - \sin^2\lambda_0} - \cos\lambda_0\right] \quad [10]$$

where: t = shear
$d = l/l_0$ where: l_0 = original length
l = final length

χ_0 and λ_0 as above for original orientation.

The value of the elastic shear at the critical resolved shear stress[10] (i.e. maximum elastic deformation) follows from the equation:

$$\gamma_{yz} = \frac{4}{3}\left[(S_{11} - S_{12}) + \frac{1}{3}S_{44}\right]\tau_{yz} + \frac{\sqrt{2}}{3}\left[S_{44} - 2(S_{11} - S_{12})\right]\tau_{xy} \quad [11]$$

where: $\tau_{yz} = \frac{P}{A}\sin\chi\cos\lambda$

(i.e. critical resolved shear stress)

and

$$\tau_{xy} = \frac{P}{A}\cos\lambda\sqrt{\sin^2\lambda - \sin^2\chi}$$

Experimental Procedure: Single crystals 9/16 in. in diam were made by Bridgman's method[11] of slow solidification from the melt, at a rate of 4.8 in. per hr. Crystals made in this manner were then given an homogenization anneal of 22 hr at 800°C to minimize chemical coring.

Orientations of the crystals were obtained by the back-reflection Laue technique as developed and described by Greninger.[12] Usually at least four X ray photograms were taken at 90° intervals around the circumference of the crystal at the center, and the resulting orientation values averaged. The probable accuracy of the orientation determinations in all cases is better than 1°, and in most cases is probably within ½° of the true orientation.

The lineage structure (13) type of crystal imperfection was noted in almost all crystals from the multiplicity of Laue spots appearing on the X ray photograms. The maximum spread between spots from a single plane was 5°. The average maximum value of lineage structure observed on all crystals was 1½°.

Specimen Preparation: Machining the crystals in a lathe followed by a suitable electrolytic polish was found to be the most expedient means of preparing the crystals for test. The tension specimens were machined to the following dimensions: 6 in. long with a reduced section 2¼ in. long by ½ in. diam. The torsion specimens, which contained no

reduced section, were machined to 5/16 in. diam by 5½ in. long. The crystals were turned at slow speeds taking a chip of approximately 0.002 in. in the early stages and 0.001 in. in the finishing operation.

Subsequent to machining operations, the gauge length of the crystal was electrolytically polished to produce a smooth, stress-free surface which was suitable for microscopic examination. An electrolyte, suggested by Rodda,[14] of chromic acid (200 g per liter of water) was contained in a stainless steel cathode pot suitably masked with paraffin at the bottom, in order to minimize the tapering effect brought about by its shape. The crystals were polished at one minute intervals for 15 min., utilizing a current density of 6.5 amp per sq in., while agitating the solution constantly. A total of approximately 0.026 in. was removed from the diameter of each specimen.

To ascertain that all crystals were free from machining effects prior to testing them, three or four X rays were taken at the center of each crystal at 90° positions on the periphery. Absence of Laue spot distortion was interpreted as evidence that the crystals were free from significant measurable strains exceeding the elastic limit.

Tension Tests: The tensile specimens were extended in a Southwark Emery testing machine at a rate of loading of approximately 100 lb per min. Load values could be estimated to 5 lb and the scale was accurate within ± 1 pct.

Strain measurements were made with SR-4 bonded resistance wire strain gauges (A-1 and A-8 types) in all cases except Crystal No. 6, in which case two Huggenberger extensometers were utilized. An SR-4 portable strain indicator, Type K, was used for the measurements with the wire gauges. With such equipment strain readings of increments as small as 2½ millionths of an inch per inch can be estimated without difficulty. The accuracy of the strain readings is within ± 1 pct, as determined by the manufacturer's calibration of the gauge factor. These gauges thus provide high sensitiveness for observation of the small strains encountered, sufficient accuracy for the definition of the modulus to ± 1 pct and can be cemented to the specimen without marking the surface or producing high local stresses such as occur at the points of attachment of mechanical extensometers.

Particular care was taken in these tests to obtain accurate axial alignment of load and specimens axis. The maximum stress, S, produced by a load P eccentric by an amount "e" in a specimen of circular section is

$$S = \frac{P}{A}\left(1 + \frac{2e}{r}\right)$$

where A is area and r is radius of the section. Thus for a ½ in. diam specimen, the maximum stress is increased 0.8 pct above the average $\frac{P}{A}$ for each 0.001 in. eccentricity. Since plastic deformation will occur when the maximum stress becomes sufficient, yielding will start at an unduly low average stress dependent upon the amount of eccentricity. This can result in the appearance of a false anelastic portion of the stress-strain curve, and misleading values of critical resolved shear stress. If average strain is measured and plotted against average stress, then the slope of the curves and value of E will remain correct for the straight line portion despite eccentricity of load.

The tensile grips used here consisted of ball bearing supported gimbals holding the clamps on the ends of the specimen. For the relatively light loads in these experiments friction in the gimbal supports was found to be negligible. The specimen fixed in its clamps could be adjusted by set screws to position the specimen axis accurately with respect to the crossing axis of the gimbal bearings. This adjustment was made by trial until the strains were equal around the specimens.

Either three or four SR-4 gauges were suitably placed on each crystal by means of nitrocellulose cement at 90° intervals around the circumference of the crystal. Two were placed perpendicular to the plane containing the specimen axis and the

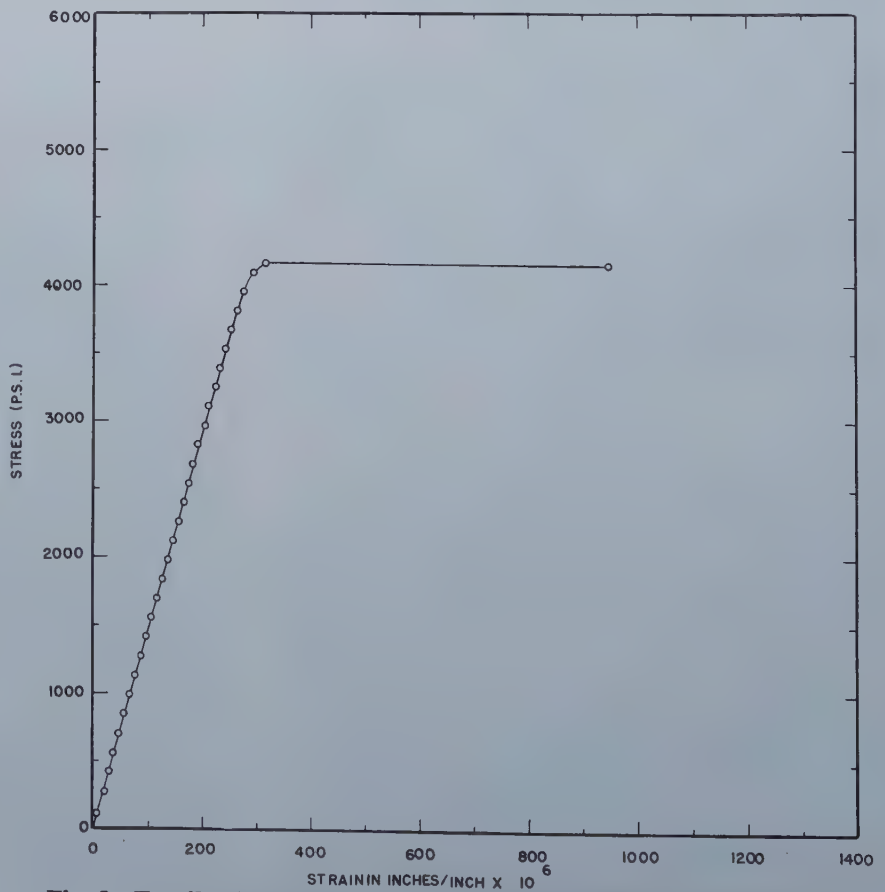

Fig. 3—Tensile stress-strain curve for single crystal of alpha brass.

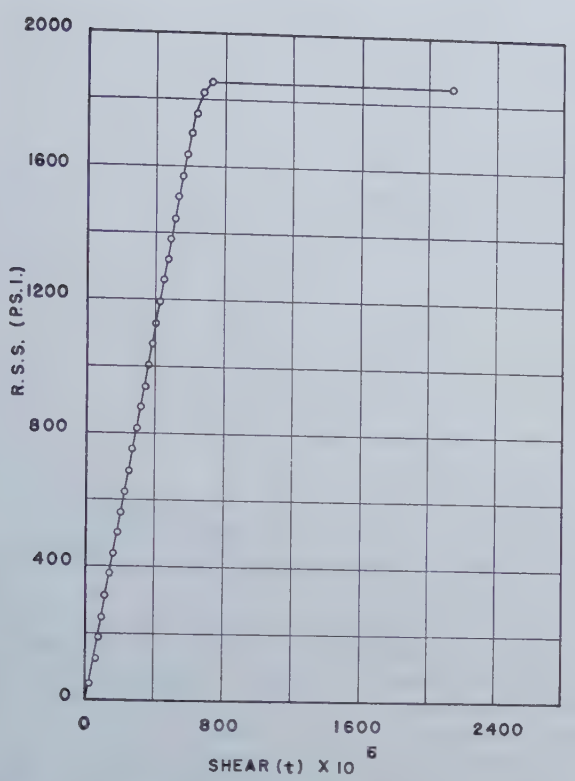

Fig. 4—Tensile shear-strengthening curve for single crystal of alpha brass No. 31.

slip direction in order to assure comparable deformational measurements in the plastic range. The strains of these two gauges were compared with each other in the strain indicator box. Upon loading the crystal, both gauges would change resistance at the same rate, producing zero deflection of the indicator needle, if the specimen axis and the stress axis were in alignment. If perfect alignment were not obtained, the strain indicator needle would deflect in proportion to the applied load and the amount of eccentricity. Therefore, by loading to 200-300 lb in the elastic range, the alignment could be readjusted by means of the set screws so that there was no deflection of the indicator needle.

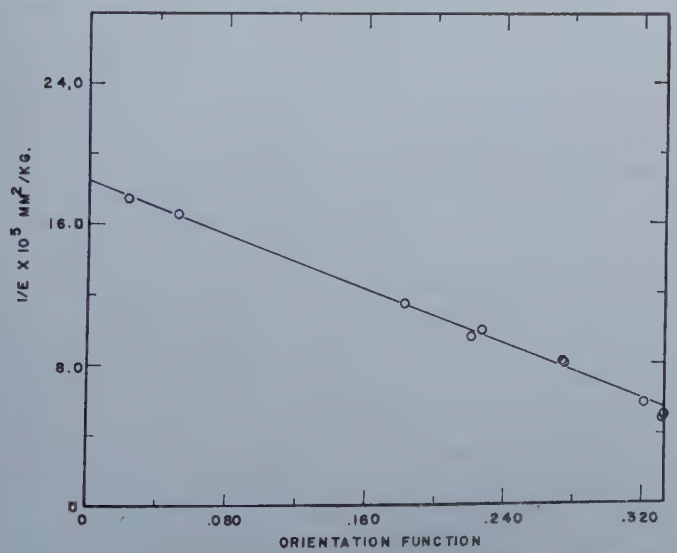

Fig. 5—Effect of orientation on reciprocal elastic modulus for tension (71 pct copper alloy).

If the indicator needle remained undeflected as the load was removed, this indicated that the alignment was satisfactory in one direction. It then remained to obtain satisfactory alignment in the direction at 90° from these gauges. This was accomplished by matching the third gauge against one of the first two, or, when the crystal had four gauges, matching the two remaining gauges against each other. The variation in strain readings around the specimen was held to about 1 pct.

Torsion Tests: A torsion balance similar to that of Goen's[15] was constructed in order to obtain the free torsion modulus. The torsion wheel was mounted on precision ball bearings which had a considerable amount of end play. This arrangement gave a no-load sensitivity of 0.3 g (7.7 g per cm torsion moment).

Torsion measurements were obtained by measuring the deflection of a beam of light reflected from two mirrors which were fastened to the surface of the specimen along the same cylindrical element. Two calibrated traveling microscopes were read to 0.001 mm permitting twist measurements within one second of arc.

The load was applied by means of calibrated weights added at intervals which permitted accurate reading of the microscopes. The alignment of the stress axis with the specimen axis was accomplished by centering the grips on the torsion wheel axis (torsion axis) and then sliding the axis sufficiently to permit subsequent insertion of the specimen.

Chemical Analysis: All crystals were analyzed for copper to determine the amount of zinc which had been lost by vaporization and the amount of segregation which occurred during the melting and solidification, respectively. The electrolytic method was used for the determination of copper, as described by the A.S.T.M. Standards.[16] A spectrographic analysis for impurities showed the Pb, Fe, Si to be less than 0.01 pct.

Experimental Results

Tension: Typical stress-strain and shear-strengthening curves are shown in fig. 3 and 4, respectively. The large number of observations in the elastic range together with the close definition of the line illustrates the sensitiveness of the apparatus used. Sharp yield points as illustrated were obtained on most crystals. However, some specimens showed a marked anelastic region resulting in slow yielding, the cause of which is not apparent. Eccentricity, rate of loading and faulty application of gauges are possible causes. It is apparently not an inherent function of orientation, since it was found with crystals in different portions of the stereographic triangle. In one case, the same crystal produced a gradual yield and later after loading adjustments, a sharp yield.

Reciprocal Young's modulus is plotted against the direction cosines in fig. 5 for crystals averaging 71 pct copper (68.3-73.9 pct). These data closely define a straight line, which, when extrapolated to zero value of the orientation function, gives an intercept value of 18.82×10^{-13} cm² per dyne which is the value of the elastic coefficient S_{11}.

The values of critical resolved shear stress (C.R.S.S.) were calculated for all crystals whose data were suitable for this purpose. Seven crystals having a composition of 71.2 ± 1.25 pct copper gave an average C.R.S.S. value of 1900 psi (1.33 kg per mm²) with an average error of ± 1 pct (table I). In view of the relatively complete coverage in the stereographic triangle (fig. 6) it is considered that these values are a strong substantiation of the

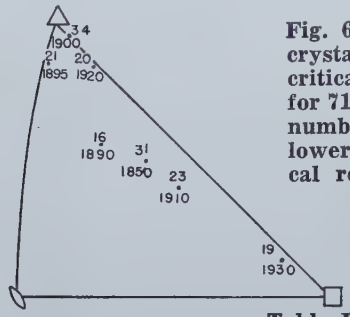

Fig. 6—Orientation of single crystals used to determine critical resolved shear stress for 71 pct copper alloy. Upper number indicates crystal; lower number indicates critical resolved shear stress in psi.

Table I.
Critical Resolved Shear Stress and Elastic Shear

Crystal	Average Copper Content	C.R.S.S. (psi)	C.R.S.S. Kg per mm²	Elastic Shear $\gamma_{yz} \times 10^{-5}$	Orientation Function
16	72.5	1890	1.33	44.05	0.275
19	70.5	1930	1.35	45.9	0.023
20	70.0	1920	1.35	33.3	0.321
21	70.2	1895	1.33	30.3	0.333
23	71.3	1910	1.34	53.7	0.182
31	71.9	1850	1.30	47.6	0.227
34	72.3	1900	1.33	25.3	0.332
Av.	71.2	1900	1.33	40.0	0.242

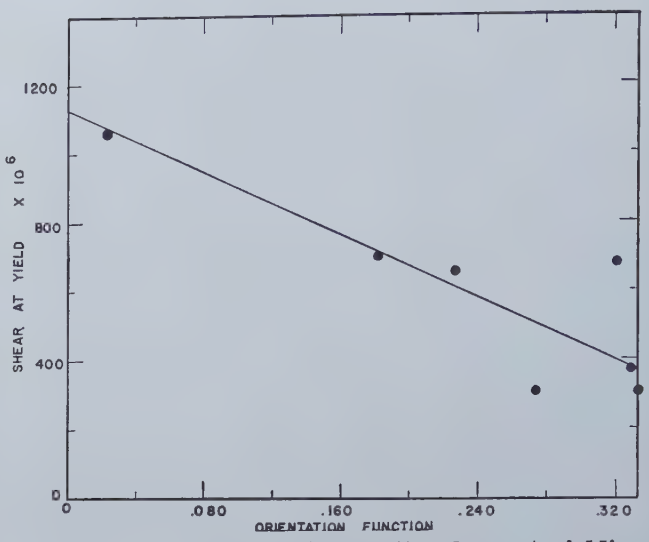

Fig. 7—Effect of orientation on the shear at yielding (71 pct copper alloy).

critical resolved shear stress formulation of Schmid and Boas[8] for specimens of circular cross-section. It appears therefore that the large variations in critical resolved shear stress previously reported are entirely the result of surprisingly large experimental differences.

Also in table I are the values of the elastic shear at the critical resolved shear stress (γ_{yz}). The elastic shear is approximately constant only for orientation functions (direction cosines) below about 0.24, above which the shear decreases due

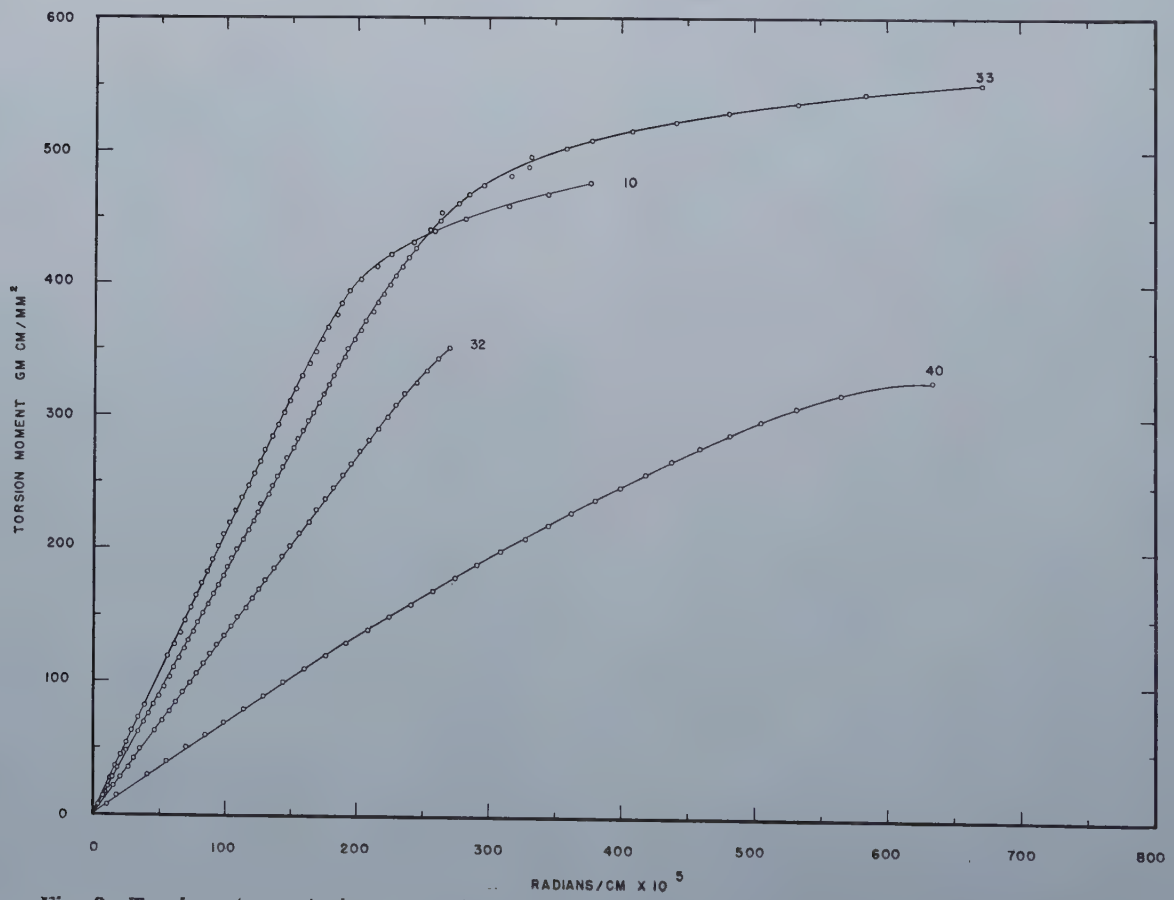

Fig. 8—Torsion stress-strain curves for single crystals of alpha brass (71 pct copper alloy).

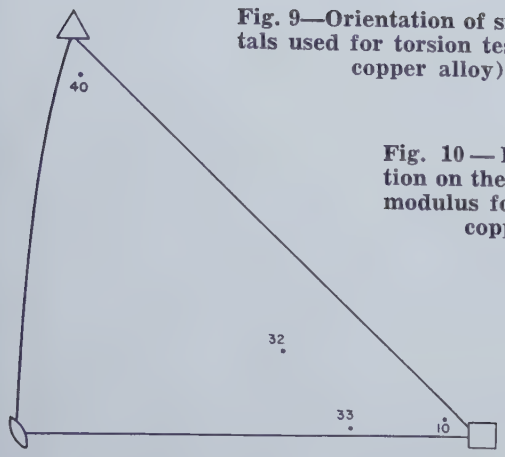

Fig. 9—Orientation of single crystals used for torsion tests (71 pct copper alloy).

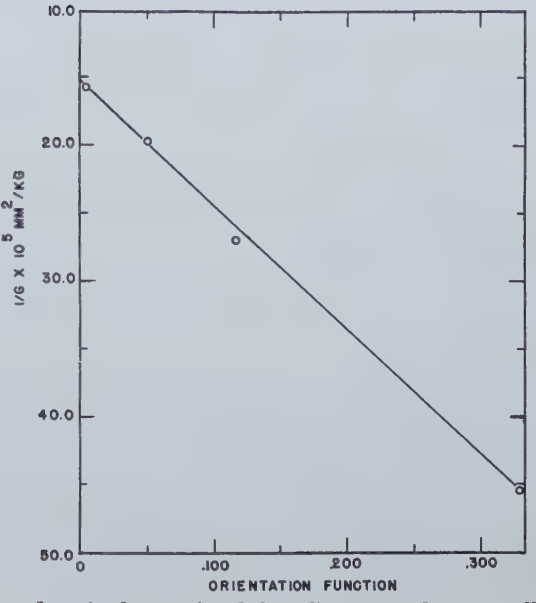

Fig. 10 — Effect of orientation on the reciprocal elastic modulus for torsion (71 pct copper alloy).

to the increase in the value of the second term of Eq 11. The average value (40.0×10^{-5}) is lower than that of Masima and Sachs[1] (43.3×10^{-5}) which may be explained by their critical resolved shear stress (1.44 kg per mm²) compared to the lower value (1.33 kg per mm²) used in the present investigation.

Resolved shear (t of Eq 10) at the critical resolved shear stress shows a decrease with increasing value of direction cosines (fig. 7). The significance of these data is questionable, since the calculation assumes a crystallographic elastic deformation mechanism just before yielding the same as that occurring during plastic deformation. These values of resolved shear are not constant, and the scatter of points suggests that it is not of basic importance to the slip process.

Torsion: Although the torsion balance was constructed so as to allow flexure torsion coupling,

Table II. Elastic Coefficients

Average Copper Content, pct	S_{11}	S_{12}	S_{44}	S_{11}	S_{12}	S_{44}
	10^{-13} cm² per dyne			10^{-5} mm² per kg		
71.2	18.82	−9.45	15.55	18.45	−9.27	15.25
77.4	17.10	−8.28	14.90	16.75	−8.07	14.60

specimens whose torsion axes corresponded to cubic, dedecahedral or octahedral poles were chosen for the torsion tests whenever possible because their symmetry minimized the error for deviations from free torsion. Fig. 8 shows the results of the torsion tests on crystals having an average of 71.9 ± 1.2 pct Cu with orientations as shown in fig. 9. An extrapolation of the reciprocal torsion modulus to zero value of direction cosine (fig. 10) gives an intercept value of 15.55×10^{-13} cm² per dyne, the value of S_{44}. Substitution in Eq 4 and 5 gives -9.45×10^{-13} cm² per dyne for the elastic coefficient S_{12}.

Effect of Composition: Zinc loss during remelting resulted in a group of crystals having an average copper content of 77.4 ± 1.0 pct. Fig. 11 and 12 show the results of the tension and torsion tests, respectively, on these crystals. The effect of increasing the copper content is to decrease the reciprocal Young's modulus and also the reciprocal torsion modulus. The values obtained for the elastic coefficients of the higher copper alloy are listed in table II. This decrease in S_{11} with increasing copper content substantiates the value ($S_{11} = 13.3 \times 10^{-13}$ cm² per dyne) determined by Goens and Weerts[17] for unalloyed copper rather than that of Kimura[18] (16.4×10^{-13}).

Discussion of Results

The values for the elastic coefficients of alpha brass (71.2 pct Cu) shown in table II are somewhat lower than those reported by Masima and Sachs.[1] However, there would be rather good agreement between these two sets of values if the extrapolations of Masima and Sachs had been drawn through their experimental points rather than above them as shown in fig. 1. The reason for their choice of extrapolation is not apparent.

The values for the elastic coefficients for alpha brass (77.4 pct Cu) shown in table II indicate that the numerical values of these coefficients increase with increasing zinc content. These data are consistent with the values for unalloyed copper reported by Goens and Weerts,[17] which, when plotted against weight percent zinc in alpha brass, approximated the following linear relationships (unit: 10^{-13} cm² per dyne):

$$S_{11} = 14.9 + 0.118 \text{ (wt pct Zn)}$$
$$S_{12} = -6.3 - 0.095 \text{ (wt pct Zn)}$$
$$S_{44} = 13.3 + 0.074 \text{ (wt pct Zn)}$$

The evaluations of elastic anisotropy in table III indicate that increasing zinc content increases both the elastic anisotropy and Poisson's ratio for alpha brass, as would be expected. Again using Goen's and Weert's[17] values for unalloyed copper, the following linear relationships were approximated:

$S_{44} - 2(S_{11} - S_{12}) = -29.04 - 0.30$ (wt pct Zn)

$\mu = -S_{12}/S_{11} = 0.420 + 0.0028$ (wt pct Zn)

Unit: 10^{-13} cm² per dyne

The value of 1.33 kg per mm² for the critical resolved shear stress of alpha brass (71.2 pct Cu) is lower than the values of Masima and Sachs,[1] von Göler and Sachs,[7] Burghoff[2] and Martin,[4] but higher than the values of Maddin, Mathewson and Hibbard.[5, 6] The accuracy of the experimental method and the small average deviation (0.01 kg per mm²) of the values strongly substantiates the critical resolved shear stress law of Boas and Schmid.[8] The average elastic shear at the critical resolved shear stress was 40.0×10^{-5}, somewhat

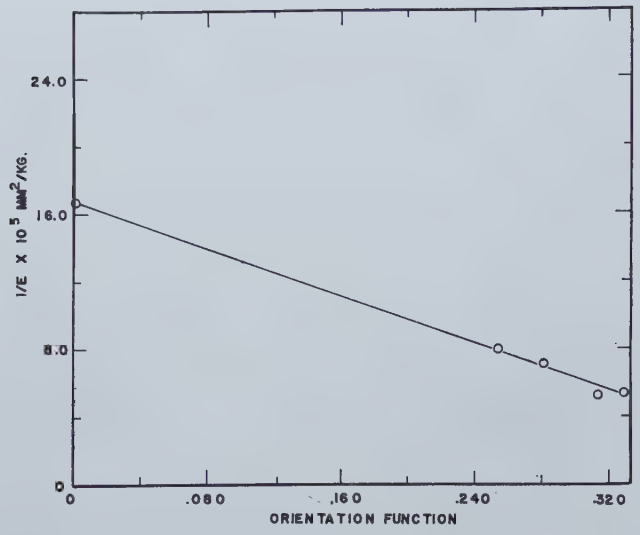

Fig. 11—Effect of orientation on the reciprocal elastic modulus for tension (77 pct copper alloy).

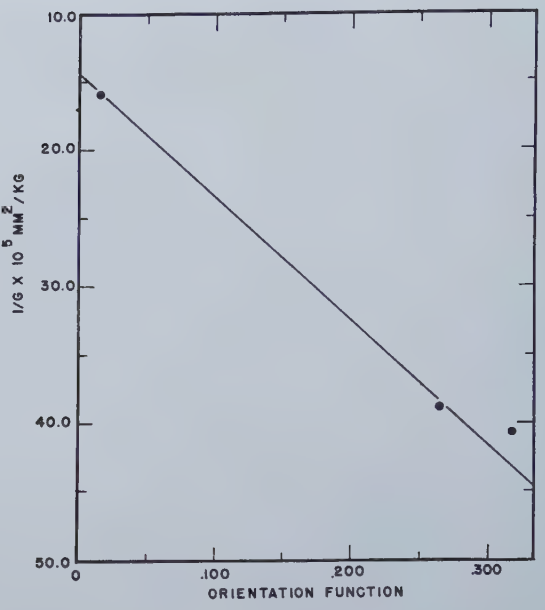

Fig. 12—Effect of orientation on the reciprocal elastic modulus for torsion (77 pct copper alloy).

lower than the values of Masima and Sachs[1] as might be expected from their higher values for the critical resolved shear stress and elastic coefficients. The variation in this elastic shear was as predicted from the critical resolved shear stress law.

Summary: From tension and torsion experiments on single crystals of alpha brass, the following values were obtained for elastic coefficients: (Unit: 10^{-13} cm² per dyne)

Table III. Measure of Elastic Anisotropy

Per Cent Copper	E. Max. kg per mm² Direction 111	E. Min. kg per mm² Direction 100	G. Max. kg per mm² Direction 100	G. Min. kg per mm² Direction 111	$S_{44}-2(S_{11}-S_{12})$ Cm² per dyne x 10^{-13}	Poisson's Ratio $\frac{S_{12}}{S_{11}}$
71.2	19050	5420	6550	2180	−40.99	0.502
77.4	19400	5960	6850	2230	−35.7	0.482

		71.2 pct Copper	77.4 pct Copper
	S_{11}	18.82	17.10
	S_{12}	−9.45	−8.23
	S_{44}	15.55	14.90
Elastic anisotropy	$S_{44}-2(S_{11}-S_{12})$	−40.99	−35.7
Poisson's ratio	$-S_{12}/S_{11}$	0.502	0.482

Using the values of Goens and Weerts[18] for unalloyed copper, approximate linear relationships were found for the change in the elastic coefficients with composition.

A value of 1.33 kg per mm² (1900 psi) was determined for the critical resolved shear stress of alpha brass (71.2 pct Cu). The small average deviation of 0.01 kg per mm² strongly substantiates the critical resolved shear stress law of Boas and Schmid.[8] The elastic shear at the critical resolved shear stress averaged 40.0 x 10^{-5} and varied from 25.3 x 10^{-5} to 53.7 x 10^{-5}, depending upon orientation.

Acknowledgments

The authors wish to acknowledge the interest and helpful discussions of Professor C. H. Mathewson and Professor L. W. McKeehan. Mr. Gustav Nelson assisted in the construction of the torsion apparatus and the preparation of single crystal specimens. The Bridgeport Brass Co., Bridgeport, Conn., and the American Brass Co., Torrington, Conn., kindly furnished the brass rod from which the single crystals were made. The Type K strain indicator was a gift to Hammond Laboratory from the Yale Metallurgical Alumni.

References

[1] M. Masima and G. Sachs: *Ztsch. Phys.* (1928) **50**, 161.
[2] H. L. Burghoff: D. Eng. Dissertation, Yale Univ., 1939.
[3] R. G. Treuting and R. M. Brick: *Trans.* AIME (1942) **147**, 128.
[4] D. L. Martin: Unpublished Research, Yale Univ., 1940.
[5] R. Maddin, C. H. Mathewson and W. R. Hibbard, Jr.: *Trans.* AIME (1948) **180**. *Metals Tech.*, Feb. 1948, TP 2331.
[6] R. Maddin, C. H. Mathewson and W. R. Hibbard, Jr.: *Trans.* AIME (1949) **185**, 527. *Jnl. of Metals*, Aug. 1949, TP 2658.
[7] F. von Göler and G. Sachs: *Ztsch. Phys.* (1929) **55**, 581.
[8] W. Boas and E. Schmid: *Ztsch. Phys.* (1933) **86**, 828.
[9] R. F. S. Hearmon: *Rev. Mod. Phys.* (1946) **18**, 409.
[10] E. Schmid and W. Boas: Kristallplastizität. J. Springer, Berlin (1935).
[11] P. W. Bridgman: *Proc.* Am. Acad. (1925) **60**, 305.
[12] A. B. Greninger: *Trans.* AIME (1933) **117**, 61.
[13] M. J. Buerger: *Ztsch. Kristal.* (1934) **89**, 195.
[14] J. L. Rodda: *Trans.* AIME (1942) **147**, 128.
[15] E. Goens: *Ann. d. Phys.* (1933) **16**, 793.
[16] ASTM Standard E8-46.
[17] E. Goens and J. Weerts: *Ztsch. Phys.* (1936) **37**, 321.
[18] R. Kimura: Tohoku Univ. Sci. Rpt. Ser. I, (1933) **22**, 553.

Uranium-Aluminum and Uranium-Iron

The phase diagrams for the systems uranium-aluminum and uranium-iron have been determined. For each system several intermetallic compounds occur. The solid solubility in the terminal phases is very limited in all cases.

by Paul Gordon and A. R. Kaufmann

THE large-scale manufacture and use of uranium in conjunction with the atomic energy development during the war led to a need for knowing the equilibrium diagrams of uranium with various other metals. The alloys of uranium with aluminum and with iron were among the first that were studied for this purpose. Much of the work was done in the manner of a survey since it was necessary to determine the important features of the phase diagrams rather than to obtain completely detailed results. For this reason no attempt was made to locate exactly such features as liquidus lines, solid solubility limits and compound and eutectic compositions. It is believed, however, that there are no great inaccuracies in the diagrams reported here and that no important points were overlooked.

PAUL GORDON is Asst. Professor of Phys. Metallurgy, Illinois Institute of Technology and A. R. KAUFMANN is Assoc. Professor of Metallurgy, Massachusetts Institute of Technology.

This work was carried out at the M.I.T. Metallurgical Project during the year 1943 under the sponsorship of the Manhattan Project. (Contract #W7405-eng-175)

AIME New York Meeting, Feb. 1950.

TP 2764 E. Discussion (2 copies) may be sent to Transactions *AIME before Apr. 1, 1950, and is scheduled for publication Nov. 1950. Manuscript received Oct. 14, 1949.*

Earlier work on alloys of uranium with aluminum and iron is almost nonexistent and in each case is considered to have been of little value by M. Hansen.[1] It is interesting to note, however, that the compound UAl_3 was first reported in 1902 by L. Guillet.

Experimental Procedure

Materials: The uranium used for making most of the aluminum alloys was obtained from material prepared by Metal Hydrides, Inc., and melted in vacuum at M.I.T. Because of the lack of an adequate supply of metal, it was necessary to use material from several different batches and hence it is impossible to state an exact analysis. However, a few results indicated about 0.01 to 0.03 pct iron and probably about 0.03 to 0.05 pct carbon. Toward the end of the work a small amount of metal was obtained from Brown University and from Iowa State College and this was used in determining the transformations in pure metal and in some dilute alloys. All of the aluminum used in this investigation came from a supply of high purity metal (greater than 99.9 pct aluminum) which was obtained through the courtesy of Dr. Mehl of the Carnegie Institute of Technology.

The uranium used for making the alloys with iron was produced by the bomb reduction process which has been described by J. Chipman.[2] This metal, after vacuum melting, contained about 99.9 pct uranium by weight with carbon and iron as the chief impurities. Electrolytic iron containing about 0.012 pct carbon, 0.020 pct nickel and 0.009 pct copper was used in making the melts.

Melting Equipment: The melting of the alloys went through a stage of development which culminated in the use of beryllia or beryllia-lined crucibles and in the use of high frequency heating in either vacuum or in an atmosphere of argon. It was found that uranium at a few hundred degrees above its melting point would pick up aluminum and to a lesser extent silicon from an alundum thimble while aluminum above 1000°C would extract silicon from the impure alundum. No reaction of either metal with beryllia was noted at temperatures as high as 1800°C. The distillation of aluminum from the aluminum-rich alloys was quite troublesome at temperatures above about 1300°C and was only partially avoided by the use of argon instead of vacuum. Melting in resistance furnaces,

without the benefit of eddy current stirring, was found to produce worthless alloys because the extreme difference in density of the metals made the attainment of a homogeneous alloy very difficult. Induction heating largely overcame this difficulty, although a considerable amount of segregation occurred during the solidification of the melt in the crucible. No attempt was made to cast the alloys which were only about 1 or 2 cu in. in volume. The final ingots were sufficiently homogeneous for all but the most exacting studies and for such purposes it was usually possible, by means of metallographic inspection, to select a satisfactory portion of the specimen for closer examination.

Fig. 1 shows the melting equipment which was used extensively with a 20 KVA Ecco converter. The apparatus worked satisfactorily for melting by direct induction up to 1800°C. There was vigorous eddy current stirring which usually broke the oxide skin at the top of the metal. A vacuum of about 10^{-3} mm Hg could be obtained in this equipment with mercury diffusion pumps, although during the initial heating the pressure often rose as high as 10^{-1} mm Hg. The materials to be melted were placed into the cold crucible and then either heated to a specified temperature or heated until the stirring of the metal indicated a thorough mixing of the liquid, after which solidification was allowed to take place.

Examination of Specimens: The ingots as solidified were examined for segregation and poor alloying by grinding and polishing a flat portion the length of the specimen, followed by metallographic examination. If the alloy passed this inspection, a portion was cut off for chemical analysis and for a more detailed metallographic and X ray examination while the remainder was used for thermal analysis.

Most of the alloys were given a chemical analysis and usually the results were fairly close to the intended composition. However, there were a number of discrepancies which were caused partly by inhomogeneity in the alloy and partly by unsatisfactory chemical technique. This was particularly true in the aluminum-rich alloys where the chemical procedure failed completely. It was necessary to use spectrographic analysis in such cases, and this had an added advantage in that small regions of the alloy could be selected under the microscope and then be broken out for analysis. The uncertainty as to the exact composition of some of the alloys made it difficult to fix the precise location of some of the phases, but with the aid of X ray diffraction patterns and critical metallographic examinations, it was possible to arrive at fairly satisfactory conclusions.

Metallographic polishing was accomplished by mounting the specimens in bakelite and then going through the usual series of abrasive papers and ending on a silk-covered wheel with magnesia as abrasive. The specimens containing large amounts of intermetallic compounds had to be handled carefully in the rough grinding in order to prevent tearing out the brittle phases. The alloys containing up to 67 at. pct aluminum or iron were usually given a brief electrolytic etch in a solution of 5

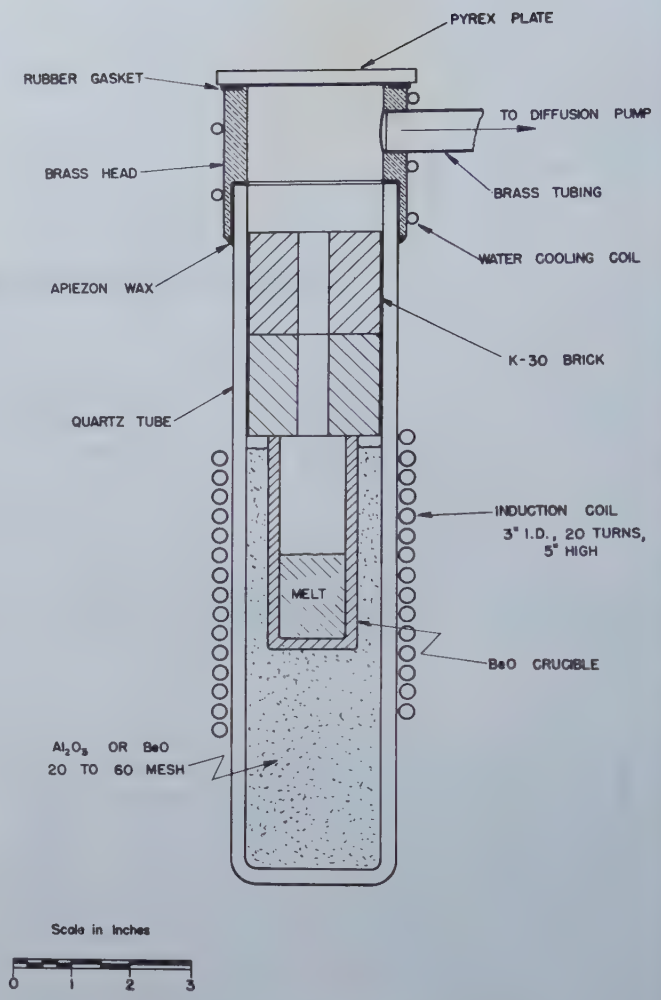

Fig. 1—Induction melting furnace.

parts phosphoric acid, 5 parts ethylene glycol and 8 parts ethyl alcohol, while the higher aluminum alloys were etched with a 1 pct hydrofluoric acid solution. The high iron alloys were etched with nital.

X ray diffraction patterns were made in a Debye-Sherrer camera, using powders formed by filing the softer alloys and by grinding the brittle compounds in an agate mortar. It was necessary to anneal the filings in evacuated quartz tubes to get sharp lines, but the grindings gave satisfactory patterns without any treatment. The uranium-rich powders usually gave a weak pattern of UO_2, but this did not interfere with observation of the lines due to the metal. Several attempts were made to quench uranium-rich powders from about 1000°C by breaking the quartz capsule under water, but this always yielded nothing but UO_2. Calibration of the X ray film was done by means of tungsten lines.

Heat-treatment of Specimens: Most of the alloys were examined as solidified but in certain cases it was necessary to heat-treat and quench. This was accomplished by sealing off specimens, which were about ⅛ in. diam, in an evacuated quartz tube which was broken under water for the quench. The quartz tube was fastened to a block of nickel which

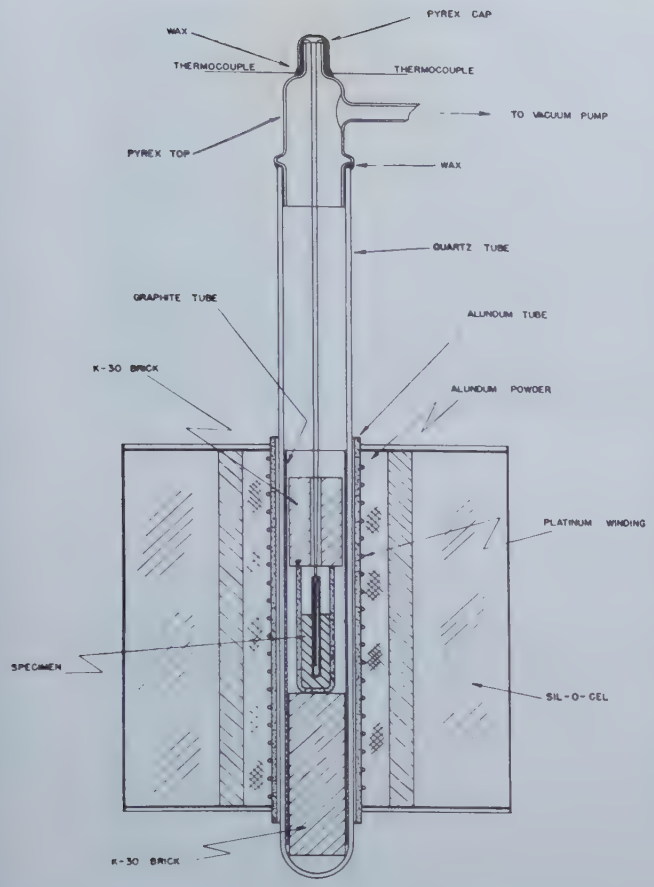

served both to give a uniform temperature in the furnace and to act as a hammer for breaking the quartz.

It was found that the uranium-rich alloys would react with the quartz at temperatures above 1000°C and pick up enough silicon to alter the microstructure. In order to avoid this, the specimens were placed inside tiny cups of BeO and then sealed up as before. This technique was satisfactory up to about 1300°C, at which temperature the devitrification of the quartz became serious. A small amount of heat-treatment at temperatures up to 1400°C was carried out in an atmosphere of purified helium which was maintained under slight pressure inside a Zircofrax tube. This arrangement gave sufficient protection from oxidation to allow at least several hours heat-treatment. Some of the aluminum-rich alloys were heat-treated at 500° to 600°C for as long as a week in a vacuum of about 10^{-2} mm Hg without serious oxidation.

Fig. 2—Apparatus for thermal measurements.

Fig. 3 (below)—Uranium-Aluminum equilibrium diagram.

[•] Thermal measurement determinations. Determinations by chemical analysis of liquid in equilibrium with solid. Numbered circles indicate X ray and microscopic determinations. 1. Uranium and UAl_2. 2. Uranium. 3. Liquid. 4. Liquid and UAl_2. 5. UAl_2 and UAl_3. 6. UAl_3 and UAl_5. 7. Liquid and UAl_3. 8. Liquid and UAl_5. 9. UAl_5 and Aluminum.

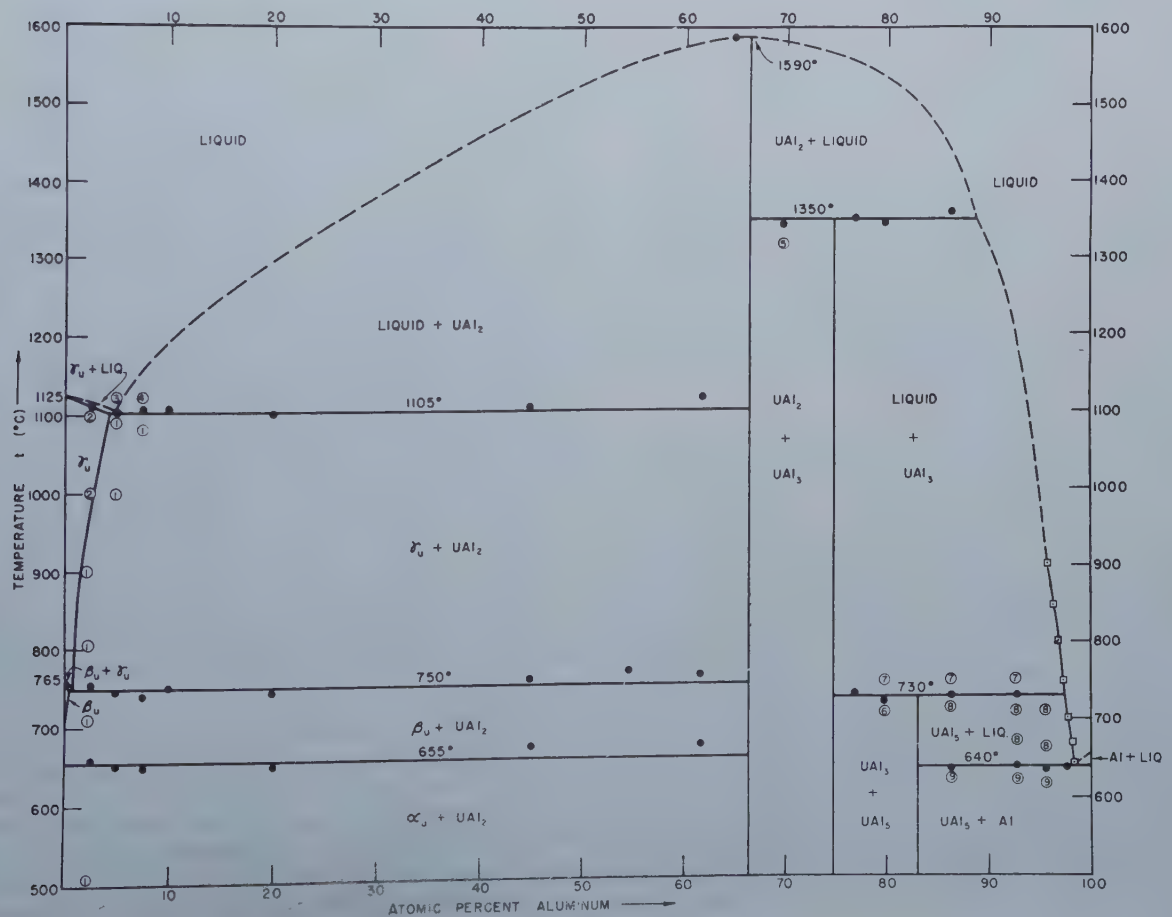

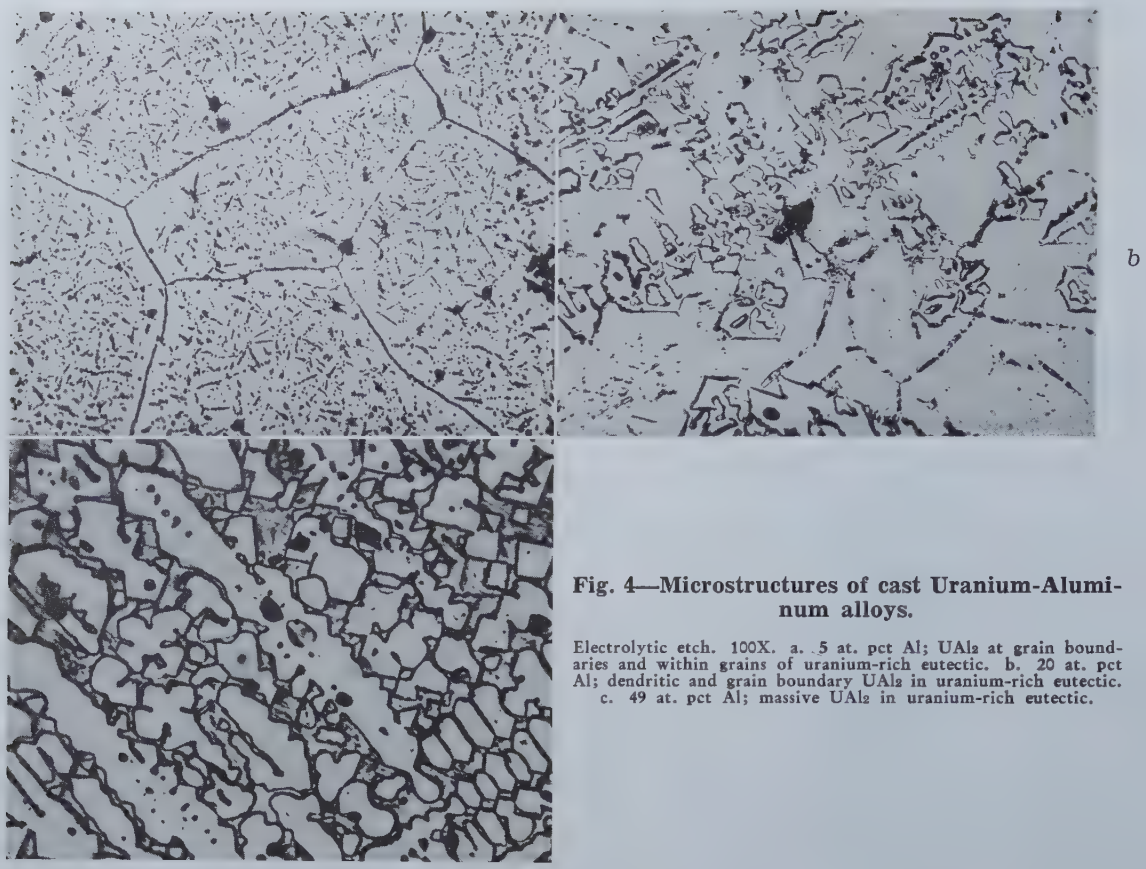

Fig. 4—Microstructures of cast Uranium-Aluminum alloys.

Electrolytic etch. 100X. a. 5 at. pct Al; UAl_2 at grain boundaries and within grains of uranium-rich eutectic. b. 20 at. pct Al; dendritic and grain boundary UAl_2 in uranium-rich eutectic. c. 49 at. pct Al; massive UAl_2 in uranium-rich eutectic.

Thermal Measurements: After removing a portion of the ingot for metallographic examination, the remainder of the specimen was used for thermal analysis. A hole was drilled into the softer specimens to receive the thermocouple while the harder and more brittle alloys were crushed to a powder which was packed around the thermocouple. A bare thermocouple was used for some of the lower temperature measurements in the solid state, while a magnesia tube was used for protection against the uranium-rich alloys at higher temperatures and a quartz tube inside a magnesia tube was used for the high-aluminum alloys. This amount of protection was necessary because of the aluminum vapors which quickly attacked the platinum-platinum-rhodium thermocouple.

Observations were made in a resistance furnace using the inverse rate method and taking readings every 5°C, although this was sometimes reduced to 1°C. The heating or cooling rate generally was about 5° to 10°C per min, but sometimes was as low at 1°C per min. Several attempts were made to secure a constant rate of heating or cooling. One of these consisted of using a temperature controller and two thermocouples to maintain a constant temperature difference between the specimen and the furnace. This procedure was satisfactory in the lower ranges of temperature, but led to spurious effects above about 1200°C. A variation of the technique was to maintain the temperature difference manually instead of with a controller and this was more satisfactory since it avoided the small fluctuations due to the on-and-off cycle of the controller. Another method consisted of driving the temperature setting of the controller slowly up or down, but this again did not give a sufficiently smooth variation. The procedure which was finally adopted was simply to raise or lower the voltage applied to the furnace by increments large enough to effect a change of about 200° to 400°C in the temperature and then to conduct readings during the time that the rate of change of temperature was satisfactory. This meant a certain amount of repetition in order to get the temperature ranges to overlap but the method still was considered more satisfactory than the others.

The thermal measurements up to about 1550°C were made in the apparatus shown in fig. 2. Most of the work was done in a vacuum of the order of 10^{-3} mm Hg, but occasionally an argon atmosphere was used. The quartz tube, which formed the vacuum chamber, was prevented from collapsing at the high temperatures by the thin graphite tube inside of it. The quartz lasted a long time at temperatures up to 1300°C, but was good for only about 10 to 20 hr at 1400°C and 2 to 4 hr at 1500°C. A few rough observations were made at temperatures above 1550°C using induction heating in the regular melting furnace and reading temperature as a function of time.

Experimental Results—Aluminum Alloys

The results of all the work are indicated in the equilibrium diagram given in fig. 3. This may be briefly summarized with the statements that the solid transformations and melting point of uranium are not greatly altered by aluminum, that three intermetallic compounds with the formulas UAl_2,

Fig. 5—Microstructures of quenched 2.5 at. pct Aluminum alloy.

Electrolytic etch. a. 100X. Quenched from 900°C.; UAl_2 in uranium-rich matrix. b. 500X. Quenched from 1000°C; UAl_2 completely in solution. (Small particles are inclusions.)

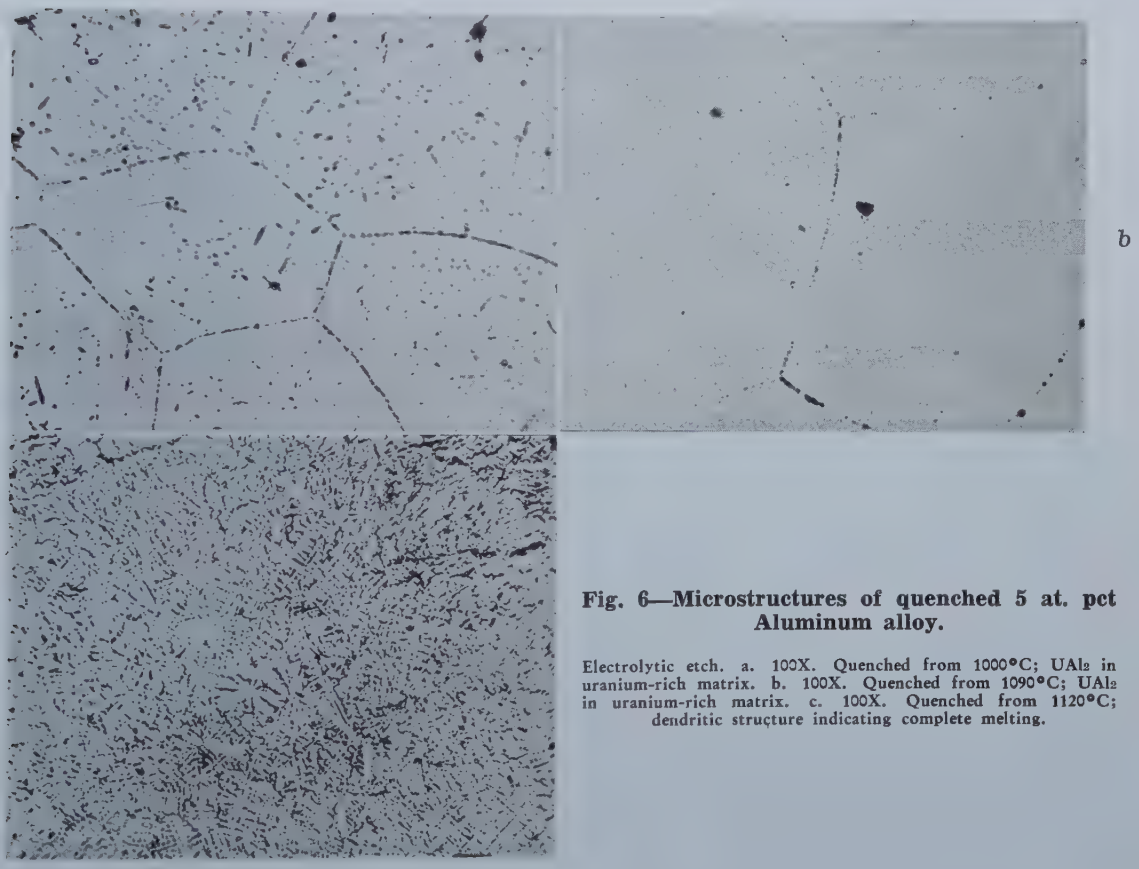

Fig. 6—Microstructures of quenched 5 at. pct Aluminum alloy.

Electrolytic etch. a. 100X. Quenched from 1000°C; UAl_2 in uranium-rich matrix. b. 100X. Quenched from 1090°C; UAl_2 in uranium-rich matrix. c. 100X. Quenched from 1120°C; dendritic structure indicating complete melting.

UAl_3, and UAl_5 occur in the system and that there is no extensive solid solubility of either metal in the other. The black points in fig. 3 give the results of thermal measurements during heating and the numbered circles in conjunction with the legend indicate the phases observed by X ray and microscopic examination of specimens quenched from the temperatures shown by the circles. Micrographs and X ray diffraction patterns in support of the diagram will be described below.

The solid transformations and melting point of uranium occur at about the temperatures shown in the diagram, that is, alpha to beta at 655°C, beta to gamma at 765°C, and gamma to liquid at 1125°C. All attempts to fix these temperatures more accurately gave inconclusive results, presumably because of insufficient purity of the metal. The rate of heating or cooling influences the temperature of transformation and accordingly several heating runs were made at the slow rate of 1°C per min. Under these conditions the transformations seemed to occur over a range of about 5°C instead of at a definite temperature as was the case when the heating rate was greater. A sample of metal (from Brown University), which was alleged to be pure, gave more difficulty in this respect than some of the Metal Hydrides material. The former material seemed to melt as high as 1135°C, but the latter,

which was used for the bulk of the alloys, melted around 1125°C.

The solid transformations of uranium persisted without any great change in the aluminum alloys up to the first compound, UAl_2. Because of the uncertainty in the transformation temperatures of the pure metal, it was difficult to decide if any significant change did occur in the alloys. The data indicate about 15°C lowering of the beta to gamma transformation to about 750°C and no change in the alpha to beta transformations. Quenching of the pure metal or the aluminum alloys did not retain any high temperature phases and thus was useless for obtaining the precise transformation temperatures.

A second phase is apparent in even the most dilute aluminum alloys as cast, and the amount of this phase increases continuously with the aluminum content until at about 67 at. pct aluminum the alloy becomes one phase. These changes are illustrated in the micrographs of fig. 4.

The solidus temperature of the uranium-rich alloys is lowered to about 1105°C as shown by the thermal measurements and since this temperature remains the same all the way to UAl_2 it is believed that a eutectic reaction occurs. No typical eutectic structure is apparent in the uranium-rich alloys and this makes it difficult to fix the eutectic composition by microscopic examination. The lack of such a structure is believed to be caused by the fact that the eutectic occurs so much closer to uranium than to UAl_2 that the amount of the latter phase is very small at this composition. However, the thermal measurements (shown in fig. 3) and various quenching experiments, to be described below, fix the general locality of the eutectic at about 5 at. pct aluminum. Liquidus lines were not satisfactorily observed at this portion of the diagram and hence these could not be used to locate the eutectic composition.

The maximum solid solubility of aluminum in gamma uranium was determined to be about 4 to 5 at. pct at 1105°C as shown by the quenching experiments illustrated in fig. 5 and 6. It can be seen that some precipitated UAl_3 persists up to the eutectic temperature in the 5 at. pct alloy, but that it all goes into solution in the 2.5 at. pct specimen. The existence of the eutectoid at the beta to gamma transformation has been assumed on the basis of a slight lowering of the transformation temperature in the alloys but the exact location of it is unknown. No precision lattice parameter measurements were attempted, so it is not known to what extent the aluminum remains in the alpha uranium after quenching. However, an age hardening effect, which will be described later, indicates that the aluminum does remain in solution.

X ray diffraction patterns of alloys with increasing aluminum content substantiate the conclusion that no additional phases exist between uranium and the compound UAl_2. The identification of this compound as UAl_2 is based on microscopic examination of the alloys and on the crystal structure determined by X rays. Because of the difficulty with chemical analysis and inhomogeneity in the alloys the micro-examination could not fix the location to better than about ± 2 at. pct. The X ray crystal structure analysis was not carried out far enough to give a unique molecular formula for the compound, but comparison of the density obtained by direct measurement with that calculated from the measured unit cell gave fairly good substantiation to the formula UAl_2; values of $\sin^2\theta$ using copper K-alpha radiation are given table I. The lines may be indexed on a diamond cubic pattern with $a_0 = 7.74$ Å. This must mean that there are 8 uranium atoms to a unit cell, since the scattering from the aluminum atoms is very small, and hence there would be 16 aluminum atoms in a unit cell if the formula UAl_2 is correct. With this number of atoms to a cell, the X ray density is 8.38 g per cm^3, while the measured density is 8.21 g per cm^3. This is a fairly good check considering the experimental difficulty of getting a sound and homogeneous alloy, but the result probably is not good enough to prove the formula UAl_2. A calculation of line intensities, which would prove this point, was not made at M.I.T.

The melting point of UAl_2 was not uniquely determined because of the difficulties encountered at high temperature. The thermal effect shown at about 1590°C is believed to be significant, but it was obtained under poor conditions using induction heating. No evidence of an appreciable solid solution range on either side of this compound was found.

The next phase on the aluminum side of UAl_2 is the compound UAl_3, and in this case the formula has been proven to be correct by an X ray crystal structure determination. The $\sin^2\theta$ values together with the line intensities and indices for the diffraction pattern of UAl_3 are given in table II. The pattern is that of a simple cube with relatively small deviation from the expected line intensities. This must mean that the uranium atoms are at the corners of a cube and, if aluminum atoms are placed at the faces of the cube, the calculated line intensities check very closely with the observed values. The lattice parameter of the cube is 4.27 Å and,

Table I. X Ray Diffraction Results for UAl_2: Diamond Cubic Lattice: $a_0 = 7.74$ Å (true unit).

$Sin^2\theta$*	hkl	Line Intensity‡
0.0314	111	W to M
0.0816	220	S
0.1126	311	S
0.1615	400	W
0.1922	331	M
0.2425	422	S
0.2714	511,333	S
0.3208	440	M
0.3505	531	M
0.3994	620	M
0.4305	533	M to W
0.4790	444	W
0.5088	711,551	W to M
0.5574	642	S
0.5868	731,553	S
0.6362	800	VW
0.6660	733	VW
0.7113†	822	M to S
0.7408†	555	M to S
0.7882†	840	M
0.8174†	911	M
0.8645†	664	M
0.8940†	931	M

* Values obtained with Cu-K alpha radiation
† Last six values obtained with Cu-K $alpha_1$ radiation
‡ VW—Very Weak
W—Weak
M—Medium
S—Strong

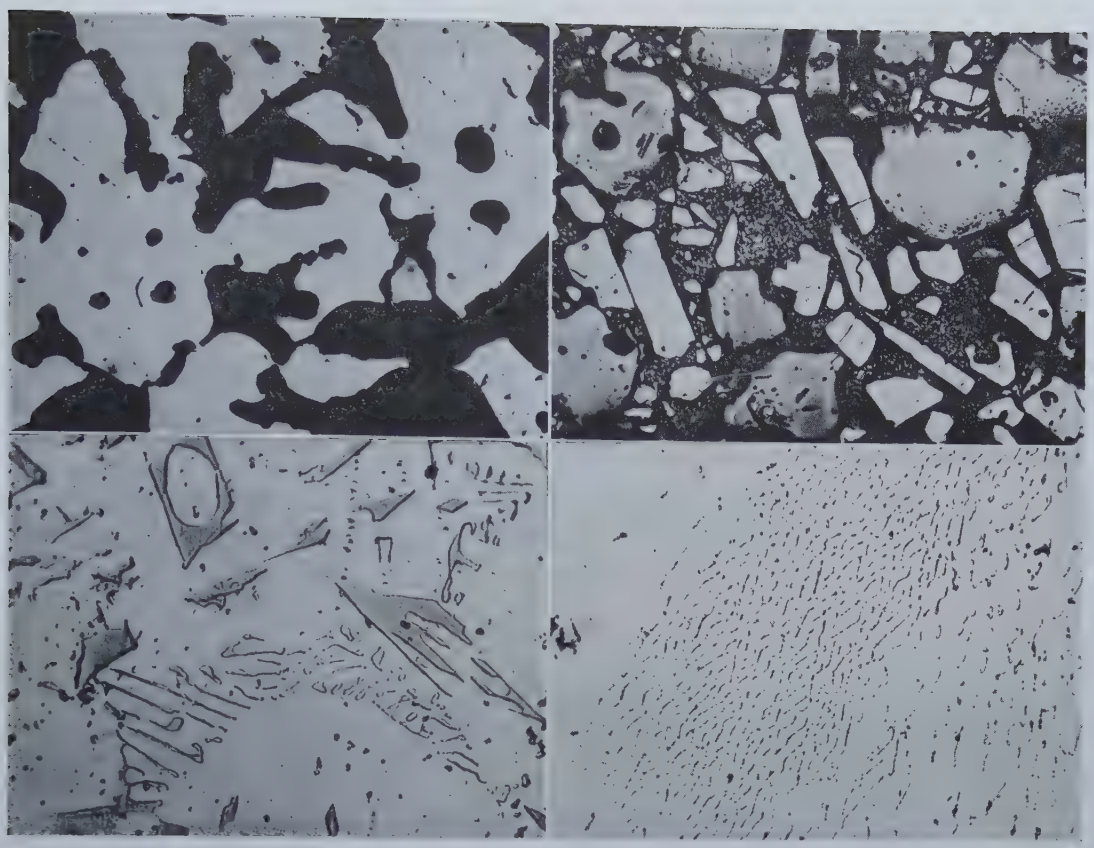

Fig. 7—Microstructures of cast Uranium-Aluminum alloys.

One pct HF acid etch. a. 100X. 70 at. pct Al; massive UAl_2 and UAl_3. b. 100X. 80 at. pct Al, heated to 710°C for 40 hr; massive UAl_3 (dark) and massive UAl_3 (light). Matrix is one or both of the two compounds finely divided. c. 500X. 92.5 at. pct Al; massive UAl_3 and coarse eutectic of UAl_3 and Al. d. 99 at. pct Al; eutectic of UAl_3 and Al.

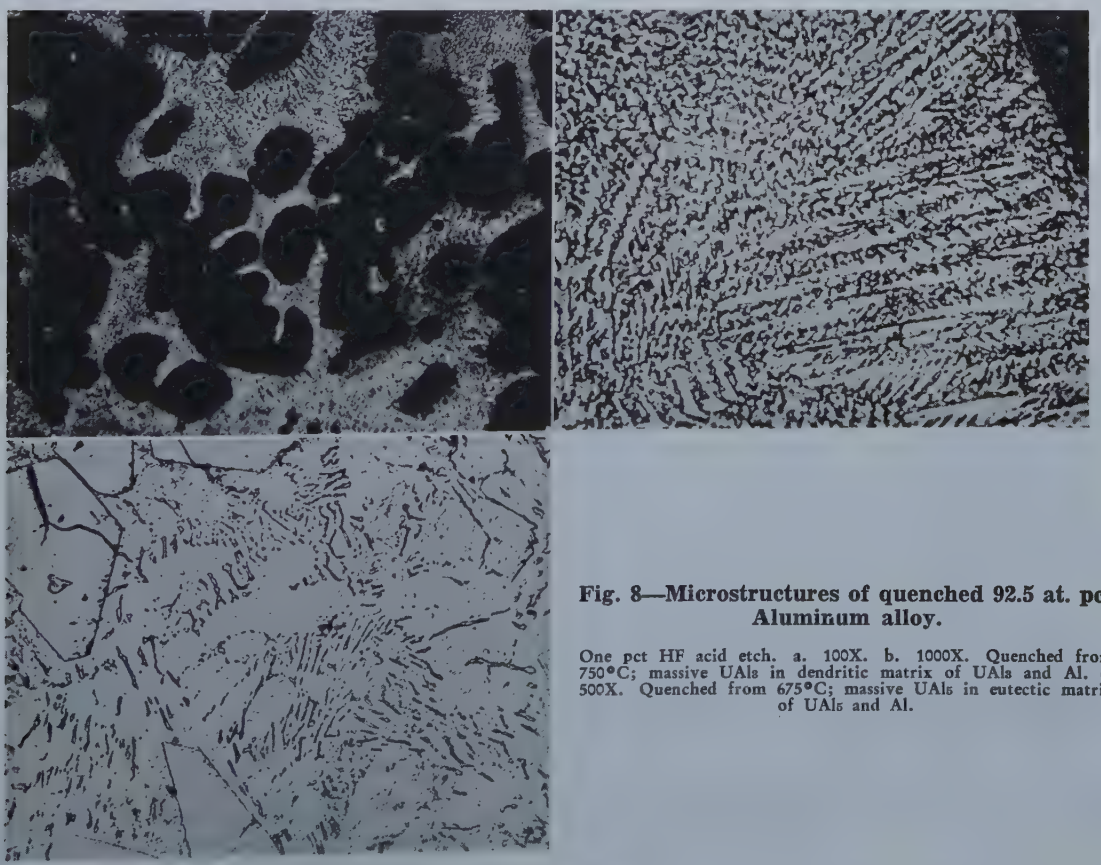

Fig. 8—Microstructures of quenched 92.5 at. pct Aluminum alloy.

One pct HF acid etch. a. 100X. b. 1000X. Quenched from 750°C; massive UAl_3 in dendritic matrix of UAl_3 and Al. c. 500X. Quenched from 675°C; massive UAl_3 in eutectic matrix of UAl_3 and Al.

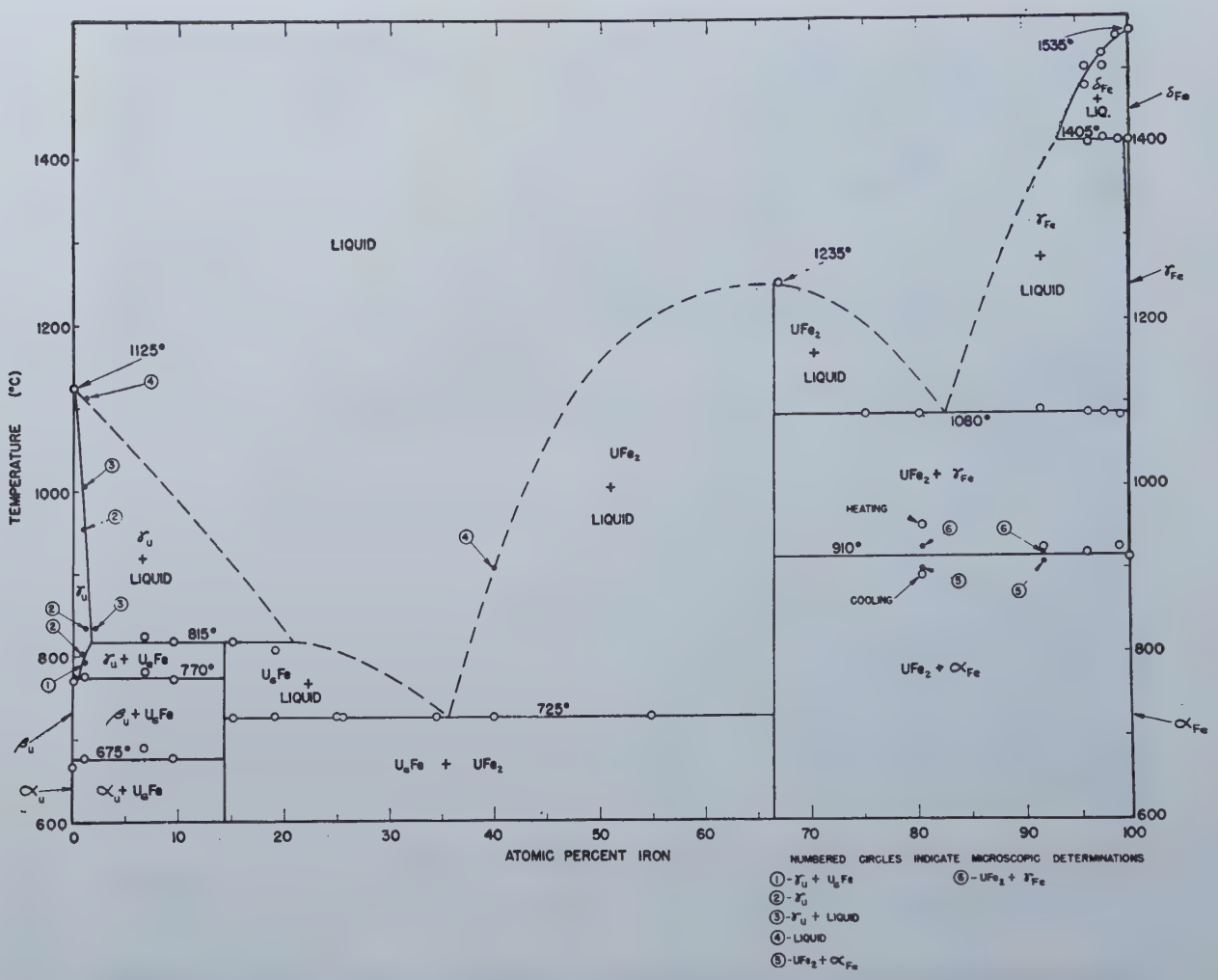

Fig. 9—Uranium-Iron equilibrium diagram.
°—Thermal measurement determinations.

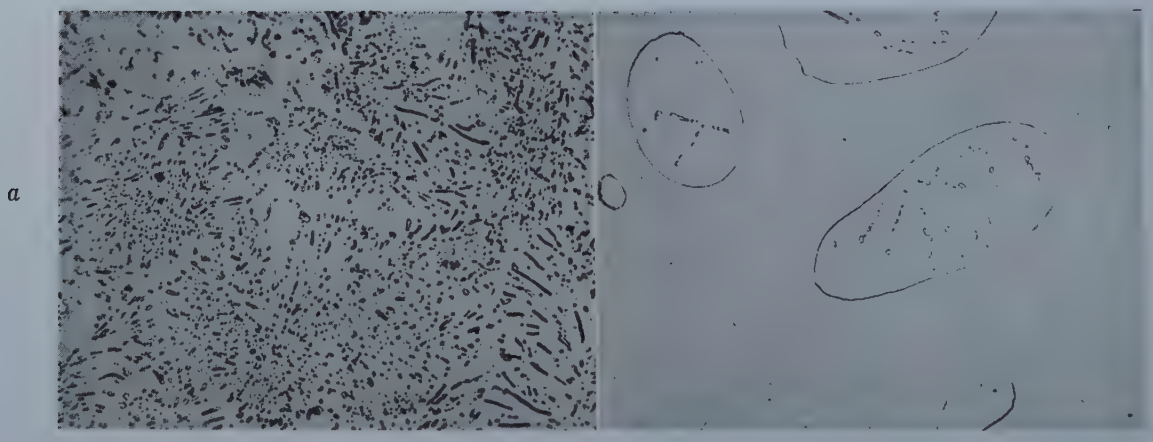

Fig. 10—Microstructures of Uranium-Iron alloys in the as-cast condition.
Electrolytic etch. a. 500X. 1.0 at. pct iron; largely eutectoid of U6Fe and U. Matrix is uranium phase. b. 500X. 9.65 at. pct iron; peritectic structure; large globules of U in U6Fe matrix; precipitated U6Fe particles in U globules.

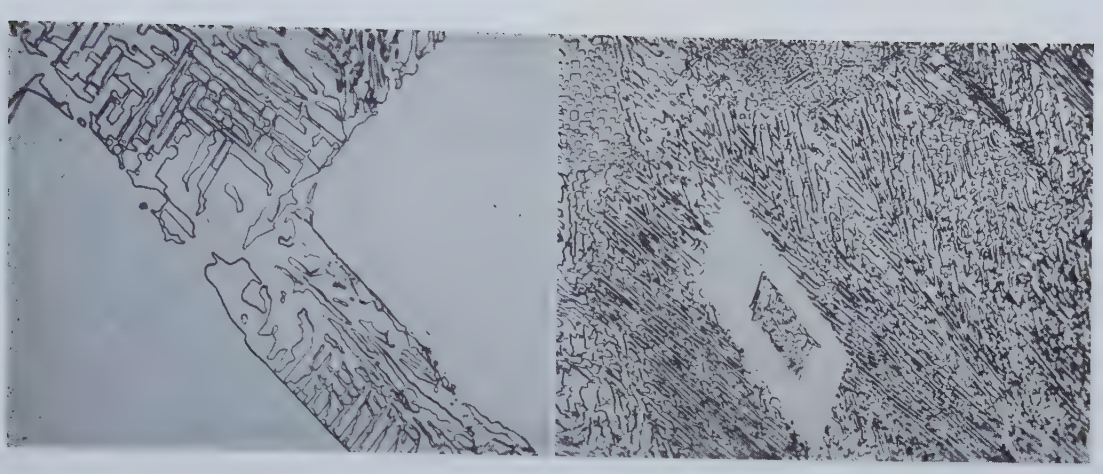

Fig. 11—Microstructures of Uranium-Iron alloys in the as-cast condition.

Electrolytic etch. a. 500X. 25.6 at. pct iron; massive U_6Fe plus eutectic of UFe_2 in U_6Fe. b. 500X. 34.5 at. pct iron; massive U_6Fe plus eutectic of UFe_2 in U_6Fe.

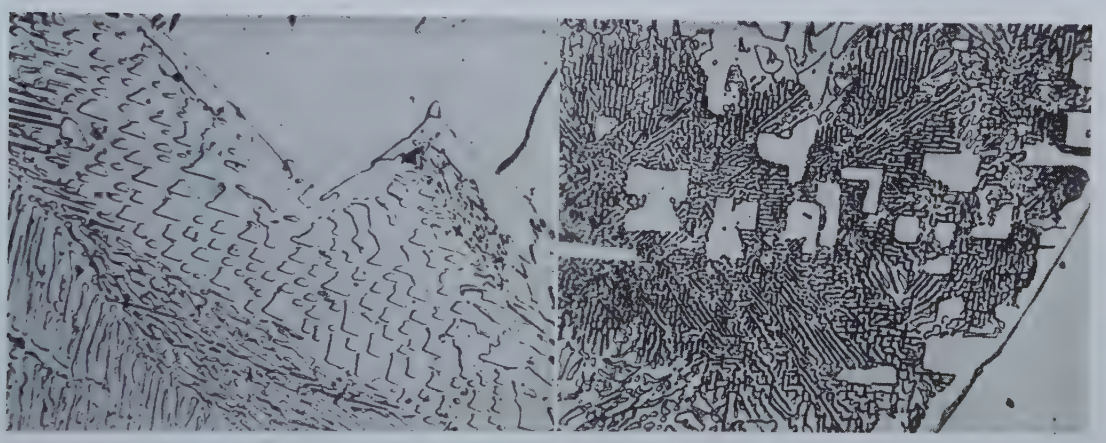

Fig. 12—Microstructures of Uranium-Iron alloys in the as-cast condition.

Electrolytic etch. a. 500X. 39.8 at. pct iron; massive UFe_2 plus eutectic of UFe_2 in U_6Fe. b. 500X. 54.7 at. pct iron; massive UFe_2 plus eutectic UFe_2 in U_6Fe.

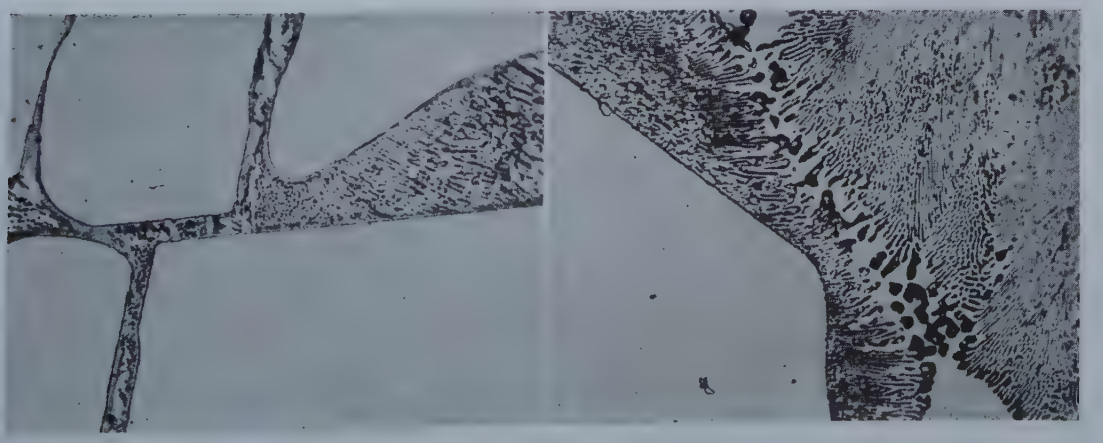

Fig. 13—Microstructures of Uranium-Iron alloys in the as-cast condition.

a. 500X. 64.9 at. pct iron; massive UFe_2 plus grain boundary eutectic of UFe_2 in U_6Fe. Electrolytic etch. b. 500X. 75.3 at. pct iron; massive UFe_2 plus eutectic of Fe in UFe_2. Nital etch.

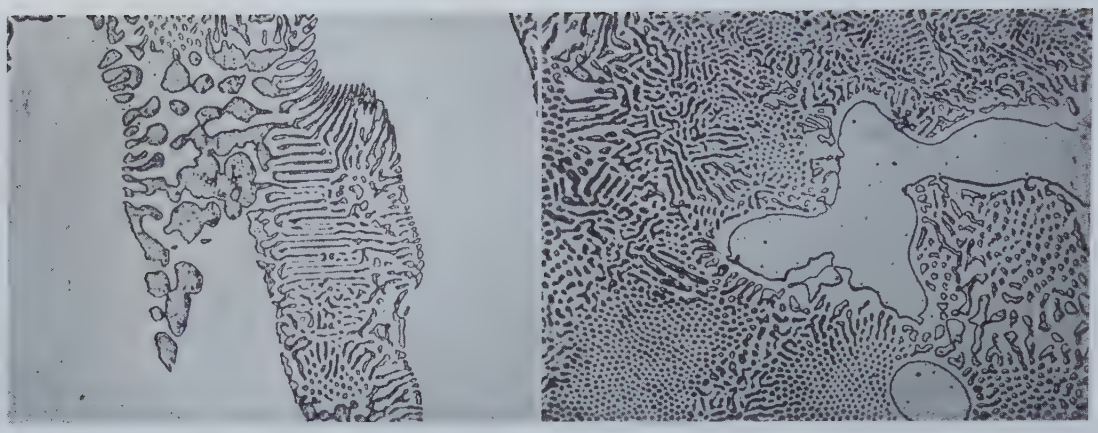

Fig. 14—Microstructures of Uranium-Iron alloys in the as-cast condition.

Nital etch. a. 500X. 80.5 at. pct iron; massive UFe_2 plus eutectic of Fe in UFe_2. b. 500X. 85.7 at. pct iron; massive Fe plus eutectic of Fe in UFe_2.

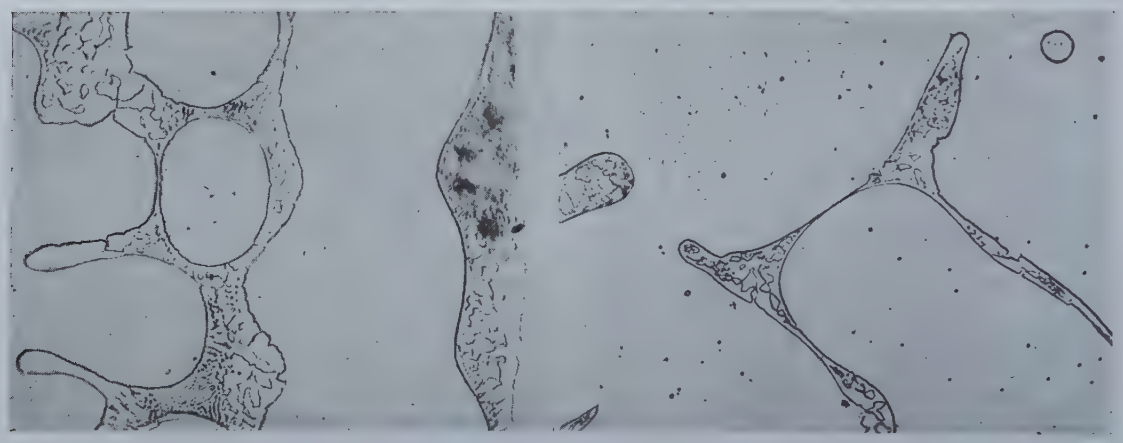

Fig. 15—Microstructures of Uranium-Iron alloys in the as-cast condition.

Nital etch. a. 500X. 96.1 at. pct iron; massive Fe plus eutectic of Fe in UFe_2. b. 99.0 at. pct iron; massive Fe plus eutectic of Fe in UFe_2.

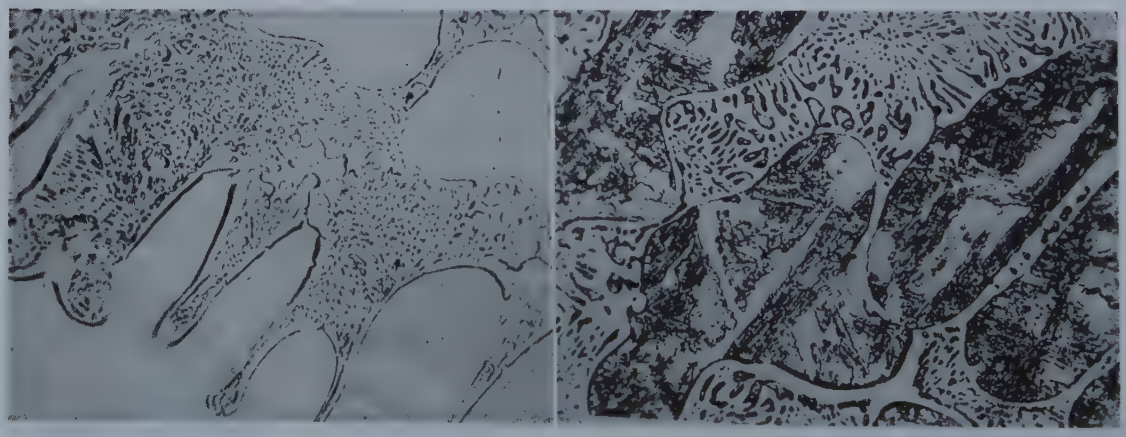

Fig. 16—Microstructures of Uranium-Iron alloy containing 91.8 at. pct iron:

after quenching from just below and just above the transformation temperature (910°C) for alpha to gamma iron Nital etch. a. Alloy quenched from 904°C. 500X. b. Alloy quenched from 917°C. Widmanstatten structures in iron phase indicate steel has passed through the alpha to gamma transformation. 500X.

Table II. X Ray Diffraction Results for UAl_3: Simple Cubic Lattice: $a_0 = 4.27$ Å (true unit)

$Sin^2\theta$*	hkl	Line Intensity†
0.0345	100	S
0.0679	110	S
0.1007	111	S
0.1343	200	S
0.1667	210	S
0.2005	211	S
0.2621	220	M to S
0.2951	300,221	M to S
0.3290	310	M
0.3622	311	S
0.3944	222	W to M
0.4269	320	M
0.4599	321	M to S
0.5262	400	W
0.5574	410,322	M to S
0.5886	411,330	M
0.6227	331	M
0.6561	420	M
0.6872	421	M
0.7176	332	W to M
0.7839	422	M to S
0.8147	500,430	W to M
0.8499	510,431	M to S
0.8797	511,333	W to M

* Values obtained with Cu-K alpha radiation
† VW—Very Weak
W—Weak
M—Medium
S—Strong

Table III. X Ray Diffraction Results for UAl_5: Structure not Determined

$Sin^2\theta$*	Line Intensity†	$Sin^2\theta$*	Line Intensity†
0.0166	W	0.3689	W to M
0.0345	W	0.3893	W
0.0454	W	0.4012	VW
0.0529	VW to W	0.4081	VW
0.0602	M to S	0.4184	W to M
0.0965	M	0.4269	W to M
0.1126	M	0.4408	VW
0.1243	VW to W	0.4948	VW
0.1255	VW to W	0.5035	VW
0.1427	VW to W	0.5245	M
0.1477	VW	0.5349	M to S
0.1615	W	0.5679	VW
0.1693	W	0.5834	W
0.1720	W	0.5954	W to M
0.1746	W	0.6039	W
0.1827	W	0.6260	W
0.1853	VW	0.6429	W
0.2033	VW	0.6595	M
0.2189	VW	0.6693	W
0.2380	S	0.6824	W
0.2500	VW	0.7254	W
0.2652	M	0.7486	W
0.2824	W to M	0.7737	W
0.2903	W to M	0.7854	W to M
0.2951	W to M	0.8078	W to M
0.3078	W to M	0.8306	W
0.3192	VW	0.8460	W
0.3290	VW	0.8692	M
0.3439	W to M	0.8864	W
0.3488	W to M	0.8983	W
0.3605	M to S		

* Values obtained with Cu-K alpha radiation
† VW—Very Weak
W—Weak
M—Medium
S—Strong

taking one uranium atom and three aluminum atoms to a unit cell, a calculated density of 6.8 g per cm^3 is obtained. The measured density is only 6.4 g per cm^3, but the disagreement with the calculated value is due to the difficulty in getting a homogeneous specimen of fairly large size.

Alloys between UAl_2 and UAl_3 show a two-phase structure with each constituent in massive form as shown in the micrograph, fig. 7a. This structure, along with the clear-cut thermal data shown in fig. 3, proves that UAl_3 forms by means of a peritectic reaction between UAl_2 and liquid. The peritectic temperature, as observed on alloys during heating, is located at about 1350°C. No attempt was made to determine the exact extent of the peritectic line into the liquid field.

A third compound, which is considered to be UAl_5, occurs on the aluminum side of UAl_3. The chief evidence for the existence of this compound is given by X ray diffraction patterns and by the consistent thermal data, which indicate a peritectic reaction between UAl_3 and liquid at about 730°C (fig. 3). The formula UAl_5 has not been definitely proven since the crystal structure has not been obtained from the X ray diffraction pattern; the $\sin^2\theta$ values and line intensities, however, are listed in table III. Metallographic examination places the compound in the vicinity of UAl_5, but again difficulties with inhomogeneity and chemical analysis precluded a more precise determination.

Cast alloys between UAl_3 and UAl_5 exhibited a rather indecisive two-phase structure which contained the two compounds in massive form in a matrix composed largely of the same two phases in a finely divided state. This microstructure persisted even after a fairly long heat treatment just below the peritectic temperature as shown in fig. 7b. Some of this matrix probably also was aluminum due to the peritectic reaction not having gone to completion, but there was not enough of it to appear in the diffraction patterns. Thermal measurements usually gave a weak indication of the eutectic at 640°C (between UAl_5 and Al) in the alloys lying between UAl_3 and UAl_5 and this was apparently due to residual aluminum. An 80 pct aluminum specimen which was annealed at 700°C for about a week gave only a very feeble effect at 640°C, whereas in the cast condition this thermal break had been much stronger.

Alloys on the aluminum side of UAl_5 exhibit a strong thermal effect at 640°C (fig. 3) which is due to a eutectic reaction between UAl_5 and aluminum as revealed by the micrographs in fig. 7c and 7d. The eutectic composition has been placed at about 1.7 at. pct uranium (13 wt pct) by noting the intersection of one of the liquidus lines with the eutectic horizontal. Points on the liquidus line in this instance were obtained by chemical analysis of samples of the liquid which were in thermal equilibrium with the compound at a series of temperatures.* These results have been plotted in fig. 3 and the undetermined portion of the liquidus line has been drawn to join the known part.

The existence of the eutectic and peritectic reactions in this range of alloys was further checked by metallographic and X ray examination of specimens quenched from above and below these temperatures. The results of this examination are indicated in fig. 3 and are illustrated by the micrographs of fig. 8. Specimens quenched from above the peritectic temperature were especially revealing since the diffraction pattern of UAl_5 would disappear and be replaced by that of UAl_3 and aluminum.

* This work was done several years after the phase diagram determination and was carried out by G. Bitsianes and E. Hayes at Massachusetts Institute of Technology under contract #W-7405-eng-175.

Table IV. X Ray Diffraction Results for UFe_2: Diamond Cubic Lattice, $a_0 = 7.050$ Å (true unit)

$Sin^2\theta$*	hkl	Line Intensity†
0.0483	111	VW
0.0718		VVW
0.1044		VVW
0.1290	220	W to M
0.1766	311	M
0.1928		VW
0.2447		VVW
0.2567	400	VW
0.3054	331	W
0.3858	422	W to M
0.4330	511,333	W to M
0.5148	440	W to M
0.5627	531	W
0.6436	620	W to M
0.6914	533	W
0.7098		VVW
0.7716	444	VW
0.8187	711,551	W
0.8987	642	S

* Values obtained with Cu-K alpha radiation
† VVW—Very, Very Weak
VW—Very Weak
W—Weak
M—Medium
S—Strong

Table V. X Ray Diffraction Results for U_6Fe: Lattice Structure Undetermined

$Sin^2\theta$*	Line Intensity†
0.0807	W to M
0.0975	VW
0.1065	VW
0.1175	VW
0.1278	M
0.1949	W
0.2139	W
0.2707	VW
0.2934	W to M
0.3102	VW
0.3605	W to M
0.3765	W
0.3875	W
0.4277	W
0.4948	VW
0.5061	VW
0.5383	VW
0.5799	M
0.6961	W
0.7215	W
0.7401	W
0.7522	W
0.8125	W to M
0.8294	W to M
0.8460	W to M
0.8692	W to M
0.8830	W to M

* Values obtained with Cu-K alpha radiation
† VW—Very Weak
W—Weak
M—Medium
S—Strong

No attempt was made to determine the solid solubility, if any, of uranium in aluminum since all evidence indicated that it must be very small.

Experimental Results—Iron Alloys

It was found, as shown in fig. 9, that there are eight solid phases comprising the uranium-iron system: alpha, beta and gamma uranium; alpha, gamma and delta iron; and two intermetallic compounds. No X ray evidence of the existence of the beta and gamma uranium phases and of the gamma and delta iron phases was obtained because even brine quenching of very small specimens failed to retain these phases at room temperature.

One intermetallic compound was located at the composition UFe_2 (66.7 at. pct iron). Microscopic examination revealed a virtually one-phase structure at 67 at. pct iron. Furthermore, it was found possible to index the main lines in the X ray photogram of this compound on a diamond cubic lattice (see table IV). The lattice parameter was then determined to be $a_0 = 7.050$ Å. Using this parameter and assuming a cell made up of 8 uranium and 16 iron atoms, the density of the compound was calculated as 13.2. This is a reasonably good check with the measured density 13.0 of an alloy containing 67 at. pct iron. In view of the rapid variation of density with composition in the uranium-iron system the small discrepancy between the calculated and measured densities may be largely attributable to the fact that the measured density was obtained on an alloy somewhat high in iron. Several very weak lines appear in the X ray photogram of the UFe_2 compound which cannot be fitted into the diamond cubic pattern. The reason for the presence of these lines is somewhat obscure. They are not due to oxide, and although one of the lines coincides with an alpha iron position, it cannot be ascribed to alpha iron because other strong alpha iron lines do not appear.

The formula U_6Fe of the other compound has been established chiefly on the basis of microscopic measurements. A homogenized 15 at. pct iron alloy still showed traces of the eutectic structure typical of the compositions between the two compounds. On this evidence, the composition of the compound high in uranium was placed at the nearest simple formula below 15 at. pct iron. The lines in the X ray photogram of this compound were measured and their $\sin^2\theta$ values listed in table V, but attempts to index these lines on a definite pattern were unsuccessful.

A study of the diagram of fig. 9 and the micrographs of fig. 10 to 16 reveals the following pertinent facts about the uranium-iron system:

1. The solubility of iron in gamma uranium is appreciable, reaching a maximum of about 1.5 to 2 at. pct iron at 815°C. A homogeneous alloy containing 1 at. pct iron does not begin to melt until a temperature of 975°C is reached, and it is not completely molten until 1115°C is attained.

2. The solubility of iron in alpha and beta uranium, and of uranium in alpha iron is practically negligible.

3. The gamma iron field is quite limited. Its actual extent has not been determined, but is known to be less than 0.5 at. pct of uranium.

4. At the uranium-rich end, there is a peritectic reaction which occurs at 815°C involving the phases gamma uranium, liquid and U_6Fe.

5. At 770°C, a eutectoid reaction takes place between the phases gamma uranium, beta uranium, and U_6Fe. The eutectoid composition has been placed somewhat below 1 at. pct iron in view of the fact that specimens of the 1.0 at. pct iron alloy quenched from above the eutectoid temperature still show the presence of some U_6Fe in the form of globules quite a bit larger than the eutectoid particles in fig. 10a.

6. A phase change between alpha and beta uranium appears at 675°C in the composition range be-

tween almost pure uranium and the compound U_6Fe.

7. Between the two compounds U_6Fe and UFe_2 a eutectic transformation occurs at the surprisingly low temperature of 725°C.

8. The compound UFe_2 melts at 1235°C creating an open maximum in the diagram.

9. At 1080°C another eutectic transformation appears, involving UFe_2 gamma iron, and liquid.

10. The alpha to gamma transformation in iron occurs at about 910°C. In this case, the thermal data were somewhat inconsistent. The thermal holds obtained on the alloys containing 91.8 at. pct iron and above were all somewhat high. The 80.5 at. pct iron alloy showed the alpha to gamma break only after complete homogenizing, and even then a large spread between the thermal holds of cooling and heating appeared as indicated in fig. 9. The microscopic evidence of this transformation was quite definite, however. Specimens of the 80.5, 91.8, and 99.0 at. pct iron alloys were quenched from just below and just above 910°C. The resulting microstructures for the 91.8 at. pct iron alloy are illustrated in fig. 16. The Widmanstätten structure appearing in the iron phase of the specimens quenched from just above 910°C is good proof that the iron has undergone a phase change. There is some sign of very finely dispersed precipitated particles in the iron phase, which is probably a result of the alpha to gamma transformation (see fig. 14b, 15a and 15b).

11. The details of the diagram in the vicinity of the delta iron transformation and the melting point of iron are somewhat doubtful. It is believed that the calibration of the thermocouple used was inconsistently low in this high temperature range. The melting point of iron, the temperature of the gamma-delta transformation and the melting point of nickel in a check run were all from 15° to 25°C lower than the standard values given for these points. The thermal points plotted in fig. 9 for the high iron alloys at and above the gamma transformation have therefore been plotted higher than the experimentally determined values by an amount (25°C) sufficient to bring the melting point of iron up to the accepted value of 1535°C. In all the alloys exhibiting the gamma-delta transformation, the temperature of this reaction remains the same as in pure iron, thus signifying negligible solid solubility of uranium in delta iron.

Properties of Uranium-Aluminum and Uranium-Iron Alloys

No systematic attempt was made to determine the physical properties of the uranium-aluminum alloys, but a few observations made in the course of the phase diagram study are worthy of mention. With regard to the three intermetallic compounds it may be said that all of them are brittle enough to be readily crushed with a hammer, but that none of them is hard enough to scratch glass. The densities of UAl_2 and UAl_3 are about 8.3 and 6.8 g per cm^3 respectively, while that of UAl_5 was not determined.

The possibility of age hardening the uranium-rich alloys after quenching from the gamma solid solution was explored with some care. For this purpose two alloys were prepared, one with 2.5 and the other with 5 at. pct aluminum. The former was successfully forged at about 600°C into a one-half-inch square bar, but the latter broke up during this operation and hence was available only in the cast condition for the later heat treatments.

Specimens of the 2.5 pct alloy were quenched from 1040°C and microscopic examination showed that all of the UAl_2 was in solution. The gamma phase was not retained by this treatment and hence the specimens consisted of supersaturated alpha uranium. This quenched material had an average Rockwell "C" hardness of about 29 to 31 which is greater than the as-cast value of about 25.

The specimens were reheated for one-half hour at successively increasing temperatures and the hardness again measured. It was found that the Rockwell "C" hardness decreased progressively to a value of about 25 as the aging temperature was raised to 300°C and then increased to a maximum value of about 35 after the 500°C treatment. This represents a hardening from minimum to maximum of about 9 to 10 R_C units. Other specimens were heated at 500°C for increasing times to determine the optimum treatment. The maximum hardness, 36 R_C, was reached in about 3 hr, after which softening occurred.

The 5 pct aluminum specimen was found to be quite brittle after quenching from 1040°C and also 1090°C and micro-examination showed that some grain boundary UAl_2 still was undissolved. The hardness of this alloy as cast was about 25 R_C after the quench. Aging for 2.5 hr at 500°C further increased the hardness to about 45 R_C which is a substantial increase over the annealed value. However, the hardening of this particular alloy could not be usefully employed to increase the strength of uranium because of the extreme brittleness which was manifest both in quenching cracks and in spalling under the hardness indenter.

It is possible that an aged 3 to 4 at. pct aluminum alloy would be sufficiently ductile to come within the range of a usable material and at the same time exhibit a substantial increase in hardness and tensile strength over that of pure uranium.

Only a few casual observations of the properties of the uranium-iron alloys were made. Both of the compounds U_6Fe and UFe_2 are hard and brittle but do not scratch glass. A rough measurement with a permanent magnet indicated that UFe_2 is not ferromagnetic at room temperature. It is worthwhile to point out that small amounts of iron will produce a liquid phase in uranium above 815°C and that this condition may lead to hot shortness in fabrication operations at such temperatures.

References

[1] M. Hansen: Aufbau der Zweistofflegierungen, (1943), pp. 160, 750.

[2] J. Chipman: Metallurgy in the Development of Atomic Power. Declassified Document #MDDC-539, Dept. of Commerce, Washington, D. C.

The Alloy Systems Uranium-Tungsten, Uranium-Tantalum and Tungsten-Tantalum

by C. H. Schramm, P. Gordon and A. R Kaufmann

The constitutions of the uranium-tungsten and uranium-tantalum alloy systems have been determined and the resulting phase diagrams constructed. The relationship between lattice parameter and composition for tantalum-tungsten solid solutions has been delineated. In addition, two phases of the uranium-tantalum-carbon ternary system have been discovered and described.

AS a part of the general program on alloys of uranium carried out at the Massachusetts Institute of Technology under contract W-7405-eng-175 for the Manhattan Project during the recent war, it was considered desirable to investigate the boundary binary phase diagrams of the ternary alloy system uranium-tungsten-tantalum. Previous work on these alloys was practically nonexistent. A brief statement to the effect that tantalum and tungsten form a continuous series of solid solutions was found in a general paper on tantalum by W. V. Bolton[1] but no information was available on the uranium-tungsten and uranium-tantalum systems. The research to be described in this paper has served to delineate the main features of the uranium-tungsten, uranium-tantalum phase diagrams and to check Bolton's work on the tungsten-tantalum diagram.

C. H. SCHRAMM is Research Associate, Harvard University, P. GORDON is Assistant Prof. of Metallurgy, Illinois Inst. of Technology, and A. R. KAUFMANN, Member AIME, is Assoc. Prof. of Metallurgy and Director of the M.I.T. Metallurgical Project, Mass. Inst. of Technology.

New York Meeting, Feb. 1950.

TP 2765 E. Discussion (2 copies) may be sent to Transactions *AIME before Apr. 1, 1950, and will be published Nov. 1950. Manuscript received Oct. 14, 1949.*

Experimental Details

Metals: The tungsten and tantalum used for preparing the alloys were 99.96 and 99.65 pct pure, respectively. The chief impurities in the metals were about 0.02 pct molybdenum in the tungsten, and 0.2 pct columbium, 0.05 pct tungsten, 0.02 pct barium and 0.01 pct silicon in the tantalum. The uranium used was 99.9 pct pure, with the main contaminants being iron and carbon. (An appreciable amount of magnesium was present in the uranium as received, but this distilled off during melting and so is not reported as an impurity.)

The composition of specimens indicated in the subsequent figures and tables of this paper are the results of chemical analyses on the cast alloys except for the tantalum-tungsten alloys. For the latter, chemical analysis was not very reliable as a result of the difficulty of separating tungsten and tantalum chemically. Consequently, the nominal

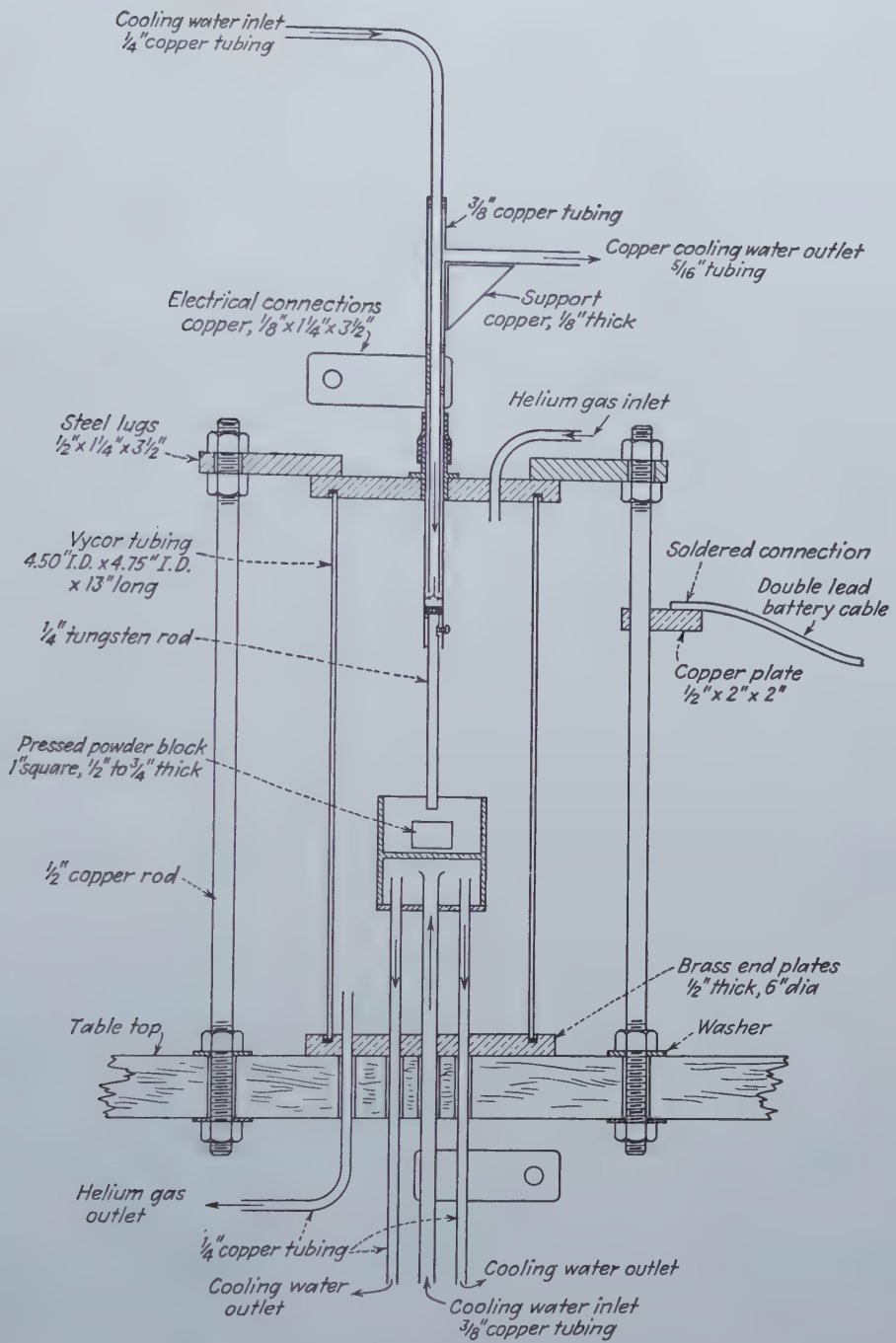

Fig. 1—Scale Drawing of Arc-melting Apparatus.

compositions of these specimens, believed to be accurate within 1 pct of either element, were used.

Melting Apparatus: Because of the high melting points of tungsten and tantalum, special techniques for the preparation and heat-treatment of the alloys had to be developed. Attempts to prepare even the uranium-rich alloys by conventional melting methods using BeO, ZrO_2 and TiC crucibles inside an induction-heated graphite shell met with little success. In each case the metal was found to have reacted with the crucible when heating was carried to about 2200°C.

The apparatus which proved most satisfactory for melting purposes is illustrated in fig. 1. The specimen in the form of a powder compact of the two metals (mixed and pressed in a dry box to prevent oxidation of the uranium powder) was placed in a water-cooled copper cup and made the positive terminal of a dc arc with a ¼-in. diam tungsten (or tantalum, depending on the alloy being made) rod as the negative electrode. This assembly was contained within a Vycor tube in which an atmosphere of helium was maintained. The upper electrode holder fitted through a tight rubber tube, giving an air tight seal and allowing the electrode to be lowered and raised for starting the arc and also

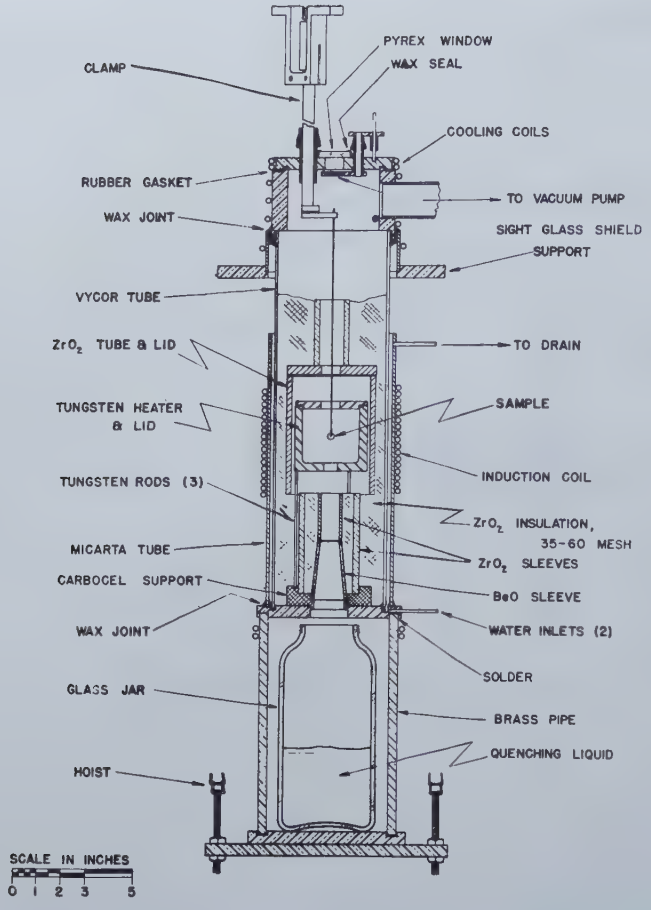

Fig. 2—Scale Drawing of Induction Heating Unit.

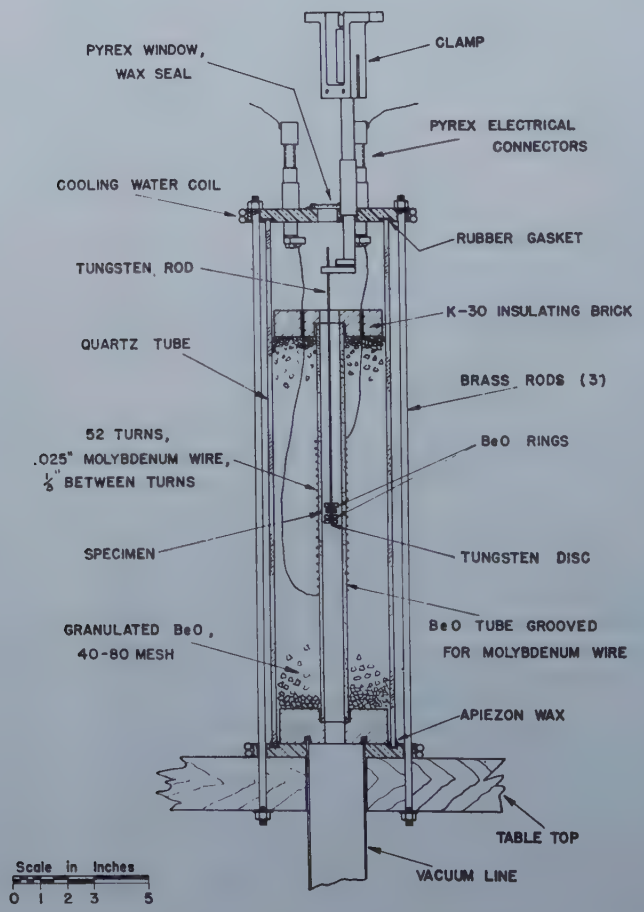

Fig. 3—Scale Drawing of Resistance Heating Unit.

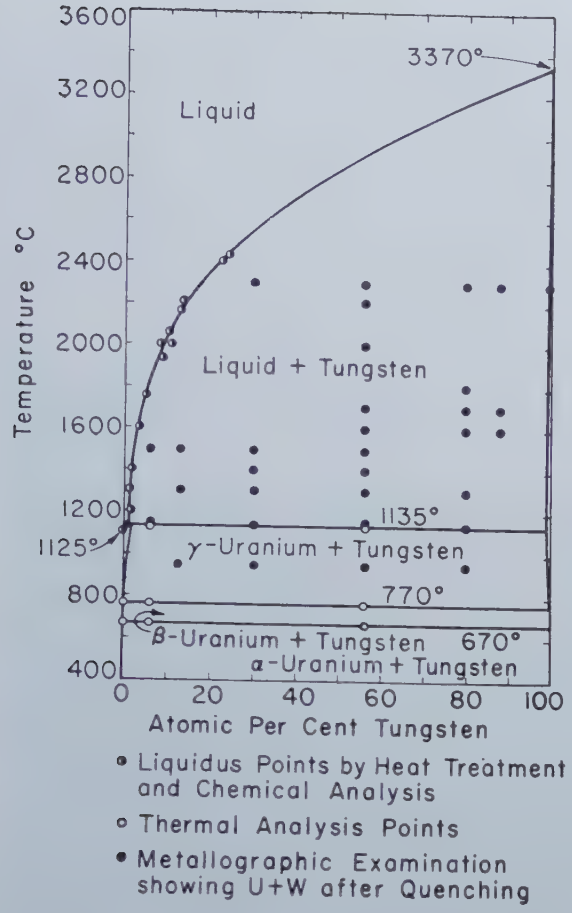

Fig. 4—The Uranium-Tungsten Phase Diagram.

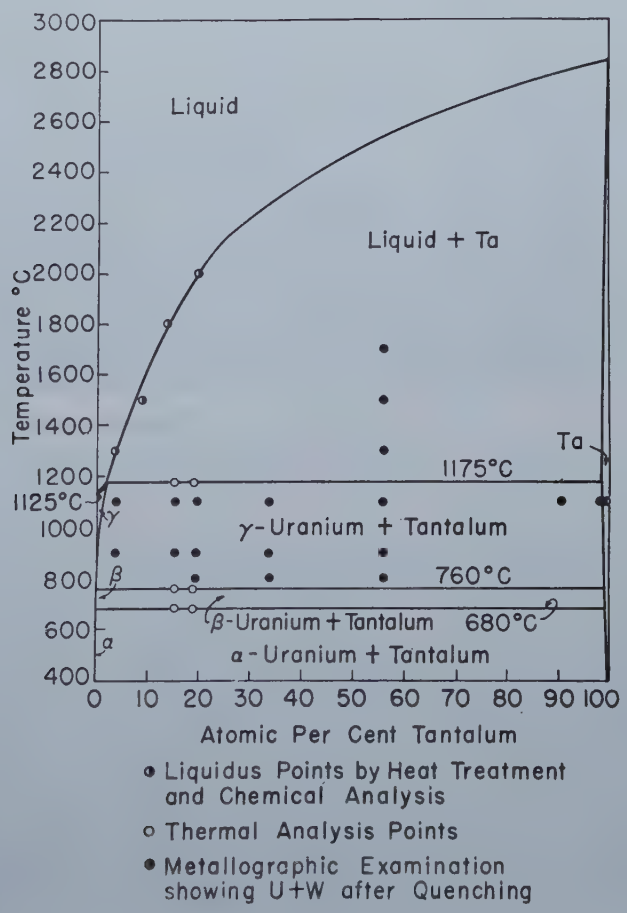

Fig. 5—The Uranium-Tantalum Phase Diagram.

tilted to move the arc over the surface of the specimen. The arc required 15 to 20 v and the current could be varied from 200 to 700 amp.

With the arrangement just described, the upper portion of the specimen was readily melted, while the under side, being in contact with the copper, remained relatively cool. This necessitated turning the specimen over for a second heating in order to complete the fusion. However, the problem of refractories, which was the principal obstacle in this high temperature work, was neatly side-stepped. Pure tungsten (m.p. = 3370°C) was readily melted in the arc. Alloy specimens prepared were essentially homogeneous in composition as determined by metallographic examination. The pick-up of impurities during melting was limited to copper by the a tungsten wire, the wire being held by a clamp in the upper part of the unit. After heating, quenching was carried out when desired merely by loosening the clamp by means of its parts above and outside the furnace and allowing the specimen and wire to drop into a Silicone oil bath. The whole operation was carried out in vacuum, the pressure being 10^{-3} mm mercury during heating and 10^{-4} mm during the hold at temperature.

With the apparatus shown in fig. 2 connected to a 20 kva Ecco high frequency oscillator, temperatures up to just below the melting point of zirconia (2700°C) were readily obtained. A previous arrangement using graphite in place of both the tungsten chamber and the zirconia insulation had allowed temperatures up to 3000°C to be reached.

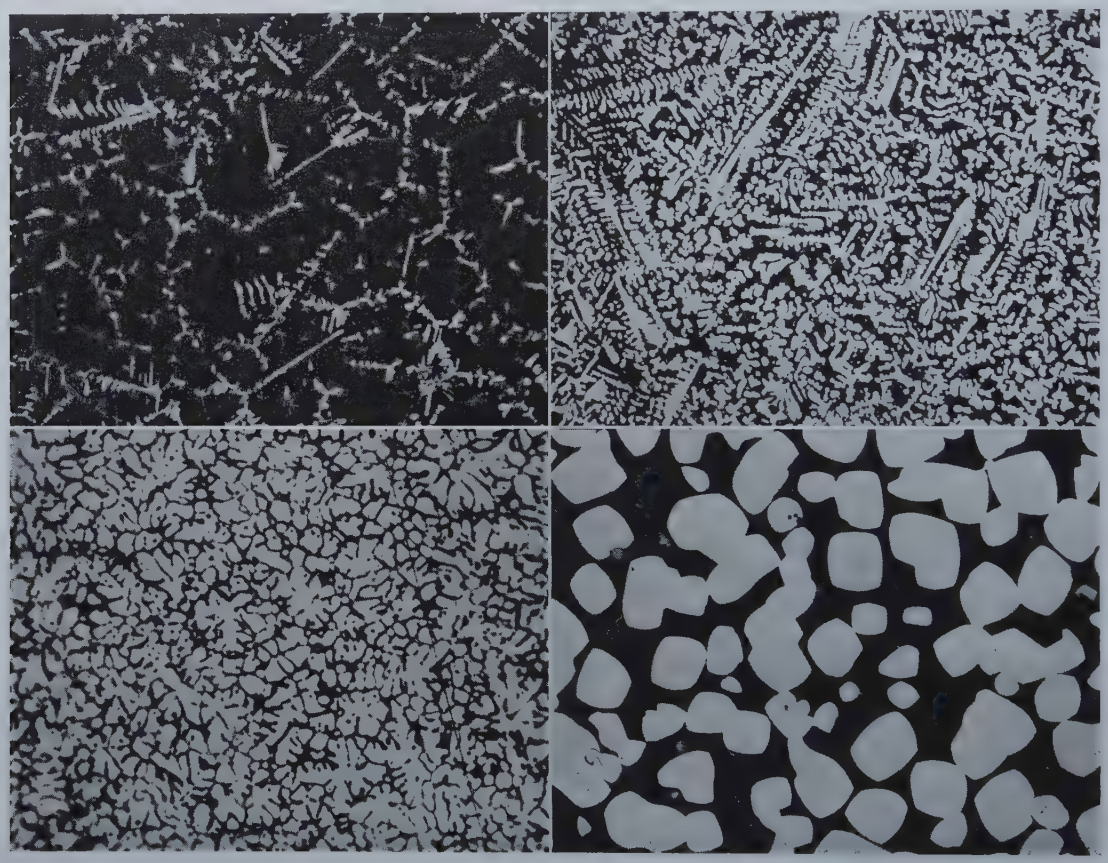

Fig. 6—Typical Microstructure of As-melted and Heat-treated Uranium-Tungsten Alloys.

Etchant-heat tinting. 150X. White phase is tungsten, dark phase uranium. a. 12.5 at. pct tungsten. As-melted. b. 56.0 at. pct tungsten. As-melted. c. 80.0 at. pct tungsten. As-melted. d. 56.0 at. pct tungsten. Quenched from 1400°C.

nature of the apparatus (assuming a nonreactive atmosphere) and all evidence, including chemical analysis, indicated that the copper pickup was negligible.

Induction Heat-treating Equipment: In order to facilitate the heat-treatment of alloy samples at high temperatures and to make possible quenching from these temperatures, an induction heating unit was constructed as shown in fig. 2. The principal feature of the furnace was a tungsten heating chamber within a zirconia tube having openings at both top and bottom leading through zirconia sleeves to give a through passageway. The specimen was suspended within the heating chamber on It was found, however, that the carbon vapor prevailing in the heating chamber atmosphere reacted quite rapidly with the specimens above 2300°C and hence this construction was discarded.

Resistance-wound Heat-treating Equipment: Because the induction unit described above was limited to relatively short heating periods, a high-vacuum resistance-heated unit was constructed for lengthy heat-treatments at temperatures up to about 1900°C. This unit consisted of a bank of three identical, molybdenum wound resistance furnaces. A detailed drawing of one of the furnaces is shown in fig. 3. By controlling the power input to these fur-

naces with voltage stabilizers and variac transformers, it was possible to maintain temperatures to ± 3°C over long periods of time in the range 1000° to 1900°C. The vacuum system included a 4 in. oil diffusion pump backed by a mechanical pump. With all three furnaces operating at temperatures between 1100° and 1700°C pressures as low as 3 x 10^{-5} mm of mercury were obtainable with this pumping system.

When it was desired to quench the specimens being heat-treated, the clamp holding the sample (see fig. 3) was opened and the sample dropped through the furnace tube and copper tee into a standard-taper tube containing mercury or Silicone oil. "NV" grade Silicone oil was used for quenching since it has a very high degree of thermal stability and an extremely low vapor pressure. This oil was used for quenching metal powders which would otherwise become contaminated with mercury. Mercury was used for quenching solid samples and when so used a thin film of Silicone oil was placed on the mercury to lower the vapor pressure of the latter in the system.

Temperatures in both the induction and resistance heat-treating units were measured with an optical pyrometer of the disappearing filament type. The accuracy of measurement was within about 20°C.

Metallographic Technique: The preparation of specimens for metallographic examination was done by standard laboratory methods. The specimens were ground through 3/0 emery paper and polished on lead laps with two grades of levigated alumina.

Three different etching techniques were employed to distinguish the phases present in the alloys. Most of the uranium-tungsten alloys were etched by heat tinting, that is, accelerated oxidation of the uranium (see fig. 6). In addition, two etching procedures were used to aid in ascertaining the presence of free tungsten. One was an electrolytic etch in a 15 pct aqueous solution of sodium hydroxide which attacks free tungsten quite vigorously but has little or no effect on the other phases involved. The second was an electrolytic etch in a solution of ethyl alcohol, ethylene glycol, and phosphoric acid (8:5:5 parts by volume). With 20 to 40 v across the cell this etch deposits a thin film on the tungsten ranging in color from brown to purple, the color depending on the voltage used. It was found that tantalum is affected similarly by this etch, and most of the uranium-tantalum specimens were etched in this way (see fig. 7). The color film does not form on uranium, nor on any of the extraneous phases (oxides, carbides, etc.) encountered in the specimens.

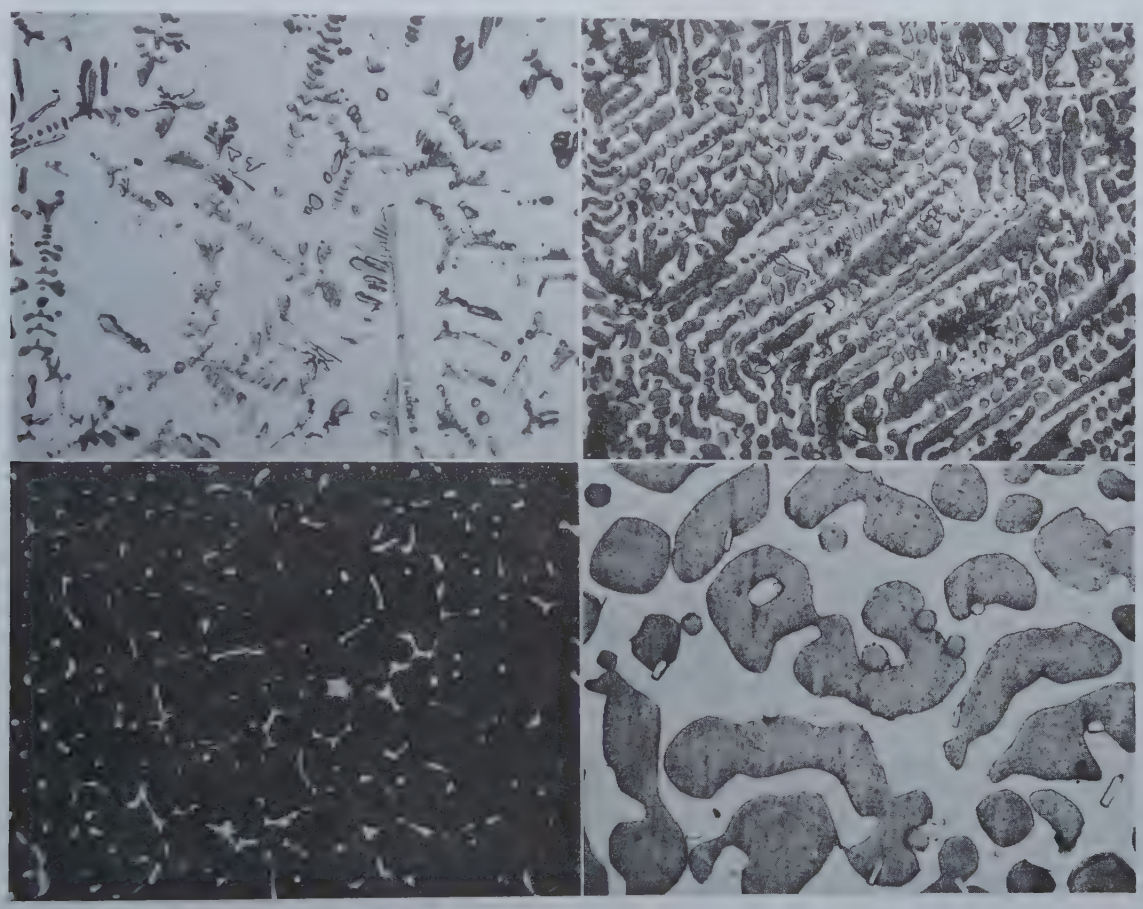

Fig. 7—Typical Microstructures of As-melted and Heat-treated Uranium-Tantalum Alloys.

Electrolytic etch in ethyl alcohol-ethylene glycol-phosphoric acid solution. 500X. White phase is uranium, dark phase tantalum. a. 14.9 at. pct tantalum. As-melted. b. 56.4 at. pct. tantalum. As-melted. c. 89.5 pct tantalum. As-melted. d. 56.4 at. pct tantalum. Quenched from 1300°C.

X Ray Techniques: Powder X ray examination with a Debye-Scherrer camera was employed to

confirm the identity of the phases present, and also for some measurements of lattice parameters. Precision parameter measurements were made on pure tungsten, uranium and tantalum, on some heat-treated dilute alloys of uranium and tungsten, and on the 20 at. pct tantalum-in-tungsten alloy* by means of a symmetrical focusing back reflection camera. Cohen's[2] method for analytical extrapolation was used to eliminate systematic errors. In all cases copper radiation was employed with the wave lengths: K alpha$_1$ = 1.54050, K alpha$_2$ = 1.54435, K beta = 1.39216 Å.

* Because of the broadening effect of the solid solution on X ray lines, precision measurements on the other tantalum-tungsten alloys were not obtainable.

Thermal Analysis Technique: The procedure for thermal analysis is described adequately elsewhere[3]. Briefly, it consisted of obtaining time temperature curves during heating and cooling of the alloys, phase changes being indicated by holds in the curves. The reported temperatures of transformation are those determined during heating. Temperature was measured to an accuracy of about ±5°C with a platinum-platinum-rhodium thermocouple protected from reaction with the specimen by a thin layer of slip-cast beryllia.

Discussion of Results

The Uranium-Tungsten and Uranium-Tantalum Systems: The tungsten-uranium and tantalum-uranium phase diagrams are qualitatively much alike, differing only by relatively minor shifts in the exact temperature-composition coordinates at which transformations and reactions occur. As shown in fig. 4 and 5, each consists of four solid phases; namely, alpha, beta and gamma uranium plus either tungsten or tantalum, and a single liquid solution, at high temperatures, of the two metals concerned.

In view of the high chemical affinity of uranium for a great many materials, the most striking feature of both systems is the complete absence of intermediate phases. Melting of the alloys in the arc was carried out at temperatures in the range 3000° to 4000°C. The microstructures of several of the as-melted alloys are shown in fig. 6 and 7. Microstructures typical of the as-melted alloys are shown in fig. 6 and 7. Heat-treatments of as long as several hundred hours followed by quenching (see fig. 4 and 5) were carried out covering the temperature range 800°C to 2300°C, but no evidence for the formation of intermediate phases was found. Some typical quenched structures are included in fig. 6 and 7. Just as for the as-melted alloys, it may be seen that the heat treated structures consist essentially of free tungsten or free tantalum embedded in uranium. Only the shape and size of the primary particles change after heat-treatment, the particles growing and becoming spheroidized with increasing temperature and time treatment. No sign of rimming of either the tungsten or the tantalum is noticed, a phenomenon which would be expected if some sluggish reaction between the uranium and the second metal had begun. X ray evidence corroborated the conclusion that the two important constituents in any alloy were uranium and either tungsten or tantalum.

A few extraneous gray particles may be noted in some of the micrographs. These particles are believed to be an oxide of uranium, probably UO_2. Other extraneous phases were occasionally found in alloys after heat treatment, but in every case these phases were confined strictly to the uranium matrix and no sign was ever observed that the tungsten or tantalum entered into the reaction at all.

The terminal solid solubilities in both the uranium-tungsten and the uranium-tantalum systems were revealed to be very limited. No careful attempt was made to determine the exact values of these solubilities, but metallographic and X ray evidence was obtained to establish the order of magnitude of solid solution limits. For the uranium-tungsten alloys the evidence placed the elevated temperature solution limits at probably less than one atomic percent at both ends of the diagram. The lattice parameters of the pure metals were found to be:

$a_0 = 3.1651 \pm 0.0001$Å for tungsten and $a_0 = 2.8540$Å, $b_0 = 5.8683$Å, $c_0 = 4.9576$Å ± 0.01 pct for alpha uranium.

X ray measurements on dilute alloys in both the tungsten-rich and uranium-rich regions revealed small changes in these parameters as a result of quenching*. The tungsten lattice constant increased by approximately 0.02 pct. In the case of uranium the magnitude of the maximum change was not definitely determined because the nonuniform shift of the X ray lines made the indexing of many of the closely spaced lines at best uncertain. However, calculations made on the basis of line indices which seemed most probably correct indicated that the decrease in the lattice parameters of the uranium might be of the order of 0.04 to 0.10 pct.

* It was not found possible to suppress the formation of alpha uranium by quenching.

The high temperature solid solubility limits of tantalum in uranium and uranium in tantalum were both indicated to be less than about 2 at. pct. A 3.6 at. pct tantalum alloy showed little change in the quantity of tantalum dendrites present even after quenching following a heat-treatment of 7 days at 1100°C. At the tantalum-rich end of the diagram the 99.2 and 98.5 at. pct tantalum alloys both revealed a small number of very fine grain boundary particles after a similar heat treatment. The exact identity of these particles could not be determined, but they were undoubtedly either uranium or uranium oxide. X ray parameter measurements on these two alloys gave the results listed in table I.

Table I.
Increase of Tantalum Parameter on Heat-Treatment

Alloy (at. pct Ta)	a_0 in Angstroms	
	Not Heat-treated	Quenched from 1100°C
Pure Tantalum	3.308	3.312
99.2		3.320
98.5	3.311	3.327

That there is some increase in the solid solubility of uranium in tantalum with temperature is readily

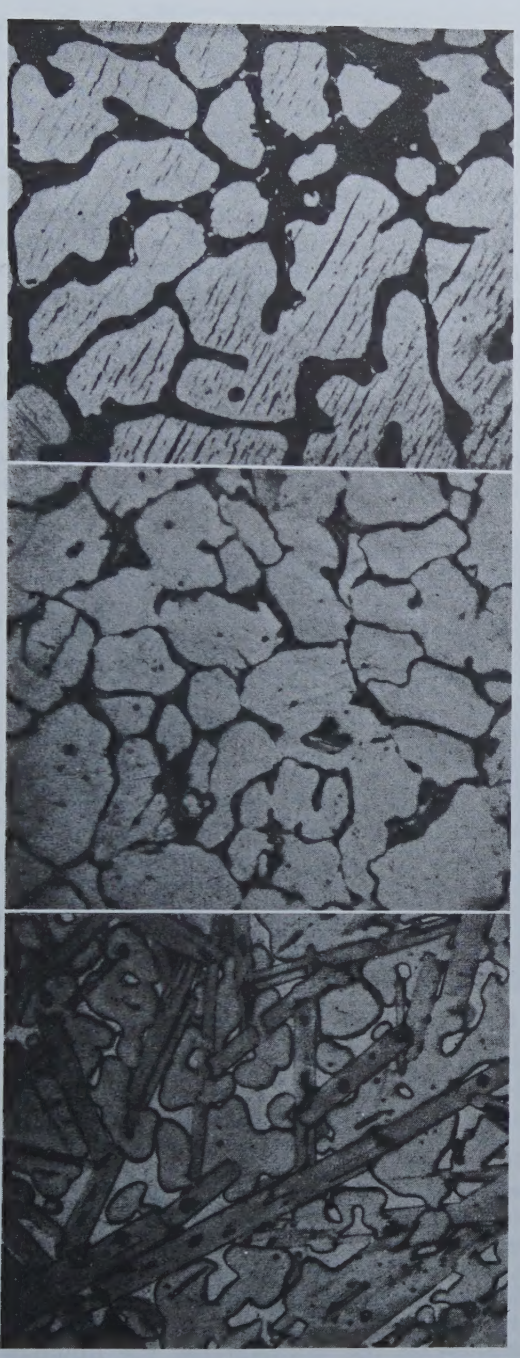

Fig. 8—Microstructures of Some Ternary Uranium-Tantalum-Carbon Alloys.

Etchant—electrolytic etch in alcohol-glycol-phosphoric solution. 250X. a. 76Ta-5U-19C (at. pct) alloy.* Massive $UTa_{10}C_4$ (light) plu Ta. b. 67.3. Ta-6.7U-26.0C (at. pct) alloy. Largely $UTa_{10}C_4$ (light). c. 55.5 Ta-9.4U-35.1C (at. pct) alloy $UTa_{10}C_4$ plus face-centered cubic phase (white).
* Approximate composition. No analysis available.

seen. However, the maximum solubility must be of the order of 2 at. pct uranium, for measurements on alloys of higher uranium content showed no further increase in the tantalum parameter.

Thermal measurements placed the alpha-beta and beta-gamma uranium phase transformations and the solidus lines at the temperatures indicated in fig. 4 and 5. The solid-solid transformations in the uranium were located in each case at approximately the same temperatures as those found for the corresponding phase changes in unalloyed uranium. The solidus in the tantalum system is clearly marked as a peritectic transformation by its appearance at a temperature 50°C higher than the melting point of uranium (1125°C). The nature of the tungsten solidus reaction is, however, in some doubt. On the basis of the slight raising of the temperature of the beginning of melting for the alloys as compared with the melting point of uranium (1135°C compared with 1125°C), this solidus reaction is tentatively also described as a peritectic transformation.

Establishment of the liquidus lines up to a temperature of 2400°C for the uranium-tungsten system and up to 2000°C for the uranium-tantalum system was accomplished in the induction unit by heating tungsten, or tantalum, in contact with molten uranium at a series of predetermined temperatures and then analyzing the solidified uranium chemically. In the case of tungsten, uranium specimens were machined into cylinders so as just to fill small tungsten crucibles, heated in the crucibles to the desired temperatures above the solidus and held there for a period of time long enough to attain the equilibrium solution of tungsten (from the crucible) in the uranium. After cooling, the crucible was broken away from the specimen and the surface of the latter ground to remove any traces of the crucible adhering to the alloy. In addition, a 1/64 in. layer was ground from the specimen to eliminate any tungsten particles which may have gotten into the uranium not by solution but by intergranular attack of the uranium on the tungsten. Such tungsten particles were easily distinguishable under the microscope by their angular or spheroidal shapes from the dendritic tungsten resulting from solution in and rejection from the uranium. Metallographic examination revealed that these nondendritic tungsten particles were almost exclusively confined to a region within 1/64 in. of the crucible wall.

For determination of the solubility of tantalum in molten uranium, the procedure described for tungsten had to be modified because of two difficulties encountered. First, it developed that molten uranium attacked (intergranularly) the tantalum crucibles available so vigorously even at temperatures only 100°-200°C above the uranium melting

Table II.
X ray Diffraction Lines for $UTa_{10}C_4$ CuKα Radiation

$Sin^2\theta$	Intensity*	$Sin^2\theta$	Intensity*
0.05626	VW	0.3828	VVW
0.06285	VW	0.3964	M
0.07524	VW	0.4327	W
0.08468	W	0.4779	M
0.1024	S	0.5538	M
0.1112	S	0.5806	VVW
0.1206	W	0.6045	M
0.1481	VW	0.6418	S
0.1575	VW	0.6775	W
0.1848	M	0.6969	S
0.2008	VVW	0.7230	W
0.2189	VVW	0.7436	W
0.2497	M	0.7989	S
0.2775	VVW	0.8413	M
0.2910	VVW	0.8800	M
0.3077	S	0.9386	S
0.3215	VVW	0.9596	S
0.3345	VVW	0.9706	VW
0.3500	M	0.9859	W-M
0.3593	W-M		

*S — Strong
M — Medium
W — Weak
VW — Very Weak
VVW — Very Very Weak

point that the whole uranium melt drained through the crucible and was lost in a short time. Hence, beryllia crucibles were substituted for the tantalum crucibles. The tantalum for alloying was introduced by inserting a tantalum rod into the molten uranium and withdrawing the rod prior to allowing the alloy to solidify. This technique was satisfactory at temperatures up to 1800°C, and was used to obtain the results given for tantalum in fig. 5 at 1300°, 1500° and 1800°C. Contamination of the melts with beryllium from the crucibles was negligible at these temperatures. At higher temperatures, reaction of the uranium with the crucible became appreciable so that beryllia crucibles could no longer be used. The value for the solubility of tantalum in uranium at 2000°C given in fig. 5 was obtained by melting uranium in a tantalum crucible which was itself placed in a close-fitting tungsten crucible. The uranium penetrated the tantalum crucible but was prevented from draining away by the comparatively stable tungsten crucible. Even this technique failed, however, at higher temperatures, and, thus, no results are reported for tantalum above 2000°C.

The second difficulty encountered was concerned with the carbon impurity present in the uranium. In the liquidus determination technique involving the insertion of a tantalum rod into the molten uranium, it was found that a layer of some new phase formed on the surface of the tantalum rod. This intervening layer markedly decreased the solution rate of tantalum in uranium and thus prevented the attainment of chemical equilibrium in reasonable times. Investigation showed that the interfering layer was a tantalum-uranium-carbon ternary phase very near the composition 67.3 at. pct Ta, 6.7 at. pct U, and 26.0 at. pct C (approximating closely the formula $UTa_{10}C_4$). Micrographs of several ternary alloys at and near this composition are shown in fig. 8. The corresponding powder X ray patterns are reproduced in fig. 9. The crystal symmetry of the phase is quite low, so that its structure was not determinable from the pattern shown in fig. 9b. The measured $\sin^2\theta$ values of the lines and the line intensities using Cu K α radiation are listed in table II. It may be of interest to note that another phase of the Ta-U-C system was identified incidental to this investigation. This phase gave a face-centered cubic pattern ($a_0 = 4.41$Å) and may be observed as the second (white) constituent in fig. 8.

In the course of the work establishing the identity of the $UTa_{10}C_4$ ternary phase, it was revealed that this carbide is considerably more stable than the binary carbides of uranium and tantalum. It has a very high melting point, probably well above 2500°C. Its deliberate formation was thus used as a means of decarburizing the uranium prior to making a liquidus determination. This was done by heating the molten uranium in contact with a tantalum rod (at the temperature at which this same uranium would later be used for a tantalum solution run), withdrawing the rod before allowing the uranium to solidify. In this way the carbon remaining in the uranium was reduced to a value too low to be detected by ordinary chemical analysis, that is, to less than 0.002 wt pct. Using this relatively carbon-free uranium, no further difficulty was encountered in obtaining solution of the tantalum in the uranium for the liquidus determinations.

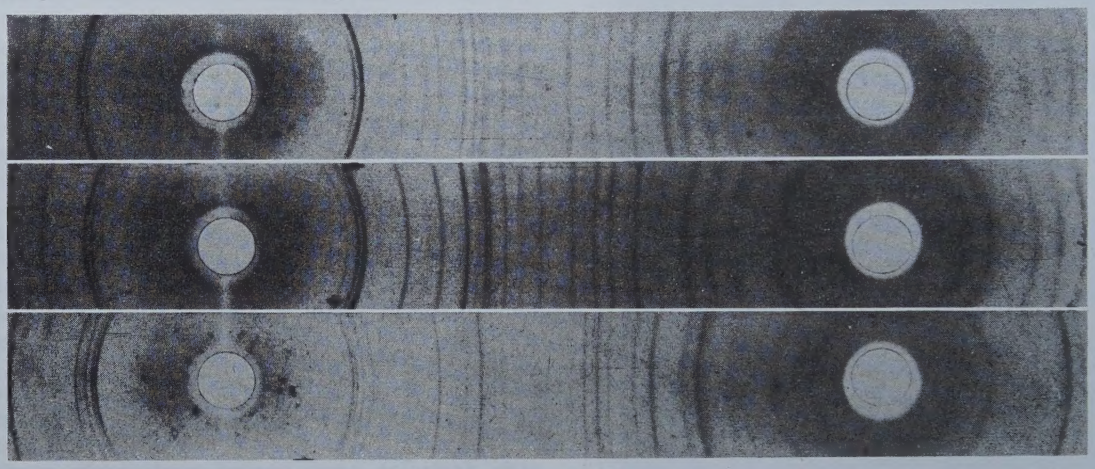

Fig. 9—Reproduction of Powder X Ray Photograms of the Three Ternary Alloys Shown in Fig. 8.

a. 76 Ta-5 U-19C (at. pct) alloy.* $UTa_{10}C_4$ and tantalum lines. b. 67.3 Ta-6.7 U-26.0 C (at. pct) alloy. Only $UTa_{10}C_4$ lines. c. 55.5 Ta-9.4U-35.1C (at. pct) alloy. $UTa_{10}C_4$ and face centered cubic phase lines.
* Approximate composition. No analysis available.

The Tantalum-Tungsten System: As reported by Bolton[1] tantalum and tungsten form a complete series of solid solutions. Since the two elements follow one another in the periodic table, have the same face-centered cubic crystal structure, and have lattice dimensions differing by only 4.4 pct, the continuous solid solution series is to be expected on the basis of the well-known Hume-Rothery rules. In the present work, no effort was made actually to fix the position of the solidus and liquidus lines, because of the extremely high temperatures involved. However, since it became necessary in connection with other work to know the variation in the lattice parameters of tantalum-tungsten alloys as a function of composition, this information was obtained and served to corroborate Bolton's conclusion.

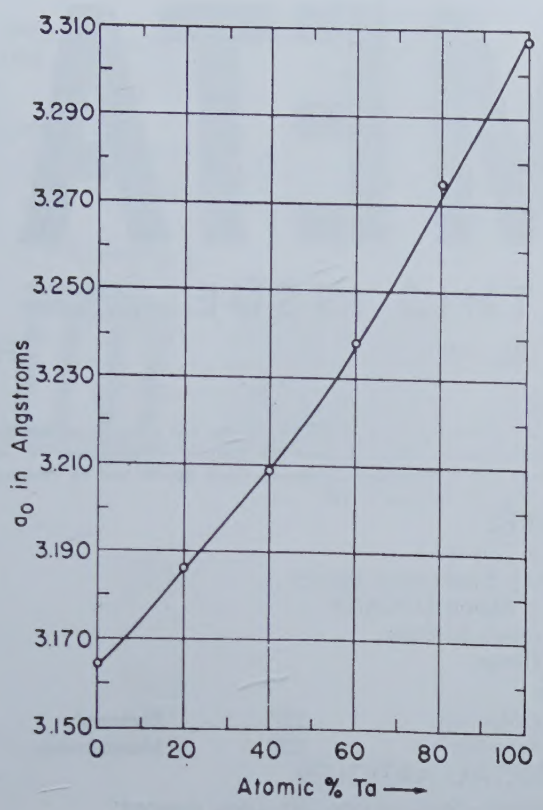

Fig. 10—Lattice Parameter of Tantalum-Tungsten Solid Solutions as a Function of Composition.

Alloys containing 20, 40, 60 and 80 at. pct tantalum, respectively, were prepared in the arc-melting apparatus. These alloys were then homogenized in vacuo for 5 hr at 2000°C. Powder for the X ray samples was obtained by crushing and sifting through a 200-mesh screen. The powders were stress relieved at 1300°C in vacuo.

As mentioned previously under *X Ray Techniques*, the parameters were measured both with a Debye-Scherrer type camera and with a back reflection symmetrical focusing camera. The results obtained are given in table III along with values for the pure metals listed by Barrett[4], and are plotted in fig. 10. The experimental parameter value for tantalum, 3.3077Å, may be seen to be somewhat higher than Barrett's value, 3.3026. The former value has been used in fig. 10 for two reasons: first, because the chief impurities in the tantalum used in this work were tungsten and columbium, both of which would tend to lower, rather than raise, the tantalum parameter; and second, because the shape and slope of the parameter-composition curve (fig. 10) indicate a value for the lattice constant of pure tantalum appreciably higher than that given by Barrett.

Table III. X Ray Parameter Values for Tantalum-Tungsten System

Nominal Atomic Pct Tantalum	X Ray Technique	a_0 in Angstroms
0	Barrett	3.1650
0	B. R. S. F*	3.1650
20	Debye-Scherrer	3.1861
20	B. R. S. F.*	3.1866
40	Debye-Scherrer	3.2098
60	Debye-Scherrer	3.2378
80	Debye-Scherrer	3.2744
100	Barrett	3.3026
100	Debye-Scherrer	3.3074
100	B. R. S. F.*	3.3077

* Back-reflection symmetrical focusing camera.

It is clear from the continuous, smooth nature of the curve in fig. 10 that tantalum and tungsten undoubtedly form a continuous series of solid solutions.

Conclusions

1. The constitutions of the uranium-tungsten and uranium-tantalum alloy systems have been determined and have been set forth in the phase diagrams of fig. 4 and 5.
2. Two phases of the uranium-tantalum-carbon ternary system have been discovered, one approximating the formula $UTa_{10}C_4$, having a low crystal symmetry and an extremely high melting point, and the other being a face-centered cubic phase with $a_0 = 4.41$Å.
3. The tantalum-tungsten system has been indicated to be a continuous series of solid solutions. The relationship between lattice parameter and composition for the tantalum-tungsten solid solutions has been determined.

References

[1] W. V. Bolton: *Ztsch. f. Electrochemie* (1905) **11**, 51.

[2] M. V. Cohen: *Rev. Sci. Instr.* (1935) **6**, 68; *Ibid.* (1936) **7**, 155.

[3] P. Gordon and A. R. Kaufmann: Alloys of Uranium and Aluminum. **12B**, Plutonium Project Record (Div. IV of Nat'l. Nuclear Energy Series).

[4] C. S. Barrett: Structure of Metals. McGraw-Hill Book Co., New York and London, (1943).